

DISSERTATION

**Targeted protein degradation in the pathogenesis and therapy  
of multiple myeloma**

**Gezielte Proteindegradation in der Pathogenese und Therapie  
des Multiplen Myeloms**

zur Erlangung des akademischen Grades  
Doctor of Philosophy (PhD)

vorgelegt der Medizinischen Fakultät  
Charité – Universitätsmedizin Berlin

von

**Yuen Lam Dora Ng**

Erstbetreuung: Prof. Dr. Jan Krönke

Datum der Promotion: February 28, 2025





## Table of contents

List of tables .....	iii
List of figures .....	iv
List of abbreviations.....	v
Abstract .....	6
1. Introduction .....	9
1.1 Pathogenesis .....	9
1.2 Prognosis .....	10
1.3 Treatment .....	10
1.4 Immunomodulatory drugs .....	11
1.5 IMiD-resistance mechanisms .....	11
1.6 Apoptosis modulators.....	12
1.7 Proteolysis targeting chimeras (PROTACs) .....	13
2. Methods.....	15
2.1 Study cohort .....	15
2.2 Proteomics and phosphoproteomics.....	15
2.3 RNA-sequencing .....	16
2.4 <i>In vivo</i> .....	16
2.5 Cell culture .....	16
2.6 Plasmids and transduction.....	17
2.7 Cell viability assay .....	18
2.8 Immunoblotting.....	19
2.9 Chemical synthesis.....	20
2.10 Software and statistical analyses .....	21
3. Results .....	22
3.1 Proteomic profiling identifies CDK6 protein upregulation in relapse myeloma patients...22	
3.2 Overexpression of CDK6 in myeloma cells confers IMiD-resistance.....	23

---

3.3 Combined targeting of CDK6 and IKZF1/3 is synergistic in multiple myeloma cells .....	24
3.4 CDK6 inhibition with IMiDs is highly efficacious in <i>in vivo</i> myeloma model .....	25
3.5 Targeting CDK6 reverses a relapse protein signature in multiple myeloma .....	26
3.6 Proteogenomic landscape of multiple myeloma and signatures of primary translocations t(11;14), t(4;14), and chr1q gain .....	28
3.7 Proteomic-based outcome prediction .....	29
3.8 Identification of UBE2Q1 as a driver for high-risk 1q gain myeloma.....	30
3.9 Identification of myeloma-specific drivers for potential therapeutic targeting.....	31
3.10 Design, generation, and quantitative evaluation of pan-IAP degraders .....	32
3.11 Protein degradation and cell viability from pan-IAP degraders.....	34
4. Discussion .....	36
Reference list.....	42
Statutory Declaration.....	50
Declaration of own contribution to the publications .....	51
Excerpt from Journal Summary List .....	53
Printing copies of the publications_Ng, Ramberger <i>et al.</i> 2022 .....	56
Printing copies of the publications_Ramberger <i>et al.</i> 2024 .....	84
Printing copies of the publications_Ng, Bricelj <i>et al.</i> 2023 .....	116
Curriculum Vitae.....	170
Publication list.....	171
Acknowledgments .....	173

**List of tables**

Table 1. List of oligonucleotide sequences. ....	17
Table 2. List of reagents.....	18
Table 3. List of primary and secondary antibodies. ....	19

## List of figures

Figure 1. Proteomic profiling identifies CDK6 protein upregulation in relapsed multiple myeloma patients..	23
Figure 2. Overexpression of CDK6 in myeloma cells confers IMiD-resistance.	24
Figure 3. Combined targeting of CDK6 and IKZF1/3 is synergistic in multiple myeloma cells.	25
Figure 4. Targeting CDK6 with IMiDs is highly efficacious in <i>in vivo</i> myeloma model.....	26
Figure 5. Targeting CDK6 reverses a relapse protein signature in multiple myeloma.....	27
Figure 6. Proteogenomic landscape of multiple myeloma and signatures of primary translocations t(11;14), t(4;14), and chr1q gain.	28
Figure 7. Proteomic-based outcome prediction.....	29
Figure 8. Identification of UBE2Q1 as a driver for high-risk 1q gain myeloma.....	31
Figure 9. Identification of myeloma-specific drivers for potential therapeutic targeting..	32
Figure 10. Design, generation, and quantitative evaluation of IAP-targeting PROTAC series....	33
Figure 11. Protein degradation and cell viability from pan-IAP degraders..	35

---

## List of abbreviations

ASCT	Autologous stem cell transplantation
BCMA	B-cell maturation antigen
BiTE	Bi-specific T-cell engagers
CAR-T	Chimeric antigen receptor T-cell
CRBN	Cereblon
CUL4A	Cullin 4A
DDB1	DNA damage-binding protein 1
HRD	hyperdiploidy
IAP	Inhibitor of apoptosis
IFN $\gamma$	Interferon-gamma
IKZF1	Ikaros family zinc finger protein-1
IKZF3	Ikaros family zinc finger protein-3
IL-2	Interleukin-2
IMiD	Immunomodulatory drug
ISS	International Staging System
MACS	Magnetic activated cell sorting
MGUS	monoclonal gammopathy of unknown significance
OS	Overall survival
PFS	Progression-free survival
PROTAC	Proteolysis targeting chimera
R-ISS	Revised International Staging System
ROC1	Regulator of cullins 1
SMM	smoldering multiple myeloma
PCL	plasma cell leukemia
TMT	tandem mass tag

## Abstract

The rediscovery of the immunomodulatory drug thalidomide as an effective therapy for multiple myeloma, along with the development of its more potent analogs, lenalidomide and pomalidomide, has significantly advanced the therapeutic armamentarium for multiple myeloma. Thalidomide analogs bind to the protein cereblon (CRBN) and alter the E3 ubiquitin ligase complex's substrate specificity, leading to ubiquitination and proteasomal degradation of Ikaros transcription factors. Despite these advances, the disease remains incurable as most patients relapse due to acquired treatment resistance. Although genetic alterations have been extensively studied, they do not account for the majority of resistance cases, necessitating the exploration of non-genetic mechanisms. This study aimed to investigate the role of post-transcriptional and -translational regulation of proteins in multiple myeloma in the context of pathogenesis and therapy resistance.

Applying deep quantitative proteomics on primary multiple myeloma samples, we identified post-transcriptional upregulation of the cyclin-dependent kinase 6 (CDK6) protein as a targetable non-genetic resistance mechanism in lenalidomide-resistant patients. We demonstrated that CDK6 regulates a relapse-associated protein signature, and that inhibiting CDK6 acts synergistically with pomalidomide in myeloma cells both *in vitro* and *in vivo*.

In a subsequent study, we performed a proteogenomic study on a large cohort of 138 myeloma patients at first diagnosis to investigate the proteomic landscape of multiple myeloma. The findings revealed that genetic alterations and post-transcriptional regulation contribute to a highly deregulated proteome in myeloma cells compared to healthy plasma cells. We uncovered the post-translational regulator ubiquitin-conjugating enzyme E2 Q1 (UBE2Q1) as an oncogenic driver on chromosome 1q that is associated with therapy resistance. By integrating proteomics and functional CRISPR screens, we also uncovered additional potential therapeutic targets for multiple myeloma.

Among other findings, we identified a strong deregulation of apoptosis-related proteins in the t(11;14) subset of myeloma patients. In addition, inhibitor of apoptosis (IAP) genes *BIRC2* and *BIRC3* are frequently deleted in relapsed/refractory myeloma cases, indicating a possible higher sensitivity to apoptosis-modulating drugs. We therefore developed novel pan-IAP protein degraders that are more effective than conventional IAP inhibitors in inhibiting the growth of multiple myeloma cells and other hematologic cancers.

In summary, this work has uncovered significant insights into the role of the ubiquitin-proteasome system in the pathogenesis and therapy of multiple myeloma, which has the potential to improve patient outcomes in multiple myeloma and other cancers in the future.

## Zusammenfassung

Die Wiederentdeckung des immunmodulatorischen Medikaments Thalidomid als effektive Therapie beim Multiplen Myelom und die daraus entwickelten stärkeren Analoga Lenalidomid und Pomalidomid erweiterten das therapeutische Arsenal für das Multiple Myelom stark. Thalidomid und seine Analoga binden an das Protein Cereblon (CRBN) und verändern die Substratspezifität des CRBN-E3-Ubiquitin-Ligase-Komplexes, was zur Ubiquitinierung und proteasomalen Abbau von Ikaros-Transkriptionsfaktoren führt. Obwohl nahezu alle Patienten auf die Therapie ansprechen, erleiden die meisten einen Rückfall aufgrund erworbener Therapieresistenz. Genetische Veränderungen wie Mutationen in *CRBN* erklären weniger als 10% der Resistenz. Ziel dieser Arbeit war es, die Rolle von post-transkriptioneller und -translationaler Regulation von Proteinen beim Multiplen Myelom im Kontext der Therapieresistenz zu untersuchen.

Durch die Anwendung quantitativer Proteomik an primären Proben des Multiplen Myeloms konnten wir die post-transkriptionelle Hochregulierung des Proteins Cyclin-abhängige Kinase 6 (CDK6) als einen nicht-genetischen Resistenzmechanismus bei Lenalidomid-resistenten Patienten identifizieren. Wir wiesen nach, dass CDK6 eine Resistenz-assoziierte Proteinsignatur reguliert, dessen Hemmung durch Inhibitoren sowohl *in vitro* als auch *in vivo* synergistisch mit Pomalidomid auf Myelomzellen wirkt.

In einer darauf aufbauenden Studie erstellten wir eine proteogenomische Studie an einer großen Kohorte von Myelompatienten zum Zeitpunkt der Erstdiagnose. Diese zeigte, dass sowohl genetische Veränderungen und post-transkriptionelle Regulation zu einem stark deregulierten Proteom in Myelomzellen im Vergleich zu gesunden Plasmazellen beitragen. Mit dem Ubiquitin-konjugierendem Enzym E2 Q1 (UBE2Q1) konnten wir einen post-translationalen Regulator als onkogenen Treiber auf Chromosom 1q aufdecken, der mit Therapieresistenz assoziiert ist. Durch die Integration von Proteomik und funktionellen CRISPR-Screens identifizierten wir zudem weitere potenzielle therapeutische Ziele für das Myelom.

Unter anderem fanden wir eine starke Deregulierung apoptosebezogener Proteine in der t(11;14)-Subgruppe von Myelompatienten. Die Apoptoseinhibitor (IAP)-Gene *BIRC2* und *BIRC3* sind darüber insbesondere bei rezidierten/refraktären Myelomfällen häufig deletiert, was zu einer möglichen höheren Sensitivität auf apoptosemodulierende Medikamente führt. Daher entwickelten wir neuartige pan-IAP-Protein-Degrader, die wirksamer als herkömmliche IAP-Inhibitoren das Wachstum von Multiplen Myelomzellen hemmten.

Zusammenfassend konnte diese Arbeit wesentliche Erkenntnisse über die Rolle des Ubiquitin-Proteasom-Systems bei der Pathogenese und Therapie des Multiplen Myeloms aufdecken, die das

Potential haben, die Behandlungsergebnisse beim Multiplen Myelom und anderen Krebserkrankungen in Zukunft zu verbessern.



## 1. Introduction

Multiple myeloma is a genetically heterogeneous plasma cell neoplasia and is the second most prevalent hematologic malignancy. The disease is characterized by the infiltration of abnormal, cancerous plasma cells in the bone marrow and the production and secretion of monoclonal immunoglobulins termed paraproteins. Clinically, multiple myeloma presents with hypercalcemia, renal insufficiency, anemia, and osteolytic lesions, caused by excessive paraprotein production and the aggressive growth of malignant cells. Cytogenetic abnormalities and the bone marrow microenvironment also play a crucial role in the disease's progression. Despite the introduction of novel therapies, such as immunomodulatory drugs, proteasome inhibitors, monoclonal antibodies, and cellular immunotherapies such as chimeric antigen receptor (CAR) T cells and bispecific antibodies, leading to prolonged survival, multiple myeloma to date remains incurable due to the frequent development of therapy resistance.

### *1.1 Pathogenesis*

Plasma cells are terminally differentiated, antibody-secreting effector cells derived from the B-cell lymphoid lineage and play a crucial role in the humoral immune response. In multiple myeloma, the accumulation and dissemination of these plasma cells in the bone marrow leads to the production of abnormal amounts of monoclonal immunoglobulin, which can be detected in serum or urine and cause a variety of clinical manifestations and complications<sup>1</sup>. Multiple myeloma is preceded by two precursor conditions: monoclonal gammopathy of undetermined significance (MGUS), a premalignant asymptomatic condition characterized by the presence of a small amount of monoclonal protein in the blood and no detectable end-organ damage<sup>2-4</sup>, and smoldering multiple myeloma (SMM), an intermediate stage with clonal plasma cells in the bone marrow expanding past 10 % but without myeloma-defining events<sup>1,5</sup>. The progression of the disease to multiple myeloma is characterized by the CRAB criteria (hypercalcemia, renal failure, anemia, and bone marrow lesions) or other myeloma-defining events. A rare and aggressive form of multiple myeloma, secondary plasma cell leukemia (PCL), is present when >20% circulating plasma cells are detected in the peripheral blood and is typically associated with a poorer prognosis<sup>1,6</sup>.

The genetic architecture of multiple myeloma is complex, involving various genetic abnormalities that drive tumor development and progression. Primary genetic events that initiate the development of overt disease frequently involve the translocation of immunoglobulin heavy chain (IgH) on chromosome 14 with oncogenes *MMSET/FGFR3* (t(4;14)), *CCND1* (t(11;14)), *MAF* (t(14;16)),

and MAFB (t(14;20)), or hyperdiploidy (HRD), particularly trisomy of odd-numbered chromosomes. Secondary genetic events occur later in the pathogenesis of the disease and comprise the acquisition of genomic aberrations such as chromosomal gains or lesions, secondary translocations, and somatic mutations. The most frequently mutated genes in multiple myeloma include *KRAS*, *NRAS*, *FAM46C*, *BRAF*, *TP53*, and *DIS3*, resulting in dysregulation of pathways such as the MAPK, NF- $\kappa$ B, and DNA-damage pathways<sup>7-9</sup>. *BIRC2* and *BIRC3*, encoding cIAP1 and cIAP2 respectively, are located on chromosome 11q and are detected in 7% of multiple myeloma cases<sup>10</sup>. The deletions are significantly enriched in t(4;14) cases compared to non-t(4;14) cases and are more frequently detected in relapse patients<sup>11</sup>. *BIRC2/BIRC3* deletions contribute to the clonal expansion under therapeutic selection<sup>12</sup> and lead to constitutive activation of the non-canonical NF- $\kappa$ B pathway, resulting in poor prognosis<sup>9,13,14</sup>.

### 1.2 Prognosis

Prognostic evaluation in multiple myeloma requires the assessment of several factors, including tumor burden according to Durie-Salmon Staging (DSS)<sup>15</sup> and the International Staging System (ISS)<sup>16</sup>, molecular subtypes such as del(17p), gain(1q), or del(1p)<sup>17,18</sup>, response to treatment<sup>19</sup>, elevation of serum lactate dehydrogenase (LDH), and presence of circulating plasma cells. The Revised International Staging System (R-ISS) integrates these predictive factors to provide a comprehensive prognostic staging algorithm<sup>20</sup>. Risk stratification in multiple myeloma is a dynamic and evolving field, driven by ongoing research and emerging treatment options, and is essential for personalizing treatment approaches and improving patient outcomes.

### 1.3 Treatment

The treatment landscape for multiple myeloma has evolved significantly over the past few decades, resulting in improved patient outcomes and prolonged survival. The introduction of new effective therapies has substantially improved outcomes in multiple myeloma over the past decade with a median life expectancy of >10 years in younger patients. Current treatment modalities largely incorporate intensive chemotherapy supported by autologous stem cell transplantation (ASCT), proteasome inhibitors, corticosteroids, and immunomodulatory drugs. Other targeted therapies such as venetoclax, a BCL-2 inhibitor clinically used in the treatment of acute myeloid leukemia for the modulation of apoptosis, are also used, although not approved, in specific genetic contexts in multiple myeloma<sup>21,22</sup>. In the past years, immunotherapies have emerged as an advanced approach in the treatment of multiple myeloma and include monoclonal antibodies, antibody-drug conjugates,

chimeric antigen receptor T-cell (CAR-T) therapy, and bi-specific T-cell engagers (BiTEs) targeting CD38<sup>23</sup>, SLAMF7<sup>24–26</sup>, as well as B-cell maturation antigen (BCMA)<sup>27–31</sup>.

#### *1.4 Immunomodulatory drugs*

Immunomodulatory drugs (IMiDs) have a fascinating history that spans decades of research, controversy, and remarkable clinical advancements. The discovery of thalidomide's immunomodulatory properties in the 1990s marked a pivotal turning point in the treatment of multiple myeloma, despite its earlier tragic use as a sedative in the 1950s, which led to severe birth defects in >10,000 newborn children during the so-called Contergan catastrophe and its subsequent market withdrawal<sup>32–34</sup>. Thalidomide analogs, lenalidomide and pomalidomide, were developed with enhanced immunological and anti-cancer effects and are clinically used in the treatment of multiple myeloma<sup>35</sup>, as well as myelodysplastic syndrome<sup>36</sup>, chronic lymphocytic leukemia, and non-Hodgkin's lymphoma<sup>37</sup>. Currently, efforts are underway to develop more potent analogs, such as avadomide<sup>38</sup>, iberdomide<sup>39,40</sup>, and mezigdomide<sup>41–43</sup>, which are currently tested in clinical trials.

The mechanism of action of IMiDs involves the modulation of E3 ubiquitin ligase complex cereblon (CRBN)<sup>34</sup>. CRBN, together with DNA damage-binding protein 1 (DDB1), Cullin 4A (CUL4A), and regulator of cullins 1 (ROC1), facilitates the targeted degradation of key transcription factors Ikaros family zinc finger protein-1 (IKZF1) and -3 (IKZF3) upon binding of thalidomide analogs<sup>44</sup>. As IKZF1 and IKZF3 are important regulators for lymphoid differentiation and transcriptionally regulate IRF4 and c-Myc, which are essential for the growth and survival of multiple myeloma cells, the depletion of these proteins results in anti-myeloma effects<sup>45</sup>. IMiDs also possess immunostimulatory effects via enhancing T- and natural killer (NK)- cell proliferation and cytokines interleukin-2 (IL-2) and interferon-gamma (IFN $\gamma$ ) production due to the negative regulation by IKZF1 and IKZF3<sup>46–49</sup>.

#### *1.5 IMiD-resistance mechanisms*

Sequencing studies and functional genetic screens in relapsed multiple myeloma have identified acquired genetic alterations in members of the CRBN-CRL4 E3 ligase complex in 10 – 20% of relapsed patients as an IMiD-resistance mechanism<sup>50–53</sup>. Similarly, mutations in the degron sites of IKZF1/3 have been found to disrupt their interaction with CRBN in the presence of IMiDs, thereby leading to resistance<sup>54</sup>. In addition to mutations within the CRBN-IKZF axis, functional CRISPR/Cas9 screens have identified CSN9 signalosome as a regulator of CRBN expression levels<sup>51</sup> and ChIP-seq have shed light on how c-FOS transactivates IRF4 and SLAMF7<sup>55</sup> as well as

ETV4 sustaining transcription of *MYC* independent of IKZF1<sup>56</sup>, mediating IMiD-resistance. Epigenetics have also been described to mediate resistance towards IMiDs. Aberrant CRBN methylation was described to be correlated with reduced CRBN expression levels in IMiD-refractory multiple myeloma<sup>57</sup>. Other studies have reported that IMiD-resistance is associated with enhanced genome-wide DNA methylation and reduced chromatin accessibility, thus EZH2 inhibition can overcome IMiD resistance in both cereblon-dependent and –independent manner<sup>58,59</sup>. While previous research has leveraged sequencing to uncover genetic resistance mechanisms, the majority of resistance remains unexplained. In various cancer studies, protein and RNA levels often show a low correlation<sup>60–62</sup>. This discrepancy emphasizes the general need for integrating proteomic and genomic approaches in cancer research, as relying solely on RNA expression studies may overlook important functional changes at the protein level. The low correlation can result from post-transcriptional and post-translational regulation such as ubiquitination, as well as differences in the stability of protein and RNA and translation efficiency. As protein levels often correlate more closely with cellular phenotypes and drug responses than mRNA levels, incorporating proteomic profiling is crucial for identifying potential therapeutic targets and biomarkers. Only a few proteomic studies with low sample numbers on multiple myeloma have been previously reported, including research on resistance towards bortezomib-based therapy<sup>63</sup>, understanding metabolic adaptations of myeloma cells in the bone marrow tumor microenvironment<sup>64</sup>, and investigating lipid metabolism changes in the pathogenesis of multiple myeloma<sup>65</sup>. Integrating proteomic analyses may facilitate the identification of non-genetic resistance mechanisms by providing insights into protein expression, post-translational modifications, and protein networks. Elucidating these resistance pathways is imperative for developing effective strategies to manage and overcome IMiD resistance in multiple myeloma. Comprehensive research is required to delineate these mechanisms and optimize therapeutic approaches.

### *1.6 Apoptosis modulators*

While apoptosis modulators have demonstrated high clinical efficacy in other cancers, the efficacy in multiple myeloma is limited. BCL2-selective inhibitor venetoclax, a BH3 mimetic, is FDA-approved for the targeting of chronic lymphocytic leukemia (CLL)<sup>66,67</sup> and acute myeloid leukemia (AML)<sup>68,69</sup>. Venetoclax binds selectively to anti-apoptotic BCL2 proteins, displacing proapoptotic proteins BAX and BAK, thereby initiating apoptosis. The administration of venetoclax has shown remarkable efficacy, achieving high response rates and improved remission in relapsed/refractory CLL<sup>70,71</sup>, and demonstrating improved remission rates when used in combination

with hypomethylating agents in newly diagnosed AML patients who are unfit for intensive chemotherapy<sup>68,72</sup>. In multiple myeloma, however, venetoclax only demonstrated efficacy in a subset of patients<sup>21,22</sup>. There is ongoing research aiming to elucidate factors modulating venetoclax-sensitivity in multiple myeloma, one of which suggests that expression of B-cell markers is associated with BCL2 dependency<sup>73,74</sup>.

Another class of apoptosis modulators is SMAC mimetics. Second mitochondria-derived activator of caspases (SMAC) mimetics are a class of drugs that promotes apoptosis by inhibiting IAPs through the binding to the BIR3 domain<sup>75,76</sup>. Inhibitor of apoptosis (IAP) proteins cellular IAP1 (*BIRC2*, cIAP1), cellular IAP2 (*BIRC3*, cIAP2), and X-chromosome-linked IAP (*BIRC4*, XIAP) are important ubiquitin E3 ligases that regulate programmed cell death through the inhibition of caspases and modulation of NF- $\kappa$ B and TNF receptor signaling<sup>77-79</sup>. Upregulation of the IAP protein family, including XIAP, is often associated with poor prognosis, worse overall survival, and increased resistance to therapies<sup>80-83</sup>. Monovalent and bivalent IAP antagonists have been developed and were in early-phase clinical trials but with limited clinical efficacy as monotherapy<sup>84-86</sup>. These antagonists lead to the autoubiquitination and degradation of cIAP1 and cIAP2 while XIAP is inhibited but not degraded<sup>87-89</sup>.

### *1.7 Proteolysis targeting chimeras (PROTACs)*

Proteolysis targeting chimeras (PROTACs) represent a novel modality for targeted protein degradation and has gained increasing prominence in recent years. These heterobifunctional molecules consist of two distinct ligands: one that binds to a specific target protein, and another that recruits an E3 ubiquitin ligase, connected by a linker. The induced proximity between the target protein and E3 ligase facilitates polyubiquitination of the target protein, marking it for degradation via the cell's intrinsic ubiquitin-proteasome system. This approach represents a highly selective and targeted strategy and the potential to enable degradation of disease-causing proteins that have been challenging to target with small-molecule inhibitors has gained significant interest and investment from both the academic research community and the pharmaceutical industry.

Compared to traditional small-molecule inhibitors, PROTACs offer several distinct advantages. They degrade disease-relevant proteins instead of inhibiting their activity, are effective at lower doses due to event-driven processes instead of occupancy-driven mechanisms, and are versatile as they can target proteins without active sites. Consequently, the discovery and rapid advancement of PROTACs have expanded the human druggable proteome, potentially offering more potent and durable therapeutic effects.

PROTACs targeting androgen receptors and estrogen receptors have already entered Phase II clinical trials for the treatment of prostate and breast cancer<sup>90</sup>. While PROTACs show great promise, their clinical development is still in the early stages. Challenges such as improving cell-specific delivery, identifying additional E3 ligases for optimal target degradation, and enhancing tissue specificity need to be addressed to fully realize their therapeutic potential. The ongoing advancements in PROTAC technology are poised to revolutionize the landscape of drug discovery and development. PROTACs are expected to become a valuable tool in precision medicine, offering new avenues for the treatment of a wide range of diseases that currently lack effective therapeutic options.

## **Research aim**

This work aims to leverage proteomics to comprehensively profile the proteome of multiple myeloma and identify potential therapeutic targets and biomarkers, as well as actionable targets that can overcome treatment resistance. Additionally, we seek to explore and develop PROTACs for targeted protein degradation to advance treatment strategies.

## 2. Methods

This section outlines the principle methodologies applied in the publications featured in this dissertation, with emphasis on the major techniques applied and experiments to which I contributed. Comprehensive details of the methods used for each study can be found in the respective publications<sup>91–93</sup>.

### 2.1 Study cohort

Five multiple myeloma patients who underwent treatment regimens including lenalidomide were included in the proteomic study by Ng, Ramberger *et al.*<sup>91</sup>. Multiple myeloma cells collected by bone marrow aspiration at diagnosis and relapse were enriched by CD138+ magnetic activated cell sorting (MACS) (Miltenyi, #130-051-031, Germany) and subjected to quantitative proteomic profiling. An independent cohort of thirteen newly diagnosed and relapsed/refractory patient samples was used for the validation of the proteomic findings. Patient characteristics and treatment undergone are included in Supplementary Figure 1 of Ng, Ramberger *et al.*<sup>91</sup>. Patient samples were chosen based on sample availability.

The proteomics study by Ramberger *et al.*<sup>93</sup> comprised 138 patients, of which 114 were newly diagnosed myeloma, 17 were plasma cell leukemia, and 7 were MGUS<sup>93</sup>. Of the samples from newly diagnosed patients, 100 were obtained from the DSMM XII-XIV clinical trials (NCT00925821, NCT01090089, NCT01685814)<sup>94–96</sup>. All samples were collected via bone marrow aspiration, other than plasma cell leukemia, which was obtained from peripheral blood. All primary samples either had an average CD138+ purity of 85% or enriched by CD138+ MACS. Patient samples were chosen based on the availability of sufficient and high-quality myeloma cells for proteomic and genetic analyses, as well as the accessibility of FISH-based cytogenetics and clinical data.

Written informed consent was obtained from all patients according to the Declaration of Helsinki and approved by the Institutional Review Board (IRB). The studies were approved by the responsible ethics committees Ulm University (136/20, 307/08) and Charité Universitätsmedizin Berlin (EA2/142/20).

### 2.2 Proteomics and phosphoproteomics

Proteomic analysis of all primary myeloma samples and cell lines was performed with tandem mass tag (TMT) technique. In brief, samples were lysed and protein peptides were isobarically labeled with tandem mass tags (Thermo Scientific, 90406, A44520, USA). Q-Exactive HF-X

(Thermo Scientific, USA) was used for the acquisition of mass spectrometry raw data. The data was then analyzed by MaxQuant (Version 1.6.3.3<sup>91</sup> and Version 2.0.3.0<sup>93</sup>) and searched against the human reference proteome (UniProt). Further details on protein extraction and digestion, TMT labeling, peptide fractionation, phosphopeptide enrichment, liquid chromatography-mass spectrometry, and raw data search and analysis can be found in the methods section of respective publications<sup>91,93</sup>.

Processed proteomics data is available on ProteomeXchange Consortium via the PRIDE partner repository with accession numbers PXD021265<sup>91</sup>, PXD038437<sup>93</sup>, and PXD043580<sup>93</sup>.

### 2.3 RNA-sequencing

Library preparation on RNA samples in the studies conducted in Ng, Ramberger *et al.*<sup>91</sup> and Ramberger *et al.*<sup>93</sup> was performed using the TruSeq Stranded Exome RNA Kit (Illumina, USA). Sequencing was performed on HiSeq2000 (Illumina, USA) with 50 bp single-end reads with an average coverage of  $36.6 \times 10^6$  reads per sample. RNA-seq data was aligned and quantified using STAR<sup>97</sup>, and quantitative data was processed similarly to proteomic data for enhanced comparability. GSEA and MSigDB were used for gene set enrichment analysis.

RNA sequencing expression data is available at Gene Expression Omnibus (GEO) with accession numbers GSE162403<sup>91</sup> and GSE222727<sup>93</sup>.

### 2.4 *In vivo*

6-8 week-old female NOD/Shi-scid/IL2R $\gamma^{\text{null}}$  mice were subcutaneously injected with  $1 \times 10^7$  MM.1S human myeloma cells. Tumors reached 200 mm<sup>3</sup> after 19 days and were subsequently randomized for treatment initiation. Pomalidomide and palbociclib were administered daily by oral gavage, at 5 mg/kg and 50mg/kg respectively. Dual-targeting PROTAC YKL-06-102 was administered daily via intraperitoneal injection at 5 mg/kg. The animals underwent 17 days of treatment followed by 11 days of observation. Mice were euthanized upon reaching study termination of a maximum tumor size of 1200 mm<sup>3</sup>. The animal study adhered to the guidelines set forth by the United Kingdom Coordinated Committee on Cancer Research and received approval and authorization from the Landesamt für Gesundheit und Soziales, Berlin, Germany (approval No. G 0333/18).

### 2.5 Cell culture

All cell lines were purchased from American Type Culture Collection (ATCC) (Virginia, USA) or German Collection of Microorganisms and Cell Cultures GmbH (DSMZ) (Leibniz, Germany).



Cells were maintained either in RPMI-1640 or DMEM medium containing 10% fetal bovine serum (FBS) and 1% penicillin/streptomycin. NCI-H929 cells were additionally supplemented with 50  $\mu$ M beta-mercaptoethanol and 1 mM sodium pyruvate, and INA-6 cells were cultured in the presence of 10 ng/ml hIL-6 (PeproTech, USA). Cells were cultured at 37 °C with 5% CO<sub>2</sub> in humidified atmosphere. All cell lines were authenticated with short tandem repeat (STR) profiling and molecular markers were compared against the STR profile database DMSZ CellDive. All cell lines were tested negative in regular mycoplasma tests.

## 2.6 Plasmids and transduction

For virus production, HEK293T cells were transfected with constructs along with their respective packaging and envelope plasmids using Trans-LT1 transfection reagent (Mirus Bio, USA). Virus was harvested 48 h post-transfection and passed through 0.45  $\mu$ m filters. Packaging and envelope plasmids used include pSPAX2, pVPack-GP, and pMD2.G.

Vectors used in the studies pertaining to CRISPR/Cas9-mediated genetic knockout include pLKO5d.SSF.SpCas9.P2a.BSD and pLKO5.hU6.sgRNA.dTom. Sequences of sgRNAs are included in Table 1. For the ectopic overexpression of protein candidates, pRSF91-GFP-T2A-Puro and pLenti.6.2.V5-DEST were used as backbone with respective cDNAs cloned in.

Table 1. List of oligonucleotide sequences. List is own representation adapted from Ng, Ramberger *et al.* and Ng, Bricelj *et al.*<sup>91,92</sup>.

Oligonucleotides	Sequence
CRISPR/Cas9 sgRNA	
<i>Rb1</i> sgRNA #1	TGAACTACTTACGAACTGCT
<i>CRBN</i> sgRNA #1	GTCCTGCTGATCTCCTTCGC
<i>CRBN</i> sgRNA #2	GGATTCACATAAGCTGCCAT
<i>BIRC2</i> sgRNA	ATGCTATGTCAGAACACCGG
<i>BIRC3</i> sgRNA	TTTCGTTATTCATTGCACAG
<i>BIRC4</i> sgRNA	ATGACA ACTAAAGCACCGCA
qPCR	
TRIP13_forward	ACTGTTGCACTTCACATTTTCCA
TRIP13_reverse	TCGAGGAGATGGGATTTGACT
RRM1_forward	GCTGAAACAGCTGCAACCTT
RRM1_reverse	ACCATGGGAGAGTGTTTGCC
MCM3_forward	TACCTGGACTTCCTGGACGA

MCM3_reverse	AAGGCAACCAGCTCCTCAAA
MCM5_forward	CCAAGTGTCCACGTTGGATG
MCM5_reverse	TGCTCCGGGTATTTCTGCTT
PRPS2_forward	AGGTAGGAGAGAGTCGTGCC
PRPS2_reverse	CCACTCGGCAATGTTTTCCC

### 2.7 Cell viability assay

Cells were plated in 96-well or 384-well plates and incubated at 37 °C for 96 h with respective treatments. For assays involving the investigation of inhibitors towards IAP proteins, TNF- $\alpha$  was added at 1 ng/ml. Cell viability was assessed using CellTiter-Glo® Luminescent Cell Viability Assay (Promega, USA) and measured with Synergy LX Multi-Mode plate reader (BioTek, USA) or POLARStar Omega plate reader (BMG LabTech, Germany). All results were normalized to the DMSO-treated control. Data represents the mean  $\pm$  standard deviation (s.d.) of independent biological triplicates. All reagents used are included in Table 2.

Table 2. List of reagents. List is own representation adapted from Ng, Ramberger *et al.*, Ramberger *et al.*, and Ng, Bricelj *et al.*<sup>91-93</sup>.

Reagent	Source	Catalog #
Inhibitors		
AZD5582	MedChemExpress	HY-12600
Birinapant	MedChemExpress	HY-16591
Bortezomib	SelleckChem	S1013
BV6	MedChemExpress	HY-16701
Carfilzomib	SelleckChem	S2853
Dexamethasone	SelleckChem	S1322
Erdafitinib	Hözel Diagnostics	S8401-5
LCL161	MedChemExpress	HY-15518
Lenalidomide	SelleckChem	S1029
Melphalan	SelleckChem	S8266
MG132	SelleckChem	S2619
MLN4924	SelleckChem	S7109
MLN7243	SelleckChem	S8341
NT157	Selleckchem	S8228
Palbociclib	SelleckChem	S4482
Pomalidomide	SelleckChem	S1567

PROTACs		
BSJ-03-123	Synthesized according to Brand <i>et al.</i> 2019 and Steinebach <i>et al.</i> 2020 <sup>98,99</sup>	
CST528	Synthesized according to Brand <i>et al.</i> 2019 and Steinebach <i>et al.</i> 2020 <sup>98,99</sup>	
YKL-06-102	Synthesized according to Brand <i>et al.</i> 2019 and Steinebach <i>et al.</i> 2020 <sup>98,99</sup>	
Cytokines		
hTNF- $\alpha$	Miltenyi Biotec	130-094-014

### 2.8 Immunoblotting

Respective cell lines were treated correspondingly and lysed in Pierce lysis buffer. Subsequently, SDS-PAGE was carried out and proteins were transferred onto Immobilon®-P PVDF Membrane (Merck, Germany). Blotted membranes were blocked and incubated overnight at 4 °C in primary antibodies. Secondary HGP-conjugated antibodies were incubated at room temperature for 1 h, followed by protein detection with Immobilon Western Chemiluminescent HRP Substrate (Merck, Germany) or WesternBright ECL HRP substrate (Advansta, USA). Chemiluminescence was detected and imaged with LAS-4000x Luminescent Image Analyzer (Fujifilm, Japan) or ChemiDoc XRS+ System (Bio-Rad, Germany). For subsequent protein detections, membranes were subjected to incubation with Restore Western Blot Stripping Buffer (Thermo Scientific, USA) and re-activation with methanol. List of immunoblotting antibodies used can be found in Table 3.

Table 3. List of primary and secondary antibodies. List is own representation adapted from Ng, Ramberger *et al.* and Ng, Bricelj *et al.*<sup>91-93</sup>.

Antibody	Source	Catalog #	Clone
Primary antibodies			
BIRC2	BioRad	VMA00532	AB01/3B4
Aiolos	Cell Signaling	15103S	D1C1E
beta-actin	Sigma-Aldrich	A1978	
CDK4	Cell Signaling	12790	D9G3E
CDK6	Cell Signaling	3136	DCS83
CDK6	Santa Cruz Biotechnology	sc-7961	B-10
cIAP2	Cell Signaling	3130S	58C7
c-Myc	Cell Signaling	5605	D84C12
CRBN	Sigma-Aldrich	SAB2106014	

HIF-1 $\alpha$	BDBioSciences	610958	54
Ikaros	Cell Signaling	14859S	D6N9Y
IRF4	Cell Signaling	4299	D43H10
Phospho-Rb (Ser807/811)	Cell Signaling	9308	
Rb	Cell Signaling	9309	4H1
RRM1	Cell Signaling	8637	D12F12
RRM2	Cell Signaling	65939	E7Y9J
TRIP13	Santa Cruz Biotechnology	sc-514285	A-7
VHL	Cell Signaling	68547S	
XIAP	Cell Signaling	14334S	D2Z8W
$\alpha$ -tubulin	Sigma-Aldrich	T5168	B512
Secondary antibodies			
anti-rabbit IgG HRP-linked antibody	Cell Signaling	7074	
anti-mouse IgG HRP-linked antibody	Cell Signaling	7076	

### 2.9 Chemical synthesis

In brief, two parallel libraries of 8 linkers varying in length and chemical composition were prepared. The first series consisted of chloro to carboxylic acid (Cl-to-COOH) linkers, whereas the second series contained methane-sulfonate to chloro (OMs-to-Cl) linkers. Four different E3 ligase ligands were then prepared, two of which target the von Hippel-Lindau (VHL) ligase, one for binding to inhibitor of apoptosis (IAP) proteins, and 4-fluorothalidomide, which represents the cereblon (CRBN) binding moiety.

The first series of heterobifunctional molecules consists of a VHL ligand coupled with chloro to carboxylic acid linkers. The second VHL series was prepared utilizing a VHL ligand with an alternate exit vector, which presumably leads to differently oriented ternary complexes, and methane-sulfonate to chloro linkers were conjugated via the alkylation of phenol of VHL ligand. The VHL-linker conjugates were reacted with the IAP ligand and then Boc-protected under acidic conditions. Lastly, the IAP ligand was first *O*-alkylated for the CRBN-IAP heteroPROTACs series, where the chloro-linker-IAP ligand conjugates were CRBN-binding moiety connected to the CRBN-binding moiety by reacting 4-fluorothalidomide with the amino conjugates in a nucleophilic aromatic substitution. Removal of the Boc protecting group yielded the envisioned heteroPROTACs.

After identifying the most potent compounds, appropriate negative controls were prepared by incorporating structurally modified ligands for the chosen E3 ligases, which abolished their binding affinity. All of the prepared products were purified either through column chromatography or by using an automated flash chromatography system. The purity and identity of compounds were confirmed via  $^1\text{H}$  and  $^{13}\text{C}$  NMR spectroscopy, an LC/MSD system, high-resolution mass spectrometry (HRMS), and ultra-performance liquid chromatography (UPLC).

The chemical synthesis section was completed with generous help from Aleša Bricelj from the Faculty of Pharmacy at University of Ljubljana.

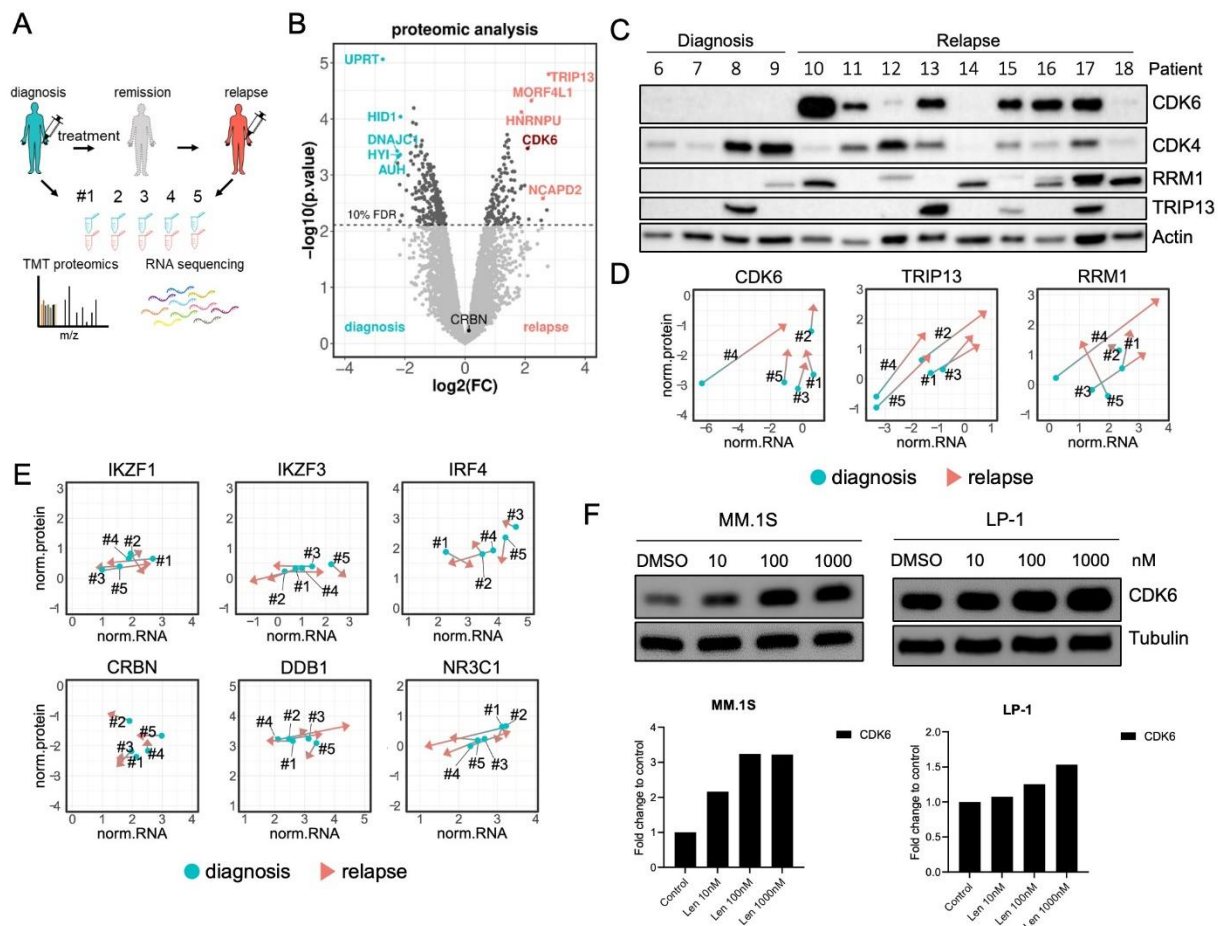
### *2.10 Software and statistical analyses*

Raw proteomics data was analyzed with with MaxQuant (Version 1.6.3.3 or 2.0.3.0) or with DI-ANN 1.8.1. RNA sequencing data was aligned with STAR 2.7 and quantified with RSEM 1.3.0. Further analysis on processed proteomics or transcriptomics data was analysed with R(4.0.3) and R studio (V 1.3.1093 or 4.1.1). Statistical analyses of cell viability experiments were performed with GraphPad Prism v8 and v9.1.0. Western blot quantification was performed using ImageJ (1.53o) software.

### 3. Results

#### 3.1 Proteomic profiling identifies CDK6 protein upregulation in relapse myeloma patients

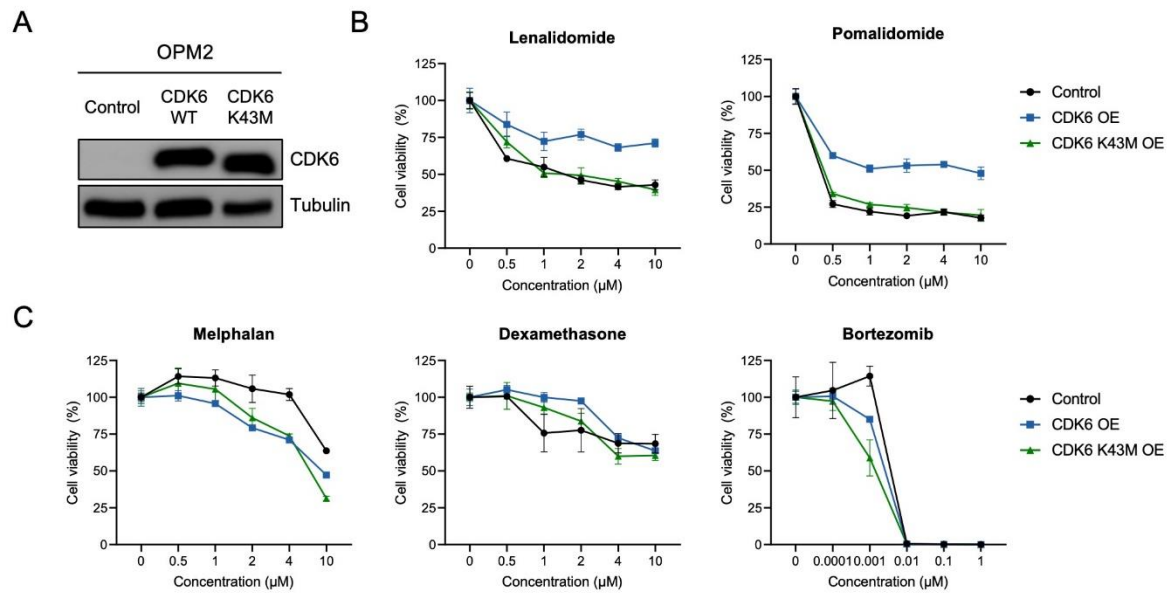
Genetic alterations in CRBN and other members of the IMiD pathway account for approximately 20% of IMiD resistance<sup>50–53</sup>. To explore potential non-genetic IMiD resistance mechanisms, we performed integrated quantitative proteomics and transcriptomics on longitudinal samples from five patients, collected at both diagnosis and relapse under lenalidomide therapy and subjected to CD138 enrichment for multiple myeloma cells (Figure 1A). We detected a total of 6,095 proteins and identified the deregulation of more than 450 proteins between pre-treatment and relapse samples using an FDR cutoff of 0.10 (Figure 1B). Of the top upregulated proteins, TRIP13 and RRM1 have been described to be implicated in the pathogenesis of multiple myeloma<sup>100–102</sup> and are part of the validated GEP70 and GEP5 multiple myeloma high-risk signature<sup>103,104</sup>, and CDK6 is targetable where its inhibitors have demonstrated activity in pre-clinical myeloma studies<sup>105–108</sup>. An independent cohort of thirteen patient samples with four obtained at diagnosis and nine obtained at relapse further validated the upregulation of TRIP13, RRM1, and CDK6 protein expression levels (Figure 1C). The overall protein-RNA correlation of all protein/RNA pairs was weak, indicated by a Pearson correlation coefficient (PCC) of 0.34. TRIP13 demonstrated the highest RNA/protein correlation with a PCC of 0.84 while RRM1 and CDK6 showed a RNA to protein correlation of 0.6 and 0.39 respectively (Figure 1D). While CDK4 acts as a regulator of the cell cycle together with CDK6, we did not detect any significant changes in the protein levels of CDK4. As all patients received lenalidomide-comprising treatment, we also examined the RNA/protein correlation of IMiD-associated proteins<sup>34,44,109</sup>. We did not detect any changes in the protein levels of IKZF1/3, IRF4, CRBN, DDB1, and NR3C1 (Figure 1E). To further validate the proteomic findings, multiple myeloma cell lines were cultured in the presence of lenalidomide *in vitro* over the course of six weeks. Induced lenalidomide-resistant cells demonstrated elevated levels of CDK6 protein, corroborating the proteomic findings in myeloma patients (Figure 1F).



**Figure 1. Proteomic profiling identifies CDK6 protein upregulation in relapsed multiple myeloma patients.** (A) Quantitative proteomic analysis and RNA-sequencing of five paired multiple myeloma patient bone marrow samples collected at diagnosis and at relapse. (B) Average  $\log_2(\text{fold change})$  of proteins at relapse/ diagnosis is plotted against its  $-\log_{10}(\text{p-value})$ . (C) Western blot validation of top-upregulated proteins at relapse in an independent patient cohort ( $n=13$ ). (D) Normalized protein intensities ( $\log_2$  TMT intensities) of CDK6, TRIP13, RRM1, and (E) IMiD-associated proteins in all 10 samples were plotted against their respective normalized RNA expression levels ( $\log_2$  TPM values). Samples from the same patient are connected. (F) CDK6 protein expression levels of induced lenalidomide-resistant MM.1S and LP-1 cells as displayed via Western blotting and corresponding quantification. Figure is own representation adapted from Ng, Ramberger *et al.*<sup>91</sup>.

### 3.2 Overexpression of CDK6 in myeloma cells confers IMiD-resistance

To investigate the role of CDK6 in multiple myeloma drug resistance, retroviral overexpression vectors were used on myeloma cell lines (Figure 2A). High CDK6 expression conferred reduced sensitivity towards lenalidomide and pomalidomide across various cell lines (Figure 2B). The sensitivity impairment from CDK6 was kinase-dependent as the introduction of kinase-dead mutant K43M did not alter drug sensitivity. The effect of CDK6-overexpressing cells on melphalan, dexamethasone, and bortezomib sensitivity was not as pronounced and was cell-line specific (Figure 2C). These data imply that the kinase function of CDK6 selectively impairs IMiD-sensitivity in myeloma cells.

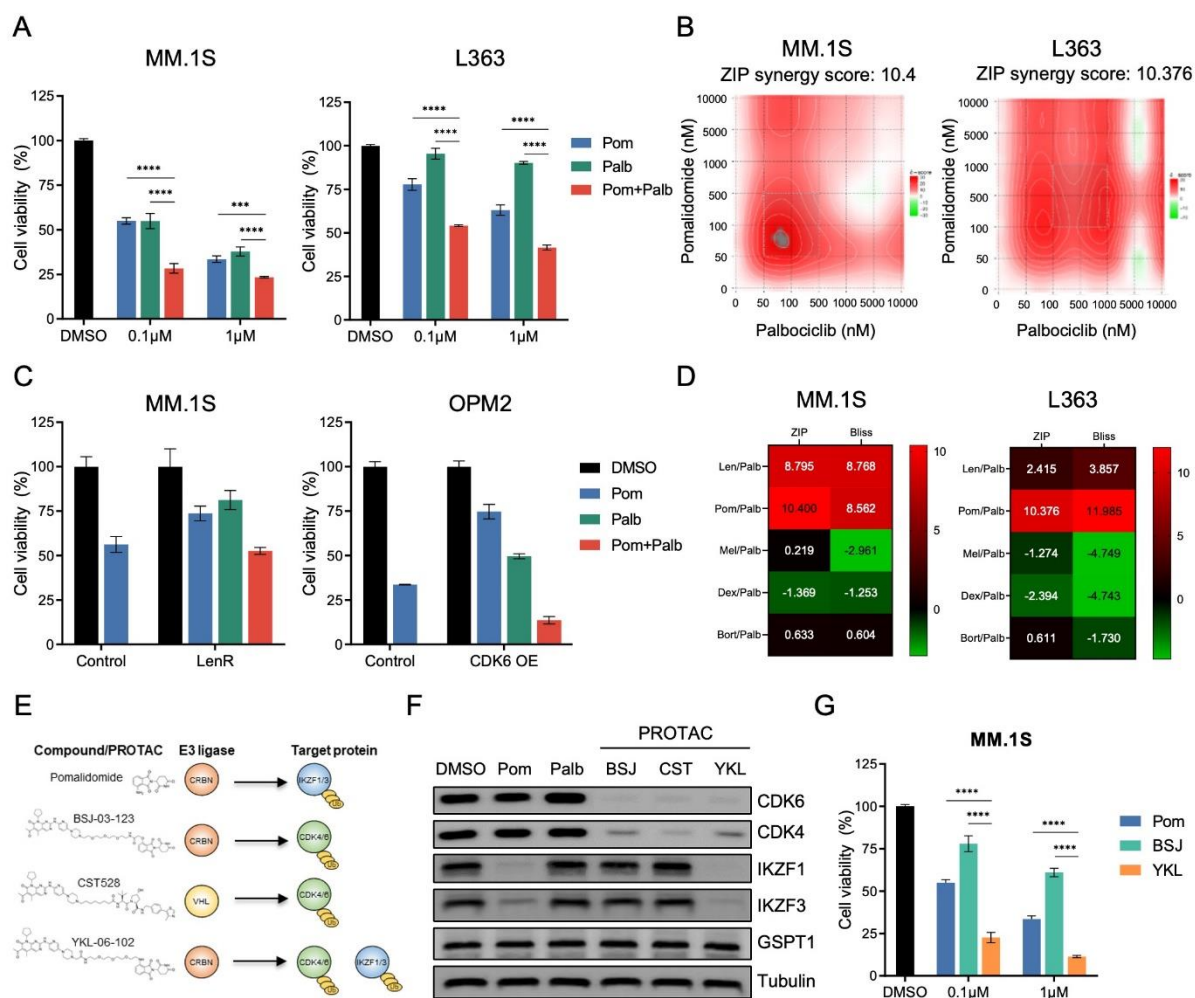


**Figure 2. Overexpression of CDK6 in myeloma cells confers IMiD-resistance.** (A) Overexpression of CDK6 WT or kinase-impaired mutant K43M in myeloma cell line OPM2 utilizing retroviral vectors confirmed via Western blot. (B) Cell viability of OPM2 cells expressing CDK6 WT or K43M upon IMiD lenalidomide and pomalidomide, (C) melphalan, dexamethasone, and bortezomib treatment for 96 h at indicated concentrations. Control indicates empty vector. Cell viability values are normalized to respective DMSO conditions. Data represent the mean  $\pm$ SD of biological triplicates. Figure is own representation adapted from Ng, Ramberger *et al*<sup>91</sup>.

### 3.3 Combined targeting of CDK6 and IKZF1/3 is synergistic in multiple myeloma cells

As induced CDK6 expression reduced IMiD-sensitivity, we next explored the effects of CDK6 inhibitor palbociclib on myeloma cell lines. While palbociclib alone exhibited moderate inhibitory effects across all multiple myeloma cell lines, the addition of palbociclib enhanced the anti-myeloma effects of IMiDs while used in combination in both IMiD-sensitive and –resistant cell lines (Figure 3A), with synergy achieved at lower concentrations (Figure 3B). Palbociclib and pomalidomide combination treatment was able to restore IMiD-sensitivity in induced IMiD-resistant cells and CDK6-overexpressing cells (Figure 3C). The addition of palbociclib synergizes with lenalidomide and pomalidomide, while the effect with other myeloma drugs was mostly additive (Figure 3D). We then utilized PROTACs that degrade CDK4/6 with or without retaining the effects of IKZF degradation (Figure 3E, 3F). PROTAC YKL-06-102, which retains pomalidomide activity and degrades both CDK4/6 and IKZF1/3, showed significant inhibition across all multiple myeloma cell lines, demonstrating intramolecular synergy (Figure 3G).



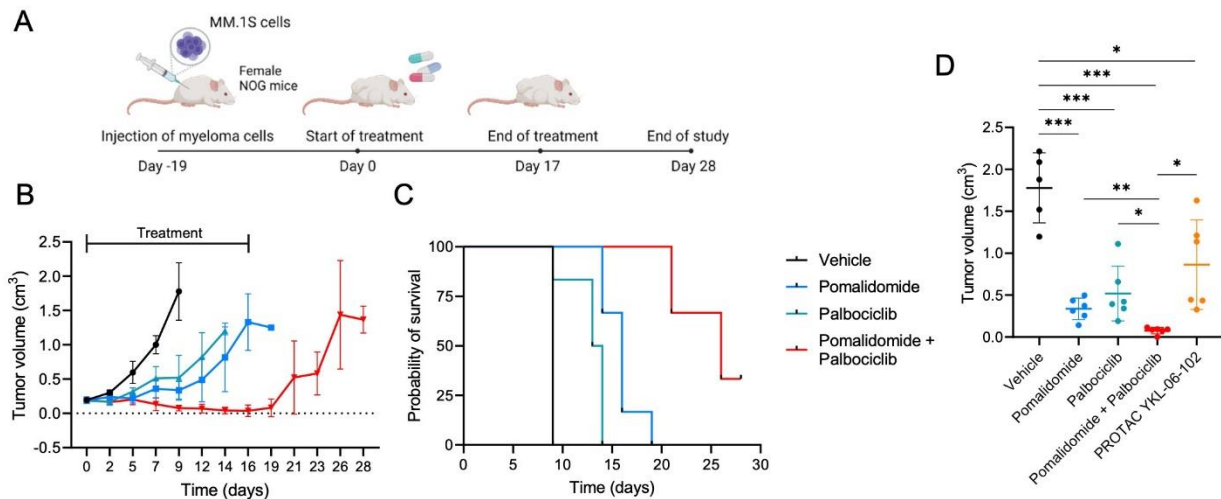


**Figure 3. Combined targeting of CDK6 and IKZF1/3 is synergistic in multiple myeloma cells.** (A) Cell viability of IMiD-sensitive cell line MM.1S and IMiD-resistant cell line L363 treated with Pom, Palb, and in combination for 96 h. (B) Synergy matrix of MM.1S and L363 cells treated with palbociclib and pomalidomide at indicated concentrations. (C) Cell viability of MM.1S LenR cells and OPM2 CDK6 OE cells treated with Pom, Palb, and in combination. (D) Heatmap of synergy scores of palbociclib treated in combination with clinical drugs indicated for multiple myeloma in MM.1S and L363 cells. (E) Chemical structure and E3 targets of pomalidomide and CDK6-targeting PROTACs. (F) Western blot analysis of MM.1S cells treated with Pom, Palb, BSJ, CST, and YKL for 16 h at 1  $\mu$ M. (G) Cell viability of MM.1S cells with Pom, BSJ, and YKL for 96 h. Pom = pomalidomide; Palb = palbociclib; BSJ = BSJ-03-123; CST = CST528; YKL = YKL-06-102. LenR = lenalidomide-resistant; OE = overexpression. Synergy levels are indicated with ZIP or Bliss synergy scores. Synergy maps were created with SynergyFinder. Cell viability values are normalized to respective DMSO conditions. Data represent the mean  $\pm$ SD of biological triplicates. Figure is own representation adapted from Ng, Ramberger *et al.*<sup>91</sup>.

### 3.4 CDK6 inhibition with IMiDs is highly efficacious in *in vivo* myeloma model

To examine if the combination treatment of CDK6 with IMiDs has *in vivo* therapeutic efficacy, a xenograft experiment was performed (Figure 4A). Myeloma cells MM.1S were injected subcutaneously into NOG mice and randomized prior to treatment. Treatment was administered p.o. for 17 days and observed until day 28. Monotherapy of pomalidomide and palbociclib significantly delayed tumor growth, while combination therapy led to the reduction of myeloma growth to un-

detectable levels and consequently, significant improvement in survival (Figure 4B, 4C). However, recurrence of myeloma occurred upon treatment termination, indicating that prolonged and continuous therapy might be required for the prevention of relapse. CDK4/6 and IKZF1/3 dual targeting PROTAC was administered intraperitoneally at maximal applicable dosage of 5 mg/kg/day due to low solubility. There was a significant delay in tumor growth of YKL-treated mice compared to vehicle-treated mice, however, the effects were not prominent in contrast to monotherapies, which can be attributed to the lower *in vivo* bioavailability (Figure 4D).

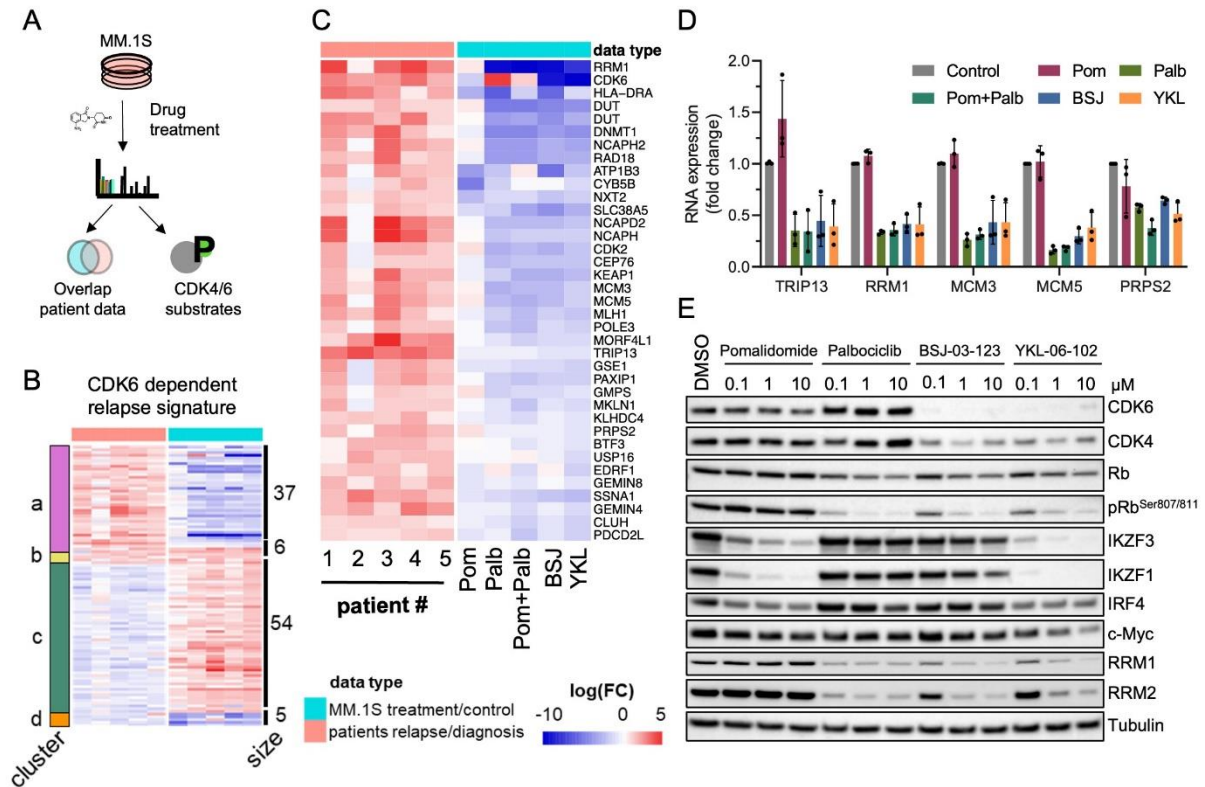


**Figure 4. Targeting CDK6 with IMiDs is highly efficacious in *in vivo* myeloma model.** (A) Schematic representation of *in vivo* experimental setup. MM.1S cells were injected s.c. into NOG mice. Treatment was administered p.o. for 17 days and observed until day 28. (B) Tumor growth of MM.1S xenograft mice with monotherapy pomalidomide (5 mg/kg), palbociclib (50 mg/kg), and in combination. (C) Kaplan-Meier curve of the four treatment groups. Data was analyzed by log-rank Mantel-Cox test. (D) Tumor size of various treatment groups on day 9, analyzed by unpaired t-tests with Welch's correction. Group size for vehicle-treated mice is  $n = 5$  and  $n = 6$  for all other treatment groups. P values indicated are as follows: \* =  $P \leq 0.05$ ; \*\* =  $P \leq 0.01$ ; \*\*\* =  $P \leq 0.001$ . Figure is own representation adapted from Ng, Ramberger *et al.*<sup>91</sup>.

### 3.5 Targeting CDK6 reverses a relapse protein signature in multiple myeloma

To investigate the effects of CDK6 inhibition on multiple myeloma cells, MM.1S cell line was treated with pomalidomide, palbociclib, or in combination and subjected to proteomic analyses (Figure 5A). The significantly deregulated proteins from the cell perturbation data was overlaid with patient data, where we identified four distinct clusters of protein expression (Figure 5B). We demonstrated that CDK6 inhibition alone, using inhibitors such as palbociclib or with degraders such as PROTACs, could reverse a protein signature specific to the relapse patients. Specifically, in cluster a, we were able to show that high-risk multiple myeloma markers TRIP13 and RRM1 are upregulated in relapse samples but are downregulated by CDK6 inhibition (Figure 5C). The phosphorylation levels of these proteins did not differ upon palbociclib treatment, proposing that these proteins are not direct CDK6 kinase substrates. Further RT-qPCR experiments demonstrated

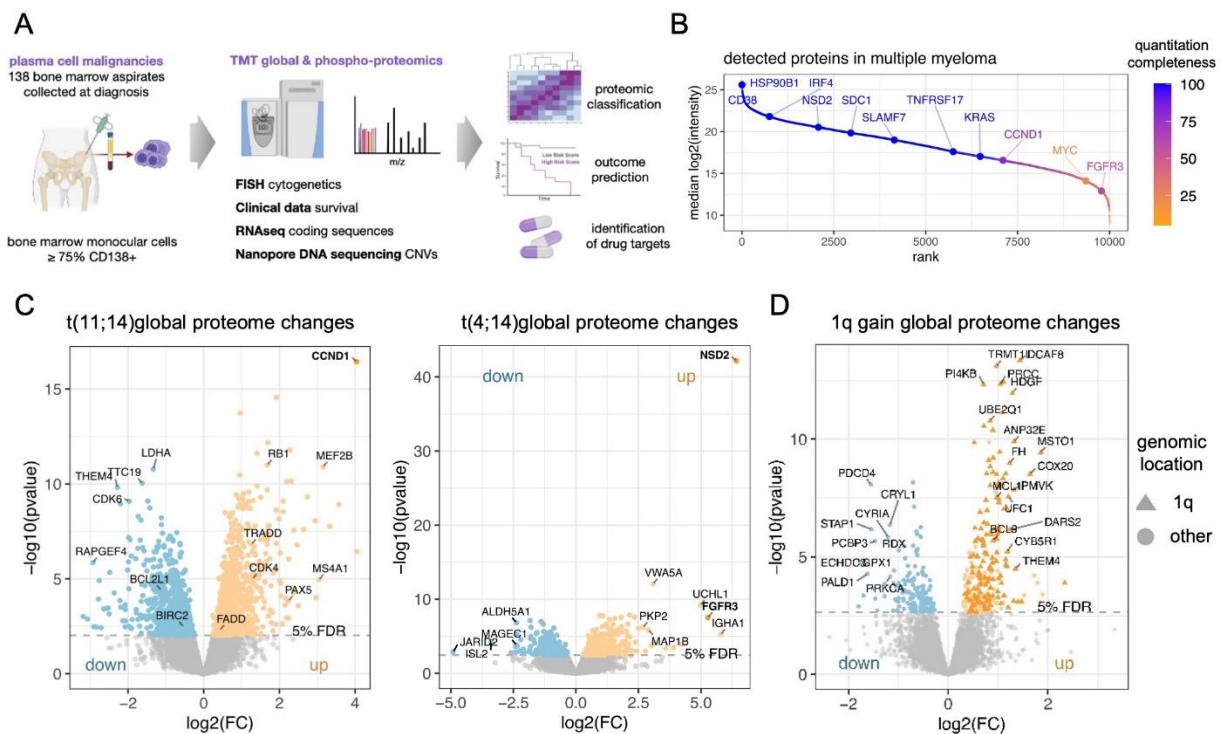
reduced mRNA levels of TRIP13, RRM1, and other proteins upon CDK6 inhibition, suggesting a CDK6-dependent transcriptional regulation of these oncoproteins (Figure 5D). Additionally, we observed more potent degradation of essential myeloma transcription factors IKZF1/3 from combined targeting of CDK6 and IKZF1/3 using PROTAC YKL (Figure 5E). These results suggest that CDK6 regulates a myeloma relapse-associated signature and its inhibition potentiates the effect of IMiDs via enhanced degradation of IKZF1/3, which likely underlies the synergy of the combination therapy.



**Figure 5. Targeting CDK6 reverses a relapse protein signature in multiple myeloma.** (A) Schematic figure of myeloma cell drug perturbation. MM.1S cells were treated with various drugs and combinations, cells were then *analyzed* for their proteomic and phosphoproteomic changes with TMT-based proteomics. (B) Protein expression levels of paired-patient data was combined with cell perturbation data. Heatmap displays protein levels passing FDR levels of  $< 0.1$ . (C) Cluster a of Figure 5B. (D) mRNA levels of candidates regulated by CDK6. (E) Western blot analysis of MM.1S cells treated with respective treatments at indicated concentrations. Pom = pomalidomide; Palb = palbociclib; BSJ = BSJ-03-123; YKL = YKL-06-102. Figure is own representation adapted from Ng, Ramberger *et al.*<sup>91</sup>.

### 3.6 Proteogenomic landscape of multiple myeloma and signatures of primary translocations $t(11;14)$ , $t(4;14)$ , and $chr1q$ gain

Our pilot study has successfully demonstrated the feasibility of applying in-depth proteomic analysis on primary multiple myeloma samples<sup>91</sup>. The low RNA-to-protein correlation also implies a high degree of post-transcriptional or post-translational regulation in myeloma, highlighting the limitation of examining DNA or RNA expression alone and the need for a more comprehensive proteogenomic study. Here, we extended the proteogenomic analysis to a total of 138 patients, with 114 newly diagnosed multiple myeloma (NDMM), 7 MGUS, and 17 plasma cell leukemia (Figure 6A). In addition to global proteomics and phospho-proteomics, FISH, RNA sequencing, and whole-genome DNA sequencing were integrated with clinical data. In total, over 10,000 proteins and 50,000 phosphopeptides were identified, including key plasma cell markers CD138 (*SDC1*), CD38, BCMA (*TNFRSF17*), and IRF4 (Figure 6B). As chromosomal aberrations are involved in the initiation of oncogenic events in multiple myeloma, we examined the proteome changes primary translocations  $t(11;14)$  and  $t(4;14)$  as well as the high-risk marker  $amp(1q)$  (Figure 6C, 6D). As  $t(11;14)$  is the only genetic subset of multiple myeloma that is sensitive to BCL2 inhibitor venetoclax<sup>21,22</sup>, proteins involved in apoptotic pathways were examined. A total of 102 apoptosis-associated proteins were significantly deregulated in  $t(11;14)$  compared to non- $t(11;14)$  cohort (FDR < 0.05), including downregulation of cIAP1 (*BIRC2*) and BCLxL (*BCL2L1*)<sup>93</sup>.



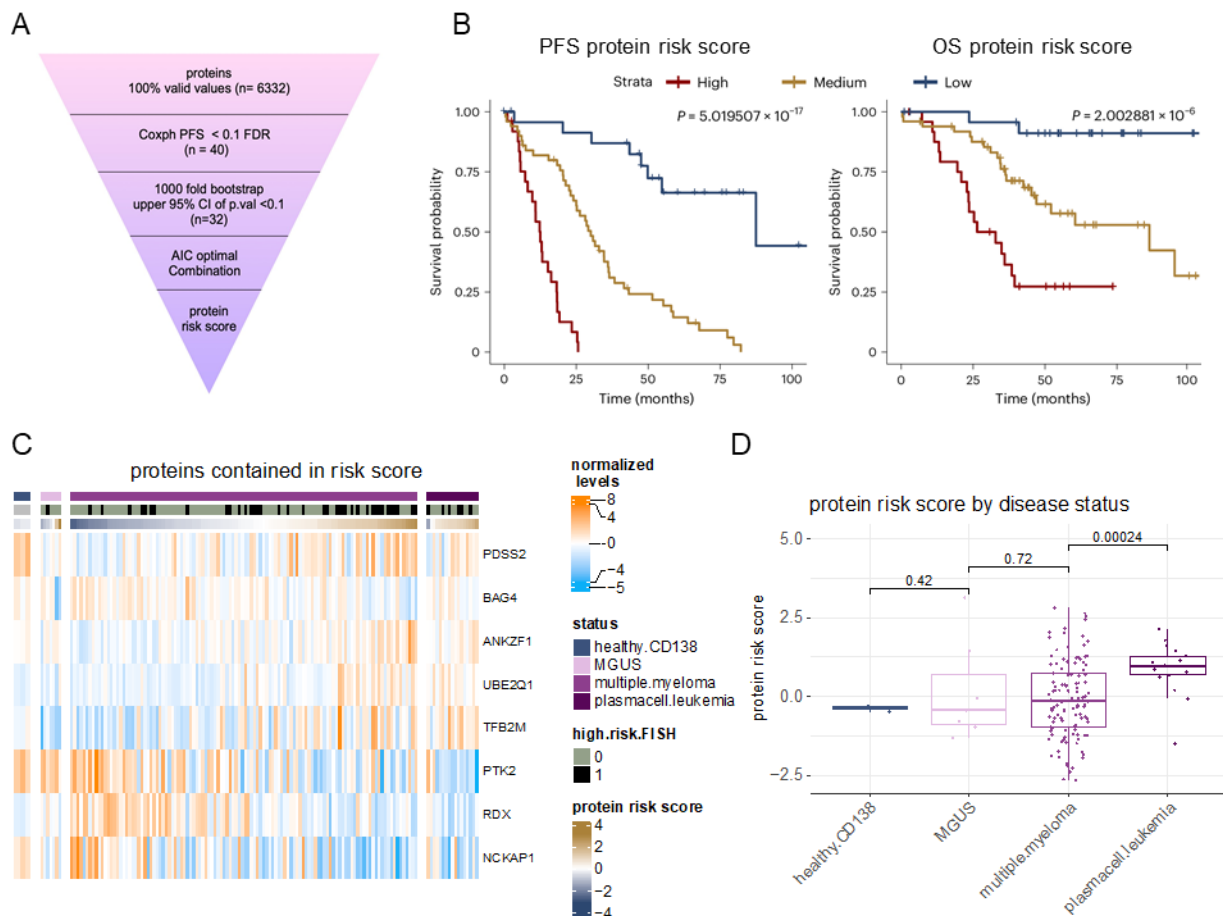
**Figure 6. Proteogenomic landscape of multiple myeloma and signatures of primary translocations  $t(11;14)$ ,  $t(4;14)$ , and  $chr1q$  gain.** (A) Schematic presentation of analyzed patient cohort and study workflow. (B) Rank plot of median intensity of proteins detected by TMT-based mass spectrometry, with key markers of multiple myeloma in



highlight. (C) Protein levels of primary translocations t(11;14), t(4;14), and chr1 gain. Multiple myeloma patient samples with primary translocations t(11;14) (n=27) were compared against non-t(11;14) samples (n=87); and t(4;14) samples (n=19) were compared against non-t(4;14) samples (n=95). (D) Myeloma samples with chr1q gain (n=46) was compared against samples without 1q copy number gain (n=68). Comparisons were performed with 2-sided, moderated 2-sample t-tests. Log<sub>2</sub>(fold change) of proteins is plotted against its  $-\log_{10}(\text{p-value})$ . Figure is own representation adapted from Ramberger *et al.*<sup>93</sup>.

### 3.7 Proteomic-based outcome prediction

To evaluate if proteomics and phosphoproteomics can provide additional prognostic insights beyond the revised International Staging System (R-ISS) for risk stratification, bootstrapping analysis and model optimization were applied using proteomics and clinical data from 100 patients (Figure 7A). A protein risk score comprising of eight proteins, including Ubiquitin-Conjugating Enzyme E2 Q1 (UBE2Q1), was defined. Applying the protein risk score on the 100 patients, we were able to stratify patients into high risk (n=25), median risk (n=50), and low risk (n=25), with



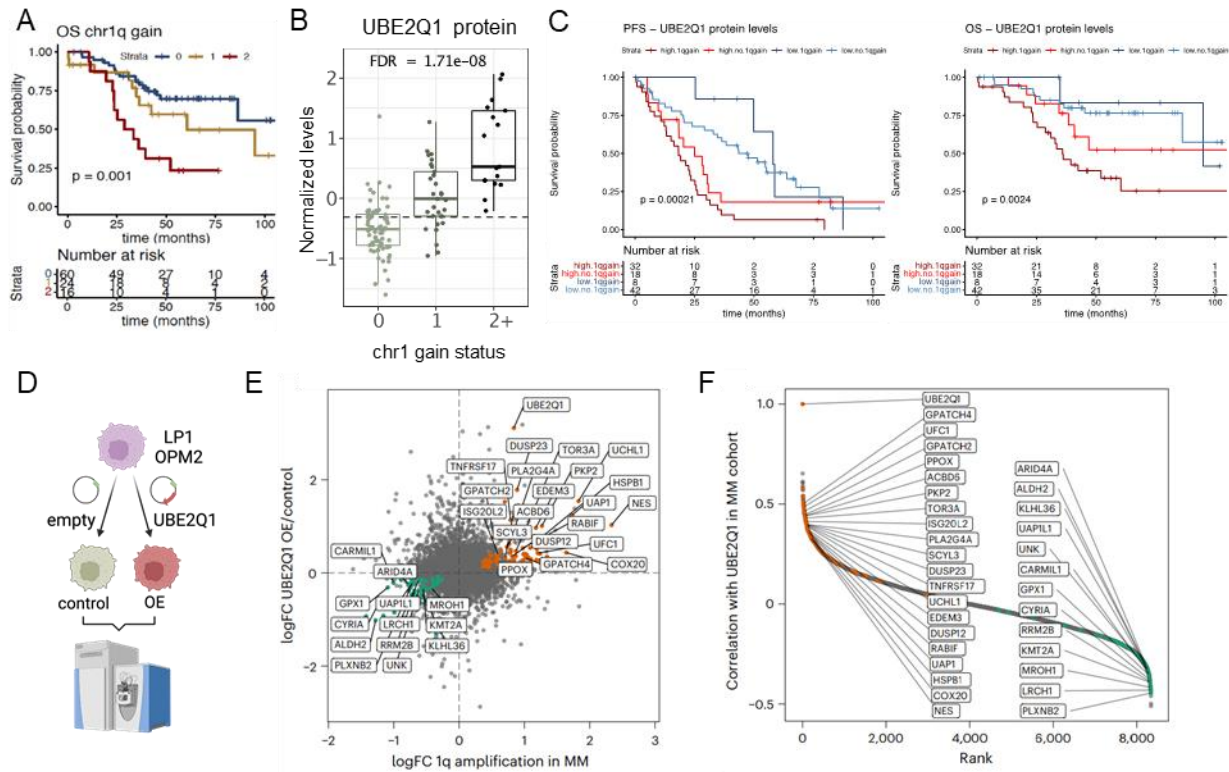
**Figure 7. Proteomic-based outcome prediction.** (A) Schematic diagram of protein risk score generation from newly diagnosed myeloma patients receiving lenalidomide-based treatment (n=100). (B) Kaplan-Meier curves of progression-free survival and overall survival of patients stratified by protein risk score quartile (low, n=25; median, n=50; high, n=25). P-value was calculated with log rank test. (C) Protein expression levels of eight proteins in risk score across various myeloma progression status. (D) Box plot of protein risk score across myeloma progression status. Boxes indicate median, 25<sup>th</sup>, and 75<sup>th</sup> percentile and whiskers indicate minimum and maximum. Healthy plasma cells, n=3; MGUS, n=7; MM, n=114; PCL, n=17. Two-sided student's t-test was applied. Figure is own representation adapted from Ramberger *et al.*<sup>93</sup>.

median PFS of 12.5, 30.0, and 87.4 months respectively (Figure 7B). In addition to the prognostic impact on survival, the protein risk score was in line with disease progression from healthy plasma cells, MGUS, multiple myeloma, to plasma cell leukemia (Figure 7C, 7D).

### 3.8 Identification of *UBE2Q1* as a driver for high-risk 1q gain myeloma

Chromosomal amplification of the 1q arm is an established high-risk cytogenetic abnormality in multiple myeloma and is associated with shorter overall survival and adverse outcomes<sup>110,111</sup>. In our study, patients with increasing copies of chr1q had significantly worse overall survival, consistent with previous studies<sup>110,111</sup> (Figure 8A). The majority of the proteins upregulated in the amp(1q) cohort are located on the 1q arm, suggesting regulation in *cis*, including one of the top candidates upregulated in the chr1q cohort, *UBE2Q1* (Figure 8B). Out of the upregulated proteins in 1q gain, *UBE2Q1* was the only candidate where protein expression levels are associated with significantly worse progression-free survival (PFS) and overall survival (OS) (Figure 8C). Survival outcomes were independent of 1q gain status, implicating the significance of *UBE2Q1* protein levels as a universal prognostic marker.

As *UBE2Q1* is involved in the ubiquitin-proteasome system, we explored its effect by overexpressing *UBE2Q1* in multiple myeloma cell lines and subjected them to global proteome analysis (Figure 8D). Comparing the *UBE2Q1*-overexpressed proteome to that of primary myeloma patients, we identified an overlap of dysregulated proteins that were also differentially expressed in the cohort of patients with 1q amplification (Figure 8E). The analysis was extended across all genetic subtypes in the primary myeloma cohort and we observed deregulation of proteins that had a high correlation with *UBE2Q1* protein expression levels (Figure 8F). These data imply that *UBE2Q1* is a regulator of other proteins significantly deregulated in 1q gain patients and is potentially an oncogenic driver of aberrant expression of proteins implicated in the pathogenesis of multiple myeloma.

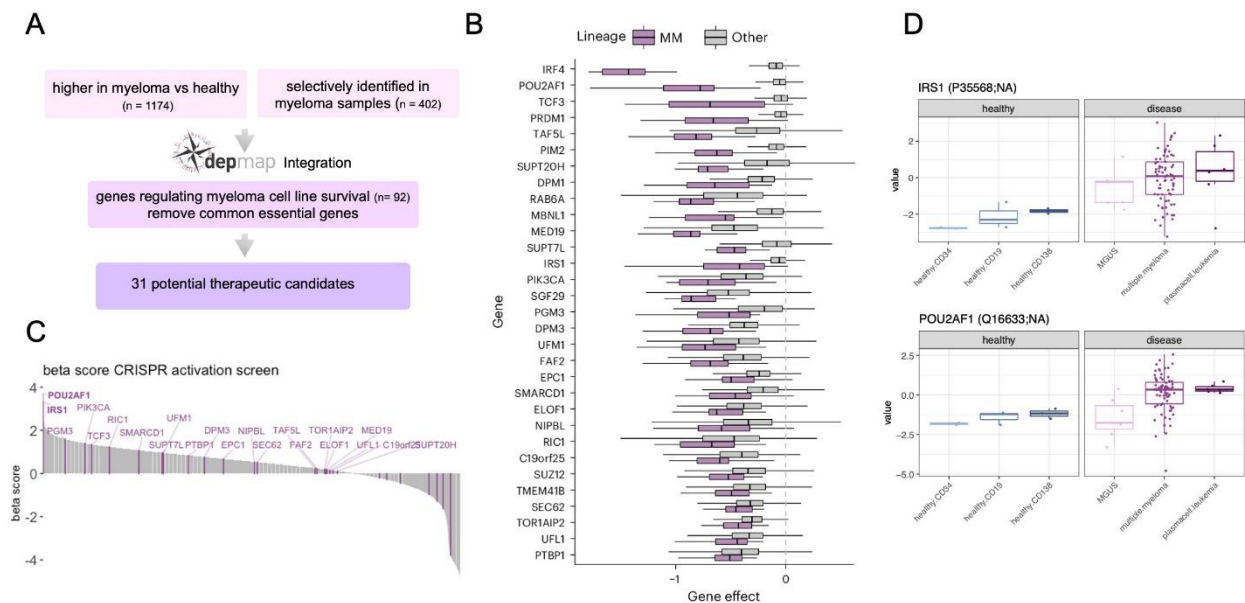


**Figure 8. Identification of UBE2Q1 as a driver for high-risk 1q gain myeloma.** (A) Kaplan-Meier curve showing overall survival of myeloma patients ranked by 1q gain status ( $n=100$ ). Log rank test was used for p-value calculation. (B) Box plot demonstrating UBE2Q1 protein levels in myeloma patients grouped by 1q gain status. Boxes indicate median, 25th, and 75th percentile. (C) Kaplan-Meier curve showing overall survival of myeloma patients ranked by UBE2Q1 protein expression levels and 1q gain status. Log rank test was applied to obtain p-value. (D) Graphical presentation of proteomic profiling of UBE2Q1 overexpression in myeloma cell lines. LP-1 and OPM2 cells were transduced with empty or UBE2Q1-overexpressing vector and analyzed with DIA mass spectrometry ( $n=4$ ). (E) Protein expression profile of UBE2Q1-overexpressing LP-1 cells (y-axis) was compared to the profile of multiple myeloma patients with chr1q amplification (x-axis). Proteins highlighted are past FDR threshold of 0.05 and 0.1 for UBE2Q1-overexpression cells and 1q gain myeloma patients respectively, and correlating with UBE2Q1 protein levels in primary myeloma samples ( $r > 0.3$  or  $r < -0.3$ ). (F) Rank plot of Pearson correlation analysis of UBE2Q1 expression levels with other proteins in multiple myeloma patient cohort. Highlighted proteins are identical to those in Figure 8E. Figure is own representation adapted from Ramberger *et al.*<sup>93</sup>.

### 3.9 Identification of myeloma-specific drivers for potential therapeutic targeting

To identify potential myeloma-specific therapeutic targets, proteins significantly and selectively upregulated in myeloma samples compared to healthy CD19, CD34, and CD138 cells were integrated with genetic dependency data (<https://depmap.org/portal/>) for myeloma-specific vulnerabilities (Figure 9A). The analysis yielded a list of 31 proteins that passed the cut-off based on essential myeloma transcription factors IKZF1/3 (Figure 9B). A genome-wide CRISPR activation screen was performed in myeloma cell line MM.1S to evaluate the role of potential protein targets identified (Figure 9C). *POU2AF1* and *IRS1* were top candidates driving myeloma proliferation,

and their role was further validated with protein expression levels increasing with disease progression (Figure 9D). Overall, our proteomic analysis combined with functional genetics uncovered potential myeloma therapeutic targets.



**Figure 9. Identification of myeloma-specific drivers for potential therapeutic targeting.** (A) Diagram of myeloma-specific therapeutic candidates from upregulated or selectively-expressed proteins in multiple myeloma. (B) Gene dependency scores of multiple myeloma cell lines (n=18) and all other cell lines (n=1082) of the candidates identified in Figure 9A. CRISPR scores were obtained from DepMap (<https://depmap.org/portal>). (C) Plot of beta scores from genome-wide CRISPR activation screen. Gene/protein names of potential therapeutic candidates are indicated. (D) Protein levels of IRS1 and POU2AF1 in healthy and disease samples. Figure is own representation adapted from Ramberger *et al.*<sup>93</sup>.

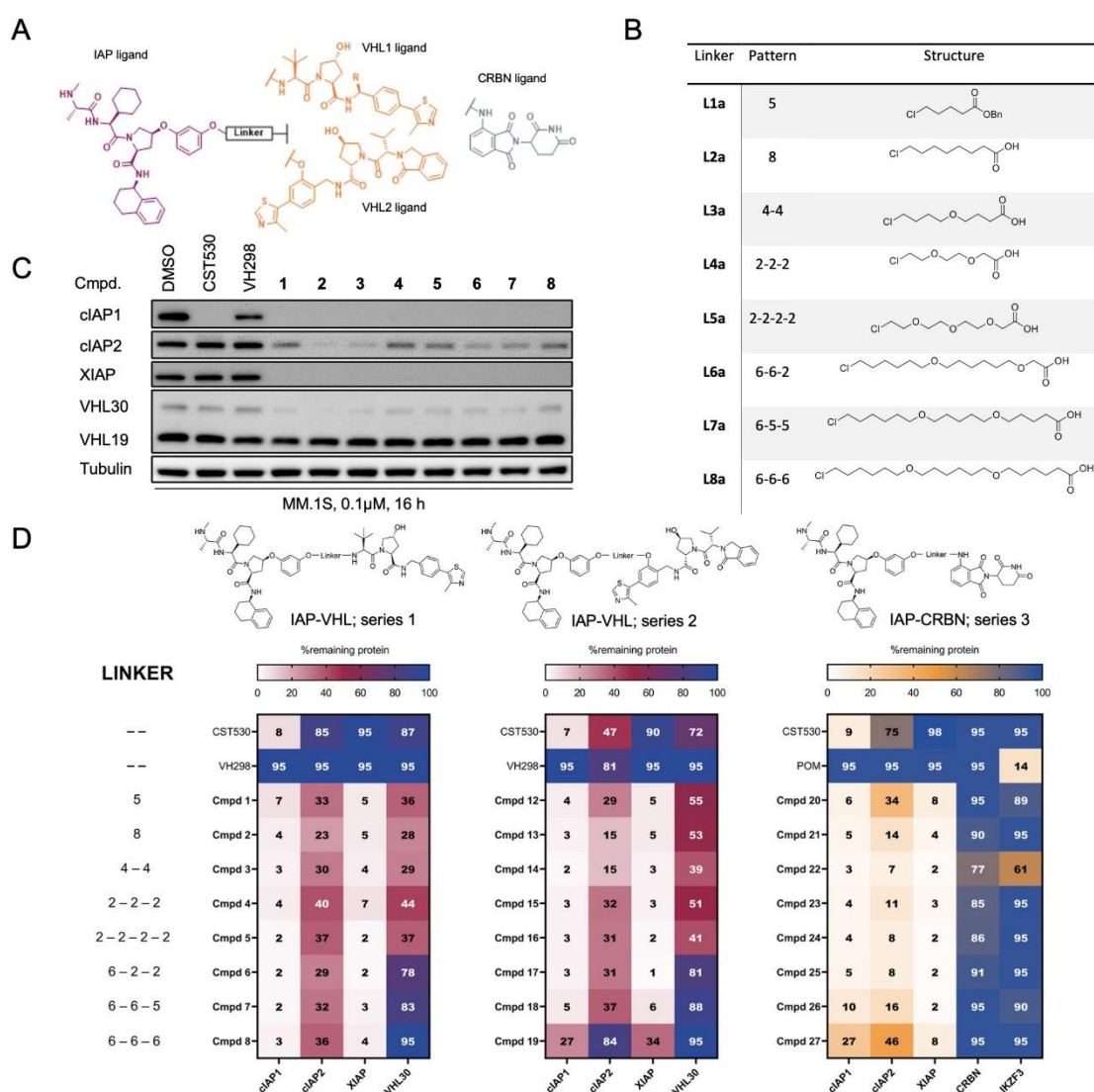
### 3.10 Design, generation, and quantitative evaluation of pan-IAP degraders

Apoptosis-related proteins were found to be highly deregulated in the t(11;14) subset of multiple myeloma patients in our proteogenomics studies<sup>93</sup>. The clinical application of BCL2 inhibitor venetoclax in multiple myeloma demonstrated efficacy only in multiple myeloma patients with t(11;14)<sup>21,22</sup>, suggesting a vulnerability to apoptosis modulators. On the other hand, *BIRC2* and *BIRC3*, encoding cellular inhibitor of apoptosis 1 (cIAP1) and 2 (cIAP2), are found to be deleted in some multiple myeloma cases<sup>10</sup>. Pan-IAP inhibitors may be an effective therapeutic strategy in *BIRC2/BIRC3* deleted cells should there be an enhanced dependency on the remaining IAP proteins. Current IAP antagonists lead to the degradation of cIAP1 and cIAP2 proteins and possess an affinity for XIAP inhibition, however, have limited clinical efficacy as single agent<sup>84,85</sup>. The need to develop more potent IAP inhibitors against all IAPs remains<sup>112,113</sup>.

To generate IAP-targeting PROTACs, three series of hetero-bifunctional compounds were designed and synthesized, each series with 8 various linker structures (Figure 10A, 10B). As



cIAP1/2, VHL, and CRBN are all E3 ligases, in addition to assessing IAP degradation, we examined the protein expression levels of VHL and CRBN where degradation might be attributed to E3 crosstalk (Figure 10C). All three series of PROTACs were capable of degrading cIAP1, cIAP2, and XIAP (Figure 10D). Our hetero-PROTACs were able to degrade cIAP1 at a similar or increased level compared to IAP ligand CST530 alone due to the autoubiquitination of cIAP1. While the IAP ligand was able to only slightly decrease cIAP2 protein levels and not XIAP, all compounds in the three series were able to enhance cIAP2 degradation to various extents and markedly lower XIAP levels.

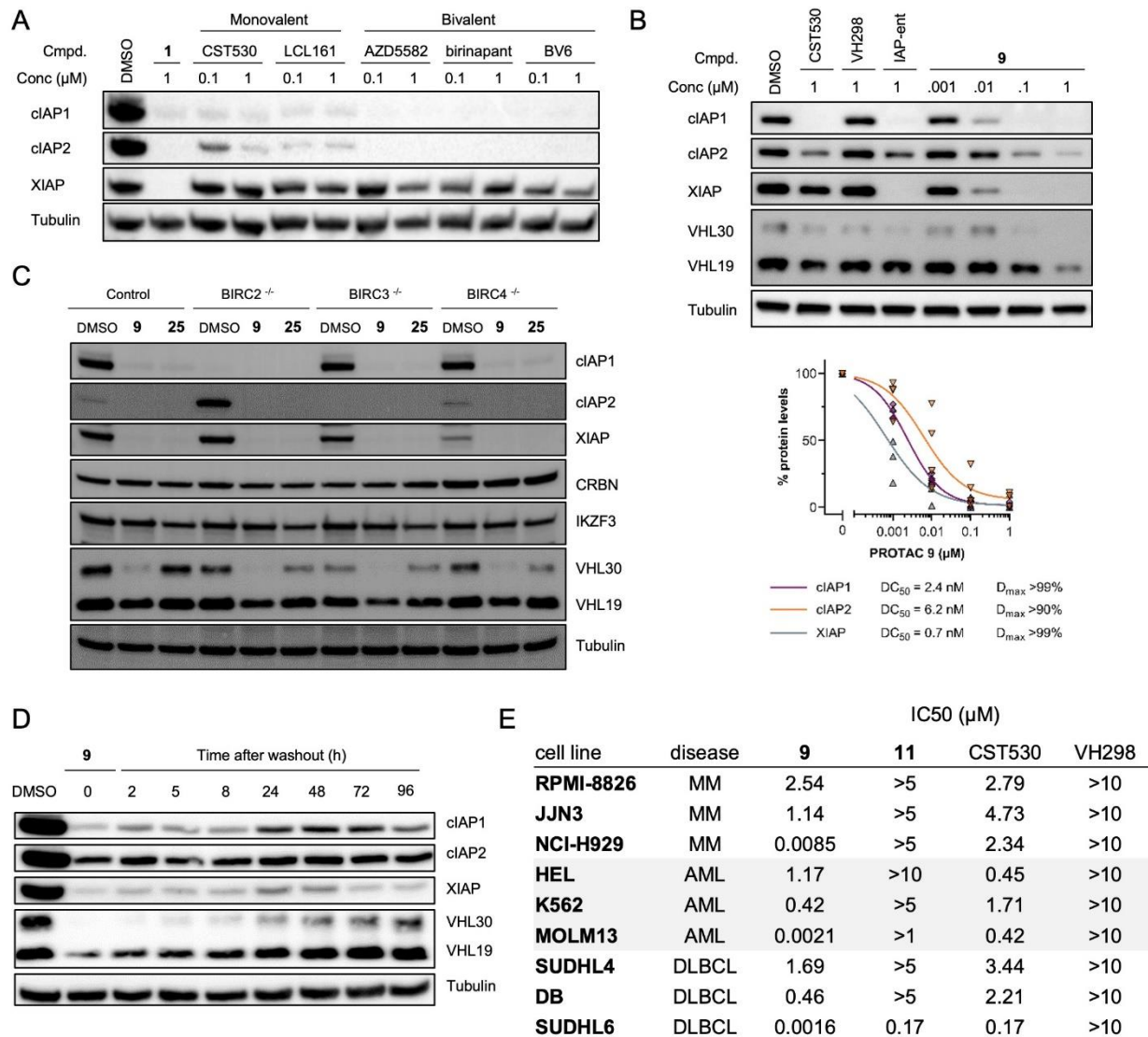


**Figure 10. Design, generation, and quantitative evaluation of IAP-targeting PROTAC series.** (A) Schematic representation of the design of three compound series targeting IAP proteins. (B) Linker structures for the generation of series 1 compounds consisting of IAP-VHL PROTACs. (C) Exemplary western blot analysis of IAP-targeting PROTACs. MM.1S cells were treated for 16 h with IAP-VHL series 1 PROTACs at 0.1  $\mu$ M with corresponding ligands as controls. (D) Degradation profile of all three series IAP-targeting hetero-PROTACs on cIAP1, cIAP2, XIAP, VHL30, CRBN, and IKZF3 protein expression levels. MM.1S cells were treated with each compound and respective controls for 16 h at 0.1  $\mu$ M. Degradation percentage indicates remaining protein levels after treatment. Values are normalized to respective loading controls and vehicle-treated control. Data represents the mean of three

independent biological replicates. CST530 = IAP ligand; VH298 = VHL ligand. Figure is own representation adapted from Ng, Bricelj *et al.*<sup>92</sup>.

### 3.11 Protein degradation and cell viability from pan-IAP degraders

The monovalent and bivalent IAP antagonists LCL161, AZD5582, birinapant, and BV6 were able to cause substantial degradation of cIAP1 and cIAP2, but not XIAP. In contrast, heteroPROTAC **1** led to pan-IAP degradation (Figure 11A). Compound **1** was optimized to enhance binding affinities and the resulting compound **9** demonstrated further enhanced pan-IAP degradation (Figure 11B). To mechanistically understand if the degradation of IAPs is mediated by cIAP1 alone and to examine if pan-IAP degradation can be achieved in *BIRC2* or *BIRC3* knockout cells, we generated *BIRC2*, *BIRC3*, and *BIRC4* knockout cells. In *BIRC2* knockout cells, pan-IAP and VHL degradation were induced by the treatment of hetero-PROTACs, demonstrating the E3 ligase activity of VHL and showcasing that cIAP2 can compensate for the loss of cIAP1 and facilitate VHL protein degradation through its E3 ubiquitin ligase function (Figure 11C). Having demonstrated the potency of hetero-PROTACs, we next investigated the persistence of IAP degradation. The reduced IAP levels were sustained up to 96 h after a single exposure of compound **9** (Figure 11D). To evaluate if the potent IAP degradation translates to inhibitory effects in cells, hematologic cell lines from multiple myeloma, acute myeloid leukemia, and lymphoma were tested. IAP degrader **9** outperformed monovalent agonist CST530 in all cell lines (Figure 11E). In NCI-H929 cells, compound **9** surpassed AZD5582 and competitively lowered the IC<sub>50</sub> profiles in MOLM13 and SUDHL6 to 2.1 nM and 1.6 nM. These data demonstrate the potential therapeutic efficacy of heteroPROTACs and support further development of IAP-targeting heterobifunctional compounds.



**Figure 11. Protein degradation and cell viability from pan-IAP degraders.** (A) Comparison of hetero-PROTAC 9 against monovalent IAP antagonists CST530, LCL161, and bivalent IAP antagonists AZD5582, birinapant, and BV6. MM.1S cells were treated for 16 h at indicated concentrations. (B) Characterization of dose-dependent protein degradation of IAP proteins and VHL30 from compound 9. (C) Treatment of hetero-PROTACs 9 and 25 at 0.1 μM for 16 h in IAP knockout MM.1S cell lines. (D) MM.1S cells were treated with compound 9 at 1 μM for 16 h before washout (t = 0). IAP protein levels were investigated at indicated time points post-washout. (E) IC<sub>50</sub> values from cell viability screening with respective controls using multiple myeloma (MM), acute myeloid leukemia (AML), and lymphoma (DLBCL) cell lines. Viability assays were performed in the presence of TNF-α and values are normalized to vehicle-treated control. Data represents mean of three independent biological replicates. CST530 = IAP ligand; VH298 = VHL ligand. Figure is own representation adapted from Ng, Bricelj *et al.*<sup>92</sup>.

## 4. Discussion

Despite significant advances in the treatment of multiple myeloma leading to improved patient outcomes, the disease remains incurable due to acquired resistance to therapies or less frequently primary resistance. The mechanisms underlying drug resistance are multifactorial, involving genetics, epigenetics, and potentially also post-transcriptional regulation. While some genetic mutations and alterations associated with resistance have been identified, they do not adequately account for the development of resistance in most cases, suggesting the involvement of non-genetic mechanisms. Therefore, there is an urgent need to better define the molecular mechanisms of resistance for existing drugs to predict, prevent, and overcome resistance, as well as to develop more robust and durable therapeutic approaches for multiple myeloma.

Although extensive genomic information derived from sequencing studies and functional genetic screens have led to new insights towards IMiD-resistance in relapsed multiple myeloma, only a fraction of the relapse cases could be explained. Our integrated proteomics and transcriptomics approach using longitudinal primary multiple myeloma samples encompass over 6,000 proteins and 20,000 phosphopeptides, demonstrating the feasibility and clinical significance of in-depth proteomic profiling in primary myeloma<sup>91</sup>. Similar to previous studies, we observed a low correlation between protein and RNA levels<sup>60-62</sup>. Interestingly, the key proteins involved in the mechanism of IMiDs were not found to be dysregulated at relapse following lenalidomide treatment. Instead, we identified CDK6 protein levels to be upregulated in relapse multiple myeloma despite no corresponding increase in RNA levels. High expression of CDK6 is commonly observed in cancers due to their role in cell cycle progression and is often associated with increased tumor aggressiveness<sup>108,114-119</sup>. We demonstrated that elevated CDK6 protein levels reduced the sensitivity of IMiDs in multiple myeloma. Targeting CDK6 with clinically-approved inhibitors such as palbociclib or PROTACs was able to overcome IMiD-resistance and showed strong synergistic effects with lenalidomide and pomalidomide both *in vitro* and *in vivo*. The subdued *in vivo* response by the dual CDK4/6 and IKZF1/3-targeting PROTAC was likely attributed to the limited bioavailability, resulting in less potent effects compared to *in vitro* studies. The general low solubility of these large molecules and unfavorable physiochemical properties also constrain the application dosage. Significant efforts are required to improve the bioavailability of PROTACs for *in vivo* and clinical use. Further cell perturbation experiments revealed a targetable CDK6-regulated protein signature in multiple myeloma patients, including the regulation of high-risk myeloma markers TRIP13 and RRM1<sup>120,121</sup>. In summary, CDK6 was identified as a key regulator in treatment-resistant multiple myeloma, supporting the clinical investigation of combining CDK6

inhibition with IMiDs as a therapeutic strategy. The study also demonstrated the proof-of-principle for the utility of quantitative proteomic approach in primary myeloma samples.

Proteomics analysis was applied to a larger cohort of multiple myeloma patients with protein expression levels integrated with genomic and transcriptomic data<sup>93</sup>. Our study provides a comprehensive proteome analysis of newly diagnosed, untreated multiple myeloma, covering the major genetic alterations of this disease which has not been characterized previously. Our comparison of healthy cells, MGUS, newly-diagnosed multiple myeloma, and plasma cell leukemia, along with clinical data, allows us to explore myeloma-specific proteins associated with the pathogenesis. Furthermore, exploration of the proteome changes in the common cytogenetic abnormalities provides insights into the molecular landscape of each genetic subtype, which could potentially facilitate the identification of actionable vulnerabilities and personalized therapeutic strategies. Again, a general low protein-to-RNA correlation was observed, consistent with previous studies<sup>60-62,91</sup>.

Our study further investigated whether proteomics and phosphoproteomics could provide additional prognostic information beyond the R-ISS for risk stratification. Utilizing proteomics and clinical data from 100 patients, a protein risk score with eight proteins was defined, including Ubiquitin-conjugating enzyme E2 Q1 (UBE2Q1). The proteins comprising the risk signature are distinct from genetic-based risk signatures and known drug mechanisms, underscoring the additional value the proteomic approach provides. The risk score was closely associated with disease progression and was also further validated in an independent cohort of myeloma patients<sup>122</sup>. Given the high degree of post-transcriptional regulation revealed from our study, multiple myeloma characterization using proteins may offer greater predictive power compared to genetics-based approach. Integrating proteomic data on proteins upregulated in myeloma samples compared to healthy hematopoietic cells and a genome-wide CRISPR activation screen, POU2AF1 and IRS1 were identified to be myeloma-selective targets driving disease progression, of which POU2AF1 has been independently described to regulate an oncogenic transcription network and IRS1 promotes myeloma growth through PI3K signaling<sup>123,124</sup>.

Amplification of the 1q chromosomal arm is a well-established high-risk cytogenetic alteration in multiple myeloma, associated with poorer overall survival and less favorable clinical outcomes<sup>110,111</sup>. Candidates on chromosome 1q have been studied for their association with adverse effects from gene expression profiling, including *CKS1B*<sup>125</sup>, *MCL-1*<sup>126</sup>, *ETV3*<sup>127</sup>, and *ADARI*<sup>128</sup>. Chr1q gain is also associated with drug resistance, with a high expression of 1q genes conferring resistance to chemotherapies<sup>129,130</sup>, and patients having shorter median PFS and OS upon lenalidomide-, bortezomib-, and daratumumab- comprising therapy<sup>131</sup>. While only a subset of t(11;14) myeloma patients respond to venetoclax<sup>21,22</sup>, the concurrent presence of 1q gain with t(11;14) is

associated with significantly worse progression-free survival<sup>132</sup>. To further uncover protein candidates in chr1q gain patients that contribute to the advanced disease, the relationship between 1q protein expression levels and progression-free and overall survival was examined. UBE2Q1 was identified to be a prognostic marker of survival outcome, as well as an oncogenic driver in 1q gain patients and master regulator of a network of proteins found to be dysregulated in multiple myeloma. UBE2Q1 has been described to be an oncogene highly expressed in some solid tumors and its upregulation is associated with poor prognosis due to its role in cell proliferation regulation<sup>133–137</sup>. As an E2 ubiquitin-conjugating enzyme, UBE2Q1 can facilitate the ubiquitination of proteins along with an E3 substrate adaptor. This post-translational modification may partially contribute to the observed discrepancy between RNA and protein levels. The identification of the E3 ligase engaging with UBE2Q1 as well as the corresponding substrate would aid in the understanding of how UBE2Q1 contributes to the pathogenesis and drug resistance in multiple myeloma. It has been reported that UBE2Q1 interacts with p53 and the repression of this tumor suppressor may contribute to the promotion of tumor growth and dysregulation in gene expression patterns<sup>138</sup>. While there are currently limited inhibitors targeting E2 enzymes, the identification of the E1 and E3 proteins associated with UBE2Q1 would greatly facilitate the design and development of inhibitors, expanding the search to disrupting the interactions between the E1-E2 or E2-E3 protein<sup>139,140</sup>. This would benefit not only multiple myeloma patients but also patients of other cancer subtypes as gain of 1q chromosomal arm is a common cytogenetic alteration<sup>141,142</sup>.

While the use of immunotherapy in the management of multiple myeloma has demonstrated efficacy in multi-drug resistant patients, antigen escape has emerged as a significant challenge leading to resistance, underscoring the need to identify additional targets for immunotherapy<sup>143,144</sup>. Other mass-spectrometry studies have demonstrated the integration of myeloma surfaceome data with proteomics and transcriptomics to identify novel immunotherapy antigens for myeloma<sup>145,146</sup>. Our integration of proteomics data and single-cell RNA sequencing with the Cancer Surfaceome Atlas allowed for the identification of selective and highly expressed Fc receptor-like 2 (FCRL2) on myeloma and B cells in addition to the currently explored targets BCMA and FCRL5<sup>147,148</sup>.

Overall, the proteomic landscape of multiple myeloma serves as a valuable resource, providing insights into the molecular characteristics of genetic subtypes, identifying key oncogenic drivers, developing a robust prognostic protein-based risk score for disease stratification, and uncovering novel potential therapeutic targets. These findings require validation in future studies with larger patient cohorts, preferably in the context of clinical trials with defined treatment regimens and available outcome data.

Previous proteogenomic studies in multiple myeloma are constrained by relatively small sample sizes. Our study of 138 multiple myeloma patients<sup>93</sup>, while significant, remains limited in comparison to larger genomic studies. While our pilot study included matched pre-treatment and relapsed samples<sup>91</sup>, longitudinal data that captures proteogenomic changes throughout the course of treatment and disease progression remains lacking. Moreover, the comprehensive nature of proteogenomic analysis, which necessitates specialized equipment and reagents, renders it cost-prohibitive and limits its widespread clinical implementation. Current technological advancements have led to increased throughput and efficiency from mass spectrometry approaches. The development of miniaturized mass spectrometry, such as micro-scaled or nano-scaled proteomics, demonstrates improved detection sensitivity and could lead to cost reductions in reagents as well as lowering the amount of required starting analyte, showing the potential of making this powerful analytical technique affordable, accessible, and suited for clinical samples where patient material is limited<sup>149</sup>. Proteogenomic studies offer valuable insights into protein expression patterns, yet they may fall short of fully elucidating the functional status of proteins, including their activity and intricate cellular interactions. While such studies can uncover promising therapeutic targets or biomarkers, they often lack comprehensive target assessment in appropriate biological models. Moreover, the increasing application of omics is generating vast amounts of data. The ongoing challenge lies in navigating this extensive data landscape and translating these big data into actionable, clinically relevant knowledge. Addressing these limitations will be crucial for advancing the field of proteogenomics in multiple myeloma and realizing its potential for improving patient care and treatment strategies.

Taken together, a multi-faceted approach combining genetic and proteomic analyses holds promise for a deeper understanding of multiple myeloma biology, revealing new potential therapeutic targets, providing insights into resistance mechanisms, and offering a more comprehensive understanding of the molecular landscape in multiple myeloma. By integrating these insights with drug development, clinicians can potentially develop more effective and personalized treatment strategies tailored to each patient's unique molecular profile and advance multiple myeloma therapy.

Of the apoptosis modulators that target the intrinsic apoptotic pathway, BH3 mimetics represent a new class of anti-cancer therapeutics targeting the BCL2 family members. Despite significant clinical efficacy in the treatment of CLL and AML<sup>68,70–72</sup>, venetoclax is only effective in a subset of multiple myeloma patients harboring t(11;14) translocation<sup>21,22</sup>. Previous studies have found that venetoclax-sensitive t(11;14) multiple myeloma exhibits higher expression of B-cell associated genes due to enhanced chromatin accessibility, contributing to an increase in B-cell depend-

ency<sup>73,74</sup>. Our proteogenomic study identified 102 apoptosis-associated proteins that are significantly deregulated in t(11;14) myeloma patients, including the enrichment of B cell markers, consistent with prior research<sup>73</sup>, and the downregulation of *BIRC2/cIAP1*<sup>93</sup>. *BIRC2* and *BIRC3*, encoding cIAP1 and cIAP2 respectively, are also frequently deleted in relapsed/refractory myeloma patients<sup>11</sup>. The dysregulation of proteins involved in apoptotic pathways provides a potential susceptibility towards apoptotic modulators. It is hypothesized that there might be a functional overlap between these proteins, evidenced by the compensatory increase in cIAP2 protein levels upon *BIRC2/cIAP1* knockout (Figure 11C). Similar to the shift in *BCL2* dependency in t(11;14), it is speculated that IAP knockout cells are more dependent on the remaining IAPs. Moreover, XIAP has been found to be associated with myeloma drug resistance and tumor development<sup>150</sup>, and targeting XIAP leads to increased cell death in multiple myeloma<sup>151</sup>. Therefore, we aimed to develop protein degraders that can lead to pan-IAP degradation that can be used in t(11;14) myeloma patients, as well as in patients harboring *BIRC2* or *BIRC3* deletion.

We designed and synthesized three series of hetero-bifunctional compounds, each with eight unique linker structures. While the monovalent and bivalent IAP inhibitors were able to induce autoubiquitination of cIAP1 and degrade cIAP2 to variable levels, XIAP protein levels remain unchanged. In contrast, our IAP-targeting PROTACs degraded cIAP1, enhanced cIAP2 degradation, and also led to XIAP degradation, and outperformed the highly potent IAP inhibitor AZD5582. The targeted degradation of XIAP facilitated by the PROTAC technology, which was previously not achieved by conventional inhibitors, underscores the potential of this pharmacologic modality. Protein degradation of XIAP may disrupt downstream signaling and inhibit cell proliferation at lower concentrations compared to inhibitors. In addition, the degradation of proteins provides a more sustained reduction of signaling response. While the development of pan-IAP degraders shows promise for apoptosis-targeting in cancer treatment, the inhibitory effects were not observed consistently across all the cell-based evaluations and warrants the exploration of the sensitivity of different cell types towards IAP inhibition. While some studies have demonstrated the induction of apoptosis in myeloma cells via the targeting of IAPs, another study has reported that IAP inhibition by monomeric LCL161 suppressed *in vivo* myeloma growth through the induction of type-I interferon signaling which led to tumor cell phagocytosis by dendritic cells and macrophages and not direct cell death<sup>152,153</sup>. Taken together, these results warrant further exploration of our IAP PROTACs in the context of anti-tumor immunity. In conclusion, we have developed hetero-bifunctional PROTACs targeting the therapeutically relevant IAP proteins and



evaluated their capacity for IAP degradation and cell viability inhibition. Further research is required to elucidate the specific disease contexts or identify molecular markers where the pan-IAP degraders demonstrate the greatest therapeutic potential.

In summary, our research utilized proteomics to identify the upregulation of CDK6 as a non-genetic resistance mechanism towards IMiDs, which can be overcome by combining CDK6 inhibitors or protein degraders with IMiDs. Furthermore, our proteogenomic analysis of multiple myeloma uncovered valuable insight into the underlying biology of the disease, revealing a high level of post-transcriptional regulation in multiple myeloma cells. We identified distinct protein signatures associated with various genetic aberrations, established a prognostic protein-based risk score, determined oncogenic drivers of the disease, and uncovered novel myeloma-specific therapeutic targets. Moreover, we developed and systematically evaluated heterobifunctional PROTACs capable of pan-IAP degradation as a potential approach to target cancer cells with dysregulated apoptotic pathways. Collectively, this research exemplifies the utility of proteomics in elucidating disease pathophysiology and uncovering resistance mechanisms, which may potentially be addressed through targeted protein degradation strategies.

## Reference list

1. Rajkumar, S. V., Dimopoulos, M. A., Palumbo, A., Blade, J., Merlini, G., Mateos, M. V., Kumar, S., Hillengass, J., Kastiris, E., Richardson, P., Landgren, O., Paiva, B., Dispenzieri, A., Weiss, B., LeLeu, X., Zweegman, S., Lonial, S., Rosinol, L., Zamagni, E., Jagannath, S., Sezer, O., Kristinsson, S. Y., Caers, J., Usmani, S. Z., Lahuerta, J. J., Johnsen, H. E., Beksac, M., Cavo, M., Goldschmidt, H., Terpos, E., Kyle, R. A., Anderson, K. C., Durie, B. G. M. & Miguel, J. F. S. International Myeloma Working Group updated criteria for the diagnosis of multiple myeloma. *Lancet Oncol* **15**, e538–e548 (2014).
2. Bird, S. A. & Boyd, K. Multiple myeloma: an overview of management. *Palliat Care Soc Pract* **13**, (2019).
3. Landgren, O., Kyle, R. A., Pfeiffer, R. M., Katzmann, J. A., Caporaso, N. E., Hayes, R. B., Dispenzieri, A., Kumar, S., Clark, R. J., Baris, D., Hoover, R. & Rajkumar, S. V. Monoclonal gammopathy of undetermined significance (MGUS) consistently precedes multiple myeloma: a prospective study. *Blood* **113**, 5412–5417 (2009).
4. Weiss, B. M., Abadie, J., Verma, P., Howard, R. S. & Kuehl, W. M. A monoclonal gammopathy precedes multiple myeloma in most patients. *Blood* **113**, 5418–5422 (2009).
5. Rajkumar, S. V., Kumar, S., Lonial, S. & Mateos, M. V. Smoldering multiple myeloma current treatment algorithms. *Blood Cancer Journal* **2022** *12*:9 **12**, 1–7 (2022).
6. Fernández de Larrea, C., Kyle, R., Rosiñol, L., Paiva, B., Engelhardt, M., Usmani, S., Caers, J., Gonsalves, W., Schjesvold, F., Merlini, G., Lentzsch, S., Ocio, E., Garderet, L., Moreau, P., Sonneveld, P., Badros, A., Gahrton, G., Goldschmidt, H., Tuchman, S., Einsele, H., Durie, B., Wirk, B., Musto, P., Hayden, P., Kaiser, M., Miguel, J. S., Bladé, J., Rajkumar, S. V. & Mateos, M. V. Primary plasma cell leukemia: consensus definition by the International Myeloma Working Group according to peripheral blood plasma cell percentage. *Blood Cancer Journal* **2021** *11*:12 **11**, 1–5 (2021).
7. Lohr, J. G., Stojanov, P., Carter, S. L., Cruz-Gordillo, P., Lawrence, M. S., Auclair, D., Sougnez, C., Knoechel, B., Gould, J., Saksena, G., Cibulskis, K., McKenna, A., Chapman, M. A., Straussman, R., Levy, J., Perkins, L. M., Keats, J. J., Schumacher, S. E., Rosenberg, M., Getz, G. & Golub, T. R. Widespread genetic heterogeneity in multiple myeloma: Implications for targeted therapy. *Cancer Cell* **25**, 91–101 (2014).
8. Walker, B. A., Boyle, E. M., Wardell, C. P., Murison, A., Begum, D. B., Dahir, N. M., Proszek, P. Z., Johnson, D. C., Kaiser, M. F., Melchor, L., Aronson, L. I., Scales, M., Pawlyn, C., Mirabella, F., Jones, J. R., Brioli, A., Mikulasova, A., Cairns, D. A., Gregory, W. M., Quartilho, A., Drayson, M. T., Russell, N., Cook, G., Jackson, G. H., Leleu, X., Davies, F. E. & Morgan, G. J. Mutational spectrum, copy number changes, and outcome: Results of a sequencing study of patients with newly diagnosed myeloma. *Journal of Clinical Oncology* **33**, 3911–3920 (2015).
9. Keats, J. J., Fonseca, R., Chesi, M., Schop, R., Baker, A., Chng, W. J., Van Wier, S., Tiedemann, R., Shi, C. X., Sebag, M., Braggio, E., Henry, T., Zhu, Y. X., Fogle, H., Price-Troska, T., Ahmann, G., Mancini, C., Brents, L. A., Kumar, S., Greipp, P., Dispenzieri, A., Bryant, B., Mulligan, G., Bruhn, L., Barrett, M., Valdez, R., Trent, J., Stewart, A. K., Carpten, J. & Bergsagel, P. L. Promiscuous mutations activate the noncanonical NF-kappaB pathway in multiple myeloma. *Cancer Cell* **12**, 131–144 (2007).
10. Walker, B. A., Leone, P. E., Chiecchio, L., Dickens, N. J., Jenner, M. W., Boyd, K. D., Johnson, D. C., Gonzalez, D., Dagrada, G. P., Protheroe, R. K. M., Konn, Z. J., Stockley, D. M., Gregory, W. M., Davies, F. E., Ross, F. M. & Morgan, G. J. A compendium of myeloma-associated chromosomal copy number abnormalities and their prognostic value. *Blood* **116**, 56–65(2010).
11. Chavan, S. S., He, J., Tytarenko, R., Deshpande, S., Patel, P., Bailey, M., Stein, C. K., Stephens, O., Weinhold, N., Petty, N., Steward, D., Rasche, L., Bauer, M., Ashby, C., Peterson, E., Ali, S., Ross, J., Miller, V. A., Stephens, P., Thanendraran, S., Schinke, C., Zangari, M., Van Rhee, F., Barlogie, B., Mughal, T. I., Davies, F. E., Morgan, G. J. & Walker, B. A. Bi-allelic inactivation is more prevalent at relapse in multiple myeloma, identifying RB1 as an independent prognostic marker. *Blood Cancer J* **7**, 1–7 (2017).
12. Keats, J. J., Chesi, M., Egan, J. B., Garbitt, V. M., Palmer, S. E., Braggio, E., Van Wier, S., Blackburn, P. R., Baker, A. S., Dispenzieri, A., Kumar, S., Rajkumar, S. V., Carpten, J. D., Barrett, M., Fonseca, R., Stewart, A. K. & Bergsagel, P. L. Clonal competition with alternating dominance in multiple myeloma. *Blood* **120**, 1067–1076 (2012).
13. Annunziata, C. M., Davis, R. E., Demchenko, Y., Bellamy, W., Gabrea, A., Zhan, F., Lenz, G., Hanamura, I., Wright, G., Xiao, W., Dave, S., Hurt, E. M., Tan, B., Zhao, H., Stephens, O., Santra, M., Williams, D. R., Dang, L., Barlogie, B., Shaughnessy, J. D., Kuehl, W. M. & Staudt, L. M. Frequent engagement of the classical and alternative NF-kappaB pathways by diverse genetic abnormalities in multiple myeloma. *Cancer Cell* **12**, 115–130 (2007).
14. Shah, V., Sherborne, A. L., Walker, B. A., Johnson, D. C., Boyle, E. M., Ellis, S., Begum, D. B., Proszek, P. Z., Jones, J. R., Pawlyn, C., Savola, S., Jenner, M. W., Drayson, M. T., Owen, R. G., Houlston, R. S., Cairns, D. A., Gregory, W. M., Cook, G., Davies, F. E., Jackson, G. H., Morgan, G. J. & Kaiser, M. F. Prediction of outcome in newly diagnosed myeloma: a meta-analysis of the molecular profiles of 1905 trial patients. *Leukemia* **32**, 102 (2018).
15. Durie, B. G. M. & Salmon, S. E. A clinical staging system for multiple myeloma- Correlation of Measured Myeloma Cell M a s s with Presenting Clinical Features, Response to Treatment, and Survival. *Cancer* **36**, 842–54 (1975).
16. Greipp, P. R., Miguel, J. S., Dune, B. G. M., Crowley, J. J., Barlogie, B., Bladé, J., Boccadoro, M., Child, J. A., Harousseau, J. L., Kyle, R. A., Lahuerta, J. J., Ludwig, H., Morgan, G., Powles, R., Shimizu, K., Shustik, C., Sonneveld, P., Tosi, P., Turesson, I. & Westin, J. International staging system for multiple myeloma. *Journal of Clinical Oncology* **23**, 3412–3420 (2005).
17. Kumar, S., Fonseca, R., Ketterling, R. P., Dispenzieri, A., Lacy, M. Q., Gertz, M. A., Hayman, S. R., Buadi, F. K., Dingli, D., Knudson, R. A., Greenberg, A., Russell, S. J., Zeldenrust, S. R., Lust, J. A., Kyle, R. A., Bergsagel, L. & Rajkumar, S. V. Trisomies in multiple myeloma: impact on survival in patients with high-risk cytogenetics. *Blood* **119**, 2100–2105 (2012).

18. Kumar, S. K., Mikhael, J. R., Buadi, F. K., Dingli, D., Dispenzieri, A., Fonseca, R., Gertz, M. A., Greipp, P. R., Hayman, S. R., Kyle, R. A., Lacy, M. Q., Lust, J. A., Reeder, C. B., Roy, V., Russell, S. J., Detweiler Short, K. E., Stewart, A. K., Witzig, T. E., Zeldenrust, S. R., Dalton, R. J., Rajkumar, S. V. & Bergsagel, P. L. Management of newly diagnosed symptomatic multiple myeloma: updated Mayo Stratification of Myeloma and Risk-Adapted Therapy (mSMART) consensus guidelines. *Mayo Clin Proc* **84**, 1095–1110 (2009).
19. Vu, T., Gonsalves, W., Kumar, S., Dispenzieri, A., Lacy, M. Q., Buadi, F., Gertz, M. A. & Rajkumar, S. V. Characteristics of exceptional responders to lenalidomide-based therapy in multiple myeloma. *Blood Cancer J* **5**, e363(2015).
20. Palumbo, A., Avet-Loiseau, H., Oliva, S., Lokhorst, H. M., Goldschmidt, H., Rosinol, L., Richardson, P., Caltagirone, S., Lahuerta, J. J., Facon, T., Bringhen, S., Gay, F., Attal, M., Passera, R., Spencer, A., Offidani, M., Kumar, S., Musto, P., Lonial, S., Petrucci, M. T., Orłowski, R. Z., Zamagni, E., Morgan, G., Dimopoulos, M. A., Durie, B. G. M., Anderson, K. C., Sonneveld, P., Miguel, J. S., Cavo, M., Rajkumar, S. V. & Moreau, P. Revised International Staging System for Multiple Myeloma: A Report From International Myeloma Working Group. *J Clin Oncol* **33**, 2863–2869 (2015).
21. Kumar, S., Kaufman, J. L., Gasparetto, C., Mikhael, J., Vij, R., Pegourie, B., Benboubker, L., Facon, T., Amiot, M., Moreau, P., Punnoose, E. A., Alzate, S., Dunbar, M., Xu, T., Agarwal, S. K., Enschede, S. H., Levenson, J. D., Ross, J. A., Maciag, P. C., Verdugo, M. & Touzeau, C. Efficacy of venetoclax as targeted therapy for relapsed/refractory t(11;14) multiple myeloma. *Blood* **130**, 2401–2409 (2017).
22. Badawi, M., Coppola, S., Eckert, D., Gopalakrishnan, S., Engelhardt, B., Doelger, E., Huang, W., Dobkowska, E., Kumar, S., Menon, R. M. & Salem, A. H. Venetoclax in biomarker-selected multiple myeloma patients: Impact of exposure on clinical efficacy and safety. *Hematol Oncol* **42**, (2024).
23. Gozzetti, A., Ciofini, S., Simoncelli, M., Santoni, A., Pacelli, P., Raspadori, D. & Bocchia, M. Anti CD38 monoclonal antibodies for multiple myeloma treatment. *Hum Vaccin Immunother* **18**, (2022).
24. Hsi, E. D., Steinle, R., Balasa, B., Szmania, S., Draksharapu, A., Shum, B. P., Huseni, M., Powers, D., Nanisetti, A., Zhang, Y., Rice, A. G., Van Abbema, A., Wong, M., Liu, G., Zhan, F., Dillon, M., Chen, S., Rhodes, S., Fuh, F., Tsurushita, N., Kumar, S., Vexler, V., Shaughnessy, J. D., Barlogie, B., Van Rhee, F., Hussein, M., Afar, D. E. H. & Williams, M. B. CS1, a Potential New Therapeutic Antibody Target for the Treatment of Multiple Myeloma. *Clin Cancer Res* **2775–2784** (2008).
25. Gogishvili, T., Danhof, S., Prommersberger, S., Rydzek, J., Schreder, M., Brede, C., Einsele, H. & Hudecek, M. SLAMF7-CAR T cells eliminate myeloma and confer selective fratricide of SLAMF7+ normal lymphocytes. *Blood* **130**, 2838–2847 (2017).
26. Lonial, S., Dimopoulos, M., Palumbo, A., White, D., Grosicki, S., Spicka, I., Walter-Croneck, A., Moreau, P., Mateos, M.-V., Magen, H., Belch, A., Reece, D., Beksac, M., Spencer, A., Oakervee, H., Orłowski, R. Z., Taniwaki, M., Röllig, C., Einsele, H., Wu, K. L., Singhal, A., San-Miguel, J., Matsumoto, M., Katz, J., Bleickardt, E., Poulart, V., Anderson, K. C. & Richardson, P. Elotuzumab Therapy for Relapsed or Refractory Multiple Myeloma. *New England Journal of Medicine* **373**, 621–631 (2015).
27. Moreau, P., Garfall, A. L., van de Donk, N. W. C. J., Nahi, H., San-Miguel, J. F., Oriol, A., Nooka, A. K., Martin, T., Rosinol, L., Chari, A., Karlin, L., Benboubker, L., Mateos, M.-V., Bahlis, N., Papat, R., Besemer, B., Martínez-López, J., Sidana, S., Delforge, M., Pei, L., Trancucci, D., Verona, R., Girgis, S., Lin, S. X. W., Olyslager, Y., Jaffe, M., Uhlar, C., Stephenson, T., Van Rempelbergh, R., Banerjee, A., Goldberg, J. D., Kobos, R., Krishnan, A. & Usmani, S. Z. Teclistamab in Relapsed or Refractory Multiple Myeloma. *New England Journal of Medicine* **387**, 495–505 (2022).
28. Ma, T., Shi, J. & Liu, H. Chimeric antigen receptor T cell targeting B cell maturation antigen immunotherapy is promising for multiple myeloma. *Ann Hematol* **98**, 813–822 (2019).
29. Lin, Q., Zhao, J., Song, Y. & Liu, D. Recent updates on CAR T clinical trials for multiple myeloma. *Mol Cancer* **18**, (2019).
30. Moreau, P., Usmani, S. Z., Garfall, A. L., van de Donk, N. W. C. J., Nahi, H., San-Miguel, J., Oriol, A., Nooka, A. K., Martin, T., Rosinol, L., Chari, A., Karlin, L., Benboubker, L., Mateos, M.-V., Bahlis, N. J., Papat, R., Besemer, B., Martínez-López, J., Sidana, S., Pei, L., Trancucci, D., Verona, R. I., Girgis, S., Olyslager, Y., Jaffe, M., Uhlar, C. M., Stephenson, T., Van Rempelbergh, R., Banerjee, A., Goldberg, J. D., Kobos, R. & Krishnan, A. Y. Updated Results from MajesTEC-1: Phase 1/2 Study of Teclistamab, a B-Cell Maturation Antigen x CD3 Bispecific Antibody, in Relapsed/Refractory Multiple Myeloma. *Blood* **138**, 896–896 (2021).
31. Lee, L., Bounds, D., Paterson, J., Herledan, G., Sully, K., Seestaller-Wehr, L. M., Fieles, W. E., Tunstead, J., McCahon, L., Germaschewski, F. M., Mayes, P. A., Craigen, J. L., Rodriguez-Justo, M. & Yong, K. L. Evaluation of B cell maturation antigen as a target for antibody drug conjugate mediated cytotoxicity in multiple myeloma. *Br J Haematol* **174**, 911–922 (2016).
32. Davies, S. Teratogenic effects of thalidomide in rabbits, rats... *Journal of Nutritional Medicine* **1**, 231 (1990).
33. Matyskiela, M. E., Couto, S., Zheng, X., Lu, G., Hui, J., Stamp, K., Drew, C., Ren, Y., Wang, M., Carpenter, A., Lee, C. W., Clayton, T., Fang, W., Lu, C. C., Riley, M., Abdubek, P., Blease, K., Hartke, J., Kumar, G., Vessey, R., Rolfe, M., Hamann, L. G. & Chamberlain, P. P. SALL4 mediates teratogenicity as a thalidomide-dependent cereblon substrate. *Nat Chem Biol* **14**, 981–987 (2018).
34. Ito, T., Ando, H., Suzuki, T., Ogura, T., Hotta, K., Imamura, Y., Yamaguchi, Y. & Handa, H. Identification of a primary target of thalidomide teratogenicity. *Science* **327**, 1345–1350 (2010).
35. Richardson, P., Mitsiades, C., Laubach, J., Schlossman, R., Ghobrial, I., Hideshima, T., Munshi, N. & Anderson, K. Lenalidomide in multiple myeloma: an evidence-based review of its role in therapy. *Core Evid* **4**, 215 (2009).
36. List, A., Dewald, G., Bennett, J., Giagounidis, A., Raza, A., Feldman, E., Powell, B., Greenberg, P., Thomas, D., Stone, R., Reeder, C., Wride, K., Patin, J., Schmidt, M., Zeldis, J. & Knight, R. Lenalidomide in the Myelodysplastic Syndrome with Chromosome 5q Deletion. *New England Journal of Medicine* **355**, 1456–1465 (2006).

37. Wiernik, P. H., Lossos, I. S., Tuscano, J. M., Justice, G., Vose, J. M., Cole, C. E., Lam, W., McBride, K., Wride, K., Pietronigro, D., Takeshita, K., Ervin-Haynes, A., Zeldis, J. B. & Habermann, T. M. Lenalidomide monotherapy in relapsed or refractory aggressive non-Hodgkin's lymphoma. *Journal of Clinical Oncology* **26**, 4952–4957 (2008).
38. Rasco, D. W., Papadopoulos, K. P., Pourdehnad, M., Gandhi, A. K., Hagner, P. R., Li, Y., Wei, X., Chopra, R., Hege, K., DiMartino, J. & Shih, K. A First-in-Human Study of Novel Cereblon Modulator Avadomide (CC-122) in Advanced Malignancies. *Clin Cancer Res* **25**, 90–98 (2019).
39. Bjorklund, C. C., Kang, J., Amatangelo, M., Polonskaia, A., Katz, M., Chiu, H., Couto, S., Wang, M., Ren, Y., Ortiz, M., Towfic, F., Flynt, J. E., Pierceall, W. & Thakurta, A. Iberdomide (CC-220) is a potent cereblon E3 ligase modulator with antitumor and immunostimulatory activities in lenalidomide- and pomalidomide-resistant multiple myeloma cells with dysregulated CRBN. *Leukemia* **2019 34:4 34**, 1197–1201 (2019).
40. Lonial, S., Popat, R., Hulin, C., Jagannath, S., Oriol, A., Richardson, P. G., Facon, T., Weisel, K., Larsen, J. T., Minnema, M. C., Abdallah, A. O., Badros, A. Z., Knop, S., Stadtmauer, E. A., Cheng, Y., Amatangelo, M., Chen, M., Nguyen, T. V., Amin, A., Peluso, T. & van de Donk, N. W. C. J. Iberdomide plus dexamethasone in heavily pretreated late-line relapsed or refractory multiple myeloma (CC-220-MM-001): a multicentre, multicohort, open-label, phase 1/2 trial. *Lancet Haematol* **9**, e822–e832 (2022).
41. Hansen, J. D., Correa, M., Nagy, M. A., Alexander, M., Plantevin, V., Grant, V., Whitefield, B., Huang, D., Kercher, T., Harris, R., Narla, R. K., Leisten, J., Tang, Y., Moghaddam, M., Ebinger, K., Piccotti, J., Havens, C. G., Cathers, B., Carmichael, J., Daniel, T., Vessey, R., Hamann, L. G., Leftheris, K., Mendy, D., Baculi, F., Lebrun, L. A., Khambatta, G. & Lopez-Girona, A. Discovery of CRBN E3 Ligase Modulator CC-92480 for the Treatment of Relapsed and Refractory Multiple Myeloma. *J Med Chem* **63**, 6648–6676 (2020).
42. Richardson, P. G., Trudel, S., Quach, H., Popat, R., Lonial, S., Orłowski, R. Z., Kim, K., Mateos, M.-V., Pawlyn, C., Ramasamy, K., Martinez-Lopez, J., Spirli, A., Casas-Avilés, I., Gong, J., Amatangelo, M., Katz, J., Maciag, P., Peluso, T. & Bahlis, N. J. Mezigdomide (CC-92480), a Potent, Novel Cereblon E3 Ligase Modulator (CELMoD), Combined with Dexamethasone (DEX) in Patients (pts) with Relapsed/Refractory Multiple Myeloma (RRMM): Preliminary Results from the Dose-Expansion Phase of the CC-92480-MM-001 Trial. *Blood* **140**, 1366–1368 (2022).
43. Gaffney, B., Shi, Y., de Jong, P., Sanchez, M., Fontanillo, C., Lopez-Girona, A., Boss, I. W., Kurtova, A., Carrancio, S., Wong, L. & Pierce, D. W. Mezigdomide (CC-92480), a Novel Cereblon E3 Ligase Modulator, Induces Vulnerability of Multiple Myeloma Cells to T-Cell-Mediated Killing. *Blood* **140**, 7108–7109 (2022).
44. Krönke, J., Udeshi, N. D., Narla, A., Grauman, P., Hurst, S. N., McConkey, M., Svinkina, T., Heckl, D., Comer, E., Li, X., Ciarlo, C., Hartman, E., Munshi, N., Schenone, M., Schreiber, S. L., Carr, S. A. & Ebert, B. L. Lenalidomide causes selective degradation of IKZF1 and IKZF3 in multiple myeloma cells. *Science* **343**, 301–305 (2014).
45. Lu, G., Middleton, R. E., Sun, H., Naniong, M. V., Ott, C. J., Mitsiades, C. S., Wong, K. K., Bradner, J. E. & Kaelin, W. G. The myeloma drug lenalidomide promotes the cereblon-dependent destruction of ikaros proteins. *Science* **343**, 305–309 (2014).
46. Krönke, J., Fink, E. C., Hollenbach, P. W., MacBeth, K. J., Hurst, S. N., Udeshi, N. D., Chamberlain, P. P., Mani, D. R., Man, H. W., Gandhi, A. K., Svinkina, T., Schneider, R. K., McConkey, M., Järås, M., Griffiths, E., Wetzler, M., Bullinger, L., Cathers, B. E., Carr, S. A., Chopra, R. & Ebert, B. L. Lenalidomide induces ubiquitination and degradation of CK1α in del(5q) MDS. *Nature* **523**, 183–188 (2015).
47. Gandhi, A. K., Kang, J., Havens, C. G., Conklin, T., Ning, Y., Wu, L., Ito, T., Ando, H., Waldman, M. F., Thakurta, A., Klippel, A., Handa, H., Daniel, T. O., Schafer, P. H. & Chopra, R. Immunomodulatory agents lenalidomide and pomalidomide co-stimulate T cells by inducing degradation of T cell repressors Ikaros and Aiolos via modulation of the E3 ubiquitin ligase complex CRL4CRBN. *Br J Haematol* **164**, 811–821 (2014).
48. Haslett, P. A. J., Corral, L., Albert, M. & Kaplan, G. Thalidomide costimulates primary human T lymphocytes, preferentially inducing proliferation, cytokine production, and cytotoxic responses in the CD8+ subset. *J Exp Med* **187**, 6–13 (1998).
49. Davies, F. E., Raje, N., Hideshima, T., Lentzsch, S., Young, G., Tai, Y. T., Lin, B., Podar, K., Gupta, D., Chauhan, D., Treon, S. P., Richardson, P. G., Schlossman, R. L., Morgan, G. J., Muller, G. W., Stirling, D. I. & Anderson, K. C. Thalidomide and immunomodulatory derivatives augment natural killer cell cytotoxicity in multiple myeloma. *Blood* **98**, 210–216 (2001).
50. Kortüm, K. M., Mai, E. K., Hanafiah, N. H., Shi, C. X., Zhu, Y. X., Bruins, L., Barrio, S., Jedlowski, P., Merz, M., Xu, J., Stewart, R. A., Andrulis, M., Jauch, A., Hillengass, J., Goldschmidt, H., Bergsagel, P. L., Braggio, E., Stewart, A. K. & Raab, M. S. Targeted sequencing of refractory myeloma reveals a high incidence of mutations in CRBN and Ras pathway genes. *Blood* **128**, 1226–1233 (2016).
51. Liu, J., Song, T., Zhou, W., Xing, L., Wang, S., Ho, M., Peng, Z., Tai, Y. T., Hideshima, T., Anderson, K. C. & Cang, Y. A genome-scale CRISPR-Cas9 screening in myeloma cells identifies regulators of immunomodulatory drug sensitivity. *Leukemia* **33**, 171–180 (2019).
52. Bohl, S. R., Schmalbrock, L. K., Bauhuf, I., Meyer, T., Dolnik, A., Szyska, M., Blätte, T. J., Knödler, S., Röhner, L., Müller, D., Kull, M., Langer, C., Döhner, H., Letai, A., Damm, F., Heckl, D., Bullinger, L. & Krönke, J. Comprehensive CRISPR-Cas9 screens identify genetic determinants of drug responsiveness in multiple myeloma. *Blood Adv* **5**, 2391–2402 (2021).
53. Gooding, S., Ansari-Pour, N., Towfic, F., Estévez, M. O., Chamberlain, P. P., Tsai, K. T., Flynt, E., Hirst, M., Rozelle, D., Dhiman, P., Neri, P., Ramasamy, K., Bahlis, N., Vyas, P. & Thakurta, A. Multiple cereblon genetic changes are associated with acquired resistance to lenalidomide or pomalidomide in multiple myeloma. *Blood* **137**, 232–237 (2021).
54. Barrio, S., Munawar, U., Zhu, Y. X., Giesen, N., Shi, C.-X., Da Viá, M., Sanchez, R., Bruins, L., Demler, T., Müller, N., Haertle, L., Garitano, A., Steinbrunn, T., Danhof, S., Cuenca, I., Barrio-Garcia, C., Braggio, E., Rosenwald, A., Martinez-Lopez, J., Rasche, L., Raab, M. S., Stewart, A. K., Einsele, H., Stühmer, T. & Kortüm, K. M. IKZF1/3 and CRL4-CRBN E3 ubiquitin ligase mutations and IMiD resistance in multiple myeloma. *Haematologica* **105**, e240 (2020).

55. Osada, N., Kikuchi, J., Iha, H., Yasui, H., Ikeda, S., Takahashi, N. & Furukawa, Y. c-FOS is an integral component of the IKZF1 transactivator complex and mediates lenalidomide resistance in multiple myeloma. (2023). doi:10.1002/ctm2.1364
56. Neri, P., Barwick, B. G., Jung, D., Patton, J. C., Maity, R., Tagoug, I., Stein, C. K., Tilmont, R., Leblay, N., Ahn, S., Lee, H., Welsh, S. J., Riggs, D. L., Stong, N., Flynt, E., Thakurta, A., Keats, J. J., Lonial, S., Bergsagel, P. L., Boise, L. H. & Bahlis, N. J. ETV4-Dependent Transcriptional Plasticity Maintains MYC Expression and Results in IMiD Resistance in Multiple Myeloma. *Blood Cancer Discov* **5**, 56–73 (2024).
57. Haertle, L., Barrio, S., Munawar, U., Han, S., Zhou, X., Vogt, C., Fern, R. A., Bittrich, M., Ruiz-Heredia, Y., Da Vi, M., Zovko, J., Garitano-Trojaola, A., Bolli, N. O., Ruckdeschel, A., Stf Uhmer, T., Chatterjee, M., Kull, M., Krč, J., Agirre, X., Martin-Subero, J. I., Raab, P., Einsele, H., Rasche, L., Martinez-Lopez, J., Haaf, T., Martin, K. & Um, K. Cereblon enhancer methylation and IMiD resistance in multiple myeloma. *Blood* **4**, 1721–1726 (2021).
58. Dimopoulos, K., Helbo, A. S., Munch-Petersen, H. F., Sjø, L., Christensen, J., Kristensen, L. S., Asmar, F., Emil, N., Hermansen, U., O'connel, C., Gimsing, P., Liang, G., Grønbaek, K., Dimopoulos, C. K. & Grønbaek, K. Dual inhibition of DNMTs and EZH2 can overcome both intrinsic and acquired resistance of myeloma cells to IMiDs in a cereblon-independent manner. *Mol Oncol* **12**, 180–195 (2018).
59. Li, Y., Barber, A., Martin, S., Morales, S., Bird, S., Chrisochidou, Y. & Pawlyn, C. EZH2 Inhibition Overcomes Immunomodulatory Drug (IMiD) Resistance in Multiple Myeloma Cell Lines in a Cereblon Pathway Dependent Manner. *Blood* **142**, 4187–4188 (2023).
60. Mertins, P., Mani, D. R., Ruggles, K. V., Gillette, M. A., Clauser, K. R., Wang, P., Wang, X., Qiao, J. W., Cao, S., Petralia, F., Kawaler, E., Mundt, F., Krug, K., Tu, Z., Lei, J. T., Gatzka, M. L., Wilkerson, M., Perou, C. M., Yellapantula, V., Huang, K. L., Lin, C., McLellan, M. D., Yan, P., Davies, S. R., Townsend, R. R., Skates, S. J., Wang, J., Zhang, B., Kinsinger, C. R., Mesri, M., Rodriguez, H., Ding, L., Paulovich, A. G., Fenyö, D., Ellis, M. J. & Carr, S. A. Proteogenomics connects somatic mutations to signalling in breast cancer. *Nature* **534**, 55–62 (2016).
61. Nusinow, D. P., Szpyt, J., Ghandi, M., Rose, C. M., McDonald, E. R., Kalocsay, M., Jané-Valbuena, J., Gelfand, E., Schweppe, D. K., Jedrychowski, M., Golji, J., Porter, D. A., Rejtar, T., Wang, Y. K., Kryukov, G. V., Stegmeier, F., Erickson, B. K., Garraway, L. A., Sellers, W. R. & Gygi, S. P. Quantitative Proteomics of the Cancer Cell Line Encyclopedia. *Cell* **180**, 387–402.e16 (2020).
62. Tyanova, S., Albrechtsen, R., Kronqvist, P., Cox, J., Mann, M. & Geiger, T. Proteomic maps of breast cancer subtypes. *Nat Commun* **7**, 1–11 (2016).
63. Dytfeld, D., Luczak, M., Wrobel, T., Usnarska-Zubkiewicz, L., Brzeźniakiewicz, K., Jamroziak, K., Giannopoulos, K., Przybyłowicz-Chalecka, A., Ratajczak, B., Czerwinska-Rybak, J., Nowicki, A., Joks, M., Czechowska, E., Zawartko, M., Szczepaniak, T., Grzasko, N., Bochenek, M., Kubicki, T., Morawska, M., Tusznió, K. & Jakubowiak, A. Comparative proteomic profiling of refractory/relapsed multiple myeloma reveals biomarkers involved in resistance to bortezomib-based therapy. *Oncotarget* **7**, 56726–56736 (2016).
64. Janker, L., Mayer, R. L., Bileck, A., Kreutz, D., Mader, J. C., Utpatel, K., Heudobler, D., Agis, H., Gerner, C. & Slany, A. Metabolic, anti-apoptotic and immune evasion strategies of primary human myeloma cells indicate adaptations to hypoxia. *Molecular and Cellular Proteomics* **18**, 936–953 (2019).
65. Mohamed, A., Collins, J., Jiang, H., Molendijk, J., Stoll, T., Torta, F., Wenk, M. R., Bird, R. J., Marlton, P., Mollee, P., Markey, K. A. & Hill, M. M. Concurrent lipidomics and proteomics on malignant plasma cells from multiple myeloma patients: Probing the lipid metabolome. *PLoS One* **15**, 1–16 (2020).
66. Eichhorst, B., Niemann, C. U., Kater, A. P., Fürstenau, M., von Tresckow, J., Zhang, C., Robrecht, S., Gregor, M., Juliusson, G., Thornton, P., Staber, P. B., Tadmor, T., Lindström, V., da Cunha-Bang, C., Schneider, C., Poulsen, C. B., Illmer, T., Schöttker, B., Nösslinger, T., Janssens, A., Christiansen, I., Baumann, M., Frederiksen, H., van der Klift, M., Jäger, U., Leys, M. B. L., Hoogendoorn, M., Lotfi, K., Hebart, H., Gaska, T., Koene, H., Enggaard, L., Goede, J., Regelink, J. C., Widmer, A., Simon, F., De Silva, N., Fink, A.-M., Bahlo, J., Fischer, K., Wendtner, C.-M., Kreuzer, K. A., Ritgen, M., Brüggemann, M., Tausch, E., Levin, M.-D., van Oers, M., Geisler, C., Stilgenbauer, S. & Hallek, M. First-Line Venetoclax Combinations in Chronic Lymphocytic Leukemia. *New England Journal of Medicine* **388**, 1739–1754 (2023).
67. Hampel, P. J., Swaminathan, M., Rogers, K. A., Parry, E. M., Burger, J. A., Davids, M. S., Ding, W., Ferrajoli, A., Hyak, J. M., Jain, N., Kenderian, S. S., Wang, Y., Wierda, W. G., Woyach, J. A., Parikh, S. A. & Thompson, P. A. A multicenter study of venetoclax-based treatment for patients with Richter transformation of chronic lymphocytic leukemia. *Blood Adv* **8**, 2342–2350 (2024).
68. DiNardo, C. D., Jonas, B. A., Pullarkat, V., Thirman, M. J., Garcia, J. S., Wei, A. H., Konopleva, M., Döhner, H., Letai, A., Fenaux, P., Koller, E., Havelange, V., Leber, B., Esteve, J., Wang, J., Pejsa, V., Hájek, R., Porkka, K., Illés, Á., Lavie, D., Lemoli, R. M., Yamamoto, K., Yoon, S.-S., Jang, J.-H., Yeh, S.-P., Turgut, M., Hong, W.-J., Zhou, Y., Potluri, J. & Pratz, K. W. Azacitidine and Venetoclax in Previously Untreated Acute Myeloid Leukemia. *New England Journal of Medicine* **383**, 617–629 (2020).
69. Kamoda, Y., Hirao, M., Iizuka, H., Kida, M., Usuki, K. & Ichikawa, M. Improved Survival with Venetoclax in Patients with Acute Myeloid Leukemia: A Retrospective Single-Center Cohort Study. *Blood* **142**, 5936–5936 (2023).
70. Roberts, A. W., Ma, S., Kipps, T. J., Coutre, S. E., Davids, M. S., Eichhorst, B., Hallek, M., Byrd, J. C., Humphrey, K., Zhou, L., Chyla, B., Nielsen, J., Potluri, J., Kim, S. Y., Verdugo, M., Stilgenbauer, S., Wierda, W. G. & Seymour, J. F. Efficacy of venetoclax in relapsed chronic lymphocytic leukemia is influenced by disease and response variables. *Blood* **134**, 111 (2019).
71. Ysebaert, L., Troussard, X., Levy, V., Le Calloch, R., Guieze, R., Laribi, K., Lepretre, S., Michallet, A.-S., Leblond, V., Feugier, P., Lahjibi, E., Ramier, J. & Delmer, A. Real-World Efficacy and Safety of Venetoclax Alone and in Combination with Rituximab in Patients with Chronic Lymphocytic Leukemia: Interim Results of the Verone Study. *Blood* **140**, 12395–12396 (2022).

72. Zhang, K., Zhang, X., Xu, Y., Xue, S., Qiu, H., Tang, X., Han, Y., Chen, S., Sun, A., Zhang, Y., Wu, D. & Wang, Y. Efficacy of venetoclax combined with hypomethylating agents in young, and unfit patients with newly diagnosed core binding factor acute myeloid leukemia. *Blood Cancer Journal* 2023 13:1 **13**, 1–4 (2023).
73. Gupta, V. A., Barwick, B. G., Matulis, S. M., Shirasaki, R., Jaye, D. L., Keats, J. J., Oberlton, B., Joseph, N. S., Hofmeister, C. C., Heffner, L. T., Dhodapkar, M. V., Nooka, A. K., Lonial, S., Mitsiades, C. S., Kaufman, J. L. & Boise, L. H. Venetoclax sensitivity in multiple myeloma is associated with B-cell gene expression. *Blood* **137**, 3604–3615 (2021).
74. Kitadate, A., Terao, T., Kentaro Narita, |, Ikeda, S., Takahashi, Y., Tsushima, T., Miura, D., Takeuchi, | Masami, Takahashi, N. & Matsue, | Kosei. Multiple myeloma with t(11;14)-associated immature phenotype has lower CD38 expression and higher BCL2 dependence. *Cancer Sci* **112**, 3645–3654 (2021).
75. Chai, J., Du, C., Wu, J. W., Kyin, S., Wang, X. & Shi, Y. Structural and biochemical basis of apoptotic activation by Smac/DIABLO. *Nature* **406**, 855–862 (2000).
76. Bai, L., Smith, D. C. & Wang, S. Small-Molecule SMAC Mimetics as New Cancer Therapeutics. *Pharmacol Ther* **144**, 82 (2014).
77. Salvesen, G. S. & Duckett, C. S. IAP proteins: blocking the road to death's door. *Nat Rev Mol Cell Biol* **3**, 401–410 (2002).
78. Mahoney, D. J., Cheung, H. H., Lejmi Mrad, R., Plenchette, S., Simard, C., Enwere, E., Arora, V., Mak, T. W., Lacasse, E. C., Waring, J. & Korneluk, R. G. Both cIAP1 and cIAP2 regulate TNF $\alpha$ -mediated NF- $\kappa$ B activation. *Proc Natl Acad Sci U S A* **105**, 11778–11783 (2008).
79. Varfolomeev, E., Goncharov, T., Fedorova, A. V., Dynek, J. N., Zobel, K., Deshayes, K., Fairbrother, W. J. & Vucic, D. c-IAP1 and c-IAP2 are critical mediators of tumor necrosis factor alpha (TNF $\alpha$ )-induced NF- $\kappa$ B activation. *J Biol Chem* **283**, 24295–24299 (2008).
80. Hussain, A. R., Uddin, S., Ahmed, M., Bu, R., Ahmed, S. O., Abubaker, J., Sultana, M., Ajarim, D., Al-Dayel, F., Bavi, P. P. & Al-Kuraya, K. S. Prognostic significance of XIAP expression in DLBCL and effect of its inhibition on AKT signalling. *Journal of Pathology J Pathol* **222**, 180–190 (2010).
81. Augello, C., Caruso, L., Maggioni, M., Donadon, M., Montorsi, M., Santambrogio, R., Torzilli, G., Vaira, V., Pellegrini, C., Roncalli, M., Coggi, G. & Bosari, S. Inhibitors of apoptosis proteins (IAPs) expression and their prognostic significance in hepatocellular carcinoma. *BMC Cancer* **9**, 1–10 (2009).
82. Shi, Y.-H., Ding, W.-X., Zhou, J., He, J.-Y., Xu, Y., Gambotto, A. A., Rabinowich, H., Fan, J. & Yin, X.-M. Expression of X-Linked Inhibitor-of-Apoptosis Protein in Hepatocellular Carcinoma Promotes Metastasis and Tumor Recurrence. *Hepatology* **48**, (2008).
83. Macher-Goeppinger, S., Aulmann, S., Tagscherer, K. E., Wagener, N., Haferkamp, A., Penzel, R., Brauckhoff, A., Hohenfellner, M., Sykora, J., Walczak, H., Teh, B. T., Autschbach, F., Herpel, E., Schirmacher, P. & Roth, W. Prognostic Value of Tumor Necrosis Factor - Related Apoptosis-Inducing Ligand (TRAIL) and TRAIL Receptors in Renal Cell Cancer. *Clin Cancer Research* **15**, 650-659 (2009).
84. Infante, J. R., Dees, E. C., Olszanski, A. J., Dhuria, S. V., Sen, S., Cameron, S. & Cohen, R. B. Phase I dose-escalation study of LCL161, an oral inhibitor of apoptosis proteins inhibitor, in patients with advanced solid tumors. *Journal of Clinical Oncology* **32**, 3103–3110 (2014).
85. Pemmaraju, N., Carter, B. Z., Bose, P., Jain, N., Kadia, T. M., Garcia-Manero, G., Bueso-Ramos, C. E., DiNardo, C. D., Bledsoe, S., Daver, N. G., Popat, U., Konopleva, M. Y., Zhou, L., Pierce, S., Estrov, Z. E., Borthakur, G. M., Ohanian, M., Qiao, W., Masarova, L., Wang, X., Yee Mak, P., Cortes, J., Jabbour, E. & Verstovsek, S. Final results of a phase 2 clinical trial of LCL161, an oral SMAC mimetic for patients with myelofibrosis. *Blood Adv* **5**, 3163–3173 (2021).
86. Amaravadi, R. K., Schilder, R. J., Martin, L. P., Levin, M., Graham, M. A., Weng, D. E. & Adjei, A. A. A Phase I Study of the SMAC-Mimetic Birinapant in Adults with Refractory Solid Tumors or Lymphoma. *Mol Cancer Ther* **14**, 2569–2575 (2015).
87. Varfolomeev, E., Blankenship, J. W., Wayson, S. M., Fedorova, A. V., Kayagaki, N., Garg, P., Zobel, K., Dynek, J. N., Elliott, L. O., Wallweber, H. J. A., Flygare, J. A., Fairbrother, W. J., Deshayes, K., Dixit, V. M. & Vucic, D. IAP Antagonists Induce Autoubiquitination of c-IAPs, NF- $\kappa$ B Activation, and TNF $\alpha$ -Dependent Apoptosis. *Cell* **131**, 669–681 (2007).
88. Feltham, R., Bettjeman, B., Budhidarmo, R., Mace, P. D., Shirley, S., Condon, S. M., Chunduru, S. K., McKinlay, M. A., Vaux, D. L., Silke, J. & Day, C. L. Smac mimetics activate the E3 ligase activity of cIAP1 protein by promoting RING domain dimerization. *Journal of Biological Chemistry* **286**, 17015–17028 (2011).
89. Dueber, E. C., Schoeffler, A. J., Lingel, A., Elliott, J. M., Fedorova, A. V., Giannetti, A. M., Zobel, K., Maurer, B., Varfolomeev, E., Wu, P., Wallweber, H. J. A., Hymowitz, S. G., Deshayes, K., Vucic, D. & Fairbrother, W. J. Antagonists induce a conformational change in cIAP1 that promotes autoubiquitination. *Science (1979)* **334**, 376–380 (2011).
90. Liu, Z., Hu, M., Yang, Y., Du, C., Zhou, H., Liu, C., Chen, Y., Fan, L., Ma, H., Gong, Y. & Xie, Y. An overview of PROTACs: a promising drug discovery paradigm. *Molecular Biomedicine* **3**, 46(2022).
91. Ng, Y. L. D., Ramberger, E., Bohl, S. R., Dolnik, A., Steinebach, C., Conrad, T., Müller, S., Popp, O., Kull, M., Haji, M., Gütschow, M., Döhner, H., Walther, W., Keller, U., Bullinger, L., Mertins, P. & Krönke, J. Proteomic profiling reveals CDK6 upregulation as a targetable resistance mechanism for lenalidomide in multiple myeloma. *Nat Commun* **13**, (2022).
92. Ng, Y. L. D., Bricelj, A., Jansen, J. A., Murgai, A., Peter, K., Donovan, K. A., Gütschow, M., Krönke, J., Steinebach, C. & Sosis, I. Heterobifunctional Ligase Recruiters Enable pan-Degradation of Inhibitor of Apoptosis Proteins. *J Med Chem* **66**, 4703–4733 (2023).
93. Ramberger, E., Sapozhnikova, V., Ng, Y. L. D., Dolnik, A., Ziehm, M., Popp, O., Stramp, E., Kull, M., Gramp, F., Kramp, J., Benary, M., Mamp, S., Gao, X., Murgai, A., Haji, M., Schmidt, A., Lutz, R., Nogai, A., Braune, J., Laue, D., Langer, C., Khandanpour, C., Bassermann, F., Damp, H., Engelhardt, M., Straka, C., Hundemer, M., Beule, D., Haas, S., Keller, U., Einsele, H., Bullinger, L., Knop, S., Mertins, P. & Krönke, J. The proteogenomic landscape of multiple myeloma reveals insights into disease biology and therapeutic opportunities. *Nat Cancer* (2024).

94. Knop, S., Langer, C., Engelhardt, M., Mügge, L. O., Reichle, A., Rösler, W., Bassermann, F., Hertenstein, B., Kunitz, A., Röllig, C., Ostermann, H., Schäfer-Eckart, K., Ringhoffer, M., Günther, A., Junghans, C., Biersack, H., Schreder, M., Liebert, A., Held, S., Einsele, H. & Bargou, R. C. Lenalidomide, adriamycin, dexamethasone for induction followed by stem-cell transplant in newly diagnosed myeloma. *Leukemia* **31**, 1816–1819 (2017).
95. US National Library of Medicine. Combination of Lenalidomide and Dexamethasone in Treatment of Multiple Myeloma (DSM XIII). *ClinicalTrials.gov* at <<https://classic.clinicaltrials.gov/ct2/show/NCT01090089>>
96. Knop, S., Langer, C., Engelhardt, M. M., Bassermann, F., Schreder, M., Muegge, L.-O., Schaefer-Eckart, K., Blau, I. W., Wolleschak, D., Reusch, J., Metzler, I. von, Metzner, B., Dechow, T., Hertenstein, B., Duerk, H., Theurich, S., Stuebig, T., Kroenke, J., Held, S., Einsele, H. & DSMM, G. M. S. G. Bortezomib, lenalidomide, and dexamethasone (VRD) is superior to lenalidomide, adriamycin, and dexamethasone (RAD) prior to risk-adapted transplant in newly diagnosed myeloma. *Journal of Clinical Oncology* **38**, 8521–8521 (2020).
97. Dobin, A., Davis, C. A., Schlesinger, F., Drenkow, J., Zaleski, C., Jha, S., Batut, P., Chaisson, M. & Gingeras, T. R. STAR: Ultrafast universal RNA-seq aligner. *Bioinformatics* **29**, 15–21 (2013).
98. Brand, M., Jiang, B., Bauer, S., Donovan, K. A., Liang, Y., Wang, E. S., Nowak, R. P., Yuan, J. C., Zhang, T., Kwiatkowski, N., Müller, A. C., Fischer, E. S., Gray, N. S. & Winter, G. E. Homolog-Selective Degradation as a Strategy to Probe the Function of CDK6 in AML. *Cell Chem Biol* **26**, 300–306.e9 (2019).
99. Steinebach, C., Ng, Y. L. D., Sosič, I., Lee, C. S., Chen, S., Lindner, S., Vu, L. P., Bricelj, A., Haschemi, R., Monschke, M., Steinwarz, E., Wagner, K. G., Bendas, G., Luo, J., Gütschow, M. & Krönke, J. Systematic exploration of different E3 ubiquitin ligases: An approach towards potent and selective CDK6 degraders. *Chem Sci* **11**, 3474–3486 (2020).
100. Li, C., Xia, J., Franqui-Machin, R., Chen, F., He, Y., Ashby, T. C., Teng, F., Xu, H., Liu, D., Gai, D., Johnson, S. K., van Rhee, F., Janz, S., Shaughnessy, J. D., Tricot, G., Frech, I. & Zhan, F. TRIP13 modulates protein deubiquitination and accelerates tumor development and progression of B cell malignancies. *J Clin Invest* **131**, (2021).
101. Tao, Y., Yang, G., Yang, H., Song, D., Hu, L., Xie, B., Wang, H., Gao, L., Gao, M., Xu, H., Xu, Z., Wu, X., Zhang, Y., Zhu, W., Zhan, F. & Shi, J. TRIP13 impairs mitotic checkpoint surveillance and is associated with poor prognosis in multiple myeloma. *Oncotarget* **8**, 26718–26731 (2017).
102. Sagawa, M., Ohguchi, H., Harada, T., Samur, M. K., Tai, Y. T., Munshi, N. C., Kizaki, M., Hideshima, T. & Anderson, K. C. Ribonucleotide reductase catalytic subunit M1 (RRM1) as a novel therapeutic target in multiple myeloma. *Clinical Cancer Research* **23**, 5225–5237 (2017).
103. Heuck, C. J., Qu, P., Van Rhee, F., Waheed, S., Usmani, S. Z., Epstein, J., Zhang, Q., Edmondson, R., Hoering, A., Crowley, J. & Barlogie, B. Five gene probes carry most of the discriminatory power of the 70-gene risk model in multiple myeloma. *Leukemia* **28**, 2410–2413 (2014).
104. Shaughnessy, J. D., Zhan, F., Burington, B. E., Huang, Y., Colla, S., Hanamura, I., Stewart, J. P., Kordsmeier, B., Randolph, C., Williams, D. R., Xiao, Y., Xu, H., Epstein, J., Anaissie, E., Krishna, S. G., Cottler-Fox, M., Hollmig, K., Mohiuddin, A., Pineda-Roman, M., Tricot, G., Van Rhee, F., Sawyer, J., Alsayed, Y., Walker, R., Zangari, M., Crowley, J. & Barlogie, B. A validated gene expression model of high-risk multiple myeloma is defined by deregulated expression of genes mapping to chromosome 1. *Blood* **109**, 2276–2284 (2007).
105. Baughn, L. B., Di Liberto, M., Wu, K., Toogood, P. L., Louie, T., Gottschalk, R., Niesvizky, R., Cho, H., Ely, S., Moore, M. A. S. & Chen-Kiang, S. A novel orally active small molecule potently induces G1 arrest in primary myeloma cells and prevents tumor growth by specific inhibition of cyclin-dependent kinase 4/6. *Cancer Res* **66**, 7661–7667 (2006).
106. Ely, S., Di Liberto, M., Niesvizky, R., Baughn, L. B., Cho, H. J., Hatada, E. N., Knowles, D. M., Lane, J. & Chen-Kiang, S. Mutually exclusive cyclin-dependent kinase 4/cyclin D1 and cyclin-dependent kinase 6/cyclin D2 pairing inactivates retinoblastoma protein and promotes cell cycle dysregulation in multiple myeloma. *Cancer Res* **65**, 11345–11353 (2005).
107. Beaver, J. A., Amiri-Kordestani, L., Charlab, R., Chen, W., Palmby, T., Tilley, A., Zirkelbach, J. F., Yu, J., Liu, Q., Zhao, L., Crich, J., Chen, X. H., Hughes, M., Bloomquist, E., Tang, S., Sridhara, R., Kluetz, P. G., Kim, G., Ibrahim, A., Pazdur, R. & Cortazar, P. FDA Approval: Palbociclib for the Treatment of Postmenopausal Patients with Estrogen Receptor-Positive, HER2-Negative Metastatic Breast Cancer. *CCR Perspectives in Drug Approval* (2015).
108. Huang, X., Di Liberto, M., Jayabalan, D., Liang, J., Ely, S., Bretz, J., Shaffer, A. L., Louie, T., Chen, I., Randolph, S., Hahn, W. C., Staudt, L. M., Niesvizky, R., Moore, M. A. S. & Chen-Kiang, S. Prolonged early G1 arrest by selective CDK4/CDK6 inhibition sensitizes myeloma cells to cytotoxic killing through cell cycle-coupled loss of IRF4. *Blood* **120**, 1095–1106 (2012).
109. Eichner, R., Heider, M., Fernández-Sáiz, V., Van Bebber, F., Garz, A. K., Lemeer, S., Rudelius, M., Targosz, B. S., Jacobs, L., Knorn, A. M., Slawska, J., Platzbecker, U., Germing, U., Langer, C., Knop, S., Einsele, H., Peschel, C., Haass, C., Keller, U., Schmid, B., Götze, K. S., Kuster, B. & Bassermann, F. Immunomodulatory drugs disrupt the cereblon-CD147-MCT1 axis to exert antitumor activity and teratogenicity. *Nat Med* **22**, 735–743 (2016).
110. Skerget, M., Skopec, B., Zver, S. & Podgornik, H. Amplification of Chromosome 1q Predicts Poor Overall Survival in Newly Diagnosed Multiple Myeloma Patients. *J Hematol* **12**, 109–113 (2023).
111. Lemonakis, K., Olsson-Arvidsson, L., Karlsson, C., Johansson, B. & Hansson, M. Impact of 1q gains on treatment outcomes of patients with newly diagnosed multiple myeloma in a real-world Swedish population receiving modern treatment. *Eur J Haematol* **111**, 391–399 (2023).
112. Pemmaraju, N., Carter, B. Z., Bose, P., Jain, N., Kadia, T. M., Garcia-Manero, G., Bueso-Ramos, C. E., DiNardo, C. D., Bledsoe, S., Daver, N. G., Popat, U., Konopleva, M. Y., Zhou, L., Pierce, S., Estrov, Z. E., Borthakur, G. M., Ohanian, M., Qiao, W., Masarova, L., Wang, X., Yee Mak, P., Cortes, J., Jabbour, E. & Verstovsek, S. Final results of a phase 2 clinical trial of LCL161, an oral SMAC mimetic for patients with myelofibrosis. *Blood Adv* **5**, 3163–3173 (2021).
113. Abbas, R. & Larisch, S. cells Targeting XIAP for Promoting Cancer Cell Death-The Story of ARTS and SMAC. *Cells* **9**, 663 (2020).
114. Obexer, P. & Auserlechner, M. X-linked inhibitor of apoptosis (XIAP) - a critical death-resistance regulator and therapeutic target for personalized cancer therapy. *Front Oncol* **4**, 1–9 (2014).

115. Kollmann, K., Heller, G., Schneckenleithner, C., Warsch, W., Scheicher, R., Ott, R. G., Schäfer, M., Fajmann, S., Schleder, M., Schiefer, A. I., Reichart, U., Mayerhofer, M., Hoeller, C., Zöchbauer-Müller, S., Kerjaschki, D., Bock, C., Kenner, L., Hoefler, G., Freissmuth, M., Green, A. R., Moriggl, R., Busslinger, M., Malumbres, M. & Sexl, V. A kinase-independent function of CDK6 links the cell cycle to tumor angiogenesis. *Cancer Cell* **24**, 167–181 (2013).
116. Yang, C., Li, Z., Bhatt, T., Dickler, M., Giri, D., Scaltriti, M., Baselga, J., Rosen, N. & Chandralapaty, S. Acquired CDK6 amplification promotes breast cancer resistance to CDK4&6 inhibitors and loss of ER signaling and dependence. *Oncogene* **36**, 2255–2264 (2017).
117. Placke, T., Faber, K., Nonami, A., Putwain, S. L., Salih, H. R., Heidel, F. H., Krämer, A., Root, D. E., Barbie, D. A., Krivtsov, A. V., Armstrong, S. A., Hahn, W. C., Huntly, B. J., Sykes, S. M., Milsom, M. D., Scholl, C. & Fröhling, S. Requirement for CDK6 in MLL-rearranged acute myeloid leukemia. *Blood* **124**, 13 (2014).
118. Kollmann, K., Briand, C., Bellutti, F., Schicher, N., Blunder, S., Zojer, M. & Hoeller, C. The interplay of CDK4 and CDK6 in melanoma. *Oncotarget* **10**, 1346–1359 (2019).
119. Geng, B., Liang, M., Lilong Qin, |, Zhao, W., Wang, H., Wang, L., Xianhui Pan, | & Chen, | Xingwu. An TRIM59-CDK6 axis regulates growth and metastasis of lung cancer. *J Cell Mol Med* **23**, 1458–1469 (2019).
120. Zhang, Z., Li, J., Ou, Y., Yang, G., Deng, K., Wang, Q., Wang, Z., Wang, W., Zhang, Q., Wang, H., Sun, W., Sun, P. & Yang, S. CDK4/6 inhibition blocks cancer metastasis through a USP51-ZEB1-dependent deubiquitination mechanism. *Signal Transduct Target Ther* **5** (2020).
121. Tao, Y., Yang, G., Yang, H., Song, D., Hu, L., Xie, B., Wang, H., Gao, L., Gao, M., Xu, H., Xu, Z., Wu, X., Zhang, Y., Zhu, W., Zhan, F. & Shi, J. TRIP13 impairs mitotic checkpoint surveillance and is associated with poor prognosis in multiple myeloma. *Oncotarget* **8**, 26718–26731 (2017).
122. Sagawa, M., Ohguchi, H., Harada, T., Samur, M. K., Tai, Y. T., Munshi, N. C., Kizaki, M., Hideshima, T. & Anderson, K. C. Ribonucleotide reductase catalytic subunit M1 (RRM1) as a novel therapeutic target in multiple myeloma. *Clinical Cancer Research* **23**, 5225–5237 (2017).
123. Kropivsek, K., Kachel, P., Goetze, S., Wegmann, R., Festl, Y., Severin, Y., Hale, B. D., Mena, J., van Droegen, A., Dietliker, N., Tchinda, J., Wollscheid, B., Manz, M. G. & Snijder, B. Ex vivo drug response heterogeneity reveals personalized therapeutic strategies for patients with multiple myeloma. *Nat Cancer* **4**, 734–753 (2023).
124. De Matos Simoes, R., Shirasaki, R., Tang, H., Yamano, S., Barwick, B. G., Gandolfi, S., Dhimolea, E., Downey-Kopyscinski, S. L., Dashevsky, O., Glassner, B., Sheffer, M., Kansara, D., Bariteau, M., Sorrell, J., Gupta, V., Culhane, A., Tsherniak, A., Vazquez, F., Boise, L. H., Licht, J. D. & Mitsiades, C. S. POU2AF1 As a Master Regulator of Oncogenic Transcription Factor Networks in Myeloma. *Blood* **136**, 18–19 (2020).
125. Ge, N.-L. & Rudikoff, S. Insulin-like growth factor I is a dual effector of multiple myeloma cell growth. *Blood* **96**, 2856–2861 (2000).
126. Chang, H., Qi, X., Trieu, Y., Xu, W., Reader, J. C., Ning, Y. & Reece, D. Multiple myeloma patients with CKS1B gene amplification have a shorter progression-free survival post-autologous stem cell transplantation. *Br J Haematol* **135**, 486–491 (2006).
127. Samo, A. A., Li, J., Zhou, M., Sun, Y., Yang, Y., Zhang, Y., Li, J., van Duin, M., Lu, X. & Fan, X. MCL1 gene co-expression module stratifies multiple myeloma and predicts response to proteasome inhibitor-based therapy. *Genes Chromosomes Cancer* **57**, 420–429 (2018).
128. Gu, H., Zhong, Y., Zhang, E., Cao, L., Cai, Z. & He, J. Gain or Amplification of Chromosome 1q Mediate Multiple Myeloma Resistant to Xpo-1 Inhibitor Selinexor Via Transcription Factor ETV3. *Blood* **142**, 6579–6580 (2023).
129. Teoh, P. J., An, O., Chung, T. H., Chooi, J. Y., Toh, S. H. M., Fan, S., Wang, W., Koh, B. T. H., Fullwood, M. J., Ooi, M. G., de Mel, S., Soekjojo, C. Y., Chen, L., Ng, S. B., Yang, H. & Chng, W. J. Aberrant hyperediting of the myeloma transcriptome by ADAR1 confers oncogenicity and is a marker of poor prognosis. *Blood* **132**, 1304–1317 (2018).
130. Shi, L., Wang, S., Zangari, M., Xu, H., Cao, T. M., Xu, C., Wu, Y., Liu, Y., Yang, Y., Salama, M., Li, G., Tricot, G. & Zhan, F. Over-expression of CKS1B activates both MEK/ERK and JAK/ STAT3 signaling pathways and promotes myeloma cell drug-resistance. *Oncotarget* **1** (2010).
131. Inoue, J., Otsuki, T., Hirasawa, A., Imoto, I., Matsuo, Y., Shimizu, S., Taniwaki, M. & Inazawa, J. Overexpression of PDZK1 within the 1q12-q22 amplicon is likely to be associated with drug-resistance phenotype in multiple myeloma. *Am J Pathol* **165**, 71–81 (2004).
132. Schmidt, T. M., Barwick, B. G., Joseph, N., Heffner, L. T., Hofmeister, C. C., Bernal, L., Dhodapkar, M. V., Gupta, V. A., Jaye, D. L., Wu, J., Goyal, S., Chen, Z., Boise, L. H., Lonial, S., Nooka, A. K. & Kaufman, J. L. Gain of Chromosome 1q is associated with early progression in multiple myeloma patients treated with lenalidomide, bortezomib, and dexamethasone. *Blood Cancer J* **9**, (2019).
133. Lagana, A., Thibaud, S., Melnekoff, D. T., Restrepo, P., Leshchenko, V., McCafferty, J., Newman, S., Kern, A., Corrigan, D., Hantash, F., Rossi, A., Rodriguez, C., Sanchez, L., Richard, S., Chari, A., Cho, H. J., Jagannath, S., Richter, J. & Parekh, S. Gain of chr1q Portends Poor Outcomes in Multiple Myeloma Patients Treated with Venetoclax. *Blood* **140**, 4388–4390 (2022).
134. Topno, R., Singh, I., Kumar, M. & Agarwal, P. Integrated bioinformatic analysis identifies UBE2Q1 as a potential prognostic marker for high grade serous ovarian cancer. *BMC Cancer* **21** (2021).
135. Seghatoleslam, A., Nikseresht, M., Shafiee, S. M., Monabati, A., Namavari, M. M., Talei, A., Safaei, A. & Owji, A. A. Expression of the novel human gene, UBE2Q1, in breast tumors. *Mol Biol Rep* **39**, 5135–5141 (2012).
136. Shafiee, S. M., Seghatoleslam, A., Nikseresht, M., Hosseini, S. V., Alizadeh-Naeni, M., Safaei, A. & Owji, A. A. UBE2Q1 expression in human colorectal tumors and cell lines. *Mol Biol Rep* **40**, 7045–7051 (2013).
137. Chang, R., Wei, L., Lu, Y., Cui, X., Lu, C., Liu, L., Jiang, D., Xiong, Y. C., Wang, G., Wan, C. & Qian, H. Upregulated expression of ubiquitin-conjugating enzyme E2Q1 (UBE2Q1) is associated with enhanced cell proliferation and poor prognosis in human hepatocellular carcinoma. *J Mol Histol* **46**, 45–56 (2015).



138. Zhang, B., Deng, C., Wang, L., Zhou, F., Zhang, S., Kang, W., Zhan, P., Chen, J., Shen, S., Guo, H., Zhang, M., Wang, Y., Zhang, F., Zhang, W., Xiao, J., Kong, B., Friess, H., Zhuge, Y., Yan, H. & Zou, X. Upregulation of UBE2Q1 via gene copy number gain in hepatocellular carcinoma promotes cancer progression through  $\beta$ -catenin-EGFR-PI3K-Akt-mTOR signaling pathway. *Mol Carcinog* **57**, 201–215 (2018).
139. Shafiee, S. M., Rasti, M., Seghatoleslam, A., Azimi, T. & Owji, A. A. UBE2Q1 in a human breast carcinoma cell line: Overexpression and interaction with p53. *Asian Pacific Journal of Cancer Prevention* **16**, 3723–3727 (2015).
140. Mamun, M., Liu, Y., Geng, Y. P., Zheng, Y. C., Gao, Y., Sun, J. G., Zhao, L. F., Zhao, L. J. & Liu, H. M. Discovery of neddylation E2s inhibitors with therapeutic activity. *Oncogenesis* **2023** *12*:1 **12**, 1–12 (2023).
141. Qi, S., Guan, X., Zhang, J., Yu, D., Yu, X., Li, Q., Yin, W., Cheng, X. D., Zhang, W. & Qin, J. J. Targeting E2 ubiquitin-conjugating enzyme UbcH5c by small molecule inhibitor suppresses pancreatic cancer growth and metastasis. *Mol Cancer* **21**, 1–18 (2022).
142. van Belzen, I. A. E. M., van Tuil, M., Badloe, S., Strengman, E., Janse, A., Verwiël, E. T. P., van der Leest, D. F. M., de Vos, S., Baker-Hernandez, J., Groenendijk, A., de Krijger, R., Kerstens, H. H. D., Drost, J., van den Heuvel-Eibrink, M. M., Tops, B. B. J., Holstege, F. C. P., Kemmeren, P. & Hehir-Kwa, J. Y. Molecular Characterization Reveals Subclasses of 1q Gain in Intermediate Risk Wilms Tumors. *Cancers (Basel)* **14**, (2022).
143. Girish, V., Lakhani, A. A., Thompson, S. L., Scaduto, C. M., Brown, L. M., Hagenson, R. A., Sausville, E. L., Mendelson, B. E., Kandikuppa, P. K., Lukow, D. A., Yuan, M., Lou, Stevens, E. C., Lee, S. N., Schukken, K. M., Akalu, S. M., Vasudevan, A., Zou, C., Salovska, B., Li, W., Smith, J. C., Taylor, A. M., Martiensen, R. A., Liu, Y., Sun, R. & Sheltzer, J. M. Oncogene-like addiction to aneuploidy in human cancers. *Science* **381**, (2023).
144. Lee, H., Ahn, S., Maity, R., Leblay, N., Ziccheddu, B., Truger, M., Chojnacka, M., Cirrincione, A., Durante, M., Tilmont, R., Barakat, E., Poorebrahim, M., Sinha, S., McIntyre, J., M. Y. Chan, A., Wilson, H., Kyman, S., Krishnan, A., Landgren, O., Walter, W., Meggendorfer, M., Haferlach, C., Haferlach, T., Einsele, H., Kortüm, M. K., Knop, S., Alberge, J. B., Rosenwald, A., Keats, J. J., Rasche, L., Maura, F., Neri, P. & Bahlis, N. J. Mechanisms of antigen escape from BCMA- or GPRC5D-targeted immunotherapies in multiple myeloma. *Nat Med* **29**, 2295–2306 (2023).
145. Da Vià, M. C., Dietrich, O., Truger, M., Arampatzi, P., Duell, J., Heidemeier, A., Zhou, X., Danhof, S., Kraus, S., Chatterjee, M., Meggendorfer, M., Twardziok, S., Goebeler, M. E., Topp, M. S., Hudecek, M., Prommersberger, S., Hege, K., Kaiser, S., Fuhr, V., Weinhold, N., Rosenwald, A., Erhard, F., Haferlach, C., Einsele, H., Kortüm, K. M., Saliba, A. E. & Rasche, L. Homozygous BCMA gene deletion in response to anti-BCMA CAR T cells in a patient with multiple myeloma. *Nat Med* **27**, 616–619 (2021).
146. Lejeune, M., Cem Köse, M., Jassin, M., Gou, M.-J., Herbet, A., Duray, E., Cobraiville, G., Foguene, J., Boquet, D., Gothot, A., Beguin, Y., Fillet, M. & Caers, J. Integrative Analysis of Proteomics and Transcriptomics Reveals Endothelin Receptor B as Novel Single Target and Identifies New Combinatorial Targets for Multiple Myeloma. *Hemasphere* **22**, (2023).
147. Di Meo, F., Iyer, A., Akama, K., Cheng, R., Yu, C., Cesarano, A., Kurihara, N., Tenshin, H., Aljoufi, A., Marino, S., Soni, R. K., Roda, J., Sissons, J., Vu, L. P., Guzman, M., Huang, K., Laskowski, T., Broxmeyer, H. E., Roodman, D. G. & Perna, F. A target discovery pipeline identified ILT3 as a target for immunotherapy of multiple myeloma. *Cell Rep Med* **4**, (2023).
148. Hu, Z., Yuan, J., Long, M., Jiang, J., Zhang, Y., Zhang, T., Xu, M., Fan, Y., Tanyi, J. L., Montone, K. T., Tavana, O., Chan, H. M., Hu, X., Vonderheide, R. H. & Zhang, L. The Cancer Surfaceome Atlas integrates genomic, functional and drug response data to identify actionable targets. *Nature Cancer* **2**:12 **2**, 1406–1422 (2021).
149. Cohen, A. D., Harrison, S. J., Krishnan, A., Fonseca, R., Forsberg, P. A., Spencer, A., Berdeja, J. G., Laubach, J. P., Li, M., Choeurng, V., Vaze, A., Samineni, D., Sumiyoshi, T., Cooper, J., Fine, B. M. & Trudel, S. Initial Clinical Activity and Safety of BFCR4350A, a FcRH5/CD3 T-Cell-Engaging Bispecific Antibody, in Relapsed/Refractory Multiple Myeloma. *Blood* **136**, 42–43 (2020).
150. Satpathy, S., Jaehnig, E. J., Krug, K., Kim, B.-J., Saltzman, A. B., Chan, D. W., Holloway, K. R., Anurag, M., Huang, C., Singh, P., Gao, A., Namai, N., Dou, Y., Wen, B., Vasaikar, S. V., Mutch, D., Watson, M. A., Ma, C., Ademuyiwa, F. O., Rimawi, M. F., Schiff, R., Hoog, J., Jacobs, S., Malovannaya, A., Hyslop, T., Clauser, K. R., Mani, D., Perou, C. M., Miles, G., Zhang, B., Gillette, M. A., Carr, S. A. & Ellis, M. J. Microscaled proteogenomic methods for precision oncology. *Nat Commun* (2020). doi:10.1038/s41467-020-14381-2
151. Desplanques, G., Giuliani, N., Delsignore, R., Rizzoli, V., Bataille, R. & Barillé-Nion, S. Impact of XIAP protein levels on the survival of myeloma cells. *Haematologica* **94**, 87 (2009).
152. Chauhan, D., Neri, P., Velankar, M., Podar, K., Hideshima, T., Fulciniti, M., Tassone, P., Raje, N., Mitsiades, C., Mitsiades, N., Richardson, P., Zawel, L., Tran, M., Munshi, N. & Anderson, K. C. Targeting mitochondrial factor Smac/DIA-BLO as therapy for multiple myeloma (MM). *Blood* **109**, 1220–1227 (2007).
153. Ramakrishnan, V., Painuly, U., Kimlinger, T., Haug, J., Rajkumar, S. V. & Kumar, S. Inhibitor of apoptosis proteins as therapeutic targets in multiple myeloma. *Leukemia* **28**, 1519–1528 (2014).
154. Chesi, M., Mirza, N. N., Garbitt, V. M., Sharik, M. E., Dueck, A. C., Asmann, Y. W., Akhmetzyanova, I., Kosiorek, H. E., Calcinotto, A., Riggs, D. L., Keane, N., Ahmann, G. J., Morrison, K. M., Fonseca, R., Lacy, M. Q., Dingli, D., Kumar, S. K., Ailawadhi, S., Dispenzieri, A., Buadi, F., Gertz, M. A., Reeder, C. B., Lin, Y., Chanan-Khan, A. A., Stewart, A. K., Fooksman, D. & Bergsagel, P. L. IAP antagonists induce anti-tumor immunity in multiple myeloma. *Nature Medicine* **2016** *22*:12 **22**, 1411–1420 (2016).

## Statutory Declaration

I, Yuen Lam Dora Ng, by personally signing this document in lieu of an oath, hereby affirm that I prepared the submitted dissertation on the topic “Targeted protein degradation in the pathogenesis and therapy of multiple myeloma” “Gezielte Proteindegradation in der Pathogenese und Therapie des Multiplen Myeloms”, independently and without the support of third parties, and that I used no other sources and aids than those stated.

All parts which are based on the publications or presentations of other authors, either in letter or in spirit, are specified as such in accordance with the citing guidelines. The sections on methodology (in particular regarding practical work, laboratory regulations, statistical processing) and results (in particular regarding figures, charts and tables) are exclusively my responsibility.

Furthermore, I declare that I have correctly marked all of the data, the analyses, and the conclusions generated from data obtained in collaboration with other persons, and that I have correctly marked my own contribution and the contributions of other persons (cf. declaration of contribution). I have correctly marked all texts or parts of texts that were generated in collaboration with other persons.

My contributions to any publications to this dissertation correspond to those stated in the below joint declaration made together with the supervisor. All publications created within the scope of the dissertation comply with the guidelines of the ICMJE (International Committee of Medical Journal Editors; <http://www.icmje.org>) on authorship. In addition, I declare that I shall comply with the regulations of Charité – Universitätsmedizin Berlin on ensuring good scientific practice.

I declare that I have not yet submitted this dissertation in identical or similar form to another Faculty.

The significance of this statutory declaration and the consequences of a false statutory declaration under criminal law (Sections 156, 161 of the German Criminal Code) are known to me.

Date

Signature

## Declaration of own contribution to the publications

Yuen Lam Dora Ng contributed the following to the below listed publications:

Publication 1:

**Yuen Lam Dora Ng\***, Evelyn Ramberger\*, Stephan Bohl, Anna Dolnik, Oliver Popp, Christian Steinebach, Miriam Kull, Mohamad Haji, Michael Gütschow, Hartmut Döhner, Lars Bullinger, Philipp Mertins, Jan Krönke. “Proteomic profiling reveals CDK6 upregulation as a targetable resistance mechanism for lenalidomide in multiple myeloma.” *Nature Communications* 2022 (\*equal contribution)

Contribution:

- Validation in independent cohort of multiple myeloma patients shown in Figure 1C, Figure S2B
- Cell line investigation regarding the connection between CDK6 and IMiD mechanism, resulting in Figure S2C, S4A-S4C
- Exploration of overexpression of top hits with multiple myeloma drug sensitivity, demonstrated in Figure 2A-2D, S5A-S5F, S6A-S6F
- *In vitro* perturbation of CDK6 in combination with IMiDs, shown in Figure 3A-3F, 4A-4F, S7A-S7B, S8A-S8E, S9A-S9C, S10, S12
- Treatment of multiple myeloma cell line for proteome investigation outlined in Figure 6A
- Investigation of downstream effects from CDK6 inhibition and combination treatment with IMiDs, resulting in Figure 6C, 6D, S14A, S14B
- Drafting and finalizing of the manuscript

Publication 2:

Evelyn Ramberger, Valeriia Sapozhnikova, **Yuen Lam Dora Ng**, Anna Dolnik, Matthias Ziehm, Oliver Popp, Eric Sträng, Miriam Kull, Florian Grünschläger, Josefine Krüger, Manuela Benary, Sina Müller, Xiang Gao, Arunima Murgai, Mohamed Haji, Annika Schmidt, Raphael Lutz, Axel Nogai, Jan Braune, Dominik Laue, Christian Langer, Cyrus Kandhanpour, Florian Bassermann, Hartmut Döhner, Monika Engelhardt, Christian Straka, Michael Hundemer, Dieter Beule, Simon Haas, Ulrich Keller, Hermann Einsele, Lars Bullinger, Stefan Knop, Philipp Mertins, Jan Krönke. “Proteogenomic landscape of multiple myeloma.” *Nature Cancer* 2024

---

Contribution:

- Performed control experiments on myeloma cell line MM.1S with CD138 MACS enrichment that resulted in Figure S1I
- Evaluation of various multiple myeloma cell lines across various genetic subtypes for their sensitivity towards Erdafitinib, shown in Figure 2G
- Generation of UBE2Q1 genetic knockout and overexpression experiments outlined in Figure 3F, and together with proteomic analyses by Evelyn Ramberger and Valeriia Sapozhnikova produced Figure 3G, 3H, S6G
- Treatment of myeloma cell lines with IRS1/2 inhibitor NT157 for their drug sensitivity, resulting in Fig S9D

Publication 3:

**Yuen Lam Dora Ng\***, Aleša Bricelj\*, Jacqueline A. Jansen, Arunima Murgai, Kirsten Peter, Katherine A. Donovan, Michael Gütschow, Jan Krönke, Christian Steinebach, Izidor Sosič. “Heterobifunctional Ligase Recruiters Enable Pan-Degradation of Inhibitor of Apoptosis Proteins.” *Journal of Medicinal Chemistry* 2023 (\*equal contribution)

Contribution:

- Determination of degradation profiles of all heteroPROTACs and comparison to commercially available IAP antagonists, shown in Figures 2, 3, 4B, 4C, S2-S11, S13-S14, S16
- Generation of CRISPR/Cas9 knockouts of the IAP protein family and testing of PROTACs in knockout cells, demonstrated in Figure S12
- Cell viability screening to examine the effects of IAP- heteroPROTACs on growth inhibition, resulting in Figures 6, S17, Tables 1 and S8

---

Signature, date and stamp of first supervising university professor / lecturer

---

Signature of doctoral candidate

## Excerpt from Journal Summary List

Journal Data Filtered By: **Selected JCR Year: 2019** Selected Editions: SCIE,SSCI  
 Selected Categories: **"MULTIDISCIPLINARY SCIENCES"** Selected Category  
 Scheme: WoS

**Gesamtanzahl: 71 Journale**

Rank	Full Journal Title	Total Cites	Journal Impact Factor	Eigenfactor Score
1	NATURE	767,209	42.778	1.216730
2	SCIENCE	699,842	41.845	1.022660
3	National Science Review	2,775	16.693	0.009760
4	Science Advances	36,380	13.116	0.172060
5	Nature Human Behaviour	2,457	12.282	0.014190
6	Nature Communications	312,599	12.121	1.259510
7	Science Bulletin	5,172	9.511	0.014150
8	PROCEEDINGS OF THE NATIONAL ACADEMY OF SCIENCES OF THE UNITED STATES OF AMERICA	676,425	9.412	0.931890
9	Journal of Advanced Research	3,564	6.992	0.005470
10	GigaScience	4,068	5.993	0.016410
11	Scientific Data	5,761	5.541	0.028720
12	Research Synthesis Methods	2,572	5.299	0.006440
13	ANNALS OF THE NEW YORK ACADEMY OF SCIENCES	45,596	4.728	0.026370
14	FRACTALS-COMPLEX GEOMETRY PATTERNS AND SCALING IN NATURE AND SOCIETY	2,156	4.536	0.002210
15	iScience	1,410	4.447	0.004140
16	GLOBAL CHALLENGES	481	4.306	0.001440
17	Scientific Reports	386,848	3.998	1.231180
18	JOURNAL OF KING SAUD UNIVERSITY SCIENCE	1,640	3.819	0.002020
19	Journal of the Royal Society Interface	13,762	3.748	0.027670

Journal Data Filtered By: **Selected JCR Year: 2021** Selected Editions: SCIE,SSCI  
 Selected Categories: **"ONCOLOGY"** Selected Category Scheme: WoS  
**Gesamtanzahl: 246 Journale**

Rank	Full Journal Title	Total Cites	Journal Impact Factor	Eigenfaktor
1	CA-A CANCER JOURNAL FOR CLINICIANS	61,124	286.130	0.09703
2	NATURE REVIEWS CANCER	66,699	69.800	0.05330
3	Nature Reviews Clinical Oncology	22,751	65.011	0.04148
4	LANCET ONCOLOGY	79,244	54.433	0.13790
5	ANNALS OF ONCOLOGY	68,844	51.769	0.11379
6	JOURNAL OF CLINICAL ONCOLOGY	195,709	50.717	0.24244
7	Molecular Cancer	32,250	41.444	0.03386
8	CANCER CELL	57,294	38.585	0.07359
9	Cancer Discovery	31,182	38.272	0.06475
10	JAMA Oncology	27,216	33.006	0.08103
11	Nature Cancer	2,315	23.177	0.00816
12	Journal of Hematology & Oncology	15,318	23.168	0.02209
13	Journal of Thoracic Oncology	27,842	20.121	0.03995
14	Trends in Cancer	6,389	19.161	0.01397
15	SEMINARS IN CANCER BIOLOGY	14,777	17.012	0.01217
16	Cancer Communications	2,334	15.283	0.00391
17	CLINICAL CANCER RESEARCH	115,272	13.801	0.11972
18	CANCER TREATMENT REVIEWS	12,869	13.608	0.01455
19	Annual Review of Cancer Biology-Series	1,098	13.340	0.00327
20	CANCER RESEARCH	161,957	13.312	0.09051
21	NEURO-ONCOLOGY	20,825	13.029	0.02439

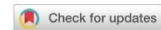
Journal Data Filtered By: **Selected JCR Year: 2021** Selected Categories: "**CHEMISTRY, MEDICINAL**"  
 Selected Editions: SCIE;SSCI Selected Category Schema: WOS Selected Open Access: N Indicator: Default

Rank	Full Journal Title	Total Citations	Journal Impact Factor
1	NATURAL PRODUCT REPORTS	14,564	15.111
2	MEDICINAL RESEARCH REVIEWS	7,973	12.388
3	JOURNAL OF MEDICINAL CHEMISTRY	92,468	8.039
4	Antioxidants	21,453	7.675
5	EUROPEAN JOURNAL OF MEDICINAL CHEMISTRY	54,556	7.088
6	EXPERT OPINION ON THERAPEUTIC PATENTS	4,626	6.714
7	PHYTOMEDICINE	18,290	6.656
8	PHYTOTHERAPY RESEARCH	22,172	6.388
9	Journal of Chemical Information and Modeling	30,162	6.162
10	Marine Drugs	25,936	6.085
11	ARCHIVES OF PHARMACAL RESEARCH	9,416	6.01
12	ACS Chemical Neuroscience	12,168	5.78
13	JOURNAL OF ENZYME INHIBITION AND MEDICINAL CHEMISTRY	8,156	5.756
14	Journal of Ginseng Research	3,740	5.735
15	ACS Infectious Diseases	5,660	5.578
16	Pharmaceuticals	9,157	5.215
17	JOURNAL OF ETHNOPHARMACOLOGY	53,915	5.195
18	MedChemComm	5,715	5.121
19	DRUG DEVELOPMENT RESEARCH	2,964	5.004
20	JOURNAL OF NATURAL PRODUCTS	34,341	4.803
21	Future Medicinal Chemistry	6,894	4.767

## Printing copies of the publications\_Ng, Ramberger *et al.* 2022



ARTICLE


<https://doi.org/10.1038/s41467-022-28515-1>

OPEN

# Proteomic profiling reveals CDK6 upregulation as a targetable resistance mechanism for lenalidomide in multiple myeloma

Yuen Lam Dora Ng <sup>1,10</sup>, Evelyn Ramberger <sup>1,2,3,10</sup>, Stephan R. Bohl<sup>4,5</sup>, Anna Dolnik<sup>1</sup>, Christian Steinebach <sup>6</sup>, Theresia Conrad<sup>7</sup>, Sina Müller<sup>1</sup>, Oliver Popp<sup>2</sup>, Miriam Kull<sup>4</sup>, Mohamed Haji<sup>2</sup>, Michael Gütschow<sup>6</sup>, Hartmut Döhner<sup>4</sup>, Wolfgang Walther<sup>8</sup>, Ulrich Keller <sup>1,3,8,9</sup>, Lars Bullinger<sup>1,3,9</sup>, Philipp Mertins <sup>2,9</sup>✉ & Jan Krönke <sup>1,3</sup>✉

The immunomodulatory drugs (IMiDs) lenalidomide and pomalidomide are highly effective treatments for multiple myeloma. However, virtually all patients eventually relapse due to acquired drug resistance with resistance-causing genetic alterations being found only in a small subset of cases. To identify non-genetic mechanisms of drug resistance, we here perform integrated global quantitative tandem mass tag (TMT)-based proteomic and phosphoproteomic analyses and RNA sequencing in five paired pre-treatment and relapse samples from multiple myeloma patients. These analyses reveal a CDK6-governed protein resistance signature that includes myeloma high-risk factors such as TRIP13 and RRM1. Overexpression of CDK6 in multiple myeloma cell lines reduces sensitivity to IMiDs while CDK6 inhibition by palbociclib or CDK6 degradation by proteolysis targeting chimeras (PROTACs) is highly synergistic with IMiDs in vitro and in vivo. This work identifies CDK6 upregulation as a druggable target in IMiD-resistant multiple myeloma and highlights the use of proteomic studies to uncover non-genetic resistance mechanisms in cancer.

<sup>1</sup>Department of Hematology, Oncology and Cancer Immunology, Charité - Universitätsmedizin Berlin, corporate member of Freie Universität Berlin and Humboldt-Universität zu Berlin, Berlin, Germany. <sup>2</sup>Proteomics Platform, Max Delbrück Center for Molecular Medicine, Berlin, Germany. <sup>3</sup>German Cancer Consortium (DKTK) partner site Berlin and German Cancer Research Center (DKFZ), Heidelberg, Germany. <sup>4</sup>Department of Internal Medicine III, Ulm University Hospital, Ulm, Germany. <sup>5</sup>Department of Medical Oncology, Dana-Farber Cancer Institute, Harvard Medical School, Boston, MA, USA. <sup>6</sup>Department of Pharmaceutical & Medicinal Chemistry, Pharmaceutical Institute, University of Bonn, Bonn, Germany. <sup>7</sup>Experimentelle Pharmakologie & Onkologie (EPO) Berlin-Buch GmbH, Berlin, Germany. <sup>8</sup>Experimental and Clinical Research Center, Charité Universitätsmedizin Berlin and Max-Delbrück-Center for Molecular Medicine, Berlin, Germany. <sup>9</sup>Berlin Institute of Health (BIH), Berlin, Germany. <sup>10</sup>These authors contributed equally: Yuen Lam Dora Ng, Evelyn Ramberger. ✉email: philipp.mertins@mdc-berlin.de; jan.kroenke@charite.de



**M**ultiple myeloma is a genetically heterogeneous malignancy of plasma cells. The immunomodulatory imide drugs (IMiDs) lenalidomide and pomalidomide are a mainstay in treating multiple myeloma<sup>1</sup>. Although the combination of IMiDs with other drugs like proteasome inhibitors, antibodies, corticosteroids, and high-dose chemotherapy can induce remissions in most patients, almost all patients eventually relapse due to acquired resistance of the multiple myeloma cells to one or several of the drugs<sup>1</sup>. IMiDs bind to cereblon (CRBN), that together with DDB1, CUL4A, and ROC1 forms the CRBN-CRL4 E3 ubiquitin ligase and modulate the substrate specificity of the enzyme<sup>2</sup>. This leads to ubiquitination and proteasomal degradation of the lymphoid transcription factors Ikaros (IKZF1) and Aiolos (IKZF3), which regulate expression of other genes such as *IRF4* and *MYC*, and are essential for the proliferation and survival of multiple myeloma cells<sup>3–7</sup>. Pomalidomide is the most potent of the approved IMiDs, both in regard to IKZF1 and IKZF3 degradation, as well as clinical activity, and is therefore a preferred treatment for relapsed multiple myeloma<sup>3,8</sup>. Sequencing studies in relapsed multiple myeloma and functional screens identified acquired genetic alterations in members of the CRBN-CRL4 E3 ligase complex that completely abrogate lenalidomide and pomalidomide activity as an IMiD-specific resistance mechanism in 10–20% of relapsed patients<sup>9–13</sup>. In single cases, IMiD-resistance was found to be caused by *IKZF1* mutations at the critical degen region, which blocks IMiD-induced IKZF1 degradation<sup>10</sup>. DNA sequencing of heavily pre-treated multiple myeloma patients identified additional recurrent mutations and aberrations enriched at relapse including homozygous inactivation of tumor-suppressor genes *TP53*, *RBI*, *FAM46C*, *BIRC3*, *TRAF3*<sup>14–16</sup>. However, only few of these aberrations have been directly linked to the activity of IMiDs or other drugs used in multiple myeloma<sup>17</sup>. Furthermore, inactivating mutations in tumor-suppressor genes are in general not amenable to pharmacologic interventions. Gene expression profiling (GEP) has found an enrichment of the GEP70 prognostically high-risk signature in relapsed cases<sup>15,18,19</sup>. Like genetic alterations, this signature was not associated with a specific treatment. In aggregate, these previous studies imply that genetic alterations alone do not fully explain the occurrence of drug resistance in multiple myeloma. In addition, protein abundance and activity frequently cannot be inferred from RNA expression analyses due to post-transcriptional regulation mechanisms in general<sup>20</sup>, and in cancer in particular, due to complex compensation effects of genetic alterations on the protein level<sup>21–23</sup>. Proteomic profiling in cell lines and pooled patient samples has been successfully applied to study drug resistance mechanisms in patients with hematological disorders such as FLT3 inhibitor-resistant acute myeloid leukemia<sup>24</sup> or bortezomib refractory multiple myeloma<sup>25,26</sup>.

Here, we apply quantitative proteomic analyses in paired, longitudinal primary multiple myeloma samples and identify CDK6 upregulation as a non-genetic resistance mechanism for IMiDs in multiple myeloma that can be overcome by pharmacologic intervention.

## Results

**Quantitative proteomic analysis identifies deregulated protein abundance levels in relapsed multiple myeloma.** To identify deregulated proteins in relapsed multiple myeloma, five patients with available longitudinal bone marrow samples were included in our study. Patients progressed during ( $N = 4$ ) or shortly after ( $N = 1$ ) lenalidomide-comprising treatment (Supplementary Fig. 1). Paired bone marrow samples obtained pre-treatment and at relapse were lysed, trypsin digested, labeled with isobaric

tandem mass tags (TMT) and analyzed with quantitative mass spectrometry (Fig. 1A).

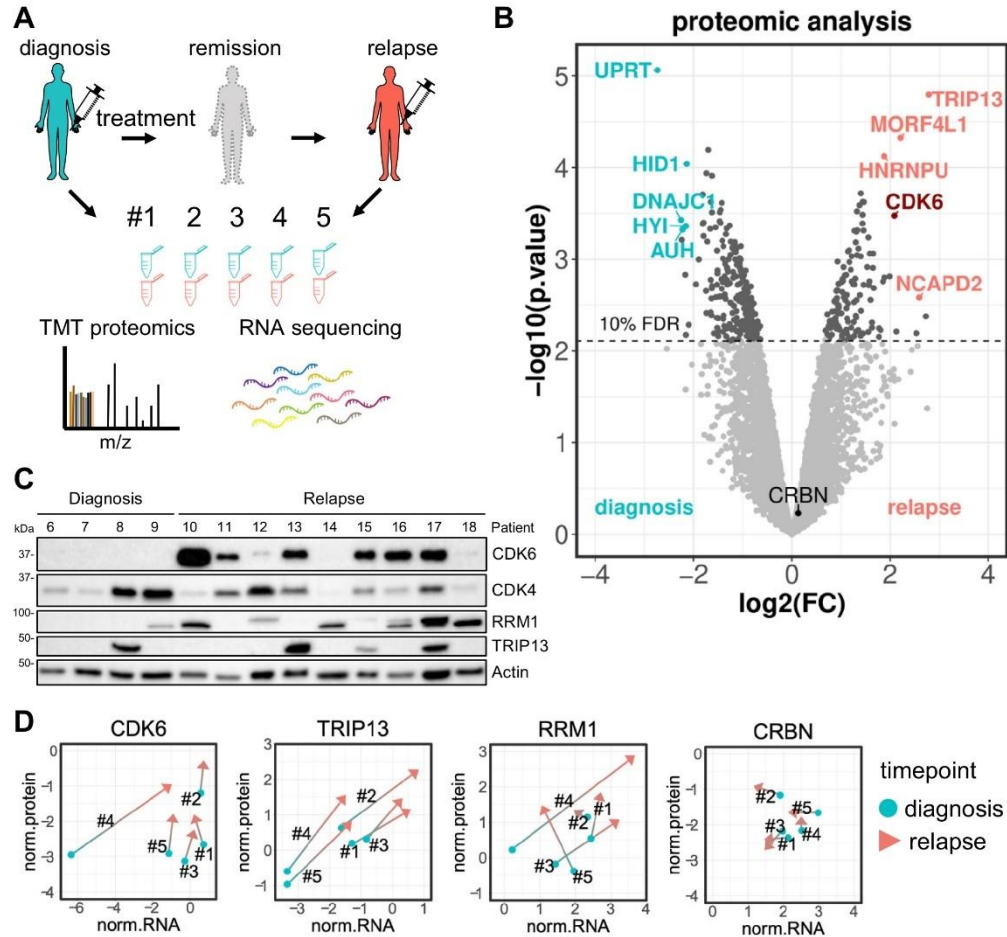
In total, we quantified 6094 proteins with at least two peptides without missing values across all samples (Supplementary Data 1). Using an FDR cutoff of 0.10, we found 130 proteins upregulated and 228 proteins downregulated in the relapse vs. pre-treatment samples (Fig. 1B). The top six upregulated proteins ranked by FC and FDR were TRIP13, RRM1, NCAPD2, NCAPH, MORF4L1, and CDK6 (Table 1), and the six most downregulated proteins were UPRT, DNAJC1, FCRL2, AUH, HYI and HID1 (Table 2). Although all five patients received lenalidomide and dexamethasone during their treatment, we did not detect changes in proteins involved in the mechanism of IMiDs (CRBN, DDB1, IKZF1, IKZF3, IRF4, BSG)<sup>2,3,27</sup> or the glucocorticoid receptor NR3C1 (Supplementary Fig. 2A). However, several of the top upregulated proteins have been previously found to be implicated in multiple myeloma and were further pursued: the ATPase TRIP13 promotes progression of B-cell malignancies<sup>28</sup> and is part of the validated GEP70 and GEP5 multiple myeloma gene expression high-risk signature<sup>29,30</sup>; RRM1 plays a role in DNA synthesis and repair, is essential for multiple myeloma cell proliferation and its expression is linked to shorter survival<sup>31</sup>; the cell-cycle regulator CDK6 is dysregulated in multiple myeloma and CDK6 inhibitors have shown activity in multiple myeloma in early clinical trials<sup>32–34</sup>. Protein analyses by western blot in an independent cohort with four samples obtained from patients at first diagnosis and nine samples from patients obtained at relapse confirmed that CDK6, TRIP13, and RRM1 proteins are more frequently detected in the relapse samples as compared to the pre-treatment samples (Fig. 1C, Supplementary Fig. 1).

**Comparison of proteome, phosphoproteome, and RNA expression analyses.** To determine whether the differential expression of the proteins was accompanied by changes in RNA expression levels, we performed RNA sequencing of the five paired samples analyzed by proteomics (Supplementary Data 2). The top upregulated RNAs at relapse versus pre-treatment samples were *ADGRG3*, *FCAR*, *CAMP* and *GOS2*. Only two of the downregulated RNA transcripts, *PAIP2B* and *ZBTB20* had an FDR below 0.1 (Supplementary Fig. 3A).

The general correlation of protein and RNA expression changes between pre-treatment and relapse among all protein/RNA pairs was weak with a median Pearson correlation coefficient (PCC) of 0.34 with a high degree of variation (range  $-1$  to  $1$ ) (Supplementary Fig. 3B). Of the top upregulated proteins, the mitosis regulatory protein TRIP13 showed the highest level of correlation for RNA/protein expression (PCC = 0.84), followed by NCAPH (0.84) and NCAPD2 (0.67). RRM1 and CDK6 had an RNA to protein correlation of 0.6 and 0.39, respectively (Fig. 1D).

In addition to analyzing the global proteome, we also performed an immobilized metal affinity chromatography (IMAC) phosphopeptide enrichment with 9 of the 10 samples. We detected 24,796 phosphopeptides derived from 5698 proteins (Supplementary Fig. 3C, Supplementary Data 1). In total, 134 phosphopeptides passed the 0.12 FDR significance cutoff. The majority of the proteins, that the significant phosphopeptides originated from, were also detected in the global proteome analysis of patient samples (92 out of 112). However, only 15 of the significant phosphopeptides belonged to proteins that were also significantly regulated on the global protein level.

The complementary nature of the different datasets was also reflected by highly significant single sample gene set enrichment analysis (ssGSEA) signatures observed in the phosphoproteomic data and, to a lesser extent, in the proteomic data (Supplementary Fig. 3D). SsGSEA revealed upregulation of cell cycle-



**Fig. 1** Identification of CDK6 protein upregulation in relapsed multiple myeloma patients. **A** Bone marrow samples of five multiple myeloma patients were obtained at diagnosis and at relapse. Samples were subjected to TMT-based quantitative proteomic analysis and RNA sequencing. **B** Protein level changes at relapse/diagnosis were determined for each patient ( $N = 5$ ) and analyzed with a moderated 1-sample  $t$ -test. Average  $\log_2$ (fold change) of each protein is plotted against its  $-\log_{10}(p\text{-value})$ . Top regulated proteins passing the 0.1 FDR significance cutoff are highlighted in color. **C** Western blot validation of top candidates in an independent patient cohort of primary patient samples obtained pre-treatment and at relapse ( $N = 13$  patient samples). **D** Median normalized protein intensities ( $\log_2$  TMT intensities) of CDK6, TRIP13, RRM1 and CRBN in all 10 samples were plotted against their respective normalized RNA expression levels ( $\log_2$  TPM values). Samples from the same patient are connected. Source data are provided as a Source Data file.

related, replication, and chromosome maintenance signatures in relapse samples and downregulation of phosphorylation, ATP synthesis, N-glycan biosynthesis and unfolded protein response signatures. The gene signatures significantly enriched in the proteomic and phosphoproteomic data were not corroborated by the RNA sequencing data, indicating post-translational regulatory mechanisms.

**Protein expression of CDK6, TRIP13, and RRM1 is independent of CRBN.** As impaired CRBN-CRL4 E3 ligase activity due to mutation, deletion or downregulation leads to altered IMiD-sensitivity in multiple myeloma cell lines and patients<sup>9–11</sup>, we examined its status in the five patients included in our proteomic analyses. No difference in CRBN RNA, protein or phosphorylation

levels were observed between pre-treatment and relapsed patient samples (Fig. 1D). Four out of five patient samples were analyzed also by exome sequencing and none was found to harbor mutations in members of the CRBN-CRL4 E3 ligase complex<sup>17</sup>. In our independent patient sample cohort, we did not observe any correlation between CRBN and CDK6, TRIP13, or RRM1 protein levels (Supplementary Fig. 2B). Consistently, CRISPR/Cas9-mediated knockout of *CRBN* in myeloma cell lines did not alter expression levels of these proteins (Supplementary Fig. 2C). Furthermore, no association was observed between genetic alterations and CDK6, TRIP13, or RRM1 protein expression in patient samples.

**CDK6 protein is upregulated in in vitro generated, lenalidomide-resistant multiple myeloma cells.** In order to mimic IMiD



**Table 1 Top upregulated proteins detected in global proteomics with their RNAseq profile.**

Gene	uniprot	log2(FC.protein)	FDR(protein)	log2(FC.RNA)	FDR(RNA)
TRIP13	Q15645	2.78	0.03	1.56	0.15
RRM1	P23921	2.72	0.08	0.59	0.77
NCAPD2	Q15021	2.59	0.07	0.39	0.83
NCAPH	Q15003	2.53	0.09	0.97	0.73
MORF4L1	Q9UBU8	2.21	0.06	0.24	0.74
CDK6	Q00534	2.08	0.06	0.30	0.69
BAZ1B	Q9UIG0-2	1.99	0.07	-0.07	0.94
CHTF18	Q8WVB6	1.88	0.07	1.75	0.15
HNRNPU	Q00839-2	1.87	0.06	0.32	0.63
KEAP1	Q14145	1.46	0.06	0.43	0.71

Proteins passing the 0.1 FDR significance cutoff were ranked by their fold change and FDR. The corresponding fold changes and FDR from RNAseq are displayed.

**Table 2 Top downregulated proteins detected in global proteomics with their RNAseq profile.**

Gene	uniprot	log2(FC.protein)	FDR(protein)	log2(FC.RNA)	FDR(RNA)
UPRT	Q96BW1	-2.73	0.03	-0.67	0.45
DNAJC1	Q96KC8	-2.26	0.06	-0.82	0.43
FCRL2	Q96LA5	-2.24	0.06	-1.33	0.18
AUH	Q13825	-2.23	0.06	0.16	0.90
HY1	Q5T013	-2.16	0.06	-0.98	0.55
HID1	Q8IV36-2	-2.14	0.06	-1.29	0.24
GSTP1	P09211	-1.81	0.06	-0.29	0.76
GLO1	Q04760-2	-1.74	0.06	-0.01	1.00
CYP20A1	Q6UW02	-1.70	0.06	-0.96	0.52
USO1	O60763	-1.63	0.06	-0.77	0.31

Proteins passing the 0.1 FDR significance cutoff were ranked by their fold change and FDR. The corresponding fold changes and FDR from RNAseq are displayed.

resistance in vitro, we cultured MM.1S and LP-1 cells in the presence of different concentrations of lenalidomide. Cells cultured in the presence of 100 nM lenalidomide for several weeks had enhanced levels of CDK6 protein and were partially resistant to lenalidomide, highly consistent with the findings in lenalidomide-treated myeloma patients (Supplementary Fig. 4A).

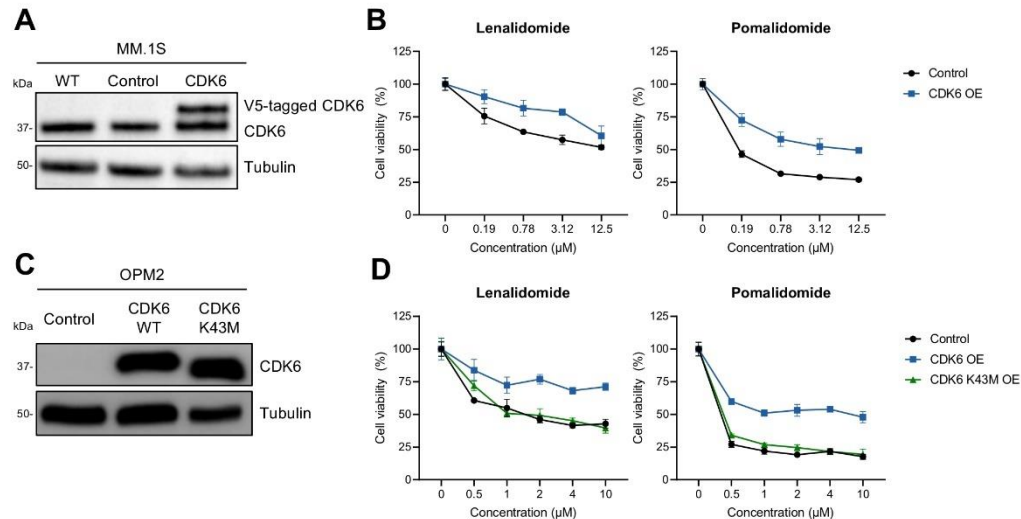
In contrast, short-term treatment with lenalidomide or proteasome inhibitors for up to 72 h had no effect or even decreased protein levels of CDK6, showing that their expression is not directly induced by the drugs (Supplementary Fig. 4B, C).

**Overexpression of CDK6 impairs IMiD sensitivity.** To investigate whether upregulation of CDK6, TRIP13, and RRM1 protein levels are causally linked to drug resistance, we induced their expression in MM.1S and OPM2 cell lines using lenti- and retroviral expression vectors (Fig. 2A, C, Supplementary Fig. 5A). TRIP13 overexpression did not alter drug sensitivity in MM.1S cells (Supplementary Fig. 5B–F). In contrast, both CDK6 and RRM1 overexpression in MM.1S and OPM2 cells reduced sensitivity to lenalidomide as well as to pomalidomide (Fig. 2B, D, Supplementary Fig. 5B, C). The effect of CDK6 was kinase-dependent since the introduction of a kinase-dead mutant CDK6 K43M<sup>35</sup> was not able to rescue cells from lenalidomide exposure (Fig. 2D). High CDK6 expression levels slightly enhanced sensitivity towards melphalan and dexamethasone in one cell line each (Supplementary Fig. 6). No effect was observable for bortezomib. In aggregate, these data imply that high CDK6 and RRM1 expression selectively reduce IMiD sensitivity in multiple myeloma cell lines.

**CDK6 kinase inhibition sensitizes multiple myeloma cells to IMiDs.** Given that CDK6 upregulation was found in lenalidomide-resistant patients and induced expression reduced lenalidomide-

sensitivity, we next tested the effects of the CDK6 inhibitor palbociclib<sup>36,37</sup> in multiple myeloma cell lines. Palbociclib had no to moderate activity in multiple myeloma cell lines with 5 out of 10 responding (Fig. 3A, C, Supplementary Fig. 7A). However, palbociclib markedly enhanced the anti-multiple myeloma effects of IMiDs when both drugs were combined with high synergy scores (Fig. 3A, B, Supplementary Figs. 7A, 8A, B, E). This effect was observed across all cell lines expressing CDK6 at various levels (Supplementary Fig. 7B). Remarkably, this included multiple myeloma cell lines that are naturally insensitive to IMiDs like L363 (Fig. 3C, D) and AMO-1, and synergy was observed at low drug concentrations corresponding to plasma levels in treated patients<sup>38</sup>. In acquired lenalidomide-resistant cells with increased CDK6 protein levels, as well as in CDK6 overexpressing cells, the addition of palbociclib restored IMiD-sensitivity to levels similar as in parental cells (Fig. 3E, F). These data show that palbociclib treatment increases the sensitivity to lenalidomide and pomalidomide in multiple myeloma cells. In contrast, combined treatment of palbociclib and melphalan, bortezomib or dexamethasone was mostly additive (Supplementary Fig. 8C, D).

**Bifunctional PROTACs degrading CDK6 and IKZF1/3 possess intramolecular synergy.** We next investigated an alternative way to inactivate CDK6 using protein degradation. Proteolysis targeting chimeras (PROTACs) are bifunctional molecules which comprise two linker-connected moieties that simultaneously bind a target protein and an E3 ubiquitin ligase<sup>39</sup>. Like IMiDs, PROTACs hijack E3 ubiquitin ligases and induce ubiquitination and degradation of the target protein. We and others have recently described PROTACs that effectively target CDK6 for proteasomal degradation through hijacking the CRBN- or von Hippel-Lindau (VHL) E3 ligase (Fig. 4A, B)<sup>40,41</sup>. We tested the anti-proliferative effects of the CDK6-selective, CRBN-recruiting PROTAC BSJ-03-



**Fig. 2 High expression levels of CDK6 confers augmented IMiD-resistance.** **A** Overexpression of CDK6 in MM.1S cells using lentiviral transduction confirmed through western blot analysis. **B** Cell viability of CDK6-overexpressing MM.1S cells upon 96 h treatment with lenalidomide and pomalidomide at indicated concentrations. ( $N = 3$  biologically independent replicates). **C** Overexpression of CDK6 in OPM2 cells using retroviral transduction confirmed through western blot analysis. **D** Cell viability of CDK6 WT or K43M-overexpressing OPM2 cells upon 96 h treatment with lenalidomide and pomalidomide at indicated concentrations. ( $N = 3$  biologically independent replicates) Control denotes empty vector. Cell viability is normalized to respective DMSO conditions. Data represent the mean  $\pm$  SD of biological triplicates. Source data are provided as a Source Data file.

123 or the VHL-recruiting PROTAC CST528 that degrades both CDK4 and CDK6. Consistent with the results for the kinase inhibitor palbociclib, PROTAC-mediated CDK6 degradation reduced multiple myeloma cell growth in a subset of cell lines. Combination of IMiDs with the VHL-recruiting PROTAC CST528 had synergistic effects with IMiDs consistent with the results observed for the CDK6 kinase inhibitor palbociclib (Fig. 4C, D)<sup>41</sup>. In contrast, combination of IMiDs with a CRBN-hijacking, CDK6-specific PROTAC (BSJ-03-123) showed antagonistic effects that are likely due to the competition for the CRBN E3-ligase (Supplementary Fig. 9).

We next tested a CRBN-hijacking, pomalidomide-based PROTAC, YKL-06-102, that retains the activity of pomalidomide and potentially induces both degradation of CDK6 and IMiD neosubstrates IKZF1 and IKZF3<sup>40</sup>. YKL-06-102 significantly reduced viability in all ten multiple myeloma cell lines tested, including those with a low IMiD sensitivity (Fig. 4E and F, Supplementary Fig. 10). These results show that CRBN-hijacking PROTACs targeting CDK6, IKZF1, and IKZF3 simultaneously are highly effective in multiple myeloma cells through intramolecular synergy.

**Combination treatment of pomalidomide and palbociclib is highly effective in vivo.** To test whether the combination of IMiDs with CDK6 inhibition has therapeutic efficacy in vivo, we conducted a study in the MM.1S xenograft model (Fig. 5A). MM.1S cells were injected subcutaneously and mice were randomized for treatment groups after 19 days when tumors reached 200 mm<sup>3</sup>. Treatment was performed for 17 days, with pomalidomide and palbociclib being orally administered at 5 and 50 mg/kg, respectively. Pomalidomide and palbociclib as monotherapy significantly delayed tumor growth, while combination therapy reduced tumor volumes below detection limits after 2 weeks (Fig. 5B, Supplement Fig. 11). After cessation of treatment, tumor

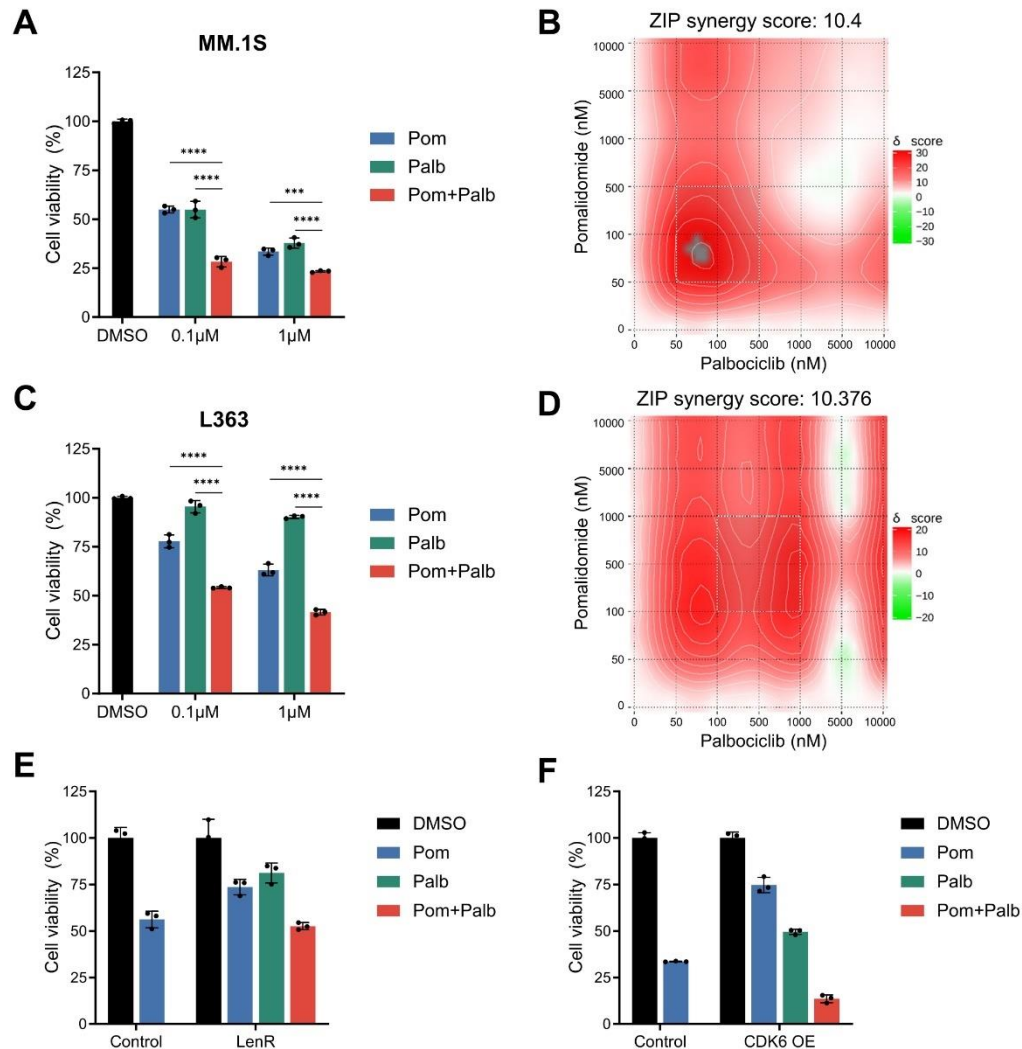
growth resumed, indicating that prolonged treatment with both drugs is necessary to prevent multiple myeloma relapse. The potent suppression of tumor growth in the combination group translated to a significant improvement in survival as compared to mice that received pomalidomide or palbociclib alone (Fig. 5C).

Intraperitoneal application of the CDK6/IKZF1/IKZF3-degrading PROTAC YKL-06-102 at a maximal applicable dosage of 5 mg/kg per day (due to low solubility) significantly delayed tumor growth as compared to control treated mice, yet the effect was not better than pomalidomide or palbociclib alone, likely due to lower bioavailability in vivo (Supplementary Fig. 11).

**The synergistic effect of IMiDs and CDK6 inhibition is independent of RB1 and cell cycle progression.** RB1 is one of the major substrates of CDK6 and palbociclib treatment resulted in reduced phosphorylation of RB1 and G1 cell cycle arrest in MM cell lines, consistent with previous studies in cancer<sup>42,43</sup>. Heterozygous chromosome 13q/RB1 deletions are among the most frequent genetic alterations in multiple myeloma and complete loss is observed in heavily treated patients, implying that it contributes to drug resistance<sup>14</sup>. We therefore tested whether RB1 knockout through CRISPR/Cas9 affects sensitivity to pomalidomide, palbociclib or the combination treatment with CDK6 inhibition or degradation in MM.1S cell line. In line with studies in breast cancer, RB1 knockout reduced sensitivity to palbociclib (Supplementary Fig. 12). However, the synergistic effects of CDK6 inhibition and IMiDs were retained in RB1 knockout cells, demonstrating that the sensitization to IMiDs is independent of functional RB1.

**CDK6 inhibition reverses a relapse-associated protein signature.** To investigate the effects of CDK6 inhibition and the basis for the synergy with IMiDs in multiple myeloma, we



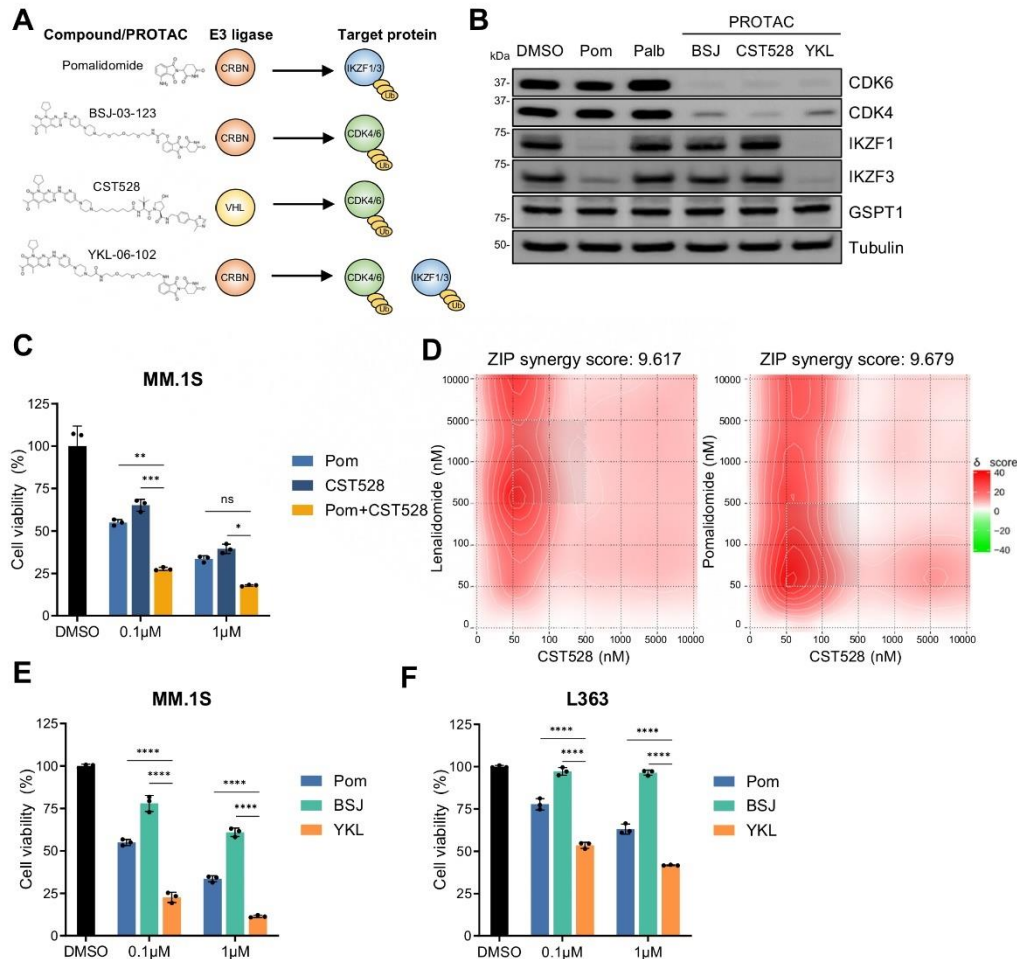


**Fig. 3** CDK6 inhibition by palbociclib synergizes with IMiD treatment of multiple myeloma cells. **A** Cell viability of MM.1S cells treated 96 h with pomalidomide (pom), palbociclib (palb), or in combination. ( $N = 3$  biologically independent replicates). **B** Synergy map of MM.1S cells treated with palbociclib in combination with lenalidomide or pomalidomide. **C** Cell viability of L363 cells treated with pomalidomide, palbociclib, or in combination ( $N = 3$  biologically independent replicates). **D** Synergy map of L363 cells treated with palbociclib in combination with lenalidomide or pomalidomide. **E** Cell viability of MM.1S LenR cells ( $N = 3$  biologically independent replicates) and **F** OPM2 CDK6 OE cells upon combination treatment of pomalidomide and palbociclib ( $N = 3$  biologically independent replicates) Synergy levels are indicated with ZIP synergy scores. Synergy maps were generated with SynergyFinder<sup>75</sup>. Cell viability is normalized to respective DMSO conditions. Data represent the mean  $\pm$  SD of biological triplicates. One-way ANOVA is applied.  $P$  values are displayed as follows: n.s. =  $P > 0.05$ ; \* $P \leq 0.05$ ; \*\* $P \leq 0.01$ ; \*\*\* $P \leq 0.001$ ; \*\*\*\* $P \leq 0.0001$ . Source data are provided as a Source Data file.

performed quantitative proteomic and phosphoproteomic analyses in MM.1S cells treated with pomalidomide, palbociclib, and CDK6-specific PROTACs alone or in combination (Fig. 6A, Supplementary Data 3). Global proteome analysis of drug-treated MM.1S cells identified 7460 proteins, of which 240 and 179 were significantly regulated by treatment with 24 h pomalidomide or palbociclib, respectively (0.1 FDR). In line with previous results,

CRBN neo-substrates IKZF1, IKZF3, and ZFP91 were the most downregulated proteins in pomalidomide treated samples. The effect of palbociclib and the CDK6-specific PROTAC BSJ-03-123 on protein levels highly correlated (Supplementary Fig. 13A, B).

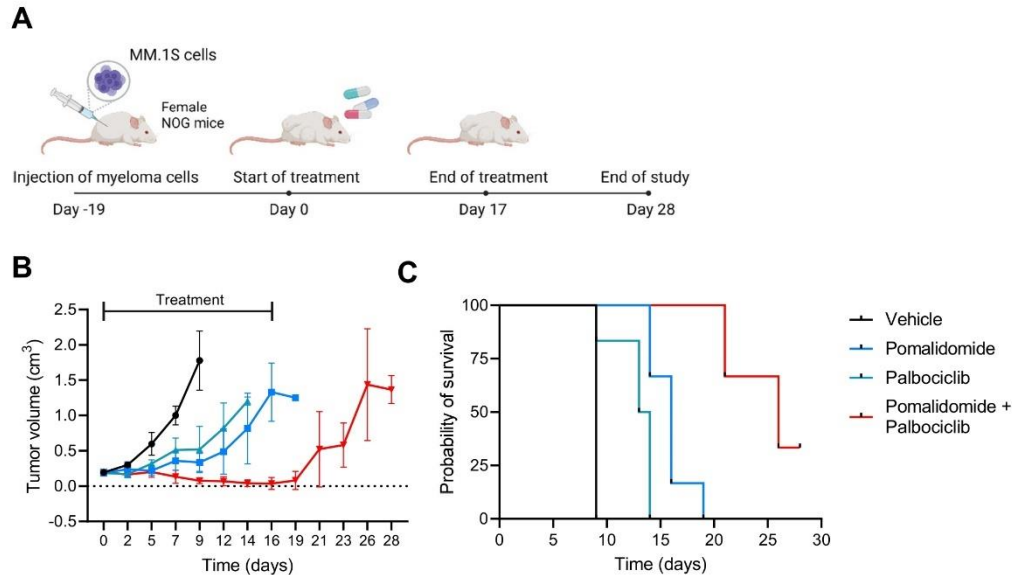
When we compared the significantly regulated proteins in patient samples and drug-treated MM.1S cells, we observed a striking pattern where proteins upregulated in patient samples at



**Fig. 4** CDK6 inhibition synergizes with IKZF1/3 degradation. **A** Chemical structure, hijacked E3 ligase, and targets of pomalidomide (pom), PROTAC BSJ-03-123 (BSJ), PROTAC CST528, and PROTAC YKL-06-102 (YKL). **B** Western blot analysis of MM.1S cells treated with 1  $\mu$ M of pomalidomide, palbociclib, BSJ-03-123, CST528, and YKL-06-102 for 16 h ( $N = 3$  biologically independent replicates). **C** Cell viability of MM.1S cells treated 96 h with pomalidomide, CST528 and in combination ( $N = 3$  biologically independent replicates). **D** Synergy map of MM.1S cells treated with CST528 in combination with lenalidomide or pomalidomide. **E** Cell viability of 96 h treatment with pomalidomide, BSJ-03-123 and YKL-06-102 in MM.1S cells ( $N = 3$  biologically independent replicates) and **F** L363 cells ( $N = 3$  biologically independent replicates). Synergy levels are indicated with ZIP synergy scores. Synergy maps were generated with SynergyFinder<sup>75</sup>. Cell viability is normalized to respective DMSO conditions. Data represent the mean  $\pm$  SD of biological triplicates. One-way ANOVA is applied.  $P$  values are displayed as follows: n.s. =  $P > 0.05$ ; \* $P \leq 0.05$ ; \*\* $P \leq 0.01$ ; \*\*\* $P \leq 0.001$ ; \*\*\*\* $P \leq 0.0001$ . Source data are provided as a Source Data file.

relapse were downregulated by CDK6 inhibition or degradation in MM.1S cells and vice versa (Fig. 6B, Supplementary Data 4). In detail, we found an overlap of 37 proteins upregulated in the relapse samples and downregulated by CDK6 inhibition (cluster a), as well as 54 proteins significantly downregulated in relapse and upregulated by CDK6 inhibition (cluster c) (Supplementary Fig. 13C). Among the CDK6 regulated proteins included in the signature were the two top upregulated proteins in relapse, TRIP13 and RRM1<sup>30,31</sup>. Other proteins upregulated in relapse and targeted by CDK6 inhibition are comprised of cell cycle-related genes (CDK2, MCM3/5, NCAPH, NCAPD2, PDCD2L,

USP16), DNA damage regulators (PAXIP1, RAD18, and MLH1) and transcriptional/epigenetic regulators (DNMT1, BTF3, EDRF1, KEAP1, MORF4L1). Upregulation of the genome integrity safeguard PAXIP1 links CDK6 to a factor that has been identified to be highly selective for myeloma cell survival in the Dependency Map studies<sup>44</sup> and the higher abundance of the oxidative stress sensing E3 ligase KEAP1 may indicate a connection to oxidative metabolism. The downregulated proteins in cluster c are dominated by 27 mitochondrial genes including key factors for leucine catabolic metabolism (AUH), TCA cycle (IDH3B), the electron transport chain (NDUFA10, COX5B),



**Fig. 5** Combination treatment of pomalidomide and palbociclib has high therapeutic efficacy in multiple myeloma in vivo. **A** MM.1S cells were injected into NOG mice and treatment started 19 days after injection of myeloma cells when tumors were  $\sim 0.2 \text{ cm}^3$ . Mice were treated on a daily basis with vehicle control, pomalidomide (5 mg/kg), palbociclib (50 mg/kg) or the combination p.o. for 17 days and observed until day 28. **B** Tumor growth in treated mice of monotherapy of pomalidomide and palbociclib, and in combination. Mice were taken out of the study when tumors exceeded a size of  $1.2 \text{ cm}^3$ . **C** Survival of the four groups. Statistical differences were analyzed by log-rank Mantel-Cox test. All comparisons of survival curves resulted in  $P$ -values  $< 0.01$ . Data represent mean  $\pm$  SD of biological replicates. Group size:  $n = 5$  for vehicle group;  $n = 6$  for pomalidomide treatment group;  $n = 6$  for palbociclib treatment group;  $n = 6$  for pomalidomide + palbociclib treatment group. Figure **A** was created with BioRender.com. Source data are provided as a Source Data file.

ATP synthase (ATP5D, ATP5J), and fatty acid metabolism (ACAD9, ECHS1, HADHB, MLYCD, MCEE). Similar to the effects observed here it has been reported that the signaling axis CDK4-RB1-E2F represses mitochondrial oxidative metabolism<sup>45</sup>.

We also observed lower levels of IKZF1/3 and MYC in the combined treatments as compared to single treatments alone. (Fig. 6C, Supplementary Fig. 14A, B). The enhanced inactivation of essential multiple myeloma transcription factors likely contributes to the synergistic effects of IMiDs and CDK6 inhibition.

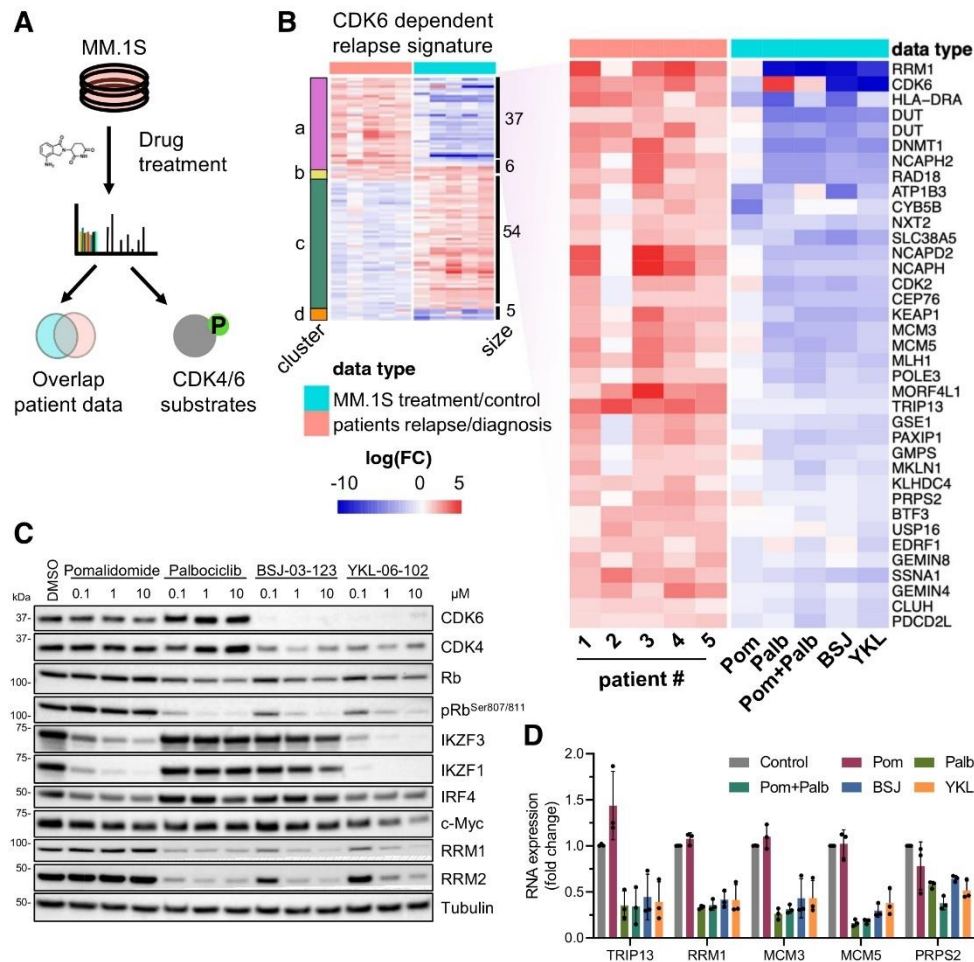
**Identification of CDK6 substrates by phosphoproteomics in multiple myeloma.** To identify CDK6 substrates in multiple myeloma, we performed phosphoproteomics analyses in MM.1S cells treated with palbociclib or the CDK6-specific PROTAC BSJ-03-123. We identified 29,811 phosphopeptides across all samples of which 122 phosphopeptides on 96 proteins were significantly downregulated after 3 h of palbociclib or BSJ-03-123 treatment (0.1 FDR). In addition, phosphorylation status of 558 proteins (1022 phosphopeptides) not regulated on global protein level was specifically downregulated after 24 h palbociclib treatment, with an overlap of 45 proteins to the 3 h timepoint, which we deemed particularly interesting, since these phosphosites were downregulated at an early time point and in a sustained manner (Supplementary Data 3, Supplementary Fig. 15A). The effect of palbociclib and the CDK6-specific PROTAC BSJ-03-123 on phosphopeptide levels was highly correlated (Supplementary Fig. 15B). Identified phosphorylation targets comprised the known CDK4/6 substrates RB1, RBL1, RBL2, and CDKN1A as well as several proteins that were deregulated in relapse samples (DNTM1, GMPS, KLHDC4, NCAPD2, NCAPH, GLYR1,

NOP56), providing a functional link between CDK6 kinase function and CDK6-regulated protein levels. In addition, lower phosphorylation levels were observed in palbociclib treated cells in several transcriptional regulators including RNF169 and ZBTB38, as well as known CDK6 interactors and substrates JUN and FOXM1 (Supplementary Data 3)<sup>46,47</sup>. However, for many proteins deregulated on the protein level, including RRM1 and TRIP13, we did not detect lower phosphorylation levels after CDK6 inhibition, indicating that these proteins are not direct CDK6 substrates. RT-qPCR analyses revealed that TRIP13, RRM1 and other proteins tested had reduced mRNA levels after CDK6 inhibition or inactivation, implying CDK6-dependent transcriptional regulation as has been previously reported (Fig. 6D)<sup>46</sup>.

## Discussion

Drug resistance is one of the biggest challenges in cancer therapy. Genetic alterations revealed in comprehensive sequencing studies do not sufficiently explain the emergence of resistance in most cases, implying non-genetic mechanisms<sup>48</sup>. Here we applied an integrated proteomics and transcriptomics approach in primary multiple myeloma matched pre-treatment/resistant samples that identified and validated a targetable CDK6 governed protein resistance signature. Only a few proteomic studies of multiple myeloma have been previously published<sup>26,49,50</sup>. Our dataset containing over 6000 proteins and 20,000 phosphopeptides represents a deep proteomic study of longitudinal samples from relapsed multiple myeloma patients. It provides proof of principle for feasibility and clinical relevance of in-depth proteomic analysis in multiple myeloma. We observed a low correlation of protein and RNA levels implying a high degree of post-





**Fig. 6 Targeting CDK6 in myeloma cells reverses a relapse protein signature.** **A** Proteomic and phosphoproteomic changes of MM.1S cells treated with different drugs and combinations were assessed with TMT-based proteomics. **B** Combined heatmap displaying protein levels of paired-patient data and cell perturbation data. MM.1S cells were treated for 24 h with pomalidomide (pom), palbociclib (palb), in combination (pom + palb), BSJ-03-123 (BSJ), and YKL-06-102 (YKL). **C** Western blot analysis of MM.1S cells treated for 16 h with respective treatments at indicated concentrations ( $N = 3$  biologically independent replicates). **D** mRNA levels of downstream CDK6 targets in MM.1S cells upon treatment of 1  $\mu\text{M}$  with pomalidomide, palbociclib, or in combination, BSJ-03-123 and YKL-06-102 ( $N = 3$  biologically independent replicates). mRNA expression is normalized to respective GAPDH levels and DMSO conditions. Data represent the mean  $\pm$  SD of biological triplicates. Source data are provided as a Source Data file.

transcriptional and post-translational regulation in multiple myeloma. Indeed, the most upregulated and functionally relevant proteins identified by our proteomics approach would have been missed by RNA sequencing. This is in line with previous studies in other tumors highlighting that protein level and activity cannot necessarily be inferred from RNA expression<sup>21,51,52</sup>.

Unexpectedly, proteins known to be involved in pathways targeted by routinely used myeloma drugs like CRBN, IKZF1, proteasome subunits, or the glucocorticoid receptor were not found deregulated at relapse. However, several of the proteins we identified as significantly deregulated have been previously implicated in multiple myeloma. TRIP13, an AAA-ATPase involved in genome stability<sup>53</sup>, is among the top-ranking genes included in the GEP70, a

highly validated high-risk RNA expression signature in multiple myeloma<sup>18,29,30</sup>. TRIP13 overexpression is a driver of B-cell malignancies<sup>28</sup> and is functionally linked to drug resistance in multiple myeloma and other cancers<sup>30</sup>, and inhibition of TRIP13 is toxic to multiple myeloma cells<sup>54</sup>. RRM1, together with RRM2, forms the ribonucleotide reductase heterodimeric tetramer that is involved in DNA damage repair<sup>55</sup>. Multiple myeloma cells were shown to be dependent on RRM1 and high RRM1 RNA expression is associated with an adverse outcome<sup>31</sup>. In line with this, we found RRM1 overexpression to reduce IMiD sensitivity in multiple myeloma cells.

CDK6, together with CDK4, is a vital regulator of the cell cycle through regulation of RB1<sup>42,56–58</sup>. CDK6 has been found



upregulated in a wide range of cancer, including multiple myeloma<sup>32,46,59</sup>. We found that CDK6 overexpression reduces sensitivity to IMiDs, but not to other drugs in multiple myeloma. Blocking CDK6 through palbociclib or by protein degradation via PROTACs inhibited cell cycle progression and proliferation consistent with previous reports<sup>32,36</sup>. Palbociclib was able to overcome IMiD resistance and showed strong synergy with lenalidomide and pomalidomide *in vitro* and *in vivo*. CDK6-specific PROTACs hijacking CRBN were antagonistic with IMiDs due to E3 ligase competition. This issue could be overcome by either hijacking two different E3 ligases, CRBN and VHL, or a PROTAC, such as YKL-06-102, that simultaneously targets IKZF1, IKZF3, and CDK6, achieving intramolecular synergistic effects even in IMiD-insensitive multiple myeloma cells. However, the low activity of this PROTAC in the MM.1S xenograft model shows that the pharmacologic properties of PROTACs need to be optimized for application *in vivo*.

Our data imply that the effects of CDK6 in multiple myeloma depend on its kinase function but are independent of RB1, the CDK4/6 substrate which is most relevant for other cancers. Our proteomic analyses in multiple myeloma cell lines revealed that CDK6 governs many of the proteins deregulated at relapsed/resistant disease, either through direct phosphorylation of proteins or by indirect alterations of the transcriptional activity of genes including TRIP13 and RRM1, and is thus a master regulator of a relapse-associated program. The CDK6-dependent relapse signature contains proteins connected to DNA damage repair, cell cycle, and metabolic pathways including electron transport chain, energy transfer, and fatty acid metabolism. Antagonizing this signature by CDK6 inactivation in conjunction with IMiDs resulted in a significant and fast downregulation of the essential transcription factor MYC, further highlighting the synergistic effects of IKZF1/3 and CDK6 inactivation. While many of the relapse-associated proteins are regulated by CDK6, the mechanism that drives elevated CDK6 protein expression itself is not clear. We couldn't find any associations with genetic alterations and the lack of correlation with RNA expression implies post-transcriptional and/or post-translational mechanisms. This, as well as the exact downstream functions of CDK6 in resistant multiple myeloma, needs to be evaluated in detail in future studies.

Several CDK4/6 inhibitors are approved by the FDA and EMA for advanced breast cancer and are being investigated in hematologic malignancies including acute lymphoblastic leukemia<sup>60</sup> and acute myeloid leukemia<sup>33,61,62</sup>. In multiple myeloma, a phase I/II clinical trial that combined palbociclib with bortezomib and dexamethasone showed that this regimen is feasible and has antitumor activity<sup>63</sup>. Here, we show that combining CDK6 inhibition with IMiDs is particularly synergistic in multiple myeloma. Although both drugs cause cytopenia as an unwanted side-effect, our data suggest that low dosages of palbociclib may be sufficient to sensitize multiple myeloma cells to IMiDs. PROTACs have recently entered clinical trials<sup>64</sup> and PROTACs with combined IKZF1/IKZF3/CDK6 activity provide an attractive alternative with single drug synergistic effects. CDK6 protein levels may provide a biomarker to identify patients who would benefit most from this therapeutic combination. In conclusion, our results identify CDK6 as a master regulator in treatment-resistant relapsed multiple myeloma and provide a strong rationale for further investigating CDK6 inhibition together with IMiDs in multiple myeloma.

## Methods

**Study cohort.** Five multiple myeloma patients with paired pre-treatment and relapsed samples were included in the proteomics study. Additional 13 samples from an independent cohort of newly diagnosed or relapsed/refractory multiple

myeloma patients were analyzed with western blotting. Patient characteristics and treatment are summarized in Supplementary Fig. 1. All samples were obtained from the iliac crest of patients and were CD138+ enriched by MACS (Miltenyi, Cologne, Germany). For patients #1, #3, #4, and #5 whole-exome sequencing data is reported in a previous study<sup>17</sup>. All patients provided written informed consent according to the Declaration of Helsinki and the study was approved by the institutional review board (IRB) of Ulm University.

**Cell culture.** Multiple myeloma cell lines MM.1S, OPM2, NCI-H929, L363, LP1, RPMI-8226, AMO-1, INA-6, JN3, and KMS12BM were obtained from ATCC (Manassas, Virginia, USA) and the German Collection of Microorganisms and Cell Cultures GmbH (DSMZ, Braunschweig, Germany), and maintained in RPMI-1640 medium (Merck KGaA, Darmstadt, Germany) containing 10% fetal bovine serum (FBS) and supplemented with 1% penicillin/streptomycin and 1% L-glutamine. INA-6 cells were supplemented with IL-6. Cells were maintained at 37 °C with 5% CO<sub>2</sub> in humidified atmosphere.

**Treatment of MM1S for proteomic and phosphoproteomic analysis.** MM.1S WT cells were subjected to respective treatments for either 3 or 24 h in biological duplicates. Pomalidomide treatment was administered at a final concentration of 10 μM, while palbociclib, BSI-03-123, and YKL-06-102 were administered at 1 μM. Control cells were treated with solvent only. Cells were pelleted and washed three times with cold 1 × PBS.

**Proteomics and phosphoproteomics sample preparation.** Samples for global proteome and phospho-proteome profiling were analyzed with isobaric TMT<sup>21</sup>. Samples were lysed at 4 °C with urea lysis buffer (8 M urea, 50 mM Tris (pH 8), 150 mM NaCl) supplemented with protease inhibitors (2 μg/ml aprotinin, 10 μg/ml leupeptin 1 mM phenylmethylsulfonylfluoride) and phosphatase inhibitors (10 mM NaF, phosphatase inhibitor cocktail 1 and 2, Sigma Aldrich). Extracted proteins were reduced with 5 mM dithiothreitol for 1 h and alkylated with 10 mM iodoacetamide for 45 min in the dark. Sequencing grade LysC (Wako) was added at a weight to weight ratio of 1:50. After 2 h, samples were diluted 1:4 with 50 mM Tris-HCl pH 8 and sequencing grade trypsin (Promega) was added at a weight to weight ratio of 1:50. Digestion was completed overnight and subsequently acidified samples were desalted with Sep-Pak C18 cc Cartridges (Waters). Dried samples were resuspended in 10 mM HEPES (pH 8.5) and peptide concentration was determined. For relative quantification of proteins in multiple myeloma patient samples, 10 μg peptides for each sample were labeled with 10-plexing TMT (TMT-10; Thermo Fisher Scientific) and combined into one TMT plex. For quantification of phosphopeptides in multiple myeloma patient samples, 150 μg of peptides for the samples 1–9 and 23 μg of starting material for sample 10 were labeled with TMT-10 reagents and combined into a second plex. TMT-channel annotation of patient proteomic data is available in Supplementary Data 1. For global and phosphoproteome analysis of MM.1S drug-treated cells, 200 μg peptides of each sample were labeled with 11-plexing TMT (TMT-11; Thermo Fisher Scientific) and the samples were randomly distributed into two TMT plexes. For the MM.1S experiment, an internal reference sample composed of equal amounts of peptide material from all samples was included in each TMT 11-plex to provide a standard for relative quantification. TMT-channel annotation of MM.1S proteomic data is available in Supplementary Data 3. Combined TMT samples were fractionated off-line into 24 fractions using high-pH reversed phase chromatography. For analysis of the global proteome, 500 ng peptides of each fraction were analyzed with LC-MS/MS. The remaining material was pooled into 12 fractions for each plex and subjected to phosphopeptide enrichment with immobilized metal affinity chromatography (IMAC) automated on an AssayMap Bravo System (Agilent)<sup>65</sup>.

**Liquid chromatography mass spectrometry.** Mass spectrometry raw data was acquired on a Q-Exactive HF-X connected to an EASY-nLC 1200 system (both Thermo Fisher Scientific). Each H<sub>2</sub>O fraction was measured individually as a single LC-MS injection. Samples were separated online on a 25 cm column packed in-house with C18-AQ 1.9 μm beads (Dr. Maisch Reprosil-Pur 120). A gradient of mobile phase A (0.1% formic acid and 3% acetonitrile in water) and mobile phase B (0.1% formic acid, 90% acetonitrile in water) was used to separate the samples online at a flow rate of 250 μl/min. Mobile phase B was ramped from 4% to 30% in the first 88 min, followed by an increase to 60% B in 10 min and a plateau of 90% B for 5 min. Temperature of the column was kept constant at 45 °C. MS data was acquired in data-dependent acquisition and profile centroid mode. MS1 scans were acquired at 60,000 resolution, scan range of 350–1500 *m/z*, automatic gain control (AGC) target value of 3e6 and maximum injection time (IT) of 10 ms. The 20 most abundant ions were picked for fragmentation with normalized collision energy (NCE) set to 32 and 0.7 *m/z* isolation window. MS2 scans were acquired at 45,000 resolution, fixed first mass 120 *m/z*, AGC target value of 3e5 and maximum IT of 86 ms. Ions with charge state 1, 6 or higher were excluded from fragmentation and dynamic exclusion was set to 30 s. LC-MS parameters for phosphoproteomic analysis was the same with the exception of MS2 maximum IT that was set to 120 ms.



**Mass spectrometry raw data searching with MaxQuant.** Raw data was analyzed with MaxQuant (Version 1.6.3.3)<sup>66</sup> and searched against the human reference proteome (UP000005640) downloaded from UniProt in 01/2017 ([https://ftp.uniprot.org/pub/databases/uniprot/previous\\_releases/](https://ftp.uniprot.org/pub/databases/uniprot/previous_releases/)) and default protein contaminants included in MaxQuant. PIF filter was set to 0.5. Fixed modifications were set to carbamidomethylation of C. Variable modifications were set to M-oxidation and acetylation of protein N-termini including neo protein N-terms after cleavage of first methionine. A maximum of 5 modification per peptide were allowed. N-terminal acetylation and M-oxidation were used in protein quantification (unmodified counterpart discarded). Unique and razor peptides were used for quantification. TMT correction factors supplied by the manufacturer were applied.

**Mass spectrometry data analysis.** Analysis of MaxQuant output was performed with R(4.0.3) and R studio (Version 1.3.1093) statistical software environment. Statistical analysis in R was aided by the ProTIGY application provided by the Broad Institute on GitHub (<https://github.com/broadinstitute/protigy>)<sup>67</sup>. Protein group files were filtered for reverse hits, potential contaminants and proteins only identified by site. Resulting proteins were filtered for proteins identified with at least two peptides and at least one unique peptide. Phosphoproteomic data was analyzed in a separate MaxQuant run and filtered for valid values across all samples. Due to limited protein amounts of the patient 5 diagnosis sample, patient 5 was excluded from the analysis of the phosphoproteomic data. For the analysis of multiple myeloma patient samples, log<sub>2</sub> ratios (relapse/diagnosis) of proteins and phosphopeptides were calculated for each patient and normalized with median-MAD normalization. The processed data was analyzed with a two-sided moderated one-sample *t*-test (limma package)<sup>68</sup>. Prior to applying multiple testing correction with the Benjamini-Hochberg method, data was subjected to reproducibility filtering to remove outliers (global proteome 99% confidence interval; phosphoproteome 95% confidence interval with linear mixed effect models). As expected, the phosphoproteome showed higher variability compared to the global proteome, which is more stable towards dynamic modifications. We therefore applied a stronger outlier filter and more relaxed cutoff for the phosphoproteomic data. A cutoff of 0.1 and 0.12 FDR was implemented for global proteome (Fig. 1B) and phosphoproteome (Supplementary Fig. 3C) analysis of patients samples respectively. For the analysis of MM.1S drug treated cells, the log<sub>2</sub> ratios (sample/internal standard) were calculated and normalized with median-MAD normalization. The resulting ratios were subsequently normalized to the control sample and analyzed with a two-sided moderated one-sample *t*-test. Resulting *p*-values were corrected for multiple testing with the Benjamini-Hochberg method. MM.1S phosphoproteomic data was subjected to reproducibility filtering (99% confidence interval) with Bland-Altman filtering to remove outliers prior to *p*-value correction. For MM.1S derived data, a 0.1 FDR significance cutoff was applied. The Phosphosite plus (PSP) database was used for identifying known CDK6 targets<sup>69</sup>. The processed proteomics data as well as TMT channel annotation is available in supplementary data files. The mass spectrometry proteomics data and search results have been deposited to the ProteomeXchange Consortium via the PRIDE partner repository<sup>70</sup> with the dataset identifier PXD021265.

**RNA-sequencing.** Library preparation was performed from 100 ng of input total RNA using the TruSeq Stranded Exome RNA Kit (Illumina, San Diego, CA, USA) according to the manufacturer's instructions. The pooled RNA libraries were sequenced on an Illumina HiSeq2000 with 50 bp single-end reads with an average coverage of  $36.6 \times 10^6$  reads per sample. RNA-Seq data were aligned and quantified with STAR<sup>71</sup> and mRNA reads were identified using an in-house analysis pipeline detecting exons in a shuffled order. To increase comparability with proteomics data, TPM RNAseq data was processed like TMT-proteomics data and median-MAD normalized log<sub>2</sub> ratios (relapse/diagnosis) were analyzed with a two-sided moderated one-sample *t*-test. RNA transcripts were matched with the protein groups file and Pearson correlation of individual genes to proteins was calculated across all 10 samples (median normalized values). Processed RNAseq data is available in the supplements. Gene set enrichment analysis was performed using GSEA and the Molecular Signatures Database (MsigDB)<sup>72</sup>. RNA-sequencing data is available on Gene Expression Omnibus (accession number GSE162403).

**Fluorescence in situ hybridization (FISH).** Fluorescence in situ hybridization was performed on plasma cells isolated from patients. Genetic regions of interest specific for the diagnosis for multiple myeloma and their translocation partners were detected. FISH was performed according to standardized protocols using commercially available probes (Abbott Laboratories, Chicago, United States; MetaSystems, Altlußheim, Germany)<sup>73</sup>.

**In vivo experiment.**  $1 \times 10^7$  MM.1S cells were injected subcutaneously into 6–8-week-old female NOG mice (strain: NOD.Cg-Prkdc<sup>scid</sup> Il2rg<sup>tm1Sug</sup>/JcTac). Mice for the study were obtained from Taconic (Leverkusen, Germany). The in vivo experiments were performed at EPO GmbH Berlin, Germany. The animals were group-housed (max. 5 mice/cage) in individually ventilated cages (IVC type GM 500, Techniplast) at temperature of  $22 \pm 2$  °C, humidity of  $50 \pm 10\%$ , at 12 h dark-light cycles.

Tumor-bearing mice were randomized after 19 days when tumors reached 200 mm<sup>3</sup> and treatments were started. Pomalidomide was administered at 5 mg/kg

while palbociclib was administered at 50 mg/kg. Both drugs were administered daily via oral gavage. YKL-06-102 was administered daily at 5 mg/kg via intraperitoneal injections. Treatment was performed for 17 days and thereafter, remaining animals were observed for another 11 days. Mice were euthanized when tumor volume reached 1200 mm<sup>3</sup>. The animal study was conducted in compliance with the United Kingdom Coordinated Committee on Cancer Research guidelines and have been approved and authorized by the Landesamt für Gesundheit und Soziales, Berlin, Germany (approval No. G 0333/18).

**Generation of lenalidomide-resistant cell lines.** MM.1S and LP-1 myeloma cells were cultured for over 3 weeks in the continuous presence of lenalidomide at 10, 100 and 1000 nM. Lenalidomide-resistance was confirmed with drug sensitivity assay with lenalidomide treatment.

**Plasmids and viral transduction.** The following plasmids were used: pLenti.6.2.V5-DEST, pRSP91-GFP-T2A-Puro, pLKO5d.SSF.SpCas9.P2a.BSD and pLKO5.hU6.sgRNA.dTom<sup>61,74</sup>. Complementary DNA (cDNA) of CDK6 and TRIP13 were cloned into pRSP91-GFP-T2A-Puro plasmid. pLenti.6.2.V5-DEST containing CDK6 WT and CDK6 K43M mutant were kind gifts from Claudia Scholl (National Center for Tumor Diseases and German Cancer Research Center (DKFZ)). sgRNAs targeting *RBI* were cloned into pLKO5.hU6.sgRNA.dTom.

For generation of lentiviral and retroviral vectors, HEK293T cells were transfected with constructs along with their respective packaging and envelope vectors. Viral supernatants were harvested 48 h after transfection and were used to transduce human multiple myeloma cell lines.

**Generation overexpressing and knockout cells.** Human multiple myeloma cell lines were transduced with virus containing with or without the CDK6 construct in backbones pLenti.6.2.V5-DEST and pRSP91-GFP-T2A-Puro. Transduced cells were selected with blasticidin and puromycin (InvivoGen, San Diego, USA) respectively.

Human multiple myeloma cell lines were transduced with virus containing pLKO5d.SSF.SpCas9.P2a.BSD and cells were selected with blasticidin (InvivoGen, San Diego, USA). Cells were then transduced with respective *CRBN* and *RBI* sgRNA constructs cloned into pLKO5.hU6.sgRNA.dTom, along with luciferase and POLR2A controls. Transduction success was confirmed through FACS analysis 48 h post-transduction with a minimum efficiency of 95% tomato fluorescence. *CRBN* and *RBI* knockout was confirmed through Western blot analysis. *CRBN*-targeting sgRNAs are as follow: 5'-GTCTGCTGATCTCCCTCCG-3' and 5'-GGATTACATAAGCTGCCAT-3'; *RBI*-targeting sgRNA is as follow: 5'-GGTTCTTGAGCAACATGGG-3'.

**Reagents and antibodies.** Lenalidomide, pomalidomide, palbociclib, melphalan, bortezomib and dexamethasone were obtained from SelleckChem. BSJ-03-123, YKL-06-102 and CST528 were synthesized according to Brand et al. 2019 and Steinebach et al. 2020.

Primary antibodies used for Western blotting from Cell Signaling (Danvers, USA) include CDK6 (clone DCS83, #3136, RRID:AB\_2229289, 1:2000), CDK4 (clone D9G3E, #12790, RRID:AB\_2631166, 1:1000), Rb (clone 4H1, #9309, RRID:AB\_823629, 1:1000), Phospho-Rb (Ser807/811) (#9308, RRID:AB\_331472, 1:1000), IKZF3 (clone D1C1E, #15103, RRID:AB\_2744524, 1:1000), IKZF1 (clone D6N9Y, #14859, RRID:AB\_2744523, 1:1000), IRF4 (clone D43H10, #4299, RRID:AB\_10547141, 1:1000), c-Myc (clone D84C12, #5605, RRID:AB\_1903938, 1:1000), RRM1 (clone D12F12, #8637, RRID:AB\_11217623, 1:1000), RRM2 (clone E7Y9J, #65939, 1:1000), anti-rabbit IgG HRP-linked antibody (#7074, 1:5000), anti-mouse IgG HRP-linked antibody (#7076, 1:5000); antibodies from Sigma-Aldrich (St. Louis, USA) include anti- $\alpha$ -Tubulin (#T5168, RRID:AB\_477579, 1:7000); antibodies from Santa Cruz Biotechnology (Dallas, USA) include CDK6 (clone B-10, sc-7961, 1:1000), TRIP13 (clone A-7, sc-514285, 1:1000); antibodies from Abcam (Cambridge, UK) include anti- $\beta$ -actin (ab20272, 1:10,000).

**Immunoblotting.** Cells were treated with respective drugs for 16 h and treated cells were washed and lysed in Pierce IP lysis buffer. SDS-PAGE was performed with 10–20  $\mu$ g of proteins loaded per sample. Proteins were then transferred onto PVDF membranes. Blotted membranes were blocked with 5% milk in tris-buffered saline/Tween20 (TBST) for one hour, followed by three times 10 min washes in TBST. Primary antibodies were diluted in 5% BSA in TBST and incubations were performed overnight at 4 °C. After further washes, respective secondary HRP-conjugated antibodies diluted in 5% milk were incubated for one hour at room temperature. Detection of proteins on PVDF was carried out using WesternBright ECL HRP substrate or WesternBright Sirius HRP substrate (Advansta, San Jose, USA) and imaged with ChemiDoc XRS + System (Bio-Rad, Munich, Germany). Membranes were subjected to 10 min incubation with Restore<sup>™</sup> Western Blot Stripping Buffer (Thermo Fisher Scientific, Waltham, USA) followed by TBST washes. After brief re-activation with methanol, membranes were blocked, and further probing of proteins was carried out.

**Quantitative RT-PCR.** MM.1S cells were treated with drugs at indicated times and concentrations. mRNA from cells were extracted using Qiagen RNeasy Kit and was performed according to manufacturer's instructions. Reverse transcription PCR



## ARTICLE

NATURE COMMUNICATIONS | <https://doi.org/10.1038/s41467-022-28515-1>

(RT-PCR) were carried out using TaqMan Reverse Transcription Reagents (Thermo Fisher Scientific, Waltham, USA).

Real-time quantitative PCR (RT-qPCR) were performed with SYBR Green Master Mix (Thermo Fisher Scientific, Waltham, USA) and StepOnePlus Real-Time PCR System. qPCR standard protocol was 95 °C for 5 min, followed by 45 cycles of 95 °C for 10 s and 60 °C for 30 s. Expression fold change was calculated with  $2^{-\Delta\Delta C_T}$ .

Primer pair sequences are as follow: 5'-ACTGTTGCACTTCACATTTTCCA-3' and 5'-TCGAGGAGATGGGATTGACT-3' for TRIP13; 5'-GCTGAAACAGCTGCAACCTT-3' and 5'-ACCATGGGAGAGTGTTTGC-3' for RRM1; 5'-TACCTGGACTTCCTGGACGA-3' and 5'-AAGGAACACGCTCCTCAA-3' for MCM3; 5'-CCAAGTGTCCACGTTGGATG-3' and 5'-TGCTCCGGGTATTCTGCTT-3' for MCM5; 5'-AGGTAGGAGAGATCGTCC-3' and 5'-CCACTCGGCAATGTTTCCC-3' for PRPS2; 5'-CAATGACCCCTTATTGACC-3' and 5'-GACAAGCTTCCCGTTCTCAG-3' for GAPDH.

**Cell viability assay.** Cells were seeded in 96-well or 384-well plates with respective treatments and plates were incubated at 37 °C for 96 h. Cell viability readout was measured using CellTiter-Glo® Luminescent Cell Viability Assay (Promega, Madison, USA) and measured with POLARStar Omega plate reader (BMG Lab-Tech, Ortenberg, Germany). All conditions were normalized to the dimethyl sulfoxide (DMSO) (Sigma Aldrich, Taufkirchen, Germany) treated control. Data represents the mean ± SD of biological triplicates.

**Software and statistical analysis.** Mass spectrometry raw data was searched with MaxQuant (Version 1.6.3.3)<sup>66</sup>. RNA-Seq data were aligned and quantified with STAR<sup>71</sup>. Analysis of proteomics and RNAseq data was performed with R(4.0.3) and R studio (Version 1.3.1093) statistical software environment. Statistical analysis of omics data in R was aided by the protigy application provided by the Broad institute on GitHub (<https://github.com/broadinstitute/protigy>). Statistical and graphical analyses of in vitro and in vivo experiments were performed with Prism version 8 and 9.1.0 (GraphPad Software, San Diego, CA, USA). Statistical differences were analyzed by one-way ANOVA, unpaired *t* tests with Welch's correction and log-rank Mantel-Cox tests. *P* values are displayed as follows: n.s. = *P* > 0.05; \**P* ≤ 0.05; \*\**P* ≤ 0.01; \*\*\**P* ≤ 0.001; \*\*\*\**P* ≤ 0.0001. For the generation of synergy maps, SynergyFinder was used, and ZIP and Bliss reference models were utilized<sup>72</sup>.

**Reporting summary.** Further information on research design is available in the Nature Research Reporting Summary linked to this article.

### Data availability

The mass spectrometry proteomics data and search results generated in this study have been deposited to the ProteomeXchange Consortium via the PRIDE partner repository<sup>70</sup> with the dataset identifier PXD021265. The human reference proteome (UP000005640) was downloaded from UniProt in 01/2017 ([https://ftp.uniprot.org/pub/databases/uniprot/previous\\_releases/](https://ftp.uniprot.org/pub/databases/uniprot/previous_releases/)). The RNA-sequencing data generated in this study are available on Gene Expression Omnibus under accession number GSE162403. Processed proteomics data are available in Supplementary Data 1 (patient proteomics data) and Supplementary Data 3 (MMIS proteomics data); processed patient RNAseq data is available in Supplementary Data 2. The remaining data are available within the Article, Supplementary Information or Source Data file. Source data are provided with this paper.

Received: 22 January 2021; Accepted: 26 January 2022;

Published online: 23 February 2022

### References

- Kumar, S. K., Rajkumar, V., Kyle, R. A., Van Duin, M. & Sonneveld, P. Multiple myeloma. *Nat. Rev. Dis. Prim.* **3**, 1–20 (2017).
- Ito, T. et al. Identification of a primary target of thalidomide teratogenicity. *Science* **327**, 1345–1350 (2010).
- Krönke, J. et al. Lenalidomide causes selective degradation of IKZF1 and IKZF3 in multiple myeloma cells. *Science* **343**, 301–305 (2014).
- Lu, G. et al. The myeloma drug lenalidomide promotes the cereblon-dependent destruction of ikaros proteins. *Science* **343**, 305–309 (2014).
- Zhu, Y. X. et al. Identification of cereblon-binding proteins and relationship with response and survival after IMiDs in multiple myeloma. *Blood* **124**, 536–545 (2014).
- Shaffer, A. L. et al. IRF4 addiction in multiple myeloma. *Nature* **454**, 226–231 (2008).
- Fischer, E. S. et al. Structure of the DDB1-CRBN E3 ubiquitin ligase in complex with thalidomide. *Nature* **512**, 115–124 (2014).
- Miguel, J. S. et al. Pomalidomide plus low-dose dexamethasone versus high-dose dexamethasone alone for patients with relapsed and refractory multiple myeloma (MM-003): A randomised, open-label, phase 3 trial. *Lancet Oncol.* **14**, 1055–1066 (2013).
- Kortüm, K. M. et al. Targeted sequencing of refractory myeloma reveals a high incidence of mutations in CRBN and Ras pathway genes. *Blood* **128**, 1226–1233 (2016).
- Barrio, S. et al. IKZF1/3 and CRL4-CRBN E3 ubiquitin ligase mutations and IMiD resistance in multiple myeloma. *Haematologica* **105**, e240 (2020).
- Liu, J. et al. A genome-scale CRISPR-Cas9 screening in myeloma cells identifies regulators of immunomodulatory drug sensitivity. *Leukemia* **33**, 171–180 (2019).
- Lu, G. et al. UBE2G1 governs the destruction of cereblon neomorphic substrates. *Life* **7**, 1–24 (2018).
- Sievers, Q. L., Gasser, J. A., Cowley, G. S., Fischer, E. S. & Ebert, B. L. Genome-wide screen identifies cullin-RING ligase machinery required for lenalidomide-dependent CRL4CRBN activity. *Blood* **132**, 1293–1303 (2018).
- Chavan, S. S. et al. Bi-allelic inactivation is more prevalent at relapse in multiple myeloma, identifying RB1 as an independent prognostic marker. *Blood Cancer J.* **7**, 1–7 (2017).
- Weinhold, N. et al. Clonal selection and double-hit events involving tumor suppressor genes underlie relapse in myeloma. *Blood* **128**, 1735–1744 (2016).
- Lohr, J. G. et al. Widespread genetic heterogeneity in multiple myeloma: Implications for targeted therapy. *Cancer Cell* **25**, 91–101 (2014).
- Bohl, S. R. et al. Comprehensive CRISPR-Cas9 screens identify genetic determinants of drug responsiveness in multiple myeloma. *Blood Adv.* **5**, 2391–2402 (2021).
- Shaughnessy, J. D. et al. A validated gene expression model of high-risk multiple myeloma is defined by deregulated expression of genes mapping to chromosome 1. *Blood* **109**, 2276–2284 (2007).
- Nair, B. et al. Gene expression profiling of plasma cells at myeloma relapse from tandem transplantation trial Total Therapy 2 predicts subsequent survival. *Blood* **113**, 3572–3575 (2009).
- Schwanhüusser, B. et al. Global quantification of mammalian gene expression control. *Nature* **473**, 337–342 (2011).
- Mertins, P. et al. Proteogenomics connects somatic mutations to signaling in breast cancer. *Nature* **534**, 55–62 (2016).
- Vasaikar, S. et al. Proteogenomic analysis of human colon cancer reveals new therapeutic opportunities. *Cell* **177**, 1035–1049.e19 (2019).
- Zhang, H. et al. Integrated proteogenomic characterization of human high-grade serous ovarian cancer. *Cell* **166**, 755–765 (2016).
- Morales, M. L. et al. MEK inhibition enhances the response to tyrosine kinase inhibitors in acute myeloid leukemia. *Sci. Rep.* **9**, 18630 (2019).
- Zaal, E. A. et al. Bortezomib resistance in multiple myeloma is associated with increased serine synthesis. *Cancer Metab.* **5**, 1–12 (2017).
- Dytfeld, D. et al. Comparative proteomic profiling of refractory/relapsed multiple myeloma reveals biomarkers involved in resistance to bortezomib-based therapy. *Oncotarget* **7**, 56726–56736 (2016).
- Eichner, R. et al. Immunomodulatory drugs disrupt the cereblon-CD147-MCT1 axis to exert antitumor activity and teratogenicity. *Nat. Med.* **22**, 735–743 (2016).
- Li, C. et al. TRIP13 modulates protein deubiquitination and accelerates tumor development and progression of B cell malignancies. *J. Clin. Invest.* **131**, e146893 (2021).
- Heuck, C. J. et al. Five gene probes carry most of the discriminatory power of the 70-gene risk model in multiple myeloma. *Leukemia* **28**, 2410–2413 (2014).
- Tao, Y. et al. TRIP13 impairs mitotic checkpoint surveillance and is associated with poor prognosis in multiple myeloma. *Oncotarget* **8**, 26718–26731 (2017).
- Sagawa, M. et al. Ribonucleotide reductase catalytic subunit M1 (RRM1) as a novel therapeutic target in multiple myeloma. *Clin. Cancer Res.* **23**, 5225–5237 (2017).
- Huang, X. et al. Prolonged early G1 arrest by selective CDK4/CDK6 inhibition sensitizes myeloma cells to cytotoxic killing through cell cycle-coupled loss of IRF4. *Blood* **120**, 1095–1106 (2012).
- Bellutti, F. et al. CDK6 antagonizes P53-induced responses during tumorigenesis. *Cancer Discov.* **8**, 884–897 (2018).
- Leone, P. E. et al. Deletions of CDKN2C in multiple myeloma: biological and clinical implications. *Clin. Cancer Res.* **14**, 6033–6041 (2008).
- Hu, M. G. et al. CDK6 kinase activity is required for thymocyte development. *Blood* **117**, 6120–6131 (2011).
- Baughn, L. B. et al. A novel orally active small molecule potently induces G1 arrest in primary myeloma cells and prevents tumor growth by specific inhibition of cyclin-dependent kinase 4/6. *Cancer Res.* **66**, 7661–7667 (2006).
- Fry, D. W. et al. Specific inhibition of cyclin-dependent kinase 4/6 by PD 0332991 and associated antitumor activity in human tumor xenografts. *Mol. Cancer Ther.* **3**, 1427–1437 (2004).
- Chen, N., Zhou, S. & Palmisano, M. Clinical Pharmacokinetics and Pharmacodynamics of Lenalidomide. *Clin. Pharmacokinet.* **56**, 139–152 (2017).

39. Burslem, G. M. & Crews, C. M. Proteolysis-targeting chimeras as therapeutics and tools for biological discovery. *Cell* **181**, 102–114 (2020).
40. Brand, M. et al. Homolog-selective degradation as a strategy to probe the function of CDK6 in AML. *Cell Chem. Biol.* **26**, 300–306.e9 (2019).
41. Steinebach, C. et al. Systematic exploration of different E3 ubiquitin ligases: an approach towards potent and selective CDK6 degraders. *Chem. Sci.* **11**, 3474–3486 (2020).
42. Connell-Crowley, L., Harper, J. W. & Goodrich, D. W. Cyclin D1/Cdk4 regulates retinoblastoma protein-mediated cell cycle arrest by site-specific phosphorylation. *Mol. Biol. Cell* **8**, 287–301 (1997).
43. Finn, R. S. et al. PD 0332991, a selective cyclin D kinase 4/6 inhibitor, preferentially inhibits proliferation of luminal estrogen receptor-positive human breast cancer cell lines in vitro. *Breast Cancer Res.* **11**, 1–13 (2009).
44. Dempster, J. M. et al. Extracting biological insights from the project achilles genome-scale CRISPR screens in cancer cell lines. *bioRxiv* <https://doi.org/10.1101/720243> (2019).
45. Blanchet, E. et al. E2F transcription factor-1 regulates oxidative metabolism. *Nat. Cell Biol.* **13**, 1146–1154 (2011).
46. Kollmann, K. et al. A kinase-independent function of CDK6 links the cell cycle to tumor angiogenesis. *Cancer Cell* **24**, 167–181 (2013).
47. Anders, L. et al. A systematic screen for CDK4/6 substrates links FOXM1 phosphorylation to senescence suppression in cancer cells. *Cancer Cell* **20**, 620–634 (2011).
48. Marine, J. C., Dawson, S. J. & Dawson, M. A. Non-genetic mechanisms of therapeutic resistance in cancer. *Nat. Rev. Cancer* **20**, 743–756 (2020).
49. Janker, L. et al. Metabolic, anti-apoptotic and immune evasion strategies of primary human myeloma cells indicate adaptations to hypoxia. *Mol. Cell. Proteom.* **18**, 936–953 (2019).
50. Mohamed, A. et al. Concurrent lipidomics and proteomics on malignant plasma cells from multiple myeloma patients: probing the lipid metabolome. *PLoS ONE* **15**, 1–16 (2020).
51. Nusinow, D. P. et al. Quantitative proteomics of the cancer cell line encyclopedia. *Cell* **180**, 387–402.e16 (2020).
52. Tyanova, S. et al. Proteomic maps of breast cancer subtypes. *Nat. Commun.* **7**, 1–11 (2016).
53. Alfieri, C., Chang, L. & Barford, D. Mechanism for remodelling of the cell cycle checkpoint protein MAD2 by the ATPase TRIP13. *Nature* **559**, 274–278 (2018).
54. Wang, Y. et al. A small-molecule inhibitor targeting TRIP13 suppresses multiple myeloma progression. *Cancer Res.* **80**, 536–548 (2020).
55. Niida, H. et al. Essential role of Tip60-dependent recruitment of ribonucleotide reductase at DNA damage sites in DNA repair during G1 phase. *Genes Dev.* **24**, 333–338 (2010).
56. Kato, J., Matsushime, H., Hiebert, S. W., Ewen, M. E. & Sherr, C. J. Direct binding of cyclin D to the retinoblastoma gene product (pRb) and pRb phosphorylation by the cyclin D-dependent kinase CDK4. *Genes Dev.* **7**, 331–342 (1993).
57. Ewen, M. E. et al. Functional interactions of the retinoblastoma protein with mammalian D-type cyclins. *Cell* **73**, 487–497 (1993).
58. Dowdy, S. F. et al. Physical interaction of the retinoblastoma protein with human D cyclins. *Cell* **73**, 499–511 (1993).
59. Ely, S. et al. Mutually exclusive cyclin-dependent kinase 4/cyclin D1 and cyclin-dependent kinase 6/cyclin D2 pairing inactivates retinoblastoma protein and promotes cell cycle dysregulation in multiple myeloma. *Cancer Res.* **65**, 11345–11353 (2005).
60. De Dominicis, M. et al. Selective inhibition of Ph-positive ALL cell growth through kinase-dependent and -independent effects by CDK6-specific PROTACs. *Blood* **135**, 1560–1573 (2020).
61. Placke, T. et al. Requirement for CDK6 in MLL-rearranged acute myeloid leukemia. *Blood* **124**, 13–23 (2014).
62. Martinez-Soria, N. et al. The oncogenic transcription factor RUNX1/ETO corrupts cell cycle regulation to drive leukemic transformation. *Cancer Cell* **34**, 626–642.e8 (2018).
63. Niesvizky, R. et al. Phase 1/2 study of cyclin-dependent kinase (CDK)4/6 inhibitor palbociclib (PD-0332991) with bortezomib and dexamethasone in relapsed/refractory multiple myeloma. *Leuk. Lymphoma* **56**, 3320–3328 (2015).
64. Petrylak, D. P. et al. First-in-human phase I study of ARV-110, an androgen receptor (AR) PROTAC degrader in patients (pts) with metastatic castrate-resistant prostate cancer (mCRPC) following enzalutamide (ENZ) and/or abiraterone (ABI). American Society of Clinical Oncology. 2020;Abstract:
65. Mertins, P. et al. Integrated proteomic analysis of post-translational modifications by serial enrichment. *Nat. Methods* **10**, 634–637 (2013).
66. Cox, J. & Mann, M. MaxQuant enables high peptide identification rates, individualized p.p.b.-range mass accuracies and proteome-wide protein quantification. *Nat. Biotechnol.* **26**, 1367–1372 (2008).
67. Udeshi, N. D. et al. Rapid and deep-scale ubiquitylation profiling for biology and translational research. *Nat. Commun.* **11**, 359 (2020).
68. Ritchie, M. E. et al. Limma powers differential expression analyses for RNA-seq and microarray studies. *Nucleic Acids Res.* **43**, e47 (2015).
69. Hornbeck, P. V. et al. PhosphoSitePlus, 2014: mutations, PTMs and recalibrations. *Nucleic Acids Res.* **43**, D512–D520 (2015).
70. Perez-Riverol, Y. et al. The PRIDE database and related tools and resources in 2019: improving support for quantification data. *Nucleic Acids Res.* **47**, D442–D450 (2019).
71. Dobin, A. et al. STAR: ultrafast universal RNA-seq aligner. *Bioinformatics* **29**, 15–21 (2013).
72. Subramanian, A. et al. Gene set enrichment analysis: a knowledge-based approach for interpreting genome-wide expression profiles. *Tien Tzu Hsueh Pao/Acta Electron. Sin.* **102**, 15545–15550 (2005).
73. Ross, F. M. et al. Report from the European myeloma network on interphase FISH in multiple myeloma and related disorders. *Haematologica* **97**, 1272–1277 (2012).
74. Heckl, D. et al. Generation of mouse models of myeloid malignancy with combinatorial genetic lesions using CRISPR-Cas9 genome editing. *Nat. Biotechnol.* **32**, 941–946 (2014).
75. Ianevski, A., Giri, A. K. & Aittokallio, T. SynergyFinder 2.0: visual analytics of multi-drug combination synergies. *Nucleic Acids Res.* **48**, W488–W493 (2020).

### Acknowledgements

This study was supported by the Deutsche Forschungsgemeinschaft (DFG) Emmy-Noether Program Kr3886/2-1 and 2-2 to J.K. and by the German Ministry of Education and Research (BMBF), as part of the National Research Node “Mass spectrometry in Systems Medicine” (MSCorSys), under grant agreement 031I0220B to P.M. Y.L.D.N. is enrolled in the doctoral program of the Berlin School of Integrative Oncology (BSIO). S.R.B. is a DFG research scholar (St5303/1-1). U.K. was supported by Deutsche Krebshilfe grants #70114425 and #111944.

### Author contributions

Contribution: J.K. and P.M. designed the study; Y.L.D.N., E.R., S.B., A.D., S.M., O.P. and M.H. performed experiments; S.B. and M.K. collected patient material; C.S. synthesized compounds; T.C. and W.W. performed and statistically analyzed mouse experiments; Y.L.D.N., E.R., S.B., A.D., C.S., S.M., O.P., M.H., M.G., H.D., L.B., U.K., P.M. and J.K. analyzed and interpreted data; Y.L.D.N., E.R., P.M. and J.K. wrote the manuscript. All authors have read and approved the manuscript.

### Funding

Open Access funding enabled and organized by Projekt DEAL.

### Competing interests

J.K. has received fees for advisory boards from BMS, Takeda, and Janssen. All other authors declare no competing interests.

### Additional information

**Supplementary information** The online version contains supplementary material available at <https://doi.org/10.1038/s41467-022-28515-1>.

**Correspondence** and requests for materials should be addressed to Philipp Mertins or Jan Krönke.

**Peer review information** *Nature Communications* thanks Georg Winter and the other, anonymous, reviewer(s) for their contribution to the peer review of this work. Peer reviewer reports are available.

**Reprints and permission information** is available at <http://www.nature.com/reprints>

**Publisher's note** Springer Nature remains neutral with regard to jurisdictional claims in published maps and institutional affiliations.



**Open Access** This article is licensed under a Creative Commons Attribution 4.0 International License, which permits use, sharing, adaptation, distribution and reproduction in any medium or format, as long as you give appropriate credit to the original author(s) and the source, provide a link to the Creative Commons license, and indicate if changes were made. The images or other third party material in this article are included in the article's Creative Commons license, unless indicated otherwise in a credit line to the material. If material is not included in the article's Creative Commons license and your intended use is not permitted by statutory regulation or exceeds the permitted use, you will need to obtain permission directly from the copyright holder. To view a copy of this license, visit <http://creativecommons.org/licenses/by/4.0/>.

© The Author(s) 2022



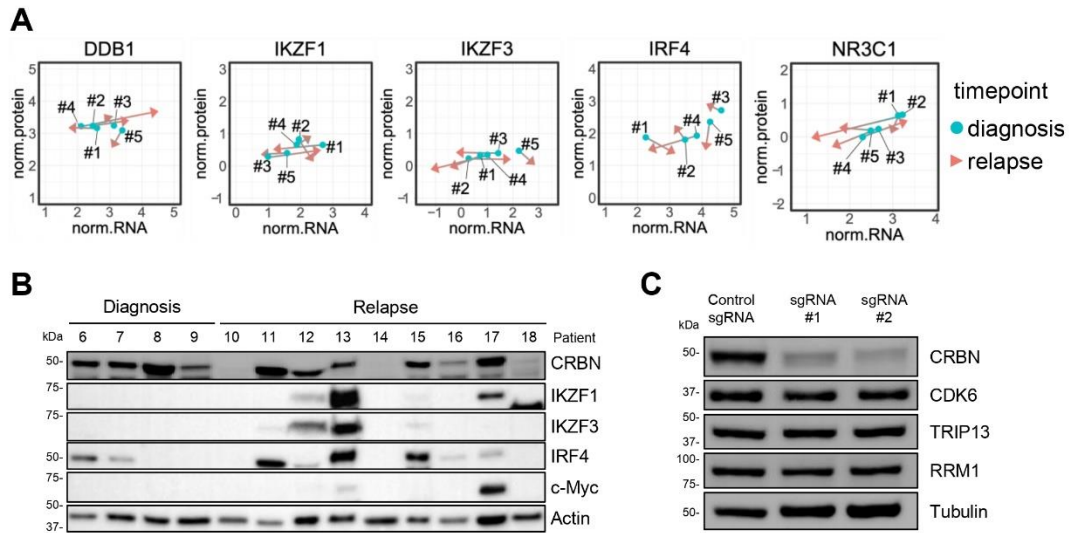
## Supplementary Figure 1

Analysis	Patient #	Sample Time point	Ig-Type	FISH Diagnosis	Treatment	Time between samples (months)	FISH Relapse
Proteomics, RNA seq, WES ID #16	1	Diagnosis + Relapse	IgA lambda	t(14;16), +17p13, penta 1q21, +1p32, tetra 9q34	Len / Dex	28	t(14;16), +17p13, tetra 1q21, +1p32, +9q34, del13q14
Proteomics, RNA seq	2	Diagnosis + Relapse	IgG kappa	+9q34, +1q21	Len / Dox / Dex HD-Mel+ Auto-SCT Len maintenance	24	+9q34, tetra 1q21
Proteomics, RNA seq, WES ID #14	3	Diagnosis + Relapse	kappa	t(11;14)	Len / Dex/ HD-Mel+ Auto-SCT Len maintenance	19	t(11;14), +1q21
Proteomics, RNA seq, WES ID #9	4	Diagnosis + Relapse	lambda	t(11;14)	Len / Dex	33	t(11;14)
Proteomics, RNA seq, WES ID #1	5	Diagnosis+ Relapse	IgA kappa	t(4;14), +1q21, del13q14	Mel / Pred Len / Dex Bort / Dex Pom / Dex/ HD-Mel+ Auto-SCT	46	t(4;14), +1q21, del13q14
Immunoblot	6	Diagnosis	lambda	t(4;14), +1q21, del13q			
Immunoblot	7	Diagnosis	IgG lambda	t(4;14), del 13q			
Immunoblot	8	Diagnosis	lambda	t(11;14)			
Immunoblot	9	Diagnosis	kappa	t(11;14), del17p13, del13q14			
Immunoblot	10	Relapse	IgG lambda		B/ HD-Mel+ Auto-SCT/ DRD		t(4;14), del13q14, +1q21
Immunoblot	11	Relapse	IgA kappa		BCD/ HD-Mel+auto Len / Dex		+9q34.2, +1q21, +17p13.1
Immunoblot	12	Relapse	IgA kappa		Carf / Mel / Pred Len / Pred		+9q34
Immunoblot	13	Relapse of #8	lambda		BCD/ HD-Mel+ Auto-SCT Len / Dex Carf / Dex/ HD-Mel+ Auto-SCT Len / Bort / Dex Dara Pom / Dex		t(11;14)
Immunoblot	14	Relapse	IgA lambda		Len / Bort / Dex 2x HD-Mel+ Auto-SCT		t(14;16), tetra 1q, del13q,
Immunoblot	15	Relapse of #7	IgG lambda		ID/ 2x HD-Mel+ Auto-SCT		t(4;14), del 13q
Immunoblot	16	Relapse	IgG lambda		BCD/ 2x HD-Mel+ Auto-SCT/B DRD		t(4;14), +1q21, del13q,
Immunoblot	17	Relapse	IgA lambda		Bort / Thal / Dex / Cis / Dox / CP / E		tetra 1q21, +13q14, del17p, t(14;16)
Immunoblot	18	Relapse	IgG lambda		BCD/ HD-Mel+ Auto-SCT/B Len maintenance Vor / Dex / Dara		+9q34

BCD= bortezomib/ cyclophosphamide/ dexamethasone; Bort = bortezomib; Carf = carfilzomib; Cis = cisplatin; CP = cyclophosphamide; Dara = daratumumab; Dex = dexamethasone; Dox = doxorubicin; DRD= daratumumab/ lenalidomide/ dexamethasone; E = etoposide; HD-Mel+ Auto-SCT = High dose melphalan with autologous stem cell transplantation; ID = idarubicine/ dexamethasone; Len = lenalidomide; Mel = melphalan; Pom = pomalidomide; Pred = prednisone; Thal = thalidomide; Vor = Vorinostat.

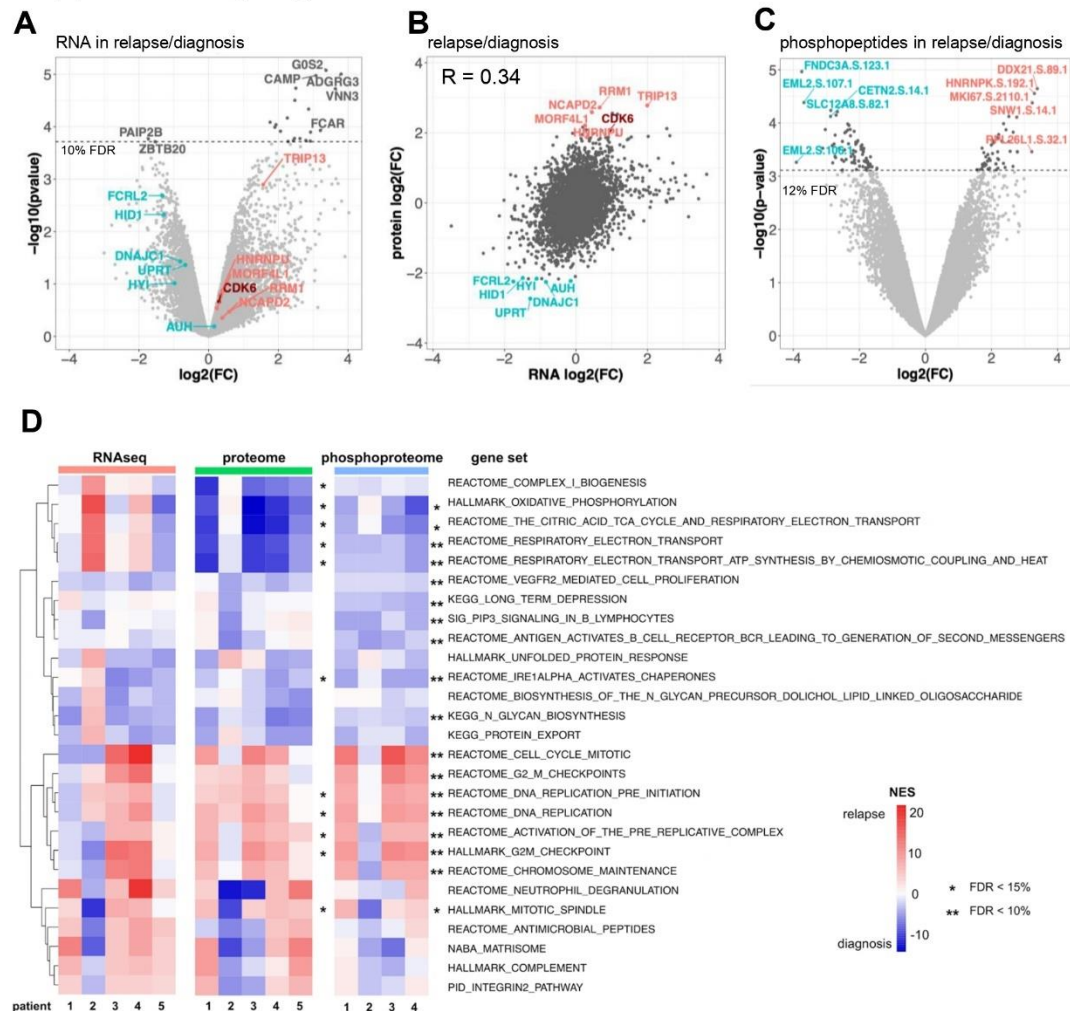
Supplementary Figure 1. Patient characteristics. WES ID is referenced to Bohl *et al.* 2021.

## Supplementary Figure 2



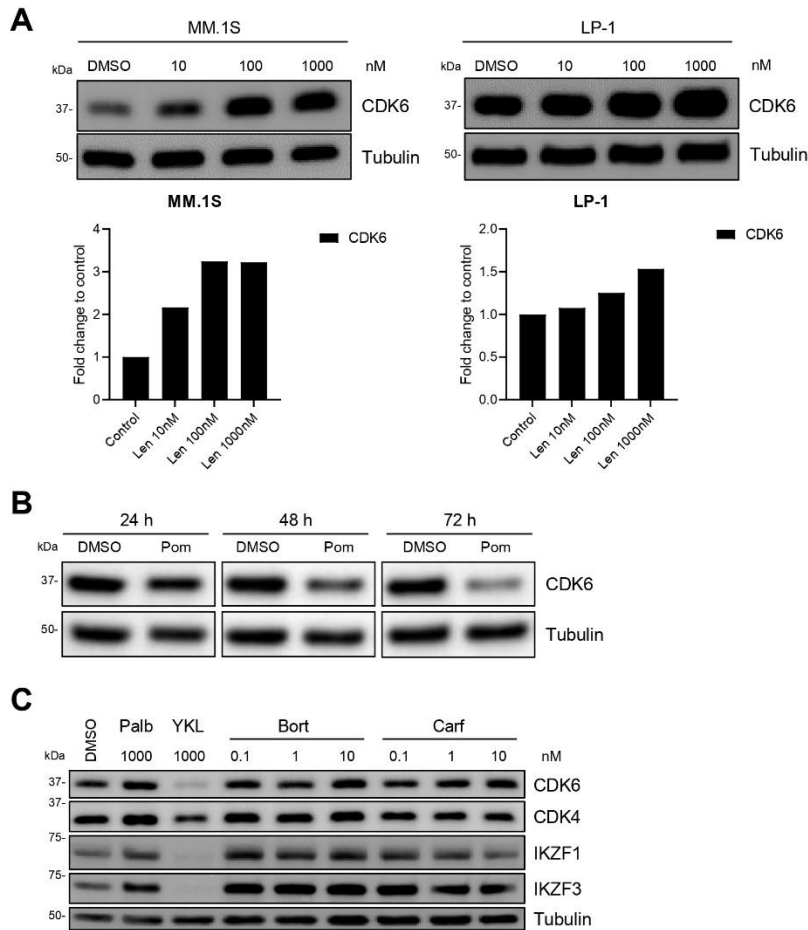
**Supplementary Figure 2. Protein and RNA expression levels of proteins involved in the mechanism of thalidomide analogs in multiple myeloma. (A)** Median normalized protein intensities (log<sub>2</sub> TMT intensities) of DDB1, IKZF1, IKZF3, IRF4 and NR3C1 in all 10 samples were plotted against their respective normalized RNA expression levels (log<sub>2</sub> TPM values). Samples from the same patient are connected. **(B)** Western blot of additional patient cohort for expression of IMiD-related proteins. (N=13 patient samples) **(C)** CRISPR/Cas9-mediated knockout of CRBN and protein levels of CDK6, TRIP13, and RRM1 detected by western blot. (N=3 biologically independent replicates)

## Supplementary Figure 3



**Supplementary Figure 3. RNA sequencing, phosphoproteomic analysis, and top deregulated gene signatures in paired multiple myeloma patient samples.** (A) RNA expression changes at relapse/diagnosis were determined for each patient and analyzed with a two-sided moderated 1-sample t-test. Average  $\log_2$ (fold change) of each transcript is plotted against its  $-\log_{10}(\text{p-value})$ . The corresponding transcripts of the 6 most up and down regulated proteins are highlighted in color. (B) Correlation of average fold changes ( $\log_2(\text{FC})$ ) of protein and RNA expression levels. (C) Phosphopeptide abundance level changes at relapse/diagnosis were determined for each patient and analyzed with a two-sided moderated 1-sample t-test. Average  $\log_2$ (fold change) of each phosphopeptide is plotted against its  $-\log_{10}(\text{p-value})$ . (D) Single sample gene set enrichment analysis (ssGSEA) of relapse/diagnosis ratios in each patient. Heatmap displays the normalized enrichment scores (NES) of the most regulated gene sets in RNAseq, global proteome and phosphoproteome datasets for each patient. Significance of terms in each dataset is indicated with stars. Significance was determined with a one-sample moderated t-test.

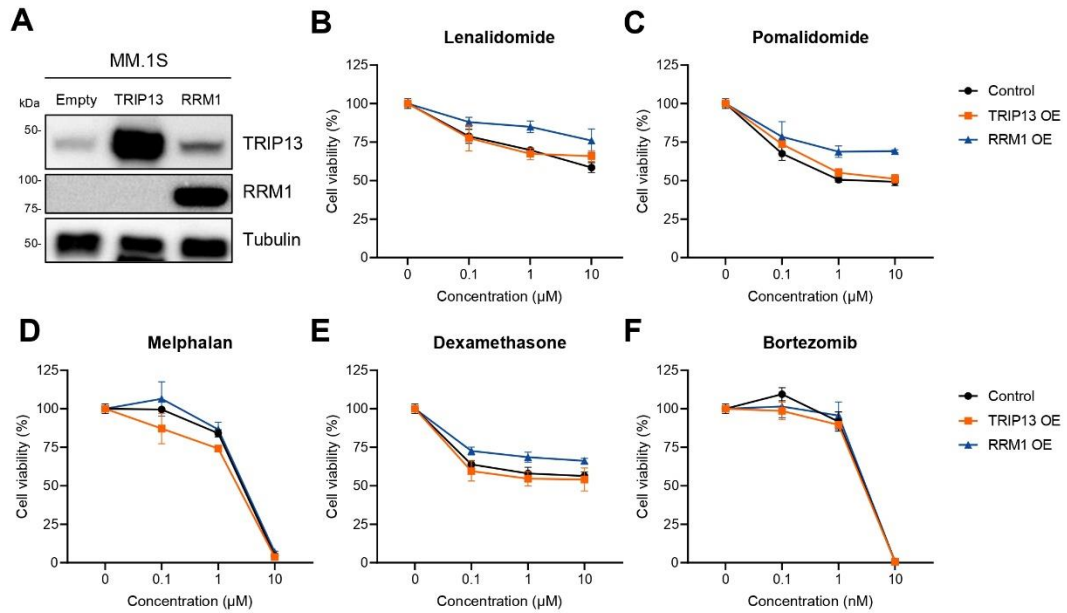
## Supplementary Figure 4



**Supplementary Figure 4. CDK6 protein levels in multiple myeloma cells treated with IMiDs and proteasome inhibitors.** Multiple myeloma cells MM.1S and LP-1 were cultured in the presence of respective concentrations of lenalidomide (len) to induce drug-resistance. (A) CDK6 protein levels of lenalidomide-resistant (lenR) cells and respective quantification. CDK6 protein levels were normalized to respective loading controls and to treatment control. (B) Treatment of MM.1S cells with 1 μM of pomalidomide (pom) for 24, 48, or 72 h. (C) Treatment of MM.1S with palbociclib (palb), YKL-06-102 (YKL), and proteasome inhibitors bortezomib (bort) and carfilzomib (carf) at respective concentrations for 4 h. (N=3 biologically independent replicates)

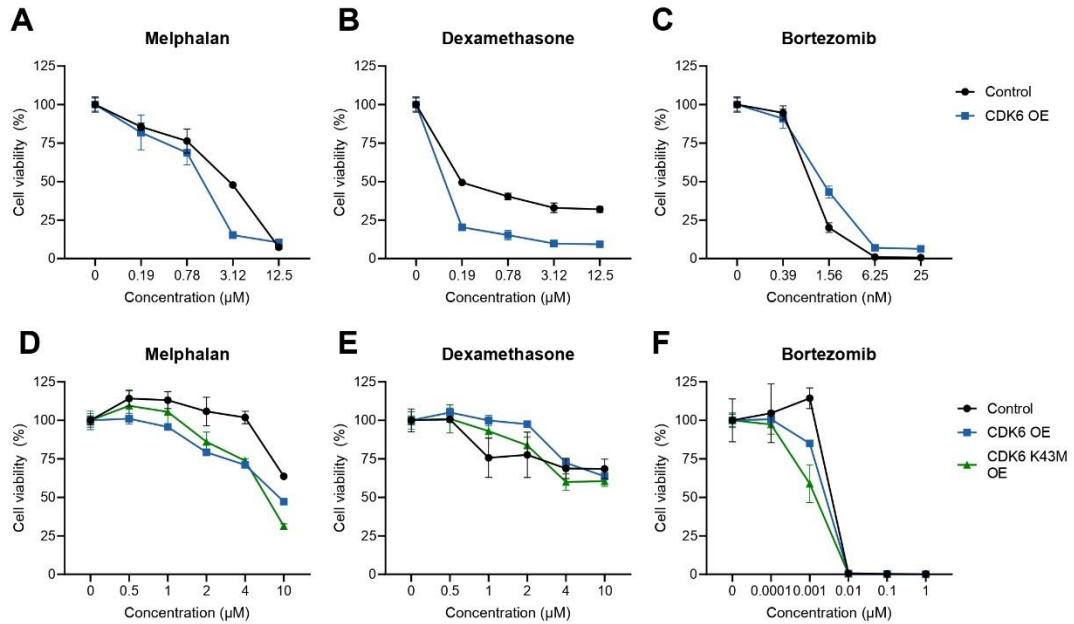


## Supplementary Figure 5



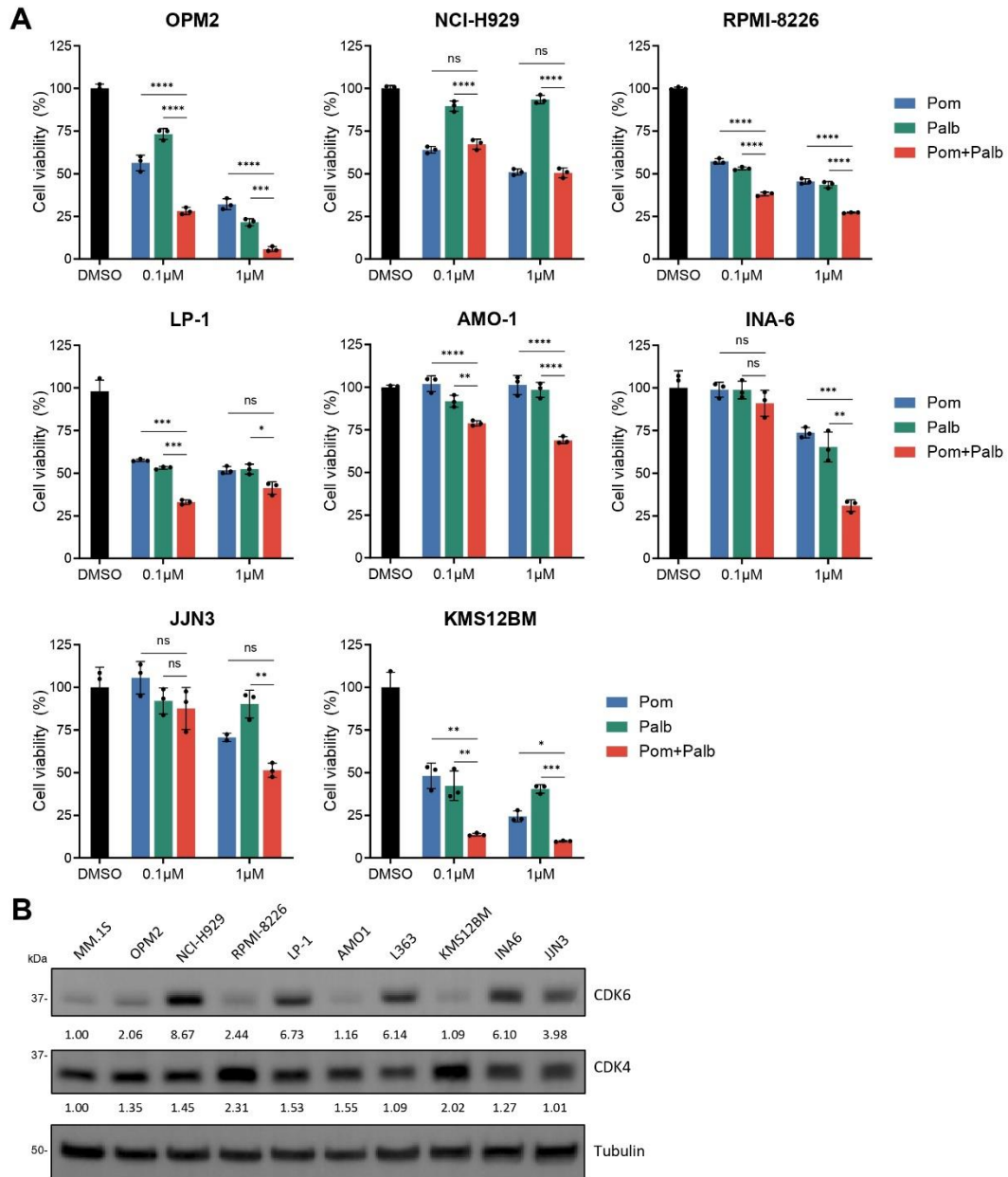
**Supplementary Figure 5. Effects of elevated TRIP13 or RRM1 protein expression on cell viability in response to multiple myeloma therapies.** (A) Overexpression of TRIP13 and RRM1 in MM.1S cells using retroviral transduction confirmed through western blot analysis. (B) Cell viability of RRM1- and TRIP13-overexpressing MM.1S cells after subjected to 96 h treatment with lenalidomide, (C) pomalidomide, (D) melphalan, (E) dexamethasone, and (F) bortezomib. (N=3 biologically independent replicates) Control denotes empty vector. Cell viability is normalized to respective DMSO conditions. Data represent the mean  $\pm$ SD of biological triplicates.

## Supplementary Figure 6



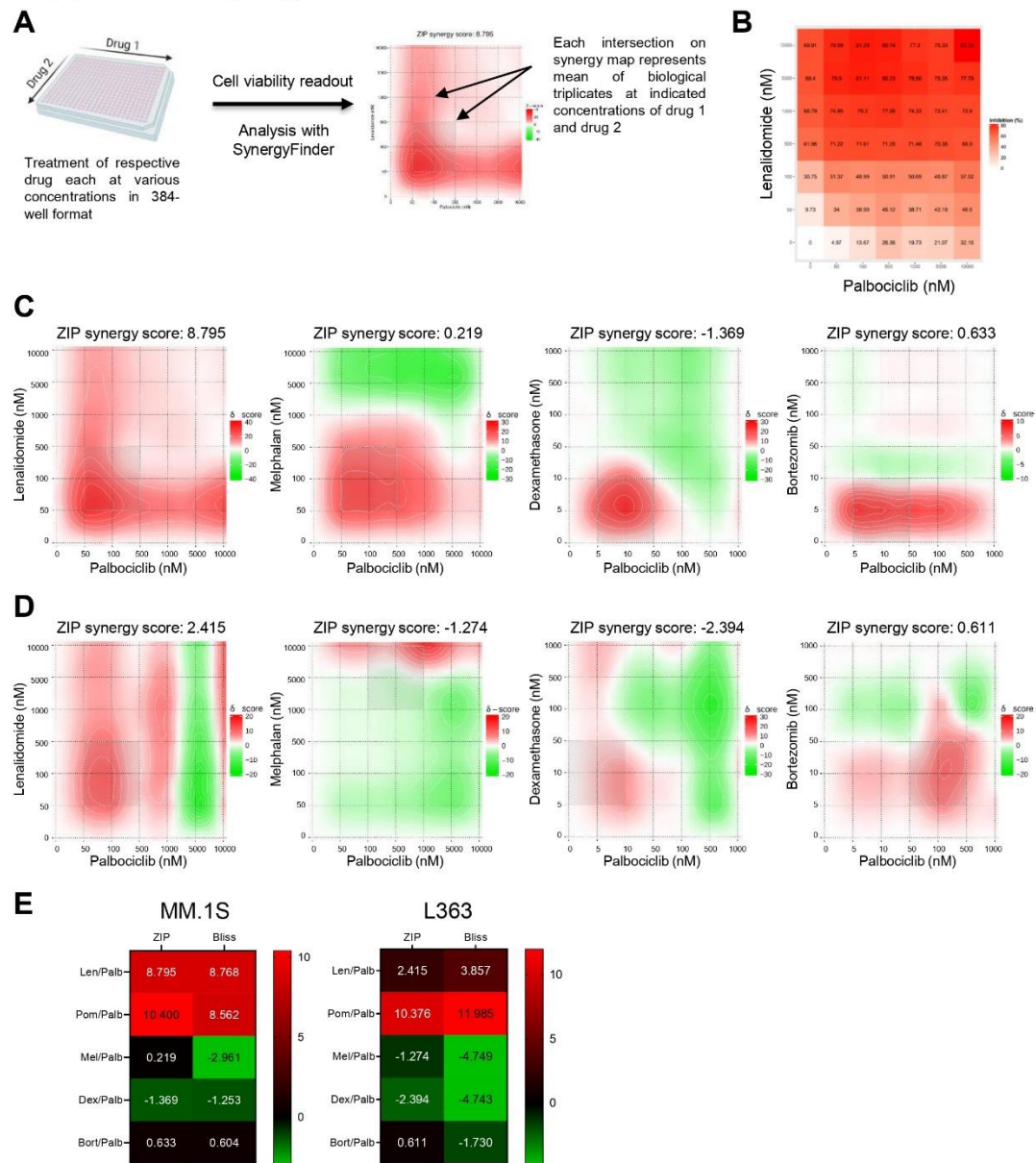
**Supplementary Figure 6. Effects of CDK6 overexpression in response to multiple myeloma therapies.** (A-C) Cell viability of 96 h treatment with melphalan, dexamethasone and bortezomib in MM.1S cells overexpressing CDK6 WT and in (D-F) OPM2 cells overexpressing CDK6 WT and CDK6 K43M mutant. (N=3 biologically independent replicates) Control denotes empty vector. Cell viability is normalized to respective DMSO conditions. Data represent the mean  $\pm$ SD of biological triplicates.

## Supplementary Figure 7



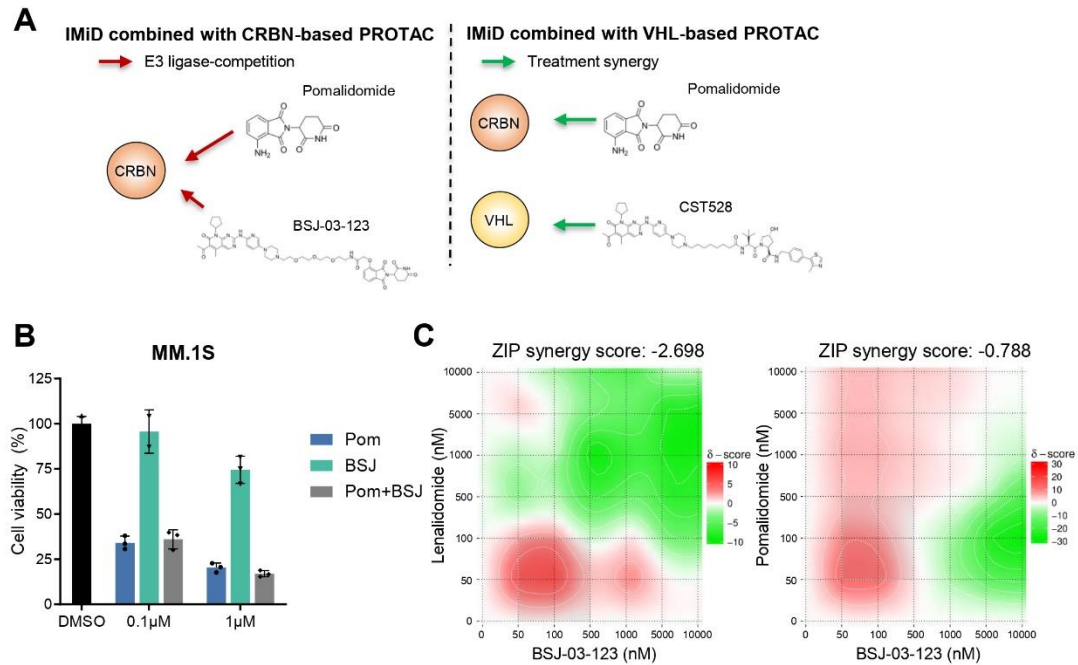
**Supplementary Figure 7. CDK6 inhibition by palbociclib sensitizes multiple myeloma cells to IMiDs.** (A) Cell viability of IMiD-sensitive and -resistant multiple myeloma cell lines when treated for 96 h with pomalidomide (pom), palbociclib (palb), and in combination (pom+palb). (N=3 biologically independent replicates) (B) Endogenous levels of CDK6 across all multiple myeloma cell lines. Cell viability is normalized to respective DMSO conditions. Data represent the mean  $\pm$ SD of biological triplicates. One-way ANOVA is applied. P values are displayed as follows: n.s. =  $P > 0.05$ ; \* =  $P \leq 0.05$ ; \*\* =  $P \leq 0.01$ ; \*\*\* =  $P \leq 0.001$ ; \*\*\*\* =  $P \leq 0.0001$ . Quantification of CDK6 and CDK4 is normalized to tubulin and to MM.1S.

## Supplementary Figure 8



**Supplementary Figure 8. Drug synergy analyses of palbociclib with multiple myeloma drug treatments.** (A) Workflow for obtaining synergy plots. (B) MM.1S cell viability upon combination treatment of palbociclib with lenalidomide. (C) Synergy plots of 96 h treatment of palbociclib in combination with lenalidomide, melphalan, dexamethasone, and bortezomib in MM.1S and (D) L363 cells. (E) Heatmap of synergy scores of combination treatments with palbociclib. Synergy plots, ZIP score and Bliss score calculations were generated and performed with SynergyFinder.<sup>75</sup> Data is normalized to respective DMSO conditions and represent the mean of biological triplicates.

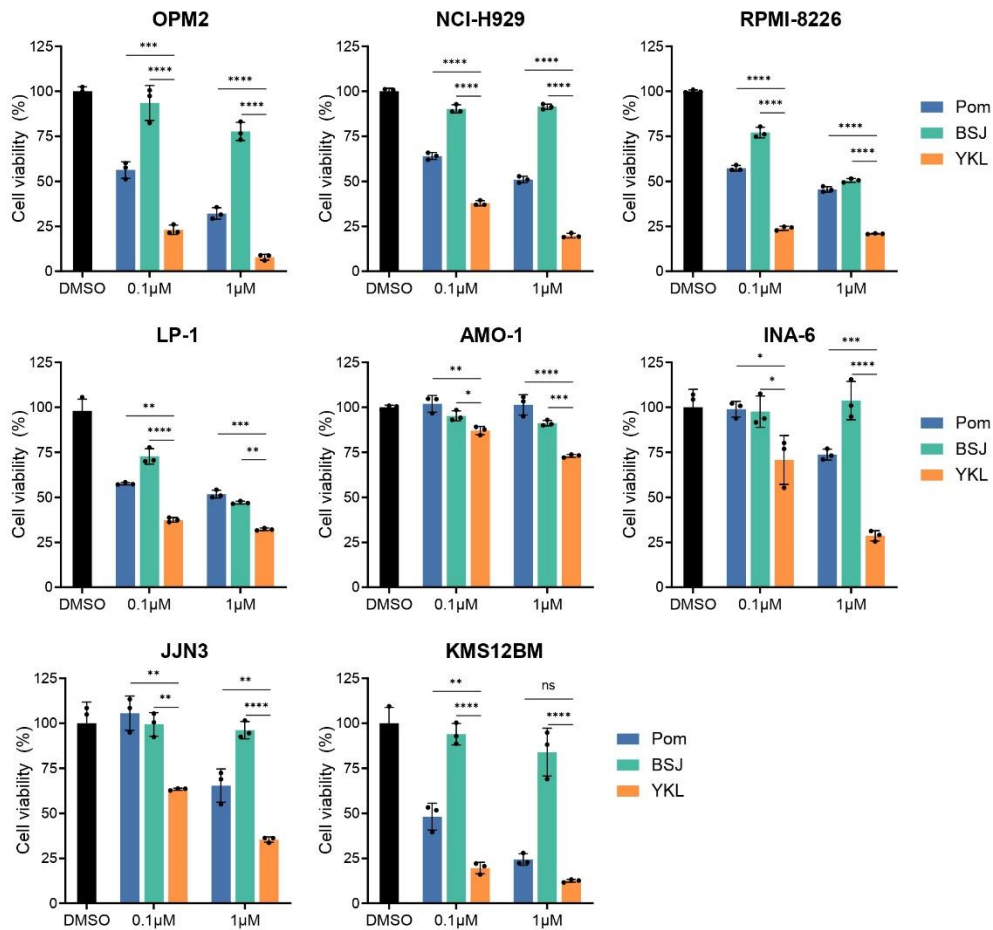
## Supplementary Figure 9



**Supplementary Figure 9. Overcoming antagonism by CRBN-based PROTACs with VHL-based CDK6 PROTAC.** (A) Schematic diagram of E3 ligase competition upon combination treatment of IMiD with CRBN-based PROTAC versus synergistic treatment with VHL-based PROTAC. (B) Cell viability of MM.1S after 96 h treatment of pomalidomide (pom), BSJ-03-123 (BSJ), or in combination (pom+BSJ). (N=3 biologically independent replicates) (C) Synergy map of MM.1S cells treated with BSJ-03-123 in combination with lenalidomide and pomalidomide. Synergy levels are indicated with ZIP synergy scores. Synergy maps were generated with SynergyFinder.<sup>75</sup> Viability data represent the mean  $\pm$ SD of biological triplicates. Synergy data represent the mean of biological triplicates.

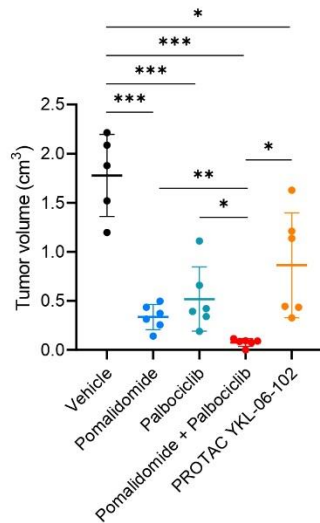


## Supplementary Figure 10



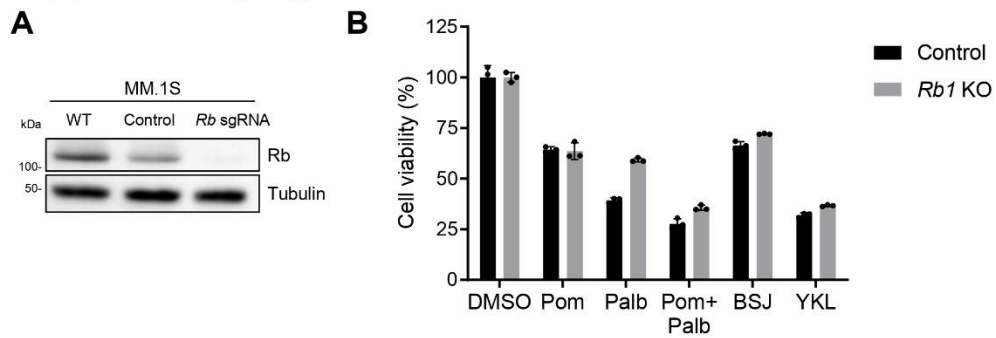
**Supplementary Figure 10. YKL-06-102 shows high level of intramolecule synergism via CDK6, IKZF1, and IKZF3 degradation.** Cell viability of IMiD-sensitive and -resistant multiple myeloma cell lines after 96 h treatment with pomalidomide (pom), BSJ-03-123 (BSJ), and YKL-06-102 (YKL). (N=3 biologically independent replicates) Cell viability is normalized to respective DMSO conditions. Data represent the mean  $\pm$ SD of biological triplicates. One-way ANOVA is applied. P values are displayed as follows: n.s. =  $P > 0.05$ ; \* =  $P \leq 0.05$ ; \*\* =  $P \leq 0.01$ ; \*\*\* =  $P \leq 0.001$ ; \*\*\*\* =  $P \leq 0.0001$ .

## Supplementary Figure 11



**Supplementary Figure 11. *In vivo* effects of pomalidomide, CDK6 inhibition and CDK6/IKZF1/IKZF3-targeting PROTAC.** Tumor size on day 9. Differences in tumor volumes were analyzed by unpaired t-tests with Welch's correction. Data represent the mean  $\pm$ SD of biological replicates. Group size: n=5 for vehicle group; n=6 for pomalidomide treatment group; n=6 for palbociclib treatment group; n=6 for pomalidomide + palbociclib treatment group; n=6 for YKL-06-102 treatment group. P values are displayed as follows: \* =  $P \leq 0.05$ ; \*\* =  $P \leq 0.01$ ; \*\*\* =  $P \leq 0.001$ .

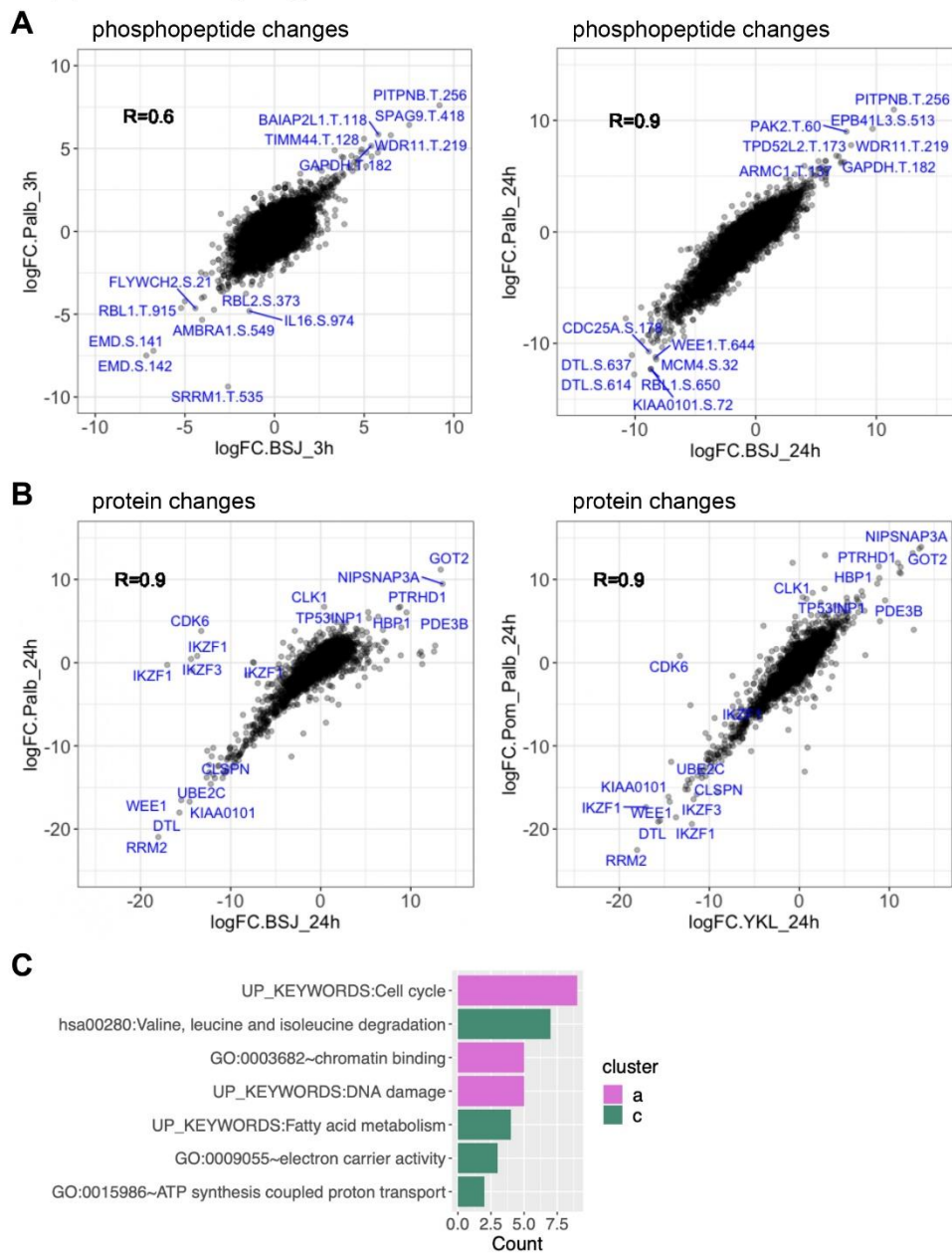
## Supplementary Figure 12



**Supplementary Figure 12. Combination treatment is independent of *Rb1*.** (A) Western blot analysis for confirmation of CRISPR/Cas9-mediated knockout of *Rb1* in MM.1S cells. (B) Cell viability of various single or combined treatments in MM.1S control or *Rb1* KO cells at 1  $\mu$ M each. Cells were treated for 96 h with pomalidomide (pom), palbociclib (palb), in combination (pom+palb), BSJ-03-123 (BSJ), and YKL-06-102 (YKL). (N=3 biologically independent replicates) Control denotes Cas9- cells transduced with luciferase sgRNA. Cell viability is normalized to respective DMSO conditions. Data represent the mean  $\pm$ SD of biological triplicates.

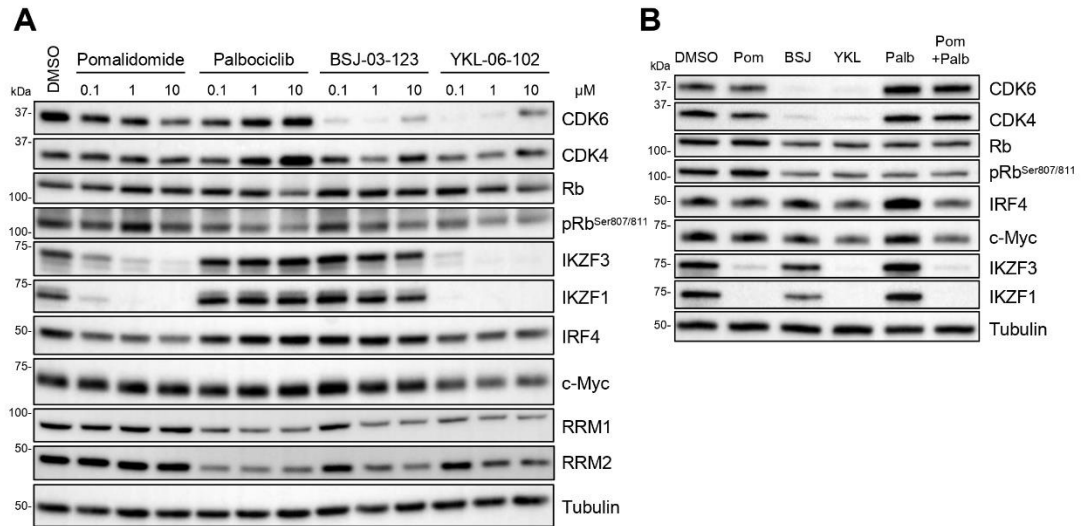


## Supplementary Figure 13



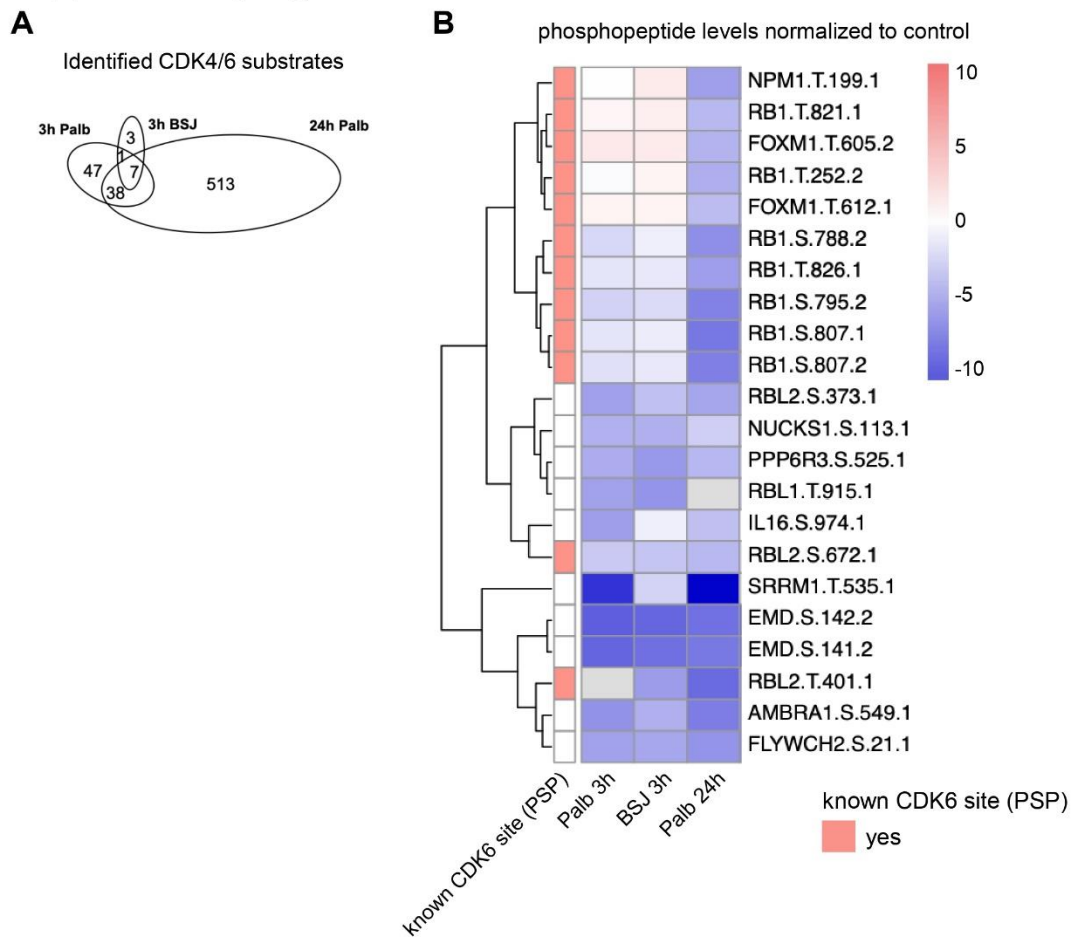
**Supplementary Figure 13. Correlation of CDK6 inhibition by palbociclib and CDK6 degradation by PROTACs.** MM.1S cells were treated for 3 h or 24 h as indicated. Dotplots show correlation of fold changes of (A) phosphopeptides or (B) proteins relative to control treated cells. (C) Representative GO annotation of proteins in cluster a and cluster c of Figure 6B. Pom = pomalidomide; Palb = palbociclib; BSJ = BSJ-03-123; YKL = YKL-06-102.

## Supplementary Figure 14



**Supplementary Figure 14. Protein analyses of multiple myeloma cells treated with pomalidomide, CDK6 inhibitors and PROTACs.** (A) Western blot analysis of OPM2 cells treated for 16 h with pomalidomide, palbociclib, BSJ-03-123, and YKL-06-102 at indicated concentrations. (N=3 biologically independent replicates) (B) Western blot analysis of MM.1S cells after subjected to respective drug treatments at 1 μM for 16 h. Cells were treated with pomalidomide (pom), palbociclib (palb), in combination (pom+palb), BSJ-03-123 (BSJ), and YKL-06-102 (YKL). (N=3 biologically independent replicates)

## Supplementary Figure 15



**Supplementary Figure 15. Phosphoproteomic analysis of drug-treated MM.1S cells identifies potential CDK4/6 substrates in multiple myeloma cells.** (A) Overlap of putative CDK4/6 substrates in MM.1S cells. (B) Fold change relative to control of most regulated phosphopeptides and known CDK6 targets from phosphosite plus (PSP). Palb = palbociclib; BSJ = BSJ-03-123.



# The proteogenomic landscape of multiple myeloma reveals insights into disease biology and therapeutic opportunities

Received: 21 December 2022

Accepted: 15 May 2024

Published online: 28 June 2024

Check for updates

A list of authors and their affiliations appears at the end of the paper

Multiple myeloma (MM) is a plasma cell malignancy of the bone marrow. Despite therapeutic advances, MM remains incurable, and better risk stratification as well as new therapies are therefore highly needed. The proteome of MM has not been systematically assessed before and holds the potential to uncover insight into disease biology and improved prognostication in addition to genetic and transcriptomic studies. Here we provide a comprehensive multiomics analysis including deep tandem mass tag-based quantitative global (phospho)proteomics, RNA sequencing, and nanopore DNA sequencing of 138 primary patient-derived plasma cell malignancies encompassing treatment-naïve MM, plasma cell leukemia and the premalignancy monoclonal gammopathy of undetermined significance, as well as healthy controls. We found that the (phospho) proteome of malignant plasma cells are highly deregulated as compared with healthy plasma cells and is both defined by chromosomal alterations as well as posttranscriptional regulation. A prognostic protein signature was identified that is associated with aggressive disease independent of established risk factors in MM. Integration with functional genetics and single-cell RNA sequencing revealed general and genetic subtype-specific deregulated proteins and pathways in plasma cell malignancies that include potential targets for (immuno)therapies. Our study demonstrates the potential of proteogenomics in cancer and provides an easily accessible resource for investigating protein regulation and new therapeutic approaches in MM.

Multiple myeloma (MM), the second most frequent hematologic malignancy, is characterized by expansion of monoclonal plasma cells in the bone marrow. Patients suffer from bone lesions, renal insufficiency, hypercalcemia and bone marrow failure<sup>1</sup>. The introduction of effective therapies including thalidomide analogs, proteasome inhibitors and immunotherapies such as chimeric antigen receptor (CAR)-T cells in the past decade substantially extended survival in MM. However, MM is still considered incurable and those patients with high-risk characteristics have a particularly poor outcome<sup>1</sup>.

Chromosomal alterations are the initiating step in the pathogenesis of MM that are already present in the premalignant stage of monoclonal gammopathy of undetermined significance (MGUS). Primary genetic events define the cytogenetic subgroups of MM<sup>2</sup> and are associated with a distinct gene expression profile<sup>3,4</sup>. Half of the patients exhibit translocations involving the immunoglobulin heavy chain (*IgH*) enhancer on chromosome 14, predominantly with oncogenes *CCND1* (t(11;14)), *NSD2* and *FGFR3* (t(4;14)) and *MAFB* (t(14;16)). Patients without these translocations typically have a hyperdiploid

✉ e-mail: [stefan.knop@klinikum-nuernberg.de](mailto:stefan.knop@klinikum-nuernberg.de); [philipp.mertins@mdc-berlin.de](mailto:philipp.mertins@mdc-berlin.de); [jan.kroenke@charite.de](mailto:jan.kroenke@charite.de)



(HRD) karyotype with trisomies primarily of the odd-numbered chromosomes. Secondary genetic events occur later in the pathogenesis of MM and include del(13q) comprising *RBI*, del(17p) comprising *TP53*, gain or amplification of chromosome 1q and mutations in *NRAS*, *KRAS*, *TP53*, *TENTSC* (*FAM46C*) and *DIS3* (refs. 5–7). Genetics together with blood protein levels of albumin, b2-microglobulin and lactate dehydrogenase are incorporated in the revised international staging system (R-ISS), the current standard for risk classification and therapy stratification in MM<sup>8</sup>.

Proteomics has recently emerged as a technology to study cancer biology, generate prognostic and predictive models and identify new therapeutic targets<sup>9</sup>. Proteogenomic studies integrating genomics and transcriptomics in solid tumors<sup>9–11</sup> and in hematologic malignancies<sup>12–14</sup> revealed low correlation between RNA and protein expression, demonstrating that inferring the activity of proteins merely based on studying RNA expression is limited. While many proteogenomic studies contribute to the general understanding of disease mechanisms, only a few of them have connected proteome alterations to clinical outcome<sup>10,12,15,16</sup>. For MM, a limited number of proteomic studies have been conducted in small cohorts<sup>17–21</sup>, while comprehensive proteogenomic studies that evaluate how the proteome is influenced by genetic alterations, disease stage and how protein expression impact outcomes, are currently missing. In this Resource, to address this gap, we performed an integrated multiomics study, including tandem isobaric mass tag (TMT)-based quantitative global- and phosphoproteomic analysis, RNA sequencing and whole-genome nanopore DNA sequencing to assess copy number alterations (CNAs) of 138 patients with plasma cell malignancies of different disease stages including MGUS, newly diagnosed multiple myeloma (NDMM) and plasma cell leukemia (PCL), a highly aggressive form of plasma cell dyscrasias.

## Results

### Proteomic landscape of newly diagnosed MM

To characterize the proteomic landscape of treatment-naive symptomatic MM we analyzed plasma cells isolated from 114 patients with NDMM (Fig. 1a and Supplementary Table 1). The frequency of primary and secondary chromosomal alterations, as assessed by fluorescence in situ hybridization (FISH) was distributed according to the described incidence in MM<sup>6</sup>. RNA sequencing (Supplementary Table 2) and nanopore whole-genome DNA sequencing (Supplementary Table 3) were conducted for the majority of samples to assess gene expression and CNAs, respectively, which largely aligned with the genetic alterations detected by FISH (Fig. 1b and Supplementary Table 3). Global proteome and phosphoproteome levels were quantified with TMT. The number of identified proteins and phosphopeptides across TMT plexes was comparable (Extended Data Fig. 1a) and in total, over 10,000 proteins and 50,000 phosphopeptides were identified, of which 8,336 proteins and 25,131 phosphopeptides were quantified in at least half of the samples (Fig. 1c). The phosphoproteomic data extended the number of detected proteins to 11,297 proteins (Fig. 1c and Extended Data Fig. 1b). Technical replicates showed a good correlation, and no batch effects of TMT plexes were observed (Extended Data Fig. 1c). Key plasma cell markers, including the transcription factor *IRF4*, surface proteins *CD38*, *TNFRSF17* (*BCMA*) and *SDC1* (*CD138*) and translocation partners *NSD2*,

*FGFR3* and *CCND1* were identified (Fig. 1c). Immunoglobulin heavy and light chain protein levels corresponded to clinical metadata (Extended Data Fig. 1d). Compensation effects of CNAs from RNA to protein levels were especially observed for ribosomal, spliceosome and proteasome proteins as well as proteins located on 1q (Extended Data Fig. 1e,f). RNA-to-protein correlation was moderate, with a median Pearson correlation coefficient of 0.29 (Fig. 1d) and proteins affected by translocations, as well as key cell surface proteins and transcription factors, displayed above-average correlation (Fig. 1d). Single sample gene set enrichment analysis (ssGSEA) of ranked RNA–protein correlations revealed enrichment of individual signaling pathways and negative enrichment of genes associated with splicing, proteasomal degradation and oxidative phosphorylation (Fig. 1e). These data imply extensive posttranscriptional regulation in MM. We observed varying levels of immune cell signatures as contaminants arising from differences in *CD138*<sup>+</sup> sorting status and efficiency, but these did not compromise the major distinctions we identified between the different genetic subgroups (Extended Data Fig. 1g,h). The *CD138*<sup>+</sup> cell enrichment procedure itself had no effect on the (phospho)proteome of malignant plasma cells as assessed in the myeloma cell line MM.1S (Extended Data Fig. 1i and Supplementary Tables 4 and 5).

Unsupervised nonnegative matrix factorization (NMF) clustering of phosphoproteomics-derived pathways (Extended Data Fig. 2a) identified a distinct subcluster of patients with lower survival probability (Extended Data Fig. 2b). This cluster was independent of genetic alterations and characterized by upregulation of proliferation and cell cycle signatures, alongside downregulation of *TNF- $\alpha$*  and *ERBB* signaling pathways (Extended Data Fig. 2c).

### Genetic alterations affect protein levels in *cis* and *trans*

Given the central role of chromosomal aberrations in disease initiation, biology and prognosis in MM, we determined the impact of common genetic alterations on the (phospho)proteome with differential expression analysis. Most translocations, HRD, +1q and del(13q), had a profound effect on the expression levels of proteins in *cis* and in *trans*. Less regulation was observed by t(14;16), del(1p) or del(17q) although this could in part be explained by the smaller sample numbers and thus reduced statistical power (Fig. 1f and Supplementary Tables 6 and 7). The most significant proteins and phosphopeptides in the genetic subtypes are IgH translocation partners and proteins encoded on chromosomes affected by CNAs (Fig. 1g). SsGSEA of global and phosphoproteomic data confirmed significant regulation of myeloma molecular subgroups previously defined by RNA expression studies<sup>3</sup> (Extended Data Fig. 2d).

In cases with t(11;14) cell cycle regulators were highly deregulated, including high expression of the translocation partner *CCND1*, increased *CDK4* protein levels and *RB1* phosphorylation, with concomitantly decreased *CDK6* protein levels (Fig. 2a,b). In non-t(11;14) cases, high *RB1* phosphorylation was instead associated with *CDK6* protein expression and/or high levels of *CCND2* and *CCND3* RNA and phosphoprotein (Fig. 2b). T(11;14) myeloma is the only genetic subgroup sensitive to venetoclax, a selective inhibitor of *BCL2* (ref. 22). Of note, we found 102 apoptosis-related proteins deregulated in t(11;14) myeloma, including downregulation of apoptosis inhibitor *BIRC2* and *BCL2L1* (*BCL-XL*) and upregulation of proapoptotic proteins such

**Fig. 1 | Proteogenomic landscape of newly diagnosed MM.** **a**, Overview of the proteogenomic study. **b**, A heat map of CNVs detected by nanopore sequencing in 109 cases of NDMM sorted by primary genetic subgroup: HRD, t(11;14), t(4;14) and t(14;16) translocations. Cytogenetic alterations, including deletions, amplifications and translocations were detected by FISH. **c**, Proteins and phosphopeptides detected by TMT-based mass spectrometry ranked by median intensity. **d**, Ranked gene symbol-wise Pearson correlation of mRNA–protein levels across MM samples ( $n = 8,511$  RNA–protein pairs with at least ten valid values in both datasets). **e**, ssGSEA of the mRNA–protein correlations for KEGG pathways ( $n = 165$  ranked pathways). Gene sets were ranked by their normalized

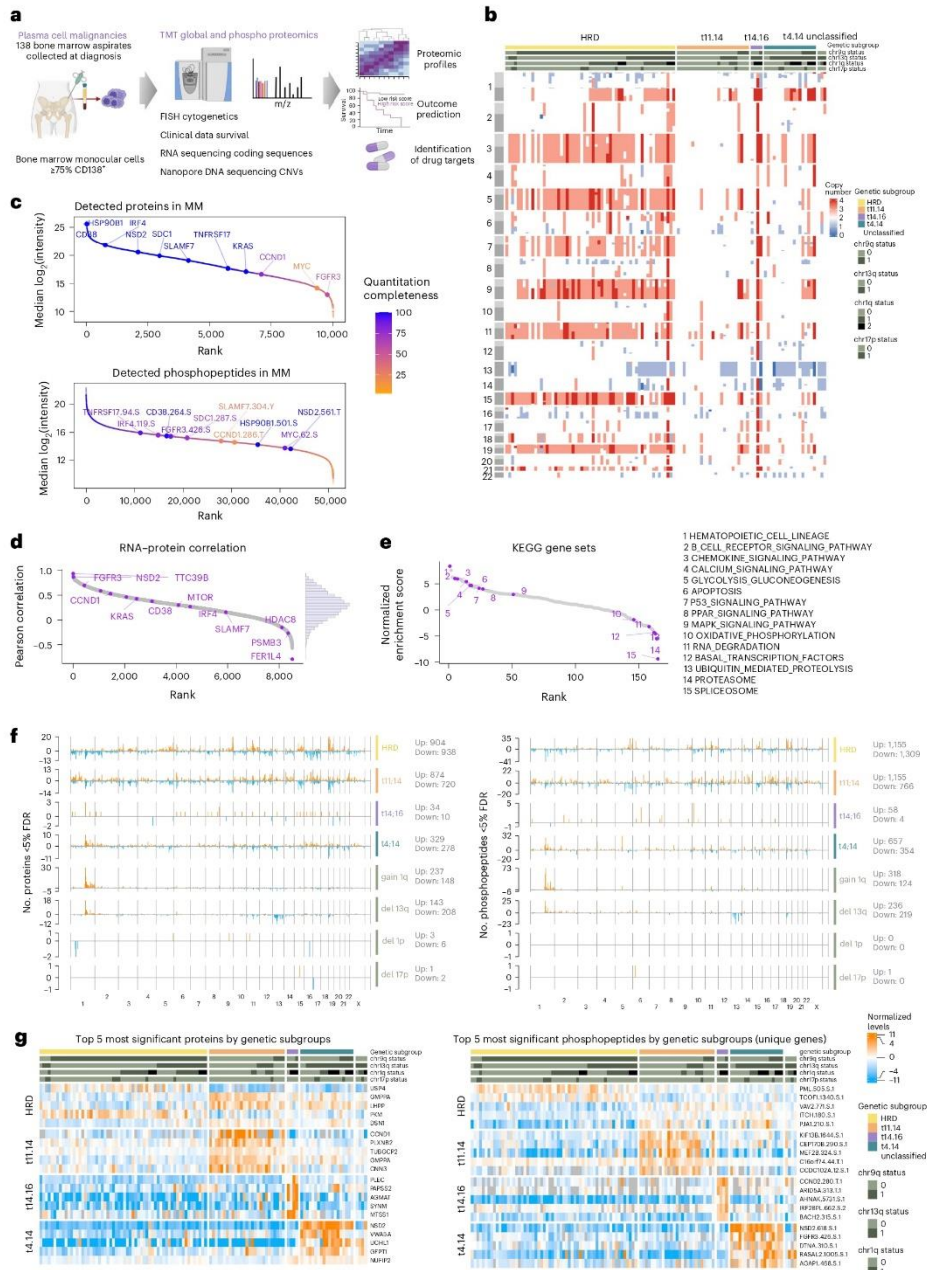
enrichment score and informative pathways are annotated with purple circles. **f**, Differentially regulated proteins (left) and phosphopeptides (right) in each cytogenetic subgroup were determined with a two-sided, moderated two-sample *t*-test comparing subsets of samples against all other samples. The number of significant hits (FDR < 0.05) in each group is plotted across genomic location. **g**, Heat maps displaying the five most significant proteins (left) and phosphopeptides (right) in each genetic subgroup across MM samples. For phosphopeptides mapping to the same protein, only the most significant entry is displayed. Phosphopeptides are annotated with gene name, position, amino acid and number of phosphorylations present.

Resource

<https://doi.org/10.1038/s43018-024-00784-3>

as TRADD and FADD (Fig. 2a and Extended Data Fig. 3a,b). We also detected elevated protein levels of several B cell markers and genes present in the myeloma CD2 gene set<sup>3</sup> (Extended Data Fig. 3c), which may also be linked to BCL2 dependency in t(11;14) myeloma<sup>3,23,24</sup>.

Translocation *t(4;14)* leads to integration of the *IgH* enhancer upstream of *NSD2* (*MMSET*) and *FGFR3* (Extended Data Fig. 3d). *NSD2* was selectively and strongly upregulated on RNA, protein and phosphoprotein levels in all t(4;14) patients (Fig. 2c,d). In contrast, *FGFR3*





## Resource

<https://doi.org/10.1038/s43018-024-00784-3>

was not uniformly expressed and could be detected only in 12/19 (63%) samples with t(4;14) (Fig. 2d and Extended Data Fig. 4e), consistent with RNA data (Extended Data Fig. 3f) and previous findings<sup>25–27</sup>. SsGSEA of phosphoproteomic data revealed upregulation of the FGFR3 signaling pathway in samples with elevated FGFR3 protein independent of t(4;14) status (Fig. 2e). FGFR3 protein expression highly correlated with dependency on FGFR3 while NSD2 knockout (KO) shows no effect on survival in MM cell lines (Fig. 2f)<sup>28,29</sup>. Accordingly, the FGFR inhibitor erdafitinib was highly effective in the t(4;14) positive/FGFR3 high cell line OPM2, but ineffective in FGFR3-negative cells irrespective of t(4;14) status (Fig. 2g). Among the top upregulated proteins in t(4;14) cases in *trans* is the deubiquitinating enzyme ubiquitin C terminal hydrolase L1 (UCHL1) (Fig. 2c and Extended Data Fig. 3e). UCHL1 has been previously shown to be essential for MM and other B cell malignancies and is associated with aggressive disease<sup>30</sup>.

In HRD myeloma cases, we detected changes in the proteome that reflect characteristic patterns of aneuploidy (Extended Data Fig. 4a,b). Most significantly upregulated proteins include the deubiquitinase USP4 (chr3), as well as the redox regulator TXN (chr9) and pyruvate kinase PKM (chr15) (Extended Data Fig. 4c). Pathway analysis revealed upregulation of the tricarboxylic acid cycle and oxidative phosphorylation, and downregulation of mitotic cell cycle gene signatures (Extended Data Fig. 4d).

For secondary genetic alterations, we mostly found proteins regulated in *cis*. Del(13q) comprises the known tumor suppressor genes *RBI* and *DIS3*, and their RNA and protein levels were consistently downregulated (Extended Data Fig. 5a,b). The most significantly downregulated protein was MYC binding protein 2 (MYCBP2), located on 13q (Extended Data Fig. 5a). MYCBP2 acts as an E3 ubiquitin ligase, playing a crucial role in modulating MYC transcriptional activity<sup>31</sup>. In patients with del(1p), we found downregulation of tumor suppressor and apoptosis regulator FAS-associated factor 1 (FAF1), as previously reported<sup>29</sup> (Extended Data Fig. 5c,d). Deletion of 17p always comprises the tumor suppressor *TP53*, which was only detected in 18% of samples in our proteomic data. The most significantly downregulated protein in del(17p) cases was FXR2 (located 100 kb downstream of *TP53*), which is often codeleted with *TP53* in cancer (Extended Data Fig. 5e,f)<sup>32</sup>.

### The E2 ubiquitin ligase UBE2Q1 is a candidate oncoprotein in MM with 1q amplification

Amplification of the long arm of chromosome 1 (+1q) is a well-established high-risk marker in MM and, consistent with previous studies, the number of 1q copies correlated with shorter overall survival (OS) in our cohort (Extended Data Fig. 6a)<sup>6</sup>. A large fraction of the upregulated proteins (147/237, 62%) is regulated in *cis* (on 1q), including many of the proteins previously suggested as potential oncogenic drivers such as ANP32E, BCL9 and MCL1 (Fig. 3a and Extended Data Fig. 6b)<sup>33</sup>. We observed only partial correlation of 1q status with protein levels of the

clinical trial stage drug target MCL1 (Fig. 3b) and confirmed this finding with reanalysis of previously published expression data<sup>34</sup> (Extended Data Fig. 6c). Several proteins involved in proteasomal degradation, proteostasis and protein folding pathways were upregulated in MM with 1q gain/amplification including proteins regulated in *cis* such as the E2 ligase UBE2Q1 (Fig. 3c) and the E3 ligase DCAF8 as well as in *trans* such as members of the chaperonin containing TCP-1 complex and E2 ligases UBE2G2 and UBE2H (Extended Data Fig. 6d). Although correlation of 1q genes from copy number (CN) to RNA and protein was in general high, many genes exhibited buffering effects of CNAs (Fig. 3d). The E2 ligase UBE2Q1 was the only 1q protein significantly associated with both adverse OS and progression-free survival (PFS) after false discovery rate (FDR) correction. The prognostic impact of UBE2Q1 protein expression was independent of 1q status, predicting outcomes even in patients without 1q chromosomal gain or amplification (Fig. 3e). Additionally, high RNA expression levels of UBE2Q1 were associated with shorter OS in an independent patient cohort<sup>3</sup> (Extended Data Fig. 6e). Analysis of clustered regularly interspaced short palindromic repeat (CRISPR) KO screening data in MM cell lines revealed a correlation between UBE2Q1 genetic dependency and copy number status (Extended Data Fig. 6f). Given the role of UBE2Q1 in ubiquitination-mediated protein degradation, we evaluated the effect of UBE2Q1 overexpression in two MM cell lines (Fig. 3f). In UBE2Q1 overexpressing LPI cells, we observed deregulation of proteins that also correlated with UBE2Q1 level expression in primary MM and were also differentially expressed in primary myeloma patients with 1q gain (Fig. 3g,h). These included the cell surface protein BCMA (TNFRSF17), ubiquitin hydrolase UCHL1, heat shock protein HSPB1, dual specificity phosphatases DUSP23 and DUSP12 and the stem cell marker nestin (NES). We also observed an overlap of regulated proteins in UBE2Q1 overexpressing OPM2 cells, although the effect was less pronounced (Extended Data Fig. 6g and Supplementary Table 8). These data imply that UBE2Q1, which is deregulated by DNA amplification of its gene, modulates protein levels of other proteins and points toward a role of UBE2Q1 in MM pathogenesis.

### Protein signatures in MGUS and PCL

MM develops from the premalignant state MGUS defined by the presence of less than 10% monoclonal plasma cells in the bone marrow and the absence of symptoms. Patients can remain in this state for >10 years without treatment. Proteomic analyses of seven MGUS cases revealed only a few differences to NDMM with deregulation of 20 proteins and 509 phosphopeptides (Fig. 4a and Extended Data Fig. 7a). Within the differentially expressed proteins, the histone methyltransferase KMT2D, a known tumor suppressor in B cell malignancies, was found at higher abundance in MGUS (Fig. 4a and Extended Data Fig. 7c)<sup>35</sup>.

PCL is a highly aggressive form of extramedullary myeloma with a poor outcome, where plasma cells acquire independence of the

**Fig. 2 | (Phospho)proteomic profiles of primary translocations t(11;14) and t(4;14).** **a**, Global protein levels in newly diagnosed MM cases with t(11;14) ( $n = 27$ ) were compared against cases without t(11;14) ( $n = 87$ ) with a two-sided, moderated two-sample  $t$ -test. The  $\log_2$  fold change (FC) of each protein is plotted against its  $P$  value.  $P$  values were adjusted with the Benjamini–Hochberg method and the significance threshold of 0.05 FDR is indicated. **b**, The heat map displays the normalized expression of *RBI*, *CDK4*, *CDK6*, *CCND1*, *CCND2* and *CCND3* on RNA and protein level and *RBI* phosphopeptides. Phosphopeptides are annotated with protein name, position, amino acid and number of phosphorylations. **c**, Global protein levels in cases with t(4;14) ( $n = 19$ ) were compared against other MM cases ( $n = 95$ ) with a two-sided, moderated two-sample  $t$ -test. The  $\log_2$  FC of each protein is plotted against its  $P$  value.  $P$  values were adjusted with the Benjamini–Hochberg method and the significance threshold of 0.05 FDR is indicated. **d**, Protein, phosphoprotein and RNA expression levels of FGFR3 and NSD2 in samples with ( $n = 19$ ) or without t(4;14) ( $n = 95$ ). For phosphopeptide data, the peptide with the least missing values

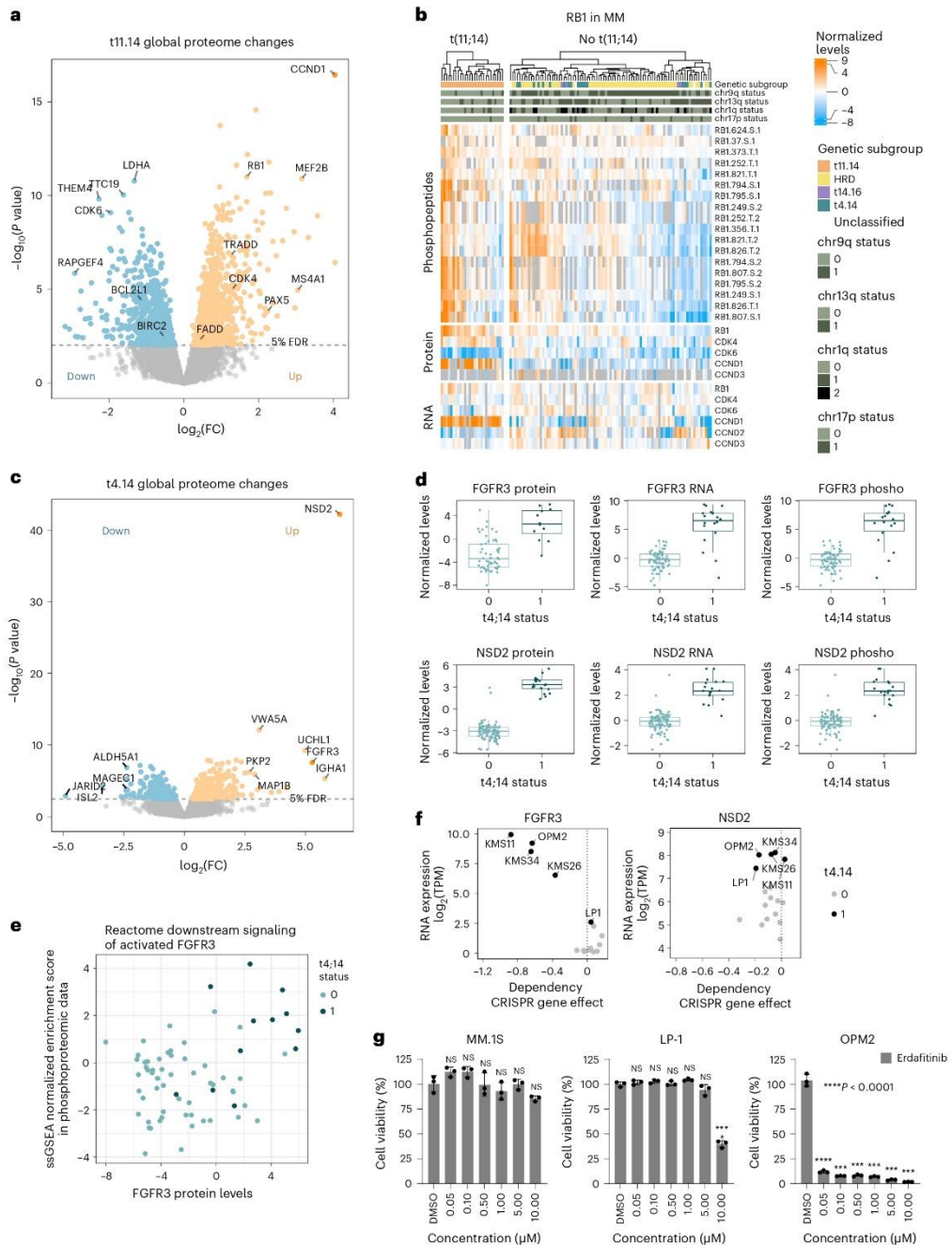
was selected for a graphical representation (FGFR3.S.425; NSD2.S.618). FDRs of the comparison between the two groups are indicated. Box plots show median (middle line), 25th and 75th percentiles, whiskers extend to minimum and maximum excluding outliers (values greater than  $1.5 \times$  interquartile range (IQR)). **e**, FGFR3 protein levels in MM samples are plotted against the ssGSEA normalized enrichment score of the Reactome gene set ‘Downstream signaling of activated FGFR3 in phosphoproteomic data’. Normalized TMT ratios in each sample were used as input for ssGSEA. **f**, FGFR3 and NSD2 RNA expression and CRISPR–Cas9 KO screening data in MM cell lines were extracted from the depmap portal (depmap.org). RNA expression is plotted against the CRISPR KO gene effect. **g**, Cell viability of MM cell lines after treatment with FGFR3 inhibitor erdafitinib for 96 h at indicated concentrations ( $n = 3$ , independent replicates). Data are plotted as mean  $\pm$  s.d. Drug treatments of each cell line were compared to respective DMSO controls with a Dunnett’s test. \*\*\*\* $P$  value < 0.0001. Exact  $P$  values listed in the source table.

Resource

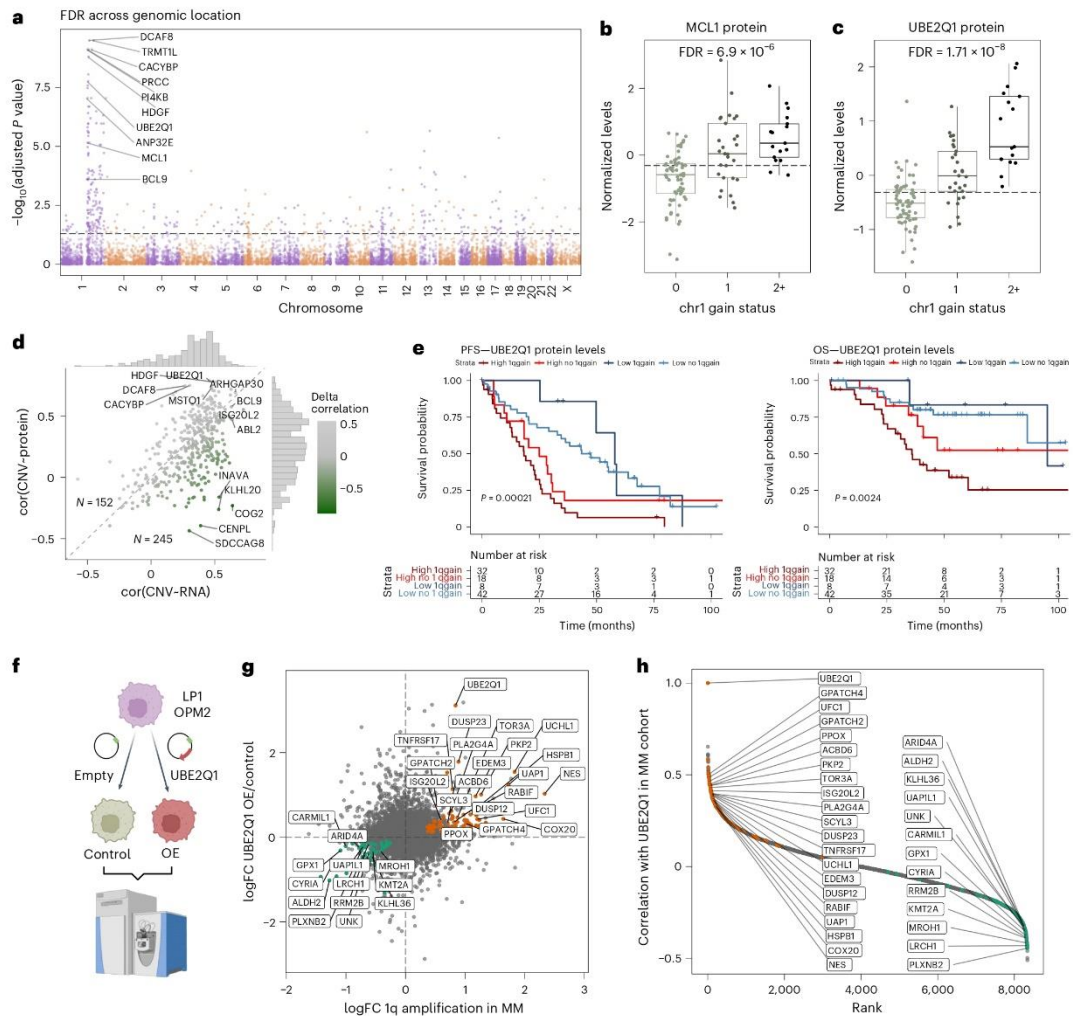
<https://doi.org/10.1038/s43018-024-00784-3>

bone marrow microenvironment and enter the bloodstream. While genetically similar, the (phospho)proteome of PCL and MM differs significantly as demonstrated by principal component analysis (PCA) (Fig. 4b) and statistical comparison (Fig. 4c and Extended Data Fig. 7a),

irrespective of whether the PCL cells were obtained from blood ( $n = 12$ ) or bone marrow ( $n = 5$ ) (Extended Data Fig. 7b,c). SsGSEA analysis revealed a gradual enrichment of proliferative and MYC target signatures from MGUS to MM to PCL (Fig. 4d). Among the most upregulated





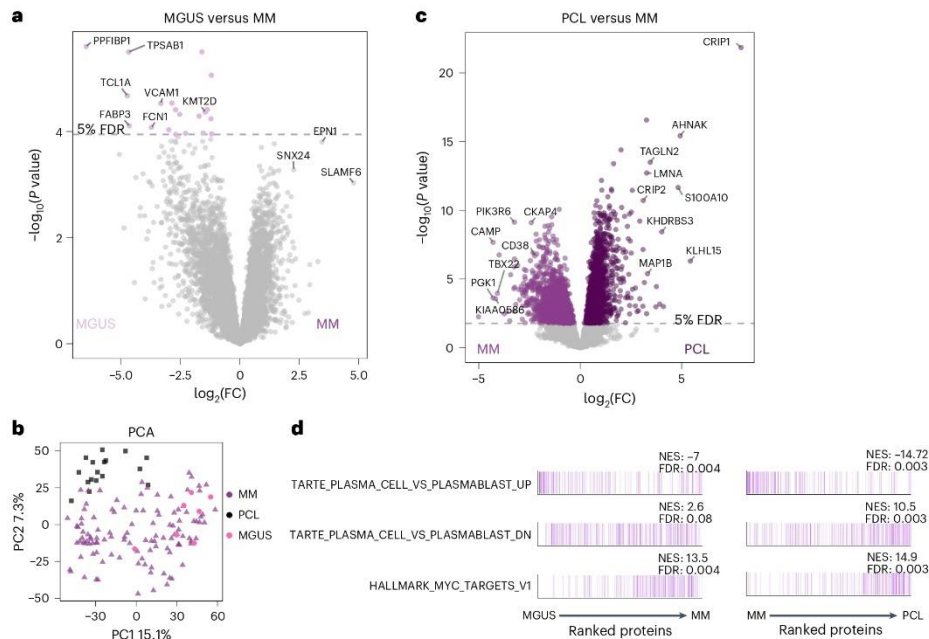


**Fig. 3 | Identification of UBE2Q1 as a candidate protein for the aggressive phenotype of MM with gain/amp of chromosome 1q.** **a**, Global protein levels in MM samples with 1q copy number gain ( $n = 46$ ) were compared against all other samples ( $n = 68$ ) with a two-sided, moderated two-sample  $t$ -test. The  $-\log_{10}(\text{FDR})$  of each protein is plotted across genomic location. The significance threshold of 0.05 FDR is indicated. **b**, MCL1 protein levels in patients with MM grouped by 1q gain status. FDR for the comparison 1q gain versus no 1q gain is indicated (0:  $n = 68$ ; 1:  $n = 29$ ; 2+:  $n = 17$ ). Box plots show median (middle line), 25th and 75th percentiles, whiskers extend to minimum and maximum excluding outliers (values greater than  $1.5 \times \text{IQR}$ ). **c**, UBE2Q1 protein levels in patients with MM grouped by 1q gain status. FDR for the comparison 1q gain versus no 1q gain is indicated (0:  $n = 68$ ; 1:  $n = 29$ ; 2+:  $n = 17$ ). Box plot shows median (middle line), 25th and 75th percentiles, whiskers extend to minimum and maximum excluding outliers (values greater than  $1.5 \times \text{IQR}$ ). **d**, Genes located on chromosome 1q with at least ten valid value pairs in all datasets (RNA, DNA

and protein) were extracted ( $n = 397$  genes). The Pearson correlation coefficient of copy number determined by nanopore sequencing with RNA expression level ( $\text{cor}(\text{CNV-RNA})$ ) is plotted against the Pearson correlation coefficient of copy number with protein expression level ( $\text{cor}(\text{CNV-protein})$ ). **e**, Kaplan–Meier plots show survival of patients grouped by UBE2Q1 protein levels (median) and 1q gain status. Survival in the different groups is compared by a log rank test. **f**, UBE2Q1 was overexpressed in LP1 and OPM2 cell lines. Empty vectors were used as a control. Cell lines were analyzed with label-free DIA proteomics ( $n = 4$ , biological replicates). **g**, Correlation of protein FCs in 1q gain myeloma patients (x axis) and UBE2Q1 overexpressing LP1 cells compared with control (y axis). Proteins regulated in LP1 cells ( $<0.05$  FDR) and patients with 1q gain ( $<0.1$  FDR) and correlating with UBE2Q1 protein levels in myeloma cohort ( $r > 0.3$  or  $r < -0.3$ ) are indicated. **h**, Correlation analysis of UBE2Q1 with all other protein levels in newly diagnosed MM. Proteins are ranked by their Pearson correlation coefficient. The same proteins as in **g** are highlighted.

proteins in PCL are cysteine-rich protein 1 (CRIP1) and CRIP2, a protein also highly expressed in acute myeloid leukemia<sup>36</sup>. Further upregulated proteins in PCL include AHNAK, TAGLN2 and LMNA, which are linked

to metastasis and aggressive disease in solid cancer (Extended Data Fig. 7c)<sup>37</sup>. Conversely, PCL cases displayed lower levels of the monoclonal antibody target CD38 (Fig. 4c).



**Fig. 4 | Proteome profiles of MGUS and PCL.** **a**, Global protein levels in newly diagnosed MM samples ( $n = 114$ ) were compared with those in pre-malignant MGUS samples ( $n = 7$ ) with a two-sided, moderated two-sample  $t$ -test. The  $\log_2$ FC of each protein is plotted against its  $P$  value.  $P$  values were adjusted with the Benjamini–Hochberg method and the significance threshold of 0.05 FDR is indicated. **b**, PCA of global proteome data of newly diagnosed MM, MGUS and PCL samples. **c**, Global protein levels in MM samples ( $n = 114$ ) were compared against PCL ( $n = 17$ ) with a two-sided, moderated two-sample  $t$ -test. The  $\log_2$  fold

change of each protein is plotted against its  $P$  value.  $P$  values were adjusted with the Benjamini–Hochberg method and the significance threshold of 0.05 FDR is indicated. **d**, The mean  $\log_2$  fold change of proteins in MM versus MGUS or PCL versus MM or samples was used as input for an ssGSEA analysis. The plot shows proteins ordered by their rank; proteins belonging to the respective gene set are marked by color. The normalized enrichment score (NES) and FDR of each gene set are indicated.

### Proteomic-based outcome prediction

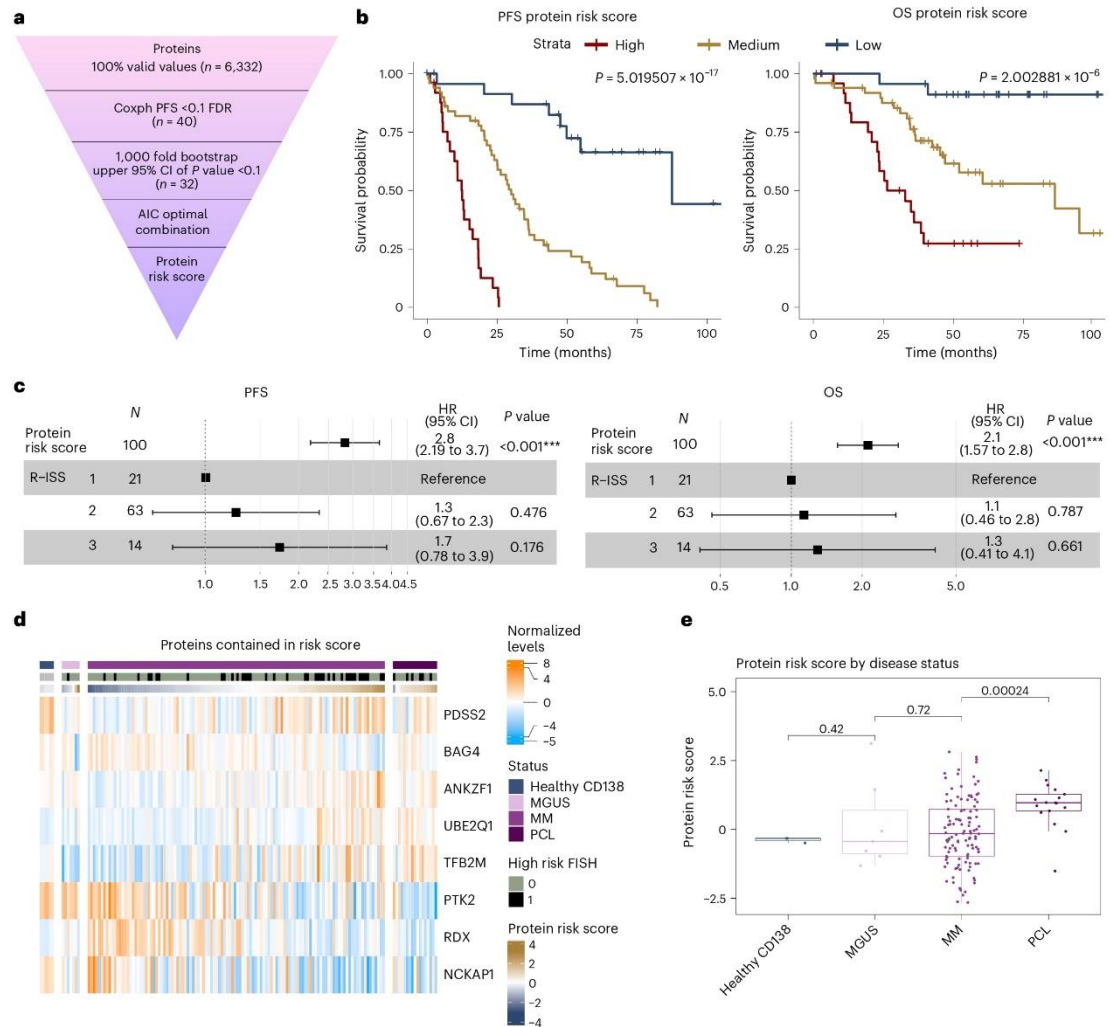
Risk stratification of NDMM is currently based on R-ISS and in our cohort we concordantly observed a significant impact of R-ISS on survival while other parameters had no effect (Extended Data Fig. 8b,c). We evaluated whether proteomics and phosphoproteomics provide prognostic information in addition to R-ISS, the current standard for risk stratification in MM. We conducted single-variable Cox regression analysis on PFS and OS using fully quantified proteins and phosphopeptides in 100 patients treated in the Deutsche Studiengruppe Multiples Myelom (DSMM) XII, XIII and XIV clinical trials. Despite variations in induction therapy, all patients were scheduled to receive a lenalidomide-based induction, high-dosage melphalan with autologous stem cell transplantation (auto-SCT) and lenalidomide maintenance therapy (for details, see Methods). In total, 40 proteins and 4 phosphopeptides had FDR < 0.1 and one protein FDR < 0.05 (Supplementary Table 9 and Extended Data Fig. 8a). Applying a bootstrapping approach and model optimization (Fig. 5a), we defined a protein risk score containing protein level information of eight proteins with differing weights, including the 1q protein UBE2Q1 (Supplementary Table 9). Patients with a high protein risk score ( $n = 25$ ) had a median PFS of 12.5 months as compared with 30.0 months in patients with a median score ( $n = 50$ ), and 87.4 months in patients with a low score ( $n = 25$ ), which translated to a median OS of 29.6, 86.3 and 108.1 months, respectively (Fig. 5b). The prognostic value of the protein risk score remained consistent across CD138-enriched and nonenriched samples (Extended Data Fig. 8d) and was independent of R-ISS (Fig. 5c). Strikingly, the protein risk score gradually increased

following disease aggressiveness from MGUS (median score  $-0.43$ ) to NDMM (median score  $-0.15$ ) and PCL (median score  $0.97$ ) (Fig. 5d,e). The proteomic risk signature had a significant impact on outcome in an independent, external cohort of patients with NDMM recently published by Kropivsek et al.<sup>21</sup> despite the small number of patients as well as differences in treatment and proteomic data acquisition (Extended Data Fig. 8e).

### Identification of MM-selective and essential proteins

We utilized TMT-based proteomics with a booster channel to identify proteins specific to MM cells compared with hematopoietic stem and progenitor cells (CD34<sup>+</sup>), B cells (CD19<sup>+</sup>) and plasma cells (CD138<sup>+</sup>) isolated from the bone marrow of healthy donors (Fig. 6a). Key hematopoietic lineage markers behaved as expected with higher levels of PAX5 in B cells, CD34 in stem/progenitor cells and IRF4 in CD138<sup>+</sup> plasma cells (Fig. 6b). A comparison of MM cells with each of the three healthy populations revealed 1,475, 1,350 and 1,187 significantly regulated proteins (FDR < 0.1) in MM as compared with CD34<sup>+</sup>, CD19<sup>+</sup> and CD138<sup>+</sup> healthy cells, respectively (Fig. 6c and Extended Data Fig. 9a). Among the proteins consistently upregulated in MM were ribosomal proteins and heat shock proteins (Extended Data Fig. 9a). Several markers of plasma cell differentiation including PRDM1, CD56 (NCAM1) and BCMA (TNFRSF17) were higher expressed in MM cells while for CD138 (SDC1) and CD38 no major differences were observed (Extended Data Fig. 9b). We combined the list of significantly upregulated proteins in any of the three comparisons (Fig. 6c) with proteins selectively identified in myeloma

## Resource

<https://doi.org/10.1038/s43018-024-00784-3>

**Fig. 5 | A proteomic risk score predicts outcome in NDMM. a**, The workflow for the generation of a proteomic risk score in patients with NDMM who received a lenalidomide-based intensive treatment within clinical trials ( $n = 100$ ). **b**, Kaplan-Meier plots show PFS and OS for patients according to the protein risk signature score divided by lowest quartile (low,  $n = 25$ ), second and third quartile (medium,  $n = 50$ ) and highest quartile (high,  $n = 25$ ). Survival in the different groups is compared by the log rank test. **c**, Multivariable Cox regression analysis for PFS and OS including the protein risk score as continuous variable (hazard ratio (HR) per 1 point increase) and R-ISS. Data are represented as hazard ratio with 95%

confidence interval (CI). Significance was tested with a Wald test. **d**, Expression of proteins contained in the protein high-risk score across samples from healthy donors, patients with premalignancy MGUS, MM and PCL. **e**, Protein risk score values calculated for the proteome data of healthy plasma cells, MGUS, MM and PCL samples.  $P$  values from a two-sided Student's  $t$ -test are indicated. Healthy CD138:  $n = 3$ ; MGUS:  $n = 7$ ; MM:  $n = 114$ ; PCL:  $n = 17$ . Box plots show median (middle line), 25th and 75th percentiles, whiskers extend to minimum and maximum excluding outliers (values greater than  $1.5 \times$  IQR).

cells (402 proteins) and performed integrated analysis with genetic dependency data (depmap.org)<sup>38</sup> (Fig. 6d). To detect myeloma-specific vulnerabilities, genes were filtered by their median dependency in myeloma versus nonmyeloma cell lines applying a cutoff based on the lenalidomide targets IKZF1 and IKZF3 (refs. 39,40). This resulted in a candidate target list of 31 proteins that included known MM survival factors such as transcription factors IRF4 and PRDM1 and kinases PIM2 and PIK3CA (Fig. 6e)<sup>41</sup>. Among the proteins not previously linked to

MM were three members (TAF5L, SUPT7L and SUPT20H) of the SAGA complex, a posttranslational regulator of MYC transcriptional activity that is important for myeloma growth. Two additional SAGA subunits, SUPT3H and TAF12, were also upregulated in MM but did not pass the filter for selective dependency<sup>42</sup>. The candidate list further included members of the dolichol-phosphate mannosylase complex DPM1 and DPM3 and the ubiquitin-like modifier UFM1 as well as its ligase UFL1. To further evaluate the role of proteins in MM, we performed a



## Resource

<https://doi.org/10.1038/s43018-024-00784-3>

complementary whole-genome CRISPR activation screen in the MM.1S cell line (Fig. 6f and Supplementary Table 10). Strikingly, the top genes driving MM cell growth were POU2AF1 and IRS1, two proteins highly expressed and essential for MM (Fig. 6g, h). *POU2AF1*, encoding the OCA-B transcriptional coactivator, is a B cell differentiation factor essential for germinal center formation and several B cell neoplasias, including lymphoma<sup>43</sup> and MM<sup>44</sup>. IRS1 is a downstream signaling protein of insulin growth factor 1 receptor (IGF1R) and is highly phosphorylated in MM cells when IGF1 binds to IGF1R<sup>45</sup>. Expression of IRS1 and POU2AF1 in MM cell lines extracted from the Cancer Cell Line Encyclopedia and the pan cancer proteomic map<sup>46</sup> is highly correlated with genetic dependency (Extended Data Fig. 9c). Treatment with the IRS1 inhibitor NT157 (ref. 47) reduced proliferation in MM cell lines, highlighting IRS1 as a potential selective target for therapy (Extended Data Fig. 9d). In aggregate, these data demonstrate that integrated proteomic analysis in primary patient cells with functional genetics in cell lines reveals potential therapeutic vulnerabilities in MM.

#### Proteomics reveals candidates for immunotherapies

Immunotherapies such as CAR-T cells and bispecific antibodies targeting BCMA and GPCR5D are approved and highly effective treatments for MM<sup>48,49</sup>. To identify additional MM selective cell surface proteins, we integrated our comparison of healthy and malignant plasma cells with the cancer surface proteome resource<sup>50</sup> (Fig. 7a). While TNFRSF17 (BCMA) was highly specific for myeloma samples, other immunotherapy targets such as CD38, CD138 (SDC1) and SLAMF7 were not or only moderately higher expressed in MM versus healthy plasma cells. In addition, we detected several proteins with expression levels higher in MM cells, including Fc receptor-like 2 and 5 (FCRL2 and 5), receptor tyrosine kinase like orphan receptor 2 (ROR2), signaling lymphocytic activation molecule family member 1 (SLAMF1) and lysosomal associated membrane protein 3 (LAMP3) (Fig. 7b). All proteins displayed good RNA-to-protein correlation in our dataset (Extended Data Fig. 9e) and evaluation of these targets in single-cell RNA sequencing data<sup>51</sup> further confirmed their selective and higher expression in malignant plasma cells (Fig. 7c). FCRL5 is currently being explored as an immunotherapy target in MM in clinical trials<sup>52</sup>. Leveraging single-cell RNA sequencing data from the protein atlas (<https://www.proteinatlas.org/>)<sup>53</sup> revealed ROR2, LAMP3 and SLAMF1 to be expressed in non-hematopoietic tissue and we thus chose to further evaluate FCRL2, which is only expressed on plasma and B cells. Flow cytometry in primary patient and healthy donor bone marrow confirmed FCRL2 surface expression on MM cells in 7 of 11 patients and showed moderate or low expression on healthy plasma and B cells and other hematopoietic cells, respectively (Fig. 7d, e and Extended Data Fig. 9f, g).

#### Discussion

We provide a proteogenomic landscape of newly diagnosed, untreated MM, covering the major cytogenetic alterations of this disease. Including comparisons with healthy cells, MGUS and PCL, and correlation with clinical data, MM-specific proteins can be explored in the context of disease progression. Analysis of >100 well-annotated primary patient samples and integration with DNA and RNA sequencing allowed us to map the consequences of recurrent genetic alterations to the (phospho) proteome. A low correlation of RNA to protein levels was observed in myeloma cells, consistent with proteogenomic studies in other types of hematologic and solid cancer<sup>9-11,13</sup>. This was especially true for the proteins involved in protein homeostasis, such as proteasome formation, ubiquitination and splicing. In contrast, RNA and protein levels of regulators of B cell differentiation, IgH translocation partners and those encoded in CNAs showed higher correlation. Multiple genetic alterations affecting cell cycle regulation, including cyclin D translocations or upregulation of Rb1 phosphorylation as well as *Rb1* deletions, had a major impact on the (phospho)proteome, highlighting cell cycle dysregulation as a hallmark of MM. In patients with primary IgH

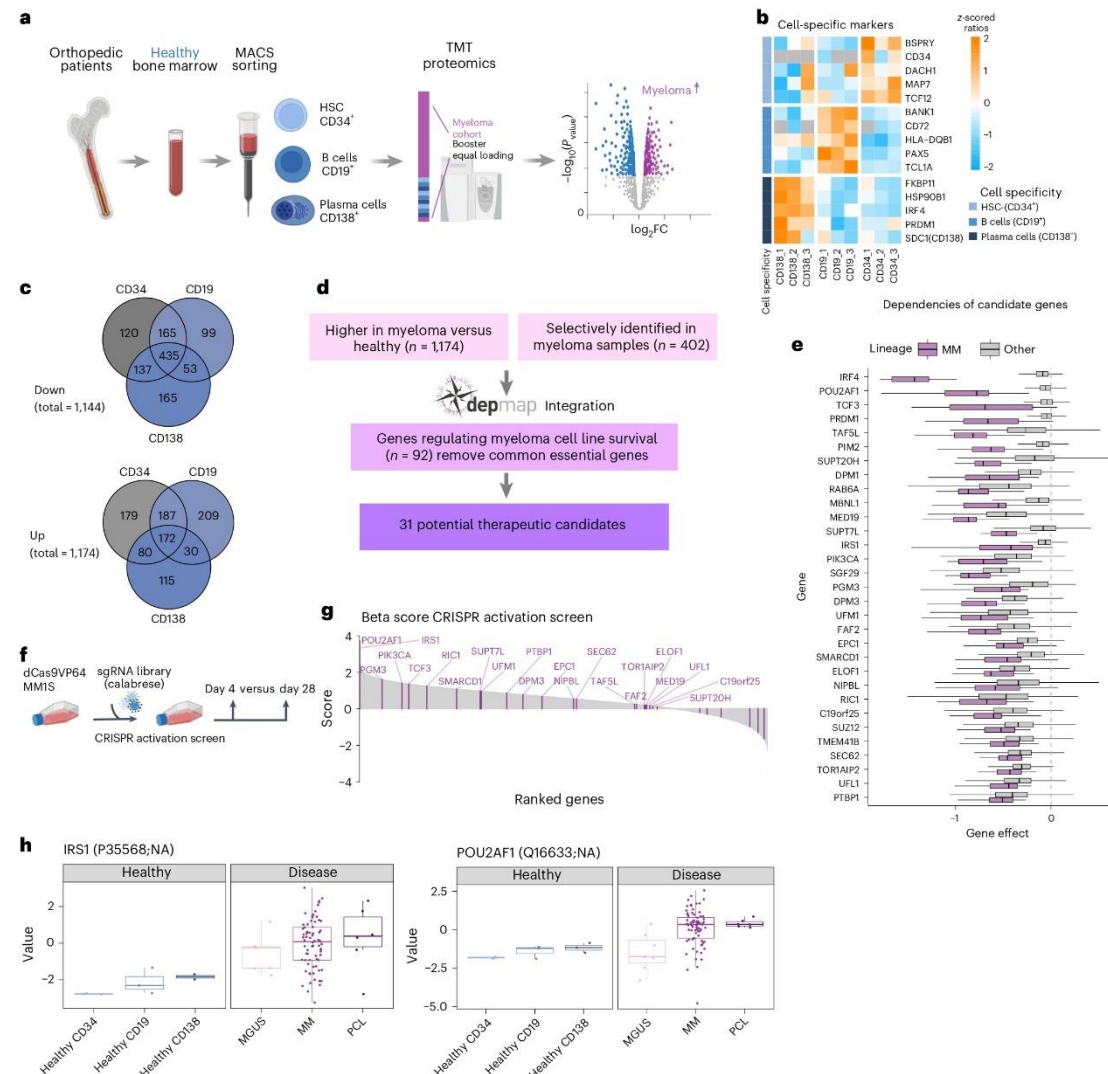
translocations, the recurrent translocation partners were, in general, the most upregulated proteins and RNA transcripts, with the exception of FGFR3, which was only elevated in a subset of cases with t(4;14). FGFR3 protein abundance independent of t(4;14) was predictive of downstream signaling and sensitivity to FGFR3 inhibition. The pronounced deregulation of proteins involved in the apoptosis pathway and B cell markers observed in t(11;14) myeloma provides a possible link to the enhanced sensitivity of these cases to BCL2 inhibition<sup>22</sup>. These findings may guide future studies to find more reliable predictive protein-based biomarkers for personalized treatment in MM. In line with this, proteomic-based prediction for ex vivo drug sensitivity in primary MM cells has recently been demonstrated by Kropivsek et al.<sup>21</sup>.

Amplification of chromosome 1q is an established high-risk marker in MM and also other types of cancer. However, which of the proteins encoded on 1q confer therapy resistance is not completely understood<sup>6</sup>. While several previously described 1q candidates such as ANP32E, BCL9 and MCL1 were found upregulated on the protein level in +1q cases, our integrated analysis identified the E2 ubiquitin ligase UBE2Q1 as a 1q protein highly correlated with outcome. Consistent with our findings in MM, high UBE2Q1 expression levels are associated with shorter survival in other cancers indicating a tumor-agnostic role in conferring therapy resistance<sup>54-56</sup>. E2 ubiquitin ligases, which as enzymes are in principle amenable for pharmacologic intervention, mediate ubiquitin transfer to a substrate protein via an E3 ligase and thus can regulate their substrate proteins on the posttranslational level. Consistently, we show that UBE2Q1 regulates many of the proteins also found differentially expressed in patient samples with 1q gain. The E3 ubiquitin ligase(s) for UBE2Q1 as well as its substrates implicated in drug resistance are currently not known and warrant further studies. In addition to UBE2Q1, we found other members of the ubiquitin-proteasome system deregulated either directly by chromosomal events in *cis* or through *trans* effects including E3 ligases DCAF8 (Chr 1q) and MYCBP2 (Chr 13q), the deubiquitinating enzymes UCHL1 and USP4 (Chr 3) and ubiquitin-like modifiers UFL1 and UFM1. Conceivably, altered levels of these enzymes lead to posttranslational regulation of their substrates, which to some extent may explain the low RNA-protein correlation observed in MM.

Outcome prediction is of high clinical relevance in cancer to identify patients with aggressive disease and to personalize therapy. We identified a protein risk signature that was highly predictive for outcome and independent of the R-ISS in patients with NDMM from three consecutive DSMM clinical trials that incorporated the major therapy principles still included in current first-line therapies. The proteins in the risk signature, which include the 1q protein UBE2Q1, are not associated with known drug mechanisms and do not overlap with genes from RNA-based risk signatures such as GEP70 or SKY92, highlighting additional value provided by proteomics<sup>4,57</sup>. Furthermore, our protein risk signature was associated with disease stage and could be validated in an independent cohort<sup>21</sup> that was treated with different treatment modalities, further implying that these proteins are associated with aggressive disease. These findings need to be evaluated in larger patient cohorts in the context of currently applied therapy regimens to determine clinical applicability. While we could only investigate a small but representative subset of patients of the DSMM trials due to sample availability, technically, (phospho)proteomics could be performed for the majority of myeloma patients, similar to cytogenetic and RNA expression analysis. Since the reliability of global analyses of bulk tumor samples in general depends on tumor cell purity, we show that our results including outcome and conclusions are robust and independent of sorting status if a cutoff of 75% tumor cell purity is applied.

We found the premalignancy MGUS and symptomatic MM to be almost indistinguishable on the proteome level, which in part may be explained by the strong impact of genetic alterations that are already present in MGUS<sup>35</sup>. In contrast, PCLs have a more distinct protein

## Resource

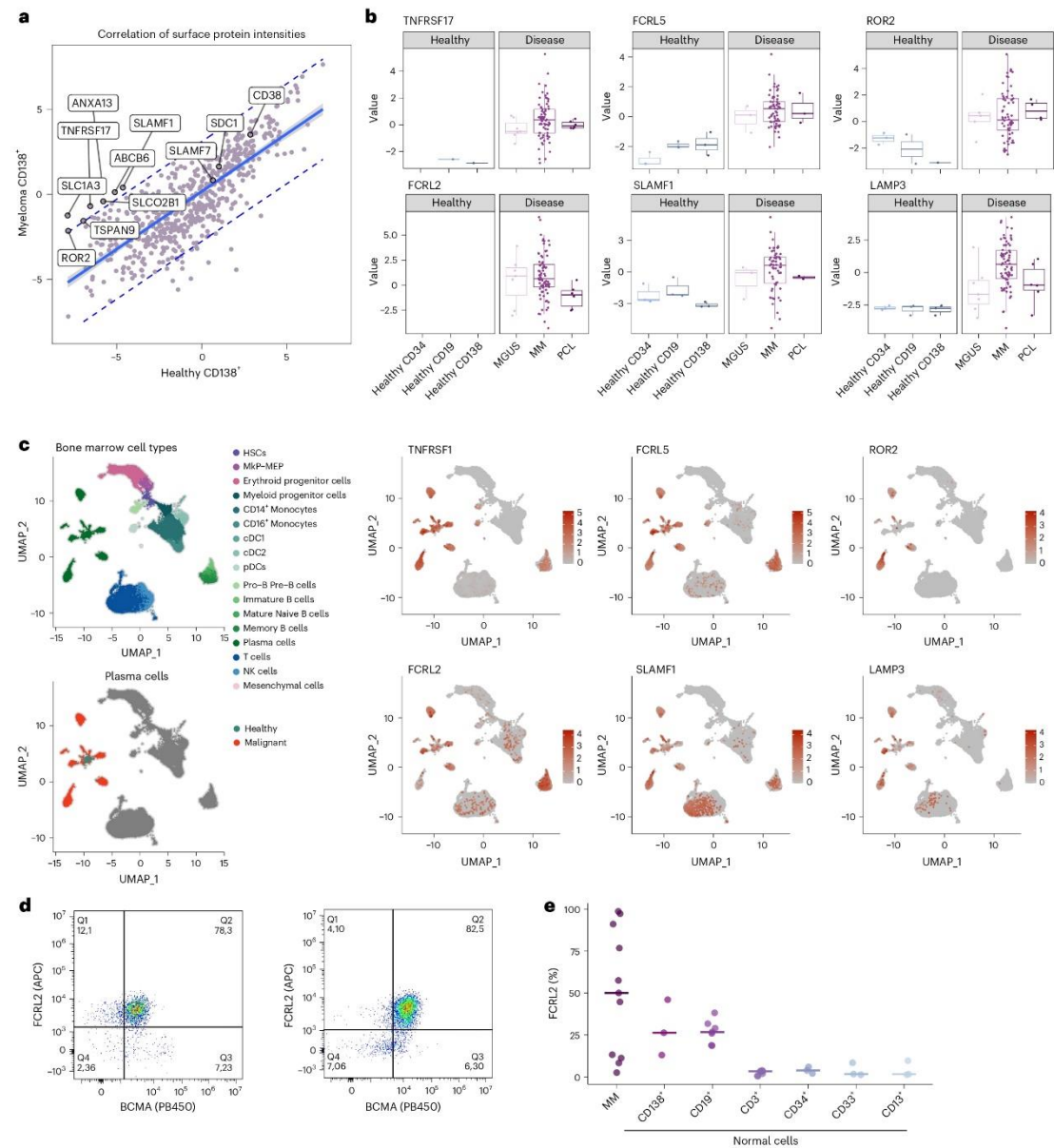
<https://doi.org/10.1038/s43018-024-00784-3>

**Fig. 6 | Integrated proteomic and genetic screens reveal drivers of MM cell growth.** **a**, Hematopoietic cell populations were sorted using MACS enrichment for the surface markers CD34 (hematopoietic stem and progenitor cells (HSCs)), CD19 (B cells) and CD138 (plasma cells) from bone marrow of individuals without hematologic malignancy ( $n = 3$ ). Proteins were quantified via TMT with a booster channel approach. Booster and equal loading control were identical to the internal standard used for TMT analysis of cohort samples. **b**, Protein levels of cell lineage-specific markers in healthy samples. z-scored TMT ratios are displayed. **c**, Proteins in MACS sorted healthy bone marrow and CD138<sup>+</sup> sorted MM samples were compared with a two-sided, moderated two-sample *t*-test. *P* values were adjusted with the Benjamini–Hochberg method. The total number of regulated proteins is indicated, the Venn diagrams show overlap of up- and downregulated proteins in MM samples compared with healthy samples ( $FDR < 0.1$ ). **d**, Data analysis workflow to identify potential therapeutic candidates from myeloma upregulated or specifically expressed proteins. **e**, Gene dependency scores from

CRISPR–Cas9 KO screening data from the depmap portal. The gene effect of potential therapeutic targets in myeloma ( $n = 18$ ) and other cell lines ( $n = 1,082$ ) is displayed. The RNA to protein correlation in myeloma cohort is indicated for each candidate gene. Box plot shows median (middle line), 25th and 75th percentiles, whiskers extend to minimum and maximum excluding outliers (values greater than  $1.5 \times IQR$ ). **f**, The workflow for a genome-wide CRISPR–Cas9 activation screen using the Calabrese library performed in the MM cell line MM.1S. **g**, Gene effect on proliferation ranked by beta score. A higher beta score indicates expansion of cells carrying the indicated sgRNAs. The MAGeCK MLE algorithm was applied for the analysis of beta scores and *P* values. Potential targets identified by proteomic analysis are marked in purple. **h**, Protein levels of IRS1 and POU2AF1 across healthy and malignant cell populations. Healthy CD138:  $n = 3$ ; healthy CD19:  $n = 3$ ; healthy CD34:  $n = 3$ ; MGUS:  $n = 7$ ; MM:  $n = 114$ ; PCL:  $n = 17$ . Box plot shows median (middle line), 25th and 75th percentiles, whiskers extend to minimum and maximum excluding outliers (values greater than  $1.5 \times IQR$ ).



## Resource

<https://doi.org/10.1038/s43018-024-00784-3>

**Fig. 7 | Identification of surface proteins on MM cells. a**, The identified surface proteins from the healthy to disease comparison were extracted by integrating proteomics data with the cancer surfaceome atlas. The plot shows the correlation of median-normalized raw intensities of surface proteins in CD138<sup>+</sup> sorted MM and healthy bone marrow samples. The 95% confidence interval is indicated with a blue line, the 95% prediction interval is indicated with dashed blue lines. **b**, Protein levels of selected surface proteins in healthy hematopoietic cells and malignant plasma cells. Healthy CD138:  $n = 3$ ; healthy CD19:  $n = 3$ ; healthy CD34:  $n = 3$ ; MGUS:  $n = 7$ ; MM:  $n = 114$ ; PCL:  $n = 17$ . Box plot shows median (middle line), 25th and 75th percentiles, whiskers extend to minimum and maximum excluding

outliers (values greater than  $1.5 \times \text{IQR}$ ). **c**, UMAP plots showing single-cell RNA sequencing data of bone marrow from healthy and patients with MM. Cells are colored by cell type, malignancy status or by normalized RNA expression levels of selected surface proteins. **d**, FACS analysis of BCMA (TNFRSF17) (x axis) and FCRL2 (y axis) expression in MM samples. Two representative examples of patients with MM with high FCRL2 expression were selected. **e**, The percentage of FCRL2-positive cells in MM cells and minimal to no expression in other normal hematologic cell populations,  $n = 19$ . MkP, megakaryocyte progenitor; MAP, megakaryocyte/erythrocyte progenitor; DC, dendritic cell; NK, natural killer.



## Resource

<https://doi.org/10.1038/s43018-024-00784-3>

expression profile and we observed some overlap of upregulated proteins to other disseminated, aggressive malignancies such as acute leukemia<sup>36</sup>.

Proteomic profiling of healthy and malignant plasma cells and integration with CRISPR dependency data revealed myeloma-specific vulnerabilities. Besides well-established B cell differentiation regulators, including IRF4 and PRDM1, we found the transcriptional coactivator POU2AF1 (OCA-B, BOB1) as a highly expressed protein and essential in MM. These findings are in line with a recent study describing POU2AF1 as a regulator of genes important for MM proliferation<sup>38</sup>. We detected insulin response substrate-1 (IRS1) as another potential drug target in MM. Insulin growth factor signaling leads to the activation of AKT, which has been shown to promote myeloma growth<sup>45</sup> but is also important for other tissues. Our data indicate that IRS1 as compared with IGF-1R1 is a highly selective target of this pathway in MM cells. Our integrated analyses further point to a potential role of the SAGA complex in MM that, among other functions, is a posttranslational regulator of MYC, providing a potential link to the transformation of plasma cells<sup>58</sup>.

T cell therapies such as CAR-T and bispecific antibodies are revolutionizing MM treatment, showing remarkable effectiveness in multidrug resistant patients. However, resistance can arise from loss or mutation of targeted surface proteins, as shown for BCMA and GPCRS<sup>59,60</sup>, highlighting the need for additional targets. Our combined proteomic and single-cell RNA sequencing approach reliably detected MM-specific surface proteins, including candidates recently found by an orthogonal approach using surface biotinylation or glycoprotein capture<sup>61,62</sup>. We validated FCRL2 as a surface protein on primary MM cells. FCRL2 is also expressed on chronic lymphocytic leukemia cells<sup>63</sup> and may be exploited as a potential immunotherapy target in myeloma and other B cell malignancies.

Collectively, the proteomic landscape of plasma cell malignancies described here provides a powerful resource that can easily be assessed through an online tool for interactive self-exploration (<https://myelomaprot.mdc-berlin.de>) to promote research on MM biology, risk stratification and novel therapies.

## Methods

### Study cohort

A total of 138 patients were included in the proteomics study (114 NDMM, 17 PCL and 7 MGUS cases). Inclusion criteria were the availability of myeloma cells of appropriate quantity and quality for proteomic and genetic analyses and available information on FISH-bases cytogenetics and clinical parameters. All patients provided written informed consent according to the Declaration of Helsinki. The study was approved by the responsible ethic committees Ulm University (136/20, 307/08) and Charité Universitätsmedizin Berlin (EA2/142/20). Clinical trials of the DSMM and sample collection were approved by the ethics committee of Würzburg University (2008-000007-28, 145-11).

Patient characteristics are summarized in Supplementary Table 1. One hundred out of 114 newly diagnosed patients were treated within one of the DSMM XII–XIV clinical trial and had available outcome data (NCT00925821, NCT01090089 and NCT01685814)<sup>64</sup>. All of these 100 patients were scheduled to receive a lenalidomide-based intensive therapy within a clinical trial.

DSMM XII/NCT00925821 (*N* = 12): induction therapy with four cycles lenalidomide/adriamycin/dexamethasone. All patients were scheduled to receive high-dose melphalan/auto-SCT, while the nature of the second SCT was determined by risk stratification: high-risk patients (cytogenetics, ISS) were scheduled to undergo allogeneic stem cell transplantation (*N* = 3) followed by lenalidomide maintenance while standard-risk patients received a second auto-SCT followed by lenalidomide maintenance for 1 year<sup>64</sup>.

DSMM XIII, arm A2/NCT01090089 (*N* = 20): induction therapy with three cycles of lenalidomide/dexamethasone followed by two

cycles of high-dose melphalan/auto-SCT and lenalidomide maintenance until progression.

DSMM XIV/NCT01685814 (*N* = 68): induction therapy randomized between four cycles lenalidomide/adriamycin/dexamethasone (*N* = 36) or three cycles lenalidomide/bortezomib/dexamethasone (*N* = 32) followed by high-dose melphalan/auto-SCT, second randomization in patients with very good partial response (VGPR) or better directly to lenalidomide maintenance until progression or a second cycle of high-dose melphalan/auto-SCT followed by lenalidomide maintenance for 3 years. Patients not achieving VGPR after the first high-dose melphalan/auto-SCT were randomized to receive a second cycle of high-dose melphalan/auto-SCT followed by lenalidomide maintenance for 3 years or allogeneic stem cell transplantation (*N* = 3) followed by 1 year of lenalidomide maintenance.

No significant difference was observed for PFS and OS across the patients treated in the three different trials.

Healthy control cells were obtained from orthopedic surgery patients without evidence for malignancy. The median age of the healthy donors was 63 years (range, 57–78 years). All donors provided written informed consent according to the Declaration of Helsinki and the study was approved by the responsible ethic committee Charité – Universitätsmedizin Berlin (EA4/115/21).

### Cell isolation

Except for 12 PCL samples from peripheral blood, all samples were collected from bone marrow aspiration. Mononuclear cells were isolated with a Ficoll gradient and plasma cell content was determined morphologically. The majority of samples (89/138) were enriched for CD138<sup>+</sup> cells via magnetic-activated cell sorting (MACS) directly after mononuclear cell isolation using magnetic beads conjugated to a human CD138-specific antibody (130-051-301, Miltenyi). Non-MACS enriched samples (49/138) were selected for a plasma cell content >75% and had an average CD138<sup>+</sup> purity of 85%. Healthy bone marrow mononuclear cells were isolated by Ficoll gradient and CD34<sup>+</sup>, CD19<sup>+</sup> and CD138<sup>+</sup> cells were enriched with MACS antibody bead conjugates (all Miltenyi), according to the manufacturer's protocol. For each cell population of healthy bone marrow cells, three replicates were obtained. Replicates one and two were obtained from separate individuals and replicate three was obtained by pooling material from three different donors due to limitations in sample material.

### FISH analysis

FISH in combination with immunofluorescent detection of light chain-restricted plasma cells was performed on plasma cells from patients. Genetic regions of interest for the diagnosis of MM and their translocation partners were detected. FISH was performed according to standardized protocols using commercially available probes (Abbott Laboratories and MetaSystems).

### DNA preparation and nanopore sequencing

DNA was isolated with the AllPrep DNA/RNA kit (QIAGEN, 80204). RNA and DNA were extracted from the same sample while protein was extracted from a different aliquot of the same patient/time point sample. Nanopore DNA sequencing was performed with the Oxford Nanopore Technologies (ONT) platform. Libraries containing either a pool of three samples or just a single sample were prepped with the Rapid Barcoding Sequencing kit (SQK-RBK004, ONT) using approximately 350 ng starting material for each sample in a pool of three or 400 ng of starting material for a single run (Rapid Sequencing kit, SQK-RAD004). A maximum amount of 850 ng library was loaded onto the flow cell (FLO-MINI06D, R 9.4.1, ONT) and sequenced on a GridION sequencer (ONT), according to the manufacturer's instructions.

### RNA sequencing library preparation and sequencing

RNA was isolated with the AllPrep DNA/RNA kit (QIAGEN, 80204). Library preparation was performed from 20 to 100 ng of input total



## Resource

<https://doi.org/10.1038/s43018-024-00784-3>

RNA per sample using the TruSeq Stranded Exome RNA kit (Illumina), according to the manufacturer's instructions. The pooled RNA libraries were sequenced on an Illumina HiSeq2000 with 50-bp single-end reads with an average coverage of  $36.6 \times 10^6$  reads per sample.

#### Protein extraction and digestion

Samples were lysed at 4 °C with urea lysis buffer as previously described<sup>65</sup>. Protein lysates were reduced with 5 mM dithiothreitol for 1 h and alkylated with 10 mM iodoacetamide for 45 min in the dark. Samples were subsequently diluted 1:4 with 50 mM Tris-HCl, pH 8 and sequencing grade LysC (Wako Chemicals) was added at a weight-to-weight ratio of 1:50. After 2 h, sequencing grade trypsin (Promega) was added at a weight-to-weight ratio of 1:50 and digestion was completed overnight. Samples were acidified with formic acid and centrifuged to remove precipitated material (20,000g, 15 min). The supernatant was desalted with Sep-Pak C18 cc Cartridges (Waters).

#### TMTpro labeling of peptides

Desalted and dried peptides were labeled with TMTpro 16 plex reagents (Thermo Scientific) according to the manufacturer's instructions and at a sample-to-tag ratio of 1:7 (*w/w*). After confirming successful labeling, TMT-labeled peptides of cohort samples were randomly combined into ten TMTpro plexes (see Supplementary Table 11 for TMT channel allocation). For TMT plex 1–9, 75 µg peptides per channel were used and 45 µg of peptides per channel were used for TMT plex 10. An equal loading internal standard that consisted of a mix of all cohort samples was included in each TMT plex. Samples from healthy bone marrow donors were analyzed in an 11th TMTpro plex with 10 µg peptides per sample and an equal loading internal standard that was the same as for the cohort samples. The 11th TMT plex also contained a booster channel (500 µg peptides) that was identical to the internal standard and the two TMT channels next to it were left empty to prevent signal spillover. Combined TMT samples were dried down and resuspended in liquid chromatography sample buffer (3% acetonitrile (ACN), 0.1% formic acid) before desalting with Sep-Pak C18 cc Cartridges (Waters).

#### Peptide fractionation of TMT-labeled samples

Dried TMT-labeled samples were resuspended in high pH buffer A (5 mM ammonium formate, 2% ACN) before offline high pH reverse phase fractionation by high-performance liquid chromatography (HPLC) on an UltiMate 3000 HPLC (Thermo Scientific) with an XBridge Peptide BEH C18 (130 Å, 3.5 µm; 4.6 mm × 250 mm) column (Waters) as previously described (Mertins et al.<sup>65</sup>). Each fractionated TMT plex was pooled into 24 or 28 fractions and 10% of each fraction was reserved for global proteome measurements. The remaining fractions were further pooled into 12 or 14 fractions per TMT plex for phosphoproteomics. Dried global proteome fractions or immobilized metal affinity chromatography-enriched phosphopeptides were reconstituted in liquid chromatography sample buffer before mass spectrometric measurements.

#### Phosphopeptide enrichment

Phosphopeptide enrichment was performed with immobilized metal affinity chromatography automated on an AssayMap Bravo System (Agilent) equipped with AssayMAP Fe(III)-NTA cartridges.

#### Liquid chromatography–mass spectrometry

Samples were fractionated online with a 25-cm column packed in-house with C18-AQ1.9 µm beads (Dr. Maisch Reprosil-Pur 120). Samples were separated with a gradient of mobile phase A (0.1% formic acid and 3% acetonitrile in water) and mobile phase B (0.1% formic acid, 90% acetonitrile in water) at a flow rate of 250 µl min<sup>-1</sup>. TMT samples were separated with an EASY nLC 1200 HPLC system and temperature of the column was controlled by a column oven set to 45 °C. For a 2 h gradient, mobile phase B was increased from 4% to 30% in the first 88 min,

followed by an increase to 60% B in 10 min and a plateau of 90% B for 5 min, followed by 50% buffer B for 5 min. For a 4 h gradient, mobile phase B was increased from 3% to 30% in the first 192 min followed by an increase to 60% B in 10 min, a plateau of 90% B for 5 min and 5 min 50% buffer B. All TMT fractions were measured with a 2 h gradient. To boost identification in the 11th TMT plex with healthy bone marrow samples, fractions of plex 11 were additionally measured with a 4 h gradient. MS data of TMT samples was acquired in profile centroid mode and data-dependent acquisition on a QExactive HF-X (Thermo Fisher). MS1 scans were acquired at 60,000 resolution, scan range of 350–1,500 *m/z*, maximum injection time (IT) of 10 ms and automatic gain control (AGC) target value of 3e6. The 20 most abundant ion species were picked for fragmentation, normalized collision energy (NCE) was set to 32 and the isolation window was at 0.7 *m/z*. MS2 scans were acquired at 45,000 resolution, fixed first mass 120 *m/z*, AGC target value of 3e5 and maximum IT of 86 ms. Dynamic exclusion was set to 30 s and ions with charge state 1, 6 or higher were excluded from fragmentation. For analysis of phosphoproteomic fractions of TMT-labeled samples the liquid chromatography–mass spectrometry parameters were the same, with the exception of MS2 maximum IT that was set to 120 ms.

#### TMT raw data search and processing

All TMT mass spectrometry raw files were analyzed together in one MaxQuant (v.2.0.3.0)<sup>66</sup> run. Data were searched against the human reference proteome (UP000005640) downloaded from UniProt in January 2021 ([https://ftp.uniprot.org/pub/databases/uniprot/previous\\_releases/](https://ftp.uniprot.org/pub/databases/uniprot/previous_releases/)) and default protein contaminants. TMT correction factors were applied and the minimum reporter precursor intensity fraction was set to 0.5. Fixed modifications were set to carbamidomethylation of C and variable modifications were set to M oxidation and acetylation of protein N-termini. TMT global proteome and phosphopeptides fractions were analyzed in the same MaxQuant run in separate parameter groups using the same settings, except for including also phospho (STY) as a variable modification when searching phosphopeptide fractions. A maximum of five modifications per peptide were allowed. N-terminal acetylation and M-oxidation were used in protein quantification. Only unique and razor peptides were used for protein quantification. Protein FDR was set to 0.01. Protease specificity was set to Trypsin/P. MaxQuant output files were further analyzed in R studio (v.4.1.1). The protein groups file was filtered for reverse hits, potential contaminants and proteins only identified by site. Protein groups were further filtered for at least two peptides and at least one unique or razor peptide. The TMT-based phosphosite table was expanded by multiplicity and reverse database hits and potential contaminants were removed. Corrected reporter ion intensity columns of both tables were log<sub>2</sub> transformed and normalized by subtraction of the internal standard channel contained in each TMT plex. The resulting TMT ratios were normalized via median–median absolute deviation (MAD) normalization. Before differential expression analysis, data were filtered for detection in more than 49% of cohort samples. For comparing healthy and malignant samples, only MACS-sorted samples were compared. Proteomic results are available in Supplementary Table 6 (global proteome) and Supplementary Table 7 (phosphoproteome).

#### Label-free proteomic analysis of cell lines

CD138 MACS sorted and unsorted cell line samples were fractionated online with a 2 h gradient and mass spectrometry data were acquired on a QExactive Plus mass spectrometer in data dependent acquisition (DDA) mode (top ten). MS1 scans were acquired at 70,000 resolution, scan range of 350–2000 *m/z*, maximum IT of 50 ms and AGC target value of 3e6. NCE was set to 26 and the isolation window was at 1.6 *m/z*. MS2 scans were acquired at 17,500 resolution, fixed first mass 120 *m/z*, AGC target value of 5e4 and maximum IT of 50 ms. Dynamic exclusion was set to 30 s and ions with charge state 1, 6 or higher were excluded from fragmentation. Label-free DDA data were analyzed in MaxQuant 2.0.1.1.



## Resource

<https://doi.org/10.1038/s43018-024-00784-3>

using default parameters. The LFQ and match between run options were enabled. Phospho (STY) was included as a variable modification for searching the phosphoproteome data. MaxQuant LFQ intensities were  $\log_2$  transformed and filtered for contaminants, identified by side, as well as valid values (minimum three per experimental group). The missing values were imputed from a normal distribution with a width of 0.3 times the standard deviation in the sample and a downshift of 1.8 from the observed mean. LFQ intensities were median normalized before differential expression analysis and experimental groups (control and MACS) were compared using a two-sided moderated two-sample *t*-test.

UBE2Q1 overexpressing samples were analyzed as described previously using data-independent acquisition (DIA)<sup>67</sup>. Label-free DIA data were searched using DIA-NN 1.8.1 software against the human UniProt reference proteome<sup>68</sup>. The search was performed in library-free mode with the *in silico* FASTA digest parameter enabled. The peptide length range was set to 7–30, and the precursor charge range was set to 1–4. The *m/z* range for precursors was set to 340–1,650, and for fragment ions, it was set to 200–1,800. The rest of parameters were set to default with reannotate and match between run being enabled. LFQ protein intensities from the DIA-NN pg output table were log<sub>2</sub> transformed and filtered for contaminants and peptides per protein (>1), as well as valid values (>70%). Imputation was performed as described above and resulting intensities were median normalized before differential expression analysis. Experimental groups (empty overexpression vector (empty OE) and UBE2Q1 overexpression (UBE2Q1 OE)) were compared using a two-sided moderated two-sample *t*-test.

#### Cell culture

All cell lines were obtained from the American Type Culture Collection (ATCC) or DSMZ German Collection of Microorganisms and Cell Cultures and were maintained in RPMI-1640 medium containing 10% fetal bovine serum (FBS) and supplemented with 1% penicillin/streptomycin and 1% L-glutamine. NCI-H929 cells were cultured in media supplemented with beta-mercaptoethanol and sodium pyruvate, and INA-6 cells were cultured in media supplemented with IL-6. Cells were maintained at 37 °C with 5% CO<sub>2</sub> in the humidified atmosphere.

#### CRISPR–Cas9 activation screen

Lentiviral plasmid dCAS-VP64 Blast was a gift from Feng Zhang (Addgene plasmid #61425)<sup>69</sup> and was used to stably transduce MM.1S cells. The human Calabrese CRISPR activation pooled library set A was a gift from David Root and John Doench (Addgene #92379)<sup>70</sup>. Lentivirus was produced using HEK293T cells via transfection of the guide library with pSPAX2 and pMD2.G. Virus titration was performed to achieve a MOI of ~0.3 in MM.1S dCas-VP64 cells. A total of  $1 \times 10^8$  MM.1S dCas-VP64 cells were transduced, and  $3 \times 10^7$  cells were collected for baseline comparison. The remaining cells were maintained and the media were refreshed every 3 days. On day 28, all cells were collected for genomic DNA analysis. Genomic DNA extraction was performed with Wizard Genomic DNA Purification Kit (A1120). The guide RNA library was amplified and cleaned up with AMPure XP beads. Library single guide (sg)RNAs were sequenced on a NextSeq 500 instrument (Illumina). The MAGeCK algorithm (<https://www.bioconductor.org/packages/release/bioc/html/MAGeCKFlute.html>) was utilized for analyzing normalized reads and beta score. The beta score indicates the difference in sgRNA abundance between day 4 and day 28, a high score indicating a survival advantage of the respective gene.

#### Generation of UBE2Q1 overexpression cell lines

UBE2Q1 cDNA was cloned into retroviral vector pRSF91-FLAG-GW-IRES-GFP-T2A-Puro via a Gateway reaction. Retroviral vectors containing empty or UBE2Q1 constructs generated in HEK293T cells were used to stably transduce MM cell lines OPM2 and LP-1. Seven days posttransduction, cells were placed under puromycin selection. At the

time of analysis, the purity of stable cell lines was 99% GFP fluorescence as determined by flow cytometry.

#### Inhibitor treatment and viability assays

NT157 was obtained from SelleckChem (S8228), erdafitinib was purchased from Hölzel Diagnostics (HY-18708). Cells were seeded in 384-well plates with respective treatments and plates were incubated at 37 °C for 96 h. Cell viability readout was measured using CellTiter-Glo Luminescent Cell Viability Assay on a POLARstar Omega plate reader.

#### FACS analysis of FCRL2 expression

FCRL2 fluorescence-activated cell sorting (FACS) analysis was performed on primary cells, of 14 samples from patients with MM (13 bone marrow aspirates and one ascitic fluid) and 7 healthy donor samples (6 bone marrow samples and one peripheral blood). All samples contained isolated mononuclear cells and were stained with allophycocyanin (APC) anti-FCRL2 (Miltenyi Biotec, 130-107-439). For myeloma cell identification, we used BV421 anti-BCMA (BioLegend, 357519) and FITC anti-SLAMF7 (BioLegend, 331818). The different subpopulations of immune cells were distinguished by PE anti-CD138 (BD Pharmingen, 552026), FITC anti-CD19, PE anti-CD3 (both from BioLegend, 302206 and 344806) as well as PC7 anti-CD13, PE anti-CD33 and PE anti-CD34 (all from Beckman Coulter, B19714, A07775 and A07776). All antibodies were used in a dilution of 1:40. Data analysis was performed with FlowJo v10. Unstained controls were used to set the gates for the fluorochromes.

#### Survival analysis with bootstrapping and risk score calculation with AIC-optimal model

The analysis was restricted to patients with MM treated with lenalidomide in induction and maintenance therapy as well as high-dose melphalan/auto-SCT within DSMM clinical trials ( $N = 100$  patients). For each fully quantified protein and phosphopeptide, a continuous variable Cox proportional hazard model for PFS was calculated and resulting *P* values were corrected with Benjamini–Hochberg. We combined the FDR-controlled approach with 1,000-fold bootstrapping to identify the most reproducibly significant proteins in a cohort of the same size randomly sampled with replacement from our data, that is, allowing multiple occurrences of samples in the bootstrap cohort. The 95% confidence interval of *P* values from the bootstrapping was calculated. Proteins with an upper confidence interval of *P* values <0.1 and an FDR <0.1 ( $n = 32$ ) were selected as candidates for the final risk score. A multi-protein Cox PH model was constructed by step-wise addition of optimal proteins based on the Akaike Information Content (AIC), balancing increased model performance versus increased model complexity. The final risk score was calculated on the AIC-optimal multi-protein model, by linear combination of the protein abundance scaled by the model coefficients. This resulted in a protein score containing protein-level information of eight proteins with differing weights. The inclusion of additional proteins or phosphopeptides into the model only led to marginal improvement in the survival prediction accuracy. Differences in survival were analyzed with a log-rank test. For validation, we calculated the protein risk score on untreated myeloma samples analyzed by Kropivsek et al.<sup>21</sup> based on the provided protein quantifications ('CD138 cells' quantification). The term for PDSS2 was omitted from the risk score since it was not quantified in the Kropivsek et al. cohort. No other adaptations of the risk score were employed. Survival curves were stratified by the median risk score of the respective cohort.

#### RNA–protein correlation and CNV buffering analysis

For RNA–protein correlation analysis RNAseq samples were filtered for a minimum plasma cell content of 80% and a mapped read count higher than 20 million. Proteome data were collapsed to gene-level information via median and RNA and protein datasets were matched



## Resource

<https://doi.org/10.1038/s43018-024-00784-3>

by gene name. Copy number variation (CNV) data were matched with RNA and protein data via the cytogenetic band of the corresponding gene locus. For calculating Pearson correlation across MM samples, the resulting data matrix was filtered for at least ten paired values. To estimate the buffering of CNVs from RNA to protein level we calculated a customized score with the following formula:

$$\text{buffering score}_g = \left[ \text{corr}(\text{RNA}_g, \text{CN}_g) - \text{corr}(\text{protein}_g, \text{CN}_g) \right] \times |\text{CN}_g - 2|$$

For each gene ( $g$ ) we subtracted the Pearson correlation ( $\text{corr}$ ) of protein to copy number (CN) from the Pearson correlation ( $\text{corr}$ ) of RNA to CN. The resulting delta was corrected with the average copy number effect diverging from a diploid genotype. Pearson correlations and buffering scores were subjected to ssGSEA analysis as described below.

### ssGSEA

The ssGSEA implementation available on <https://github.com/broadinstitute/ssGSEA2.0> was used to separately project protein and phosphopeptide abundance changes to signaling pathways. The normalized ratio or fold change matrix was collapsed to gene level information via median and subjected to ssGSEA. For ssGSEA of normalized TMT ratios, the gene set databases containing curated gene sets (C2.all.v7.0.symbols.gmt), oncogenic signature gene sets, (c6.all.v7.0.symbols.gmt) and hallmark gene sets (h.all.v7.0.symbols.gmt) were used. For ssGSEA of RNA to protein correlations, the Kyoto Encyclopedia of Genes and Genomes (KEGG) gene sets (c2.cp.kegg.v7.0.symbols.gmt) were used. For ssGSEA of buffering of CNVs from RNA to protein level, databases containing positional genesets (c1.all.v7.0.symbols.gmt) and KEGG gene sets (c2.cp.kegg.v7.0.symbols.gmt) were used. The following parameters were used for all ssGSEA analyses: sample.norm.type = 'rank', weight = 0.75, statistic = 'area.under.RES', output.score.type = 'NES', nperm = 1,000, min.overlap = 10, correl.type = 'z.score'

### NMF clustering of ssGSEA enrichment scores

Normalized ssGSEA scores of phosphoproteomic data were used as input for NMF with the NMF R package (v.0.23.0)<sup>71</sup> as previously described<sup>72</sup>. The following parameters were used:  $K = 2:7$ , method = 'brunet', nrun = 50. The cophenetic correlation coefficient was used to evaluate the clustering quality. After determining the optimal factorization rank  $k$ , we repeated the NMF analysis using 500 iterations with random initializations and performed partitioning of samples into clusters.

### GO term analysis with Metascape

Gene Ontology (GO) term enrichment analysis of a gene list corresponding to proteins regulated in Iq gain not located on chromosome 1q was performed with the Metascape<sup>73</sup> online tool.

### Integration of Depmap data

Proteins significantly upregulated in myeloma versus healthy samples (<0.1 FDR) or selectively identified in myeloma samples were further filtered for potential therapeutic targets by integrating the depmap CRISPR KO database (gene effect download file<sup>74</sup>). First, genes coding proteins in our candidate list were filtered for median dependency in myeloma cell lines <-0.4 (median dependency of the myeloma therapeutic targets IKZF1 and IKZF3). Common essential genes (DepMap Public 22Q2) were excluded from the target list. In addition, genes were filtered for having a minimum difference of median dependency in myeloma versus median dependency in nonmyeloma cell lines >0.1.

### RNA sequencing data analysis

RNA sequencing data were aligned and quantified with STAR and messenger RNA reads were identified using an in-house analysis pipeline detecting exons in a shuffled order. To increase comparability to TMT

data, RNA gene-level transcripts per million (TPM) values were further normalized as described previously<sup>75</sup>. First, TPM gene-level data were normalized via median subtraction (by gene) and, subsequently, each sample was normalized by median-MAD normalization. The normalized data are available in Supplementary Table 2.

### Nanopore DNA sequencing data analysis

After basecalling, the sequenced reads were aligned with minimap2 (ref. 76) to the University of California, Santa Cruz (UCSC) hg19 genome reference (<https://www.ncbi.nlm.nih.gov/grc>) without haplotype specific scaffolds. After conversion of the alignment files (SAMtools v.0.1.19, <https://github.com/samtools/>) SAM format, (<https://samtools.github.io/hts-specs/SAMv1.pdf>) sorting and indexing to binary alignment format (BAM format, <https://samtools.github.io/hts-specs/SAMv1.pdf>) the copy number profiles were generated with the absolute copy number estimate package<sup>77</sup> in R (4.2.1, <https://cran.r-project.org/>) with a bin size of 1 million base pairs. Errors were estimated with 'maximum absolute error' and only autosomes were called. The resulting copy number aberrations were reported on to genomic band level to the nearest integer. Ambiguous copy numbers were called by the most prevalent copy number on the particular band. Bands with insufficient reads were marked as NA. For subclonal events, the nearest natural number was chosen, except in the vicinity of two where a deviation threshold of 0.35 was used to maximize the concordance with FISH results.

Ploidy and cellularity (relevant local minimum used) of each sample in absolute copy number estimate were matched to existing FISH data. If FISH data were not available, the profiles were chosen for plausibility, minimizing the number of aberrations and avoiding scaffolds with copy number 0. The processed data are available in Supplementary Table 2. Four additional cases without 9q amplification were assigned to the hyperdiploidy group based on nanopore sequencing

### Validation by single-cell sequencing data

Expression of candidates from the proteomic analysis was further validated with single-cell RNA sequencing data of bone marrow from healthy individuals and patients with MM from Lutz et al.<sup>51</sup>. Uniform manifold approximation and projection (UMAP) plots highlighting normalized expression for genes of interest were generated in R using the FeaturePlot() function from the Seurat package<sup>78</sup>.

### Statistics and reproducibility

No statistical method was used to predetermine sample size, samples were chosen based on availability. As the study focuses on newly diagnosed samples, four TMT labeled samples corresponding to relapse cases were excluded from the analysis. In the TMT plex analyzing healthy cells, carrier channels containing the booster channel and unsorted mononuclear cells were excluded from further analysis; they were present in the TMT plex to increase coverage of low abundant proteins. Patient samples were randomly distributed across TMT plexes. Technical replicates of eight samples were differentially labeled and included in different TMT plexes. Replicates clustered together as expected and had an average Pearson correlation coefficient of 0.8 for global proteome and 0.77 for phosphoproteomic normalized ratios, respectively. We performed four or three biological replicates of cell culture experiments for proteomics or inhibitor treatments, respectively. All attempts of replication were successful and no replicate was excluded from analysis. Differentially expressed proteins were determined with a two-sided moderated two-sample  $t$ -test (limma package). The resulting  $P$  values were corrected with the Benjamini-Hochberg method. Drug treatments of each cell line were compared to respective dimethyl sulfoxide (DMSO) controls with a Dunnett's test. For analyzing CRISPR-Cas9 activation screen data, the MAGeCK maximum-likelihood estimation (MLE) algorithm was applied for the analysis of beta scores and  $P$  values.

## Resource

<https://doi.org/10.1038/s43018-024-00784-3>

## Reporting summary

Further information on research design is available in the Nature Portfolio Reporting Summary linked to this article.

## Data availability

Data that support the findings of this study have been deposited in the following repositories. Mass spectrometry data have been deposited on PRIDE with the accession numbers [PXD038437](https://www.ebi.ac.uk/pride/archive/projects/PXD038437) and [PXD043580](https://www.ebi.ac.uk/pride/archive/projects/PXD043580). Processed proteomics data of patient samples can be interactively explored at <https://myelomaprot.mdc-berlin.de/>. RNA sequencing expression data are available at the Gene Expression Omnibus under accession number [GSE222727](https://www.ncbi.nlm.nih.gov/geo/query/acc.cgi?acc=GSE222727). Previously published microarray data that were reanalyzed here are available under accession code [GSE2658](https://www.ncbi.nlm.nih.gov/geo/query/acc.cgi?acc=GSE2658) ref. 34. Proteomics data were searched against the human reference proteome (UP000005640) downloaded from UniProt in January 2021 ([https://ftp.uniprot.org/pub/databases/uniprot/previous\\_releases/](https://ftp.uniprot.org/pub/databases/uniprot/previous_releases/)). Source data are provided with this paper. All other data supporting the findings of this study are available from the corresponding author on reasonable request.

## Code availability

The data were processed as described in Methods. All used R packages are public and are freely available online. No new code or mathematical algorithms were generated from this manuscript.

## References

- van de Donk, N. W. C. J., Pawlyn, C. & Yong, K. L. Multiple myeloma. *Lancet* **397**, 410–427 (2021).
- Manier, S. et al. Genomic complexity of multiple myeloma and its clinical implications. *Nat. Rev. Clin. Oncol.* **14**, 100–113 (2017).
- Zhan, F. et al. The molecular classification of multiple myeloma. *Blood* <https://doi.org/10.1182/blood-2005-11-013458> (2006).
- Shaughnessy, J. D. Jr et al. A validated gene expression model of high-risk multiple myeloma is defined by deregulated expression of genes mapping to chromosome 1. *Blood* **109**, 2276–2284 (2007).
- Lohr, J. G. et al. Widespread genetic heterogeneity in multiple myeloma: implications for targeted therapy. *Cancer Cell* **25**, 91–101 (2014).
- Walker, B. A. et al. Mutational spectrum, copy number changes, and outcome: results of a sequencing study of patients with newly diagnosed myeloma. *J. Clin. Oncol.* **33**, 3911–3920 (2015).
- Chapman, M. A. et al. Initial genome sequencing and analysis of multiple myeloma. *Nature* **471**, 467–472 (2011).
- Mani, D. R. et al. Cancer proteogenomics: current impact and future prospects. *Nat. Rev. Cancer* **22**, 298–313 (2022).
- Vasaikar, S. et al. Proteogenomic analysis of human colon cancer reveals new therapeutic opportunities. *Cell* **177**, 1035–1049.e19 (2019).
- Satpathy, S. et al. A proteogenomic portrait of lung squamous cell carcinoma. *Cell* **184**, 4348–4371.e40 (2021).
- Mertins, P. et al. Proteogenomics connects somatic mutations to signalling in breast cancer. *Nature* **534**, 55–62 (2016).
- Jayavelu, A. K. et al. The proteogenomic subtypes of acute myeloid leukemia. *Cancer Cell* **40**, 301–317.e12 (2022).
- Meier-Abt, F. et al. The protein landscape of chronic lymphocytic leukemia. *Blood* **138**, 2514–2525 (2021).
- Herbst, S. A. et al. Proteogenomics refines the molecular classification of chronic lymphocytic leukemia. *Nat. Commun.* **13**, 6226 (2022).
- Petralia, F. et al. Integrated proteogenomic characterization across major histological types of pediatric brain cancer. *Cell* **183**, 1962–1985.e31 (2020).
- Griffen, T. L. et al. Proteomic profiling based classification of CLL provides prognostication for modern therapy and identifies novel therapeutic targets. *Blood Cancer J.* **12**, 43 (2022).
- Janker, L. et al. Metabolic, anti-apoptotic and immune evasion strategies of primary human myeloma cells indicate adaptations to hypoxia. *Mol. Cell. Proteomics* **18**, 936–953 (2019).
- Mohamed, A. et al. Concurrent lipidomics and proteomics on malignant plasma cells from multiple myeloma patients: probing the lipid metabolome. *PLoS ONE* **15**, e0227455 (2020).
- Ng, Y. L. D. et al. Proteomic profiling reveals CDK6 upregulation as a targetable resistance mechanism for lenalidomide in multiple myeloma. *Nat. Commun.* **13**, 1009 (2022).
- Koomen, D. C. et al. Metabolic changes are associated with melphalan resistance in multiple myeloma. *J. Proteome Res.* **20**, 3134–3149 (2021).
- Kropivsek, K. et al. Ex vivo drug response heterogeneity reveals personalized therapeutic strategies for patients with multiple myeloma. *Nat. Cancer* **4**, 734–753 (2023).
- Kumar, S. et al. Efficacy of venetoclax as targeted therapy for relapsed/refractory t(11;14) multiple myeloma. *Blood* **130**, 2401–2409 (2017).
- Kitadate, A. et al. Multiple myeloma with t(11;14)-associated immature phenotype has lower CD38 expression and higher BCL2 dependence. *Cancer Sci.* **112**, 3645–3654 (2021).
- Gupta, V. A. et al. Venetoclax sensitivity in multiple myeloma is associated with B-cell gene expression. *Blood* **137**, 3604–3615 (2021).
- Santra, M., Zhan, F., Tian, E., Barlogie, B. & Shaughnessy, J. A subset of multiple myeloma harboring the t(4;14)(p16;q32) translocation lacks FGFR3 expression but maintains anIGH/MMSET fusion transcript. *Blood* <https://doi.org/10.1182/blood-2002-09-2801> (2003).
- Walker, B. A. et al. A compendium of myeloma-associated chromosomal copy number abnormalities and their prognostic value. *Blood* **116**, e56–e65 (2010).
- Keats, J. J. et al. In multiple myeloma, t(4;14)(p16;q32) is an adverse prognostic factor irrespective of FGFR3 expression. *Blood* **101**, 1520–1529 (2003).
- Ghandi, M. et al. Next-generation characterization of the Cancer Cell Line Encyclopedia. *Nature* **569**, 503–508 (2019).
- DepMap, B. DepMap 22Q2 public. *Figshare* <https://doi.org/10.6084/m9.figshare.19700056.v2> (2022).
- Hussain, S., Bedekovics, T., Chesi, M., Bergsagel, P. L. & Galarzy, P. J. UCHL1 is a biomarker of aggressive multiple myeloma required for disease progression. *Oncotarget* **6**, 40704–40718 (2015).
- Guo, Q., Xie, J., Dang, C. V., Liu, E. T. & Bishop, J. M. Identification of a large Myc-binding protein that contains RCC1-like repeats. *Proc. Natl Acad. Sci. USA* **95**, 9172–9177 (1998).
- Fan, Y. et al. FXR1 regulates transcription and is required for growth of human cancer cells with homozygous deletion. *eLife* **6**, e26129 (2017).
- Schmidt, T. M., Fonseca, R. & Usmani, S. Z. Chromosome 1q21 abnormalities in multiple myeloma. *Blood Cancer J.* **11**, 83 (2021).
- Slomp, A. et al. Multiple myeloma with 1q21 amplification is highly sensitive to MCL-1 targeting. *Blood Adv.* **3**, 4202–4214 (2019).
- Zhang, J. et al. Disruption of KMT2D perturbs germinal center B cell development and promotes lymphomagenesis. *Nat. Med.* **21**, 1190–1198 (2015).
- Raffel, S. et al. Quantitative proteomics reveals specific metabolic features of acute myeloid leukemia stem cells. *Blood* **136**, 1507–1519 (2020).
- Sohn, M. et al. Ahnak promotes tumor metastasis through transforming growth factor- $\beta$ -mediated epithelial-mesenchymal transition. *Sci. Rep.* **8**, 14379 (2018).
- de Matos Simoes, R. et al. Genome-scale functional genomics identify genes preferentially essential for multiple myeloma cells compared to other neoplasias. *Nat. Cancer* **4**, 754–773 (2023).



## Resource

<https://doi.org/10.1038/s43018-024-00784-3>

39. Krönke, J. et al. Lenalidomide causes selective degradation of IKZF1 and IKZF3 in multiple myeloma cells. *Science* **343**, 301–305 (2014).
40. Lu, G. et al. The myeloma drug lenalidomide promotes the cereblon-dependent destruction of Ikaros proteins. *Science* **343**, 305–309 (2014).
41. Shaffer, A. L. et al. IRF4 addiction in multiple myeloma. *Nature* **454**, 226–231 (2008).
42. Herbst, D. A. et al. Structure of the human SAGA coactivator complex. *Nat. Struct. Mol. Biol.* **28**, 989–996 (2021).
43. Chapuy, B. et al. Discovery and characterization of super-enhancer-associated dependencies in diffuse large B cell lymphoma. *Cancer Cell* **24**, 777–790 (2013).
44. Zhao, C. et al. POU2AF1, an amplification target at 11q23, promotes growth of multiple myeloma cells by directly regulating expression of a B-cell maturation factor, TNFRSF17. *Oncogene* **27**, 63–75 (2008).
45. Ge, N. L. & Rudikoff, S. Insulin-like growth factor I is a dual effector of multiple myeloma cell growth. *Blood* **96**, 2856–2861 (2000).
46. Gonçalves, E. et al. Pan-cancer proteomic map of 949 human cell lines. *Cancer Cell* **40**, 835–849.e8 (2022).
47. Garofalo, C. et al. Preclinical effectiveness of selective inhibitor of IRS-1/2 NT157 in osteosarcoma cell lines. *Front. Endocrinol.* **6**, 74 (2015).
48. Berdeja, J. G. et al. Ciltacabtagene autoleucel, a B-cell maturation antigen-directed chimeric antigen receptor T-cell therapy in patients with relapsed or refractory multiple myeloma (CARTITUDE-1): a phase 1b/2 open-label study. *Lancet* **398**, 314–324 (2021).
49. Munshi, N. C. et al. Idecabtagene vicleucel in relapsed and refractory multiple myeloma. *N. Engl. J. Med.* **384**, 705–716 (2021).
50. Hu, Z. et al. The Cancer Surfaceome Atlas integrates genomic, functional and drug response data to identify actionable targets. *Nat. Cancer* **2**, 1406–1422 (2021).
51. Lutz, R. et al. Multiple myeloma long-term survivors display sustained immune alterations decades after first line therapy. Preprint at *bioRxiv* <https://doi.org/10.1101/2023.05.27.542555> (2023).
52. Cohen, A. D. et al. Initial clinical activity and safety of BFCR4350A, a FcRH5/CD3 T-cell-engaging bispecific antibody, in relapsed/refractory multiple myeloma. *Blood* **136**, 42–43 (2020).
53. Karlsson, M. et al. A single-cell type transcriptomics map of human tissues. *Sci. Adv.* **7**, eabh2169 (2021).
54. Chang, R. et al. Upregulated expression of ubiquitin-conjugating enzyme E2Q1 (UBE2Q1) is associated with enhanced cell proliferation and poor prognosis in human hepatocellular carcinoma. *J. Mol. Biol.* **46**, 45–56 (2015).
55. Topno, R., Singh, I., Kumar, M. & Agarwal, P. Integrated bioinformatic analysis identifies UBE2Q1 as a potential prognostic marker for high grade serous ovarian cancer. *BMC Cancer* **21**, 220 (2021).
56. Li, C. et al. Genetic analysis of multiple myeloma identifies cytogenetic alterations implicated in disease complexity and progression. *Cancers* **13**, 517 (2021).
57. Kuiper, R. et al. A gene expression signature for high-risk multiple myeloma. *Leukemia* **26**, 2406–2413 (2012).
58. Patel, J. H. et al. The c-MYC oncoprotein is a substrate of the acetyltransferases hGCN5/PCAF and TIP60. *Mol. Cell. Biol.* **24**, 10826–10834 (2004).
59. Lee, H. et al. Mechanisms of antigen escape from BCMA- or GPRC5D-targeted immunotherapies in multiple myeloma. *Nat. Med.* **29**, 2295–2306 (2023).
60. Da Viá, M. C. et al. Homozygous BCMA gene deletion in response to anti-BCMA CAR T cells in a patient with multiple myeloma. *Nat. Med.* **27**, 616–619 (2021).
61. Anderson, G. S. F. et al. Unbiased cell surface proteomics identifies SEMA4A as an effective immunotherapy target for myeloma. *Blood* **139**, 2471–2482 (2022).
62. Ferguson, I. D. et al. The surfaceome of multiple myeloma cells suggests potential immunotherapeutic strategies and protein markers of drug resistance. *Nat. Commun.* **13**, 4121 (2022).
63. Li, F. J. et al. FCRL2 expression predicts IGHV mutation status and clinical progression in chronic lymphocytic leukemia. *Blood* **112**, 179–187 (2008).
64. Knop, S. et al. Lenalidomide, adriamycin, dexamethasone for induction followed by stem-cell transplant in newly diagnosed myeloma. *Leukemia* **31**, 1816–1819 (2017).
65. Mertins, P. et al. Reproducible workflow for multiplexed deep-scale proteome and phosphoproteome analysis of tumor tissues by liquid chromatography–mass spectrometry. *Nat. Protoc.* **13**, 1632–1661 (2018).
66. Cox, J. & Mann, M. MaxQuant enables high peptide identification rates, individualized p.p.b.-range mass accuracies and proteome-wide protein quantification. *Nat. Biotechnol.* **26**, 1367–1372 (2008).
67. Wang, Z. et al. Direct-to-biology, automated, nano-scale synthesis, and phenotypic screening-enabled E3 ligase modulator discovery. *Nat. Commun.* **14**, 8437 (2023).
68. Demichev, V., Messner, C. B., Vernardis, S. I., Lilley, K. S. & Ralser, M. DIA-NN: neural networks and interference correction enable deep proteome coverage in high throughput. *Nat. Methods* **17**, 41–44 (2020).
69. Konermann, S. et al. Genome-scale transcriptional activation by an engineered CRISPR–Cas9 complex. *Nature* **517**, 583–588 (2015).
70. Sanson, K. R. et al. Optimized libraries for CRISPR–Cas9 genetic screens with multiple modalities. *Nat. Commun.* **9**, 5416 (2018).
71. Gaujoux, R. & Seoighe, C. A flexible R package for nonnegative matrix factorization. *BMC Bioinformatics* **11**, 367 (2010).
72. Gillette, M. A. et al. Proteogenomic characterization reveals therapeutic vulnerabilities in lung adenocarcinoma. *Cell* **182**, 200–225.e35 (2020).
73. Zhou, Y. et al. Metascape provides a biologist-oriented resource for the analysis of systems-level datasets. *Nat. Commun.* **10**, 1523 (2019).
74. Pacini, C. et al. Integrated cross-study datasets of genetic dependencies in cancer. *Nat. Commun.* **12**, 1–14 (2021).
75. Krug, K. et al. Proteogenomic landscape of breast cancer tumorigenesis and targeted therapy. *Cell* **183**, 1436–1456.e31 (2020).
76. Li, H. Minimap2: pairwise alignment for nucleotide sequences. *Bioinformatics* **34**, 3094–3100 (2018).
77. Poell, J. B. et al. ACE: absolute copy number estimation from low-coverage whole-genome sequencing data. *Bioinformatics* **35**, 2847–2849 (2019).
78. Hao, Y. et al. Integrated analysis of multimodal single-cell data. *Cell* **184**, 3573–3587.e29 (2021).

### Acknowledgements

This study was supported by funding through a grant of Deutsche Konsortium für Translationale Krebsforschung to J. Krönke and U.K., the Deutsche Forschungsgemeinschaft to J. Krönke (Emmy-Noether Program Kr3886/2-2, KR 3886/7-1 and SBF-1074) and S.H. (HA 8790/3-1), the Wilhelm Sander Stiftung to J. Krönke, the German Ministry of Education and Research, as part of the National Research Node ‘Mass spectrometry in Systems Medicine’ (MSCorSys), under grant agreement O31L0220B to P.M., and from Berliner Krebsgesellschaft for A.D., L.B., J. Krönke, P.M. and J.B. Y.L.D.N. is enrolled in the doctoral program of the Berlin School of Integrative Oncology. We thank



**Resource**<https://doi.org/10.1038/s43018-024-00784-3>

K. Holzmann and K. Lanz from the Core Facility Genomics of Ulm University for technical support with RNA sequencing. Figures were, in part, created with Biorender.

**Author contributions**

J. Krönke, P.M. and E.R. designed the study; E.R., A.D., Y.L.D.N., A.S., S.M., X.G., J. Krüger, V.S. and M.H. performed experiments; E.R., A.D., Y.L.D.N., E.S., V.S., M.B., M.Z., O.P., F.G., M.H., A.M. and R.L. analyzed, interpreted and visualized data. J. Krönke, P.M., L.B., S.H. and D.B. provided supervision. S.K., M.K., A.N., J.B., D.L., C.L., U.K., C.K., F.B., H.D., M.E., C.S. and H.E. collected patient material. J. Krönke. and E.R. wrote the manuscript with input from all authors. All authors have read and approved the manuscript.

**Funding**

Open access funding provided by Max-Delbrück-Centrum für Molekulare Medizin in der Helmholtz-Gemeinschaft (MDC).

**Competing interests**

J.K. received speaker and/or advisory board honoraria from Bristol-Myers Squibb/Celgene, Sanofi, Abbvie, Takeda, Pfizer and Janssen. S.K. received honoraria from Amgen, Bristol-Myers Squibb, Celgene, Janssen, Takeda, Sanofi and Oncoceptides; served as a consultant or in an advisory role for Amgen, Bristol-Myers Squibb, Celgene, Janssen and Takeda; and received research funding from Amgen, Bristol-Myers Squibb, Celgene, Janssen and Takeda. The other authors declare no competing interests.

**Additional information**

**Extended data** is available for this paper at <https://doi.org/10.1038/s43018-024-00784-3>.

**Supplementary information** The online version contains supplementary material available at <https://doi.org/10.1038/s43018-024-00784-3>.

**Correspondence and requests for materials** should be addressed to Stefan Knop, Philipp Mertins or Jan Krönke.

**Peer review information** *Nature Cancer* thanks Bruno Paiva and the other, anonymous, reviewer(s) for their contribution to the peer review of this work.

**Reprints and permissions information** is available at [www.nature.com/reprints](http://www.nature.com/reprints).

**Publisher's note** Springer Nature remains neutral with regard to jurisdictional claims in published maps and institutional affiliations.

**Open Access** This article is licensed under a Creative Commons Attribution 4.0 International License, which permits use, sharing, adaptation, distribution and reproduction in any medium or format, as long as you give appropriate credit to the original author(s) and the source, provide a link to the Creative Commons licence, and indicate if changes were made. The images or other third party material in this article are included in the article's Creative Commons licence, unless indicated otherwise in a credit line to the material. If material is not included in the article's Creative Commons licence and your intended use is not permitted by statutory regulation or exceeds the permitted use, you will need to obtain permission directly from the copyright holder. To view a copy of this licence, visit <http://creativecommons.org/licenses/by/4.0/>.

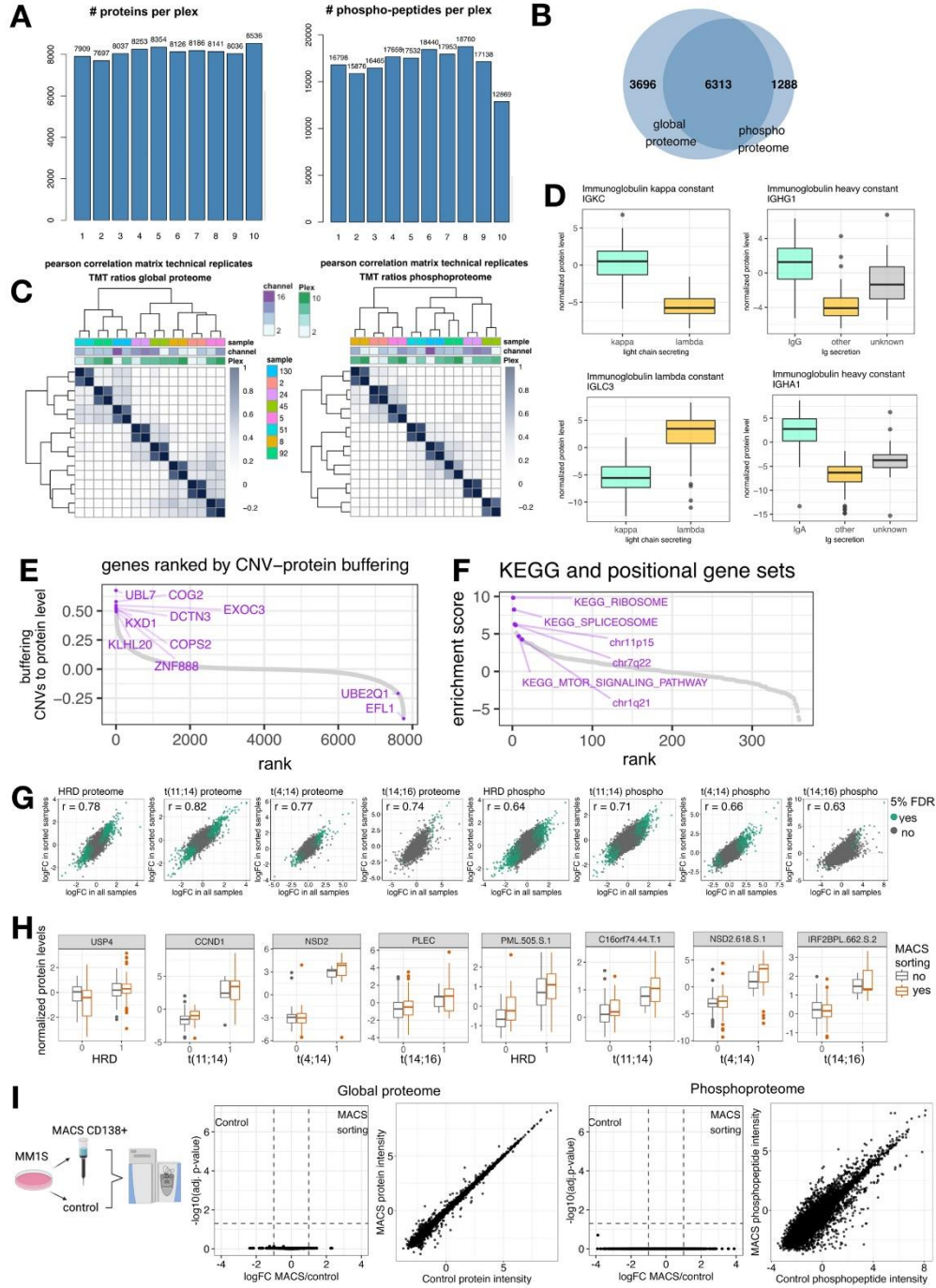
© The Author(s) 2024

**Evelyn Ramberger** <sup>1,2,3</sup>, **Valeriia Sapozhnikova** <sup>1,2,3</sup>, **Yuen Lam Dora Ng**<sup>1</sup>, **Anna Dolnik**<sup>1</sup>, **Matthias Ziehm** <sup>2,4</sup>, **Oliver Popp**<sup>2,4</sup>, **Eric Sträng**<sup>1</sup>, **Miriam Kull**<sup>5</sup>, **Florian Grünschlager** <sup>6,7,8</sup>, **Josefine Krüger** <sup>1</sup>, **Manuela Benary** <sup>4</sup>, **Sina Müller** <sup>1</sup>, **Xiang Gao**<sup>5</sup>, **Arunima Murgai** <sup>1,3</sup>, **Mohamed Hajj**<sup>2,4</sup>, **Annika Schmidt**<sup>1</sup>, **Raphael Lutz**<sup>6,7,9</sup>, **Axel Nogai**<sup>1</sup>, **Jan Braune** <sup>1</sup>, **Dominik Laue** <sup>1</sup>, **Christian Langer**<sup>5</sup>, **Cyrus Khandanpour**<sup>10</sup>, **Florian Bassermann** <sup>11</sup>, **Hartmut Döhner** <sup>5</sup>, **Monika Engelhardt** <sup>12</sup>, **Christian Straka**<sup>13</sup>, **Michael Hundemer** <sup>9</sup>, **Dieter Beule** <sup>4</sup>, **Simon Haas** <sup>1,2,3,4,6,7</sup>, **Ulrich Keller** <sup>1,2,3</sup>, **Hermann Einsele** <sup>14</sup>, **Lars Bullinger**<sup>1,3</sup>, **Stefan Knop** <sup>14,15,16</sup>  , **Philipp Mertins** <sup>2,4</sup>   & **Jan Krönke** <sup>1,3</sup> 

<sup>1</sup>Charité – Universitätsmedizin Berlin, Corporate member of Freie Universität Berlin and Humboldt-Universität zu Berlin, Berlin, Germany. <sup>2</sup>Max Delbrück Center for Molecular Medicine, Berlin, Germany. <sup>3</sup>German Cancer Consortium (DKTK), partner site Berlin, DKFZ and Charité – Universitätsmedizin Berlin, Berlin, Germany. <sup>4</sup>Berlin Institute of Health, Berlin, Germany. <sup>5</sup>Internal Medicine III, University Hospital Ulm, Ulm, Germany. <sup>6</sup>German Cancer Research Center (DKFZ), Heidelberg, Germany. <sup>7</sup>Heidelberg Institute for Stem Cell Technology and Experimental Medicine, Heidelberg, Germany. <sup>8</sup>Faculty of Biosciences, Heidelberg University, Heidelberg, Germany. <sup>9</sup>Department of Medicine V, Hematology, Oncology and Rheumatology, Heidelberg University Hospital, Heidelberg, Germany. <sup>10</sup>Department of Medicine A, Hematology, Oncology and Pneumology, University Hospital Muenster, Muenster, Germany. <sup>11</sup>Department of Medicine III, Technical University of Munich, Klinikum rechts der Isar, Munich, Germany. <sup>12</sup>Freiburg University Hospital, Freiburg, Germany. <sup>13</sup>Medizinische Klinik, München Klinik Schwabing, Munich, Germany. <sup>14</sup>Department of Internal Medicine II, University Hospital Würzburg, Würzburg, Germany. <sup>15</sup>Nuremberg General Hospital, Nuremberg, Germany. <sup>16</sup>Paracelsus Medical School, Nuremberg, Germany.  
✉ e-mail: [stefan.knop@klinikum-nuernberg.de](mailto:stefan.knop@klinikum-nuernberg.de); [philipp.mertins@mdc-berlin.de](mailto:philipp.mertins@mdc-berlin.de); [jan.kroenke@charite.de](mailto:jan.kroenke@charite.de)

Resource

<https://doi.org/10.1038/s43018-024-00784-3>



Extended Data Fig. 1 | See next page for caption.

## Resource

<https://doi.org/10.1038/s43018-024-00784-3>
**Extended Data Fig. 1 | Quality control and influence of cell sorting. a:**

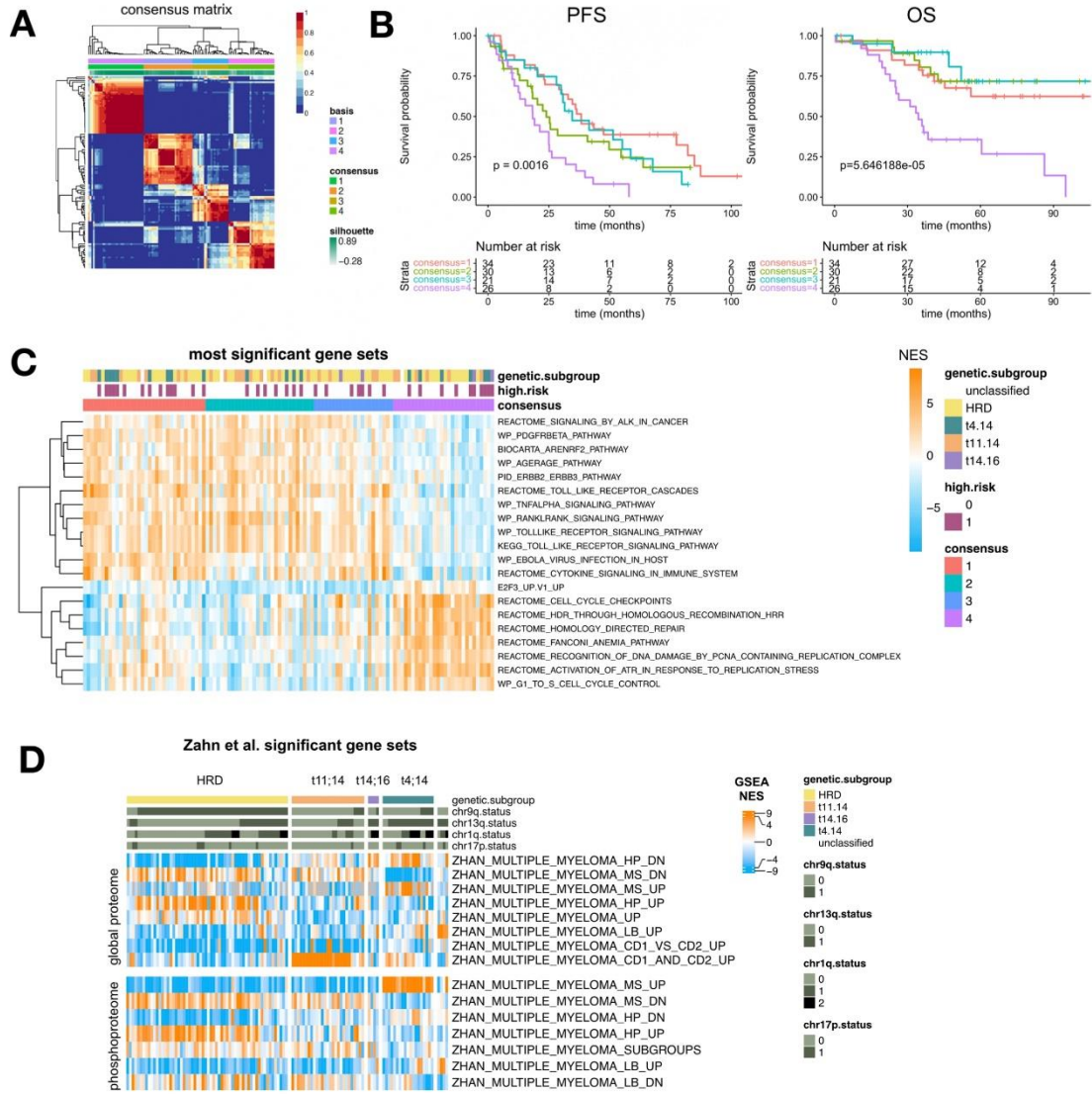
Numbers of proteins and phosphopeptides detected in each TMT plex. **b:** Overlap of detected protein IDs in the proteome and phosphoproteome datasets. **c:** Correlation matrix showing Pearson correlation of technical replicates (normalized TMT ratios). **d:** Immunoglobulin constant light chain protein levels. Predominant light chain kappa  $n = 83$ , lambda  $n = 39$ . Predominant immunoglobulin constant IgG  $n = 68$ , IgA  $n = 32$ ; other  $n = 24$ , unknown  $n = 14$ . Boxplots show median (middle line), 25th and 75th percentiles, whiskers extend to minimum and maximum excluding outliers (values outside of 1.5 times the interquartile range (IQR)). **e:** Genes ranked by the buffering score of CNVs from RNA to protein level. The buffering score was calculated with a customized score and for each gene ( $g$ ) the Pearson correlation of protein to copy number (CN) was subtracted from the Pearson correlation of RNA to CN. The resulting delta was corrected with the average copy number effect diverging from a diploid genotype. Genes are ranked from highest (high buffering of CNVs from RNA to protein level) to lowest score. **f:** SsGSEA of the protein-CNV buffering score in SIE for KEGG and positional pathways ( $n = 359$  ranked pathways) showing that CNVs of certain pathways are buffered from RNA to protein level. **g:** Correlation

of protein and phosphopeptides changes in each genetic subgroup in all samples (x-axis) and MACS-sorted samples (y-axis) in MM cohort. Regulated proteins ( $< 0.05$  FDR) are indicated in green. **h:** Levels of top-regulated proteins and phosphopeptides in each genetic subgroup in MM samples with and without MACS sorting. HRD sorted  $n = 35$ , HRD unsorted  $n = 25$ , HRDneg sorted  $n = 41$ , HRDneg unsorted  $n = 13$ ; t(11.14) sorted  $n = 24$ , t(11.14) unsorted  $n = 3$ , t(11.14)neg sorted  $n = 52$ , t(11.14)neg unsorted  $n = 35$ ; t(14.16) sorted  $n = 3$ , t(14.16) unsorted  $n = 1$ , t(14.16)neg sorted  $n = 73$ , t(14.16)neg unsorted  $n = 37$ ; t(4.14) sorted  $n = 11$ , t(4.14) unsorted  $n = 8$ , t(4.14)neg sorted  $n = 65$ , t(4.14)neg unsorted  $n = 30$ ; Boxplots show median (middle line), 25th and 75th percentiles, whiskers extend to minimum and maximum excluding outliers (values outside of 1.5\*IQR). **i:** MMIS cells were sorted with CD138 + MACS and the global proteome and phosphoproteome were analyzed with label-free proteomics ( $n = 4$ , biological replicates). MACS-sorted samples were compared against the control with a moderated 2-sample t-test. No significant differences between MACS-sorted and non-sorted MM.1S cells were detected ( $< 0.05$  FDR). Plots show results of moderated 2-sample t-test and correlation of averaged normalized intensities in both groups.



Resource

<https://doi.org/10.1038/s43018-024-00784-3>

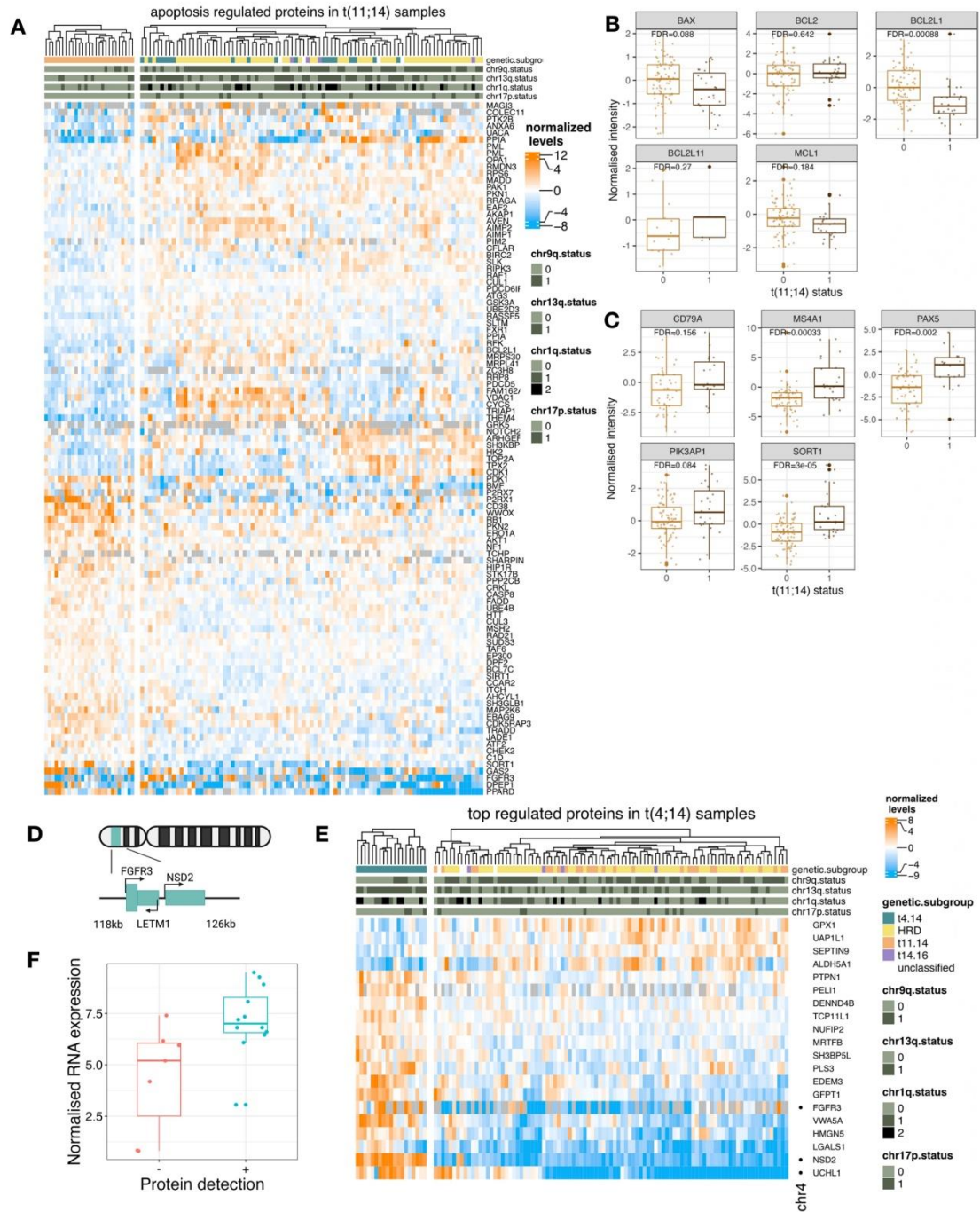


**Extended Data Fig. 2 | Unsupervised clustering of phosphoproteomic data.** **a:** SsGSEA normalized enrichment scores of phosphoproteomic data were used as input for non-negative matrix factorization (NMF) clustering. NMF consensus map is shown. **b:** Kaplan-Meier plots show progression-free survival (PFS) and overall survival (OS) of MM patients grouped by consensus cluster as shown in A. Survival in different groups was compared with a log-rank test. **c:** Gene sets of phosphoproteomic data most significantly different between consensus

cluster 4 and other clusters (moderated t-test, the 20 most significant gene sets (FDR < 0.05) are shown). **d:** TMT ratios were analyzed with ssGSEA using the gene sets C2.all.v7.0.symbols.gmt, c6.all.v7.0.symbols.gmt and h.all.v7.0.symbols.gmt. Heatmaps display ssGSEA normalized enrichment scores (NES) of Zahn et al. gene sets significant between myeloma genetic subgroups (ANOVA; FDR < 0.14). Global proteome data (top) and phosphoproteome data (bottom) are shown.

Resource

<https://doi.org/10.1038/s43018-024-00784-3>



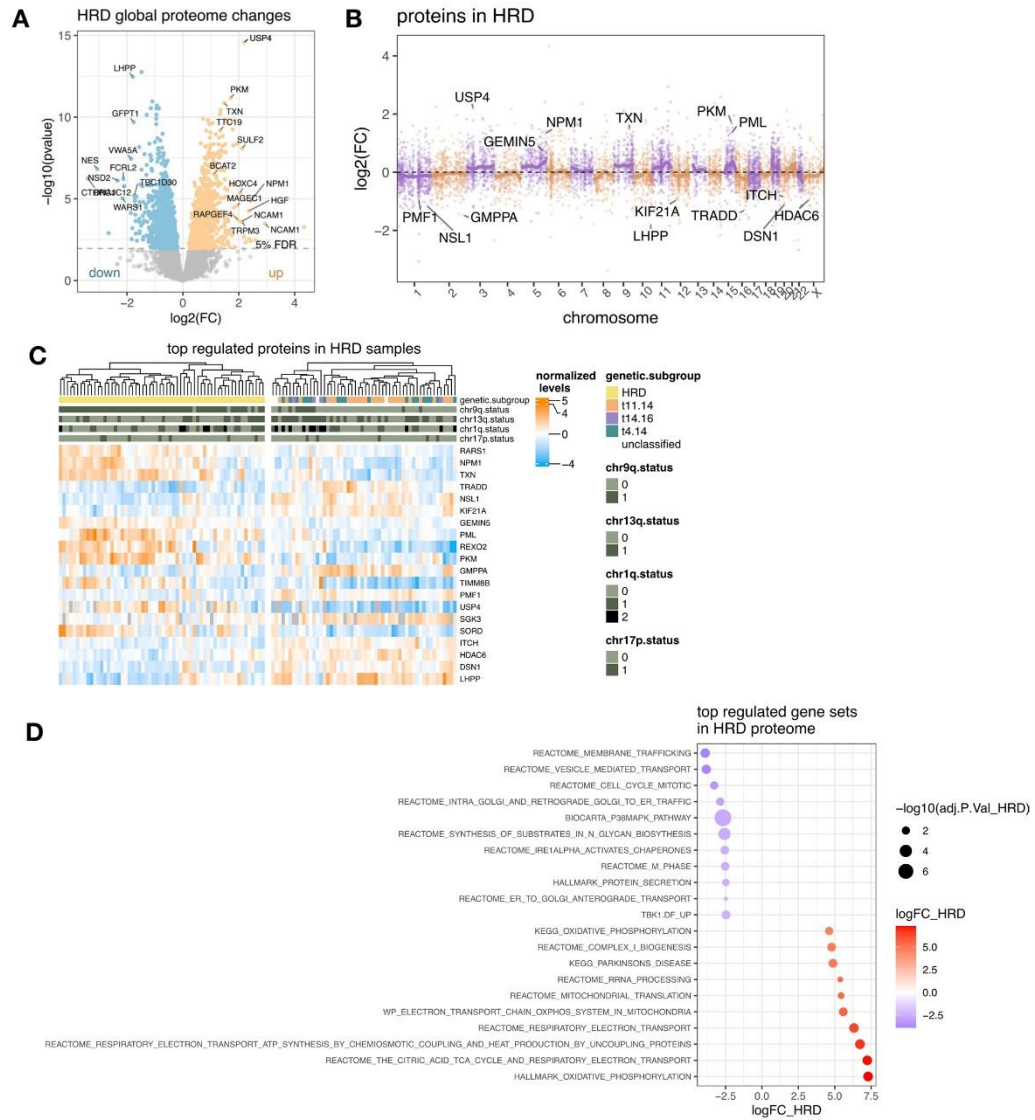
Extended Data Fig. 3 | See next page for caption.



**Resource**<https://doi.org/10.1038/s43018-024-00784-3>

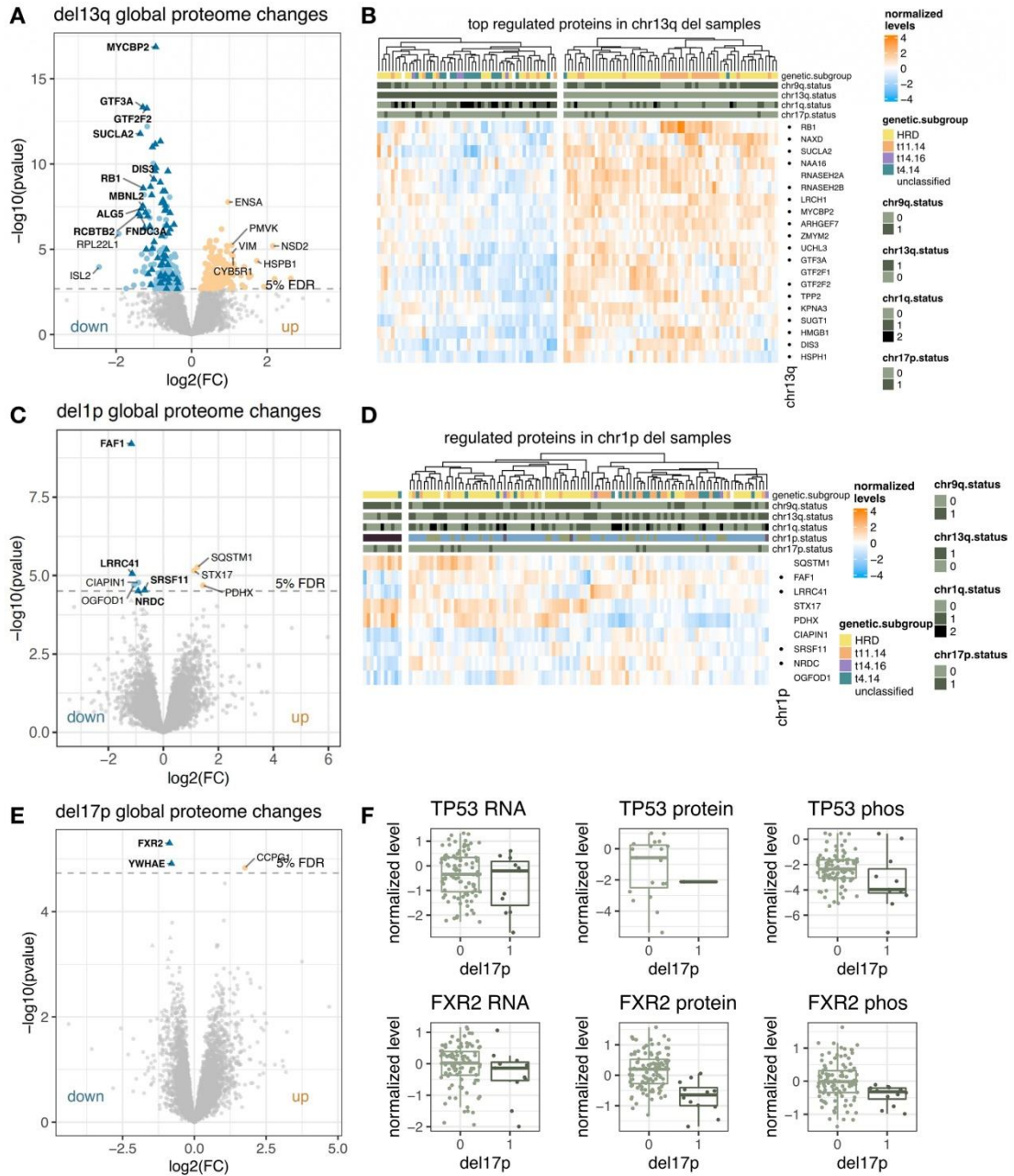
**Extended Data Fig. 3 | Protein level changes in multiple myeloma patients with translocations t(11;14) and t(4;14).** **a:** Significantly regulated proteins in t(11;14) (FDR < 0.05) with the GO term annotation apoptosis. **b:** Levels of proteins involved in venetoclax response in patients with (n = 27) and without (n = 87) t(11;14). FDR is indicated. Boxplot shows median (middle line), 25th and 75th percentiles, whiskers extend to minimum and maximum excluding outliers (values greater than 1.5 times the interquartile range). **c:** Protein levels of selected B cell markers and genes in CD2 gene set in patients with (n = 27) and without (n = 87) t(11;14). FDR is indicated. Boxplot shows median (middle line),

25th and 75th percentiles, whiskers extend to minimum and maximum excluding outliers (values greater than 1.5 times the interquartile range). **d:** Schematic representation of the chromosomal locus on 4p16 affected by t(4;14). **e:** Levels of the most regulated proteins in t(4;14) samples (top 20 by FDR). Row annotation: dots indicate proteins located on chromosome 4. **f:** Normalized FGFR3 RNA levels in t(4;14) patients with (n = 13) or without (n = 7) FGFR3 protein detection. FDR is indicated. Boxplot shows median (middle line), 25th and 75th percentiles, whiskers extend to minimum and maximum excluding outliers (values greater than 1.5 times the interquartile range).



**Extended Data Fig. 4 | Proteins deregulated in hyperdiploid myeloma. a:** Global protein levels in HRD samples without translocation were compared against all other samples with a 2-sided, moderated 2-sample t-test. The  $\log_2$  of fold change of each protein is plotted against its p-value. P-values were adjusted with the Benjamini-Hochberg method and the significance threshold of 0.05 FDR is indicated. **b:**  $\log_2$  fold changes of proteins in HRD samples mapped to the chromosomal location. Line indicates smoothed conditional mean. The 15 most significantly regulated proteins in HRD samples are indicated by gene

name. **c:** Protein levels (normalized TMT ratios) of the most regulated proteins in HRD samples (top 20 by FDR). **d:** Normalized TMT ratios were used as input for an ssGSEA with the gene sets C2.all.v7.0.symbols.gmt, c6.all.v7.0.symbols.gmt and h.all.v7.0.symbols.gmt. Normalized enrichment scores in HRD samples were compared against HRD samples with a 2-sided, moderated 2-sample t-test. The most 10 most up and down regulated significant gene sets (< 0.05 FDR) are displayed.



Extended Data Fig. 5 | See next page for caption.

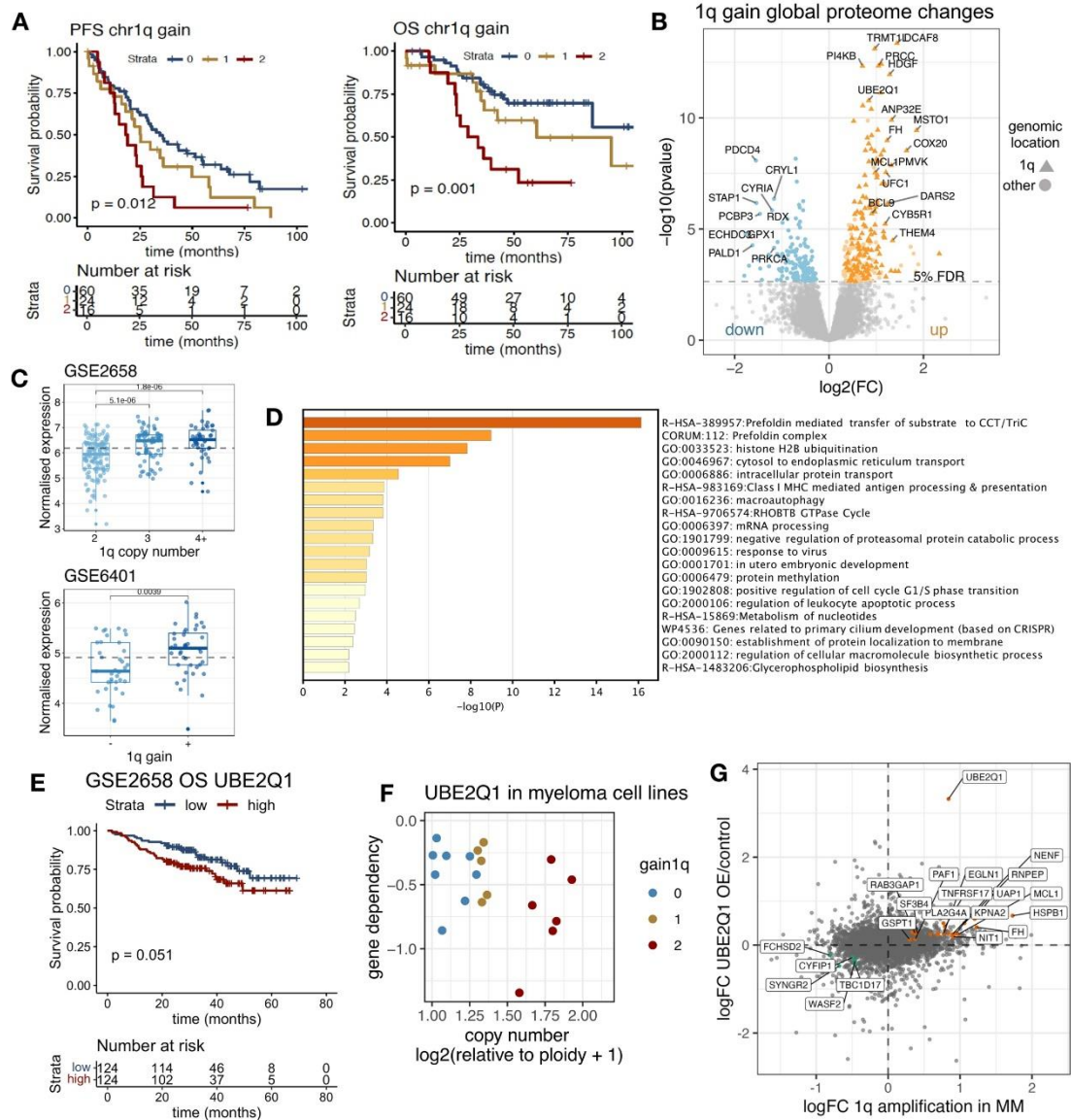
---

**Resource**<https://doi.org/10.1038/s43018-024-00784-3>

**Extended Data Fig. 5 | Proteins deregulated in del13q, del1p and del17p myeloma.** **a:** Global protein levels in del13q samples were compared against all other samples with a 2-sided, moderated 2-sample t-test. The log<sub>2</sub> of fold change of each protein is plotted against its p-value. P-values were adjusted with the Benjamini-Hochberg method and the significance threshold of 0.05 FDR is indicated. Proteins located on 13q are indicated with a triangle. **b:** Protein levels of the most regulated proteins in del13q samples (top 20 by FDR). Row annotation indicates proteins located on chromosome 13q. **c:** Global protein levels in del1p samples were compared against all other samples with a 2-sided, moderated 2-sample t-test. The log<sub>2</sub> of fold change of each protein is plotted against its p-value. P-values were adjusted with the Benjamini-Hochberg method and the significance threshold of 0.05 FDR is indicated. Proteins located on 1p are

indicated with a triangle. **d:** Protein levels of significantly regulated proteins in del1p samples. Row annotation indicates proteins located on chromosome 1p. **e:** Global protein levels in del17p samples were compared against all other samples with a 2-sided, moderated 2-sample t-test. The Log<sub>2</sub> of fold change of each protein is plotted against its p-value. P-values were adjusted with the Benjamini-Hochberg method and the significance threshold of 0.05 FDR is indicated. Proteins located on chromosome 17p are indicated with a triangle. **f:** RNA, protein, and phosphoprotein levels of TP53 and FXR2 in samples with (n = 12) and without (n = 102) del17p. Boxplot shows median (middle line), 25th and 75th percentiles, whiskers extend to minimum and maximum excluding outliers (values greater than 1.5\*IQR).

## Resource

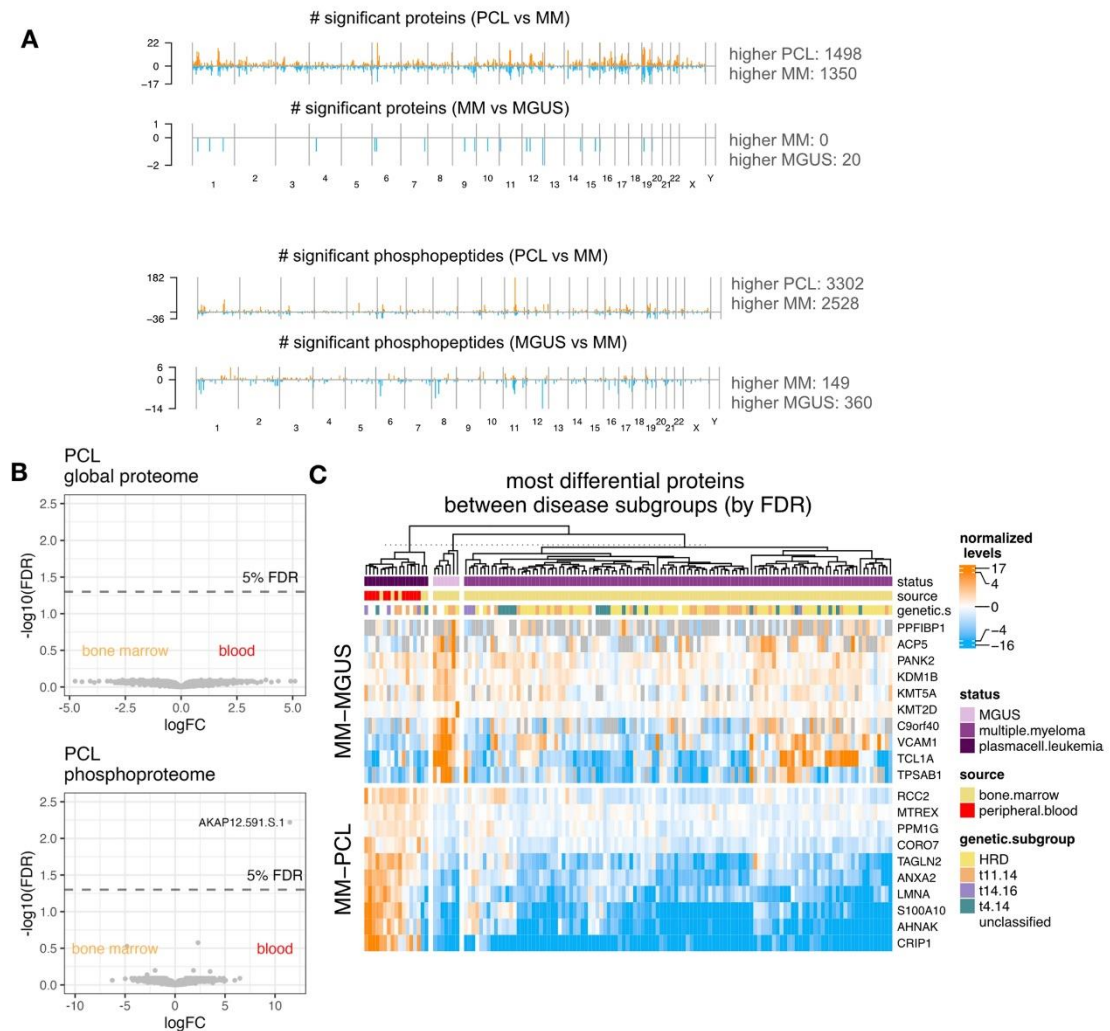
<https://doi.org/10.1038/s43018-024-00784-3>


**Extended Data Fig. 6 | Influence of 1q amplifications on the proteome. a:** Kaplan-Meier plot showing progression free and overall survival of myeloma patients stratified by chr1q gain ( $n = 100$  patients). P-values were calculated with a log-rank test. **b:** Global protein levels in multiple myeloma samples with 1q copy number gain ( $n = 46$ ) were compared against all other samples ( $n = 68$ ) with a 2-sided, moderated 2-sample t-test. The  $\log_2$  of fold change of each protein is plotted against its p-value. Proteins located on 1q are denoted with a triangle. P-values were adjusted with the Benjamini-Hochberg method and the significance threshold of 0.05 FDR is indicated. **c:** MCL1 RNA expression in multiple myeloma extracted from microarray datasets GSE2658 (2:  $n = 134$ ; 3:  $n = 70$ , 4+:  $n = 44$ ) and GSE6401 (1q gain  $n = 40$ , no 1q gain  $n = 37$ ). Boxplot shows median (middle line), 25th and 75th percentiles, whiskers extend to minimum and maximum excluding outliers (values greater than  $1.5 \times IQR$ ). The levels of

MCL1 were compared by the two-sided t-test, p-values are indicated above the boxplots. P-values are adjusted using Bonferroni correction. **d:** Metascape GO term enrichment of proteins upregulated in 1q samples ( $< 0.05$  FDR) that are not located on 1q. **e:** UBE2Q1 expression was extracted from Zhan et al. Microarray dataset (GSE2658). Kaplan-Meier plot shows overall survival of myeloma patients stratified by median UBE2Q1 expression. Survival in the groups is compared by the log rank test. **f:** Multiple myeloma cell line dependency data extracted from the depmap portal. The DNA copy number of UBE2Q1 is plotted against the genetic dependency. 1q copy number gains are indicated by color. **g:** Correlation of protein fold changes in 1q gain myeloma patients (x-axis) and UBE2Q1 overexpressing OPM2 compared to control (y-axis). Proteins regulated in OPM2 ( $< 0.05$  FDR) and in 1q patients ( $< 0.1$  FDR) are indicated by color.



## Resource

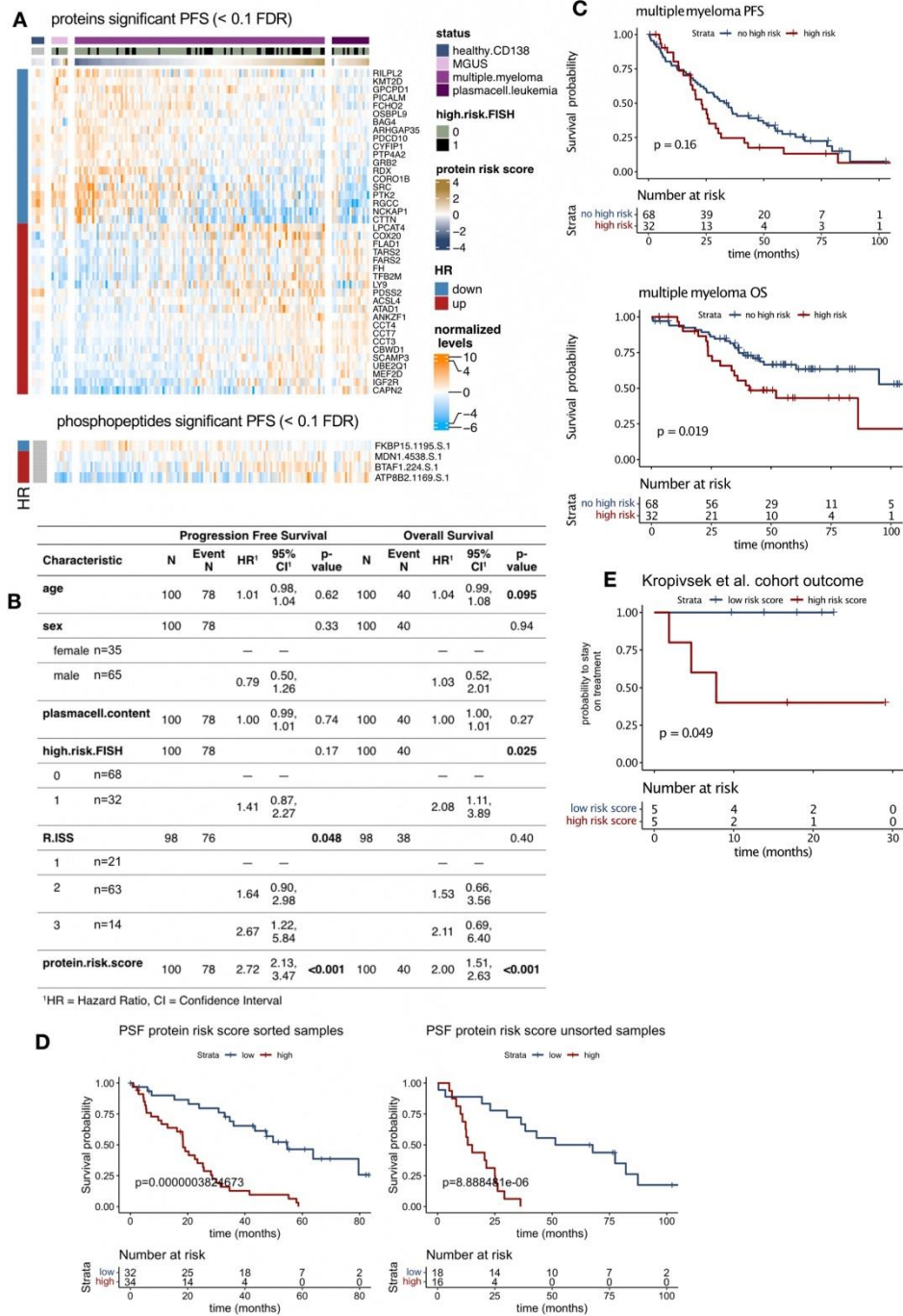
<https://doi.org/10.1038/s43018-024-00784-3>

**Extended Data Fig. 7 | Differential protein levels in plasma cell leukemias indicate a highly proliferative phenotype.** **a:** Global protein or phosphopeptide levels in multiple myeloma samples ( $n = 114$ ) were compared against MGUS ( $n = 7$ ) or plasma cell leukemia ( $n = 17$ ) samples with a 2-sided, moderated 2-sample t-test. P-values were adjusted with the Benjamini-Hochberg method. Significant ( $< 0.05$  FDR) proteins or phosphopeptides in each comparison are plotted across their genomic location. **b:** Global protein levels in plasma cell leukemia samples

isolated from blood ( $n = 12$ ) or bone marrow ( $n = 5$ ) were compared with a 2-sided, moderated 2-sample t-test. The  $\log_2$  of fold change of each protein is plotted against its p-value. P-values were adjusted with the Benjamini-Hochberg method and the significance threshold of 0.05 FDR is indicated. Bottom plot shows the same analysis for phosphoproteomic data. **c:** Heatmap displays normalized levels of the most significantly regulated proteins between MM and PCL or MM and MGUS (by FDR).

Resource

<https://doi.org/10.1038/s43018-024-00784-3>



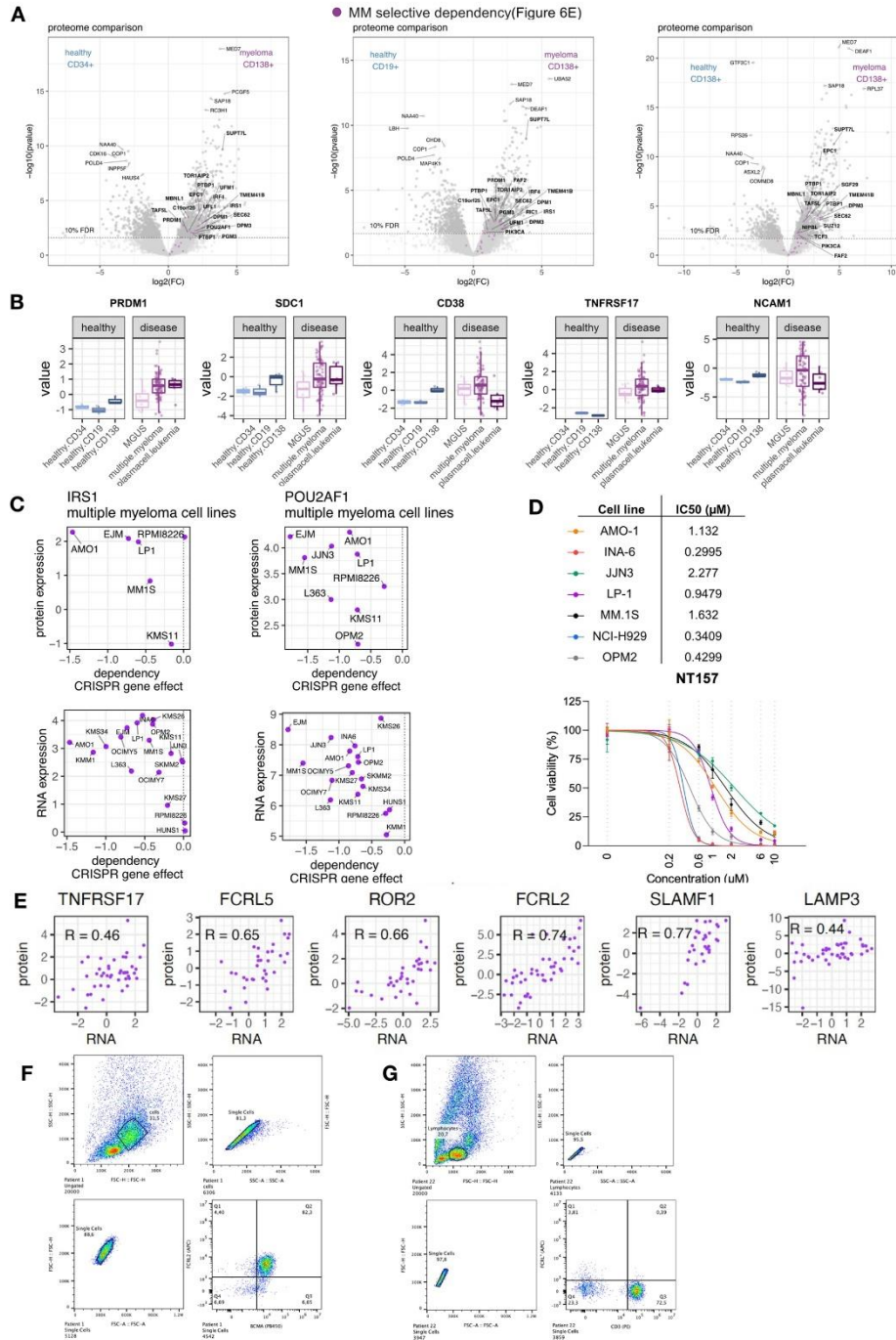
Extended Data Fig. 8 | See next page for caption.

---

**Resource**<https://doi.org/10.1038/s43018-024-00784-3>

**Extended Data Fig. 8 | Proteins and phosphopeptides associated with outcome.** **a:** Fully quantified proteins and phosphopeptides were investigated for their correlation with progression-free survival with a univariate Cox regression analysis as a continuous variable. The resulting p-values were subjected to multiple testing control with Benjamini-Hochberg. Normalized expression levels of proteins and phosphopeptides passing the 0.1 FDR cutoff are plotted as a heatmap. Row annotation indicates hazard ratios > 1 (up) or < 1 (down). **b:** Table showing the impact of clinical parameters and protein risk score on progression-free survival (PFS) and overall survival (OS). P-values were calculated with univariate Cox regression analysis. **c:** Kaplan-Meier plots showing PFS and OS curves of patients with (blue) and without (red) at least one high-risk FISH marker (del(17p), t(4;14), +1q21). P-values were calculated with a log-rank

test. Patients treated within the DSMM clinical trials that received a lenalidomide-based induction therapy followed by high-dose melphalan/autologous hematopoietic stem cell transplantation and lenalidomide maintenance were included (n = 100) in the survival analysis. **d:** Kaplan-Meier plots showing progression-free survival (PFS) for patients according to the protein risk signature score in samples with and without CD138 MACS sorting. Survival in the groups is compared by the log rank test. **e:** Proteomics data was extracted from Kropivsek et al. and protein risk score was calculated for untreated myeloma patients (n = 10). Kaplan-Meier plot shows time to the next treatment or death for myeloma patients stratified by median risk score. Survival in the groups is compared by the log rank test.



Extended Data Fig. 9 | See next page for caption.

**Resource**<https://doi.org/10.1038/s43018-024-00784-3>

**Extended Data Fig. 9 | Comparison of multiple myeloma with healthy bone marrow reveals potential therapeutic targets.** **a:** Global protein levels of multiple myeloma samples (MACS sorted samples only, n = 76) and healthy bone marrow cells sorted for CD138+ (plasma cells, n = 3), CD19+ (B cells, n = 3) and CD34+ (HSC, n = 3) were compared with a 2-sided, moderated 2-sample t-test. The log<sub>2</sub> of fold change of each protein is plotted against its p-value. P-values were adjusted with the Benjamini-Hochberg method and the significance threshold of 0.1 FDR is indicated. Data was integrated with the depmap database and potential therapeutic targets (Fig. 6d) are indicated as purple stars. **b:** Protein levels of selected plasma cell-specific proteins in healthy and disease samples. Healthy CD138: n = 3; healthy CD19: n = 3, healthy CD34: n = 3; MGUS:

n = 7; MM: n = 114; PLC: n = 17. Boxplot shows median (middle line), 25th and 75th percentiles, whiskers extend to minimum and maximum excluding outliers (values greater than 1.5\*IQR). **c:** Protein (top) or RNA (bottom) expression of IRS1 and POU2AF1 in multiple myeloma cell lines plotted against genetic dependency. Data was extracted from the depmap database and Goncalves et al. **d:** Cell viability of multiple myeloma cell lines treated for 96 h with the IRS1 inhibitor NT157 in biological triplicates. Concentration is indicated in  $\mu$ M. Data is represented as mean  $\pm$  standard deviation. **e:** RNA to protein correlation of selected surface markers in myeloma samples displayed in Fig. 7. **f** and **g:** Representative plot showing gating strategy for the FACS analysis in Fig. 7d-f: Multiple myeloma cells, G: non-malignant cells on example of T cells.



## Heterobifunctional Ligase Recruiters Enable pan-Degradation of Inhibitor of Apoptosis Proteins

Yuen Lam Dora Ng,<sup>¶</sup> Aleša Bricelj,<sup>¶</sup> Jacqueline A. Jansen, Arunima Murgai, Kirsten Peter, Katherine A. Donovan, Michael Gütschow, Jan Krönke, Christian Steinebach,\* and Izidor Sosič\*Cite This: *J. Med. Chem.* 2023, 66, 4703–4733

Read Online

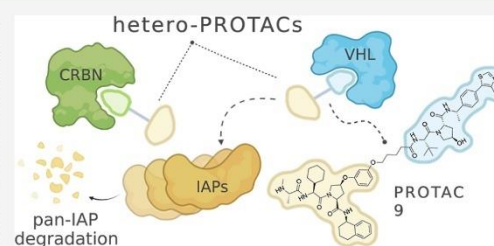
ACCESS |

Metrics &amp; More

Article Recommendations

Supporting Information

**ABSTRACT:** Proteolysis targeting chimeras (PROTACs) represent a new pharmacological modality to inactivate disease-causing proteins. PROTACs operate via recruiting E3 ubiquitin ligases, which enable the transfer of ubiquitin tags onto their target proteins, leading to proteasomal degradation. However, several E3 ligases are validated pharmacological targets themselves, of which inhibitor of apoptosis (IAP) proteins are considered druggable in cancer. Here, we report three series of heterobifunctional PROTACs, which consist of an IAP antagonist linked to either von Hippel-Lindau- or cereblon-recruiting ligands. Hijacking E3 ligases against each other led to potent, rapid, and preferential depletion of cellular IAPs. In addition, these compounds caused complete X-chromosome-linked IAP knockdown, which was rarely observed for monovalent and homobivalent IAP antagonists. In cellular assays, hit degrader **9** outperformed antagonists and showed potent inhibition of cancer cell viability. The hetero-PROTACs disclosed herein are valuable tools to facilitate studies of the biological roles of IAPs and will stimulate further efforts toward E3-targeting therapies.



## INTRODUCTION

In the last decade, significant advancements have been made in the field of proteolysis targeting chimeras (PROTACs). PROTACs are now recognized as one of the most promising modalities with the potential to promote the development of targeted therapy drugs.<sup>1–6</sup> Classical PROTACs are heterobifunctional compounds comprising a ligand that binds to a target protein of interest, a ligand that binds to and recruits an E3 ubiquitin ligase, and a linker tether. Such molecules can facilitate the formation of a ternary target–PROTAC–E3 ligase complex, followed by ubiquitination of the target protein and its subsequent degradation by the proteasome.<sup>7</sup> PROTACs possess several advantages over conventional inhibitors as they exert their action catalytically, resulting in a potent intracellular degradation of the target proteins. Moreover, PROTACs can discriminate between similar proteins within the same family or even protein isoforms, thus allowing exclusive target-selective degradation.<sup>8,9</sup>

E3 ubiquitin ligases orchestrate protein turnover via facilitating substrate proximity and ubiquitin transfer. They encompass a diverse group of more than 600 enzymes, with most E3 ligases belonging to the really interesting new gene (RING) family. Many have crucial roles in various biological processes<sup>10</sup> but are also implicated in multiple diseases. Therefore, targeting E3 ligases is considered an attractive approach for small-molecule drugs.<sup>11–15</sup> Cellular RING E3

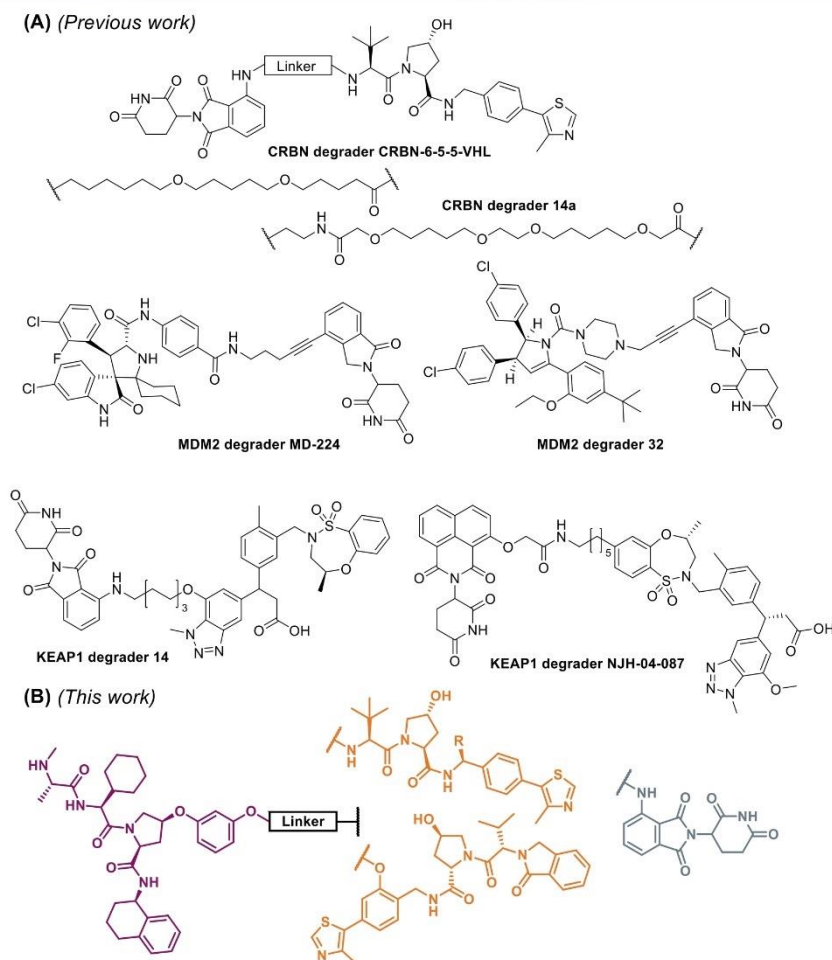
ligases are large multi-subunit complexes but usually do not possess a defined ligand-binding site rendering the inhibitor design difficult. Nevertheless, traditional approaches yielded potent compounds targeting murine double minute 2 (MDM2), von Hippel-Lindau (VHL), and inhibitor of apoptosis (IAP) proteins.<sup>11</sup> The consequence of binding to these E3 ligases is disrupting protein–protein interactions between ligases and their respective substrates. E3 ligases can also be degraded via proximity-induced ubiquitination. Namely, several homodimeric E3 degraders have been developed by linking two identical E3 ligase ligands.<sup>16–19</sup>

Directing different E3 ligases against each other by heterodimeric PROTACs also proved to be a productive strategy for their depletion. We recently reported preferential degradation of cereblon (CRBN) over VHL with molecules assembled from pomalidomide-based CRBN binders and a VHL ligand (CRBN-6-5-5-VHL, Figure 1A).<sup>20</sup> The prevalence of VHL over CRBN was also observed in a separate study by Ciulli and colleagues (14a, Figure 1A).<sup>21</sup> On the contrary,

Received: November 7, 2022

Published: March 30, 2023





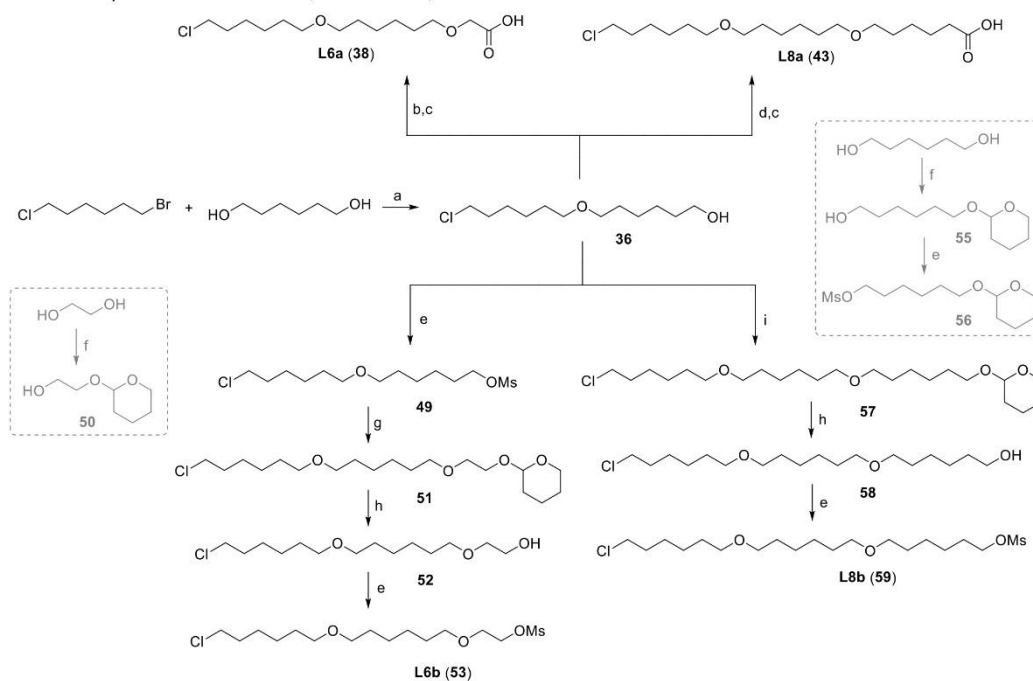
**Figure 1.** (A) Examples of heterobifunctional E3 ligase degraders. CRBN-6-5-5-VHL and 14a were shown to be potent CRBN degraders which utilize VHL as the recruited ligase,<sup>20,21</sup> whereas MD-224 and PROTAC 32 cause depletion of MDM2 via CRBN-mediated ubiquitination.<sup>18,23</sup> PROTAC 14 and NJH-04-087 exhibited degradation of KEAP1 over CRBN.<sup>24,25</sup> (B) Schematic representation of the designed compounds in this work.

linking MDM2 inhibitors to lenalidomide resulted in MDM2 degradation (MD-224 and PROTAC 32, Figure 1A).<sup>22,23</sup> Of note, CRBN levels were not monitored for the latter two examples, thereby not entirely confirming the unilateral degradation of MDM2. Recently, the compendium of heterobifunctional ligase degraders was extended by KEAP1-CRBN recruiters (PROTAC 14 and NJH-04-087, Figure 1A) that preferentially degrade KEAP1.<sup>24,25</sup>

Cellular IAP1 (cIAP1/BIRC2), cellular IAP2 (cIAP2/BIRC3), and X-chromosome-linked IAP (XIAP/BIRC4) have been studied in great detail because of their critical role in controlling the apoptotic machinery.<sup>26</sup> Their overexpression has been linked to tumor progression, resistance to anti-cancer therapies, and poor prognosis.<sup>27–29</sup> This clinical significance has translated to the development of numerous mimetics of the

IAP-binding motif (i.e., the *N*-terminal Ala-Val-Pro-Ile moiety)<sup>30–32</sup> of the second mitochondria-derived activator of caspases (SMAC), which functions as an endogenous IAP antagonist.<sup>33,34</sup> Several SMAC-mimicking IAP monovalent and bivalent antagonists have entered into clinical trials for the treatment of various cancers (Figure S1).<sup>35,36</sup> However, they demonstrated low efficacy as single agents, and current clinical evaluations are limited to combination studies with other cytotoxic drugs, radiation, and immunotherapy.<sup>37</sup>

IAP antagonists have profound effects on cIAPs levels. Both monovalent and bivalent SMAC mimetics bind to the baculoviral IAP repeat (BIR) type 3 domain of IAPs. This event promotes a rapid and ubiquitin- and proteasome-dependent loss of cIAP1 and cIAP2.<sup>38,39</sup> It was suggested that BIR3-binding IAP antagonists destabilize a closed/

Scheme 1. Syntheses of Linkers L6a, L8a and L6b, L8b<sup>4f</sup>

<sup>4f</sup>Reagents and conditions: (a) 50% NaOH (aq), DMSO, rt, 24 h; (b) *tert*-butyl bromoacetate, NaH, DMF/THF, 0 °C to rt, 18 h; (c) TFA, CH<sub>2</sub>Cl<sub>2</sub>, 40 °C, 2 h; (d) *tert*-butyl 6-bromohexanoate (**41**), toluene, 50% NaOH (aq), TBAHS, rt, 18 h; (e) MsCl, DIPEA, CH<sub>2</sub>Cl<sub>2</sub>, rt, 2 h; (f) 3,4-dihydro-2H-pyran, CuSO<sub>4</sub> × 5 H<sub>2</sub>O, MeCN, rt, 4 h; (g) **50**, TBAHS, 50% NaOH (aq), toluene, rt, 18 h; (h) *p*TsOH × H<sub>2</sub>O, MeOH, rt, 20 h; (i) **56**, TBAHS, 50% NaOH (aq), toluene, rt, 18 h.

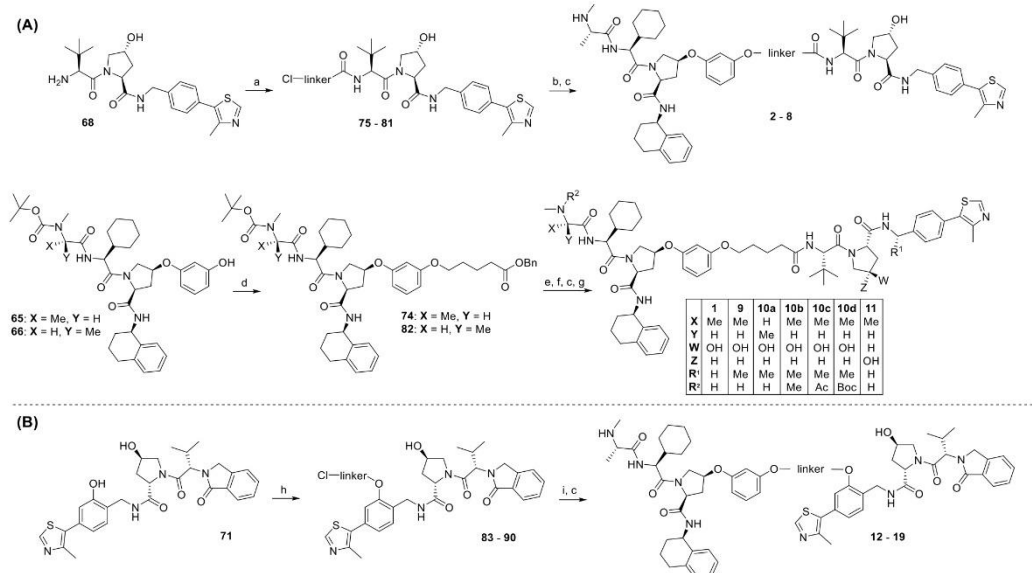
autoinhibited form of cIAP (by blocking the crucial BIR3-RING domain interactions), resulting in dimerization, E3 ubiquitin ligase activation, autoubiquitination, and proteasomal degradation.<sup>40,41</sup> Although most IAP antagonists do also possess an affinity for the BIR3 domain of XIAP, this rarely results in XIAP autodegradation.<sup>38</sup> IAP antagonists such as bestatin and more recently the improved LCL161 also represent valuable E3-recruiter moieties for the assembly of heterobifunctional protein degraders.<sup>42</sup>

Encouraged by our successful outcomes with heterodimerizing PROTACs and the fact that IAPs are validated anti-cancer targets, we decided to include IAPs in the hetero-PROTAC approach for E3 modulation (Figure 1B). We systematically designed three series of bifunctional molecules. Two series were assembled by linking the selected IAP ligand<sup>43</sup> to two VHL ligands with differently oriented exit vectors. In the third series, the CRBN ligand pomalidomide was incorporated into hetero-PROTACs (for E3 ligand structures, see Table S1). Our efforts to induce IAP degradation through hijacking another E3 ligase via hetero-PROTACs led to selective depletion of IAPs, including XIAP, and, in one case, also to selective XIAP degradation. Notably, the pan-IAP deficit could translate into very potent inhibitors of cancer cell viability, thus further substantiating the rationale of our strategy.

## RESULTS AND DISCUSSION

**Design and Synthesis of Bifunctional IAP PROTACs.** It is widely accepted that linkers play a significant role in PROTAC activity, as even subtle differences in length or composition influence the degradation activity and selectivity.<sup>44,45</sup> Three libraries of heterobifunctional PROTACs were systematically designed with eight linkers of varying length and chemical composition in each library (Tables S2–S6). The synthesis of the first series of IAP-VHL hetero-PROTACs (Series 1) was accomplished by a straightforward approach employing chloro to carboxylic acid (Cl-to-CO<sub>2</sub>H) linkers **L1a–L8a** (Table S2). Most of the linkers were acquired by a BAIB/TEMPO-mediated oxidation of the appropriate primary alcohol precursors. In contrast, **L6a**, **L7a**, and **L8a** were prepared by elongating C6–O–C6 or C6–O–C5 alcohols with *tert*-butyl bromoacetate, *tert*-butyl 5-bromopentanoate, or *tert*-butyl 6-bromohexanoate (Schemes 1 and S1), respectively, followed by deprotection of the *tert*-butyl ester. Linkers **L2a–L8a** were first coupled to the VHL ligand VH032 (VHL1 ligand, **68**),<sup>46</sup> and the obtained conjugates **75–81** were applied to alkylate the Boc-protected IAP ligand **65** (Scheme 2A). Because intramolecular cyclization occurred when coupling the C5 linker **L1a** to the VHL1 ligand, **L1a** was first attached to the Boc-protected IAP ligand **65** or to the negative control IAP ligand **66**. This was followed by deprotection of the terminal carboxylic acid before coupling with either VH032 (**68**) or a



Scheme 2. (A) Syntheses of the IAP-VHL Series 1 Hetero-PROTACs 2–8, 1, and 9 and Negative Controls 10a–d and 11<sup>a</sup>

<sup>a</sup>Reagents and conditions: (a) linker L2a–L8a (Table S2), HATU, DIPEA, DMF, rt, 16 h; (b) step 1: NaI, acetone, 60 °C, 48 h; step 2: 65, Cs<sub>2</sub>CO<sub>3</sub>, DMF, 60 °C, 16 h; (c) 1 M HCl in EtOAc, rt, 4 h; (d) step 1: linker L1a (Table S2), NaI, acetone, 60 °C, 48 h; step 2: Cs<sub>2</sub>CO<sub>3</sub>, DMF, 60 °C, 16 h; (e) Pd/C, H<sub>2</sub>, EtOAc, rt, 18 h; (f) 68 or 69, HATU, DIPEA, DMF, rt, 16 h; (g) 9, formaldehyde, Pd/C, H<sub>2</sub>, DMF, rt, 16 h (for compound 10b) or 9, Ac<sub>2</sub>O, DIPEA, CH<sub>2</sub>Cl<sub>2</sub>, 0 °C to rt, 16 h (for compound 10c); (B) synthesis of the IAP-VHL series 2 hetero-PROTACs 12–19. Reagents and conditions: (h) linker L1b–L8b (Table S3), Cs<sub>2</sub>CO<sub>3</sub>, DMF, rt, 16 h, then 60 °C, 3 h; (i) step 1: NaI, acetone, 60 °C, 48 h and step 2: 65, Cs<sub>2</sub>CO<sub>3</sub>, DMF, 60 °C, 16 h.

methylated VHL ligand (Me-VHL1, 69) which is known to enhance the VHL-binding affinity.<sup>47</sup> The desired hetero-PROTACs 1–9 and controls 10a and 11 were obtained following Boc deprotection of the corresponding IAP ligands (Scheme 2A). Additional control compounds were obtained by derivatization of PROTAC 9 into dimethyl- (10b) or acetyl- (10c) bearing analogues.

For the second IAP-VHL series (Series 2), a different exit vector at the VHL side was employed, presumably leading to differently oriented ternary complexes.<sup>48,49</sup> For this subseries, methane-sulfonate to chloro (OMs-to-Cl) linkers L1b–L8b (Table S3) were utilized as crucial building blocks. Most of these (L1b–L5b) were prepared by subjecting the selected alcohols to mesylation. At the same time, L6b, L7b, and L8b were obtained through elongation of C6–O–C6 or C6–O–CS mesylates with the corresponding tetrahydropyranyl (THP)-protected diols. Following cleavage of the THP-protecting group, mesylates were prepared (Schemes 1 and S5–S7). The obtained linkers were attached to the phenolic VHL ligand (VHL2 ligand, 71) through O-alkylation. These ligand–linker conjugates 83–90 were then connected to the IAP ligand 65, followed by removing the Boc-protecting group under acidic conditions to yield hetero-PROTACs 12–19 (Scheme 2B).

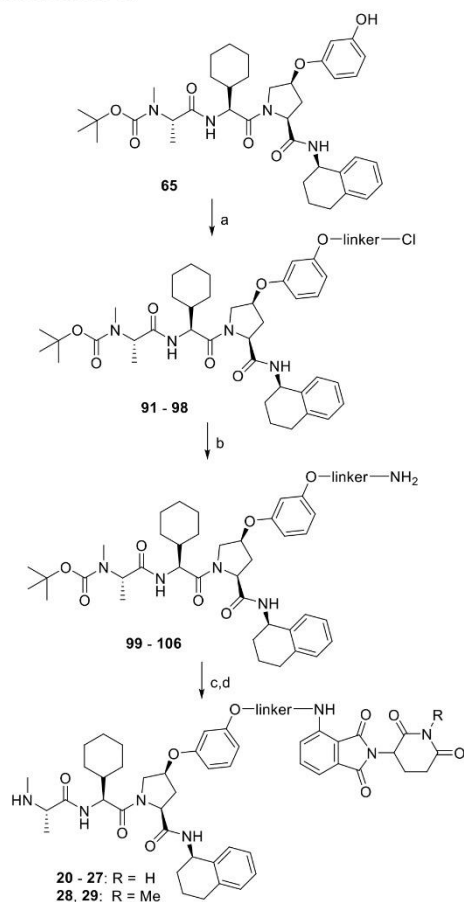
In the third series of hetero-PROTACs, OMs-to-Cl linkers were used to alkylate the IAP ligand 65, and the resulting chloro-linker-IAP ligand conjugates 91–98 were converted to amino-functionalized building blocks via azidolysis and hydrolysis. Finally, these amine building blocks 99–106 were

reacted with 4-fluorothalidomide (72) in a nucleophilic aromatic substitution. Removal of the Boc protecting group yielded the envisioned IAP-CRBN heterobifunctional PROTACs 20–27. For the assembly of negative control compounds 28 and 29, an N-methylated thalidomide derivative 73 was used in place of 4-fluorothalidomide (72) (Scheme 3).

The physicochemical properties of all hetero-PROTACs (Tables S4–S6) and known IAP inhibitors (Table S7) are provided in the Supporting Information. Despite encompassing a wide range in terms of lipophilicity (log *D*<sub>7.4</sub> from 3.4 to 5.8), a similar activity window was observed for IAP-VHL Series 1 PROTACs. In Series 2, the most lipophilic hetero-PROTAC 19 showed the lowest IAP degradation levels at 0.1 μM, whereas for IAP-CRBN series, high PROTAC lipophilicity led to XIAP-selective depletion (Figure 2 and Table S6).

**Hetero-PROTACs Induce Potent pan-IAP Degradation.** At the outset of our studies, we were aware of the different outcomes possible, as the E3 ligase crosstalk can result in a favored degradation of one ligase or depletion of both E3s in the case of simultaneous cross- and/or autoubiquitination. In the case of preferred ubiquitination of IAP(s), our compounds might be degraders of either cIAP1, cIAP2, XIAP, or of two or even three IAPs. To evaluate the capability of our panel of hetero-PROTACs for E3 ligase degradation, VHL19, VHL30, CRBN, cIAP1, cIAP2, and XIAP levels were quantified by western blot analyses. For each series, MM.1S cells were treated with 0.1 or 1 μM of each compound

Scheme 3. Synthesis of the IAP-CRBN Series Hetero-PROTACs 20–29<sup>a</sup>



<sup>a</sup>Reagents and conditions: (a) linkers L1b–L8b (Table S3), K<sub>2</sub>CO<sub>3</sub>, DMF, 70 °C, 20 h; (b) step 1: NaN<sub>3</sub>, DMF, 80 °C, 4 h; step 2: Pd/C, H<sub>2</sub>, MeOH, rt, 3 h; (c) 72 or 73, DIPEA, DMSO, 90 °C, 20 h; (d) 1 M HCl in EtOAc, rt, 4 h.

for 16 h. Original blots are provided in the Supporting Information (Figures S2–S4), and an overview is given in Figure 2. The IAP antagonists LCL161, AZD5582, birinapant, and BV6 were assessed as comparators (Figure 3). These monovalent and bivalent IAP-targeting compounds led to substantial degradation of cIAP1 and cIAP2 at concentrations as low as 0.1 μM. The bivalent IAP antagonists performed better than the monovalent SMAC mimetics, but all of these compounds failed to degrade XIAP (Figure 3).

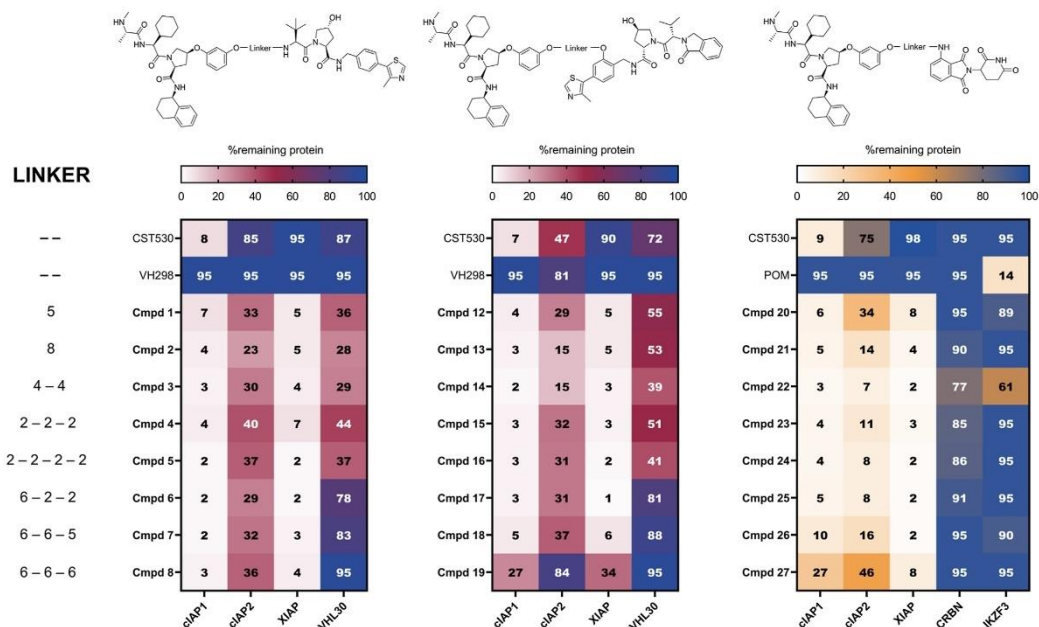
The effect of representatives from Series 1 on IAP depletion was significantly enhanced in comparison to the incorporated IAP ligand CST530 itself (Figures 2, 3, and S2), which caused only potent cIAP1 autodegradation but moderate cIAP2 depletion in MM.1S cells. As expected, treatment with the VHL inhibitor VH298 did not affect the levels of IAPs. Hetero-

PROTACs, on the other hand, induced complete cIAP1 and XIAP degradation even at 0.1 μM. In addition, a substantial reduction of cIAP2 levels was observed for these hetero-PROTACs (Figures 2 and S2–S4). We were particularly pleased with the ability of PROTACs to degrade XIAP, which was rarely down-regulated by monovalent or bivalent IAP ligands in all previous studies. Of note, after a 16 h treatment with 0.1 μM concentration, a reduction of VHL30 levels was observed for all Series 1 PROTACs (Figures 2 and S2). However, this effect was less pronounced for compounds containing long and hydrophobic linkers (i.e., PROTACs 6–8). The most profound degradation of VHL30 (71% protein degradation, as quantified by western blot) was observed for hetero-PROTAC 3, meaning that both ligases were degraded simultaneously at 0.1 μM concentration. The effect on VHL30 levels was very similar at 1 μM (Figure S5). Bidirectional degradation was in stark contrast to the properties of our CRBN-VHL hetero-PROTAC CRBN-6-5-5-VHL, which selectively degraded CRBN.<sup>20,50</sup> Similarly, the VHL-targeting homo-PROTAC CM11 only caused a reduction of the long VHL isoform but spared the 19 kDa protein.<sup>17</sup> Comparative analysis between 1, 2, and CM11 confirmed similarities between PROTACs whereby IAP-VHL hetero-PROTAC 1 also notably and dose dependently reduced VHL19 levels (42% remaining VHL19 at 1 μM, Figure S6). We estimate that the effects of IAP-VHL degraders would not be masked by the hypoxia-inducible factor (HIF)-dependent hypoxic response because recent results showed that homo-PROTAC-mediated VHL30 degradation or siRNA-mediated knockdown of VHL leads to almost undetectable stabilization of HIF-1α.<sup>17,51</sup>

After the initial PROTAC screening, 1 was selected for further optimization due to its comparatively small size and thus the higher chance to overcome PK/PD penalties.<sup>52</sup> We modified the compound by incorporating the Me-VHL ligand 69 with improved binding affinity for VHL into the hetero-PROTAC. The resulting compound 9 (Figure 4A) showed enhanced pan-IAP degradation in MM.1S cells at even lower concentrations (Figure 4B). Interestingly, also stronger VHL19 degradation was observed at 1 μM (24% remaining VHL19). Densitometric quantifications of western blotting bands after treatment with hetero-PROTAC 9 in MM.1S cells revealed DC<sub>50,16h</sub> values of 2.4 nM (cIAP1), 6.2 nM (cIAP2), and 0.7 nM (XIAP). Maximum cIAP1, cIAP2, and XIAP degradation (D<sub>max</sub>) of 99, 90, and 99%, respectively, at 0.1 μM concentration of 9 was achieved (Figure 4C). A head-to-head comparison of 9 with birinapant demonstrated that the latter caused more pronounced cIAP1 degradation, whereas 9 outperformed birinapant in depleting cIAP2 and XIAP (Figure S7A). On the other hand, AZD5582 showed stronger cIAPs degradation than IAP-VHL hetero-PROTAC 9 but did not influence XIAP levels even at 1 μM (Figure S7B).

Profiling the activities of the second series of hetero-PROTACs, where we utilized a different linker exit vector, revealed a degradation profile similar to that of the first series. Namely, hetero-PROTACs 12–14 with C5, C8, and C4–O–C4 linkers, respectively, induced the most potent pan-IAP degradation (Figures 2 and S3). Unidirectional ubiquitination between the two E3 ligases was again observed only for hetero-PROTACs with long linkers (compounds 17–19). In line with this, also no effect on VHL19 levels was seen (Figures 2 and S3). In terms of achieving degradation of a pair of IAPs, 19 seemed interesting as it caused dual cIAP1/XIAP degradation at 0.1 μM concentration in MM.1S. However, profiling of the





**Figure 2.** Degradation profiles of Series 1 (left), Series 2 (middle), and Series 3 (right) of hetero-PROTACs on cIAP1, cIAP2, XIAP, VHL30, CRBN, and IKZF3 expression levels. Percentage degradation is indicated as the remaining protein levels after MM.1S cells were subjected to 16 h treatment with each compound at 0.1  $\mu$ M. Values are normalized to respective loading controls and to DMSO-treated conditions. All data represent an average of at least three independent experiments. CST530: IAP ligand and VH298: VHL ligand.



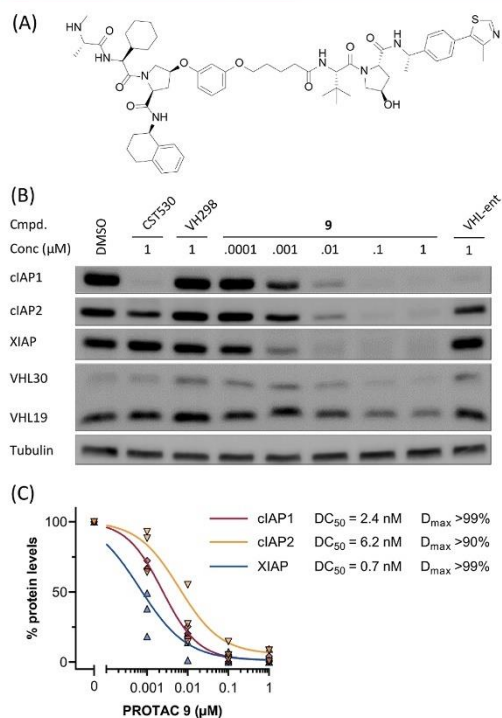
**Figure 3.** Monovalent (CST530 and LCL161) and bivalent IAP antagonists (AZD5582, binapant, and BV6) induce potent cIAP autodegradation, whereas the IAP-VHL hetero-PROTAC 1 is a pan-IAP degrader. MM.1S cells were treated at 0.1 or 1  $\mu$ M for 16 h.

concentration dependence of **19** showed pan-IAP degradation at 1  $\mu$ M and no degradation at 10 nM (Figure S8).

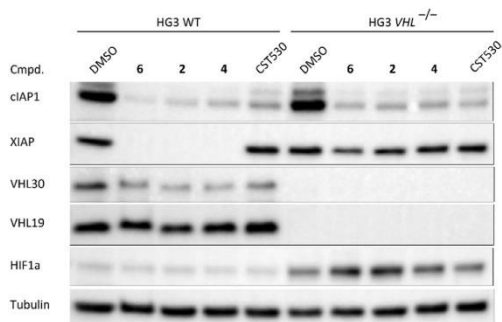
To investigate the relative ability of E3 ligases to induce degradation of each other upon treatment with the IAP-CRBN hetero-PROTACs, MM.1S cells were used. For **21**–**26**, consistent, unidirectional, and distinct degradation of all three IAPs was observed already at 0.1  $\mu$ M concentration (Figure 2). Of these, compounds **22**, **25**, and **26** showed pronounced pan-IAP depletion, and, concurrently, they induced substantial IKZF3 degradation at 1  $\mu$ M as an effect of modulating the substrate scope upon pomalidomide binding (Figure S4B). At 0.1  $\mu$ M, only **22** caused depletion of IKZF3, with approximately 40% of IKZF3 degraded after 16 h treatment. This dual mode could be useful in settings where these secondary effects are desirable. The most intriguing finding within the IAP-CRBN hetero-PROTAC series was observed for compound **27**, equipped with the longest linker.

An isoform-selective XIAP degradation was indicated after 16 h-treatment at 0.1  $\mu$ M (Figures 2 and S4A). A significant and selective decrease of XIAP levels compared to cIAP1 and cIAP2 was confirmed on a proteome level, where MM.1S cells were treated with hetero-PROTAC **27** for 3 h (see Figure 6B). This result unveils that IAP selectivity within the IAP-CRBN hetero-PROTAC series can be tuned by linker modifications.

**Mechanistic Considerations.** To understand the mechanism of E3 recruitment and ubiquitin transfer, we tested a set of control compounds with inactivated IAP- or VHL-binding motifs (Table S4). As little was known about appropriately rendering IAP ligands inoperative, we synthesized a series of putative IAP-non-binding controls **10a**–**d** (Scheme 2A and Figure S9). In **10a**, the stereochemistry of the critical *N*-methyl alanine portion was inverted or substituted with a second methyl group (**10b**). However, literature data indicated remaining affinity for the XIAP-BIR3 domain.<sup>53</sup> Indeed, **10a** and **10b** were still able to induce pan-IAP or cIAP1 and cIAP2 degradation, respectively (Figure S9). Further increasing the size of the *N*-terminal substituent and lowering the basicity in **10c** (R = acetyl) and **10d** (R = Boc) led to inactivated PROTACs. Both methylation and acetylation were performed through a convenient late-stage modification reactions of the final PROTAC **9**, highlighting the general utility of these transformations to produce inactivated IAP-recruiting PROTACs. By analogy with series **10**, hetero-PROTAC **11** (VHL-ent) possessing a VHL non-binding diastereomer only induced cIAP1 degradation (Figure 4B), which is a common attribute of IAP antagonists.



**Figure 4.** (A) Structure of pan-IAP degrader PROTAC 9. (B) IAP-VHL hetero-PROTAC 9 (CST626) induces cIAP1, cIAP2, XIAP, and VHL30 degradation in a dose-dependent manner. Hetero-PROTAC 11 (impaired VHL binding) and the monovalent IAP inhibitor CST530 induce only cIAP1 degradation. VHL inhibitor VH298 has no effects on the investigated proteins. MM.1S cells were treated with PROTACs or controls at indicated concentrations for 16 h. (C) Quantification of (B) and calculation of the  $DC_{50}$  values from repeats ( $n = 4$ ).



**Figure 5.** PROTACs 6, 2, and 4 retain degradation of cIAP1 and XIAP in chronic lymphocytic leukemia wild-type cells (HG3) and HG3 VHL-knockout cells. Cells were treated with compounds at 1  $\mu$ M for 16 h.

Next, cellular activities of hetero-PROTACs 2, 4, and 6 were evaluated in chronic lymphocytic leukemia cells (HG3), for

which a VHL-knockout cell line was created (Figure 5). In both VHL<sup>+/+</sup> and VHL<sup>-/-</sup> cells, cIAP1 autodegradation was observed after treatment with our hetero-PROTACs, demonstrating that ligand binding is the condition per quam. In contrast, recruitment of a VHL is required for XIAP degradation as this occurred only in HG3 wild-type cells. Thus, VHL knockout confirmed the involvement of E3 ubiquitin ligase CRL2<sup>VHL</sup> in the induced degradation of XIAP (and, at least in part, cIAP1) by these IAP-VHL heterobifunctional PROTACs. This provides additional evidence that the degradation of IAPs relies on the formation of a hetero-ternary complex consisting of both ligases and the degraders.

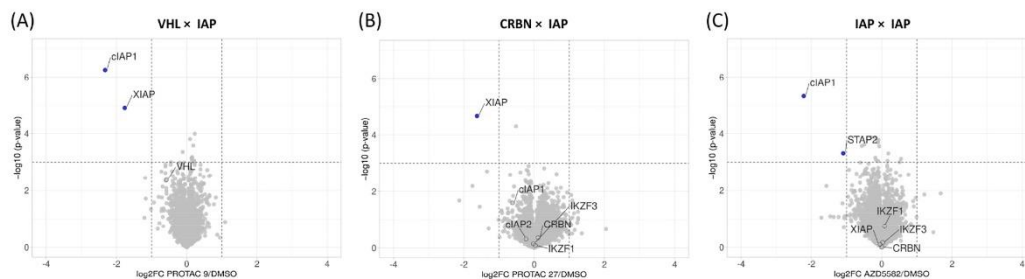
When evaluating the time dependence of hetero-PROTAC 9, we observed complete degradation of cIAP1, cIAP2, and XIAP already after 3 h at 0.1  $\mu$ M compound concentration. Interestingly, the effect on VHL30 depletion was most pronounced after 6 h of treatment in MM.1S cells (Figure S10A).

Next, we examined the persistence of IAP degradation in MM.1S cells after a single exposure to 1  $\mu$ M of 9 and subsequent removal of the compound. Results indicated a nearly full and stable pan-degradation of IAPs up to 72 h. VHL19 and VHL30 levels restored more rapidly following drug washout (Figure S11A). Nevertheless, intracellularly cycling quantities of PROTAC that remain inside the cells after washout may be sufficient to generate these characteristics. In contrast, when the system was further challenged with the competing VH298 after the washout, XIAP levels increased more rapidly (Figure S11B), consistent with an IAP antagonist mode and an unleashed resynthesis of XIAP. In a series of experiments where individual IAPs were knocked out, we observed no differences in VHL30 degradation by hetero-PROTAC 9; e.g., in cIAP1 knockout cells, VHL30 degradation could also be mediated by cIAP2 (Figure S12). A set of experiments were performed to demonstrate the involvement of the ubiquitin-proteasome system in degradation. Treatment of cells with a proteasome inhibitor MG132 completely abrogated degradation of IAPs. The reliance on CRL2<sup>VHL</sup> was assessed with a neddylation inhibitor MLN4924, which blocks the activity of CRLs (Figure S13A). Similarly, a selective ubiquitin-activating enzyme inhibitor MLN7243 also prevented the PROTAC-induced degradation of IAPs (Figure S13A).

Concentration- and time-dependent degradation of IAPs in MM.1S cells was evaluated for 25 too (Figures S14 and S10B). Complete cIAP1 and XIAP depletion occurred already at 10 nM, whereas 0.1  $\mu$ M concentration was needed for the complete depletion of all IAPs. The corresponding CRBN-non-binding control 28 failed to degrade XIAP at 1  $\mu$ M concentration but caused a significant deficit of cIAP2 (32% remaining protein, Figure S14). Pan-depletion of IAPs by 25 was also very rapid as we observed complete degradation already after 3 h at 0.1  $\mu$ M (Figure S10B). In addition, the proteasome-mediated mechanism of IAP degradation by 25 was confirmed using the same experiments as for hetero-PROTAC 9 (Figure S13B).

To analyze the proteome-wide degradation selectivity of hetero-PROTACs 9, 25, and 27, a diaPASEF-based mass spectrometry approach was employed.<sup>34</sup> MM.1S cells were treated with 100 nM PROTACs for 3 h. Of the total 7170 unique proteins identified, 9 (Figure 6A) and 25 (Figure S15) degraded cIAP1 and XIAP to levels below the detection level,





**Figure 6.** diaPASEF quantitative proteomics for (A) hetero-PROTAC 9 (CST626), (B) hetero-PROTAC 27 (SAB142), and (C) homobivalent compound AZD5582. MM.1S cells were treated with either DMSO or the mentioned compounds at 0.1  $\mu\text{M}$  for 3 h in four and two biological replicates, respectively. Downstream statistical analysis was performed using Bioconductor's limma package. The quantified proteins were plotted as log 2-fold change (compound/DMSO) versus  $-\log_{10}$  of  $p$ -value using RStudio. Note: dataset for 27 was obtained in an independent/separate proteomics run.

whereas cIAP2 could not be evaluated in this experiment as it was undetected in DMSO–vehicle treatments. Accordingly, global proteomic plots show the mathematically imputed levels of IAP proteins in treatment groups if the corresponding IAP was detected in the control treatment (see also Experimental Section). AZD5582 also depleted cIAP1 below the detection level but did not cause XIAP degradation (Figure 6C), which is in accordance with the fact that IAP antagonists have no effect on XIAP.

In a separate experiment, global proteome analysis in MM.1S cells after treatment with 27 (Figure 6B) showed selective XIAP degradation with no impact on cIAP1 and cIAP2, rendering this compound significantly more selective for XIAP over cIAP1 and cIAP2 that were only degraded at higher concentrations and after prolonged treatment times. Moreover, we did not observe changes in CRBN, IKZF1, IKZF3, and VHL levels in the proteomic data, thus further substantiating the unilateral effect of our hetero-PROTACs.

**pan-IAP Degradation Reduces Cell Viability.** To assess the pharmacological consequences of IAP depletion, the pan-IAP degraders 9 and 25, along with appropriate inactivated PROTACs, were evaluated for their cell growth inhibition in nine hematological cell lines (Figures 7 and S17), i.e., three myeloma (RPMI-8226, JLN3, and NCI-H929), three leukemia (HEL, K562, and MOLM13), and three lymphoma cells (SUDHL4, DB, and SUDHL6). We included the monovalent ligase ligands VH298 (VHL), pomalidomide (CRBN), and CST530 (IAP), as well as the homobivalent SMAC mimetic AZD5582 as reference standards. As TNF- $\alpha$  and related signaling cascades represent crucial factors for the single-agent activity of IAP-targeting compounds,<sup>29,38,39,55</sup> the viability inhibition of sensitive cell lines was evaluated in the presence and absence of this inflammatory stimulus. Co-administration of TNF- $\alpha$  potentiated the inhibitory effects of both SMAC mimetics and PROTACs for all cell lines tested, consistent with previous studies.<sup>56–59</sup> pan-IAP degraders 9 and 25 were more potent than the positive control IAP monovalent and bivalent antagonists in several cell lines (Figures 7 and S17). PROTACs 9 and 25 demonstrated superior activity over AZD5582 in NCI-H929, reaching  $\text{IC}_{50}$  values of 8.5 and 27 nM, respectively (Tables 1 and S8). In addition, PROTAC 9 demonstrated a competitive  $\text{IC}_{50}$  profile in MOLM13 cells at 2.1 nM and SUDHL6 cells at 1.6 nM. While the activity of PROTAC 25 in these two cell lines did not supersede

**Table 1.** Cell Viability Profiles ( $\text{IC}_{50}$  Values) of the VHL-Recruiting PROTAC 9, the VHL Non-Binding Control 11, as well as the Monovalent IAP Antagonist CST530 and the VHL Inhibitor VH298 for Comparison<sup>a</sup>

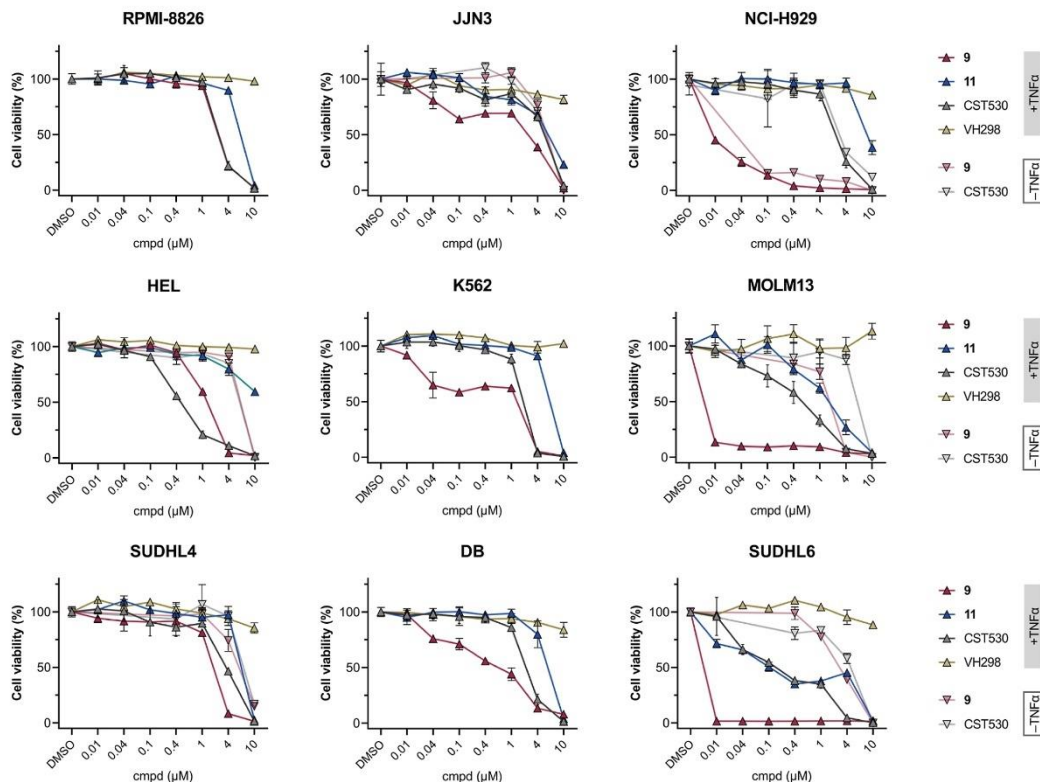
cell line	disease <sup>b</sup>	$\text{IC}_{50}$ ( $\mu\text{M}$ )			
		9	11	CST530	VH298
RPMI-8826	MM	2.54	>5	2.79	>10
JLN3	MM	1.14	>5	4.73	>10
NCI-H929	MM	0.0085	>5	2.34	>10
HEL	AML	1.17	>10	0.45	>10
K562	AML	0.42	>5	1.71	>10
MOLM13	AML	0.0021	>1	0.42	>10
SUDHL4	DLBCL	1.69	>5	3.44	>10
DB	DLBCL	0.46	>5	2.21	>10
SUDHL6	DLBCL	0.0016	0.17	0.17	>10

<sup>a</sup>Values correspond to TNF $\alpha$ -challenged conditions. <sup>b</sup>MM, multiple myeloma; AML, acute myeloid leukemia; DLBCL, diffuse large B-cell lymphoma.

PROTAC 9, it was able to induce potent cell viability reduction in other cell lines such as JLN3 and SUDHL4 (Table S8), surpassing that of IAP antagonists. These effects were independent of IAP baseline levels (Figure S16), which is in agreement with the previous studies of IAP antagonists.

## CONCLUSIONS

In this study, we designed heterobifunctional compounds assembled from an IAP antagonist linked to either a VHL- or a CRBN-recruiting ligand. The entire set of PROTACs consisted of 32 tailored members, which were subjected to in-depth biological studies. Through appropriate control experiments (chemical controls and impairment of the ubiquitin–proteasome system), we provided significant evidence for the engagement with the proposed E3 ligases and PROTAC-induced ubiquitin transfer. The accompanied heterodimerization approach led to novel E3 modulators with IAP degradation profiles that could not be reached with monomeric or homobivalent SMAC mimetics. Among the set of IAP degraders were compounds that induced depletion of the 19 and 30 kDa VHL isoforms. The described pan-IAP degraders will serve as selective tools to explore the biology of IAPs and thus open up new avenues for apoptosis research in various cellular contexts. In addition, selected compounds from our



**Figure 7.** Cell viability screenings in nine different hematological cancer cell lines with pan-IAP degrader **9**, its VHL non-binding control **11**, as well as the structurally related IAP antagonist CST530 and the VHL inhibitor VH298 as respective controls. In certain cases, viability inhibition was assessed in the presence and absence of TNF- $\alpha$ . Multiple myeloma, acute myeloid leukemia, and lymphoma cell lines were treated with the respective compounds at indicated concentrations for 96 h. Viability is normalized to their respective DMSO controls. Data represent means  $\pm$  s.d. of at least three independent biological replicates.

series warrant further appraisal as anti-cancer agents on account of their ability of depleting validated cancer-related IAPs. Preliminary cell-based evaluations of our lead hetero-PROTAC **9** demonstrated that induced degradation of IAPs supersedes the biological effects of monovalent and bivalent IAP antagonists in certain cases. Therefore, further development of IAP-targeting heterobifunctional compounds may lead to degraders with significant therapeutic benefits in the battle against cancer. Exploiting PROTAC methodology to induce the degradation of therapeutically relevant ligases raises hope to unlock this difficult-to-tackle class of drug targets. We also anticipate that the contest between two different E3s may be extendable to any other ligandable ligase.

## EXPERIMENTAL SECTION

**Chemistry General Remarks.** Preparative column chromatography was performed using Merck silica gel 60 (0.063–0.200 mm) or using an automated flash chromatography system puriFlash XS 520Plus. Melting points were determined on a Büchi 510 oil bath apparatus or on a Reichelt hot-stage apparatus and were uncorrected.  $^1\text{H}$  NMR and  $^{13}\text{C}$  NMR spectra were recorded on a Bruker Avance 400 MHz NMR spectrometer, a Bruker Avance 500 MHz NMR spectrometer, or a Bruker Avance III 600 MHz NMR spectrometer,

respectively. NMR spectra were processed and analyzed in MestReNova. Chemical shifts are given in parts per million (ppm) and are referenced to the deuterated solvent used. Coupling constants  $J$  are given in Hz, and the splitting patterns are given as s (singlet), d (doublet), t (triplet), q (quartet), or m (multiplet). In the case of overlapping extraneous solvent peaks, multiplet analyses in  $^1\text{H}$  NMR spectra were performed using qGSD (quantitative Global Spectral Deconvolution). Resonance assignments were made on the basis of one- and two-dimensional NMR techniques which include  $^1\text{H}$ ,  $^{13}\text{C}$ , DEPT, HSQC, and HMBC experiments. *Important note:* the presence of amide rotamers significantly complicated the appearance and validation of the  $^1\text{H}$  and  $^{13}\text{C}$  NMR spectra associated with synthetic intermediates and final PROTACs. The presence of rotamers was demonstrated by recording a representative  $^1\text{H}$  NMR at 80 °C (see the Supporting Information). Thus, reported resonances and integrals may have limited accuracy. High-resolution mass measurements were recorded on a Thermo Scientific Q Exactive Plus mass spectrometer (Thermo Fisher Scientific). The purity and identity of compounds were determined on an Infinity Lab LC/MSD system (Agilent) with the ESI source coupled with an HPLC 1260 Infinity II (Agilent) using an EC50/2 Nucleodur C18 Gravity 3  $\mu\text{m}$  column (Macherey-Nagel). The column temperature was 40 °C. HPLC conditions started with 90%  $\text{H}_2\text{O}$  containing 2 mM  $\text{NH}_4\text{Ac}$ . The gradient ramped up to 100% MeCN in 10 min, followed by further flushing with 100% MeCN for 5 min. The flow rate was 0.5 mL/min. The samples were dissolved in



H<sub>2</sub>O, MeOH, or MeCN (approx. 1 mg/mL), and 2  $\mu$ L of the sample solution was injected. Positive total ion scans were observed from 100 to 1000 *m/z* (or more if necessary), and UV absorption was detected from 190 to 600 nm using a diode array detector (DAD). The purity was determined at 220–600 nm. Analytical reversed-phase HPLC for PROTACs 11 and 20–27 was performed on a Thermo Scientific Dionex UltiMate 3000 UHPLC modular system (Thermo Fisher Scientific), equipped with a photodiode array detector set to 254 nm. A Waters Acquity UPLC HSS C18 SB column (1.8  $\mu$ m, 2.1 mm  $\times$  50 mm) was used and thermostated at 40 °C. The mobile phase consisted of 0.1% TFA in H<sub>2</sub>O (A) and MeCN (B), employing the following gradient: 95% A to 5% A in 10 min, then 95% B for 4 min, with a flow rate of 0.3 mL/min, and an injection volume of 5  $\mu$ L. All compounds that were evaluated in biological assays are >95% pure by HPLC analysis.

Note: To provide readers a clearer picture of all synthesized compounds and to enable easier tracking of experimental procedures, a table with structures of all intermediates is given at the end of the Supporting Information.

**General Procedures. General Procedure I: Mesylation.** To a solution of the corresponding alcohol (7 mmol) in dry CH<sub>2</sub>Cl<sub>2</sub> (15 mL), DIPEA (1.36 g, 1.79 mL, 10.5 mmol) was added under an argon atmosphere and the mixture was cooled to 0 °C. Subsequently, methanesulfonyl chloride (1.20 g, 0.81 mL, 10.5 mmol) was added dropwise at 0 °C, followed by stirring of the mixture at rt for 2 h. After the reaction was complete (monitored by TLC), MeOH (20 mL) was added to the mixture carefully. The volatiles were then evaporated, and the crude product was purified by column chromatography.

**General Procedure II: Alkylation of the IAP Ligand Using Cl-Bearing Linkers or Conjugates.** The corresponding linker or the VHL ligand–linker conjugate (0.30 mmol) was dissolved in dry acetone (15 mL), and NaI (0.45 g, 3.0 mmol) was added. The mixture was stirred at 60 °C for 48 h. After evaporation of the solvent, the residue was suspended in EtOAc (50 mL) and subsequently washed with 10% Na<sub>2</sub>SO<sub>3</sub> solution, H<sub>2</sub>O, and brine (each 25 mL). The organic layer was dried over Na<sub>2</sub>SO<sub>4</sub>, filtered, and evaporated. This intermediate was dissolved in dry DMF (5 mL), and Cs<sub>2</sub>CO<sub>3</sub> and the corresponding IAP ligand 65 or 66 (1.0 equiv based on the yield from the Finkelstein reaction) were added. The mixture was stirred at 60 °C for 18 h. After cooling, it was quenched with half-saturated brine (100 mL) and extracted with CH<sub>2</sub>Cl<sub>2</sub> (3  $\times$  50 mL). The combined organic layers were washed with 5% LiCl solution and brine (each 50 mL), dried over Na<sub>2</sub>SO<sub>4</sub>, filtered, and evaporated. The crude product was purified by column or flash chromatography.

**General Procedure III: Coupling of the VHL1 Ligand and Cl-to-COOH Linkers.** The corresponding Cl-to-COOH linker L1a–L8a (0.50 mmol) was dissolved in dry DMF (5 mL), and DIPEA (0.35 mL, 2 mmol) was added, followed by the addition of HATU (0.21 g, 0.55 mmol). After stirring for 5 min, the corresponding VHL ligand 68–70 (deprotected amine, 0.62 mmol) dissolved in dry DMF (5 mL) and DIPEA (0.35 mL, 2 mmol) were added to the mixture. The combined mixture was stirred at room temperature for 16 h, after which half-saturated brine (50 mL) was added, and the product was extracted with EtOAc (3  $\times$  50 mL). The combined organic phases were washed with saturated NH<sub>4</sub>Cl solution, 5% LiCl solution, and brine (each 50 mL), dried over Na<sub>2</sub>SO<sub>4</sub>, filtered, and concentrated in vacuo.

**General Procedure IV: Alkylation of the VHL2 Ligand Using OMs-to-Cl Linkers.** The corresponding OMs-to-Cl linker L1b–L8b (1.2 mmol) was dissolved in dry DMF (10 mL), followed by the addition of Cs<sub>2</sub>CO<sub>3</sub> (0.49 g, 1.5 mmol). Then, the phenolic VHL ligand 71 (0.55 g, 1.0 mmol) dissolved in dry DMF (5 mL) was added. The combined mixture was stirred at room temperature for 16 h and 3 h at 60 °C. After cooling, half-saturated brine (50 mL) was added, and the product was extracted with EtOAc (3  $\times$  50 mL). The combined organic phases were washed with saturated NH<sub>4</sub>Cl solution, 5% LiCl solution, and brine (each 50 mL); dried over Na<sub>2</sub>SO<sub>4</sub>, filtered, and concentrated in vacuo. The crude product was purified by column or flash chromatography.

**General Procedure V: Alkylation of the IAP Ligand Using OMs-to-Cl Linkers.** To a solution of IAP ligand 65 (0.17 g, 0.25 mmol) and K<sub>2</sub>CO<sub>3</sub> (52 mg, 0.38 mmol) in dry DMF (2 mL), a solution of the corresponding mesylate-bearing linker L1b–L8b (0.30 mmol) in dry DMF (2 mL) was added under an argon atmosphere. The mixture was stirred at 70 °C for 20 h. The volatiles were then evaporated, and the crude product was purified by column chromatography.

**General Procedure VI: Synthesis of Alkyl Azides and Subsequent Reduction to Amines.** To a solution of the corresponding IAP ligand–linker–chloro conjugate 91–98 (0.19 mmol) in dry DMF (5 mL), NaN<sub>3</sub> (25 mg, 0.38 mmol) was added under an argon atmosphere. After stirring the mixture at 80 °C for 4 h, the volatiles were removed, and H<sub>2</sub>O (40 mL) was added. The product was extracted with EtOAc (60 mL). The organic layer was washed with brine (50 mL), dried over Na<sub>2</sub>SO<sub>4</sub>, filtered, concentrated, and further dried under high vacuum. This azide intermediate was dissolved in dry MeOH (5 mL) and treated with 10% Pd/C (22 mg, 20% w/w). The reaction mixture was stirred under H<sub>2</sub> (1 atm, balloon) for 2 h. The mixture was filtered through Celite and washed with MeOH, and the filtrate was concentrated. The products were used in the next step without further purification.

**General Procedure VII: Removal of Boc Protecting Groups.** The Boc-protected PROTAC precursor was treated with 1 M HCl in EtOAc (5 mL), and the mixture was stirred at rt for 4 h. After removal of the volatiles, the oily residue was treated with Et<sub>2</sub>O (5 mL), and the mixture was stirred at rt for 1 h. If a colorless precipitate appeared, it was collected by suction filtration and washed with Et<sub>2</sub>O (2  $\times$  2 mL). Because of sufficient purity, PROTACs 2, 4, 6, 9, 10, and 12–17 were used as hydrochloride salts. For the remaining final PROTACs, additional purification by column chromatography was necessary, and those compounds were transformed into free bases.

**General Procedure VIII: Nucleophilic Aromatic Substitution.** The corresponding IAP ligand–linker–amine conjugate 99–106 (0.11 mmol) was dissolved in dry DMSO (2 mL), and DIPEA (44 mg, 56  $\mu$ L, 0.33 mmol) and the corresponding CRBN ligand 72 or 73 (32 mg, 0.11 mmol) were added. The mixture was stirred at 90 °C for 20 h. After cooling, H<sub>2</sub>O (30 mL) and saturated NaHCO<sub>3</sub> solution (10 mL) were added, and the mixture was extracted with CH<sub>2</sub>Cl<sub>2</sub> (5  $\times$  50 mL). The combined organic layers were washed with brine (200 mL), dried over Na<sub>2</sub>SO<sub>4</sub>, filtered, and concentrated. The oily residue was purified by column chromatography.

**Syntheses of Linkers. Syntheses of L1a–L8a Linkers (L1a: Cl-to-CO<sub>2</sub>Bn and L2a–L8a: Cl-to-CO<sub>2</sub>H).** L1a: Benzyl 5-Chloropentanoate (30). 5-Chlorovaleric acid (1.85 g, 13.55 mmol), benzyl bromide (2.32 g, 1.61 mL, 13.55 mmol), and Na<sub>2</sub>CO<sub>3</sub> (1.72 g, 16.26 mmol) were mixed in MeCN (20 mL) and heated to 80 °C for 18 h. After cooling, the suspension was filtered and then partitioned between H<sub>2</sub>O (100 mL) and EtOAc (2  $\times$  100 mL). The combined organic layers were washed with H<sub>2</sub>O, NaHCO<sub>3</sub> solution, and brine (each 50 mL); dried over Na<sub>2</sub>SO<sub>4</sub>; filtered; and concentrated in vacuo. The crude product was purified by column chromatography (petroleum ether/EtOAc 19:1) to give a colorless oil. Yield (1.87 g, 61%); *R*<sub>f</sub> = 0.43 (petroleum ether/EtOAc 19:1); <sup>1</sup>H NMR (600 MHz, DMSO-*d*<sub>6</sub>):  $\delta$  1.61–1.76 (m, 4H), 2.39 (t, *J* = 7.3 Hz, 2H), 3.62 (t, *J* = 6.4 Hz, 2H), 5.08 (s, 2H), 7.29–7.39 (m, 5H); <sup>13</sup>C NMR (151 MHz, DMSO-*d*<sub>6</sub>):  $\delta$  22.00, 31.46, 32.76, 40.24, 45.08, 65.54, 128.09, 128.14, 128.58, 136.39, 172.67; LC–MS (ESI) *m/z*: [M + H]<sup>+</sup> calcd for C<sub>12</sub>H<sub>16</sub>ClO<sub>2</sub>, 227.08; found, 227.1.

L2a: 8-Chlorooctanoic Acid (31). This compound was synthesized as we described previously.<sup>60</sup>

4-(4-Chlorobutoxy)butan-1-ol (32). 1,4-Butanediol (33.80 g, 375 mmol) was mixed in DMSO (50 mL) and aqueous NaOH (50%, 19.3 mL, 375 mmol). After stirring for 10 min, 1-bromo-4-chlorobutane (12.86 g, 75 mmol) was added while cooling with a water bath. The resulting suspension was vigorously stirred at rt for 24 h. After the addition of a saturated NH<sub>4</sub>Cl solution (150 mL), the mixture was extracted with CH<sub>2</sub>Cl<sub>2</sub> (3  $\times$  150 mL). The combined organic layers were washed with H<sub>2</sub>O (150 mL) and brine (150 mL), dried over Na<sub>2</sub>SO<sub>4</sub>, filtered, and concentrated. The crude product was purified by column chromatography (gradient of petroleum ether/EtOAc 2:1



to 3:2) to give a colorless oil. Yield (4.88 g, 36%);  $R_f$  = 0.31 (petroleum ether/EtOAc 1:1);  $^1\text{H NMR}$  (500 MHz, DMSO- $d_6$ ):  $\delta$  1.38–1.54 (m, 4H), 1.54–1.63 (m, 2H), 1.70–1.79 (m, 2H), 3.30–3.43 (m, 6H), 3.63 (t,  $J$  = 6.7 Hz, 2H), 4.32 (t,  $J$  = 5.2 Hz, 1H);  $^{13}\text{C NMR}$  (126 MHz, DMSO- $d_6$ ):  $\delta$  26.04, 26.76, 29.34, 29.42, 45.44, 60.71, 69.23, 70.08; LC–MS (ESI)  $m/z$ :  $[\text{M} + \text{H}]^+$  calcd for  $\text{C}_8\text{H}_{16}\text{ClO}_2$ , 181.10; found, 180.9.

**L3a: 4-(4-Chlorobutoxy)butanoic Acid (33).** Alcohol 32 (1.08 g, 6 mmol) was dissolved in MeCN (15 mL) and  $\text{H}_2\text{O}$  (15 mL). TEMPO (0.20 g, 1.32 mmol) was then added, followed by the portionwise addition of (diacetoxyiodo)benzene (4.25 g, 13.2 mmol). The orange mixture was stirred at rt for 16 h. It was neutralized by the addition of saturated  $\text{NaHCO}_3$  solution (100 mL), and the aqueous layer was washed with EtOAc (2  $\times$  100 mL). The aqueous phase was then acidified by the careful addition of 2 N HCl solution until pH = 1. The mixture was then extracted with EtOAc (2  $\times$  100 mL), and the combined organic layers were dried over  $\text{Na}_2\text{SO}_4$ , filtered, and concentrated. The crude product was purified by column chromatography (gradient of  $\text{CH}_2\text{Cl}_2$  to  $\text{CH}_2\text{Cl}_2/\text{MeOH}$  9:1) to give a brownish oil. Yield (0.89 g, 76%);  $R_f$  = 0.45 ( $\text{CH}_2\text{Cl}_2/\text{MeOH}$  9:1);  $^1\text{H NMR}$  (500 MHz, DMSO- $d_6$ ):  $\delta$  1.54–1.63 (m, 2H), 1.66–1.79 (m, 4H), 2.23 (t,  $J$  = 7.3 Hz, 2H), 3.35 (dt,  $J$  = 6.3, 8.0 Hz, 4H), 3.63 (t,  $J$  = 6.6 Hz, 2H), 11.97 (s, 1H);  $^{13}\text{C NMR}$  (126 MHz, DMSO- $d_6$ ):  $\delta$  24.88, 26.72, 29.28, 30.56, 45.45, 69.17, 69.26, 69.39, 174.38; LC–MS (ESI)  $m/z$ :  $[\text{M} + \text{H}]^+$  calcd for  $\text{C}_8\text{H}_{16}\text{ClO}_3$ , 195.08; found, 195.1.

**L4a: 2-(2-(2-Chloroethoxy)ethoxy)acetic Acid (34).** This compound was synthesized as we described previously.<sup>60</sup>

**L5a: 2-(2-(2-(2-Chloroethoxy)ethoxy)ethoxy)acetic Acid (35).** This compound was synthesized as we described previously.<sup>60</sup>

**6-((6-Chlorohexyl)oxy)hexan-1-ol (36).** This compound was synthesized as we described previously.<sup>20</sup>

**tert-Butyl 2-((6-((6-Chlorohexyl)oxy)hexyl)oxy)acetate (37).** Linker 36 (1.89 g, 8 mmol), *tert*-butyl bromoacetate (3.08 g, 3.5 mL, 24 mmol), and TBAHS (2.71 g, 8 mmol) were mixed in toluene (6 mL), followed by the addition of 50% aqueous NaOH solution (4 mL) at 0  $^\circ\text{C}$ . The mixture was vigorously stirred at rt for 18 h. The mixture was diluted with  $\text{H}_2\text{O}$  (100 mL) and extracted with EtOAc (3  $\times$  50 mL). The combined organic layers were washed with brine (50 mL), dried over  $\text{Na}_2\text{SO}_4$ , filtered, and concentrated. The crude product was purified by column chromatography (petroleum ether/EtOAc 10:1) to give a colorless oil. Yield (1.42 g, 51%);  $R_f$  = 0.48 (petroleum ether/EtOAc 10:1);  $^1\text{H NMR}$  (600 MHz, DMSO- $d_6$ ):  $\delta$  1.24–1.39 (m, 8H), 1.41 (s, 9H), 1.44–1.51 (m, 6H), 1.66–1.73 (m, 2H), 3.29–3.34 (m, 4H), 3.40 (t,  $J$  = 6.5 Hz, 2H), 3.60 (t,  $J$  = 6.6 Hz, 2H), 3.90 (s, 2H);  $^{13}\text{C NMR}$  (151 MHz, DMSO- $d_6$ ):  $\delta$  25.15, 25.58, 25.68, 26.24, 27.89, 29.22, 29.27, 29.34, 32.17, 45.47, 68.17, 69.93, 70.03, 70.65, 80.66, 169.63; LC–MS (ESI)  $m/z$ :  $[\text{M} + \text{H}]^+$  calcd for  $\text{C}_{18}\text{H}_{36}\text{ClO}_4$ , 351.23; found, 351.2.

**L6a: 2-((6-((6-Chlorohexyl)oxy)hexyl)oxy)acetic Acid (38).** This compound was produced from 37 after acidic cleavage of the *tert*-butyl ester group in  $\text{CH}_2\text{Cl}_2/\text{TFA}$  (1:1) at 40  $^\circ\text{C}$  for 2 h and was used in the next step without further purification after evaporation of the volatiles.

**tert-Butyl 5-((5-((6-Chlorohexyl)oxy)pentyl)oxy)pentanoate (39).** This compound was synthesized as we described previously.<sup>20</sup>

**L7a: 5-((5-((6-Chlorohexyl)oxy)pentyl)oxy)pentanoic Acid (40).** This compound was produced from 39 after acidic cleavage of the *tert*-butyl ester group in  $\text{CH}_2\text{Cl}_2/\text{TFA}$  (1:1) at 40  $^\circ\text{C}$  for 2 h and was used in the next step without further purification after evaporation of the volatiles.

**tert-Butyl 6-Bromohexanoate (41).** This compound was synthesized as we described previously.<sup>20</sup>

**tert-Butyl 6-((6-((6-Chlorohexyl)oxy)hexyl)oxy)hexanoate (42).** This compound was synthesized as we described previously.<sup>20</sup>

**L8a: 6-((6-((6-Chlorohexyl)oxy)hexyl)oxy)hexanoic Acid (43).** This compound was produced from 42 after acidic cleavage of the *tert*-butyl ester group in  $\text{CH}_2\text{Cl}_2/\text{TFA}$  (1:1) at 40  $^\circ\text{C}$  for 2 h and was used in the next step without further purification after evaporation of the volatiles.

**Syntheses of L1b–L8b Linkers (OMs-to-Cl).** **L1b: 5-Chloropentyl Methanesulfonate (44).** This compound was prepared using general procedure 1 and 5-chloro-1-pentanol (2.0 g, 16.3 mmol). The crude product was purified by column chromatography (EtOAc) to give a colorless oil. Yield (2.80 g, 85%);  $R_f$  = 0.60 (EtOAc);  $^1\text{H NMR}$  (400 MHz,  $\text{CDCl}_3$ ):  $\delta$  1.52–1.63 (m, 2H), 1.74–1.87 (m, 4H), 3.01 (s, 3H), 3.55 (t,  $J$  = 6.5 Hz, 2H), 4.24 (t,  $J$  = 6.4 Hz, 2H);  $^{13}\text{C NMR}$  (101 MHz,  $\text{CDCl}_3$ ):  $\delta$  22.99, 28.56, 31.97, 37.52, 44.69, 69.72; HRMS (ESI)  $m/z$ :  $[\text{M} + \text{Na}]^+$  calcd for  $\text{C}_6\text{H}_{13}\text{O}_3\text{ClSNa}$ , 223.0166; found, 223.0164.

**L2b: 8-Chlorooctyl Methanesulfonate (45).** This compound was synthesized as we described previously.<sup>60</sup>

**L3b: 4-(4-Chlorobutoxy)butyl Methanesulfonate (46).** This compound was prepared using general procedure 1 and 32 (0.41 g, 2.29 mmol). The crude product was purified by column chromatography (EtOAc/*n*-hexanes 1:1) to give a colorless oil. Yield (0.33 g, 56%);  $R_f$  = 0.22 (EtOAc/*n*-hexanes 1:2);  $^1\text{H NMR}$  (400 MHz,  $\text{CDCl}_3$ ):  $\delta$  1.65–1.74 (m, 4H), 1.79–1.89 (m, 4H), 3.00 (s, 3H), 3.43 (td,  $J$  = 6.2, 2.1 Hz, 4H), 3.56 (t,  $J$  = 6.6 Hz, 2H), 4.25 (t,  $J$  = 6.5 Hz, 2H);  $^{13}\text{C NMR}$  (101 MHz,  $\text{CDCl}_3$ ):  $\delta$  25.83, 26.37, 27.16, 29.63, 37.50, 45.09, 70.00, 70.07, 70.14; HRMS (ESI)  $m/z$ :  $[\text{M} + \text{H}]^+$  calcd for  $\text{C}_8\text{H}_{20}\text{O}_4\text{ClS}$ , 259.0765; found, 259.0764.

**L4b: 2-(2-(2-Chloroethoxy)ethoxy)ethyl Methanesulfonate (47).** This compound was synthesized as we described previously.<sup>60</sup>

**L5b: 2-(2-(2-(2-Chloroethoxy)ethoxy)ethoxy)ethyl Methanesulfonate (48).** This compound was synthesized as we described previously.<sup>60</sup>

**6-((6-Chlorohexyl)oxy)hexyl Methanesulfonate (49).** This compound was prepared using general procedure 1 and 36 (1.05 g, 3.38 mmol). The crude product was purified by column chromatography (EtOAc/*n*-hexanes 1:2) to give a colorless oil. Yield (0.75 g, 57%);  $R_f$  = 0.35 (EtOAc/*n*-hexanes 1:2);  $^1\text{H NMR}$  (400 MHz,  $\text{CDCl}_3$ ):  $\delta$  1.32–1.50 (m, 8H), 1.53–1.62 (m, 4H), 1.71–1.82 (m, 4H), 3.00 (s, 3H), 3.39 (t,  $J$  = 6.6 Hz, 4H), 3.53 (t,  $J$  = 6.7 Hz, 2H), 4.22 (t,  $J$  = 6.6 Hz, 2H);  $^{13}\text{C NMR}$  (101 MHz,  $\text{CDCl}_3$ ):  $\delta$  25.44, 25.65, 25.82, 26.84, 29.22, 29.67, 29.70, 32.68, 37.50, 45.21, 70.18, 70.76, 70.86; HRMS (ESI)  $m/z$ :  $[\text{M} + \text{H}]^+$  calcd for  $\text{C}_{17}\text{H}_{36}\text{O}_3\text{ClS}$ , 387.1967; found, 387.1960.

**2-((Tetrahydro-2H-pyran-2-yl)oxy)ethan-1-ol (50).** To a solution of ethylene glycol (3.00 g, 48.34 mmol) in dry MeCN (25 mL), 3,4-dihydro-2H-pyran (4.47 g, 48.2 mL, 53.17 mmol) was added under an argon atmosphere. Subsequently,  $\text{CuSO}_4 \times 5 \text{H}_2\text{O}$  (2.41 g, 9.67 mmol) was added, followed by stirring of the mixture at rt for 3 h. After the reaction was complete, the mixture was filtered, and the filtrate was concentrated. The crude product was purified by column chromatography (EtOAc) to give a colorless oil. Yield (1.21 g, 18%);  $R_f$  = 0.30 (EtOAc);  $^1\text{H NMR}$  (400 MHz,  $\text{CDCl}_3$ ):  $\delta$  1.49–1.60 (m, 4H), 1.73–1.89 (m, 2H), 2.80–2.86 (m, 1H), 3.51–3.58 (m, 1H), 3.66–3.81 (m, 4H), 3.88–3.97 (m, 1H), 4.55–4.59 (m, 1H);  $^{13}\text{C NMR}$  (101 MHz,  $\text{CDCl}_3$ ):  $\delta$  20.01, 25.27, 30.81, 62.24, 63.26, 70.72, 100.15; HRMS (ESI)  $m/z$ :  $[\text{M} + \text{Na}]^+$  calcd for  $\text{C}_7\text{H}_{14}\text{O}_3\text{Na}$ , 169.0835; found, 169.0837.

**2-(2-((6-((6-Chlorohexyl)oxy)hexyl)oxy)ethoxy)tetrahydro-2H-pyran (51).** To a solution of 50 (0.72 g, 4.93 mmol) and 49 (1.55 g, 4.93 mmol) in toluene (20 mL), TBAHS (1.67 g, 4.93 mmol) and 50% NaOH (aq) (2.5 mL) were added. The reaction mixture was stirred at rt for 18 h.  $\text{H}_2\text{O}$  (70 mL) was then added, and the mixture was extracted with EtOAc (3  $\times$  100 mL). The combined organic layers were further washed with  $\text{H}_2\text{O}$  and brine (each 200 mL). The organic layers were dried over  $\text{Na}_2\text{SO}_4$ , filtered, and concentrated in vacuo. The crude product was purified by column chromatography (EtOAc/*n*-hexanes 1:2) to give a colorless oil. Yield (1.08 g, 50%);  $R_f$  = 0.45 (EtOAc/*n*-hexanes 1:2);  $^1\text{H NMR}$  (400 MHz,  $\text{CDCl}_3$ ):  $\delta$  1.30–1.47 (m, 8H), 1.47–1.65 (m, 10H), 1.67–1.87 (m, 4H), 3.37 (td,  $J$  = 6.6, 2.1 Hz, 4H), 3.41–3.55 (m, 5H), 3.55–3.61 (m, 3H), 3.80–3.90 (m, 2H), 4.62 (t,  $J$  = 4.3 Hz, 1H);  $^{13}\text{C NMR}$  (101 MHz,  $\text{CDCl}_3$ ):  $\delta$  19.59, 25.55, 25.64, 26.10, 26.18, 26.83, 29.70, 29.73, 29.84, 30.67, 32.68, 45.18, 62.31, 66.73, 70.08, 70.78, 71.00, 71.44, 99.03; HRMS (ESI)  $m/z$ :  $[\text{M} + \text{H}]^+$  calcd for  $\text{C}_{19}\text{H}_{38}\text{O}_4\text{Cl}$ , 365.2453; found, 365.2445.



2-((6-((6-Chlorohexyl)oxy)hexyl)oxy)ethan-1-ol (**52**). To a solution of **51** (1.05 g, 2.88 mmol) in MeOH (10 mL),  $p\text{TsOH} \times \text{H}_2\text{O}$  (0.27 g, 1.44 mmol) was added. The reaction mixture was stirred at rt for 20 h. Saturated  $\text{NaHCO}_3$  solution (50 mL) was added, and it was extracted with  $\text{CH}_2\text{Cl}_2$  (3  $\times$  100 mL). The combined organic layers were washed with brine (200 mL). The organic layers were dried over  $\text{Na}_2\text{SO}_4$ , filtered, and concentrated in vacuo. The crude product was purified by column chromatography (EtOAc/*n*-hexanes 1:2) to give a colorless oil. Yield (0.70 g, 87%);  $R_f$  = 0.25 (EtOAc/*n*-hexanes 1:2);  $^1\text{H}$  NMR (400 MHz,  $\text{CDCl}_3$ ):  $\delta$  1.31–1.41 (m, 6H), 1.40–1.48 (m, 2H), 1.50–1.64 (m, 6H), 1.71–1.81 (m, 2H), 2.22 (t,  $J$  = 5.9 Hz, 1H), 3.38 (td,  $J$  = 6.6, 1.1 Hz, 4H), 3.42–3.48 (m, 2H), 3.48–3.54 (m, 4H), 3.65–3.74 (m, 2H);  $^{13}\text{C}$  NMR (101 MHz,  $\text{CDCl}_3$ ):  $\delta$  25.61, 26.09, 26.14, 26.81, 29.67, 29.77, 32.65, 45.17, 61.91, 70.77, 70.93, 71.40, 71.85; HRMS (ESI)  $m/z$ :  $[\text{M} + \text{H}]^+$  calcd for  $\text{C}_{14}\text{H}_{30}\text{O}_3$ , 281.1878; found, 281.1873.

**53**: 2-((6-((6-Chlorohexyl)oxy)hexyl)oxy)ethyl Methanesulfonate (**53**). This compound was prepared using general procedure I and **52** (0.68 g, 2.41 mmol). The crude product was purified by column chromatography (EtOAc/*n*-hexanes 1:2) to give a colorless oil. Yield (0.80 g, 93%);  $R_f$  = 0.18 (EtOAc/*n*-hexanes 1:2);  $^1\text{H}$  NMR (400 MHz,  $\text{CDCl}_3$ ):  $\delta$  1.29–1.48 (m, 8H), 1.50–1.62 (m, 6H), 1.72–1.81 (m, 2H), 3.04 (s, 3H), 3.38 (td,  $J$  = 6.6, 2.2 Hz, 4H), 3.44–3.49 (m, 2H), 3.52 (t,  $J$  = 6.7 Hz, 2H), 3.65–3.69 (m, 2H), 4.32–4.37 (m, 2H);  $^{13}\text{C}$  NMR (101 MHz,  $\text{CDCl}_3$ ):  $\delta$  25.62, 26.02, 26.12, 26.81, 29.60, 29.68, 29.80, 32.66, 37.75, 45.20, 68.54, 69.43, 70.80, 70.91, 71.59; HRMS (ESI)  $m/z$ :  $[\text{M} + \text{H}]^+$  calcd for  $\text{C}_{15}\text{H}_{32}\text{O}_3\text{S}$ , 359.1654; found, 359.1647.

**54**: 5-((5-((6-Chlorohexyl)oxy)pentyl)oxy)pentyl Methanesulfonate (**54**). This compound was synthesized as we described previously.<sup>60</sup>

6-((Tetrahydro-2H-pyran-2-yl)oxy)hexan-1-ol (**55**). To a solution of 1,6-hexanediol (6.00 g, 50.77 mmol) in dry MeCN (35 mL), 3,4-dihydro-2H-pyran (4.70 g, 50.8 mL, 55.85 mmol) was added under an argon atmosphere. Subsequently,  $\text{CuSO}_4 \times 5 \text{H}_2\text{O}$  (2.53 g, 10.15 mmol) was added, followed by stirring of the mixture at rt for 3 h. After the reaction was complete, the mixture was filtered, and the filtrate was concentrated. The crude product was purified by column chromatography (EtOAc/*n*-hexanes 1:1) to give a colorless oil. Yield (3.72 g, 36%);  $R_f$  = 0.18 (EtOAc/*n*-hexanes 1:1);  $^1\text{H}$  NMR (400 MHz,  $\text{CDCl}_3$ ):  $\delta$  1.34–1.42 (m, 5H), 1.47–1.64 (m, 8H), 1.67–1.75 (m, 1H), 1.77–1.88 (m, 1H), 3.38 (dt,  $J$  = 9.5, 6.5 Hz, 1H), 3.45–3.52 (m, 1H), 3.63 (t,  $J$  = 6.6 Hz, 2H), 3.73 (dt,  $J$  = 9.6, 6.8 Hz, 1H), 3.82–3.89 (m, 1H), 4.54–4.58 (m, 1H);  $^{13}\text{C}$  NMR (101 MHz,  $\text{CDCl}_3$ ):  $\delta$  19.86, 25.61, 25.68, 26.16, 29.81, 30.91, 32.83, 62.55, 63.04, 67.65, 99.04; HRMS (ESI)  $m/z$ :  $[\text{M} + \text{H}]^+$  calcd for  $\text{C}_{11}\text{H}_{22}\text{O}_3$ , 203.1642; found, 203.1638.

6-((Tetrahydro-2H-pyran-2-yl)oxy)hexyl Methanesulfonate (**56**). This compound was prepared using general procedure I and **55** (3.00 g, 14.83 mmol). The crude product was purified by column chromatography (EtOAc/*n*-hexanes 1:2) to give a colorless oil. Yield (3.81 g, 92%);  $R_f$  = 0.18 (EtOAc/*n*-hexanes 1:2);  $^1\text{H}$  NMR (400 MHz,  $\text{CDCl}_3$ ):  $\delta$  1.38–1.47 (m, 4H), 1.51–1.64 (m, 6H), 1.67–1.84 (m, 4H), 3.00 (s, 3H), 3.38 (dt,  $J$  = 9.7, 6.4 Hz, 1H), 3.46–3.53 (m, 1H), 3.74 (dt,  $J$  = 9.6, 6.7 Hz, 1H), 3.82–3.91 (m, 1H), 4.22 (t,  $J$  = 6.6 Hz, 2H), 4.54–4.58 (m, 1H);  $^{13}\text{C}$  NMR (101 MHz,  $\text{CDCl}_3$ ):  $\delta$  19.85, 25.42, 25.59, 25.87, 29.19, 29.65, 30.89, 37.48, 62.58, 67.47, 70.18, 99.08; HRMS (ESI)  $m/z$ :  $[\text{M} + \text{H}]^+$  calcd for  $\text{C}_{12}\text{H}_{22}\text{O}_3\text{S}$ , 281.1417; found, 281.1413.

2-((6-((6-Chlorohexyl)oxy)hexyl)oxy)hexyl)oxy)tetrahydro-2H-pyran (**57**). To a solution of **36** (2.11 g, 8.92 mmol) and **56** (2.50 g, 8.92 mmol) in toluene (40 mL), TBAHS (3.03 g, 8.92 mmol) and 50% NaOH (aq) (4.5 mL) were added. The reaction mixture was stirred at rt for 18 h.  $\text{H}_2\text{O}$  (70 mL) was then added, and the mixture was extracted with EtOAc (3  $\times$  100 mL). The combined organic layers were further washed with  $\text{H}_2\text{O}$  and brine (each 200 mL). The organic layers were dried over  $\text{Na}_2\text{SO}_4$ , filtered, and concentrated in vacuo. The crude product was purified by column chromatography (EtOAc/*n*-hexanes 1:2) to give a light yellow oil. Yield (1.80 g, 48%);  $R_f$  = 0.50 (EtOAc/*n*-hexanes 1:2);  $^1\text{H}$  NMR (400 MHz,  $\text{CDCl}_3$ ):  $\delta$

1.31–1.38 (m, 8H), 1.46–1.64 (m, 16H), 1.66–1.83 (m, 4H), 3.35–3.40 (m, 8H), 3.44–3.55 (m, 4H), 3.72 (dt,  $J$  = 9.6, 6.8 Hz, 1H), 3.85 (ddd,  $J$  = 11.1, 7.5, 3.2 Hz, 1H), 4.53–4.58 (m, 1H);  $^{13}\text{C}$  NMR (101 MHz,  $\text{CDCl}_3$ ):  $\delta$  19.82, 25.61, 25.66, 26.20, 26.26, 26.85, 29.72, 29.84, 30.89, 32.69, 45.20, 62.48, 67.70, 70.79, 70.98, 71.02, 98.97; MS (ESI)  $m/z$ :  $[\text{M} + \text{MeOH} + \text{H}]^+$  calcd for  $\text{C}_{24}\text{H}_{46}\text{O}_3\text{Cl}$ , 454.10; found, 454.1.

6-((6-((6-Chlorohexyl)oxy)hexyl)oxy)hexan-1-ol (**58**). To a solution of **57** (1.77 g, 4.20 mmol) in MeOH (20 mL),  $p\text{TsOH} \times \text{H}_2\text{O}$  (0.40 g, 2.10 mmol) was added. The reaction mixture was stirred at rt for 20 h. Saturated  $\text{NaHCO}_3$  solution (50 mL) was added, and it was extracted with  $\text{CH}_2\text{Cl}_2$  (3  $\times$  100 mL). The combined organic layers were washed with brine (200 mL). The organic layers were dried over  $\text{Na}_2\text{SO}_4$ , filtered, and concentrated in vacuo. The crude product was purified by column chromatography (EtOAc/*n*-hexanes 1:2) to give a light yellow oil. Yield (1.00 g, 71%);  $R_f$  = 0.20 (EtOAc/*n*-hexanes 1:2);  $^1\text{H}$  NMR (400 MHz,  $\text{CDCl}_3$ ):  $\delta$  1.29–1.47 (m, 12H), 1.50–1.62 (m, 10H), 1.72–1.81 (m, 2H), 3.38 (td,  $J$  = 6.6, 1.7 Hz, 8H), 3.52 (t,  $J$  = 6.7 Hz, 2H), 3.62 (t,  $J$  = 6.6 Hz, 2H);  $^{13}\text{C}$  NMR (101 MHz,  $\text{CDCl}_3$ ):  $\delta$  25.64, 25.71, 26.12, 26.18, 26.83, 29.69, 29.81, 32.68, 32.82, 45.20, 63.00, 70.79, 70.90, 70.98, 71.02; HRMS (ESI)  $m/z$ :  $[\text{M} + \text{H}]^+$  calcd for  $\text{C}_{18}\text{H}_{38}\text{O}_3\text{Cl}$ , 337.2504; found, 337.2497.

**59**: 6-((6-((6-Chlorohexyl)oxy)hexyl)oxy)hexyl Methanesulfonate (**59**). This compound was prepared using general procedure I and **58** (1.00 g, 2.97 mmol). The crude product was purified by column chromatography (EtOAc/*n*-hexanes 1:2) to give a colorless oil. Yield (0.79 g, 64%);  $R_f$  = 0.40 (EtOAc/*n*-hexanes 1:2);  $^1\text{H}$  NMR (400 MHz,  $\text{CDCl}_3$ ):  $\delta$  1.30–1.47 (m, 12H), 1.51–1.61 (m, 8H), 1.70–1.82 (m, 4H), 2.99 (s, 3H), 3.34–3.41 (m, 8H), 3.53 (t,  $J$  = 6.7 Hz, 2H), 4.22 (t,  $J$  = 6.5 Hz, 2H);  $^{13}\text{C}$  NMR (101 MHz,  $\text{CDCl}_3$ ):  $\delta$  25.44, 25.66, 25.82, 26.20, 26.85, 29.21, 29.68, 29.72, 29.84, 32.69, 37.48, 45.22, 70.19, 70.72, 70.80, 71.02, 71.04; HRMS (ESI)  $m/z$ :  $[\text{M} + \text{H}]^+$  calcd for  $\text{C}_{19}\text{H}_{40}\text{O}_3\text{S}$ , 415.2280; found, 415.2270.

**Synthesis of E3 Ligands. tert-Butyl N-((1S)-2-(((1S)-1-Cyclohexyl-2-((2S,4R)-4-hydroxy-2-(((1R)-tetralin-1-yl)carbamoyl)pyrrolidin-1-yl)-2-oxo-ethyl)amino)-1-methyl-2-oxo-ethyl)-N-methyl-carbamate (**60**)**. This compound was synthesized as described previously.<sup>43</sup> A colorless solid was obtained. Yield (72%);  $R_f$  = 0.18 (petroleum ether/EtOAc 1:2); mp 88–90 °C;  $^1\text{H}$  NMR (600 MHz,  $\text{DMSO}-d_6$ ):  $\delta$  0.83–1.29 (m, 8H,  $\text{CH}_2$ ), 1.39 (s, 9H,  $\text{CH}_3$ ), 1.52–1.93 (m, 11H), 1.96–2.04 (m, 1H, CH,  $\text{CH}_2$ , 2-H, 3-H, 3'-H), 2.65–2.75 (m, 2H, 4-H), 2.73 (s, 3H,  $\text{CH}_3$ ), 3.49–3.64 (m, 1H), 3.64–3.79 (m, 1H, 5'-H), 4.28–4.45 (m, 3H, CH, 2'-H, 4'-H), 4.45–4.69 (m, 1H, CH), 4.88–4.96 (m, 1H, 1-H), 5.07 (d,  $J$  = 3.6 Hz, 1H, OH), 7.03–7.20 (m, 3H), 7.29 (d,  $J$  = 7.6 Hz, 1H, Ar-H), 7.37–7.83 (m, 1H), 8.21 (d,  $J$  = 8.8 Hz, 1H, CONH);  $^{13}\text{C}$  NMR (151 MHz,  $\text{DMSO}-d_6$ ):  $\delta$  15.13 ( $\text{CH}_3$ ), 20.58 (C-3), 25.75, 25.93, 26.04, 27.82 ( $\text{CH}_2$ ), 28.18 ( $\text{C}(\text{CH}_3)_3$ ), 28.95 (C-4), 29.14 ( $\text{CH}_2$ ), 30.08 (C-2,  $\text{CH}_3$ ), 38.01 (CH, C-3'), 46.69 (C-1), 53.38, 54.75 (CH), 55.71 (C-5'), 58.97 (C-2'), 68.98 (C-4'), 79.24 ( $\text{C}(\text{CH}_3)_3$ ), 125.79, 126.71, 128.41, 128.65 (C-5 to C-8), 137.07, 137.86 (C-4a, C-8a), 155.21, 169.81, 170.51, 171.14 (CO); LC-MS (ESI) 99% purity,  $m/z$ :  $[\text{M} + \text{H}]^+$  calcd for  $\text{C}_{32}\text{H}_{49}\text{N}_4\text{O}_6$ , 585.36; found, 585.2.

**tert-Butyl N-((1R)-2-(((1S)-1-Cyclohexyl-2-((2S,4R)-4-hydroxy-2-(((1R)-tetralin-1-yl)carbamoyl)pyrrolidin-1-yl)-2-oxo-ethyl)amino)-1-methyl-2-oxo-ethyl)-N-methyl-carbamate (**61**)**. This compound was synthesized analogously to **60** but using Boc-N-Me-D-Ala-OH. A colorless solid was obtained. Yield (61%);  $R_f$  = 0.43 (EtOAc); mp 188–190 °C;  $^1\text{H}$  NMR (600 MHz,  $\text{DMSO}-d_6$ ):  $\delta$  0.85–1.21 (m, 5H), 1.24 (d,  $J$  = 7.2 Hz, 3H), 1.39 (s, 9H), 1.51–2.04 (m, 12H), 2.65–2.73 (m, 2H), 2.73 (s, 3H), 3.59 (dd,  $J$  = 2.7, 10.4 Hz, 1H), 3.62–3.79 (m, 1H), 4.33–4.43 (m, 3H), 4.57–4.83 (m, 1H) 4.88–4.98 (m, 1H), 5.04 (d,  $J$  = 3.7 Hz, 1H), 7.03–7.10 (m, 2H), 7.10–7.16 (m, 1H), 7.30 (d,  $J$  = 7.6 Hz, 1H), 7.73 (d,  $J$  = 8.9 Hz, 1H), 8.23 (d,  $J$  = 8.8 Hz, 1H);  $^{13}\text{C}$  NMR (151 MHz,  $\text{DMSO}-d_6$ ):  $\delta$  15.64, 20.58, 25.72, 25.90, 26.08, 27.72, 28.19, 28.94, 29.09, 30.05, 30.10, 37.97, 46.67, 53.55, 54.64, 55.54, 58.95, 68.87, 79.13, 125.75, 126.69, 128.43, 128.62, 137.04, 137.89, 155.12, 169.93, 171.11, 171.53; LC-MS (ESI) 99% purity,  $m/z$ :  $[\text{M} + \text{H}]^+$  calcd for  $\text{C}_{32}\text{H}_{49}\text{N}_4\text{O}_6$ , 585.36;



found, 585.5; HRMS (ESI)  $m/z$ :  $[M + H]^+$  calcd for  $C_{32}H_{49}N_4O_6$ , 585.3647; found, 585.3626.

**3-Benzoyloxyphenol (62).** Benzyl bromide (3.42 g, 2.4 mL, 20 mmol), resorcinol (4.40 g, 40 mmol), and  $K_2CO_3$  (2.76 g, 20 mmol) in DMF (20 mL) were stirred at 80 °C for 18 h. The brown oil was filtered, rinsed with EtOAc (100 mL), and washed with half-saturated brine (2 × 100 mL) and 5% LiCl solution (100 mL). The organic layer was dried over  $Na_2SO_4$ , filtered, and concentrated. The material was purified by column chromatography (petroleum ether/EtOAc 19:1) to give a brown oil. Yield (1.92 g, 48%);  $R_f$  = 0.37 (petroleum ether/EtOAc 8:1);  $^1H$  NMR (500 MHz, DMSO- $d_6$ ):  $\delta$  5.02 (s, 2H), 6.32–6.37 (m, 1H), 6.38 (t,  $J$  = 2.3 Hz, 1H), 6.42 (dd,  $J$  = 2.4, 7.9 Hz, 1H), 7.04 (t,  $J$  = 8.2 Hz, 1H), 7.27–7.34 (m, 1H), 7.34–7.41 (m, 2H), 7.39–7.47 (m, 2H), 9.35 (br s, 1H);  $^{13}C$  NMR (126 MHz, DMSO- $d_6$ ):  $\delta$  69.16, 102.27, 105.64, 108.19, 127.70, 127.86, 128.53, 129.98, 137.41, 158.70, 159.72; LC–MS (ESI) 99% purity,  $m/z$ :  $[M + H]^+$  calcd for  $C_{15}H_{13}O_2$ , 201.09; found, 210.0.

**tert-Butyl N-[[1(1S)-2-[[[(1S)-2-[(2S,4S)-4-(3-Benzoyloxyphenoxy)-2-[[[(1R)-tetralin-1-yl]carbamoyl]pyrrolidin-1-yl]-1-cyclohexyl-2-oxoethyl]amino]-1-methyl-2-oxo-ethyl]-N-methyl-carbamate (63).** Compound 60 (2.92 g, 5.0 mmol) was dissolved in dry toluene (100 mL), and it was sonicated for 10 min to remove any dissolved gases. Subsequently, the solution was transferred into a round-bottom flask equipped with a large stirring bar, and the colorless solution was purged with argon for 5 min. Then, the other substrates were added in the following order: 62 (1.05 g, 5.25 mmol), PS-TPP (1 mmol/g loading, 5.75 g), and finally DEAD (40% in toluene, 2.40 mL, 5.25 mmol). After purging for another 5 min, the vessel was closed, and the yellow suspension was stirred at rt for 18 h. The resin was filtered off, and it was washed with EtOAc (2 × 100 mL). The combined organic layers were washed with  $H_2O$  and brine (each 250 mL), dried over  $Na_2SO_4$ , filtered, and concentrated in vacuo. The crude material was purified by column chromatography as follows: the column was packed and started with petroleum ether/EtOAc 2:1. Then, the polarity was gradually increased to 1:2, and it was eluted until the complete elimination of the side product. Subsequently, the polarity was further increased to petroleum ether/EtOAc 1:4 and kept at this level. A colorless solid was obtained. Yield (1.76 g, 46%);  $R_f$  = 0.50 (petroleum ether/EtOAc 1:4); mp 66–68 °C;  $^1H$  NMR (600 MHz, DMSO- $d_6$ ):  $\delta$  1.07 (s, 3H), 1.01–1.20 (m, 6H), 1.20–1.31 (m, 1H), 1.31–1.45 (m, 12H), 1.53–1.82 (m, 4H), 2.04–2.11 (m, 1H), 2.44–2.56 (m, 1H), 2.67 (q,  $J$  = 7.8 Hz, 2H), 2.70 (s, 3H), 3.59 (dd,  $J$  = 4.3, 11.0 Hz, 1H), 4.24 (dd,  $J$  = 5.9, 10.8 Hz, 1H), 4.30 (t,  $J$  = 7.9 Hz, 1H), 4.44 (dd,  $J$  = 5.2, 9.0 Hz, 1H), 4.53 (s, 1H), 4.87–4.94 (m, 1H), 5.02 (q,  $J$  = 4.0 Hz, 1H), 5.05 (s, 2H), 6.43–6.51 (m, 1H), 6.54 (t,  $J$  = 2.4 Hz, 1H), 6.61 (dd,  $J$  = 2.4, 8.2 Hz, 1H), 7.01–7.15 (m, 4H), 7.17 (t,  $J$  = 8.2 Hz, 1H), 7.23 (d,  $J$  = 7.4 Hz, 1H), 7.28–7.34 (m, 1H), 7.34–7.45 (m, 5H), 7.83 (d,  $J$  = 8.6 Hz, 1H);  $^{13}C$  NMR (151 MHz, DMSO- $d_6$ ):  $\delta$  14.82, 16.97, 17.63, 20.14, 21.24, 24.31, 25.66, 25.83, 25.98, 28.22, 28.47, 28.95, 29.13, 29.88, 30.23, 33.72, 34.61, 40.97, 46.85, 52.18, 55.33, 58.77, 69.46, 75.16, 80.73, 102.85, 107.88, 108.30, 125.94, 126.93, 127.86, 128.04, 128.55, 128.64, 128.87, 130.31, 137.22, 137.44, 158.31, 159.78, 169.55, 170.11, 170.51; LC–MS (ESI) 97% purity,  $m/z$ :  $[M + H]^+$  calcd for  $C_{45}H_{58}N_4O_7$ , 767.43; found, 767.4.

**tert-Butyl N-[[1(1R)-2-[[[(1S)-2-[(2S,4S)-4-(3-Benzoyloxyphenoxy)-2-[[[(1R)-tetralin-1-yl]carbamoyl]pyrrolidin-1-yl]-1-cyclohexyl-2-oxoethyl]amino]-1-methyl-2-oxo-ethyl]-N-methyl-carbamate (64).** This compound was synthesized analogously to 63 but using precursor 61 (1.75 g, 3.0 mmol) and on a smaller scale (3.0 mmol). A colorless solid was obtained. Yield (1.06 g, 46%);  $R_f$  = 0.50 (petroleum ether/EtOAc 1:1); mp 84–86 °C;  $^1H$  NMR (600 MHz, DMSO- $d_6$ ):  $\delta$  0.84–0.95 (m, 2H), 1.01–1.12 (m, 4H), 1.24 (d,  $J$  = 7.2 Hz, 3H), 1.31–1.37 (m, 10H), 1.52–1.65 (m, 6H), 1.67–1.81 (m, 5H), 2.10 (br s, 1H), 2.63–2.72 (m, 2H), 2.73 (s, 2H), 3.61 (br s, 1H), 4.24–4.40 (m, 2H), 4.44 (dd,  $J$  = 5.0, 9.0 Hz, 1H), 4.88–4.94 (m, 1H), 4.96–5.05 (m, 1H), 5.06 (s, 2H), 6.45–6.51 (m, 1H), 6.52–6.56 (m, 1H), 6.61 (dd,  $J$  = 2.4, 8.0 Hz, 1H), 7.01–7.20 (m, 4H), 7.23–7.27 (m, 1H), 7.29–7.34 (m, 1H), 7.33–7.45 (m, 4H), 7.86 (s, 1H), 7.92 (s, 1H);  $^{13}C$  NMR (151 MHz, DMSO- $d_6$ ):  $\delta$  14.56,

16.06, 20.31, 20.54, 21.22, 25.93, 26.06, 26.31, 28.48, 29.20, 29.36, 30.09, 30.51, 35.00, 47.11, 52.55, 53.22, 54.61, 55.29, 58.93, 60.21, 69.72, 75.44, 79.30, 103.10, 108.14, 108.51, 126.18, 127.18, 128.12, 128.28, 128.88, 129.11, 130.55, 137.49, 137.70, 155.50, 158.56, 160.05, 170.24, 170.90, 172.42; LC–MS (ESI) 98% purity,  $m/z$ :  $[M + H]^+$  calcd for  $C_{45}H_{58}N_4O_7$ , 767.43; found, 767.5; HRMS (ESI)  $m/z$ :  $[M + H]^+$  calcd for  $C_{45}H_{58}N_4O_7$ , 767.4378; found, 767.4350.

**tert-Butyl N-[[1(1S)-2-[[[(1S)-2-[(2S,4S)-4-(3-hydroxyphenoxy)-2-[[[(1R)-tetralin-1-yl]carbamoyl]pyrrolidin-1-yl]-2-oxoethyl]amino]-1-methyl-2-oxo-ethyl]-N-methyl-carbamate (65).** Compound 63 (1.69 g, 2.2 mmol) was dissolved in dry MeOH (20 mL), and 10% Pd/C (0.17 g, 10% w/w) was added. The vessel was closed, evacuated, and refilled with nitrogen gas (3×), followed by hydrogen gas. The black mixture was stirred for 18 h at rt. The charcoal was removed by filtration, and the title compound was obtained as a colorless solid after evaporation. Yield (1.31 g, 81%);  $R_f$  = 0.43 (EtOAc); mp 92–96 °C;  $^1H$  NMR (600 MHz, DMSO- $d_6$ ):  $\delta$  0.71–1.24 (m, 9H), 1.38 (s, 9H), 1.52–1.84 (m, 10H), 2.01–2.14 (m, 1H), 2.43–2.53 (m, 1H), 2.64–2.76 (m, 5H), 3.60 (dd,  $J$  = 4.4, 10.8 Hz, 1H), 4.18–4.27 (m, 1H), 4.32 (t,  $J$  = 7.8 Hz, 1H), 4.44 (dd,  $J$  = 5.1, 9.0 Hz, 1H), 4.85–5.00 (m, 2H), 6.23–6.40 (m, 3H), 7.00–7.16 (m, 4H), 7.24 (d,  $J$  = 7.5 Hz, 1H), 7.84 (d,  $J$  = 8.5 Hz, 1H), 8.31 (d,  $J$  = 8.4 Hz, 1H), 9.40 (s, 1H);  $^{13}C$  NMR (151 MHz, DMSO- $d_6$ ):  $\delta$  15.11, 20.04, 25.61, 25.78, 25.92, 28.17, 28.90, 29.07, 29.65, 29.81, 30.16, 34.64, 39.52, 46.78, 52.25, 53.27, 55.23, 58.65, 74.96, 79.17, 103.14, 106.14, 108.55, 125.89, 126.86, 128.51, 128.79, 130.06, 137.17, 137.40, 155.27, 158.29, 158.76, 169.40, 169.97, 170.38; LC–MS (ESI) 99% purity,  $m/z$ :  $[M + H]^+$  calcd for  $C_{38}H_{53}N_4O_7$ , 677.39; found, 677.6.

**tert-Butyl N-[[1(1R)-2-[[[(1S)-2-[(2S,4S)-4-(3-hydroxyphenoxy)-2-[[[(1R)-tetralin-1-yl]carbamoyl]pyrrolidin-1-yl]-2-oxoethyl]amino]-1-methyl-2-oxo-ethyl]-N-methyl-carbamate (66).** This compound was synthesized analogously to compound 65 but using precursor 64 (1.02 g, 1.33 mmol) in dry MeOH (13 mL) and 10% Pd/C (0.10 g, 10% w/w). A colorless solid was obtained. Yield (0.87 g, 96%);  $R_f$  = 0.57 (EtOAc); mp 92–96 °C;  $^1H$  NMR (600 MHz, DMSO- $d_6$ ):  $\delta$  0.82–1.28 (m, 9H), 1.35 (s, 9H), 1.53–1.82 (m, 10H), 2.01–2.21 (m, 1H), 2.27–2.49 (m, 1H), 2.62–2.71 (m, 2H), 2.74 (s, 3H), 3.62 (br s, 1H), 4.31 (p,  $J$  = 13.5, 15.6 Hz, 2H), 4.44 (dd,  $J$  = 4.8, 9.0 Hz, 1H), 4.88–4.96 (m, 2H), 6.19–6.45 (m, 3H), 6.93–7.19 (m, 4H), 7.25 (d,  $J$  = 7.5 Hz, 1H), 7.86 (br s, 1H), 7.91 (br s, 1H), 9.39 (s, 1H);  $^{13}C$  NMR (151 MHz, DMSO- $d_6$ ):  $\delta$  15.73, 19.94, 25.59, 25.73, 25.98, 28.15, 28.88, 29.04, 29.65, 29.75, 30.19, 34.77, 46.79, 52.27, 52.84, 54.93, 58.57, 74.96, 79.23, 103.14, 106.09, 108.55, 125.88, 126.87, 128.59, 128.79, 130.06, 137.17, 137.36, 155.19, 158.24, 158.75, 169.41, 170.47, 170.99; LC–MS (ESI) 97% purity,  $m/z$ :  $[M + H]^+$  calcd for  $C_{38}H_{53}N_4O_7$ , 677.39; found, 677.7; HRMS (ESI)  $m/z$ :  $[M + H]^+$  calcd for  $C_{38}H_{53}N_4O_7$ , 677.3909; found, 677.3896.

**tert-Butyl N-[[1(1S)-2-[[[(1S)-2-[(2S,4S)-4-(3-hydroxyphenoxy)-2-[[[(1R)-tetralin-1-yl]carbamoyl]pyrrolidin-1-yl]ethyl]amino]-1-methyl-2-oxo-ethyl]-N-methyl-carbamate (67).** This compound was synthesized analogously to 63 but using phenol (99 mg, 1.05 mmol) instead of 62 and on a smaller scale (1.0 mmol). A colorless solid was obtained. Yield (185 mg, 28%);  $R_f$  = 0.22 (petroleum ether/EtOAc 1:4); mp 70–74 °C;  $^1H$  NMR (500 MHz, DMSO- $d_6$ ):  $\delta$  0.97–1.26 (m, 8H), 1.38 (s, 9H), 1.50–1.84 (m, 11H), 2.06–2.14 (m, 1H), 2.49–2.58 (m, 1H), 2.64–2.74 (m, 5H), 3.62 (dd,  $J$  = 4.4, 10.7 Hz, 1H), 4.26 (dd,  $J$  = 6.0, 10.7 Hz, 1H), 4.32 (t,  $J$  = 7.8 Hz, 1H), 4.45 (dd,  $J$  = 5.1, 9.1 Hz, 1H), 4.87–4.95 (m, 1H), 4.99–5.07 (m, 1H), 6.83–6.98 (m, 3H), 7.01–7.17 (m, 3H), 7.21–7.32 (m, 3H), 7.63 (br s, 1H), 7.82 (d,  $J$  = 8.5 Hz, 1H);  $^{13}C$  NMR (126 MHz, DMSO- $d_6$ ):  $\delta$  14.75, 20.01, 25.59, 25.76, 25.91, 28.16, 28.88, 29.09, 29.79, 30.16, 34.54, 36.86, 46.76, 52.18, 53.01, 55.24, 58.71, 75.04, 79.18, 115.70, 121.22, 125.86, 126.86, 128.51, 128.78, 129.70, 137.15, 137.38, 154.94, 157.07, 169.99, 170.43; LC–MS (ESI) 99% purity,  $m/z$ :  $[M + H]^+$  calcd for  $C_{38}H_{53}N_4O_6$ , 661.39; found, 661.5; HRMS (ESI)  $m/z$ :  $[M + H]^+$  calcd for  $C_{38}H_{53}N_4O_6$ , 661.3960; found, 661.3916.



(2*S*,4*S*)-1-((*S*)-2-Cyclohexyl-2-((*S*)-2-(Methylamino)propanamido)acetyl)-4-phenoxy-*N*-((*R*)-1,2,3,4-tetrahydronaphthalen-1-yl)pyrrolidine-2-carboxamide (CST530).<sup>52</sup> Compound 67 (70 mg, 106  $\mu$ mol) was stirred with 1 M HCl in EtOAc (3 mL) for 3 h at rt. Subsequently, it was diluted with EtOAc (25 mL) and washed with saturated NaHCO<sub>3</sub> solution and brine (each 10 mL), dried over Na<sub>2</sub>SO<sub>4</sub>, filtered, and concentrated in vacuo. The product material was purified by column chromatography (CH<sub>2</sub>Cl<sub>2</sub>/MeOH + 7 N NH<sub>3</sub>, 29:1) to give the title compound as a colorless solid. Yield (49 mg, 83%); *R*<sub>f</sub> = 0.37 (CH<sub>2</sub>Cl<sub>2</sub>/MeOH + NH<sub>3</sub>, 19:1); mp 80–84 °C; <sup>1</sup>H NMR (500 MHz, DMSO-*d*<sub>6</sub>):  $\delta$  0.88–1.18 (m, 9H), 1.52–1.85 (m, 10H), 2.16 (s, 3H), 2.04–2.13 (m, 1H), 2.50–2.59 (m, 1H), 2.62–2.77 (m, 2H), 2.87–3.00 (m, 1H), 3.64 (dd, *J* = 4.5, 10.8 Hz, 1H), 4.23–4.34 (m, 1H), 4.39 (dd, *J* = 7.1, 8.6 Hz, 1H), 4.45 (dd, *J* = 5.2, 9.0 Hz, 1H), 4.87–4.95 (m, 1H), 5.04 (p, *J* = 5.4 Hz, 1H), 6.88–6.92 (m, 2H), 6.95 (t, *J* = 7.5 Hz, 1H), 7.02–7.19 (m, 3H), 7.21–7.33 (m, 3H), 7.84 (d, *J* = 8.6 Hz, 1H), 7.89 (d, *J* = 8.7 Hz, 1H); <sup>13</sup>C NMR (126 MHz, DMSO-*d*<sub>6</sub>):  $\delta$  19.19, 19.97, 25.55, 25.75, 25.92, 27.91, 28.86, 29.18, 29.77, 34.39, 34.54, 46.73, 52.15, 54.45, 58.63, 59.28, 74.96, 115.69, 121.20, 125.86, 126.84, 128.54, 128.76, 129.69, 137.14, 137.35, 157.06, 169.98, 170.57, 174.56; LC–MS (ESI) 97% purity, *m/z*: [M + H]<sup>+</sup> calcd for C<sub>33</sub>H<sub>43</sub>N<sub>4</sub>O<sub>4</sub>, 561.34; found, 561.3.

(2*S*,4*R*)-1-((*S*)-2-Amino-3,3-dimethylbutanoyl)-4-hydroxy-*N*-(4-(4-methylthiazol-5-yl)benzyl)pyrrolidine-2-carboxamide (68). This compound was synthesized as we described previously.<sup>60</sup>

(2*S*,4*R*)-1-((*S*)-2-Amino-3,3-dimethylbutanoyl)-4-hydroxy-*N*-((*S*)-1-(4-(4-methylthiazol-5-yl)phenyl)ethyl)pyrrolidine-2-carboxamide (69). This compound was synthesized as described previously.<sup>61,62</sup>

(2*S*,4*S*)-1-((*S*)-2-Amino-3,3-dimethylbutanoyl)-4-hydroxy-*N*-(4-(4-methylthiazol-5-yl)benzyl)pyrrolidine-2-carboxamide (70). This compound was synthesized as described previously.<sup>63</sup>

(2*S*,4*R*)-4-Hydroxy-*N*-(2-hydroxy-4-(4-methylthiazol-5-yl)benzyl)-1-((*S*)-3-methyl-2-(1-oxoisindolin-2-yl)butanoyl)pyrrolidine-2-carboxamide (71). This compound was synthesized as we described previously.<sup>60</sup>

2-(2,6-Dioxopiperidin-3-yl)-4-fluoroisindoline-1,3-dione (72). This compound was synthesized as we described previously.<sup>16</sup>

4-Fluoro-2-(1-methyl-2,6-dioxo-3-piperidyl)isindoline-1,3-dione (73). This compound was synthesized as we described previously.<sup>20</sup>

**Synthesis of E3–Linker Conjugates.** Benzyl 5-(3-(((*S*,*S*)-1-((*S*)-2-((*S*)-2-((*tert*-Butoxycarbonyl)(methyl)amino)propanamido)-2-cyclohexylacetyl)-5-(((*R*)-1,2,3,4-tetrahydronaphthalen-1-yl)-carbamoyl)pyrrolidin-3-yl)oxy)phenoxy)pentanoate (74). This compound was prepared using general procedure II, linker L1a (68 mg, 0.30 mmol), and IAP ligand 65. The crude product was purified by column chromatography (CH<sub>2</sub>Cl<sub>2</sub>/MeOH 39:1) to give a colorless oil. Yield (156 mg, 60%); *R*<sub>f</sub> = 0.40 (CH<sub>2</sub>Cl<sub>2</sub>/MeOH 39:1); <sup>1</sup>H NMR (600 MHz, DMSO-*d*<sub>6</sub>):  $\delta$  0.77–1.12 (m, 6H), 1.18 (s, 3H), 1.38 (s, 9H), 1.51–1.83 (m, 14H), 2.05–2.12 (m, 1H), 2.38–2.56 (m, 3H), 2.63–2.75 (m, 5H), 3.55–3.63 (m, 1H), 3.85–3.96 (m, 2H), 4.23 (dd, *J* = 6.1, 11.0 Hz, 1H), 4.31 (t, *J* = 7.9 Hz, 1H), 4.44 (dd, *J* = 5.1, 9.1 Hz, 1H), 4.88–5.05 (m, 2H), 5.07 (d, *J* = 1.2 Hz, 2H), 6.40–6.54 (m, 3H), 7.00–7.18 (m, 4H), 7.21–7.26 (m, 1H), 7.28–7.39 (m, 5H), 7.81 (d, *J* = 8.5 Hz, 1H), 8.31 (d, *J* = 8.3 Hz, 1H); <sup>13</sup>C NMR (151 MHz, DMSO-*d*<sub>6</sub>):  $\delta$  15.28, 20.10, 21.38, 25.62, 25.78, 25.94, 28.16, 28.18, 28.90, 29.10, 29.84, 30.18, 33.27, 34.57, 46.80, 52.16, 53.47, 55.26, 58.72, 65.53, 67.20, 75.11, 79.19, 102.50, 107.50, 107.85, 125.88, 126.86, 128.08, 128.14, 128.49, 128.58, 128.81, 130.19, 136.43, 137.16, 137.41, 154.69, 158.26, 160.02, 170.04, 170.46, 172.81; LC–MS (ESI) 96% purity, *m/z*: [M + H]<sup>+</sup> calcd for C<sub>50</sub>H<sub>67</sub>N<sub>4</sub>O<sub>9</sub>, 867.49; found, 867.6; HRMS (ESI) *m/z*: [M + H]<sup>+</sup> calcd for C<sub>50</sub>H<sub>67</sub>N<sub>4</sub>O<sub>9</sub>, 867.4863; found, 867.4861.

(2*S*,4*R*)-1-((*S*)-2-(8-Chlorooctanamido)-3,3-dimethylbutanoyl)-4-hydroxy-*N*-(4-(4-methylthiazol-5-yl)benzyl)pyrrolidine-2-carboxamide (75). This compound was synthesized as we described previously.<sup>60</sup>

(2*S*,4*R*)-1-((*S*)-2-(4-(4-Chlorobutoxy)butanamido)-3,3-dimethylbutanoyl)-4-hydroxy-*N*-(4-(4-methylthiazol-5-yl)benzyl)pyrrolidine-2-carboxamide (76). This compound was prepared using general procedure III, linker L3a (97 mg, 0.50 mmol), and VHL

ligand 68 (265 mg, 0.62 mmol). The crude product was purified by column chromatography (CH<sub>2</sub>Cl<sub>2</sub>/MeOH 29:1) to give a colorless semi-solid. Yield (191 mg, 63%); *R*<sub>f</sub> = 0.35 (CH<sub>2</sub>Cl<sub>2</sub>/MeOH 19:1); <sup>1</sup>H NMR (600 MHz, DMSO-*d*<sub>6</sub>):  $\delta$  0.92 (s, 9H), 1.21–1.28 (m, 1H), 1.54–1.62 (m, 2H), 1.61–1.80 (m, 4H), 1.86–1.93 (m, 1H), 1.99–2.06 (m, 1H), 2.13–2.21 (m, 1H), 2.22–2.31 (m, 1H), 2.43 (s, 3H), 3.27–3.40 (m, 3H), 3.56–3.70 (m, 4H), 4.21 (dd, *J* = 5.5, 15.8 Hz, 1H), 4.31–4.37 (m, 1H), 4.39–4.46 (m, 2H), 4.53 (d, *J* = 9.3 Hz, 1H), 5.10 (d, *J* = 3.6 Hz, 1H), 7.35–7.45 (m, 4H), 7.84 (d, *J* = 9.3 Hz, 1H), 8.53 (t, *J* = 6.1 Hz, 1H), 8.97 (s, 1H); <sup>13</sup>C NMR (151 MHz, DMSO-*d*<sub>6</sub>):  $\delta$  16.09, 25.73, 26.53, 26.75, 29.29, 31.78, 35.38, 38.10, 40.24, 41.82, 45.49, 45.51, 56.49, 56.53, 58.86, 69.03, 69.28, 69.61, 127.60, 128.80, 129.81, 131.33, 139.67, 147.89, 151.59, 169.84, 171.95, 172.10; LC–MS (ESI) 95% purity, *m/z*: [M + H]<sup>+</sup> calcd for C<sub>30</sub>H<sub>44</sub>ClN<sub>4</sub>O<sub>5</sub>, 607.27; found, 607.3; HRMS (ESI) *m/z*: [M + H]<sup>+</sup> calcd for C<sub>30</sub>H<sub>44</sub>ClN<sub>4</sub>O<sub>5</sub>, 607.2716; found, 607.2707.

(2*S*,4*R*)-1-((*S*)-2-(2-(2-(2-Chloroethoxy)ethoxy)acetamido)-3,3-dimethylbutanoyl)-4-hydroxy-*N*-(4-(4-methylthiazol-5-yl)benzyl)pyrrolidine-2-carboxamide (77). This compound was synthesized as we described previously.<sup>60</sup>

(2*S*,4*R*)-1-((*S*)-2-(*tert*-Butyl)-14-chloro-4-oxo-6,9,12-trioxo-3-azatetradecanoyl)-4-hydroxy-*N*-(4-(4-methylthiazol-5-yl)benzyl)pyrrolidine-2-carboxamide (78). This compound was synthesized as we described previously.<sup>60</sup>

(2*S*,4*R*)-1-((*S*)-2-(2-((6-(6-Chlorohexyloxy)hexyl)oxy)acetamido)-3,3-dimethylbutanoyl)-4-hydroxy-*N*-(4-(4-methylthiazol-5-yl)benzyl)pyrrolidine-2-carboxamide (79). This compound was prepared using general procedure III, linker L6a (147 mg, 0.50 mmol), and VHL ligand 68 (265 mg, 0.62 mmol). The crude product was purified by column chromatography (CH<sub>2</sub>Cl<sub>2</sub>/MeOH 29:1) to give a colorless oil. Yield (233 mg, 66%); *R*<sub>f</sub> = 0.27 (CH<sub>2</sub>Cl<sub>2</sub>/MeOH 19:1); <sup>1</sup>H NMR (600 MHz, DMSO-*d*<sub>6</sub>):  $\delta$  0.92 (s, 9H), 1.30–1.62 (m, 14H), 1.70–1.78 (m, 2H), 2.05–2.13 (m, 1H), 2.44–2.52 (m, 1H), 2.49 (s, 3H), 3.33–3.38 (m, 4H), 3.41–3.52 (m, 4H), 3.61 (dd, *J* = 3.8, 11.2 Hz, 1H), 3.82–3.94 (m, 2H), 4.01–4.06 (m, 1H), 4.32 (dd, *J* = 5.4, 15.1 Hz, 1H), 4.46 (d, *J* = 8.7 Hz, 1H), 4.48–4.55 (m, 2H), 4.69 (t, *J* = 7.9 Hz, 1H), 7.17 (d, *J* = 8.7 Hz, 1H), 7.33 (s, 4H), 7.40 (t, *J* = 6.0 Hz, 1H), 8.76 (s, 1H). The signal for OH is missing. <sup>13</sup>C NMR (151 MHz, DMSO-*d*<sub>6</sub>):  $\delta$  15.63, 25.48, 25.90, 25.98, 26.34, 26.67, 29.40, 29.65, 32.51, 34.96, 35.90, 43.17, 45.04, 55.24, 56.62, 56.92, 58.50, 69.81, 70.07, 70.70, 70.77, 71.85, 128.14, 129.45, 130.35, 132.11, 138.40, 147.58, 150.75, 170.51, 170.76, 171.27; LC–MS (ESI) 98% purity, *m/z*: [M + H]<sup>+</sup> calcd for C<sub>36</sub>H<sub>56</sub>ClN<sub>4</sub>O<sub>6</sub>S, 707.36; found, 707.6; HRMS (ESI) *m/z*: [M + H]<sup>+</sup> calcd for C<sub>36</sub>H<sub>56</sub>ClN<sub>4</sub>O<sub>6</sub>S, 707.3604; found, 707.3592.

(2*S*,4*R*)-1-((*S*)-2-(5-((5-((6-Chlorohexyloxy)pentyl)oxy)pentanamido)-3,3-dimethylbutanoyl)-4-hydroxy-*N*-(4-(4-methylthiazol-5-yl)benzyl)pyrrolidine-2-carboxamide (80). This compound was synthesized as we described previously.<sup>60</sup>

(2*S*,4*R*)-1-((*S*)-2-(6-((6-(6-Chlorohexyloxy)hexyl)oxy)hexanamido)-3,3-dimethylbutanoyl)-4-hydroxy-*N*-(4-(4-methylthiazol-5-yl)benzyl)pyrrolidine-2-carboxamide (81). This compound was prepared using general procedure III, linker L8a (175 mg, 0.50 mmol), and VHL ligand 68 (265 mg, 0.62 mmol). The crude product was purified by column chromatography (CH<sub>2</sub>Cl<sub>2</sub>/MeOH 29:1) to give a colorless oil. Yield (225 mg, 59%); *R*<sub>f</sub> = 0.31 (CH<sub>2</sub>Cl<sub>2</sub>/MeOH 19:1); <sup>1</sup>H NMR (600 MHz, DMSO-*d*<sub>6</sub>):  $\delta$  0.92 (s, 9H), 1.20–1.32 (m, 8H), 1.33–1.40 (m, 2H), 1.40–1.55 (m, 10H), 1.65–1.72 (m, 2H), 1.86–1.93 (m, 1H), 1.98–2.05 (m, 1H), 2.06–2.13 (m, 1H), 2.21–2.29 (m, 1H), 2.43 (s, 3H), 3.24–3.33 (m, 8H), 3.60 (t, *J* = 6.6 Hz, 2H), 3.63 (d, *J* = 10.4 Hz, 1H), 3.63–3.69 (m, 1H), 4.20 (dd, *J* = 5.5, 15.8 Hz, 1H), 4.32–4.36 (m, 1H), 4.39–4.45 (m, 2H), 4.53 (d, *J* = 9.3 Hz, 1H), 5.10 (d, *J* = 3.6 Hz, 1H), 7.37 (d, *J* = 8.3 Hz, 2H), 7.41 (d, *J* = 8.1 Hz, 2H), 7.80 (d, *J* = 9.3 Hz, 1H), 8.52 (t, *J* = 6.1 Hz, 1H), 8.96 (s, 1H); <sup>13</sup>C NMR (151 MHz, DMSO-*d*<sub>6</sub>):  $\delta$  16.10, 25.17, 25.48, 25.58, 25.73, 25.76, 26.26, 26.55, 29.17, 29.25, 29.38, 29.41, 32.19, 35.03, 35.37, 38.11, 41.83, 45.51, 56.47, 56.49, 58.87, 69.04, 69.95, 70.06, 127.60, 128.81, 129.81, 131.34, 139.67, 147.89, 151.59, 169.89, 172.12, 172.23; LC–MS (ESI) 98% purity, *m/z*: [M + H]<sup>+</sup> calcd for C<sub>40</sub>H<sub>65</sub>ClN<sub>4</sub>O<sub>6</sub>S, 763.42; found, 763.9;



HRMS (ESI)  $m/z$ :  $[M + H]^+$  calcd for  $C_{40}H_{63}ClN_4O_6S$ , 763.4230; found, 763.4215.

**Benzyl 5-(3-(((3S,5S)-1-((S)-2-((R)-2-((tert-Butoxycarbonyl)-(methylamino)propanamido)-2-cyclohexylacetyl)-5-(((R)-1,2,3,4-tetrahydronaphthalen-1-yl)carbamoyl)pyrrolidin-3-yl)oxy)phenoxy)pentanoate (82).** This compound was prepared using general procedure II, linker L1a (68 mg, 0.30 mmol), and IAP ligand 66. The crude product was purified by flash chromatography (gradient from 0 to 5% MeOH in  $CH_2Cl_2$ ) to give a colorless oil. Yield (156 mg, 60%);  $R_f$  = 0.40 ( $CH_2Cl_2/MeOH$  39:1);  $^1H$  NMR (600 MHz,  $DMSO-d_6$ ):  $\delta$  0.82–1.17 (m, 6H), 1.24 (s, 3H), 1.35 (s, 9H), 1.49–1.85 (m, 14H), 2.00–2.19 (m, 1H), 2.33–2.47 (m, 3H), 2.61–2.81 (m, 5H), 3.54–3.69 (m, 1H), 3.85–3.93 (m, 2H), 4.23–4.39 (m, 2H), 4.43 (dd,  $J$  = 4.9, 9.0 Hz, 1H), 4.87–5.03 (m, 2H), 5.08 (s, 2H), 6.39–6.58 (m, 3H), 7.00–7.18 (m, 4H), 7.25 (d,  $J$  = 7.5 Hz, 1H), 7.29–7.38 (m, 5H), 7.83 (s, 1H), 7.92 (s, 1H);  $^{13}C$  NMR (151 MHz,  $DMSO-d_6$ ):  $\delta$  15.75, 20.00, 21.34, 25.60, 25.73, 25.98, 28.15, 28.87, 29.02, 29.77, 30.19, 33.26, 34.67, 46.79, 52.41, 53.80, 54.95, 58.63, 65.51, 67.18, 75.13, 78.97, 102.46, 107.52, 107.81, 125.85, 126.86, 128.06, 128.12, 128.57, 128.79, 130.17, 136.42, 137.15, 137.98, 155.18, 158.21, 160.00, 169.88, 170.43, 172.17, 172.78; LC-MS (ESI) 99% purity,  $m/z$ :  $[M + H]^+$  calcd for  $C_{50}H_{67}N_4O_9$ , 867.49; found, 867.8; HRMS (ESI)  $m/z$ :  $[M + H]^+$  calcd for  $C_{50}H_{67}N_4O_9$ , 867.4863; found, 867.4886.

**(2S,4R)-N-(2-((5-Chloropentyl)oxy)-4-(4-methylthiazol-5-yl)benzyl)-4-hydroxy-1-((S)-3-methyl-2-(1-oxoisindolin-2-yl)butanoyl)pyrrolidine-2-carboxamide (83).** This compound was prepared using general procedure IV and linker L1b (240 mg, 1.20 mmol). The crude product was purified by column chromatography ( $CH_2Cl_2/MeOH$  29:1) to give a colorless solid. Yield (346 mg, 53%);  $R_f$  = 0.30 ( $CH_2Cl_2/MeOH$  19:1); mp 84–86 °C;  $^1H$  NMR (600 MHz,  $DMSO-d_6$ ):  $\delta$  0.73 (d,  $J$  = 6.7 Hz, 3H), 0.95 (d,  $J$  = 6.6 Hz, 3H), 1.52–1.62 (m, 2H), 1.71–1.84 (m, 4H), 1.88–1.95 (m, 1H), 2.00–2.09 (m, 1H), 2.27–2.36 (m, 1H), 2.46 (s, 3H), 3.64–3.71 (m, 3H), 3.74–3.81 (m, 1H), 4.05 (t,  $J$  = 6.2 Hz, 2H), 4.17–4.36 (m, 3H), 4.37–4.58 (m, 3H), 4.70 (d,  $J$  = 10.8 Hz, 1H), 5.08 (d,  $J$  = 4.1 Hz, 1H), 6.96–7.03 (m, 2H), 7.32 (d,  $J$  = 7.7 Hz, 1H), 7.45–7.53 (m, 1H), 7.56–7.64 (m, 2H), 7.70 (d,  $J$  = 7.6 Hz, 1H), 8.36 (t,  $J$  = 5.9 Hz, 1H), 8.98 (s, 1H);  $^{13}C$  NMR (151 MHz,  $DMSO-d_6$ ):  $\delta$  16.21, 18.80, 19.06, 23.23, 28.11, 28.57, 31.94, 37.21, 38.28, 45.54, 46.99, 55.59, 57.96, 58.87, 67.71, 68.79, 111.91, 120.98, 123.20, 123.81, 127.15, 127.86, 128.09, 131.17, 131.49, 131.56, 131.77, 142.39, 148.09, 151.65, 156.10, 167.66, 168.28, 171.72; LC-MS (ESI) 98% purity,  $m/z$ :  $[M + H]^+$  calcd for  $C_{34}H_{42}ClN_4O_5S$ , 653.26; found, 653.3; HRMS (ESI)  $m/z$ :  $[M + H]^+$  calcd for  $C_{34}H_{42}ClN_4O_5S$ , 653.2559; found, 653.2548.

**(2S,4R)-N-(2-((8-Chlorooctyl)oxy)-4-(4-methylthiazol-5-yl)benzyl)-4-hydroxy-1-((S)-3-methyl-2-(1-oxoisindolin-2-yl)butanoyl)pyrrolidine-2-carboxamide (84).** This compound was synthesized as we described previously.<sup>60</sup>

**(2S,4R)-N-(2-(4-(4-Chlorobutoxy)butoxy)-4-(4-methylthiazol-5-yl)benzyl)-4-hydroxy-1-((S)-3-methyl-2-(1-oxoisindolin-2-yl)butanoyl)pyrrolidine-2-carboxamide (85).** This compound was prepared using general procedure IV and linker L3b (310 mg, 1.20 mmol). The crude product was purified by column chromatography ( $CH_2Cl_2/MeOH$  29:1) to give a colorless solid. Yield (302 mg, 60%);  $R_f$  = 0.37 ( $CH_2Cl_2/MeOH$  29:1); mp 78–80 °C;  $^1H$  NMR (600 MHz,  $DMSO-d_6$ ):  $\delta$  0.73 (d,  $J$  = 6.8 Hz, 3H), 0.95 (d,  $J$  = 6.5 Hz, 3H), 1.56–1.64 (m, 2H), 1.64–1.83 (m, 6H), 1.88–1.95 (m, 1H), 1.99–2.07 (m, 1H), 2.26–2.37 (m, 1H), 2.46 (s, 3H), 3.34–3.47 (m, 4H), 3.62 (t,  $J$  = 6.7 Hz, 2H), 3.65–3.71 (m, 1H), 3.77 (dd,  $J$  = 4.4, 10.6 Hz, 1H), 4.06 (t,  $J$  = 6.3 Hz, 2H), 4.18–4.35 (m, 3H), 4.37–4.59 (m, 3H), 4.70 (d,  $J$  = 10.9 Hz, 1H), 5.08 (d,  $J$  = 4.1 Hz, 1H), 6.96–7.01 (m, 2H), 7.32 (d,  $J$  = 7.7 Hz, 1H), 7.49 (ddd,  $J$  = 2.2, 6.2, 8.1 Hz, 1H), 7.56–7.64 (m, 2H), 7.70 (dd,  $J$  = 1.0, 7.6 Hz, 1H), 8.36 (t,  $J$  = 6.0 Hz, 1H), 8.98 (s, 1H);  $^{13}C$  NMR (151 MHz,  $DMSO-d_6$ ):  $\delta$  16.20, 18.81, 19.06, 25.86, 26.07, 26.80, 28.57, 29.35, 37.22, 38.27, 45.52, 46.99, 55.60, 57.96, 58.88, 67.74, 68.80, 69.32, 69.85, 111.88, 120.95, 123.20, 123.81, 127.15, 127.88, 128.09, 131.16, 131.49, 131.56, 131.77, 142.39, 148.07, 151.65, 156.09, 167.66, 168.28, 171.71; LC-MS (ESI) 98% purity,  $m/z$ :  $[M + H]^+$  calcd for  $C_{37}H_{48}ClN_4O_6S$ ,

711.30; found, 711.5; HRMS (ESI)  $m/z$ :  $[M + H]^+$  calcd for  $C_{37}H_{48}ClN_4O_6S$ , 711.2978; found, 711.2965.

**(2S,4R)-N-(2-(2-(2-(2-Chloroethoxy)ethoxy)ethoxy)-4-(4-methylthiazol-5-yl)benzyl)-4-hydroxy-1-((S)-3-methyl-2-(1-oxoisindolin-2-yl)butanoyl)pyrrolidine-2-carboxamide (86).** This compound was synthesized as we described previously.<sup>60</sup>

**(2S,4R)-N-(2-(2-(2-(2-Chloroethoxy)ethoxy)ethoxy)ethoxy)-4-(4-methylthiazol-5-yl)benzyl)-4-hydroxy-1-((S)-3-methyl-2-(1-oxoisindolin-2-yl)butanoyl)pyrrolidine-2-carboxamide (87).** This compound was synthesized as we described previously.<sup>60</sup>

**(2S,4R)-N-(2-(2-((6-Chlorohexyl)oxy)hexyl)oxy)ethoxy)-4-(4-methylthiazol-5-yl)benzyl)-4-hydroxy-1-((S)-3-methyl-2-(1-oxoisindolin-2-yl)butanoyl)pyrrolidine-2-carboxamide (88).** This compound was prepared using general procedure IV and linker L6b (430 mg, 1.20 mmol). The crude product was purified by flash chromatography (gradient from 0 to 5% MeOH in  $CH_2Cl_2$ ), followed by preparative HPLC (gradient from 70 to 100% MeOH) to separate the inversely attached linker–ligand side product. A colorless resin of the chloroalkane product was obtained. Yield (316 mg, 39%);  $R_f$  = 0.29 ( $CH_2Cl_2/MeOH$  19:1);  $^1H$  NMR (600 MHz,  $DMSO-d_6$ ):  $\delta$  0.73 (d,  $J$  = 6.7 Hz, 3H), 0.95 (d,  $J$  = 6.6 Hz, 3H), 1.24–1.39 (m, 8H), 1.40–1.55 (m, 6H), 1.64–1.72 (m, 2H), 1.88–1.95 (m, 1H), 1.99–2.07 (m, 1H), 2.27–2.37 (m, 1H), 2.46 (s, 3H), 3.26–3.32 (m, 4H), 3.47 (t,  $J$  = 6.5 Hz, 2H), 3.59 (t,  $J$  = 6.6 Hz, 2H), 3.65–3.80 (m, 4H), 4.13–4.36 (m, 5H), 4.37–4.60 (m, 3H), 4.71 (d,  $J$  = 10.8 Hz, 1H), 5.06 (s, 1H), 7.00 (dd,  $J$  = 1.6, 7.8 Hz, 1H), 7.05 (d,  $J$  = 1.7 Hz, 1H), 7.33 (d,  $J$  = 7.8 Hz, 1H), 7.45–7.53 (m, 1H), 7.57–7.64 (m, 2H), 7.70 (d,  $J$  = 7.6 Hz, 1H), 8.32 (t,  $J$  = 6.0 Hz, 1H), 8.97 (s, 1H);  $^{13}C$  NMR (151 MHz,  $DMSO-d_6$ ):  $\delta$  16.16, 18.76, 19.03, 25.15, 25.64, 25.72, 26.25, 28.54, 29.23, 29.36, 32.17, 37.21, 38.22, 45.49, 46.96, 55.54, 57.94, 58.86, 68.12, 68.77, 68.82, 69.93, 70.05, 70.61, 112.42, 121.21, 123.16, 123.75, 127.37, 127.85, 128.05, 131.13, 131.41, 131.54, 131.72, 142.34, 148.06, 151.58, 156.08, 167.63, 168.25, 171.68; LC-MS (ESI) 99% purity,  $m/z$ :  $[M + H]^+$  calcd for  $C_{43}H_{60}ClN_4O_7S$ , 811.39; found, 811.8; HRMS (ESI)  $m/z$ :  $[M + H]^+$  calcd for  $C_{43}H_{60}ClN_4O_7S$ , 811.3866; found, 811.3860.

**(2S,4R)-N-(2-((5-((6-Chlorohexyl)oxy)pentyl)oxy)pentyl)oxy)-4-(4-methylthiazol-5-yl)benzyl)-4-hydroxy-1-((S)-3-methyl-2-(1-oxoisindolin-2-yl)butanoyl)pyrrolidine-2-carboxamide (89).** This compound was prepared using general procedure IV and linker L7b (464 mg, 1.20 mmol). The crude product was purified by flash chromatography (gradient from 0 to 5% MeOH in  $CH_2Cl_2$ ) to give a colorless resin. Yield (411 mg, 49%);  $R_f$  = 0.35 ( $CH_2Cl_2/MeOH$  19:1);  $^1H$  NMR (600 MHz,  $DMSO-d_6$ ):  $\delta$  0.73 (d,  $J$  = 6.7 Hz, 3H), 0.95 (d,  $J$  = 6.5 Hz, 3H), 1.24–1.40 (m, 6H), 1.41–1.52 (m, 8H), 1.52–1.64 (m, 2H), 1.65–1.72 (m, 2H), 1.73–1.83 (m, 2H), 1.86–1.97 (m, 1H), 1.99–2.07 (m, 1H), 2.27–2.39 (m, 1H), 2.46 (s, 3H), 3.31–3.39 (m, 8H), 3.59 (t,  $J$  = 6.6 Hz, 2H), 3.62–3.73 (m, 1H), 3.73–3.82 (m, 1H), 4.04 (t,  $J$  = 6.3 Hz, 2H), 4.18–4.59 (m, 6H), 4.71 (d,  $J$  = 10.8 Hz, 1H), 5.06 (s, 1H), 6.96–7.02 (m, 2H), 7.32 (d,  $J$  = 7.7 Hz, 1H), 7.45–7.55 (m, 1H), 7.57–7.64 (m, 2H), 7.70 (d,  $J$  = 7.6 Hz, 1H), 8.33 (t,  $J$  = 5.9 Hz, 1H), 8.97 (s, 1H);  $^{13}C$  NMR (151 MHz,  $DMSO-d_6$ ):  $\delta$  16.15, 18.76, 19.02, 22.55, 22.68, 25.13, 26.24, 28.53, 28.64, 29.10, 29.19, 29.22, 32.17, 37.17, 38.21, 45.48, 46.96, 55.53, 57.94, 58.84, 67.86, 68.77, 69.92, 70.01, 70.04, 70.08, 111.86, 120.90, 123.16, 123.75, 127.14, 127.84, 128.04, 131.13, 131.46, 131.53, 131.72, 142.35, 148.03, 151.56, 156.10, 167.63, 168.26, 171.66; LC-MS (ESI) 94% purity,  $m/z$ :  $[M + H]^+$  calcd for  $C_{44}H_{64}ClN_4O_7S$ , 839.42; found, 839.8; HRMS (ESI)  $m/z$ :  $[M + H]^+$  calcd for  $C_{44}H_{64}ClN_4O_7S$ , 839.4179; found, 839.4160.

**(2S,4R)-N-(2-((6-((6-Chlorohexyl)oxy)hexyl)oxy)hexyl)oxy)-4-(4-methylthiazol-5-yl)benzyl)-4-hydroxy-1-((S)-3-methyl-2-(1-oxoisindolin-2-yl)butanoyl)pyrrolidine-2-carboxamide (90).** This compound was prepared using general procedure IV and linker L8b (498 mg, 1.20 mmol). The crude product was purified by column chromatography ( $CH_2Cl_2/MeOH$  29:1) to give a colorless resin. Yield (269 mg, 31%);  $R_f$  = 0.27 ( $CH_2Cl_2/MeOH$  19:1);  $^1H$  NMR (600 MHz,  $DMSO-d_6$ ):  $\delta$  0.73 (d,  $J$  = 6.7 Hz, 3H), 0.95 (d,  $J$  = 6.5 Hz, 3H), 1.24–1.41 (m, 10H), 1.42–1.55 (m, 10H), 1.64–1.71 (m, 2H), 1.71–1.79 (m, 2H), 1.88–1.95 (m, 1H), 1.99–2.06 (m, 1H), 2.27–2.35 (m, 1H), 2.46 (s, 3H), 3.27–3.36 (m, 8H), 3.59 (t,  $J$  = 6.6



H<sub>2</sub>, 2H), 3.67 (d, *J* = 10.6 Hz, 1H), 3.77 (dd, *J* = 4.5, 10.6 Hz, 1H), 4.03 (t, *J* = 6.3 Hz, 2H), 4.16–4.60 (m, 6H), 4.70 (d, *J* = 10.8 Hz, 1H), 5.06 (d, *J* = 4.1 Hz, 1H), 6.96–7.01 (m, 2H), 7.32 (d, *J* = 7.6 Hz, 1H), 7.46–7.52 (m, 1H), 7.57–7.64 (m, 2H), 7.70 (d, *J* = 7.6 Hz, 1H), 8.33 (t, *J* = 6.0 Hz, 1H), 8.97 (s, 1H); <sup>13</sup>C NMR (151 MHz, DMSO-*d*<sub>6</sub>): δ 16.17, 18.78, 19.05, 25.17, 25.58, 25.66, 25.74, 26.26, 28.55, 28.83, 29.25, 29.38, 32.20, 37.19, 38.23, 45.51, 46.99, 55.56, 57.97, 58.87, 67.86, 68.79, 69.95, 70.03, 70.06, 111.87, 120.93, 123.19, 123.77, 127.17, 127.88, 128.07, 131.15, 131.49, 131.55, 131.75, 142.37, 148.05, 151.58, 156.13, 167.66, 168.29, 171.68; LC–MS (ESI) 96% purity, *m/z*: [M + H]<sup>+</sup> calcd for C<sub>47</sub>H<sub>68</sub>ClN<sub>4</sub>O<sub>5</sub>S, 867.45; found, 867.6; HRMS (ESI) *m/z*: [M + H]<sup>+</sup> calcd for C<sub>47</sub>H<sub>68</sub>ClN<sub>4</sub>O<sub>5</sub>S, 867.4492; found, 867.4482.

**tert-Butyl ((S)-1-((S)-2-((2S,4S)-4-(3-((S)-Chloropentyl)oxy)phenoxy)-2-(((R)-1,2,3,4-tetrahydronaphthalen-1-yl)carbamoyl)pyrrolidin-1-yl)-1-cyclohexyl-2-oxoethyl)amino)-1-oxopropan-2-yl(methyl)carbamate (91).** This compound was prepared using general procedure V and linker L1b (72 mg, 0.36 mmol). The crude product was purified by column chromatography (CH<sub>2</sub>Cl<sub>2</sub>/MeOH 50:1) to give a pale yellow oil. Yield (0.18 g, 75%); *R*<sub>f</sub> = 0.20 (CH<sub>2</sub>Cl<sub>2</sub>/MeOH 50:1); <sup>1</sup>H NMR (400 MHz, CDCl<sub>3</sub>): δ 0.75–1.00 (m, 5H), 1.30 (d, *J* = 7.1 Hz, 3H), 1.37–1.42 (m, 1H), 1.47 (s, 9H), 1.49–1.57 (m, 5H), 1.71–1.88 (m, 8H), 1.98–2.10 (m, 1H), 2.26–2.37 (m, 1H), 2.68–2.81 (m, 5H), 2.92 (s, 1H), 3.52–3.60 (m, 2H), 3.71–3.84 (m, 2H), 3.89 (t, *J* = 6.3 Hz, 2H), 4.18 (dd, *J* = 11.3, 4.8 Hz, 1H), 4.42 (t, *J* = 7.9 Hz, 1H), 4.55–4.70 (m, 1H), 4.76 (d, *J* = 9.3 Hz, 1H), 4.94 (d, *J* = 4.8 Hz, 1H), 5.13 (q, *J* = 5.0 Hz, 1H), 6.33–6.43 (m, 2H), 6.53 (dd, *J* = 8.2, 2.2 Hz, 1H), 6.59 (d, *J* = 8.3 Hz, 2H), 7.02–7.19 (m, 4H), 7.27–7.32 (m, 1H); <sup>13</sup>C NMR (101 MHz, CDCl<sub>3</sub>): δ 19.89, 23.41, 25.34, 25.45, 25.71, 28.23, 28.42, 28.72, 28.85, 29.10, 29.57, 29.81, 31.27, 33.25, 34.90, 40.31, 42.34, 42.71, 47.42, 48.70, 53.49, 54.65, 59.91, 61.54, 67.42, 72.10, 76.07, 102.59, 107.29, 108.18, 125.99, 126.89, 128.54, 128.89, 129.90, 136.50, 137.25, 157.77, 160.09, 170.94, 172.37; HRMS (ESI) *m/z*: [M + H]<sup>+</sup> calcd for C<sub>44</sub>H<sub>62</sub>O<sub>7</sub>N<sub>4</sub>Cl, 781.4302; found, 781.4284.

**tert-Butyl ((S)-1-((S)-2-((2S,4S)-4-(3-((R)-Chlorooctyl)oxy)phenoxy)-2-(((R)-1,2,3,4-tetrahydronaphthalen-1-yl)carbamoyl)pyrrolidin-1-yl)-1-cyclohexyl-2-oxoethyl)amino)-1-oxopropan-2-yl(methyl)carbamate (92).** This compound was prepared using general procedure V and linker L2b (87 mg, 0.36 mmol). The crude product was purified by column chromatography (CH<sub>2</sub>Cl<sub>2</sub>/MeOH 50:1) to give a colorless oil. Yield (0.20 g, 82%); *R*<sub>f</sub> = 0.22 (CH<sub>2</sub>Cl<sub>2</sub>/MeOH 50:1); <sup>1</sup>H NMR (400 MHz, CDCl<sub>3</sub>): δ 0.75–0.97 (m, 5H), 1.30 (d, *J* = 7.1 Hz, 3H), 1.32–1.44 (m, 8H), 1.47 (s, 9H), 1.50–1.58 (m, 4H), 1.69–1.86 (m, 8H), 1.98–2.09 (m, 1H), 2.27–2.37 (m, 1H), 2.70–2.80 (m, 5H), 2.90–2.94 (m, 1H), 3.53 (t, *J* = 6.7 Hz, 2H), 3.75–3.84 (m, 2H), 3.87 (t, *J* = 6.5 Hz, 2H), 4.17 (dd, *J* = 11.5, 4.8 Hz, 1H), 4.42 (d, *J* = 7.9 Hz, 1H), 4.59–4.69 (m, 1H), 4.76 (dd, *J* = 9.7, 2.1 Hz, 1H), 4.93 (d, *J* = 5.1 Hz, 1H), 5.13 (q, *J* = 7.6 Hz, 1H), 6.31–6.41 (m, 2H), 6.51–6.55 (m, 1H), 6.58 (d, *J* = 8.3 Hz, 1H), 7.01–7.17 (m, 5H), 7.27–7.32 (m, 1H); <sup>13</sup>C NMR (101 MHz, CDCl<sub>3</sub>): δ 22.73, 25.45, 25.57, 25.82, 25.87, 26.77, 28.49, 28.78, 29.14, 29.22, 29.70, 29.93, 31.36, 33.42, 35.07, 40.46, 40.47, 42.56, 47.49, 47.54, 48.80, 53.56, 54.70, 60.04, 60.19, 67.83, 74.19, 102.68, 102.83, 107.73, 107.85, 107.97, 126.14, 127.01, 128.70, 128.99, 129.97, 136.57, 137.34, 160.38, 171.00, 172.54, 175.16; HRMS (ESI) *m/z*: [M + H]<sup>+</sup> calcd for C<sub>46</sub>H<sub>68</sub>O<sub>7</sub>N<sub>4</sub>Cl, 823.4771; found, 823.4753.

**tert-Butyl ((S)-1-((S)-2-((2S,4S)-4-(3-(4-(4-Chlorobutoxy)butoxy)phenoxy)-2-(((R)-1,2,3,4-tetrahydronaphthalen-1-yl)carbamoyl)pyrrolidin-1-yl)-1-cyclohexyl-2-oxoethyl)amino)-1-oxopropan-2-yl(methyl)carbamate (93).** This compound was prepared using general procedure V and linker L3b (165 mg, 0.64 mmol). The crude product was purified by column chromatography (CH<sub>2</sub>Cl<sub>2</sub>/MeOH 50:1) to give a colorless oil. Yield (0.30 g, 69%); *R*<sub>f</sub> = 0.35 (CH<sub>2</sub>Cl<sub>2</sub>/MeOH 50:1); <sup>1</sup>H NMR (400 MHz, CDCl<sub>3</sub>): δ 0.75–0.97 (m, 5H), 1.30 (d, *J* = 7.1 Hz, 3H), 1.37–1.44 (m, 1H), 1.47 (s, 9H), 1.49–1.59 (m, 4H), 1.69–1.89 (m, 10H), 1.98–2.08 (m, 1H), 2.28–2.38 (m, 1H), 2.71–2.79 (m, 5H), 2.86–2.93 (m, 1H), 3.42–3.52 (m, 6H), 3.57 (t, *J* = 6.6 Hz, 2H), 3.73–3.87 (m, 2H), 3.90 (d, *J* = 6.2 Hz, 2H), 4.18 (dd, *J* = 11.5, 4.8 Hz, 1H), 4.42 (t, *J* = 7.9 Hz, 1H), 4.57–4.70 (m, 1H), 4.76 (dd, *J* = 9.9, 2.2 Hz, 1H), 4.94 (dd, *J* = 82.8, 5.0 Hz,

1H), 5.09–5.16 (m, 1H), 6.32–6.42 (m, 2H), 6.51–6.55 (m, 1H), 6.58 (d, *J* = 8.4 Hz, 2H), 7.02–7.18 (m, 4H), 7.27–7.32 (m, 1H); <sup>13</sup>C NMR (101 MHz, CDCl<sub>3</sub>): δ 22.73, 25.46, 25.56, 25.83, 26.08, 26.22, 26.28, 27.01, 28.21, 28.49, 29.22, 29.68, 29.93, 31.37, 33.42, 35.00, 40.48, 42.41, 47.52, 48.81, 53.55, 54.73, 60.01, 67.60, 73.52, 102.74, 102.87, 107.52, 108.15, 126.12, 127.00, 128.73, 128.99, 129.98, 136.60, 137.36, 157.90, 160.29, 171.08, 172.51, 175.11; HRMS (ESI) *m/z*: [M + H]<sup>+</sup> calcd for C<sub>44</sub>H<sub>60</sub>O<sub>8</sub>N<sub>4</sub>Cl, 839.4720; found, 839.4703.

**tert-Butyl ((S)-1-((S)-2-((2S,4S)-4-(3-(2-(2-(2-Chloroethoxy)ethoxy)ethoxy)phenoxy)-2-(((R)-1,2,3,4-tetrahydronaphthalen-1-yl)carbamoyl)pyrrolidin-1-yl)-1-cyclohexyl-2-oxoethyl)amino)-1-oxopropan-2-yl(methyl)carbamate (94).** This compound was prepared using general procedure V and linker L4b (74 mg, 0.30 mmol). The crude product was purified by column chromatography (CH<sub>2</sub>Cl<sub>2</sub>/MeOH 50:1) to give a pale yellow oil. Yield (0.14 g, 66%); *R*<sub>f</sub> = 0.18 (CH<sub>2</sub>Cl<sub>2</sub>/MeOH 20:1); <sup>1</sup>H NMR (400 MHz, CDCl<sub>3</sub>): δ 0.78–0.95 (m, 5H), 1.30 (d, *J* = 7.1 Hz, 3H), 1.37–1.43 (m, 1H), 1.47 (s, 9H), 1.56 (s, 4H), 1.75–1.85 (m, 4H), 1.99–2.08 (m, 1H), 2.27–2.36 (m, 1H), 2.71–2.80 (m, 5H), 2.90 (d, *J* = 14.1 Hz, 1H), 3.63 (td, *J* = 5.8, 0.6 Hz, 2H), 3.68–3.82 (m, 7H), 3.82–3.87 (m, 2H), 4.07 (d, *J* = 4.6 Hz, 2H), 4.19 (dd, *J* = 11.4, 4.8 Hz, 1H), 4.41 (t, *J* = 7.9 Hz, 1H), 4.57–4.69 (m, 1H), 4.76 (d, *J* = 9.6 Hz, 1H), 4.93 (d, *J* = 4.2 Hz, 1H), 5.12 (q, *J* = 7.7 Hz, 1H), 6.37–6.42 (m, 2H), 6.56 (d, *J* = 7.2 Hz, 1H), 6.56–6.62 (m, 2H), 7.02–7.18 (m, 4H), 7.27–7.31 (m, 1H); <sup>13</sup>C NMR (101 MHz, CDCl<sub>3</sub>): δ 20.08, 25.53, 25.64, 25.89, 28.42, 28.52, 29.34, 29.82, 30.01, 33.48, 40.64, 42.84, 47.70, 53.68, 55.33, 60.18, 67.50, 69.83, 70.78, 70.88, 71.47, 76.25, 103.07, 107.72, 108.48, 126.30, 127.22, 128.73, 129.18, 130.18, 136.64, 137.47, 157.89, 160.13, 169.46, 171.68, 172.36; HRMS (ESI) *m/z*: [M + H]<sup>+</sup> calcd for C<sub>44</sub>H<sub>64</sub>O<sub>9</sub>N<sub>4</sub>Cl, 827.4356; found, 827.4340.

**tert-Butyl ((S)-1-((S)-2-((2S,4S)-4-(3-(2-(2-(2-Chloroethoxy)ethoxy)ethoxy)ethoxy)phenoxy)-2-(((R)-1,2,3,4-tetrahydronaphthalen-1-yl)carbamoyl)pyrrolidin-1-yl)-1-cyclohexyl-2-oxoethyl)amino)-1-oxopropan-2-yl(methyl)carbamate (95).** This compound was synthesized as we described previously.<sup>60</sup>

**tert-Butyl ((S)-1-((S)-2-((2S,4S)-4-(3-(2-(6-(6-Chlorohexyl)oxy)hexyl)oxy)ethoxy)phenoxy)-2-(((R)-1,2,3,4-tetrahydronaphthalen-1-yl)carbamoyl)pyrrolidin-1-yl)-1-cyclohexyl-2-oxoethyl)amino)-1-oxopropan-2-yl(methyl)carbamate (96).** This compound was prepared using general procedure V and linker L6b (118 mg, 0.33 mmol). The crude product was purified by column chromatography (CH<sub>2</sub>Cl<sub>2</sub>/MeOH 50:1) to give a colorless oil. Yield (0.15 g, 58%); *R*<sub>f</sub> = 0.30 (CH<sub>2</sub>Cl<sub>2</sub>/MeOH 50:1); <sup>1</sup>H NMR (400 MHz, CDCl<sub>3</sub>): δ 0.79–0.99 (m, 5H), 1.30 (d, *J* = 7.1 Hz, 3H), 1.33–1.43 (m, 8H), 1.47 (s, 9H), 1.50–1.58 (m, 10H), 1.72–1.86 (m, 6H), 1.99–2.08 (m, 1H), 2.26–2.37 (m, 1H), 2.70–2.81 (m, 5H), 2.90 (d, *J* = 14.1 Hz, 1H), 3.39 (td, *J* = 6.6, 1.5 Hz, 4H), 3.46–3.57 (m, 5H), 3.75 (d, *J* = 3.5 Hz, 2H), 3.80 (d, *J* = 11.5 Hz, 1H), 4.04 (t, *J* = 4.6 Hz, 2H), 4.18 (dd, *J* = 11.4, 4.9 Hz, 1H), 4.42 (t, *J* = 7.9 Hz, 1H), 4.56–4.69 (m, 1H), 4.76 (dd, *J* = 9.8, 2.2 Hz, 1H), 4.93 (t, *J* = 4.8 Hz, 1H), 5.13 (d, *J* = 6.1 Hz, 1H), 6.36–6.42 (m, 2H), 6.55 (dd, *J* = 2.3, 0.8 Hz, 1H), 6.56–6.62 (m, 2H), 7.03–7.18 (m, 4H), 7.27–7.31 (m, 1H); <sup>13</sup>C NMR (101 MHz, CDCl<sub>3</sub>): δ 22.74, 25.45, 25.56, 25.81, 25.90, 26.01, 26.73, 28.42, 28.48, 29.16, 29.22, 29.55, 29.58, 29.63, 29.70, 29.93, 31.36, 33.38, 35.08, 40.44, 42.53, 47.54, 48.79, 53.56, 54.72, 60.04, 60.20, 67.38, 69.04, 70.59, 70.80, 74.01, 102.88, 107.64, 108.32, 126.15, 127.04, 128.63, 129.00, 129.99, 136.57, 137.34, 157.81, 160.08, 170.99, 172.54, 175.19; HRMS (ESI) *m/z*: [M + H]<sup>+</sup> calcd for C<sub>53</sub>H<sub>80</sub>O<sub>9</sub>N<sub>4</sub>Cl, 939.5608; found, 939.5650.

**tert-Butyl ((S)-1-((S)-2-((2S,4S)-4-(3-(5-(5-(6-Chlorohexyl)oxy)pentyl)oxy)phenoxy)-2-(((R)-1,2,3,4-tetrahydronaphthalen-1-yl)carbamoyl)pyrrolidin-1-yl)-1-cyclohexyl-2-oxoethyl)amino)-1-oxopropan-2-yl(methyl)carbamate (97).** This compound was prepared using general procedure V and linker L7b (254 mg, 0.66 mmol). The crude product was purified by column chromatography (CH<sub>2</sub>Cl<sub>2</sub>/MeOH 50:1) to give a pale yellow oil. Yield (0.36 g, 67%); *R*<sub>f</sub> = 0.28 (CH<sub>2</sub>Cl<sub>2</sub>/MeOH 50:1); <sup>1</sup>H NMR (400 MHz, CDCl<sub>3</sub>): δ 0.77–0.98 (m, 5H), 1.29 (d, *J* = 7.1 Hz, 3H), 1.33–1.44 (m, 5H), 1.46 (s, 9H), 1.50–1.65 (m, 15H), 1.72–1.86 (m, 8H), 1.98–2.10 (m, 1H), 2.27–2.37 (m, 1H), 2.75 (d, *J* = 4.6 Hz, 5H), 2.89–2.93 (m, 1H), 3.36–3.44 (m, 8H), 3.52 (t, *J* = 6.7 Hz, 2H), 3.74–3.85 (m,



2H), 3.88 (t,  $J = 6.5$  Hz, 2H), 4.17 (dd,  $J = 11.4, 4.7$  Hz, 1H), 4.41 (t,  $J = 7.9$  Hz, 1H), 4.58–4.69 (m, 1H), 4.75 (dd,  $J = 9.8, 2.2$  Hz, 1H), 4.93 (t,  $J = 4.8$  Hz, 1H), 5.12 (q,  $J = 6.1$  Hz, 1H), 6.34–6.40 (m, 2H), 6.50–6.54 (m, 1H), 6.55–6.71 (m, 2H), 7.02–7.17 (m, 4H), 7.27–7.31 (m, 1H);  $^{13}\text{C}$  NMR (101 MHz,  $\text{CDCl}_3$ ):  $\delta$  22.73, 25.44, 25.55, 25.81, 25.90, 26.74, 28.24, 28.47, 29.04, 29.15, 29.22, 29.45, 29.51, 29.58, 29.70, 29.93, 31.36, 33.42, 35.09, 40.45, 42.53, 47.53, 48.79, 53.56, 54.70, 60.05, 60.20, 67.78, 74.83, 76.17, 102.86, 107.62, 107.82, 107.87, 126.14, 127.02, 128.62, 128.99, 129.96, 136.55, 137.33, 160.35, 167.57, 170.99, 172.53, 175.19; HRMS (ESI)  $m/z$ :  $[\text{M} + \text{H}]^+$  calcd for  $\text{C}_{54}\text{H}_{84}\text{O}_9\text{N}_5\text{Cl}$ , 967.5921; found, 967.5918.

**tert-Butyl ((S)-1-(((S)-2-((2S,4S)-4-(3-(6-((6-Chlorohexyl)oxy)hexyl)oxy)phenoxy)-2-(((R)-1,2,3,4-tetrahydronaphthalen-1-yl)carbamoyl)pyrrolidin-1-yl)-1-cyclohexyl-2-oxoethyl)amino)-1-oxopropan-2-yl)(methyl)carbamate (98).** This compound was prepared using general procedure V and linker L8b (136 mg, 0.33 mmol). The crude product was purified by column chromatography ( $\text{CH}_2\text{Cl}_2/\text{MeOH}$  50:1) to give a colorless oil. Yield (0.24 g, 88%);  $R_f = 0.25$  ( $\text{CH}_2\text{Cl}_2/\text{MeOH}$  50:1);  $^1\text{H}$  NMR (400 MHz,  $\text{CDCl}_3$ ):  $\delta$  0.78–1.01 (m, 5H), 1.30 (d,  $J = 7.1$  Hz, 3H), 1.34–1.44 (m, 12H), 1.47 (s, 9H), 1.51–1.59 (m, 10H), 1.73–1.84 (m, 8H), 1.99–2.09 (m, 1H), 2.28–2.38 (m, 1H), 2.72–2.79 (m, 5H), 2.89 (d,  $J = 14.1$  Hz, 1H), 3.37–3.43 (m, 8H), 3.49 (d,  $J = 5.2$  Hz, 2H), 3.53 (t,  $J = 6.7$  Hz, 2H), 3.77–3.85 (m, 2H), 3.87 (t,  $J = 6.5$  Hz, 2H), 4.17 (dd,  $J = 11.5, 4.8$  Hz, 1H), 4.42 (t,  $J = 8.0$  Hz, 1H), 4.57–4.69 (m, 1H), 4.76 (d,  $J = 9.6$  Hz, 1H), 4.94 (d,  $J = 4.3$  Hz, 1H), 5.14 (d,  $J = 4.8$  Hz, 1H), 6.31–6.41 (m, 2H), 6.51–6.55 (m, 1H), 6.58 (d,  $J = 8.4$  Hz, 1H), 6.68 (s, 1H), 7.03–7.18 (m, 4H), 7.28–7.31 (m, 1H);  $^{13}\text{C}$  NMR (101 MHz,  $\text{CDCl}_3$ ):  $\delta$  22.74, 25.45, 25.56, 25.81, 25.91, 25.95, 26.02, 26.76, 28.12, 28.48, 29.17, 29.23, 29.60, 29.65, 29.71, 29.93, 31.36, 33.46, 35.04, 40.46, 42.54, 47.54, 48.80, 53.56, 54.73, 60.06, 60.17, 67.85, 70.61, 70.74, 74.62, 102.88, 107.66, 107.81, 126.15, 127.03, 128.63, 129.00, 129.97, 136.56, 137.34, 157.84, 160.39, 170.96, 172.53, 175.12; HRMS (ESI)  $m/z$ :  $[\text{M} + \text{H}]^+$  calcd for  $\text{C}_{56}\text{H}_{88}\text{O}_9\text{N}_5\text{Cl}$ , 995.6234; found, 995.6230.

**tert-Butyl ((S)-1-(((S)-2-((2S,4S)-4-(3-(5-Aminopentyl)oxy)phenoxy)-2-(((R)-1,2,3,4-tetrahydronaphthalen-1-yl)carbamoyl)pyrrolidin-1-yl)-1-cyclohexyl-2-oxoethyl)amino)-1-oxopropan-2-yl)(methyl)carbamate (99).** This compound was prepared using general procedure VI and 91 (167 mg, 0.21 mmol). The crude product was used in the next step without further purification.  $R_f = 0.35$  ( $\text{CH}_2\text{Cl}_2/\text{MeOH}/\text{NH}_4\text{OH}$  9:1:0.1); HRMS (ESI)  $m/z$ :  $[\text{M} + \text{H}]^+$  calcd for  $\text{C}_{43}\text{H}_{64}\text{O}_9\text{N}_5$ , 762.4800; found, 762.4781.

**tert-Butyl ((S)-1-(((S)-2-((2S,4S)-4-(3-(8-Aminoocetyl)oxy)phenoxy)-2-(((R)-1,2,3,4-tetrahydronaphthalen-1-yl)carbamoyl)pyrrolidin-1-yl)-1-cyclohexyl-2-oxoethyl)amino)-1-oxopropan-2-yl)(methyl)carbamate (100).** This compound was prepared using general procedure VI and 92 (200 mg, 0.24 mmol). The crude product was used in the next step without further purification.  $R_f = 0.12$  ( $\text{CH}_2\text{Cl}_2/\text{MeOH}/\text{NH}_4\text{OH}$  9:1:0.1); HRMS (ESI)  $m/z$ :  $[\text{M} + \text{H}]^+$  calcd for  $\text{C}_{46}\text{H}_{70}\text{O}_9\text{N}_5$ , 804.5247; found, 804.5247.

**tert-Butyl ((S)-1-(((S)-2-((2S,4S)-4-(3-(4-(4-Aminobutoxy)butoxy)phenoxy)-2-(((R)-1,2,3,4-tetrahydronaphthalen-1-yl)carbamoyl)pyrrolidin-1-yl)-1-cyclohexyl-2-oxoethyl)amino)-1-oxopropan-2-yl)(methyl)carbamate (101).** This compound was prepared using general procedure VI and 93 (160 mg, 0.19 mmol). The crude product was used in the next step without further purification.  $R_f = 0.25$  ( $\text{CH}_2\text{Cl}_2/\text{MeOH}/\text{NH}_4\text{OH}$  9:1:0.1); HRMS (ESI)  $m/z$ :  $[\text{M} + \text{H}]^+$  calcd for  $\text{C}_{46}\text{H}_{70}\text{O}_9\text{N}_5$ , 820.5219; found, 820.5204.

**tert-Butyl ((S)-1-(((S)-2-((2S,4S)-4-(3-(2-(2-(2-Aminoethoxy)ethoxy)ethoxy)phenoxy)-2-(((R)-1,2,3,4-tetrahydronaphthalen-1-yl)carbamoyl)pyrrolidin-1-yl)-1-cyclohexyl-2-oxoethyl)amino)-1-oxopropan-2-yl)(methyl)carbamate (102).** This compound was prepared using general procedure VI and 94 (137 mg, 0.17 mmol). The crude product was used in the next step without further purification.  $R_f = 0.18$  ( $\text{CH}_2\text{Cl}_2/\text{MeOH}/\text{NH}_4\text{OH}$  9:1:0.1); HRMS (ESI)  $m/z$ :  $[\text{M} + \text{H}]^+$  calcd for  $\text{C}_{44}\text{H}_{66}\text{O}_9\text{N}_5$ , 808.4855; found, 808.4837.

**tert-Butyl ((S)-1-(((S)-2-((2S,4S)-4-(3-(2-(2-(2-Aminoethoxy)ethoxy)ethoxy)ethoxy)phenoxy)-2-(((R)-1,2,3,4-tetrahydronaphthalen-1-yl)carbamoyl)pyrrolidin-1-yl)-1-cyclohexyl-2-oxoethyl)amino)-1-oxopropan-2-yl)(methyl)carbamate (103).** This com-

pound was prepared using general procedure VI and 95 (180 mg, 0.21 mmol). The crude product was used in the next step without further purification.  $R_f = 0.35$  ( $\text{CH}_2\text{Cl}_2/\text{MeOH}/\text{NH}_4\text{OH}$  9:1:0.1); HRMS (ESI)  $m/z$ :  $[\text{M} + \text{H}]^+$  calcd for  $\text{C}_{46}\text{H}_{70}\text{O}_{10}\text{N}_5$ , 852.5117; found, 852.5097.

**tert-Butyl ((S)-1-(((S)-2-((2S,4S)-4-(3-(2-(6-((6-Aminoethyl)oxy)hexyl)oxy)ethoxy)phenoxy)-2-(((R)-1,2,3,4-tetrahydronaphthalen-1-yl)carbamoyl)pyrrolidin-1-yl)-1-cyclohexyl-2-oxoethyl)amino)-1-oxopropan-2-yl)(methyl)carbamate (104).** This compound was prepared using general procedure VI and 96 (150 mg, 0.16 mmol). The crude product was used in the next step without further purification.  $R_f = 0.18$  ( $\text{CH}_2\text{Cl}_2/\text{MeOH}/\text{NH}_4\text{OH}$  9:1:0.1); HRMS (ESI)  $m/z$ :  $[\text{M} + \text{H}]^+$  calcd for  $\text{C}_{52}\text{H}_{82}\text{O}_9\text{N}_5$ , 920.6107; found, 920.6074.

**tert-Butyl ((S)-1-(((S)-2-((2S,4S)-4-(3-(5-(5-((6-Aminoethyl)oxy)pentyl)oxy)phenoxy)-2-(((R)-1,2,3,4-tetrahydronaphthalen-1-yl)carbamoyl)pyrrolidin-1-yl)-1-cyclohexyl-2-oxoethyl)amino)-1-oxopropan-2-yl)(methyl)carbamate (105).** This compound was prepared using general procedure VI and 97 (190 mg, 0.28 mmol). The crude product was used in the next step without further purification.  $R_f = 0.22$  ( $\text{CH}_2\text{Cl}_2/\text{MeOH}/\text{NH}_4\text{OH}$  9:1:0.1); HRMS (ESI)  $m/z$ :  $[\text{M} + \text{H}]^+$  calcd for  $\text{C}_{54}\text{H}_{86}\text{O}_9\text{N}_5$ , 948.6420; found, 948.6409.

**tert-Butyl ((S)-1-(((S)-2-((2S,4S)-4-(3-(6-((6-Aminoethyl)oxy)hexyl)oxy)hexyl)oxy)phenoxy)-2-(((R)-1,2,3,4-tetrahydronaphthalen-1-yl)carbamoyl)pyrrolidin-1-yl)-1-cyclohexyl-2-oxoethyl)amino)-1-oxopropan-2-yl)(methyl)carbamate (106).** This compound was prepared using general procedure VI and 98 (230 mg, 0.23 mmol). The crude product was used in the next step without further purification.  $R_f = 0.40$  ( $\text{CH}_2\text{Cl}_2/\text{MeOH}/\text{NH}_4\text{OH}$  9:1:0.1); HRMS (ESI)  $m/z$ :  $[\text{M} + \text{H}]^+$  calcd for  $\text{C}_{56}\text{H}_{90}\text{O}_9\text{N}_5$ , 976.6733; found, 976.6696.

**Synthesis of Boc-Protected and Final PROTACs.** **tert-Butyl ((S)-1-(((S)-1-Cyclohexyl-2-((2S,4S)-4-(3-(5-(((S)-1-(2S,4R)-4-hydroxy-2-((4-(4-methylthiazol-5-yl)benzyl)carbamoyl)pyrrolidin-1-yl)-3,3-dimethyl-1-oxobutan-2-yl)amino)-5-oxopentyl)oxy)phenoxy)-2-(((R)-1,2,3,4-tetrahydronaphthalen-1-yl)carbamoyl)pyrrolidin-1-yl)-2-oxoethyl)amino)-1-oxopropan-2-yl)(methyl)carbamate (107).** The IAP ligand-linker conjugate 74 (147 mg, 0.17 mmol) was dissolved in dry EtOAc (10 mL) and treated with 10% Pd/C (10% w/w). The reaction mixture was stirred under  $\text{H}_2$  (1 atm, balloon) for 18 h. The mixture was filtered through Celite, and the filtrate was concentrated. The oily residue was dissolved in dry DMF (5 mL), and DIPEA (59  $\mu\text{L}$ , 0.34 mmol) and HATU (71 mg, 0.187 mmol) were added. After stirring at rt for 5 min, the VHL ligand 68 (90 mg, 0.20 mmol) in dry DMF (2.5 mL) and DIPEA (59  $\mu\text{L}$ , 0.34 mmol) was added. The combined mixture was stirred at rt for 16 h. Subsequently, it was quenched with half-saturated brine (50 mL) and extracted with  $\text{CH}_2\text{Cl}_2$  (3  $\times$  50 mL). The combined organic layers were washed with saturated  $\text{NH}_4\text{Cl}$  solution, 5% LiCl solution, and brine (each 50 mL); dried over  $\text{Na}_2\text{SO}_4$ ; filtered; and evaporated. The crude product was purified by column chromatography ( $\text{CH}_2\text{Cl}_2/\text{MeOH}$  29:1) to give a colorless resin. Yield (64 mg, 32%);  $R_f = 0.22$  ( $\text{CH}_2\text{Cl}_2/\text{MeOH}$  9:1). Due to the presence of the *N*-Boc protecting group resulting in an additional set of rotamers, NMR data is only provided for the deprotected final PROTAC. HRMS (ESI)  $m/z$ :  $[\text{M} + \text{H}]^+$  calcd for  $\text{C}_{65}\text{H}_{99}\text{N}_8\text{O}_{11}\text{S}$ , 1189.6366; found, 1189.6333.

**tert-Butyl ((S)-1-(((S)-1-Cyclohexyl-2-((2S,4S)-4-(3-(8-(((S)-1-(2S,4R)-4-hydroxy-2-((4-(4-methylthiazol-5-yl)benzyl)carbamoyl)pyrrolidin-1-yl)-3,3-dimethyl-1-oxobutan-2-yl)amino)-8-oxooctyl)oxy)phenoxy)-2-(((R)-1,2,3,4-tetrahydronaphthalen-1-yl)carbamoyl)pyrrolidin-1-yl)-2-oxoethyl)amino)-1-oxopropan-2-yl)(methyl)carbamate (108).** This compound was prepared using general procedure II, VHL1 ligand-linker conjugate 75 (177 mg, 0.30 mmol), and IAP ligand 65. The crude product was purified by column chromatography ( $\text{CH}_2\text{Cl}_2/\text{MeOH}$  29:1) to give a colorless solid. Yield (206 mg, 56%);  $R_f = 0.26$  ( $\text{CH}_2\text{Cl}_2/\text{MeOH}$  19:1); mp 112–116 °C. Due to the presence of the *N*-Boc protecting group resulting in an additional set of rotamers, NMR data is only provided for the deprotected final PROTAC. HRMS (ESI)  $m/z$ :  $[\text{M} + \text{H}]^+$  calcd for  $\text{C}_{68}\text{H}_{93}\text{N}_8\text{O}_{11}\text{S}$ , 1231.6836; found, 1231.6679.



*tert*-Butyl ((*S*)-1-(((*S*)-1-Cyclohexyl-2-((2*S*,4*S*)-4-(3-(4-(4-(((*S*)-1-((2*S*,4*R*)-4-hydroxy-2-((4-(4-methylthiazol-5-yl)benzyl)carbamoyl)pyrrolidin-1-yl)-3,3-dimethyl-1-oxobutan-2-yl)amino)-4-oxobutoxy)butoxy)phenoxy)-2-(((*R*)-1,2,3,4-tetrahydronaphthalen-1-yl)carbamoyl)pyrrolidin-1-yl)-2-oxoethyl)amino)-1-oxopropan-2-yl)(methyl)carbamate (**109**). This compound was prepared using general procedure II, VHL1 ligand–linker conjugate **76** (182 mg, 0.30 mmol), and IAP ligand **65**. The crude product was purified by column chromatography (CH<sub>2</sub>Cl<sub>2</sub>/MeOH 19:1) to give a colorless semi-solid. Yield (202 mg, 54%); *R*<sub>f</sub> = 0.25 (CH<sub>2</sub>Cl<sub>2</sub>/MeOH 19:1). Due to the presence of the *N*-Boc protecting group resulting in an additional set of rotamers, NMR data is only provided for the deprotected final PROTAC. HRMS (ESI) *m/z*: [M + H]<sup>+</sup> calcd for C<sub>68</sub>H<sub>95</sub>N<sub>8</sub>O<sub>15</sub>S, 1247.6785; found, 1247.6775.

*tert*-Butyl ((*S*)-1-(((*S*)-1-Cyclohexyl-2-((2*S*,4*S*)-4-(3-(2-(2-(2-(((*S*)-1-((2*S*,4*R*)-4-hydroxy-2-((4-(4-methylthiazol-5-yl)benzyl)carbamoyl)pyrrolidin-1-yl)-3,3-dimethyl-1-oxobutan-2-yl)amino)-2-oxoethoxy)ethoxy)ethoxy)phenoxy)-2-(((*R*)-1,2,3,4-tetrahydronaphthalen-1-yl)carbamoyl)pyrrolidin-1-yl)-2-oxoethyl)amino)-1-oxopropan-2-yl)(methyl)carbamate (**110**). This compound was prepared using general procedure II, VHL1 ligand–linker conjugate **77** (179 mg, 0.30 mmol), and IAP ligand **65**. The crude product was purified by column chromatography (CH<sub>2</sub>Cl<sub>2</sub>/MeOH 19:1) to give a colorless solid. Yield (263 mg, 71%); *R*<sub>f</sub> = 0.25 (CH<sub>2</sub>Cl<sub>2</sub>/MeOH 19:1); mp 96–100 °C. Due to the presence of the *N*-Boc protecting group resulting in an additional set of rotamers, NMR data is only provided for the deprotected final PROTAC. HRMS (ESI) *m/z*: [M + H]<sup>+</sup> calcd for C<sub>66</sub>H<sub>91</sub>N<sub>8</sub>O<sub>13</sub>S, 1235.6378; found, 1235.6421.

*tert*-Butyl ((*S*)-1-(((*S*)-1-Cyclohexyl-2-((2*S*,4*S*)-4-(3-(((*S*)-1-3-((2*S*,4*R*)-4-hydroxy-2-((4-(4-methylthiazol-5-yl)benzyl)carbamoyl)pyrrolidine-1-carbonyl)-14,14-dimethyl-11-oxo-3,6,9-trioxo-12-azapentadecyl)oxy)phenoxy)-2-(((*R*)-1,2,3,4-tetrahydronaphthalen-1-yl)carbamoyl)pyrrolidin-1-yl)-2-oxoethyl)amino)-1-oxopropan-2-yl)(methyl)carbamate (**111**). This compound was prepared using general procedure II, VHL1 ligand–linker conjugate **78** (192 mg, 0.30 mmol), and IAP ligand **65**. The crude product was purified by column chromatography (CH<sub>2</sub>Cl<sub>2</sub>/MeOH 19:1) to give a colorless semi-solid. Yield (134 mg, 35%); *R*<sub>f</sub> = 0.21 (CH<sub>2</sub>Cl<sub>2</sub>/MeOH 19:1). Due to the presence of the *N*-Boc protecting group resulting in an additional set of rotamers, NMR data is only provided for the deprotected final PROTAC. HRMS (ESI) *m/z*: [M + H]<sup>+</sup> calcd for C<sub>68</sub>H<sub>95</sub>N<sub>8</sub>O<sub>14</sub>S, 1279.6683; found, 1279.6676.

*tert*-Butyl ((*S*)-1-(((*S*)-1-Cyclohexyl-2-((2*S*,4*S*)-4-(3-(6-(6-(2-(((*S*)-1-((2*S*,4*R*)-4-hydroxy-2-((4-(4-methylthiazol-5-yl)benzyl)carbamoyl)pyrrolidin-1-yl)-3,3-dimethyl-1-oxobutan-2-yl)amino)-2-oxoethoxy)hexyl)oxy)hexyl)oxy)phenoxy)-2-(((*R*)-1,2,3,4-tetrahydronaphthalen-1-yl)carbamoyl)pyrrolidin-1-yl)-2-oxoethyl)amino)-1-oxopropan-2-yl)(methyl)carbamate (**112**). This compound was prepared using general procedure II, VHL1 ligand–linker conjugate **79** (212 mg, 0.30 mmol), and IAP ligand **65**. The crude product was purified by column chromatography (CH<sub>2</sub>Cl<sub>2</sub>/MeOH 19:1) to give a colorless solid. Yield (105 mg, 26%); *R*<sub>f</sub> = 0.15 (CH<sub>2</sub>Cl<sub>2</sub>/MeOH 19:1); mp 70–72 °C. Due to the presence of the *N*-Boc protecting group resulting in an additional set of rotamers, NMR data is only provided for the deprotected final PROTAC. HRMS (ESI) *m/z*: [M + H]<sup>+</sup> calcd for C<sub>74</sub>H<sub>107</sub>N<sub>8</sub>O<sub>13</sub>S, 1347.7673; found, 1347.7704.

*tert*-Butyl ((*S*)-1-(((*S*)-1-Cyclohexyl-2-((2*S*,4*S*)-4-(3-(6-(6-(5-(((*S*)-1-((2*S*,4*R*)-4-hydroxy-2-((4-(4-methylthiazol-5-yl)benzyl)carbamoyl)pyrrolidin-1-yl)-3,3-dimethyl-1-oxobutan-2-yl)amino)-5-oxopentyl)oxy)pentyl)oxy)hexyl)oxy)phenoxy)-2-(((*R*)-1,2,3,4-tetrahydronaphthalen-1-yl)carbamoyl)pyrrolidin-1-yl)-2-oxoethyl)amino)-1-oxopropan-2-yl)(methyl)carbamate (**113**). This compound was prepared using general procedure II, VHL1 ligand–linker conjugate **80** (221 mg, 0.30 mmol), and IAP ligand **65**. The crude product was purified by flash chromatography (CH<sub>2</sub>Cl<sub>2</sub>/MeOH 19:1) to give a colorless semi-solid. Yield (235 mg, 57%); *R*<sub>f</sub> = 0.22 (CH<sub>2</sub>Cl<sub>2</sub>/MeOH 19:1). Due to the presence of the *N*-Boc protecting group resulting in an additional set of rotamers, NMR data is only provided for the deprotected final PROTAC. HRMS (ESI) *m/z*: [M + H]<sup>+</sup> calcd for C<sub>72</sub>H<sub>111</sub>N<sub>8</sub>O<sub>13</sub>S, 1375.7986; found, 1375.7981.

*tert*-Butyl ((*S*)-1-(((*S*)-1-Cyclohexyl-2-((2*S*,4*S*)-4-(3-(6-(6-(5-(((*S*)-1-((2*S*,4*R*)-4-hydroxy-2-((4-(4-methylthiazol-5-yl)benzyl)carbamoyl)pyrrolidin-1-yl)-3,3-dimethyl-1-oxobutan-2-yl)amino)-5-oxopentyl)oxy)pentyl)oxy)hexyl)oxy)phenoxy)-2-(((*R*)-1,2,3,4-tetrahydronaphthalen-1-yl)carbamoyl)pyrrolidin-1-yl)-2-oxoethyl)amino)-1-oxopropan-2-yl)(methyl)carbamate (**114**). This compound was prepared using general procedure II, VHL1 ligand–linker conjugate **81** (229 mg, 0.30 mmol), and IAP ligand **65**. The crude product was purified by flash chromatography (CH<sub>2</sub>Cl<sub>2</sub>/MeOH 19:1) to give a colorless solid. Yield (219 mg, 52%); *R*<sub>f</sub> = 0.23 (CH<sub>2</sub>Cl<sub>2</sub>/MeOH 19:1); mp 74–76 °C. Due to the presence of the *N*-Boc protecting group resulting in an additional set of rotamers, NMR data is only provided for the deprotected final PROTAC. HRMS (ESI) *m/z*: [M + H]<sup>+</sup> calcd for C<sub>78</sub>H<sub>115</sub>N<sub>8</sub>O<sub>13</sub>S, 1403.8299; found, 1403.8300.

*tert*-Butyl ((*S*)-1-(((*S*)-1-Cyclohexyl-2-((2*S*,4*S*)-4-(3-(5-(((*S*)-1-((2*S*,4*R*)-4-hydroxy-2-((4-(4-methylthiazol-5-yl)phenyl)ethyl)carbamoyl)pyrrolidin-1-yl)-3,3-dimethyl-1-oxobutan-2-yl)amino)-5-oxopentyl)oxy)phenoxy)-2-(((*R*)-1,2,3,4-tetrahydronaphthalen-1-yl)carbamoyl)pyrrolidin-1-yl)-2-oxoethyl)amino)-1-oxopropan-2-yl)(methyl)carbamate (**115** = **10d**). This compound was synthesized analogously to **107** but using VHL1 ligand–linker conjugate **92** (92 mg, 0.21 mmol). A colorless solid was obtained after flash chromatography (gradient from 0 to 5% MeOH in CH<sub>2</sub>Cl<sub>2</sub>). Yield (143 mg, 70%); *R*<sub>f</sub> = 0.23 (CH<sub>2</sub>Cl<sub>2</sub>/MeOH 19:1); mp 134–138 °C; <sup>1</sup>H NMR (600 MHz, DMSO-*d*<sub>6</sub>): δ 0.93 (s, 9H), 1.03–1.10 (m, 1H), 1.18 (s, 4H), 1.24 (s, 1H), 1.34–1.41 (m, 16H), 1.56–1.71 (m, 6H), 1.72–1.83 (m, 2H), 1.96–2.03 (m, 1H), 2.05–2.11 (m, 1H), 2.14–2.22 (m, 1H), 2.28–2.35 (m, 1H), 2.44 (s, 3H), 2.50–2.56 (m, 1H), 2.64–2.75 (m, 7H), 3.56–3.64 (m, 3H), 3.85–3.93 (m, 3H), 4.21–4.30 (m, 3H), 4.31 (t, *J* = 7.8 Hz, 1H), 4.39–4.47 (m, 2H), 4.52 (d, *J* = 9.3 Hz, 1H), 4.87–4.95 (m, 3H), 5.00–5.06 (m, 1H), 5.07 (d, *J* = 3.5 Hz, 1H), 6.44 (t, *J* = 2.4 Hz, 1H), 6.44–6.55 (m, 2H), 7.00–7.19 (m, 5H), 7.24 (d, *J* = 7.5 Hz, 1H), 7.35–7.44 (m, 5H), 7.78–7.85 (m, 2H), 8.33 (d, *J* = 7.8 Hz, 1H), 8.97 (s, 1H); LC–MS (ESI) 99% purity, *m/z*: [M + H]<sup>+</sup> calcd for C<sub>66</sub>H<sub>91</sub>N<sub>8</sub>O<sub>11</sub>S, 1203.65; found, 1204.0; HRMS (ESI) *m/z*: [M + H]<sup>+</sup> calcd for C<sub>66</sub>H<sub>91</sub>N<sub>8</sub>O<sub>11</sub>S, 1203.6523; found, 1203.6508.

*tert*-Butyl ((*R*)-1-(((*S*)-1-Cyclohexyl-2-((2*S*,4*S*)-4-(3-(5-(((*S*)-1-((2*S*,4*R*)-4-hydroxy-2-((4-(4-methylthiazol-5-yl)phenyl)ethyl)carbamoyl)pyrrolidin-1-yl)-3,3-dimethyl-1-oxobutan-2-yl)amino)-5-oxopentyl)oxy)phenoxy)-2-(((*R*)-1,2,3,4-tetrahydronaphthalen-1-yl)carbamoyl)pyrrolidin-1-yl)-2-oxoethyl)amino)-1-oxopropan-2-yl)(methyl)carbamate (**116**). This compound was synthesized analogously to **107** but using IAP ligand–linker conjugate **82** (147 mg, 0.17 mmol). A colorless solid was obtained after flash chromatography (gradient from 0 to 8% MeOH in CH<sub>2</sub>Cl<sub>2</sub>). Yield (133 mg, 66%); *R*<sub>f</sub> = 0.22 (CH<sub>2</sub>Cl<sub>2</sub>/MeOH 19:1); mp 132–136 °C. Due to the presence of the *N*-Boc protecting group resulting in an additional set of rotamers, NMR data is only provided for the deprotected final PROTAC. HRMS (ESI) *m/z*: [M + H]<sup>+</sup> calcd for C<sub>65</sub>H<sub>89</sub>N<sub>8</sub>O<sub>11</sub>S, 1189.6366; found, 1189.6315.

*tert*-Butyl ((*S*)-1-(((*S*)-1-Cyclohexyl-2-((2*S*,4*S*)-4-(3-(5-(((*S*)-1-((2*S*,4*S*)-4-hydroxy-2-((4-(4-methylthiazol-5-yl)benzyl)carbamoyl)pyrrolidin-1-yl)-3,3-dimethyl-1-oxobutan-2-yl)amino)-5-oxopentyl)oxy)phenoxy)-2-(((*R*)-1,2,3,4-tetrahydronaphthalen-1-yl)carbamoyl)pyrrolidin-1-yl)-2-oxoethyl)amino)-1-oxopropan-2-yl)(methyl)carbamate (**117**). Compound **74** (225 mg, 0.26 mmol) was dissolved in dry MeOH (8 mL) and treated with 10% Pd/C (45 mg, 20% w/w). The reaction mixture was stirred under H<sub>2</sub> (1 atm, balloon) for 2 h. The mixture was filtered through Celite and washed with MeOH, and the filtrate was concentrated. The product was dissolved in dry DMF (5 mL) along with HATU (109 mg, 0.286 mmol) and DIPEA (101 mg, 133 μL) 0.78 mmol. A solution of **70** (121 mg, 0.28 mmol) in dry DMF (5 mL) was added, followed by stirring of the mixture at rt for 18 h. The volatiles were then evaporated, and the crude product was purified by column chromatography (CH<sub>2</sub>Cl<sub>2</sub>/MeOH 20:1) to give an off-white resin. Yield (275 mg, 89%); *R*<sub>f</sub> = 0.25 (CH<sub>2</sub>Cl<sub>2</sub>/MeOH 9:1). Due to the presence of the *N*-Boc protecting group resulting in an additional set of rotamers, NMR data is only provided for the deprotected final PROTAC. HRMS (ESI) *m/z*: [M + H]<sup>+</sup> calcd for C<sub>65</sub>H<sub>89</sub>O<sub>11</sub>N<sub>8</sub>S, 1189.6366; found, 1189.6350.



(2*S*,4*S*)-1-((*S*)-2-Cyclohexyl-2-((*S*)-2-(methylamino)propanamido)acetyl)-4-(3-((*S*)-1-((2*S*,4*R*)-4-hydroxy-2-((4-(4-methylthiazol-5-yl)benzyl)carbamoyl)pyrrolidin-1-yl)-3,3-dimethyl-1-oxobutan-2-yl)amino)-5-oxopentyl)oxy)phenoxy)-*N*-((*R*)-1,2,3,4-tetrahydronaphthalen-1-yl)pyrrolidine-2-carboxamide (PROTAC 1). This compound was prepared using general procedure VII and PROTAC precursor 107 (60 mg, 50  $\mu$ mol). After filtration of the solid material, the crude product was purified by column chromatography ( $\text{CH}_2\text{Cl}_2/\text{MeOH} + 7 \text{ N NH}_3$  15:1) to give a colorless solid. Yield (24 mg, 43%);  $R_f = 0.14$  ( $\text{CH}_2\text{Cl}_2/\text{MeOH} + 7 \text{ N NH}_3$  19:1); mp 76–80 °C;  $^1\text{H NMR}$  (600 MHz,  $\text{DMSO}-d_6$ ):  $\delta$  0.92 (s, 9H), 0.94–1.14 (m, 7H), 1.52–1.83 (m, 14H), 1.86–1.93 (m, 1H), 1.96–2.14 (m, 2H), 2.15 (s, 3H), 2.16–2.21 (m, 2H), 2.28–2.40 (m, 1H), 2.42 (s, 3H), 2.50–2.57 (m, 1H), 2.62–2.74 (m, 2H), 2.89–2.98 (m, 1H), 3.46–3.69 (m, 4H), 3.84–3.93 (m, 2H), 4.13–4.60 (m, 8H), 4.87–4.93 (m, 1H), 4.98–5.06 (m, 1H), 5.13 (d,  $J = 3.6$  Hz, 1H), 6.38–6.54 (m, 3H), 7.01–7.18 (m, 4H), 7.23 (d,  $J = 7.5$  Hz, 1H), 7.32–7.44 (m, 4H), 7.80 (d,  $J = 8.6$  Hz, 1H), 7.86 (d,  $J = 9.4$  Hz, 1H), 7.92 (d,  $J = 8.6$  Hz, 1H), 8.53 (t,  $J = 6.1$  Hz, 1H), 8.95 (s, 1H);  $^{13}\text{C NMR}$  (151 MHz,  $\text{DMSO}-d_6$ ):  $\delta$  16.15, 19.27, 20.14, 22.35, 25.66, 25.85, 26.02, 26.61, 28.03, 28.50, 28.97, 29.31, 29.91, 34.46, 34.65, 34.77, 35.46, 38.15, 40.23, 41.92, 46.89, 52.26, 54.63, 56.59, 56.63, 58.79, 58.96, 59.31, 67.42, 69.12, 75.17, 102.62, 107.61, 107.87, 125.99, 127.00, 127.68, 128.58, 128.89, 128.92, 129.88, 130.30, 131.43, 137.26, 137.41, 139.72, 147.96, 151.70, 158.32, 160.16, 169.97, 170.17, 170.70, 172.23, 172.26, 174.73; LC–MS (ESI) 95% purity,  $m/z$ :  $[\text{M} + \text{H}]^+$  calcd for  $\text{C}_{60}\text{H}_{81}\text{N}_8\text{O}_9\text{S}$ , 1089.58; found, 1089.8; HRMS (ESI)  $m/z$ :  $[\text{M} + \text{H}]^+$  calcd for  $\text{C}_{60}\text{H}_{81}\text{N}_8\text{O}_9\text{S}$ , 1089.5842; found, 1089.5796.

(2*S*,4*S*)-1-((*S*)-2-Cyclohexyl-2-((*S*)-2-(methylamino)propanamido)acetyl)-4-(3-((*S*)-1-((2*S*,4*R*)-4-hydroxy-2-((4-(4-methylthiazol-5-yl)benzyl)carbamoyl)pyrrolidin-1-yl)-3,3-dimethyl-1-oxobutan-2-yl)amino)-8-oxooctyl)oxy)phenoxy)-*N*-((*R*)-1,2,3,4-tetrahydronaphthalen-1-yl)pyrrolidine-2-carboxamide (PROTAC 2). This compound was prepared using general procedure VII and PROTAC precursor 108 (123 mg, 100  $\mu$ mol). The product possessed sufficient purity after filtration. A colorless solid was obtained. Yield (93 mg, 80%); mp 162–166 °C;  $^1\text{H NMR}$  (600 MHz,  $\text{DMSO}-d_6$ ):  $\delta$  0.92 (s, 9H), 1.03–1.19 (m, 3H), 1.21–1.47 (m, 10H), 1.48–1.82 (m, 8H), 1.85–1.91 (m, 1H), 1.99–2.14 (m, 3H), 2.22–2.29 (m, 1H), 2.42–2.47 (m, 7H), 2.63–2.73 (m, 3H), 3.60–3.68 (m, 3H), 3.81–3.93 (m, 4H), 4.17–4.24 (m, 2H), 4.31–4.48 (m, 6H), 4.53 (d,  $J = 9.4$  Hz, 1H), 4.87–4.94 (m, 1H), 5.00–5.09 (m, 1H), 6.39–6.55 (m, 4H), 7.02–7.18 (m, 6H), 7.22 (d,  $J = 7.5$  Hz, 1H), 7.35–7.44 (m, 6H), 7.84 (d,  $J = 9.4$  Hz, 1H), 7.89 (d,  $J = 8.6$  Hz, 1H), 8.57 (t,  $J = 6.1$  Hz, 1H), 8.75 (d,  $J = 8.1$  Hz, 1H), 8.80–8.88 (m, 1H), 9.02 (s, 1H);  $^{13}\text{C NMR}$  (151 MHz,  $\text{DMSO}-d_6$ ):  $\delta$  16.00, 16.03, 20.10, 25.58, 25.66, 25.83, 25.91, 26.58, 28.09, 28.71, 28.83, 28.94, 28.98, 29.88, 30.92, 34.68, 35.04, 35.42, 38.16, 40.24, 41.83, 46.81, 52.31, 55.64, 56.03, 56.46, 56.54, 58.76, 58.89, 67.60, 69.05, 75.12, 102.71, 107.52, 107.73, 125.94, 126.94, 127.63, 128.53, 128.84, 128.89, 129.69, 130.26, 131.52, 137.22, 137.40, 139.80, 147.63, 151.85, 158.24, 160.14, 168.72, 169.90, 169.93, 169.96, 172.17, 172.30; LC–MS (ESI) 98% purity,  $m/z$ :  $[\text{M} + \text{H}]^+$  calcd for  $\text{C}_{63}\text{H}_{87}\text{N}_8\text{O}_9\text{S}$ , 1131.63; found, 1131.8; HRMS (ESI)  $m/z$ :  $[\text{M} + \text{H}]^+$  calcd for  $\text{C}_{63}\text{H}_{87}\text{N}_8\text{O}_9\text{S}$ , 1131.6311; found, 1131.6272.

(2*S*,4*S*)-1-((*S*)-2-Cyclohexyl-2-((*S*)-2-(methylamino)propanamido)acetyl)-4-(3-((*S*)-1-((2*S*,4*R*)-4-hydroxy-2-((4-(4-methylthiazol-5-yl)benzyl)carbamoyl)pyrrolidin-1-yl)-3,3-dimethyl-1-oxobutan-2-yl)amino)-4-oxobutoxy)phenoxy)-*N*-((*R*)-1,2,3,4-tetrahydronaphthalen-1-yl)pyrrolidine-2-carboxamide (PROTAC 3). This compound was prepared using general procedure VII and PROTAC precursor 109 (80 mg, 64  $\mu$ mol). After filtration of the solid material, the crude product was purified by column chromatography ( $\text{CH}_2\text{Cl}_2/\text{MeOH} + 7 \text{ N NH}_3$  15:1) to give a colorless solid. Yield (43 mg, 58%);  $R_f = 0.33$  ( $\text{CH}_2\text{Cl}_2/\text{MeOH} + 7 \text{ N NH}_3$  15:1); mp 84–86 °C;  $^1\text{H NMR}$  (600 MHz,  $\text{DMSO}-d_6$ ):  $\delta$  0.91 (s, 9H), 0.95–1.19 (m, 7H), 1.49–1.83 (m, 17H), 1.85–1.93 (m, 1H), 1.96–2.11 (m, 2H), 2.15 (s, 3H), 2.16–2.34 (m, 3H), 2.42 (s, 3H), 2.49–2.56 (m, 1H), 2.62–2.74 (m, 2H), 2.88–2.99 (m, 1H), 3.28–3.35 (m, 2H), 3.44–3.51 (m, 2H), 3.59–3.68 (m, 3H), 3.85–

3.94 (m, 2H), 4.17–4.28 (m, 2H), 4.31–4.49 (m, 5H), 4.52 (d,  $J = 9.4$  Hz, 1H), 4.87–5.06 (m, 2H), 5.12 (d,  $J = 3.6$  Hz, 1H), 6.39–6.44 (m, 1H), 6.44–6.54 (m, 2H), 7.04–7.18 (m, 4H), 7.23 (d,  $J = 7.4$  Hz, 1H), 7.34–7.44 (m, 4H), 7.75–7.85 (m, 2H), 7.92 (d,  $J = 8.6$  Hz, 1H), 8.52 (t,  $J = 6.1$  Hz, 1H), 8.95 (s, 1H);  $^{13}\text{C NMR}$  (151 MHz,  $\text{DMSO}-d_6$ ):  $\delta$  16.13, 19.25, 20.13, 25.63, 25.80, 25.83, 26.01, 26.09, 26.58, 28.01, 28.95, 29.28, 29.89, 31.89, 34.44, 34.62, 35.44, 38.13, 40.22, 41.89, 46.87, 52.23, 54.60, 56.55, 56.64, 58.75, 58.94, 59.30, 67.52, 69.10, 69.68, 69.80, 75.16, 102.62, 107.57, 107.87, 125.97, 126.97, 127.66, 128.55, 128.87, 128.90, 129.86, 130.28, 131.40, 137.24, 137.39, 139.70, 147.94, 151.67, 158.29, 160.13, 169.92, 170.13, 170.68, 172.13, 172.21, 174.71; LC–MS (ESI) 98% purity,  $m/z$ :  $[\text{M} + \text{H}]^+$  calcd for  $\text{C}_{63}\text{H}_{87}\text{N}_8\text{O}_{10}\text{S}$ , 1147.63; found, 1148.0; HRMS (ESI)  $m/z$ :  $[\text{M} + \text{H}]^+$  calcd for  $\text{C}_{63}\text{H}_{87}\text{N}_8\text{O}_{10}\text{S}$ , 1147.6260; found, 1147.6232.

(2*S*,4*S*)-1-((*S*)-2-Cyclohexyl-2-((*S*)-2-(methylamino)propanamido)acetyl)-4-(3-((*S*)-1-((2*S*,4*R*)-4-hydroxy-2-((4-(4-methylthiazol-5-yl)benzyl)carbamoyl)pyrrolidin-1-yl)-3,3-dimethyl-1-oxobutan-2-yl)amino)-2-oxoethoxy)ethoxy)ethoxy)phenoxy)-*N*-((*R*)-1,2,3,4-tetrahydronaphthalen-1-yl)pyrrolidine-2-carboxamide (PROTAC 4). This compound was prepared using general procedure VII and PROTAC precursor 110 (78 mg, 63  $\mu$ mol). The product possessed sufficient purity after filtration. A colorless solid was obtained. Yield (71 mg, 47%); mp 164–166 °C;  $^1\text{H NMR}$  (600 MHz,  $\text{DMSO}-d_6$ ):  $\delta$  0.92 (s, 9H), 0.93–1.17 (m, 7H), 1.33 (d,  $J = 6.9$  Hz, 3H), 1.56–1.82 (m, 6H), 1.84–1.93 (m, 1H), 2.01–2.09 (m, 2H), 2.40–2.48 (m, 7H), 2.49–2.56 (m, 1H), 2.63–2.75 (m, 2H), 3.57–3.68 (m, 7H), 3.69–3.81 (m, 2H), 3.81–3.96 (m, 1H), 3.97 (s, 2H), 4.01–4.09 (m, 2H), 4.19–4.30 (m, 2H), 4.31–4.46 (m, 5H), 4.55 (d,  $J = 9.6$  Hz, 1H), 4.87–4.94 (m, 1H), 5.01 (p,  $J = 5.5$  Hz, 1H), 6.39–6.56 (m, 3H), 7.02–7.17 (m, 5H), 7.22 (d,  $J = 7.6$  Hz, 1H), 7.35–7.45 (m, 6H), 7.90 (d,  $J = 8.5$  Hz, 1H), 8.58 (t,  $J = 6.0$  Hz, 1H), 8.73 (d,  $J = 8.1$  Hz, 1H), 8.78–8.86 (m, 1H), 8.97 (s, 1H);  $^{13}\text{C NMR}$  (151 MHz,  $\text{DMSO}-d_6$ ):  $\delta$  15.92, 16.00, 20.05, 25.62, 25.78, 25.87, 26.34, 26.44, 28.04, 28.89, 28.93, 29.84, 30.88, 34.61, 35.84, 38.06, 40.24, 41.84, 46.77, 52.23, 55.59, 55.88, 56.01, 56.71, 58.67, 58.90, 67.25, 69.01, 69.13, 69.79, 69.89, 70.60, 75.01, 102.57, 107.38, 108.07, 125.88, 126.88, 127.61, 128.47, 128.83, 129.79, 130.22, 131.36, 137.17, 137.37, 139.62, 147.75, 151.65, 158.22, 159.84, 168.66, 168.75, 169.31, 169.84, 169.93, 171.92; LC–MS (ESI) 96% purity,  $m/z$ :  $[\text{M} + \text{H}]^+$  calcd for  $\text{C}_{61}\text{H}_{82}\text{N}_8\text{O}_{11}\text{S}$ , 1131.59; found, 1135.7; HRMS (ESI)  $m/z$ :  $[\text{M} + \text{H}]^+$  calcd for  $\text{C}_{61}\text{H}_{82}\text{N}_8\text{O}_{11}\text{S}$ , 1135.5897; found, 1135.5877.

(2*S*,4*R*)-1-((*S*)-2-(*tert*-Butyl)-14-(3-((*S*,5*S*)-1-((*S*)-2-cyclohexyl-2-((*S*)-2-(methylamino)propanamido)acetyl)-5-((*R*)-1,2,3,4-tetrahydronaphthalen-1-yl)carbamoyl)pyrrolidin-3-yl)oxy)phenoxy)-4-oxo-6,9,12-trioxa-3-azatetradecanoyl)-4-hydroxy-*N*-((4-(4-methylthiazol-5-yl)benzyl)pyrrolidine-2-carboxamide (PROTAC 5). This compound was prepared using general procedure VII and PROTAC precursor 111 (80 mg, 63  $\mu$ mol). After filtration of the solid material, the crude product was purified by column chromatography ( $\text{CH}_2\text{Cl}_2/\text{MeOH} + 7 \text{ N NH}_3$  19:1) to give a colorless solid. Yield (35 mg, 47%);  $R_f = 0.17$  ( $\text{CH}_2\text{Cl}_2/\text{MeOH} + 7 \text{ N NH}_3$  19:1); mp 84–86 °C;  $^1\text{H NMR}$  (600 MHz,  $\text{DMSO}-d_6$ ):  $\delta$  0.92 (s, 9H), 1.03–1.11 (m, 6H), 1.51–1.69 (m, 7H), 1.71–1.81 (m, 3H), 1.85–1.92 (m, 1H), 2.01–2.09 (m, 2H), 2.15 (s, 2H), 2.18 (s, 1H), 2.42 (s, 3H), 2.51–2.54 (m, 1H), 2.63–2.70 (m, 2H), 2.87–3.01 (m, 1H), 3.55–3.71 (m, 12H), 3.93–4.02 (m, 4H), 4.20–4.29 (m, 3H), 4.32–4.46 (m, 6H), 4.54 (d,  $J = 9.5$  Hz, 1H), 4.90 (d,  $J = 6.5$  Hz, 1H), 5.01 (t,  $J = 5.4$  Hz, 1H), 5.13–5.17 (m, 1H), 6.42–6.53 (m, 3H), 7.02–7.18 (m, 5H), 7.22 (d,  $J = 7.6$  Hz, 1H), 7.38 (d,  $J = 7.6$  Hz, 6H), 7.83 (d,  $J = 8.5$  Hz, 1H), 7.91 (d,  $J = 8.5$  Hz, 1H), 8.56 (t,  $J = 6.2$  Hz, 1H), 8.94 (s, 1H);  $^{13}\text{C NMR}$  (151 MHz,  $\text{DMSO}-d_6$ ):  $\delta$  16.10, 19.27, 20.12, 25.64, 25.83, 26.00, 26.38, 26.48, 28.00, 28.95, 29.26, 29.89, 34.45, 34.61, 35.92, 38.09, 40.22, 41.92, 46.86, 52.22, 54.59, 55.94, 56.77, 58.72, 58.98, 59.31, 67.34, 69.10, 69.12, 69.81, 69.83, 70.09, 70.14, 70.70, 75.11, 102.48, 107.54, 108.13, 125.97, 126.97, 127.69, 128.56, 128.90, 129.91, 130.31, 131.37, 137.24, 137.40, 139.63, 147.96, 151.66, 158.30, 159.93, 168.88, 169.38, 170.13, 170.67, 172.03; LC–MS (ESI) 98% purity,  $m/z$ :  $[\text{M} + \text{H}]^+$  calcd for  $\text{C}_{63}\text{H}_{87}\text{N}_8\text{O}_{12}\text{S}$ , 1179.62;



found, 1180.0; HRMS (ESI)  $m/z$ :  $[M + H]^+$  calcd for  $C_{63}H_{87}N_8O_{12}S$ , 1179.6159; found, 1179.6122.

(2*S*,4*S*)-1-((*S*)-2-cyclohexyl-2-((*S*)-2-(methylamino)propanamido)acetyl)-4-(3-((6-((*S*)-1-((2*S*,4*R*)-4-hydroxy-2-((4-(4-methylthiazol-5-yl)benzyl)carbamoyl)pyrrolidin-1-yl)-3,3-dimethyl-1-oxobutan-2-yl)amino)-2-oxoethoxy)hexyl)oxy)hexyloxy)phenoxy)-*N*-((*R*)-1,2,3,4-tetrahydronaphthalen-1-yl)pyrrolidine-2-carboxamide (PROTAC 6). This compound was prepared using general procedure VII and PROTAC precursor 112 (101 mg, 75  $\mu$ mol). The product possessed sufficient purity after filtration. A colorless solid was obtained. Yield (73 mg, 75%); mp 142–144 °C;  $^1H$  NMR (600 MHz, DMSO- $d_6$ ):  $\delta$  0.92 (s, 9H), 0.95–1.15 (m, 5H), 1.26–1.92 (m, 30H), 2.02–2.10 (m, 2H), 2.41–2.47 (m, 6H), 2.50–2.57 (m, 1H), 2.63–2.72 (m, 2H), 3.24–3.34 (m, 4H), 3.42–3.47 (m, 2H), 3.56–3.61 (m, 2H), 3.63–3.67 (m, 2H), 3.81–3.93 (m, 6H), 4.17–4.29 (m, 2H), 4.31–4.46 (m, 5H), 4.54 (d,  $J = 9.6$  Hz, 1H), 4.85–4.94 (m, 1H), 5.01–5.07 (m, 1H), 6.39–6.45 (m, 1H), 6.46–6.54 (m, 2H), 7.02–7.18 (m, 4H), 7.22 (d,  $J = 7.5$  Hz, 1H), 7.33 (d,  $J = 9.6$  Hz, 1H), 7.35–7.46 (m, 4H), 7.89 (d,  $J = 8.5$  Hz, 1H), 8.62 (t,  $J = 6.1$  Hz, 1H), 8.75 (d,  $J = 8.1$  Hz, 1H), 8.80–8.87 (m, 1H), 9.00 (s, 1H);  $^{13}C$  NMR (151 MHz, DMSO- $d_6$ ):  $\delta$  16.27, 20.36, 25.85, 25.95, 26.01, 26.10, 26.18, 26.62, 28.37, 29.11, 29.21, 29.25, 29.52, 29.67, 30.14, 31.18, 34.95, 36.33, 38.36, 40.51, 42.13, 47.08, 52.58, 55.90, 56.05, 56.30, 57.07, 59.02, 59.23, 67.82, 69.34, 69.87, 70.32, 71.32, 75.39, 103.00, 107.78, 107.98, 126.21, 127.21, 127.94, 128.80, 129.14, 130.04, 130.52, 131.74, 137.48, 137.67, 139.97, 147.96, 152.06, 158.50, 160.40, 168.99, 169.58, 170.18, 170.22, 172.25; LC–MS (ESI) 95% purity,  $m/z$ :  $[M + H]^+$  calcd for  $C_{69}H_{99}N_8O_{11}S$ , 1247.71; found, 1248.1; HRMS (ESI)  $m/z$ :  $[M + H]^+$  calcd for  $C_{69}H_{99}N_8O_{11}S$ , 1247.7149; found, 1247.7130.

(2*S*,4*S*)-1-((*S*)-2-cyclohexyl-2-((*S*)-2-(methylamino)propanamido)acetyl)-4-(3-((6-((*S*)-1-((2*S*,4*R*)-4-hydroxy-2-((4-(4-methylthiazol-5-yl)benzyl)carbamoyl)pyrrolidin-1-yl)-3,3-dimethyl-1-oxobutan-2-yl)amino)-5-oxopentyl)oxy)pentyl)oxy)hexyloxy)phenoxy)-*N*-((*R*)-1,2,3,4-tetrahydronaphthalen-1-yl)pyrrolidine-2-carboxamide (PROTAC 7). This compound was prepared using general procedure VII and PROTAC precursor 113 (80 mg, 58  $\mu$ mol). After filtration of the solid material, the crude product was purified by column chromatography ( $CH_2Cl_2$ /MeOH + 7 N  $NH_3$ , 19:1) to give a colorless solid. Yield (38 mg, 52%);  $R_f = 0.31$  ( $CH_2Cl_2$ /MeOH + 7 N  $NH_3$ , 19:1); mp 90–92 °C;  $^1H$  NMR (600 MHz, DMSO- $d_6$ ):  $\delta$  0.91 (s, 9H), 0.97–1.11 (m, 5H), 1.24–1.83 (m, 22H), 1.85–1.93 (m, 1H), 1.98–2.04 (m, 1H), 2.06–2.13 (m, 2H), 2.15 (s, 3H), 2.17–2.29 (m, 2H), 2.42 (s, 3H), 2.50–2.56 (m, 1H), 2.62–2.74 (m, 2H), 2.94 (q,  $J = 6.8$  Hz, 1H), 3.24–3.33 (m, 10H), 3.40–3.51 (m, 4H), 3.59–3.68 (m, 3H), 3.88 (t,  $J = 6.4$  Hz, 2H), 4.17–4.31 (m, 2H), 4.31–4.46 (m, 6H), 4.52 (d,  $J = 9.4$  Hz, 1H), 4.87–4.93 (m, 1H), 4.98–5.05 (m, 1H), 5.12 (d,  $J = 3.6$  Hz, 1H), 6.40 (t,  $J = 2.4$  Hz, 1H), 6.45–6.53 (m, 2H), 7.01–7.18 (m, 5H), 7.21–7.25 (m, 1H), 7.34–7.44 (m, 5H), 7.79 (d,  $J = 6.8$  Hz, 1H), 7.80 (d,  $J = 7.7$  Hz, 1H), 7.91 (d,  $J = 8.6$  Hz, 1H), 8.52 (t,  $J = 6.1$  Hz, 1H), 8.95 (s, 1H);  $^{13}C$  NMR (151 MHz, DMSO- $d_6$ ):  $\delta$  16.14, 19.28, 20.14, 22.51, 22.74, 25.60, 25.65, 25.71, 25.84, 26.02, 26.60, 28.03, 28.87, 28.97, 29.04, 29.28, 29.42, 29.91, 34.47, 34.63, 34.89, 35.44, 38.14, 40.23, 41.91, 46.89, 52.26, 54.61, 56.57, 58.78, 58.95, 59.33, 67.60, 69.11, 69.88, 70.10, 70.14, 75.20, 102.63, 107.63, 107.82, 125.98, 126.98, 127.67, 128.57, 128.87, 128.91, 129.87, 130.28, 131.42, 137.25, 137.40, 139.71, 147.95, 151.68, 158.29, 160.18, 169.96, 170.14, 170.71, 172.22, 172.34, 174.75; LC–MS (ESI) 97% purity,  $m/z$ :  $[M + H]^+$  calcd for  $C_{71}H_{103}N_8O_{11}S$ , 1275.75; found, 1276.1; HRMS (ESI)  $m/z$ :  $[M + H]^+$  calcd for  $C_{71}H_{103}N_8O_{11}S$ , 1275.7462; found, 1275.7422.

(2*S*,4*S*)-1-((*S*)-2-cyclohexyl-2-((*S*)-2-(methylamino)propanamido)acetyl)-4-(3-((6-((*S*)-1-((2*S*,4*R*)-4-hydroxy-2-((4-(4-methylthiazol-5-yl)benzyl)carbamoyl)pyrrolidin-1-yl)-3,3-dimethyl-1-oxobutan-2-yl)amino)-6-oxohexyl)oxy)hexyl)oxy)hexyloxy)phenoxy)-*N*-((*R*)-1,2,3,4-tetrahydronaphthalen-1-yl)pyrrolidine-2-carboxamide (PROTAC 8). This compound was prepared using general procedure VII and PROTAC precursor 114 (48 mg, 34  $\mu$ mol). After filtration of the solid material, the crude product was purified by column chromatography ( $CH_2Cl_2$ /MeOH +

7 N  $NH_3$ , 19:1) to give a colorless solid. Yield (18 mg, 41%);  $R_f = 0.20$  ( $CH_2Cl_2$ /MeOH + 7 N  $NH_3$ , 19:1); mp 88–90 °C;  $^1H$  NMR (600 MHz, DMSO- $d_6$ ):  $\delta$  0.91 (s, 10H), 0.96–1.14 (m, 7H), 1.14–1.83 (m, 28H), 1.85–1.93 (m, 1H), 1.95–2.05 (m, 1H), 2.05–2.12 (m, 2H), 2.15 (s, 3H), 2.16–2.28 (m, 2H), 2.42 (s, 3H), 2.67 (dd,  $J = 9.1$ , 15.4 Hz, 2H), 2.95 (p,  $J = 7.5$  Hz, 1H), 3.22–3.33 (m, 10H), 3.59–3.68 (m, 3H), 3.87 (t,  $J = 6.4$  Hz, 2H), 4.17–4.26 (m, 2H), 4.26–4.46 (m, 6H), 4.52 (d,  $J = 9.4$  Hz, 1H), 4.86–4.93 (m, 1H), 5.02 (h,  $J = 4.9$  Hz, 1H), 5.12 (d,  $J = 3.5$  Hz, 1H), 6.40 (t,  $J = 2.4$  Hz, 1H), 6.49 (ddd,  $J = 2.3$ , 8.2, 20.1 Hz, 2H), 7.01–7.19 (m, 5H), 7.20–7.25 (m, 1H), 7.34–7.46 (m, 5H), 7.75–7.82 (m, 2H), 7.92 (d,  $J = 8.6$  Hz, 1H), 8.52 (t,  $J = 6.1$  Hz, 1H), 8.95 (s, 1H);  $^{13}C$  NMR (151 MHz, DMSO- $d_6$ ):  $\delta$  16.15, 19.27, 20.15, 25.55, 25.60, 25.64, 25.72, 25.80, 25.82, 25.85, 26.03, 26.62, 28.05, 28.88, 28.98, 29.23, 29.32, 29.42, 29.45, 29.92, 34.46, 34.64, 35.13, 35.44, 38.15, 40.24, 41.92, 46.90, 52.27, 54.63, 56.56, 56.59, 58.80, 58.96, 59.32, 67.61, 69.12, 70.09, 70.14, 75.22, 102.65, 107.65, 107.83, 125.99, 126.99, 127.69, 128.58, 128.89, 128.92, 129.89, 130.30, 131.43, 137.26, 137.40, 139.72, 147.96, 151.70, 158.29, 160.19, 169.98, 170.15, 170.73, 172.24, 172.43, 174.75; LC–MS (ESI) 97% purity,  $m/z$ :  $[M + H]^+$  calcd for  $C_{73}H_{107}N_8O_{11}S$ , 1303.77; found, 1304.1; HRMS (ESI)  $m/z$ :  $[M + H]^+$  calcd for  $C_{73}H_{107}N_8O_{11}S$ , 1303.7737; found, 1303.7775.

(2*S*,4*S*)-1-((*S*)-2-cyclohexyl-2-((*S*)-2-(methylamino)propanamido)acetyl)-4-(3-((5-((*S*)-1-((2*S*,4*R*)-4-hydroxy-2-((*S*)-1-(4-(4-methylthiazol-5-yl)phenyl)ethyl)carbamoyl)pyrrolidin-1-yl)-3,3-dimethyl-1-oxobutan-2-yl)amino)-5-oxopentyl)oxy)phenoxy)-*N*-((*R*)-1,2,3,4-tetrahydronaphthalen-1-yl)pyrrolidine-2-carboxamide (PROTAC 9) (CST626). This compound was prepared using general procedure VII and PROTAC precursor 115 (100 mg, 83  $\mu$ mol). The product possessed sufficient purity after filtration. A colorless solid was obtained. Yield (90 mg, 95%); mp 64–66 °C (free base, obtained after column chromatography);  $^1H$  NMR (600 MHz, DMSO- $d_6$ ):  $\delta$  0.93 (s, 9H), 0.96–1.20 (m, 6H), 1.30–1.40 (m, 6H), 1.51–1.83 (m, 14H), 1.96–2.10 (m, 2H), 2.14–2.22 (m, 1H), 2.28–2.39 (m, 1H), 2.42–2.47 (m, 6H), 2.51–2.58 (m, 1H), 2.64–2.74 (m, 2H), 3.58–3.68 (m, 4H), 3.81–3.94 (m, 3H), 4.21 (dd,  $J = 5.9$ , 10.9 Hz, 1H), 4.24–4.30 (m, 1H), 4.37–4.47 (m, 3H), 4.51 (d,  $J = 9.2$  Hz, 1H), 4.87–4.95 (m, 2H), 5.04 (h,  $J = 4.7$  Hz, 1H), 6.43 (s, 1H), 6.46–6.56 (m, 2H), 7.03–7.19 (m, 4H), 7.23 (d,  $J = 7.5$  Hz, 1H), 7.35–7.44 (m, 4H), 7.81 (dd,  $J = 3.7$ , 9.3 Hz, 1H), 7.88 (d,  $J = 8.5$  Hz, 1H), 8.36 (d,  $J = 7.8$  Hz, 1H), 8.73 (d,  $J = 8.1$  Hz, 1H), 8.80–8.87 (m, 1H), 9.00 (s, 1H), 9.37 (s, 1H);  $^{13}C$  NMR (151 MHz, DMSO- $d_6$ ):  $\delta$  15.95, 16.05, 20.08, 22.26, 22.58, 25.63, 25.80, 25.88, 26.62, 28.07, 28.40, 28.44, 28.91, 28.96, 29.85, 30.90, 34.65, 34.69, 35.37, 37.89, 46.80, 47.88, 52.28, 55.63, 56.02, 56.42, 56.58, 58.73, 67.36, 68.91, 75.09, 102.67, 107.50, 107.79, 125.90, 126.57, 126.91, 128.49, 128.85, 128.99, 129.77, 130.23, 131.40, 137.18, 137.38, 144.88, 147.71, 151.77, 158.24, 160.10, 168.69, 169.76, 169.90, 169.96, 170.80, 172.04; LC–MS (ESI) 99% purity,  $m/z$ :  $[M + H]^+$  calcd for  $C_{61}H_{83}N_8O_9S$ , 1103.60; found, 1103.8; HRMS (ESI)  $m/z$ :  $[M + H]^+$  calcd for  $C_{61}H_{83}N_8O_9S$ , 1103.5998; found, 1103.5980.

(2*S*,4*S*)-1-((*S*)-2-cyclohexyl-2-((*R*)-2-(methylamino)propanamido)acetyl)-4-(3-((5-((*S*)-1-((2*S*,4*R*)-4-hydroxy-2-((*S*)-1-(4-(4-methylthiazol-5-yl)phenyl)ethyl)carbamoyl)pyrrolidin-1-yl)-3,3-dimethyl-1-oxobutan-2-yl)amino)-5-oxopentyl)oxy)phenoxy)-*N*-((*R*)-1,2,3,4-tetrahydronaphthalen-1-yl)pyrrolidine-2-carboxamide (PROTAC 10a). This compound was prepared using general procedure VII and PROTAC precursor 116 (100 mg, 84  $\mu$ mol). The product possessed sufficient purity after filtration. A colorless solid was obtained. Yield (95 mg, 99%); mp 140–142 °C (dec);  $^1H$  NMR (600 MHz, DMSO- $d_6$ ):  $\delta$  0.93 (s, 9H), 1.00–1.20 (m, 4H), 1.39 (d,  $J = 6.9$  Hz, 3H), 1.51–1.82 (m, 16H), 1.86–1.93 (m, 1H), 1.99–2.06 (m, 1H), 2.06–2.12 (m, 1H), 2.14–2.22 (m, 1H), 2.29–2.37 (m, 1H), 2.44 (d,  $J = 5.6$  Hz, 6H), 2.50–2.58 (m, 1H), 2.64–2.75 (m, 2H), 3.62–3.91 (m, 6H), 4.15–4.31 (m, 2H), 4.31–4.49 (m, 5H), 4.54 (d,  $J = 9.3$  Hz, 1H), 4.85–4.94 (m, 1H), 5.01–5.07 (m, 1H), 6.39–6.45 (m, 1H), 6.45–6.55 (m, 2H), 7.03–7.20 (m, 4H), 7.23 (d,  $J = 7.5$  Hz, 1H), 7.35–7.43 (m, 4H), 7.84–7.89 (m, 2H), 8.55 (t,  $J = 6.1$  Hz, 1H), 8.79–8.90 (m, 2H), 9.00 (s, 1H);  $^{13}C$  NMR (151 MHz, DMSO- $d_6$ ):  $\delta$  16.02, 16.13, 16.79, 20.09, 22.27, 25.59, 25.73, 25.91, 26.56, 28.04, 28.44, 28.90, 28.94, 29.84, 30.85, 34.68, 35.40, 38.12,



40.24, 41.83, 46.82, 52.35, 55.46, 56.03, 56.51, 58.79, 58.87, 67.36, 69.02, 75.16, 102.68, 107.49, 107.77, 125.90, 126.91, 127.61, 128.48, 128.81, 128.84, 129.72, 130.22, 131.45, 137.18, 137.39, 139.74, 147.69, 151.73, 158.23, 160.09, 168.83, 169.86, 169.90, 169.93, 172.09, 172.12; LC–MS (ESI) 99% purity,  $m/z$ :  $[M + H]^+$  calcd for  $C_{60}H_{81}N_8O_9S$ , 1089.58; found, 1089.8; HRMS (ESI)  $m/z$ :  $[M + H]^+$  calcd for  $C_{60}H_{81}N_8O_9S$ , 1089.5842; found, 1089.5823.

(2*S*,4*S*)-1-((*S*)-2-cyclohexyl-2-((*S*)-2-(dimethylamino)propanamido)acetyl)-4-(3-((*S*)-1-((2*S*,4*R*)-4-hydroxy-2-((*S*)-1-(4-(4-methylthiazol-5-yl)phenyl)ethyl)carbamoyl)pyrrolidin-1-yl)-3,3-dimethyl-1-oxobutan-2-yl)amino)-5-oxopentyl)oxy)phenoxy)-*N*-((*R*)-1,2,3,4-tetrahydronaphthalen-1-yl)pyrrolidine-2-carboxamide (PROTAC 10b). PROTAC 9 (0.11 g, 0.10 mmol) was dissolved in dry DMF (2.5 mL), and 10% Pd/C (11 mg) and formaldehyde 36% in an aqueous solution (25  $\mu$ L, 0.30 mmol) were added. The mixture was stirred under a hydrogen atmosphere at rt for 16 h. After removal of the catalyst by filtration, it was evaporated, and the crude product was purified by column chromatography ( $CH_2Cl_2$ /MeOH + 7 N  $NH_3$  9:1) to give a colorless solid. Yield (93 mg, 83%);  $R_f$  = 0.54 ( $CH_2Cl_2$ /MeOH + 7 N  $NH_3$  9:1); mp 130–132 °C;  $^1H$  NMR (600 MHz, DMSO- $d_6$ ):  $\delta$  0.93 (s, 9H), 1.04 (d,  $J$  = 6.8 Hz, 3H), 1.36 (d,  $J$  = 7.0 Hz, 3H), 1.53–1.83 (m, 17H), 1.96–2.03 (m, 1H), 2.05–2.11 (m, 1H), 2.17 (s, 6H), 2.18 (s, 1H), 2.28–2.35 (m, 1H), 2.44 (s, 3H), 2.50–2.58 (m, 1H), 2.63–2.70 (m, 1H), 2.70 (s, 1H), 2.90–2.99 (m, 1H), 3.56–3.64 (m, 3H), 3.85–3.95 (m, 3H), 4.23–4.36 (m, 2H), 4.33–4.39 (m, 1H), 4.39–4.44 (m, 1H), 4.42–4.50 (m, 1H), 4.52 (d,  $J$  = 9.4 Hz, 1H), 4.86–4.95 (m, 3H), 5.03 (h,  $J$  = 4.8 Hz, 1H), 5.07 (d,  $J$  = 3.6 Hz, 1H), 6.44 (t,  $J$  = 2.4 Hz, 1H), 6.46–6.55 (m, 2H), 7.02–7.19 (m, 5H), 7.20–7.25 (m, 1H), 7.37 (d,  $J$  = 8.2 Hz, 2H), 7.40–7.44 (m, 2H), 7.74–7.84 (m, 3H), 8.33 (d,  $J$  = 7.8 Hz, 1H), 8.97 (s, 1H);  $^{13}C$  NMR (151 MHz, DMSO- $d_6$ ):  $\delta$  12.79, 16.12, 20.07, 22.26, 22.56, 25.57, 25.77, 25.95, 26.61, 28.06, 28.42, 28.90, 29.25, 29.84, 34.57, 34.69, 35.35, 37.86, 41.89, 41.93, 46.77, 47.85, 52.16, 56.41, 56.55, 58.67, 58.70, 63.37, 67.32, 68.92, 75.06, 102.51, 107.48, 107.81, 125.89, 126.54, 126.87, 128.48, 128.81, 128.97, 129.85, 130.17, 131.26, 137.16, 137.38, 144.79, 147.91, 151.60, 158.26, 160.09, 169.77, 169.99, 170.52, 170.77, 172.00, 172.55; LC–MS (ESI) 98% purity,  $m/z$ :  $[M + H]^+$  calcd for  $C_{63}H_{88}N_8O_9S$ , 1117.62; found, 1117.9; HRMS (ESI)  $m/z$ :  $[M + H]^+$  calcd for  $C_{63}H_{88}N_8O_9S$ , 1117.6155; found, 1117.6143.

(2*S*,4*S*)-1-((*S*)-2-cyclohexyl-2-((*S*)-2-(*N*-methylacetamido)propanamido)acetyl)-4-(3-((*S*)-1-((2*S*,4*R*)-4-hydroxy-2-((*S*)-1-(4-(4-methylthiazol-5-yl)phenyl)ethyl)carbamoyl)pyrrolidin-1-yl)-3,3-dimethyl-1-oxobutan-2-yl)amino)-5-oxopentyl)oxy)phenoxy)-*N*-((*R*)-1,2,3,4-tetrahydronaphthalen-1-yl)pyrrolidine-2-carboxamide (PROTAC 10c). PROTAC 9 (0.11 g, 0.10 mmol) was dissolved in dry  $CH_2Cl_2$  (2.5 mL) and cooled to 0 °C, and DIPEA (26  $\mu$ L, 0.15 mmol) and acetic anhydride (15  $\mu$ L, 0.15 mmol) were added. The mixture was stirred at rt for 16 h. After removal of the volatiles, the crude product was purified by flash chromatography (gradient from 0 to 10% MeOH in  $CH_2Cl_2$ ) to give a colorless solid. Yield (101 mg, 88%);  $R_f$  = 0.44 ( $CH_2Cl_2$ /MeOH + 7 N  $NH_3$  9:1); mp 86–88 °C;  $^1H$  NMR (600 MHz, DMSO- $d_6$ ):  $\delta$  0.93 (s, 9H), 1.08 (d,  $J$  = 25.9 Hz, 2H), 1.13–1.16 (m, 3H), 1.19–1.26 (m, 1H), 1.36 (d,  $J$  = 7.0 Hz, 3H), 1.53–1.74 (m, 14H), 1.77 (s, 3H), 1.95–2.03 (m, 1H), 2.03–2.12 (m, 2H), 2.14–2.22 (m, 1H), 2.28–2.35 (m, 1H), 2.44 (s, 3H), 2.69 (s, 4H), 2.81 (s, 2H), 3.55–3.66 (m, 3H), 3.89–3.93 (m, 2H), 4.21–4.35 (m, 3H), 4.40–4.46 (m, 2H), 4.52 (d,  $J$  = 9.4 Hz, 1H), 4.88–4.94 (m, 2H), 4.96–5.05 (m, 2H), 5.08 (d,  $J$  = 3.6 Hz, 1H), 6.41–6.57 (m, 3H), 7.04–7.19 (m, 5H), 7.24 (d,  $J$  = 7.5 Hz, 1H), 7.33–7.47 (m, 5H), 7.79–7.86 (m, 3H), 8.33 (d,  $J$  = 7.8 Hz, 1H), 8.96 (s, 1H); LC–MS (ESI) 99% purity,  $m/z$ :  $[M + H]^+$  calcd for  $C_{63}H_{88}N_8O_{10}S$ , 1145.61; found, 1146.0; HRMS (ESI)  $m/z$ :  $[M + H]^+$  calcd for  $C_{63}H_{88}N_8O_{10}S$ , 1145.6104; found, 1145.6100.

(2*S*,4*S*)-1-((*S*)-2-cyclohexyl-2-((*S*)-2-(methylamino)propanamido)acetyl)-4-(3-((*S*)-1-((2*S*,4*S*)-4-hydroxy-2-((4-(4-methylthiazol-5-yl)benzyl)carbamoyl)pyrrolidin-1-yl)-3,3-dimethyl-1-oxobutan-2-yl)amino)-5-oxopentyl)oxy)phenoxy)-*N*-((*R*)-1,2,3,4-tetrahydronaphthalen-1-yl)pyrrolidine-2-carboxamide (PROTAC 11). This compound was prepared using general procedure VII and PROTAC precursor 117 (150 mg, 0.126 mmol). The crude product

was purified by column chromatography ( $CH_2Cl_2$ /MeOH/ $NH_4OH$  9:1:0:1) to give a colorless solid. Yield (64 mg, 47%);  $R_f$  = 0.36 ( $CH_2Cl_2$ /MeOH/ $NH_4OH$  9:1:0:1); mp 98–100 °C;  $^1H$  NMR (400 MHz,  $CDCl_3$ ):  $\delta$  0.78–0.98 (m, 6H), 1.06 (s, 9H), 1.27 (d,  $J$  = 6.9 Hz, 3H), 1.36–1.70 (m, 10H), 1.73–1.85 (m, 6H), 1.97–2.07 (m, 2H), 2.10–2.20 (m, 1H), 2.35 (s, 3H), 2.42–2.47 (m, 1H), 2.49 (s, 3H), 2.68–2.77 (m, 2H), 2.85 (d,  $J$  = 14.0 Hz, 1H), 3.03 (q,  $J$  = 7.1 Hz, 1H), 3.59–3.66 (m, 1H), 3.73–3.85 (m, 3H), 4.07–4.13 (m, 1H), 4.21–4.36 (m, 3H), 4.40 (d,  $J$  = 7.4 Hz, 1H), 4.49–4.65 (m, 2H), 4.68–4.78 (m, 2H), 4.94–4.98 (m, 1H), 5.11 (d,  $J$  = 6.2 Hz, 1H), 6.15 (d,  $J$  = 7.1 Hz, 1H), 6.34–6.52 (m, 3H), 6.62 (d,  $J$  = 8.4 Hz, 1H), 7.01–7.06 (m, 2H), 7.08–7.15 (m, 2H), 7.27–7.36 (m, 5H), 7.49 (t,  $J$  = 6.1 Hz, 1H), 7.64–7.71 (m, 1H), 8.64 (s, 1H);  $^{13}C$  NMR (101 MHz,  $CDCl_3$ ):  $\delta$  16.26, 19.69, 20.19, 22.45, 25.62, 25.75, 25.99, 26.34, 26.82, 28.50, 28.68, 29.41, 29.89, 30.12, 33.55, 34.24, 35.30, 35.68, 37.74, 40.63, 42.90, 47.78, 53.79, 54.93, 55.14, 58.71, 59.53, 60.19, 60.36, 67.72, 69.73, 76.33, 102.91, 107.58, 108.61, 126.34, 127.27, 127.68, 128.77, 129.45, 130.25, 130.67, 131.83, 136.71, 137.57, 138.69, 148.49, 150.35, 158.10, 160.28, 169.67, 171.21, 171.31, 172.69, 174.09, 175.37; HPLC (95%  $H_2O$  (with 0.1% TFA) to 95% MeCN in 10 min, then 95% MeCN for 4 min),  $t_R$  = 6.50 min, 97% purity, detection at 254 nm; HRMS (ESI)  $m/z$ :  $[M + H]^+$  calcd for  $C_{60}H_{81}O_9N_8S$ , 1089.5842; found, 1089.5818.

*tert*-Butyl ((*S*)-1-((*S*)-1-cyclohexyl-2-((2*S*,4*S*)-4-(3-((*S*)-1-((2*S*,4*R*)-4-hydroxy-1-((*S*)-3-methyl-2-(1-oxoisindolin-2-yl)-butanoyl)pyrrolidine-2-carboxamido)methyl)-5-(4-methylthiazol-5-yl)phenoxy)oxy)phenoxy)-2-(((*R*)-1,2,3,4-tetrahydronaphthalen-1-yl)carbamoyl)pyrrolidin-1-yl)-2-oxoethyl)amino)-1-oxopropan-2-yl(methyl)carbamate (118). This compound was prepared using general procedure II, VHL2 ligand–linker conjugate 83 (196 mg, 0.30 mmol), and IAP ligand 65. The crude product was purified by flash chromatography (gradient from 0 to 5% MeOH in  $CH_2Cl_2$ ) to give a colorless solid. Yield (70 mg, 18%);  $R_f$  = 0.23 ( $CH_2Cl_2$ /MeOH 19:1); mp 130–134 °C. Due to the presence of the *N*-Boc protecting group resulting in an additional set of rotamers, NMR data is only provided for the deprotected final PROTAC. LC–MS (ESI) 97% purity,  $m/z$ :  $[M + H]^+$  calcd for  $C_{72}H_{93}N_8O_{12}S$ , 1293.66; found, 1294.3; HRMS (ESI)  $m/z$ :  $[M + H]^+$  calcd for  $C_{72}H_{93}N_8O_{12}S$ , 1293.6628; found, 1293.6611.

*tert*-Butyl ((*S*)-1-((*S*)-1-cyclohexyl-2-((2*S*,4*S*)-4-(3-((*S*)-1-((2*S*,4*R*)-4-hydroxy-1-((*S*)-3-methyl-2-(1-oxoisindolin-2-yl)-butanoyl)pyrrolidine-2-carboxamido)methyl)-5-(4-methylthiazol-5-yl)phenoxy)oxy)phenoxy)-2-(((*R*)-1,2,3,4-tetrahydronaphthalen-1-yl)carbamoyl)pyrrolidin-1-yl)-2-oxoethyl)amino)-1-oxopropan-2-yl(methyl)carbamate (119). This compound was prepared using general procedure II, VHL2 ligand–linker conjugate 84 (209 mg, 0.30 mmol), and IAP ligand 65. The crude product was purified by column chromatography ( $CH_2Cl_2$ /MeOH 29:1) to give a colorless solid. Yield (208 mg, 52%);  $R_f$  = 0.24 ( $CH_2Cl_2$ /MeOH 19:1); mp 128–130 °C. Due to the presence of the *N*-Boc protecting group resulting in an additional set of rotamers, NMR data is only provided for the deprotected final PROTAC. LC–MS (ESI) 98% purity,  $m/z$ :  $[M + H]^+$  calcd for  $C_{73}H_{99}N_8O_{12}S$ , 1335.71; found, 1336.2; HRMS (ESI)  $m/z$ :  $[M + H]^+$  calcd for  $C_{73}H_{99}N_8O_{12}S$ , 1335.7098; found, 1335.7072.

*tert*-Butyl ((*S*)-1-((*S*)-1-cyclohexyl-2-((2*S*,4*S*)-4-(3-((*S*)-1-((2*S*,4*R*)-4-hydroxy-1-((*S*)-3-methyl-2-(1-oxoisindolin-2-yl)-butanoyl)pyrrolidine-2-carboxamido)methyl)-5-(4-methylthiazol-5-yl)phenoxy)oxy)phenoxy)-2-(((*R*)-1,2,3,4-tetrahydronaphthalen-1-yl)carbamoyl)pyrrolidin-1-yl)-2-oxoethyl)amino)-1-oxopropan-2-yl(methyl)carbamate (120). This compound was prepared using general procedure II, VHL2 ligand–linker conjugate 85 (213 mg, 0.30 mmol), and IAP ligand 65. The crude product was purified by column chromatography ( $CH_2Cl_2$ /MeOH 29:1) to give a colorless solid. Yield (85 mg, 21%);  $R_f$  = 0.19 ( $CH_2Cl_2$ /MeOH 19:1); mp 114–118 °C. Due to the presence of the *N*-Boc protecting group resulting in an additional set of rotamers, NMR data is only provided for the deprotected final PROTAC. LC–MS (ESI) 96% purity,  $m/z$ :  $[M + H]^+$  calcd for  $C_{73}H_{99}N_8O_{13}S$ , 1351.71; found, 1352.2; HRMS (ESI)  $m/z$ :  $[M + H]^+$  calcd for  $C_{73}H_{99}N_8O_{13}S$ , 1351.7047; found, 1351.7051.



*tert*-Butyl ((*S*)-1-((*S*)-1-Cyclohexyl-2-((2*S*,4*S*)-4-(3-(2-(2-(2-(2-((2*S*,4*R*)-4-hydroxy-1-((*S*)-3-methyl-2-(1-oxoisindolin-2-yl)-butanoyl)pyrrolidine-2-carboxamido)methyl)-5-(4-methylthiazol-5-yl)phenoxy)ethoxy)ethoxy)ethoxy)phenoxy)-2-(((*R*)-1,2,3,4-tetrahydronaphthalen-1-yl)carbamoyl)pyrrolidin-1-yl)-2-oxoethyl)amino)-1-oxopropan-2-yl(methyl)carbamate (**121**). This compound was prepared using general procedure II, VHL2 ligand-linker conjugate **86** (210 mg, 0.30 mmol), and IAP ligand **65**. The crude product was purified by column chromatography (CH<sub>2</sub>Cl<sub>2</sub>/MeOH 29:1) to give a colorless solid. Yield (104 mg, 26%); *R*<sub>f</sub> = 0.12 (CH<sub>2</sub>Cl<sub>2</sub>/MeOH 39:1); mp 96–98 °C. Due to the presence of the *N*-Boc protecting group resulting in an additional set of rotamers, NMR data is only provided for the deprotected final PROTAC. LC–MS (ESI) 97% purity, *m/z*: [M + H]<sup>+</sup> calcd for C<sub>73</sub>H<sub>93</sub>N<sub>8</sub>O<sub>14</sub>S, 1339.67; found, 1339.7; HRMS (ESI) *m/z*: [M + H]<sup>+</sup> calcd for C<sub>73</sub>H<sub>93</sub>N<sub>8</sub>O<sub>14</sub>S, 1339.6683; found, 1339.6650.

*tert*-Butyl ((*S*)-1-((*S*)-1-Cyclohexyl-2-((2*S*,4*S*)-4-(3-(2-(2-(2-(2-((2*S*,4*R*)-4-hydroxy-1-((*S*)-3-methyl-2-(1-oxoisindolin-2-yl)-butanoyl)pyrrolidine-2-carboxamido)methyl)-5-(4-methylthiazol-5-yl)phenoxy)ethoxy)ethoxy)ethoxy)phenoxy)-2-(((*R*)-1,2,3,4-tetrahydronaphthalen-1-yl)carbamoyl)pyrrolidin-1-yl)-2-oxoethyl)amino)-1-oxopropan-2-yl(methyl)carbamate (**122**). This compound was prepared using general procedure II, VHL2 ligand-linker conjugate **87** (223 mg, 0.30 mmol), and IAP ligand **65**. The crude product was purified by flash chromatography (gradient from 0 to 5% MeOH in CH<sub>2</sub>Cl<sub>2</sub>) to give a colorless solid. Yield (112 mg, 27%); *R*<sub>f</sub> = 0.15 (CH<sub>2</sub>Cl<sub>2</sub>/MeOH 29:1); mp 96–98 °C. Due to the presence of the *N*-Boc protecting group resulting in an additional set of rotamers, NMR data is only provided for the deprotected final PROTAC. LC–MS (ESI) 96% purity, *m/z*: [M + H]<sup>+</sup> calcd for C<sub>75</sub>H<sub>99</sub>N<sub>8</sub>O<sub>15</sub>S, 1383.69; found, 1384.0; HRMS (ESI) *m/z*: [M + H]<sup>+</sup> calcd for C<sub>75</sub>H<sub>99</sub>N<sub>8</sub>O<sub>15</sub>S, 1383.6945; found, 1383.6920.

*tert*-Butyl ((*S*)-1-((*S*)-1-Cyclohexyl-2-((2*S*,4*S*)-4-(3-(2-(2-(2-((2*S*,4*R*)-4-hydroxy-1-((*S*)-3-methyl-2-(1-oxoisindolin-2-yl)-butanoyl)pyrrolidine-2-carboxamido)methyl)-5-(4-methylthiazol-5-yl)phenoxy)ethoxy)hexyl)oxy)hexyl)oxy)phenoxy)-2-(((*R*)-1,2,3,4-tetrahydronaphthalen-1-yl)carbamoyl)pyrrolidin-1-yl)-2-oxoethyl)amino)-1-oxopropan-2-yl(methyl)carbamate (**123**). This compound was prepared using general procedure II, VHL2 ligand-linker conjugate **88** (243 mg, 0.30 mmol), and IAP ligand **65**. The crude product was purified by flash chromatography (gradient from 0 to 6% MeOH in CH<sub>2</sub>Cl<sub>2</sub>) to give a colorless resin. Yield (100 mg, 23%); *R*<sub>f</sub> = 0.21 (CH<sub>2</sub>Cl<sub>2</sub>/MeOH 19:1). Due to the presence of the *N*-Boc protecting group resulting in an additional set of rotamers, NMR data is only provided for the deprotected final PROTAC. LC–MS (ESI) 98% purity, *m/z*: [M + H]<sup>+</sup> calcd for C<sub>81</sub>H<sub>111</sub>N<sub>8</sub>O<sub>14</sub>S, 1451.79; found, 1452.7; HRMS (ESI) *m/z*: [M + H]<sup>+</sup> calcd for C<sub>81</sub>H<sub>111</sub>N<sub>8</sub>O<sub>14</sub>S, 1451.7935; found, 1451.7932.

*tert*-Butyl ((*S*)-1-((*S*)-1-Cyclohexyl-2-((2*S*,4*S*)-4-(3-(2-(2-(2-((2*S*,4*R*)-4-hydroxy-1-((*S*)-3-methyl-2-(1-oxoisindolin-2-yl)-butanoyl)pyrrolidine-2-carboxamido)methyl)-5-(4-methylthiazol-5-yl)phenoxy)ethoxy)hexyl)oxy)hexyl)oxy)phenoxy)-2-(((*R*)-1,2,3,4-tetrahydronaphthalen-1-yl)carbamoyl)pyrrolidin-1-yl)-2-oxoethyl)amino)-1-oxopropan-2-yl(methyl)carbamate (**124**). This compound was prepared using general procedure II, VHL2 ligand-linker conjugate **89** (252 mg, 0.30 mmol), and IAP ligand **65**. The crude product was purified by flash chromatography (gradient from 0 to 5% MeOH in CH<sub>2</sub>Cl<sub>2</sub>) to give a colorless resin. Yield (120 mg, 27%); *R*<sub>f</sub> = 0.29 (CH<sub>2</sub>Cl<sub>2</sub>/MeOH 19:1). Due to the presence of the *N*-Boc protecting group resulting in an additional set of rotamers, NMR data is only provided for the deprotected final PROTAC. LC–MS (ESI) 93% purity, *m/z*: [M + H]<sup>+</sup> calcd for C<sub>83</sub>H<sub>115</sub>N<sub>8</sub>O<sub>14</sub>S, 1479.82; found, 1479.8; HRMS (ESI) *m/z*: [M + H]<sup>+</sup> calcd for C<sub>83</sub>H<sub>115</sub>N<sub>8</sub>O<sub>14</sub>S, 1479.8248; found, 1479.8238.

*tert*-Butyl ((*S*)-1-((*S*)-1-Cyclohexyl-2-((2*S*,4*S*)-4-(3-(2-(2-(2-((2*S*,4*R*)-4-hydroxy-1-((*S*)-3-methyl-2-(1-oxoisindolin-2-yl)-butanoyl)pyrrolidine-2-carboxamido)methyl)-5-(4-methylthiazol-5-yl)phenoxy)ethoxy)hexyl)oxy)hexyl)oxy)phenoxy)-2-(((*R*)-1,2,3,4-tetrahydronaphthalen-1-yl)carbamoyl)pyrrolidin-1-yl)-2-oxoethyl)amino)-1-oxopropan-2-yl(methyl)carbamate (**125**). This compound was prepared using general procedure II, VHL2 ligand-linker conjugate **90** (260 mg, 0.30 mmol), and IAP ligand **65**. The

crude product was purified by flash chromatography (gradient from 0 to 5% MeOH in CH<sub>2</sub>Cl<sub>2</sub>) to give a colorless resin. Yield (109 mg, 24%); *R*<sub>f</sub> = 0.21 (CH<sub>2</sub>Cl<sub>2</sub>/MeOH 19:1). Due to the presence of the *N*-Boc protecting group resulting in an additional set of rotamers, NMR data is only provided for the deprotected final PROTAC. LC–MS (ESI) 84% purity, *m/z*: [M + H]<sup>+</sup> calcd for C<sub>88</sub>H<sub>119</sub>N<sub>8</sub>O<sub>14</sub>S, 1507.86; found, 1507.5; HRMS (ESI) *m/z*: [M + H]<sup>+</sup> calcd for C<sub>88</sub>H<sub>119</sub>N<sub>8</sub>O<sub>14</sub>S, 1507.8561; found, 1507.8562.

(2*S*,4*S*)-1-((*S*)-2-Cyclohexyl-2-((*S*)-2-(methylamino)propanamido)acetyl)-4-(3-((5-(2-((2*S*,4*R*)-4-hydroxy-1-((*S*)-3-methyl-2-(1-oxoisindolin-2-yl)butanoyl)pyrrolidine-2-carboxamido)methyl)-5-(4-methylthiazol-5-yl)phenoxy)ethoxy)phenoxy)-*N*-((*R*)-1,2,3,4-tetrahydronaphthalen-1-yl)pyrrolidine-2-carboxamide (PROTAC **12**). This compound was prepared using general procedure VII and PROTAC precursor **118** (35 mg, 27 μmol). The product possessed sufficient purity after filtration. A colorless solid was obtained. Yield (30 mg, 90%); mp 164–168 °C; <sup>1</sup>H NMR (600 MHz, DMSO-*d*<sub>6</sub>): δ 0.72 (d, *J* = 6.7 Hz, 3H), 0.95 (d, *J* = 6.5 Hz, 3H), 0.95–1.24 (m, 6H), 1.33 (d, *J* = 6.9 Hz, 3H), 1.50–1.86 (m, 15H), 1.88–1.95 (m, 1H), 2.00–2.11 (m, 2H), 2.25–2.57 (m, 8H), 2.61–2.74 (m, 2H), 3.66 (dd, *J* = 5.8, 10.5 Hz, 2H), 3.76 (dd, *J* = 4.5, 10.6 Hz, 1H), 3.85 (q, *J* = 6.6 Hz, 1H), 3.94 (t, *J* = 6.4 Hz, 2H), 4.04–4.09 (m, 2H), 4.15–4.62 (m, 9H), 4.70 (d, *J* = 10.8 Hz, 1H), 4.86–4.94 (m, 1H), 5.01–5.07 (m, 1H), 6.33–6.58 (m, 3H), 6.92–7.20 (m, 6H), 7.22 (d, *J* = 7.5 Hz, 1H), 7.33 (d, *J* = 7.7 Hz, 1H), 7.46–7.52 (m, 1H), 7.60 (d, *J* = 4.3 Hz, 2H), 7.70 (d, *J* = 7.6 Hz, 1H), 7.86 (d, *J* = 8.5 Hz, 1H), 8.36 (t, *J* = 5.9 Hz, 1H), 8.73 (d, *J* = 8.1 Hz, 1H), 8.79–8.86 (m, 1H), 8.99 (s, 1H), 9.26–9.33 (m, 1H); <sup>13</sup>C NMR (151 MHz, DMSO-*d*<sub>6</sub>): δ 15.93, 16.12, 18.76, 19.05, 20.07, 22.40, 25.62, 25.79, 25.87, 28.06, 28.54, 28.56, 28.89, 28.96, 29.84, 30.89, 34.63, 37.21, 38.23, 46.79, 46.97, 52.30, 55.54, 55.61, 56.02, 57.96, 58.75, 58.87, 67.57, 67.84, 68.76, 75.14, 102.74, 107.60, 107.73, 111.91, 120.97, 123.18, 123.77, 125.89, 126.89, 127.21, 127.88, 128.07, 128.47, 128.84, 130.22, 131.10, 131.53, 131.75, 137.18, 137.37, 142.35, 147.95, 151.66, 156.11, 158.22, 160.11, 167.66, 168.28, 168.68, 169.89, 169.94, 171.71; LC–MS (ESI) 98% purity, *m/z*: [M + H]<sup>+</sup> calcd for C<sub>67</sub>H<sub>85</sub>N<sub>8</sub>O<sub>10</sub>S, 1193.61; found, 1191.9; HRMS (ESI) *m/z*: [M + H]<sup>+</sup> calcd for C<sub>67</sub>H<sub>85</sub>N<sub>8</sub>O<sub>10</sub>S, 1193.6104; found, 1193.6079.

(2*S*,4*S*)-1-((*S*)-2-Cyclohexyl-2-((*S*)-2-(methylamino)propanamido)acetyl)-4-(3-((8-(2-((2*S*,4*R*)-4-hydroxy-1-((*S*)-3-methyl-2-(1-oxoisindolin-2-yl)butanoyl)pyrrolidine-2-carboxamido)methyl)-5-(4-methylthiazol-5-yl)phenoxy)ethoxy)phenoxy)-*N*-((*R*)-1,2,3,4-tetrahydronaphthalen-1-yl)pyrrolidine-2-carboxamide (PROTAC **13**). This compound was prepared using general procedure VII and PROTAC precursor **119** (100 mg, 75 μmol). The product possessed sufficient purity after filtration. A colorless solid was obtained. Yield (94 mg, 99%); mp 212–214 °C; <sup>1</sup>H NMR (600 MHz, DMSO-*d*<sub>6</sub>): δ 0.72 (d, *J* = 6.7 Hz, 3H), 0.95 (d, *J* = 6.6 Hz, 3H), 0.97–1.18 (m, 6H), 1.31–1.48 (m, 11H), 1.53–1.82 (m, 8H), 1.88–1.95 (m, 1H), 2.00–2.11 (m, 2H), 2.27–2.40 (m, 1H), 2.44–2.47 (m, 6H), 2.63–2.74 (m, 2H), 3.63–3.73 (m, 6H), 3.76 (dd, *J* = 4.5, 10.6 Hz, 2H), 3.82–3.93 (m, 3H), 4.03 (t, *J* = 6.4 Hz, 2H), 4.16–4.25 (m, 2H), 4.26–4.34 (m, 2H), 4.32–4.47 (m, 4H), 4.53 (d, *J* = 18.1 Hz, 1H), 4.70 (d, *J* = 10.8 Hz, 1H), 4.91 (q, *J* = 7.1 Hz, 1H), 5.04 (p, *J* = 5.1 Hz, 1H), 6.40–6.45 (m, 1H), 6.46–6.55 (m, 2H), 6.96–7.01 (m, 2H), 7.01–7.19 (m, 5H), 7.22 (d, *J* = 7.5 Hz, 1H), 7.32 (d, *J* = 7.7 Hz, 1H), 7.45–7.52 (m, 1H), 7.55–7.63 (m, 2H), 7.70 (d, *J* = 7.5 Hz, 1H), 7.85 (d, *J* = 8.6 Hz, 1H), 8.36 (t, *J* = 5.9 Hz, 1H), 8.73 (d, *J* = 8.1 Hz, 1H), 8.80–8.85 (m, 1H), 9.00 (s, 1H), 9.30–9.35 (m, 1H); <sup>13</sup>C NMR (151 MHz, DMSO-*d*<sub>6</sub>): δ 15.92, 16.08, 18.76, 19.03, 20.05, 25.61, 25.67, 25.71, 25.77, 25.86, 28.05, 28.52, 28.81, 28.88, 28.92, 28.95, 29.83, 30.87, 34.61, 37.16, 38.23, 46.77, 46.96, 52.29, 55.54, 55.59, 56.00, 57.94, 58.74, 58.85, 67.59, 67.90, 68.75, 75.13, 102.74, 107.52, 107.69, 111.87, 120.91, 123.16, 123.75, 125.88, 126.88, 127.20, 127.83, 128.05, 128.47, 128.82, 130.20, 131.03, 131.53, 131.56, 131.72, 137.16, 137.35, 142.33, 147.85, 151.69, 156.11, 158.19, 160.10, 167.63, 168.26, 168.66, 169.90, 171.68; LC–MS (ESI) 98% purity, *m/z*: [M + H]<sup>+</sup> calcd for C<sub>70</sub>H<sub>91</sub>N<sub>8</sub>O<sub>10</sub>S, 1235.66; found, 1235.7; HRMS (ESI) *m/z*: [M + H]<sup>+</sup> calcd for C<sub>70</sub>H<sub>91</sub>N<sub>8</sub>O<sub>10</sub>S, 1235.6573; found, 1235.6530.



(2*S*,4*S*)-1-((*S*)-2-Cyclohexyl-2-((*S*)-2-(methylamino)propanamido)acetyl)-4-(3-(4-(2-(((2*S*,4*R*)-4-hydroxy-1-((*S*)-3-methyl-2-(1-oxoisindolin-2-yl)butanoyl)pyrrolidine-2-carboxamido)methyl)-5-(4-methylthiazol-5-yl)phenoxy)butoxy)phenoxy)-*N*-((*R*)-1,2,3,4-tetrahydronaphthalen-1-yl)pyrrolidine-2-carboxamide (PROTAC 14). This compound was prepared using general procedure VII and PROTAC precursor 120 (50 mg, 37  $\mu$ mol). The product possessed sufficient purity after filtration. A colorless solid was obtained. Yield (42 mg, 88%); mp 170–174 °C;  $^1\text{H}$  NMR (600 MHz, DMSO- $d_6$ ):  $\delta$  0.72 (d,  $J$  = 6.7 Hz, 3H), 0.95 (d,  $J$  = 6.6 Hz, 3H), 0.96–1.15 (m, 6H), 1.33 (d,  $J$  = 6.9 Hz, 3H), 1.50–1.83 (m, 12H), 1.88–1.96 (m, 1H), 2.00–2.11 (m, 2H), 2.27–2.34 (m, 1H), 2.44–2.47 (m, 6H), 2.50–2.59 (m, 1H), 2.61–2.74 (m, 2H), 3.48–3.58 (m, 10H), 3.63–3.69 (m, 2H), 3.73–3.93 (m, 4H), 4.06 (t,  $J$  = 6.3 Hz, 2H), 4.17–4.53 (m, 10H), 4.70 (d,  $J$  = 10.7 Hz, 1H), 4.87–4.94 (m, 1H), 5.04 (p,  $J$  = 5.2 Hz, 1H), 6.42 (q,  $J$  = 3.5 Hz, 1H), 6.46–6.54 (m, 2H), 6.99 (s, 1H), 7.04–7.18 (m, 4H), 7.22 (d,  $J$  = 7.5 Hz, 1H), 7.33 (d,  $J$  = 7.7 Hz, 1H), 7.45–7.53 (m, 1H), 7.60 (d,  $J$  = 5.4 Hz, 2H), 7.70 (d,  $J$  = 7.5 Hz, 1H), 7.86 (d,  $J$  = 8.5 Hz, 1H), 8.36 (t,  $J$  = 5.9 Hz, 1H), 8.73 (d,  $J$  = 8.1 Hz, 1H), 8.79–8.86 (m, 1H), 8.98 (s, 1H);  $^{13}\text{C}$  NMR (151 MHz, DMSO- $d_6$ ):  $\delta$  15.93, 16.11, 18.77, 19.04, 20.06, 25.62, 25.79, 25.86, 26.07, 28.06, 28.53, 28.89, 28.96, 29.84, 30.89, 34.63, 37.20, 38.23, 40.23, 46.79, 46.97, 52.30, 55.55, 55.61, 56.02, 57.96, 58.74, 58.87, 67.45, 67.76, 68.77, 69.76, 69.85, 75.13, 102.77, 107.49, 107.74, 111.87, 120.95, 123.18, 123.76, 125.89, 126.89, 127.19, 127.89, 128.07, 128.48, 128.84, 130.21, 131.08, 131.53, 131.74, 137.18, 137.36, 142.35, 147.93, 151.66, 156.08, 158.21, 160.07, 167.65, 168.27, 168.68, 169.90, 169.92, 171.70; LC–MS (ESI) 99% purity,  $m/z$ :  $[\text{M} + \text{H}]^+$  calcd for  $\text{C}_{70}\text{H}_{91}\text{N}_8\text{O}_{15}$ , 1251.65; found, 1252.0; HRMS (ESI)  $m/z$ :  $[\text{M} + \text{H}]^+$  calcd for  $\text{C}_{70}\text{H}_{91}\text{N}_8\text{O}_{15}$ , 1251.6523; found, 1251.6488.

(2*S*,4*S*)-1-((*S*)-2-Cyclohexyl-2-((*S*)-2-(methylamino)propanamido)acetyl)-4-(3-(2-(2-(2-(((2*S*,4*R*)-4-hydroxy-1-((*S*)-3-methyl-2-(1-oxoisindolin-2-yl)butanoyl)pyrrolidine-2-carboxamido)methyl)-5-(4-methylthiazol-5-yl)phenoxy)ethoxy)ethoxy)phenoxy)-*N*-((*R*)-1,2,3,4-tetrahydronaphthalen-1-yl)pyrrolidine-2-carboxamide (PROTAC 15). This compound was prepared using general procedure VII and PROTAC precursor 121 (58 mg, 43  $\mu$ mol). The product possessed sufficient purity after filtration. A colorless solid was obtained. Yield (54 mg, 98%); mp 206–210 °C;  $^1\text{H}$  NMR (600 MHz, DMSO- $d_6$ ):  $\delta$  0.72 (d,  $J$  = 6.5 Hz, 3H), 0.91–1.13 (m, 7H), 1.31–1.37 (m, 3H), 1.53–1.83 (m, 12H), 1.87–1.94 (m, 1H), 2.00–2.10 (m, 2H), 2.27–2.39 (m, 1H), 2.41–2.47 (m, 6H), 2.51–2.71 (m, 5H), 3.67–3.81 (m, 8H), 3.81–3.94 (m, 2H), 4.02 (t,  $J$  = 4.6 Hz, 3H), 4.15–4.27 (m, 5H), 4.31 (dd,  $J$  = 5.2, 16.4 Hz, 3H), 4.37–4.46 (m, 4H), 4.70 (d,  $J$  = 10.7 Hz, 1H), 4.90 (q,  $J$  = 7.4 Hz, 1H), 6.46 (s, 1H), 6.48 (d,  $J$  = 8.2 Hz, 1H), 6.53 (d,  $J$  = 8.8 Hz, 1H), 6.98–7.18 (m, 7H), 7.22 (d,  $J$  = 7.6 Hz, 1H), 7.33 (d,  $J$  = 7.9 Hz, 1H), 7.46–7.52 (m, 1H), 7.60 (d,  $J$  = 4.4 Hz, 2H), 7.70 (d,  $J$  = 7.7 Hz, 1H), 7.89 (d,  $J$  = 8.6 Hz, 1H), 8.36 (d,  $J$  = 6.5 Hz, 1H), 8.73 (d,  $J$  = 8.2 Hz, 1H), 8.99 (d,  $J$  = 2.7 Hz, 1H);  $^{13}\text{C}$  NMR (151 MHz, DMSO- $d_6$ ):  $\delta$  15.93, 16.10, 18.76, 19.03, 20.05, 25.61, 25.78, 25.86, 28.06, 28.53, 28.88, 28.92, 29.83, 30.87, 34.61, 37.23, 38.23, 40.23, 46.77, 46.96, 52.27, 55.55, 55.61, 56.00, 57.94, 58.70, 58.87, 67.29, 68.09, 68.76, 69.10, 69.19, 70.11, 70.26, 75.06, 102.61, 107.44, 108.01, 112.35, 121.25, 123.16, 123.75, 125.88, 126.88, 127.42, 127.89, 128.05, 128.47, 128.82, 130.23, 131.06, 131.49, 131.53, 131.73, 137.16, 137.37, 142.34, 147.93, 151.70, 156.04, 158.22, 159.88, 167.63, 168.26, 168.66, 169.87, 169.93, 171.71; LC–MS (ESI) 98% purity,  $m/z$ :  $[\text{M} + \text{H}]^+$  calcd for  $\text{C}_{68}\text{H}_{87}\text{N}_8\text{O}_{15}$ , 1239.62; found, 1240.0; HRMS (ESI)  $m/z$ :  $[\text{M} + \text{H}]^+$  calcd for  $\text{C}_{68}\text{H}_{87}\text{N}_8\text{O}_{15}$ , 1239.6159; found, 1239.6109.

(2*S*,4*S*)-1-((*S*)-2-Cyclohexyl-2-((*S*)-2-(methylamino)propanamido)acetyl)-4-(3-(2-(2-(2-(((2*S*,4*R*)-4-hydroxy-1-((*S*)-3-methyl-2-(1-oxoisindolin-2-yl)butanoyl)pyrrolidine-2-carboxamido)methyl)-5-(4-methylthiazol-5-yl)phenoxy)ethoxy)ethoxy)phenoxy)-*N*-((*R*)-1,2,3,4-tetrahydronaphthalen-1-yl)pyrrolidine-2-carboxamide (PROTAC 16). This compound was prepared using general procedure VII and PROTAC precursor 122 (55 mg, 40  $\mu$ mol). The product possessed sufficient purity after filtration. A colorless solid was obtained. Yield (51 mg, 99%); mp

144–148 °C;  $^1\text{H}$  NMR (600 MHz, DMSO- $d_6$ ):  $\delta$  0.72 (d,  $J$  = 6.6 Hz, 3H), 0.93–1.17 (m, 8H), 1.33 (d,  $J$  = 6.9 Hz, 3H), 1.49–1.85 (m, 10H), 1.87–1.94 (m, 1H), 2.00–2.09 (m, 2H), 2.26–2.38 (m, 1H), 2.40–2.48 (m, 6H), 2.50–2.58 (m, 1H), 2.63–2.74 (m, 2H), 3.51–3.72 (m, 13H), 3.73–3.80 (m, 3H), 3.80–3.93 (m, 1H), 3.96–4.05 (m, 2H), 4.14–4.56 (m, 11H), 4.70 (d,  $J$  = 10.7 Hz, 1H), 4.85–4.93 (m, 1H), 5.03 (p,  $J$  = 5.3 Hz, 1H), 6.36–6.55 (m, 3H), 6.95–7.02 (m, 1H), 7.02–7.24 (m, 6H), 7.33 (d,  $J$  = 7.8 Hz, 1H), 7.43–7.52 (m, 1H), 7.54–7.63 (m, 2H), 7.70 (d,  $J$  = 7.5 Hz, 1H), 7.88 (d,  $J$  = 8.5 Hz, 1H), 8.35 (t,  $J$  = 6.0 Hz, 1H), 8.73 (d,  $J$  = 8.1 Hz, 1H), 8.79–8.86 (m, 1H), 8.99 (s, 1H);  $^{13}\text{C}$  NMR (151 MHz, DMSO- $d_6$ ):  $\delta$  15.93, 16.10, 18.77, 19.04, 20.05, 25.62, 25.79, 25.87, 28.06, 28.54, 28.89, 28.93, 29.83, 30.89, 34.62, 37.22, 38.25, 40.24, 46.78, 46.97, 52.27, 55.56, 55.61, 56.01, 57.95, 58.70, 58.87, 67.31, 68.10, 68.77, 69.06, 69.15, 70.01, 70.07, 70.24, 75.06, 102.60, 107.45, 108.02, 112.35, 121.25, 123.17, 123.76, 125.89, 126.90, 127.42, 127.88, 128.06, 128.49, 128.83, 130.24, 131.07, 131.50, 131.53, 131.74, 137.18, 137.37, 142.35, 147.95, 151.70, 156.05, 158.23, 159.88, 167.65, 168.27, 168.68, 169.88, 169.93, 171.72; LC–MS (ESI) 99% purity,  $m/z$ :  $[\text{M} + \text{H}]^+$  calcd for  $\text{C}_{70}\text{H}_{91}\text{N}_8\text{O}_{15}$ , 1283.64; found, 1283.8; HRMS (ESI)  $m/z$ :  $[\text{M} + \text{H}]^+$  calcd for  $\text{C}_{70}\text{H}_{91}\text{N}_8\text{O}_{15}$ , 1283.6421; found, 1283.6380.

(2*S*,4*S*)-1-((*S*)-2-Cyclohexyl-2-((*S*)-2-(methylamino)propanamido)acetyl)-4-(3-(6-(6-(2-(2-(((2*S*,4*R*)-4-hydroxy-1-((*S*)-3-methyl-2-(1-oxoisindolin-2-yl)butanoyl)pyrrolidine-2-carboxamido)methyl)-5-(4-methylthiazol-5-yl)phenoxy)ethoxy)hexyloxy)hexyloxy)phenoxy)-*N*-((*R*)-1,2,3,4-tetrahydronaphthalen-1-yl)pyrrolidine-2-carboxamide (PROTAC 17). This compound was prepared using general procedure VII and PROTAC precursor 123 (35 mg, 24  $\mu$ mol). The product possessed sufficient purity after filtration. A colorless solid was obtained. Yield (29 mg, 86%); mp 118–122 °C;  $^1\text{H}$  NMR (600 MHz, DMSO- $d_6$ ):  $\delta$  0.72 (d,  $J$  = 6.7 Hz, 3H), 0.95 (d,  $J$  = 6.5 Hz, 3H), 0.96–1.15 (m, 5H), 1.19–1.85 (m, 30H), 1.87–1.95 (m, 1H), 2.00–2.11 (m, 2H), 2.27–2.40 (m, 1H), 2.40–2.48 (m, 6H), 2.50–2.59 (m, 1H), 2.64–2.75 (m, 2H), 3.25–3.33 (m, 4H), 3.46 (t,  $J$  = 6.5 Hz, 2H), 3.63–3.93 (m, 8H), 4.14–4.56 (m, 11H), 4.70 (d,  $J$  = 10.8 Hz, 1H), 4.87–4.94 (m, 1H), 5.04 (p,  $J$  = 5.1 Hz, 1H), 6.39–6.44 (m, 1H), 6.46–6.54 (m, 2H), 7.00 (dd,  $J$  = 1.6, 7.8 Hz, 1H), 7.03–7.19 (m, 5H), 7.22 (d,  $J$  = 7.4 Hz, 1H), 7.33 (d,  $J$  = 7.8 Hz, 1H), 7.43–7.52 (m, 1H), 7.61 (q,  $J$  = 4.1 Hz, 2H), 7.70 (d,  $J$  = 7.5 Hz, 1H), 7.86 (d,  $J$  = 8.6 Hz, 1H), 8.34 (t,  $J$  = 6.0 Hz, 1H), 8.73 (d,  $J$  = 8.1 Hz, 1H), 8.78–8.86 (m, 1H), 8.99 (s, 1H);  $^{13}\text{C}$  NMR (151 MHz, DMSO- $d_6$ ):  $\delta$  15.91, 16.12, 18.76, 19.03, 20.04, 25.53, 25.61, 25.64, 25.72, 25.77, 25.86, 28.05, 28.53, 28.80, 28.89, 28.94, 29.36, 29.83, 30.88, 34.62, 37.20, 38.22, 40.24, 46.77, 46.96, 52.28, 55.53, 55.59, 56.00, 57.94, 58.73, 58.86, 67.53, 68.12, 68.75, 68.81, 70.00, 70.07, 70.61, 75.12, 102.73, 107.50, 107.68, 112.40, 121.22, 123.16, 123.74, 125.87, 126.87, 127.40, 127.85, 128.05, 128.47, 128.82, 130.19, 131.07, 131.47, 131.53, 131.72, 137.16, 137.35, 142.33, 147.95, 151.64, 156.08, 158.19, 160.09, 167.62, 168.24, 168.66, 169.89, 171.69; LC–MS (ESI) 98% purity,  $m/z$ :  $[\text{M} + \text{H}]^+$  calcd for  $\text{C}_{76}\text{H}_{103}\text{N}_8\text{O}_{15}$ , 1351.74; found, 1352.1; HRMS (ESI)  $m/z$ :  $[\text{M} + \text{H}]^+$  calcd for  $\text{C}_{76}\text{H}_{103}\text{N}_8\text{O}_{15}$ , 1351.7411; found, 1351.7349.

(2*S*,4*S*)-1-((*S*)-2-Cyclohexyl-2-((*S*)-2-(methylamino)propanamido)acetyl)-4-(3-(6-(5-(5-(2-(((2*S*,4*R*)-4-hydroxy-1-((*S*)-3-methyl-2-(1-oxoisindolin-2-yl)butanoyl)pyrrolidine-2-carboxamido)methyl)-5-(4-methylthiazol-5-yl)phenoxy)pentyl)oxy)pentyl)oxy)hexyloxy)phenoxy)-*N*-((*R*)-1,2,3,4-tetrahydronaphthalen-1-yl)pyrrolidine-2-carboxamide (PROTAC 18). This compound was prepared using general procedure VII and PROTAC precursor 124 (60 mg, 40  $\mu$ mol). After filtration of the solid material, the crude product was purified by column chromatography ( $\text{CH}_2\text{Cl}_2/\text{MeOH} + 7 \text{ N NH}_3$  9:1) followed by preparative HPLC (100% MeOH) to give a colorless solid. Yield (48 mg, 87%); mp 98–102 °C;  $^1\text{H}$  NMR (600 MHz, DMSO- $d_6$ ):  $\delta$  0.73 (d,  $J$  = 6.7 Hz, 3H), 0.85 (t,  $J$  = 6.9 Hz, 2H), 0.95 (d,  $J$  = 6.5 Hz, 3H), 1.07 (d,  $J$  = 6.9 Hz, 3H), 1.19–1.82 (m, 30H), 1.88–1.95 (m, 1H), 1.99–2.11 (m, 2H), 2.16 (s, 3H), 2.17–2.24 (m, 1H), 2.31 (s, 1H), 2.46 (s, 4H), 2.50–2.56 (m, 1H), 2.64–2.75 (m, 2H), 2.87–2.97 (m, 1H), 3.30–3.39 (m, 8H), 3.61 (dd,  $J$  = 4.5, 10.7 Hz, 1H), 3.65–3.70 (m, 1H), 3.74–3.79



(m, 1H), 3.82–3.92 (m, 2H), 4.03 (t,  $J = 6.3$  Hz, 2H), 4.19–4.57 (m, 10H), 4.70 (d,  $J = 10.8$  Hz, 1H), 4.88–4.94 (m, 1H), 4.99–5.08 (m, 2H), 6.42 (t,  $J = 2.4$  Hz, 1H), 6.45–6.53 (m, 2H), 6.95–7.01 (m, 2H), 7.01–7.17 (m, 5H), 7.24 (d,  $J = 7.5$  Hz, 1H), 7.32 (d,  $J = 7.7$  Hz, 1H), 7.46–7.52 (m, 1H), 7.55–7.63 (m, 2H), 7.70 (d,  $J = 7.6$  Hz, 1H), 7.82 (d,  $J = 8.6$  Hz, 1H), 7.90 (d,  $J = 8.7$  Hz, 1H), 8.33 (t,  $J = 6.0$  Hz, 1H), 8.97 (s, 1H);  $^{13}\text{C}$  NMR (151 MHz, DMSO- $d_6$ ):  $\delta$  14.10, 16.15, 18.76, 19.03, 19.22, 20.06, 22.21, 22.56, 22.67, 25.52, 25.58, 25.64, 25.76, 25.95, 27.95, 28.54, 28.65, 28.81, 28.90, 29.11, 29.20, 29.35, 29.83, 31.10, 34.41, 34.57, 37.17, 38.21, 40.24, 46.77, 46.96, 52.15, 54.47, 55.54, 57.94, 58.65, 58.85, 59.28, 67.51, 67.85, 68.77, 70.00, 70.05, 70.08, 75.05, 102.51, 107.50, 107.73, 111.86, 120.90, 123.16, 123.74, 125.87, 126.85, 127.15, 127.83, 128.04, 128.51, 128.79, 130.15, 131.12, 131.46, 131.54, 131.71, 137.14, 137.38, 142.34, 148.03, 151.54, 156.10, 158.24, 160.10, 167.62, 168.26, 170.01, 170.60, 171.66, 174.58; LC–MS (ESI) 98% purity,  $m/z$ : [M + H]<sup>+</sup> calcd for C<sub>78</sub>H<sub>107</sub>N<sub>8</sub>O<sub>12</sub>S, 1379.77; found, 1379.6; HRMS (ESI)  $m/z$ : [M + H]<sup>+</sup> calcd for C<sub>78</sub>H<sub>107</sub>N<sub>8</sub>O<sub>12</sub>S, 1379.7724; found, 1379.7662.

(2*S*,4*S*)-1-((*S*)-2-Cyclohexyl-2-((*S*)-2-(methylamino)propanamido)acetyl)-4-(3-((6-((6-((2*S*,4*R*)-4-hydroxy-1-((*S*)-3-methyl-2-(1-oxoisindolin-2-yl)butanoyl)pyrrolidine-2-carboxamido)methyl)-5-(4-methylthiazol-5-yl)phenoxy)hexyl)oxy)hexyl)oxy)hexyl)oxy)phenoxyl)-*N*-((*R*)-1,2,3,4-tetrahydronaphthalen-1-yl)pyrrolidine-2-carboxamide (PROTAC 19). This compound was prepared using general procedure VII and PROTAC precursor 125 (32 mg, 21  $\mu\text{mol}$ ). After filtration of the solid material, the crude product was purified by preparative HPLC (gradient from 60 to 100% ACN + 0.05% TFA) to give a colorless solid. Yield (23 mg, 75%); mp 102–104 °C;  $^1\text{H}$  NMR (600 MHz, DMSO- $d_6$ ):  $\delta$  0.73 (d,  $J = 6.7$  Hz, 3H), 0.95 (d,  $J = 6.5$  Hz, 3H), 0.97–1.13 (m, 5H), 1.25–1.29 (m, 5H), 1.31 (d,  $J = 6.8$  Hz, 3H), 1.33–1.82 (m, 25H), 1.87–1.96 (m, 1H), 1.98–2.12 (m, 2H), 2.27–2.43 (m, 2H), 2.45 (s, 3H), 2.50–2.74 (m, 3H), 3.26–3.36 (m, 6H), 3.69 (s, 8H), 3.76 (dd,  $J = 4.5$ , 10.6 Hz, 1H), 3.82–3.93 (m, 3H), 4.03 (t,  $J = 6.3$  Hz, 2H), 4.15–4.35 (m, 5H), 4.38–4.57 (m, 5H), 4.70 (d,  $J = 10.8$  Hz, 1H), 4.85–4.94 (m, 1H), 5.00–5.08 (m, 1H), 6.41 (t,  $J = 2.4$  Hz, 1H), 6.45–6.56 (m, 2H), 6.96–7.00 (m, 2H), 7.03–7.20 (m, 6H), 7.22 (d,  $J = 7.5$  Hz, 1H), 7.32 (d,  $J = 7.6$  Hz, 1H), 7.47–7.52 (m, 1H), 7.57–7.63 (m, 2H), 7.70 (d,  $J = 7.5$  Hz, 1H), 7.85 (d,  $J = 8.5$  Hz, 1H), 8.33 (t,  $J = 6.0$  Hz, 1H), 8.71 (d,  $J = 8.1$  Hz, 1H), 8.74–8.81 (m, 1H), 8.97 (s, 1H);  $^{13}\text{C}$  NMR (151 MHz, DMSO- $d_6$ ):  $\delta$  15.86, 16.14, 18.77, 19.04, 20.04, 25.53, 25.56, 25.61, 25.65, 25.72, 25.78, 25.87, 28.04, 28.54, 28.81, 28.90, 28.97, 29.35, 29.38, 29.84, 30.93, 34.64, 37.18, 38.22, 40.23, 46.79, 46.97, 52.29, 55.54, 55.59, 56.02, 57.96, 58.74, 58.86, 67.54, 67.85, 68.77, 70.01, 70.06, 75.13, 102.78, 107.51, 107.68, 111.86, 120.92, 123.18, 123.76, 125.89, 126.90, 127.17, 127.87, 128.07, 128.48, 128.85, 130.20, 131.13, 131.49, 131.54, 131.74, 137.19, 137.35, 142.35, 148.01, 151.59, 156.12, 158.17, 158.20, 158.41, 160.10, 167.65, 168.28, 168.72, 169.88, 171.68; LC–MS (ESI) 99% purity,  $m/z$ : [M + H]<sup>+</sup> calcd for C<sub>80</sub>H<sub>111</sub>N<sub>8</sub>O<sub>12</sub>S, 1407.80; found, 1408.8; HRMS (ESI)  $m/z$ : [M + H]<sup>+</sup> calcd for C<sub>80</sub>H<sub>111</sub>N<sub>8</sub>O<sub>12</sub>S, 1407.8037; found, 1407.8026.

*tert*-Butyl ((2*S*)-1-(((1*S*)-1-Cyclohexyl-2-((2*S*,4*S*)-4-(3-((5-((2-((2-6-dioxopiperidin-3-yl)-1,3-dioxoisindolin-4-yl)amino)pentyl)oxy)phenoxy)-2-(((*R*)-1,2,3,4-tetrahydronaphthalen-1-yl)carbamoyl)pyrrolidin-1-yl)-2-oxoethyl)amino)-1-oxopropan-2-yl)(methyl)carbamate (126). This compound was prepared using general procedure VIII, 99 (75 mg, 98  $\mu\text{mol}$ ), and 72 (27 mg, 98  $\mu\text{mol}$ ). The crude product was purified by column chromatography (EtOAc/*n*-hexanes 4:1) to give a yellow resin. Yield (51 mg, 51%);  $R_f = 0.30$  (EtOAc/*n*-hexanes 4:1). Due to the presence of the *N*-Boc protecting group resulting in an additional set of rotamers, NMR data is only provided for the deprotected final PROTAC. HRMS (ESI)  $m/z$ : [M + H]<sup>+</sup> calcd for C<sub>68</sub>H<sub>77</sub>O<sub>11</sub>N<sub>7</sub>, 1018.5284; found, 1018.5250.

*tert*-Butyl ((2*S*)-1-(((1*S*)-1-Cyclohexyl-2-((2*S*,4*S*)-4-(3-((8-((2-((2-6-dioxopiperidin-3-yl)-1,3-dioxoisindolin-4-yl)amino)octyl)oxy)phenoxy)-2-(((*R*)-1,2,3,4-tetrahydronaphthalen-1-yl)carbamoyl)pyrrolidin-1-yl)-2-oxoethyl)amino)-1-oxopropan-2-yl)(methyl)carbamate (127). This compound was prepared using general procedure VIII, 100 (70 mg, 87  $\mu\text{mol}$ ) and 72 (24 mg, 87  $\mu\text{mol}$ ). The

crude product was purified by column chromatography (EtOAc/*n*-hexanes 4:1) to give a yellow resin. Yield (55 mg, 59%);  $R_f = 0.32$  (EtOAc/*n*-hexanes 4:1). Due to the presence of the *N*-Boc protecting group resulting in an additional set of rotamers, NMR data is only provided for the deprotected final PROTAC. HRMS (ESI)  $m/z$ : [M + H]<sup>+</sup> calcd for C<sub>59</sub>H<sub>77</sub>O<sub>11</sub>N<sub>7</sub>, 1060.5754; found, 1060.5736.

*tert*-Butyl ((2*S*)-1-(((1*S*)-1-Cyclohexyl-2-((2*S*,4*S*)-4-(3-((4-((2-((2-6-dioxopiperidin-3-yl)-1,3-dioxoisindolin-4-yl)amino)butoxy)phenoxy)-2-(((*R*)-1,2,3,4-tetrahydronaphthalen-1-yl)carbamoyl)pyrrolidin-1-yl)-2-oxoethyl)amino)-1-oxopropan-2-yl)(methyl)carbamate (128). This compound was prepared using general procedure VIII, 101 (94 mg, 115  $\mu\text{mol}$ ) and 72 (32 mg, 115  $\mu\text{mol}$ ). The crude product was purified by column chromatography (CH<sub>2</sub>Cl<sub>2</sub>/MeOH 20:1) to give a yellow resin. Yield (72 mg, 58%);  $R_f = 0.35$  (CH<sub>2</sub>Cl<sub>2</sub>/MeOH 9:1). Due to the presence of the *N*-Boc protecting group resulting in an additional set of rotamers, NMR data is only provided for the deprotected final PROTAC. HRMS (ESI)  $m/z$ : [M + H]<sup>+</sup> calcd for C<sub>59</sub>H<sub>78</sub>O<sub>12</sub>N<sub>7</sub>, 1076.5703; found, 1076.5691.

*tert*-Butyl ((2*S*)-1-(((1*S*)-1-Cyclohexyl-2-((2*S*,4*S*)-4-(3-((2-((2-((2-6-dioxopiperidin-3-yl)-1,3-dioxoisindolin-4-yl)amino)ethoxy)ethoxy)ethoxy)phenoxy)-2-(((*R*)-1,2,3,4-tetrahydronaphthalen-1-yl)carbamoyl)pyrrolidin-1-yl)-2-oxoethyl)amino)-1-oxopropan-2-yl)(methyl)carbamate (129). This compound was prepared using general procedure VIII, 102 (71 mg, 88  $\mu\text{mol}$ ), and 72 (24 mg, 88  $\mu\text{mol}$ ). The crude product was purified by column chromatography (CH<sub>2</sub>Cl<sub>2</sub>/MeOH 20:1) to give a yellow resin. Yield (72 mg, 58%);  $R_f = 0.35$  (CH<sub>2</sub>Cl<sub>2</sub>/MeOH 9:1). Due to the presence of the *N*-Boc protecting group resulting in an additional set of rotamers, NMR data is only provided for the deprotected final PROTAC. HRMS (ESI)  $m/z$ : [M + H]<sup>+</sup> calcd for C<sub>57</sub>H<sub>74</sub>O<sub>13</sub>N<sub>7</sub>, 1064.5339; found, 1064.5325.

*tert*-Butyl ((2*S*)-1-(((1*S*)-1-Cyclohexyl-2-((2*S*,4*S*)-4-(3-((2-((2-((2-6-dioxopiperidin-3-yl)-1,3-dioxoisindolin-4-yl)amino)ethoxy)ethoxy)ethoxy)ethoxy)phenoxy)-2-(((*R*)-1,2,3,4-tetrahydronaphthalen-1-yl)carbamoyl)pyrrolidin-1-yl)-2-oxoethyl)amino)-1-oxopropan-2-yl)(methyl)carbamate (130). This compound was prepared using general procedure VIII, 103 (100 mg, 117  $\mu\text{mol}$ ), and 72 (32 mg, 117  $\mu\text{mol}$ ). The crude product was purified by column chromatography (CH<sub>2</sub>Cl<sub>2</sub>/MeOH 20:1) to give a yellow resin. Yield (30 mg, 23%);  $R_f = 0.35$  (CH<sub>2</sub>Cl<sub>2</sub>/MeOH 9:1). Due to the presence of the *N*-Boc protecting group resulting in an additional set of rotamers, NMR data is only provided for the deprotected final PROTAC. HRMS (ESI)  $m/z$ : [M + H]<sup>+</sup> calcd for C<sub>59</sub>H<sub>78</sub>O<sub>14</sub>N<sub>7</sub>, 1108.5601; found, 1108.5585.

*tert*-Butyl ((2*S*)-1-(((1*S*)-1-Cyclohexyl-2-((2*S*,4*S*)-4-(3-((6-((6-((2-((2-6-dioxopiperidin-3-yl)-1,3-dioxoisindolin-4-yl)amino)hexyl)oxy)hexyl)oxy)ethoxy)phenoxy)-2-(((*R*)-1,2,3,4-tetrahydronaphthalen-1-yl)carbamoyl)pyrrolidin-1-yl)-2-oxoethyl)amino)-1-oxopropan-2-yl)(methyl)carbamate (131). This compound was prepared using general procedure VIII, 104 (95 mg, 103  $\mu\text{mol}$ ), and 72 (28 mg, 98  $\mu\text{mol}$ ). The crude product was purified by column chromatography (CH<sub>2</sub>Cl<sub>2</sub>/MeOH 30:1) to give a yellow resin. Yield (86 mg, 71%);  $R_f = 0.18$  (CH<sub>2</sub>Cl<sub>2</sub>/MeOH 20:1). Due to the presence of the *N*-Boc protecting group resulting in an additional set of rotamers, NMR data is only provided for the deprotected final PROTAC. HRMS (ESI)  $m/z$ : [M + H]<sup>+</sup> calcd for C<sub>65</sub>H<sub>90</sub>O<sub>13</sub>N<sub>7</sub>, 1176.6591; found, 1176.6571.

*tert*-Butyl ((2*S*)-1-(((1*S*)-1-Cyclohexyl-2-((2*S*,4*S*)-4-(3-((5-((5-((6-((2-((2-6-dioxopiperidin-3-yl)-1,3-dioxoisindolin-4-yl)amino)hexyl)oxy)pentyl)oxy)pentyl)oxy)phenoxy)-2-(((*R*)-1,2,3,4-tetrahydronaphthalen-1-yl)carbamoyl)pyrrolidin-1-yl)-2-oxoethyl)amino)-1-oxopropan-2-yl)(methyl)carbamate (132). This compound was prepared using general procedure VIII, 105 (65 mg, 69  $\mu\text{mol}$ ), and 72 (21 mg, 69  $\mu\text{mol}$ ). The crude product was purified by column chromatography (CH<sub>2</sub>Cl<sub>2</sub>/MeOH 50:1) to give a yellow resin. Yield (47 mg, 57%);  $R_f = 0.45$  (CH<sub>2</sub>Cl<sub>2</sub>/MeOH 9:1). Due to the presence of the *N*-Boc protecting group resulting in an additional set of rotamers, NMR data is only provided for the deprotected final PROTAC. HRMS (ESI)  $m/z$ : [M + H]<sup>+</sup> calcd for C<sub>67</sub>H<sub>94</sub>O<sub>13</sub>N<sub>7</sub>, 1204.6904; found, 1204.6904.

*tert*-Butyl ((2*S*)-1-(((1*S*)-1-Cyclohexyl-2-((2*S*,4*S*)-4-(3-((6-((6-((2-((2-6-dioxopiperidin-3-yl)-1,3-dioxoisindolin-4-yl)amino)hexyl)oxy)hexyl)oxy)hexyl)oxy)phenoxy)-2-(((*R*)-1,2,3,4-tetrahydronaph-



thalen-1-yl)carbamoyl)pyrrolidin-1-yl)-2-oxoethyl)amino)-1-oxopropan-2-yl)(methyl)carbamate (**133**). This compound was prepared using general procedure VIII, **106** (142 mg, 145  $\mu$ mol), and **72** (40 mg, 145  $\mu$ mol). The crude product was purified by column chromatography ( $\text{CH}_2\text{Cl}_2/\text{MeOH}$  50:1) to give a yellow resin. Yield (51 mg, 29%);  $R_f = 0.35$  ( $\text{CH}_2\text{Cl}_2/\text{MeOH}$  20:1). Due to the presence of the *N*-Boc protecting group resulting in an additional set of rotamers, NMR data is only provided for the deprotected final PROTAC. HRMS (ESI)  $m/z$ :  $[\text{M} + \text{H}]^+$  calcd for  $\text{C}_{69}\text{H}_{98}\text{O}_{13}\text{N}_7$ , 1232.7217; found, 1232.7205.

*tert*-Butyl ((2*S*)-1-((1*S*)-1-Cyclohexyl-2-((2*S*,4*S*)-4-(3-(2-((6-((2-(1-methyl-2,6-dioxopiperidin-3-yl)-1,3-dioxoisindolin-4-yl)amino)hexyl)oxy)hexyl)oxy)ethoxy)phenoxy)-2-((*R*)-1,2,3,4-tetrahydronaphthalen-1-yl)carbamoyl)pyrrolidin-1-yl)-2-oxoethyl)amino)-1-oxopropan-2-yl)(methyl)carbamate (**134**). This compound was prepared using general procedure VIII, **104** (92 mg, 100  $\mu$ mol), and **73** (29 mg, 100  $\mu$ mol). The crude product was purified by column chromatography ( $\text{CH}_2\text{Cl}_2/\text{MeOH}$  20:1) to give a yellow resin. Yield (65 mg, 55%);  $R_f = 0.23$  ( $\text{CH}_2\text{Cl}_2/\text{MeOH}$  20:1). Due to the presence of the *N*-Boc protecting group resulting in an additional set of rotamers, NMR data is only provided for the deprotected final PROTAC. HRMS (ESI)  $m/z$ :  $[\text{M} + \text{H}]^+$  calcd for  $\text{C}_{66}\text{H}_{92}\text{O}_{13}\text{N}_7$ , 1190.6748; found, 1190.6743.

*tert*-Butyl ((2*S*)-1-((1*S*)-1-Cyclohexyl-2-((2*S*,4*S*)-4-(3-(2-((6-((2-(1-methyl-2,6-dioxopiperidin-3-yl)-1,3-dioxoisindolin-4-yl)amino)hexyl)oxy)hexyl)oxy)ethoxy)phenoxy)-2-((*R*)-1,2,3,4-tetrahydronaphthalen-1-yl)carbamoyl)pyrrolidin-1-yl)-2-oxoethyl)amino)-1-oxopropan-2-yl)(methyl)carbamate (**135**). This compound was prepared using general procedure VIII, **106** (125 mg, 128  $\mu$ mol), and **73** (37 mg, 128  $\mu$ mol). The crude product was purified by column chromatography ( $\text{CH}_2\text{Cl}_2/\text{MeOH}$  50:1) to give a yellow resin. Yield (83 mg, 52%);  $R_f = 0.30$  ( $\text{CH}_2\text{Cl}_2/\text{MeOH}$  20:1). Due to the presence of the *N*-Boc protecting group resulting in an additional set of rotamers, NMR data is only provided for the deprotected final PROTAC. HRMS (ESI)  $m/z$ :  $[\text{M} + \text{H}]^+$  calcd for  $\text{C}_{70}\text{H}_{100}\text{O}_{13}\text{N}_7$ , 1246.7374; found, 1246.7360.

(2*S*,4*S*)-1-((*S*)-2-Cyclohexyl-2-((*S*)-2-(methylamino)propanamido)acetyl)-4-(3-(4-(4-((2-(2,6-dioxopiperidin-3-yl)-1,3-dioxoisindolin-4-yl)amino)butoxy)butoxy)phenoxy)-*N*-((*R*)-1,2,3,4-tetrahydronaphthalen-1-yl)pyrrolidine-2-carboxamide (PROTAC **20**). This compound was prepared using general procedure VII and PROTAC precursor **126** (51 mg, 50  $\mu$ mol). The crude product was purified by column chromatography ( $\text{CH}_2\text{Cl}_2/\text{MeOH}/\text{NH}_4\text{OH}$  9:1:0.1) to give a yellow solid. Yield (35 mg, 76%);  $R_f = 0.45$  ( $\text{CH}_2\text{Cl}_2/\text{MeOH}/\text{NH}_4\text{OH}$  9:1:0.1); mp 64–69  $^\circ\text{C}$ ;  $^1\text{H}$  NMR (400 MHz,  $\text{CDCl}_3$ ):  $\delta$  0.82–1.00 (m, 5H), 1.28 (d,  $J = 6.9$  Hz, 3H), 1.43–1.68 (m, 8H), 1.70–1.85 (m, 6H), 1.97–2.14 (m, 2H), 2.35 (s, 3H), 2.69–2.78 (m, 4H), 2.82–2.90 (m, 2H), 3.02–3.10 (m, 1H), 3.30 (q,  $J = 6.6$  Hz, 2H), 3.60–3.67 (m, 2H), 3.74–3.83 (m, 3H), 3.92 (t,  $J = 6.2$  Hz, 1H), 4.22–4.31 (m, 1H), 4.39–4.47 (m, 1H), 4.71–4.78 (m, 1H), 4.84–4.96 (m, 2H), 5.08–5.16 (m, 1H), 6.25 (t,  $J = 5.7$  Hz, 1H), 6.36–6.42 (m, 2H), 6.48–6.55 (m, 1H), 6.61–6.72 (m, 1H), 6.88 (d,  $J = 8.6$  Hz, 1H), 7.02–7.18 (m, 5H), 7.29 (d,  $J = 7.3$  Hz, 2H), 7.45–7.52 (m, 1H), 7.67 (d,  $J = 8.9$  Hz, 1H);  $^{13}\text{C}$  NMR (101 MHz,  $\text{CDCl}_3$ , only the peaks for the major rotamer are given):  $\delta$  19.65, 20.20, 22.93, 23.73, 25.66, 25.77, 26.03, 28.73, 29.04, 29.16, 29.42, 29.89, 30.12, 31.59, 33.57, 35.22, 40.63, 42.65, 43.03, 47.74, 49.02, 53.81, 54.96, 60.22, 61.86, 67.73, 71.27, 72.42, 102.90, 107.61, 108.50, 110.06, 111.57, 116.76, 126.31, 127.21, 128.86, 129.21, 130.22, 132.64, 136.27, 136.81, 137.57, 147.08, 158.09, 160.40, 167.77, 168.55, 169.65, 171.25, 172.69, 175.24; HPLC (95%  $\text{H}_2\text{O}$  (with 0.1% TFA) to 95% MeCN in 10 min, then 95% MeCN for 4 min),  $t_R = 7.19$  min, 95% purity, detection at 254 nm; HRMS (ESI)  $m/z$ :  $[\text{M} + \text{H}]^+$  calcd for  $\text{C}_{51}\text{H}_{64}\text{O}_9\text{N}_7$ , 918.4760; found, 918.4735.

(2*S*,4*S*)-1-((*S*)-2-Cyclohexyl-2-((*S*)-2-(methylamino)propanamido)acetyl)-4-(3-(8-((2-(2,6-dioxopiperidin-3-yl)-1,3-dioxoisindolin-4-yl)amino)oxy)ethoxy)phenoxy)-*N*-((*R*)-1,2,3,4-tetrahydronaphthalen-1-yl)pyrrolidine-2-carboxamide (PROTAC **21**). This compound was prepared using general procedure VII and PROTAC precursor **127** (54 mg, 51  $\mu$ mol). The crude product was purified by column chromatography ( $\text{CH}_2\text{Cl}_2/\text{MeOH}/\text{NH}_4\text{OH}$

15:1:0.1) to give a yellow solid. Yield (42 mg, 86%);  $R_f = 0.55$  ( $\text{CH}_2\text{Cl}_2/\text{MeOH}/\text{NH}_4\text{OH}$  9:1:0.1); mp 83–85  $^\circ\text{C}$ ;  $^1\text{H}$  NMR (400 MHz,  $\text{CDCl}_3$ ):  $\delta$  0.83–1.00 (m, 5H), 1.27 (d,  $J = 6.9$  Hz, 3H), 1.34–1.54 (m, 8H), 1.54–1.70 (m, 8H), 1.72–1.84 (m, 6H), 1.98–2.14 (m, 2H), 2.29–2.35 (m, 1H), 2.36 (s, 3H), 2.67–2.81 (m, 4H), 2.82–2.91 (m, 2H), 3.01–3.08 (m, 1H), 3.25 (q,  $J = 6.6$  Hz, 2H), 3.81 (d,  $J = 11.5$  Hz, 1H), 3.85–3.90 (m, 2H), 4.21–4.29 (m, 1H), 4.38–4.46 (m, 1H), 4.71–4.78 (m, 1H), 4.85–4.96 (m, 2H), 5.13 (q,  $J = 5.9$  Hz, 1H), 6.22 (t,  $J = 5.5$  Hz, 1H), 6.36–6.41 (m, 2H), 6.50–6.54 (m, 1H), 6.64 (d,  $J = 9.2$  Hz, 1H), 6.87 (d,  $J = 8.5$  Hz, 1H), 7.02–7.17 (m, 5H), 7.30 (d,  $J = 7.8$  Hz, 1H), 7.45–7.50 (m, 1H), 7.63 (dd,  $J = 9.0, 3.0$  Hz, 1H), 8.38 (br s, 1H);  $^{13}\text{C}$  NMR (101 MHz,  $\text{CDCl}_3$ , only the peaks for the major rotamer are given):  $\delta$  19.70, 20.21, 22.93, 25.65, 25.77, 26.03, 26.98, 28.69, 29.34, 29.43, 29.90, 30.14, 31.56, 33.62, 35.28, 40.67, 42.76, 47.75, 49.00, 53.76, 54.91, 60.24, 60.40, 68.03, 102.88, 103.03, 107.93, 108.17, 109.97, 111.48, 116.77, 126.34, 127.22, 128.90, 129.19, 130.18, 132.63, 136.24, 136.78, 137.54, 147.15, 158.08, 160.58, 167.77, 168.53, 169.66, 171.20, 172.74, 175.37; HPLC (95%  $\text{H}_2\text{O}$  (with 0.1% TFA) to 95% MeCN in 10 min, then 95% MeCN for 4 min),  $t_R = 8.04$  min, 97% purity, detection at 254 nm; HRMS (ESI)  $m/z$ :  $[\text{M} + \text{H}]^+$  calcd for  $\text{C}_{54}\text{H}_{70}\text{O}_9\text{N}_7$ , 960.5230; found, 960.5201.

(2*S*,4*S*)-1-((*S*)-2-Cyclohexyl-2-((*S*)-2-(methylamino)propanamido)acetyl)-4-(3-(4-(4-((2-(2,6-dioxopiperidin-3-yl)-1,3-dioxoisindolin-4-yl)amino)butoxy)butoxy)phenoxy)-*N*-((*R*)-1,2,3,4-tetrahydronaphthalen-1-yl)pyrrolidine-2-carboxamide (PROTAC **22**). This compound was prepared using general procedure VII and PROTAC precursor **128** (71 mg, 66  $\mu$ mol). The crude product was purified by column chromatography ( $\text{CH}_2\text{Cl}_2/\text{MeOH}/\text{NH}_4\text{OH}$  15:1:0.1) to give a yellow solid. Yield (59 mg, 92%);  $R_f = 0.42$  ( $\text{CH}_2\text{Cl}_2/\text{MeOH}/\text{NH}_4\text{OH}$  9:1:0.1); mp 80–81  $^\circ\text{C}$ ;  $^1\text{H}$  NMR (400 MHz,  $\text{CDCl}_3$ ):  $\delta$  0.83–0.99 (m, 5H), 1.28 (d,  $J = 6.8$  Hz, 3H), 1.39–1.65 (m, 7H), 1.65–1.88 (m, 12H), 1.99–2.13 (m, 2H), 2.35 (s, 3H), 2.67–2.89 (m, 6H), 3.02–3.10 (m, 1H), 3.30 (q,  $J = 6.5$  Hz, 2H), 3.44–3.50 (m, 4H), 3.80 (d,  $J = 11.7$  Hz, 1H), 3.91 (d,  $J = 5.4$  Hz, 2H), 4.23–4.29 (m, 1H), 4.39–4.48 (m, 1H), 4.71–4.78 (m, 1H), 4.81–4.96 (m, 2H), 5.13 (q,  $J = 6.1$  Hz, 1H), 6.26 (t,  $J = 5.7$  Hz, 1H), 6.36–6.41 (m, 2H), 6.49–6.54 (m, 1H), 6.59–6.73 (m, 1H), 6.88 (d,  $J = 8.5$  Hz, 1H), 7.02–7.16 (m, 5H), 7.30 (d,  $J = 7.1$  Hz, 1H), 7.47 (d,  $J = 8.5$  Hz, 1H), 7.61–7.70 (m, 1H), 8.52 (br s, 1H);  $^{13}\text{C}$  NMR (101 MHz,  $\text{CDCl}_3$ , only the peaks for the major rotamer are given):  $\delta$  19.65, 20.20, 22.93, 25.66, 25.77, 26.04, 26.28, 26.42, 26.48, 27.21, 28.69, 29.42, 29.88, 30.13, 31.58, 33.62, 35.20, 40.68, 42.61, 47.73, 49.01, 53.75, 54.93, 60.22, 67.80, 70.40, 70.67, 76.35, 102.94, 103.07, 107.72, 108.36, 110.01, 111.50, 116.78, 126.32, 127.21, 128.93, 129.19, 130.18, 132.64, 136.25, 136.81, 137.56, 147.08, 158.10, 160.49, 167.78, 168.58, 169.67, 171.28, 172.71, 175.31; HPLC (95%  $\text{H}_2\text{O}$  (with 0.1% TFA) to 95% MeCN in 10 min, then 95% MeCN for 4 min),  $t_R = 7.42$  min, 97% purity, detection at 254 nm; HRMS (ESI)  $m/z$ :  $[\text{M} + \text{H}]^+$  calcd for  $\text{C}_{54}\text{H}_{70}\text{O}_{10}\text{N}_7$ , 976.5179; found, 976.5161.

(2*S*,4*S*)-1-((*S*)-2-Cyclohexyl-2-((*S*)-2-(methylamino)propanamido)acetyl)-4-(3-(2-(2-((2-(2,6-dioxopiperidin-3-yl)-1,3-dioxoisindolin-4-yl)amino)ethoxy)ethoxy)phenoxy)-*N*-((*R*)-1,2,3,4-tetrahydronaphthalen-1-yl)pyrrolidine-2-carboxamide (PROTAC **23**). This compound was prepared using general procedure VII and PROTAC precursor **129** (47 mg, 44  $\mu$ mol). The crude product was purified by column chromatography ( $\text{CH}_2\text{Cl}_2/\text{MeOH}/\text{NH}_4\text{OH}$  15:1:0.1) to give a yellow solid. Yield (40 mg, 94%);  $R_f = 0.40$  ( $\text{CH}_2\text{Cl}_2/\text{MeOH}/\text{NH}_4\text{OH}$  9:1:0.1); mp 80–82  $^\circ\text{C}$ ;  $^1\text{H}$  NMR (400 MHz,  $\text{CDCl}_3$ ):  $\delta$  0.82–1.01 (m, 5H), 1.28 (d,  $J = 6.9$  Hz, 3H), 1.37–1.71 (m, 7H), 1.74–1.84 (m, 4H), 1.99–2.10 (m, 2H), 2.33 (s, 3H), 2.62–2.89 (m, 6H), 3.02–3.13 (m, 1H), 3.40–3.51 (m, 2H), 3.68–3.76 (m, 6H), 3.77–3.82 (m, 1H), 3.82–3.88 (m, 2H), 4.02–4.10 (m, 2H), 4.23–4.32 (m, 1H), 4.40–4.48 (m, 1H), 4.72–4.77 (m, 1H), 4.80–4.93 (m, 2H), 5.09–5.17 (m, 1H), 6.36–6.44 (m, 2H), 6.47–6.56 (m, 2H), 6.70 (s, 1H), 6.90 (dd,  $J = 8.5, 1.7$  Hz, 1H), 7.01–7.17 (m, 5H), 7.27–7.32 (m, 1H), 7.45 (d,  $J = 7.8$  Hz, 1H), 7.62–7.75 (m, 1H), 8.69 (br s, 1H);  $^{13}\text{C}$  NMR (101 MHz,  $\text{CDCl}_3$ , only the peaks for the major rotamer are given):  $\delta$  14.26, 19.59, 20.19, 22.86, 25.66, 25.79, 26.03, 28.70, 29.42, 29.84, 30.11, 31.58, 33.57,



35.11, 40.60, 42.53, 47.69, 49.01, 53.76, 54.97, 60.18, 67.61, 69.69, 69.96, 70.97, 102.75, 107.69, 107.88, 110.40, 111.72, 116.94, 126.31, 127.21, 128.86, 129.20, 130.17, 132.61, 136.16, 136.87, 137.58, 146.97, 158.10, 160.22, 167.80, 168.62, 169.41, 169.68, 171.40, 172.67, 175.25; HPLC (95% H<sub>2</sub>O (with 0.1% TFA) to 95% MeCN in 10 min, then 95% MeCN for 4 min), *t*<sub>R</sub> = 6.63 min, 95% purity, detection at 254 nm; HRMS (ESI) *m/z*: [M + H]<sup>+</sup> calcd for C<sub>52</sub>H<sub>66</sub>N<sub>7</sub>, 964.4815; found, 964.4799.

(2*S*,4*S*)-1-((*S*)-2-Cyclohexyl-2-((*S*)-2-(methylamino)propanamido)acetyl)-4-(3-(2-(2-(2-((2-(2,6-dioxopiperidin-3-yl)-1,3-dioxoisindolin-4-yl)amino)ethoxy)ethoxy)ethoxy)ethoxy)phenoxy)-*N*-((*R*)-1,2,3,4-tetrahydronaphthalen-1-yl)pyrrolidine-2-carboxamide (PROTAC 24). This compound was prepared using general procedure VII and PROTAC precursor 130 (30 mg, 27 μmol). The crude product was purified by column chromatography (CH<sub>2</sub>Cl<sub>2</sub>/MeOH/NH<sub>4</sub>OH 15:1:0.1) to give a yellow solid. Yield (22 mg, 81%); *R*<sub>f</sub> = 0.35 (CH<sub>2</sub>Cl<sub>2</sub>/MeOH/NH<sub>4</sub>OH 9:1:0.1); mp 76–80 °C; <sup>1</sup>H NMR (400 MHz, CDCl<sub>3</sub>): δ 0.81–1.02 (m, 5H), 1.28 (d, *J* = 6.9 Hz, 3H), 1.38–1.70 (m, 10H), 1.74–1.84 (m, 4H), 1.99–2.13 (m, 2H), 2.36 (s, 3H), 2.62–2.78 (m, 4H), 2.78–2.90 (m, 2H), 3.05 (q, *J* = 7.5 Hz, 1H), 3.44 (q, *J* = 5.5 Hz, 2H), 3.66–3.68 (m, 3H), 3.68–3.74 (m, 5H), 3.83 (t, *J* = 4.9 Hz, 2H), 4.05 (q, *J* = 4.7 Hz, 2H), 4.24–4.31 (m, 1H), 4.44 (t, *J* = 8.0 Hz, 1H), 4.72–4.78 (m, 1H), 4.84–4.94 (m, 2H), 5.09–5.16 (m, 1H), 6.38–6.43 (m, 2H), 6.48 (q, *J* = 5.4 Hz, 1H), 6.51–6.55 (m, 1H), 6.65 (d, *J* = 7.8 Hz, 1H), 6.91 (dd, *J* = 8.5, 2.3 Hz, 1H), 7.02–7.16 (m, 5H), 7.29 (d, *J* = 7.9 Hz, 1H), 7.44–7.50 (m, 1H), 7.65 (d, *J* = 8.7 Hz, 1H), 8.57 (br s, 1H); <sup>13</sup>C NMR (101 MHz, CDCl<sub>3</sub>, only the peaks for the major rotamer are given): δ 19.67, 20.20, 22.91, 25.66, 25.78, 26.02, 28.68, 29.42, 29.88, 30.13, 31.57, 33.54, 35.24, 40.64, 42.57, 47.73, 49.02, 53.78, 54.93, 60.20, 60.35, 67.63, 69.69, 69.81, 70.83, 70.88, 70.96, 102.95, 107.73, 128.73, 110.40, 111.77, 116.97, 126.33, 127.23, 128.85, 129.21, 130.21, 132.63, 136.18, 136.81, 137.56, 147.00, 158.08, 160.19, 167.76, 168.59, 169.42, 169.66, 171.29, 172.72, 175.35; HPLC (95% H<sub>2</sub>O (with 0.1% TFA) to 95% MeCN in 10 min, then 95% MeCN for 4 min), *t*<sub>R</sub> = 6.64 min, 98% purity, detection at 254 nm; HRMS (ESI) *m/z*: [M + H]<sup>+</sup> calcd for C<sub>54</sub>H<sub>70</sub>O<sub>12</sub>N<sub>7</sub>, 1008.5077; found, 1008.5049.

(2*S*,4*S*)-1-((*S*)-2-Cyclohexyl-2-((*S*)-2-(methylamino)propanamido)acetyl)-4-(3-(2-((6-((2-(2,6-dioxopiperidin-3-yl)-1,3-dioxoisindolin-4-yl)amino)hexyl)oxy)hexyl)oxy)ethoxy)phenoxy)-*N*-((*R*)-1,2,3,4-tetrahydronaphthalen-1-yl)pyrrolidine-2-carboxamide (PROTAC 25) (SAB 141). This compound was prepared using general procedure VII and PROTAC precursor 131 (80 mg, 68 μmol). The crude product was purified by column chromatography (CH<sub>2</sub>Cl<sub>2</sub>/MeOH/NH<sub>4</sub>OH 15:1:0.1) to give a yellow solid. Yield (61 mg, 83%); *R*<sub>f</sub> = 0.42 (CH<sub>2</sub>Cl<sub>2</sub>/MeOH/NH<sub>4</sub>OH 9:1:0.1); mp 70–73 °C; <sup>1</sup>H NMR (400 MHz, CDCl<sub>3</sub>): δ 0.82–1.00 (m, 5H), 1.28 (d, *J* = 6.9 Hz, 3H), 1.34–1.45 (m, 10H), 1.51–1.71 (m, 13H), 1.72–1.84 (m, 4H), 1.98–2.15 (m, 2H), 2.36 (s, 3H), 2.67–2.80 (m, 4H), 2.82–2.90 (m, 2H), 3.01–3.07 (m, 1H), 3.25 (q, *J* = 5.9 Hz, 2H), 3.38 (dd, *J* = 6.6, 2.7 Hz, 4H), 3.51 (d, *J* = 6.7 Hz, 2H), 3.75 (t, *J* = 4.7 Hz, 2H), 3.81 (d, *J* = 11.6 Hz, 1H), 4.04 (t, *J* = 5.1 Hz, 2H), 4.26 (dd, *J* = 11.2, 4.8 Hz, 1H), 4.42 (t, *J* = 8.3 Hz, 1H), 4.75 (dt, *J* = 9.8, 2.5 Hz, 1H), 4.85–4.96 (m, 2H), 5.13 (q, *J* = 6.1 Hz, 1H), 6.22 (t, *J* = 5.6 Hz, 1H), 6.37–6.43 (m, 2H), 6.52–6.57 (m, 1H), 6.59–6.64 (m, 1H), 6.84–6.89 (m, 1H), 7.02–7.17 (m, 5H), 7.27–7.31 (m, 1H), 7.45–7.51 (m, 1H), 7.63 (d, *J* = 8.9 Hz, 1H), 8.35 (br s, 1H); <sup>13</sup>C NMR (101 MHz, CDCl<sub>3</sub>, only the peaks for the major rotamer are given): δ 19.71, 20.21, 22.94, 25.65, 25.77, 26.01, 26.11, 26.22, 26.94, 28.68, 29.36, 29.42, 29.76, 29.78, 29.84, 29.90, 30.13, 31.57, 33.58, 35.29, 40.64, 42.73, 47.74, 49.00, 53.77, 54.92, 60.24, 60.40, 67.58, 69.25, 70.80, 71.00, 71.72, 103.08, 107.84, 108.52, 108.60, 109.97, 111.50, 116.78, 126.36, 127.24, 128.83, 129.21, 130.19, 132.63, 136.26, 136.77, 137.55, 147.14, 158.02, 160.28, 167.79, 168.54, 169.66, 171.19, 172.74, 175.39; HPLC (95% H<sub>2</sub>O (with 0.1% TFA) to 95% MeCN in 10 min, then 95% MeCN for 4 min), *t*<sub>R</sub> = 8.26 min, 96% purity, detection at 254 nm; HRMS (ESI) *m/z*: [M + H]<sup>+</sup> calcd for C<sub>60</sub>H<sub>80</sub>O<sub>11</sub>N<sub>7</sub>, 1076.6067; found, 1076.6042.

(2*S*,4*S*)-1-((*S*)-2-Cyclohexyl-2-((*S*)-2-(methylamino)propanamido)acetyl)-4-(3-(5-(5-((6-((2-(2,6-dioxopiperidin-3-yl)-

1,3-dioxoisindolin-4-yl)amino)hexyl)oxy)pentyl)oxy)pentyl)oxy)phenoxy)-*N*-((*R*)-1,2,3,4-tetrahydronaphthalen-1-yl)pyrrolidine-2-carboxamide (PROTAC 26). This compound was prepared using general procedure VII and PROTAC precursor 132 (47 mg, 39 μmol). The crude product was purified by column chromatography (CH<sub>2</sub>Cl<sub>2</sub>/MeOH/NH<sub>4</sub>OH 15:1:0.1) to give a yellow solid. Yield (35 mg, 81%); *R*<sub>f</sub> = 0.20 (CH<sub>2</sub>Cl<sub>2</sub>/MeOH/NH<sub>4</sub>OH 15:1:0.1); mp 63–66 °C; <sup>1</sup>H NMR (400 MHz, CDCl<sub>3</sub>): δ 0.81–0.99 (m, 5H), 1.27 (d, *J* = 6.9 Hz, 3H), 1.34–1.53 (m, 10H), 1.54–1.71 (m, 15H), 1.72–1.84 (m, 6H), 1.99–2.15 (m, 2H), 2.36 (s, 3H), 2.66–2.81 (m, 4H), 2.82–2.91 (m, 2H), 3.00–3.07 (m, 1H), 3.25 (d, *J* = 5.8 Hz, 2H), 3.36–3.44 (m, 8H), 3.81 (d, *J* = 11.4 Hz, 1H), 3.87 (d, *J* = 6.0 Hz, 2H), 4.24 (dd, *J* = 11.5, 4.9 Hz, 1H), 4.42 (d, *J* = 8.1 Hz, 1H), 4.75 (dd, *J* = 9.8, 2.1 Hz, 1H), 4.86–4.96 (m, 2H), 5.13 (q, *J* = 6.0 Hz, 1H), 6.21 (t, *J* = 5.6 Hz, 1H), 6.34–6.40 (m, 2H), 6.50–6.53 (m, 1H), 6.61 (dd, *J* = 8.4, 3.8 Hz, 1H), 6.87 (d, *J* = 8.5 Hz, 1H), 7.02–7.17 (m, 5H), 7.30 (d, *J* = 7.5 Hz, 1H), 7.48 (t, *J* = 7.0 Hz, 1H), 7.64 (d, *J* = 8.9 Hz, 1H), 8.38 (br s, 1H); <sup>13</sup>C NMR (101 MHz, CDCl<sub>3</sub>, only the peaks for the major rotamer are given): δ 19.71, 20.21, 22.93, 25.64, 25.76, 26.01, 26.11, 26.94, 28.68, 29.24, 29.35, 29.42, 29.66, 29.72, 29.78, 29.91, 30.13, 31.56, 33.63, 35.29, 40.65, 42.73, 47.74, 48.99, 53.76, 54.91, 60.25, 60.40, 67.98, 70.84, 70.97, 76.37, 103.06, 107.83, 108.02, 108.07, 109.96, 111.49, 116.76, 126.34, 127.23, 128.83, 129.20, 130.16, 132.62, 136.24, 136.76, 137.53, 147.13, 158.04, 160.56, 167.77, 168.51, 169.66, 171.19, 172.73, 175.39; HPLC (95% H<sub>2</sub>O (with 0.1% TFA) to 95% MeCN in 10 min, then 95% MeCN for 4 min), *t*<sub>R</sub> = 8.60 min, 99% purity, detection at 254 nm; HRMS (ESI) *m/z*: [M + H]<sup>+</sup> calcd for C<sub>62</sub>H<sub>80</sub>O<sub>11</sub>N<sub>7</sub>, 1104.6380; found, 1104.6396.

(2*S*,4*S*)-1-((*S*)-2-Cyclohexyl-2-((*S*)-2-(methylamino)propanamido)acetyl)-4-(3-((6-((6-((2-(2,6-dioxopiperidin-3-yl)-1,3-dioxoisindolin-4-yl)amino)hexyl)oxy)hexyl)oxy)hexyl)oxy)phenoxy)-*N*-((*R*)-1,2,3,4-tetrahydronaphthalen-1-yl)pyrrolidine-2-carboxamide (PROTAC 27) (SAB142). This compound was prepared using general procedure VII and PROTAC precursor 133 (50 mg, 41 μmol). The crude product was purified by column chromatography (CH<sub>2</sub>Cl<sub>2</sub>/MeOH/NH<sub>4</sub>OH 15:1:0.1) to give a yellow solid. Yield (45 mg, 97%); *R*<sub>f</sub> = 0.25 (CH<sub>2</sub>Cl<sub>2</sub>/MeOH/NH<sub>4</sub>OH 15:1:0.1); mp 62–64 °C; <sup>1</sup>H NMR (400 MHz, CDCl<sub>3</sub>): δ 0.80–0.99 (m, 5H), 1.28 (d, *J* = 6.9 Hz, 3H), 1.33–1.51 (m, 12H), 1.51–1.70 (m, 17H), 1.72–1.84 (m, 6H), 1.99–2.07 (m, 1H), 2.08–2.15 (m, 1H), 2.36 (s, 3H), 2.69–2.81 (m, 4H), 2.83–2.91 (m, 2H), 3.05 (q, *J* = 6.8 Hz, 1H), 3.25 (d, *J* = 6.2 Hz, 2H), 3.38 (dd, *J* = 6.6, 2.5 Hz, 8H), 3.82 (d, *J* = 11.0 Hz, 1H), 3.87 (d, *J* = 6.5 Hz, 2H), 4.24 (dd, *J* = 11.5, 4.8 Hz, 1H), 4.43 (d, *J* = 8.2 Hz, 1H), 4.71–4.78 (m, 1H), 4.86–4.97 (m, 2H), 5.13 (d, *J* = 6.1 Hz, 1H), 6.22 (d, *J* = 5.6 Hz, 1H), 6.34–6.41 (m, 2H), 6.49–6.54 (m, 1H), 6.59–6.65 (m, 1H), 6.87 (d, *J* = 8.6 Hz, 1H), 7.02–7.17 (m, 5H), 7.27–7.31 (m, 1H), 7.48 (dd, *J* = 8.5, 7.1 Hz, 1H), 7.65 (d, *J* = 8.9 Hz, 1H), 8.31 (br s, 1H); <sup>13</sup>C NMR (101 MHz, CDCl<sub>3</sub>, only the peaks for the major rotamer are given): δ 19.68, 20.21, 22.94, 25.65, 25.76, 26.02, 26.11, 26.16, 26.23, 26.96, 28.69, 29.37, 29.43, 29.80, 29.85, 29.91, 30.14, 31.57, 33.66, 35.25, 40.66, 42.74, 47.75, 49.00, 53.77, 54.93, 60.27, 60.38, 68.05, 70.82, 70.94, 71.02, 71.05, 76.38, 103.08, 107.86, 108.02, 109.97, 111.50, 116.77, 126.35, 127.24, 128.84, 129.21, 130.17, 132.63, 136.25, 136.76, 137.54, 147.14, 158.04, 160.59, 167.78, 168.51, 169.64, 169.68, 171.17, 172.73, 175.32; HPLC (95% H<sub>2</sub>O (with 0.1% TFA) to 95% MeCN in 10 min, then 95% MeCN for 4 min), *t*<sub>R</sub> = 9.08 min, 99% purity, detection at 254 nm; HRMS (ESI) *m/z*: [M + H]<sup>+</sup> calcd for C<sub>64</sub>H<sub>90</sub>O<sub>11</sub>N<sub>7</sub>, 1132.6693; found, 1132.6669.

(2*S*,4*S*)-1-((*S*)-2-Cyclohexyl-2-((*S*)-2-(methylamino)propanamido)acetyl)-4-(3-(2-((6-((6-((2-(1-methyl-2,6-dioxopiperidin-3-yl)-1,3-dioxoisindolin-4-yl)amino)hexyl)oxy)hexyl)oxy)ethoxy)phenoxy)-*N*-((*R*)-1,2,3,4-tetrahydronaphthalen-1-yl)pyrrolidine-2-carboxamide (PROTAC 28). This compound was prepared using general procedure VII and PROTAC precursor 134 (65 mg, 55 μmol). The crude product was purified by column chromatography (CH<sub>2</sub>Cl<sub>2</sub>/MeOH/NH<sub>4</sub>OH 9:1:0.1) to give a yellow solid. Yield (41 mg, 69%); *R*<sub>f</sub> = 0.30 (CH<sub>2</sub>Cl<sub>2</sub>/MeOH/NH<sub>4</sub>OH 9:1:0.1); mp 58–61 °C; <sup>1</sup>H NMR (400 MHz, CDCl<sub>3</sub>): δ 0.79–0.99 (m, 5H), 1.28 (d, *J* = 6.9 Hz, 3H), 1.33–1.49 (m, 10H), 1.57 (s,



13H), 1.74–1.84 (m, 4H), 2.00–2.12 (m, 2H), 2.36 (s, 3H), 2.69–2.81 (m, 4H), 2.89 (d,  $J = 14.5$  Hz, 1H), 2.94–3.00 (m, 1H), 3.01–3.07 (m, 1H), 3.21 (s, 3H), 3.25 (q,  $J = 6.7$  Hz, 2H), 3.39 (td,  $J = 6.6, 2.7$  Hz, 4H), 3.51 (t,  $J = 6.7$  Hz, 2H), 3.73–3.77 (m, 2H), 3.82 (d,  $J = 11.4$  Hz, 1H), 4.04 (d,  $J = 4.9$  Hz, 2H), 4.25 (dd,  $J = 11.5, 4.8$  Hz, 1H), 4.41 (t,  $J = 8.2$  Hz, 1H), 4.76 (dd,  $J = 9.8, 2.1$  Hz, 1H), 4.87–4.96 (m, 2H), 5.13 (q,  $J = 7.0$  Hz, 1H), 6.22 (t,  $J = 5.6$  Hz, 1H), 6.37–6.44 (m, 2H), 6.53–6.57 (m, 1H), 6.59 (d,  $J = 8.5$  Hz, 1H), 6.87 (d,  $J = 8.5$  Hz, 1H), 7.03–7.19 (m, 5H), 7.29 (d,  $J = 7.7$  Hz, 1H), 7.45–7.51 (m, 1H), 7.64 (d,  $J = 8.9$  Hz, 1H);  $^{13}\text{C}$  NMR (101 MHz,  $\text{CDCl}_3$ , only the peaks for the major rotamer are given):  $\delta$  19.71, 20.20, 22.29, 25.64, 25.76, 26.01, 26.12, 26.22, 26.98, 27.40, 28.70, 29.39, 29.43, 29.77, 29.81, 29.86, 29.91, 30.14, 32.07, 33.59, 35.30, 40.64, 42.75, 47.74, 49.76, 53.80, 54.92, 60.24, 60.41, 67.57, 69.24, 70.85, 71.04, 71.74, 76.41, 103.15, 107.91, 108.50, 110.07, 111.44, 116.71, 126.37, 127.26, 128.81, 129.22, 130.20, 132.69, 136.19, 136.77, 137.54, 147.11, 157.98, 160.29, 167.94, 169.18, 169.61, 169.83, 171.40, 172.76, 175.27; HPLC (95%  $\text{H}_2\text{O}$  (with 0.1% TFA) to 95% MeCN in 10 min, then 95% MeCN for 4 min),  $t_{\text{R}} = 8.53$  min, 97% purity, detection at 254 nm; HRMS (ESI)  $m/z$ :  $[\text{M} + \text{H}]^+$  calcd for  $\text{C}_{61}\text{H}_{84}\text{O}_{11}\text{N}_7$ , 1090.6223; found, 1090.6203.

(2*S*,4*S*)-1-((*S*)-2-Cyclohexyl-2-((*S*)-2-(methylamino)propanamido)acetyl)-4-(3-((6-((2-(1-methyl-2,6-dioxopiperidin-3-yl)-1,3-dioxoisindolin-4-yl)amino)hexyl)oxy)hexyl)oxy)hexyl)oxy)phenoxy)-*N*-((*R*)-1,2,3,4-tetrahydronaphthalen-1-yl)pyrrolidine-2-carboxamide (PROTAC 29). This compound was prepared using general procedure VII and PROTAC precursor 135 (82 mg, 66  $\mu\text{mol}$ ). The crude product was purified by column chromatography ( $\text{CH}_2\text{Cl}_2/\text{MeOH}/\text{NH}_4\text{OH}$  20:1:0.1) to give a yellow solid. Yield (44 mg, 58%);  $R_{\text{f}} = 0.30$  ( $\text{CH}_2\text{Cl}_2/\text{MeOH}/\text{NH}_4\text{OH}$  20:1:0.1); mp 56–60  $^\circ\text{C}$ ;  $^1\text{H}$  NMR (400 MHz,  $\text{CDCl}_3$ ):  $\delta$  0.80–0.98 (m, 5H), 1.28 (d,  $J = 6.9$  Hz, 3H), 1.32–1.49 (m, 12H), 1.50–1.71 (m, 18H), 1.72–1.84 (m, 6H), 2.00–2.12 (m, 2H), 2.36 (s, 3H), 2.70–2.81 (m, 4H), 2.85–2.93 (m, 1H), 2.94–2.99 (m, 1H), 3.00–3.05 (m, 1H), 3.20 (s, 3H), 3.22–3.30 (m, 1H), 3.38 (dd,  $J = 6.6, 2.6$  Hz, 8H), 3.78–3.84 (m, 1H), 3.87 (t,  $J = 6.5$  Hz, 2H), 4.23 (dd,  $J = 11.5, 4.8$  Hz, 1H), 4.41 (d,  $J = 8.4$  Hz, 1H), 4.76 (dd,  $J = 9.8, 2.1$  Hz, 1H), 4.87–4.98 (m, 2H), 5.13 (d,  $J = 6.2$  Hz, 1H), 6.22 (d,  $J = 5.6$  Hz, 1H), 6.35–6.40 (m, 2H), 6.51–6.55 (m, 1H), 6.59 (d,  $J = 8.3$  Hz, 1H), 6.87 (d,  $J = 8.5$  Hz, 1H), 7.02–7.17 (m, 5H), 7.27–7.33 (m, 1H), 7.45–7.52 (m, 1H), 7.65 (d,  $J = 8.9$  Hz, 1H);  $^{13}\text{C}$  NMR (101 MHz,  $\text{CDCl}_3$ , only the peaks for the major rotamer are given):  $\delta$  19.59, 20.07, 22.16, 25.51, 25.62, 25.88, 25.98, 26.03, 26.03, 26.10, 26.85, 27.26, 28.56, 29.25, 29.30, 29.68, 29.74, 29.79, 30.00, 31.94, 33.52, 35.18, 40.53, 42.62, 47.62, 49.63, 53.67, 54.77, 60.14, 60.28, 67.92, 70.71, 70.82, 70.91, 76.29, 102.99, 107.76, 107.86, 111.31, 116.57, 126.23, 127.12, 128.68, 129.08, 130.04, 132.55, 136.06, 136.61, 137.40, 146.98, 157.88, 160.47, 167.81, 169.04, 169.50, 169.69, 171.26, 172.63, 175.17; HPLC (95%  $\text{H}_2\text{O}$  (with 0.1% TFA) to 95% MeCN in 10 min, then 95% MeCN for 4 min),  $t_{\text{R}} = 8.40$  min, 97% purity, detection at 254 nm; HRMS (ESI)  $m/z$ :  $[\text{M} + \text{H}]^+$  calcd for  $\text{C}_{63}\text{H}_{92}\text{O}_{11}\text{N}_7$ , 1146.6849; found, 1146.6812.

**Cell Lines.** All cell lines were obtained from ATCC (Manassas, Virginia, USA) and the German Collection of Microorganisms and Cell Cultures GmbH (DSMZ, Braunschweig, Germany) and maintained in RPMI-1640 medium (Merck KGaA, Darmstadt, Germany) containing 10% fetal bovine serum and supplemented with 1% penicillin/streptomycin and 1% L-glutamine. NCI-H929 cells were cultured in media supplemented with 2-mercaptoethanol and sodium pyruvate. Cells were maintained at 37  $^\circ\text{C}$  with 5%  $\text{CO}_2$  in a humidified atmosphere.

For generation of lentiviral vectors, HEK293T cells were transfected with constructs along with the packaging and envelope vectors. Viral supernatants were harvested 48 h after transfection and were used to transduce cell lines. MM1S and HG3 cells were transduced with virus containing pLKO5d.SSF.SpCas9.P2a.BSD, and cells were selected with blasticidin. Selected cells were then transduced with respective sgRNA constructs targeting VHL, cIAP1, cIAP2, XIAP, and negative control luciferase, which were cloned into pLKO5.hU6.sgRNA.dTom. Transduction success was confirmed

through FACS analysis 48 h post-transduction with a minimum efficiency of 95% tomato fluorescence.

**Immunoblotting.** Cells were treated with respective drugs for 16 h, and treated cells were washed and lysed in Pierce IP lysis buffer. SDS-PAGE was performed, and proteins were then transferred onto PVDF membranes. Blotted membranes were blocked with 5% milk in Tris-buffered saline/Tween20 (TBST). Primary antibodies were diluted in 5% BSA in TBST, and incubations were performed overnight at 4  $^\circ\text{C}$ . Secondary HRP-conjugated antibodies diluted in 5% milk were incubated for 1 h at room temperature. Detection of proteins on PVDF was carried out using the WesternBright ECL HRP substrate or the WesternBright Sirius HRP substrate (Advanta, San Jose, USA) and imaged with LAS 4000X (Fujifilm). Membranes were subjected to 10 min incubation with Restore Western Blot Stripping Buffer (Thermo Fisher Scientific, Waltham, USA), followed by TBST washes. After brief re-activation with methanol, the membranes were blocked, and further probing of proteins was carried out.

**Reagents and Antibodies.** LCL-161, AZD5363, birinapant, and BV6 were obtained from MedChemExpress. Human TNF- $\alpha$  was obtained from Miltenyi Biotec. MG132, MLN4924, and MLN7243 were purchased from SelleckChem.

Primary antibodies used for immunoblotting include BIRC2 (BioRad; VMA00532; clone AB01/3B4), cIAP2 (Cell Signaling; 3130S; clone 58C7), XIAP (Cell Signaling; 14334S; clone D2Z8W), VHL (Cell Signaling; 68547S), CRBN (Sigma-Aldrich; SAB2106014), Ikaros (Cell Signaling; 14859S; clone D6N9Y), Aiolos (Cell Signaling; 15103S; clone DIC1E), HIF-1 $\alpha$  (BD Biosciences, 610958; clone 54),  $\alpha$ -tubulin (Sigma-Aldrich; T5168; clone B512), and beta-actin (Sigma-Aldrich; A1978). Secondary antibodies include anti-rabbit IgG HRP-linked antibody (Cell Signaling; 7074) and anti-mouse IgG HRP-linked antibody (Cell Signaling; 7076).

**Cell Viability Assays.** Cells were seeded in 384-well plates with respective treatments, and plates were incubated at 37  $^\circ\text{C}$  for 96 h. Viability assays were performed with or without the addition of TNF- $\alpha$  at 1 ng/mL. The cell viability readout was measured using the CellTiter-Glo Luminescent Cell Viability Assay (Promega, Madison, USA) and measured with a Synergy LX Multi-Mode plate reader (BioTek, Vermont, USA). All conditions were normalized to the DMSO-treated control. Data represents the mean  $\pm$  SD of biological triplicates.

**Statistical Analysis.** Statistical and graphical analyses of cell viability experiments were performed with Prism version 9.1.0 (GraphPad Software, San Diego, CA, USA). Quantification of blots was performed using ImageJ software (National Institutes of Health).

**diaPASEF-Based Proteomics. Sample Preparation LFQ Quantitative Mass Spectrometry.** MM1S cells were treated with DMSO or 0.1  $\mu\text{M}$  of compound for 3 h. The cells were harvested by centrifugation and washed with phosphate-buffered saline before snap-freezing in liquid nitrogen. The cells were lysed by addition of lysis buffer (8 M urea, 50 mM NaCl, 50 mM 4-(2-hydroxyethyl)-1-piperazine-ethanesulfonic acid (EPPS) pH 8.5, protease, and phosphatase inhibitors) and homogenization by bead beating (BioSpec) for three repeats of 30 s at 2400. Bradford assay was used to determine the final protein concentration in the clarified cell lysate. 50  $\mu\text{g}$  of protein for each sample was reduced, alkylated, and precipitated using methanol/chloroform as previously described,<sup>64</sup> and the resulting washed precipitated protein was allowed to air dry. The precipitated protein was resuspended in 4 M urea, 50 mM HEPES pH 7.4, followed by dilution to 1 M urea with the addition of 200 mM EPPS, pH 8. Proteins were first digested with LysC (1:50; enzyme/protein) for 12 h at RT. The LysC digestion was diluted to 0.5 M urea with 200 mM EPPS pH 8, followed by digestion with trypsin (1:50; enzyme/protein) for 6 h at 37  $^\circ\text{C}$ . Sample digests were acidified with formic acid to a pH of 2–3 prior to desalting using C18 solid-phase extraction plates (SOLA, Thermo Fisher Scientific). Desalted peptides were dried in a vacuum centrifuge and reconstituted in 0.1% formic acid for LC–MS analysis.

Data were collected using a TimsTOF Pro2 (Bruker Daltonics, Bremen, Germany) coupled to a nanoElute LC pump (Bruker Daltonics, Bremen, Germany) via a CaptiveSpray nanoelectrospray



source. Peptides were separated on a reversed-phase C<sub>18</sub> column (25 cm × 75 μm ID, 1.6 μM, IonOpticks, Australia) containing an integrated captive spray emitter. Peptides were separated using a 50 min gradient of 2–30% buffer B (acetonitrile in 0.1% formic acid) with a flow rate of 250 nL/min and column temperature maintained at 50 °C.

Data-Dependent Acquisition (DDA) was performed in the Parallel Accumulation-Serial Fragmentation (PASEF) mode to determine effective ion mobility windows for downstream diaPASEF data collection.<sup>54</sup> The diaPASEF parameters included 100% duty cycle using accumulation and ramp times of 50 ms each, 1 TIMS-MS scan, and 10 PASEF ramps per acquisition cycle. The TIMS-MS survey scan was acquired between 100–1700 *m/z* and 1/*K*<sub>0</sub> of 0.7–1.3 V × s/cm<sup>2</sup>. Precursors with 1–5 charges were selected, and those that reached an intensity threshold of 20,000 arbitrary units were actively excluded for 0.4 min. The quadrupole isolation width was set to 2 *m/z* for *m/z* < 700 and 3 *m/z* for *m/z* > 800, with the *m/z* between 700 and 800 *m/z* being interpolated linearly. The TIMS elution voltages were calibrated linearly with three points (Agilent ESI-L Tuning Mix Ions; 622, 922, 1222 *m/z*) to determine the reduced ion mobility coefficients (1/*K*<sub>0</sub>). To perform diaPASEF, the precursor distribution in the DDA *m/z*-ion mobility plane was used to design an acquisition scheme for DIA data collection, which included two windows in each 50 ms diaPASEF scan. Data was acquired using 16 of these 25 Da precursor double window scans (creating 32 windows), which covered the diagonal scan line for doubly and triply charged precursors, with singly charged precursors able to be excluded by their position in the *m/z*-ion mobility plane. These precursor isolation windows were defined between 400–1200 *m/z* and 1/*K*<sub>0</sub> of 0.7–1.3 V × s/cm<sup>2</sup>.

**LC-MS Data Analysis.** The diaPASEF raw file processing and controlling peptide and protein level false discovery rates, assembling proteins from peptides, and protein quantification from peptides were performed using library-free analysis in DIA-NN 1.8.<sup>55</sup> The library-free mode performs an *in silico* digestion of a given protein sequence database alongside deep learning-based predictions to extract the DIA precursor data into a collection of MS<sup>2</sup> spectra. The search results are then used to generate a spectral library which is then employed for the targeted analysis of the DIA data searched against the Swiss-Prot human database (January 2021). Database search criteria largely followed the default settings for directDIA including tryptic with two missed cleavages, carbamidomethylation of cysteine, and oxidation of methionine and precursor *Q*-value (FDR) cut-off of 0.01. The precursor quantification strategy was set to Robust LC (high accuracy) with RT-dependent cross-run normalization. Proteins with poor-quality data were excluded from further analysis (summed abundance across channels of <100 and the mean number of precursors used for quantification <2), and proteins with missing values were imputed by random selection from a Gaussian distribution either with a mean of the non-missing values for that treatment group or with a mean equal to the median of the background (in cases when all values for a treatment group are missing). Protein abundances were scaled using in-house scripts in the R framework (R Development Core Team, 2014), and statistical analysis was carried out using the limma package within the R framework.

**Imputation Description.** Protein level data output from diaNN was read into R and processed using in-house scripts. Summary statistics were calculated for the replicates of each protein condition group. Missing values for each group were imputed by random selection from a Gaussian distribution with a mean of the non-missing values for that group. For protein condition groups missing all values, the values were imputed by random selection from a Gaussian distribution with a mean equal to the median of the background, defined as the lowest 1% of the dataset. The standard deviation of each distribution was based on the global relative standard deviation of the dataset, and each distribution was truncated to have a minimum value of 100 and a maximum of 1.2 times the maximum value in the entire dataset.

**Molecular Descriptor Calculations.** Predicted values for the topological polar surface area (TPSA) were calculated using MarvinSketch 17.28.0 (ChemAxon). Predicted values for the number of rotatable bonds were obtained using LigandScout 4.4.3.

**Log D Measurements.** The determination of the log *D*<sub>7.4</sub> values was performed by a chromatographic method as described previously.<sup>60,66</sup> The system was calibrated by plotting the retention times of six different drugs (atenolol, metoprolol, labetalol, diltiazem, triphenylene, and permethrin) versus their literature-known log *D*<sub>7.4</sub> in a calibration line (*R*<sup>2</sup> = 0.99). Subsequently, the mean retention times of the analytes were taken to calculate their log *D*<sub>7.4</sub> values with the aid of the calibration line. At least two independent measurements of each analyte were performed.

**Plasma Protein Binding Studies.** Plasma protein binding (% PPB) was estimated by correlating the logarithmic retention times of the analytes on a CHIRALPAK HSA 50 × 3 mm, 5 μm column with the literature-known % PPB values (converted into log *K* values) of the following drugs: warfarin, ketoprofen, budesonide, nizatidine, indomethacin, acetylsalicylic acid, carbamazepine, piroxicam, nicardipine, and cimetidine (for details, see Valko et al.).<sup>67</sup> The samples were dissolved in MeCN/DMSO 9:1 to achieve a final concentration of 0.5 mg/mL. Mobile phase A was 50 mM ammonium acetate adjusted to pH 7.4 with ammonia solution, while mobile phase B was *i*PrOH. The flow rate was set to 1.0 mL/min, the UV detector was set to 254 nm, and the column temperature was kept at 30 °C. After injecting 2 μL of the sample, a linear gradient from 100% A to 30% *i*PrOH in 5.4 min was applied. From 5.4 to 18 min, 30% *i*PrOH was kept, followed by switching back to 100% A in 1.0 min and a re-equilibration time of 6 min. With the aid of the calibration line (*R*<sup>2</sup> = 0.96), the log *K* values of new substances were calculated and converted to their % PPB values. At least two independent measurements of each analyte were performed.

## ■ ASSOCIATED CONTENT

### Supporting Information

The Supporting Information is available free of charge at <https://pubs.acs.org/doi/10.1021/acs.jmedchem.2c01817>.

Overview on physicochemical properties of compounds, selected NMR, HPLC, and MS spectra (PDF)

Recommended compound characterization checklist (XLSX)

Molecular formula strings (CSV)

Hitlist AZD5582 vs CTRLs (CSV)

Hitlist PROTAC 9 vs CTRLs (CSV)

Hitlist PROTAC 25 vs CTRLs (CSV)

Hitlist PROTAC 27 vs CTRLs (CSV)

Normalized raw abundances for 27 and pomalidomide (XLSX)

Raw precursor abundances for 27 and pomalidomide (XLSX)

Normalized raw abundances for AZD5582, 9, 25, and pomalidomide (XLSX)

Raw precursor abundances for AZD5582, 9, 25, and pomalidomide (XLSX)

## ■ AUTHOR INFORMATION

### Corresponding Authors

Christian Steinebach – Pharmaceutical Institute, Department of Pharmaceutical & Medicinal Chemistry, University of Bonn, D-53121 Bonn, Germany; [orcid.org/0000-0001-5638-1955](https://orcid.org/0000-0001-5638-1955); Email: [c.steinebach@uni-bonn.de](mailto:c.steinebach@uni-bonn.de)

Izidor Sosič – Faculty of Pharmacy, University of Ljubljana, SI-1000 Ljubljana, Slovenia; [orcid.org/0000-0002-3370-4587](https://orcid.org/0000-0002-3370-4587); Email: [izidor.sosic@ffa.uni-lj.si](mailto:izidor.sosic@ffa.uni-lj.si)

## Authors

**Yuen Lam Dora Ng** – Department of Hematology, Oncology and Cancer Immunology, Charité—Universitätsmedizin Berlin, Corporate Member of Freie Universität Berlin and Humboldt-Universität zu Berlin, D-12203 Berlin, Germany

**Aleša Bricelj** – Faculty of Pharmacy, University of Ljubljana, SI-1000 Ljubljana, Slovenia

**Jacqueline A. Jansen** – Department of Hematology, Oncology and Cancer Immunology, Charité—Universitätsmedizin Berlin, Corporate Member of Freie Universität Berlin and Humboldt-Universität zu Berlin, D-12203 Berlin, Germany

**Arunima Murgai** – Department of Hematology, Oncology and Cancer Immunology, Charité—Universitätsmedizin Berlin, Corporate Member of Freie Universität Berlin and Humboldt-Universität zu Berlin, D-12203 Berlin, Germany; German Cancer Consortium (DKTK) Partner Site Berlin and German Cancer Research Center (DKFZ), D-69120 Heidelberg, Germany

**Kirsten Peter** – Department of Hematology, Oncology and Cancer Immunology, Charité—Universitätsmedizin Berlin, Corporate Member of Freie Universität Berlin and Humboldt-Universität zu Berlin, D-12203 Berlin, Germany

**Katherine A. Donovan** – Department of Cancer Biology, Dana-Farber Cancer Institute, Boston, Massachusetts 02215, United States; Department of Biological Chemistry and Molecular Pharmacology, Harvard Medical School, Boston, Massachusetts 02215, United States; [orcid.org/0000-0002-8539-5106](https://orcid.org/0000-0002-8539-5106)

**Michael Gütschow** – Pharmaceutical Institute, Department of Pharmaceutical & Medicinal Chemistry, University of Bonn, D-53121 Bonn, Germany; [orcid.org/0000-0002-9376-7897](https://orcid.org/0000-0002-9376-7897)

**Jan Krönke** – Department of Hematology, Oncology and Cancer Immunology, Charité—Universitätsmedizin Berlin, Corporate Member of Freie Universität Berlin and Humboldt-Universität zu Berlin, D-12203 Berlin, Germany; German Cancer Consortium (DKTK) Partner Site Berlin and German Cancer Research Center (DKFZ), D-69120 Heidelberg, Germany

Complete contact information is available at:

<https://pubs.acs.org/10.1021/acs.jmedchem.2c01817>

## Author Contributions

<sup>†</sup>Y.L.D.N. and A.B. contributed equally. M.G., J.K., C.S., and I.S. contributed to conceptualization; Y.L.D.N., A.B., K.A.D., and C.S. contributed to methodology; Y.L.D.N., J.A.J., A.M., K.P., and K.A.D. contributed to validation; Y.L.D.N., J.A.J., A.M., and K.A.D. contributed to formal analysis; Y.L.D.N., J.A.J., A.M., K.P., K.A.D., C.S., and I.S. contributed to investigation; M.G., J.K., C.S., and I.S. contributed to resources; C.S. and I.S. contributed to data curation; C.S. and I.S. contributed to writing—original draft; A.B., C.S., and I.S. contributed to writing—review and editing; Y.L.D.N., A.B., J.A.J., A.M., C.S., and I.S. contributed to visualization; M.G., J.K., C.S., and I.S. contributed to supervision; C.S. and I.S. contributed to project administration; and M.G., J.K., and I.S. contributed to funding acquisition.

## Funding

We acknowledge the support by the Slovenian Research Agency (ARRS) (Program P1-0208 and grant J1-2485 to I.S.) and the DFG (Emmy-Noether Program Kr-3886/2-1 and SFB-1074 to J.K.).

## Notes

The authors declare the following competing financial interest(s): K.A.D. is a consultant to Kronos Bio and Neomorph Inc. All other authors declare no competing financial interest.

A preprint version of this study was posted on ChemRxiv preprint server.<sup>68</sup> While this manuscript was under consideration for publication, related pan-IAP degraders hijacking CRBN were published by S. Park and colleagues.<sup>69</sup>

## ACKNOWLEDGMENTS

We thank Maja Freljh for the HRMS measurements. We also thank Eric Fischer and the Fischer Lab Degradation Proteomics Initiative for the collection of the global proteomics data supported by NIH CA214608 and CA218278.

## ABBREVIATIONS

AML, acute myeloid leukemia; BAIB, (diacetoxyiodo)benzene; BIR, baculoviral IAP repeat; cIAP, cellular IAP; CRBN, cereblon; DCC, *N,N'*-dicyclohexylcarbodiimide; DEAD, diethyl azodicarboxylate; DIPEA, *N,N*-diisopropylethylamine; DLBCL, diffuse large B-cell lymphoma; DMAP, 4-dimethylaminopyridine; DMF, dimethylformamide; DMSO, dimethyl sulfoxide; HATU, 1-[bis(dimethylamino)methylene]-1*H*-1,2,3-triazolo[4,5-*b*]pyridinium 3-oxide hexafluorophosphate; HIF, hypoxia-inducible factor; HPLC, high-performance liquid chromatography; IAP, inhibitor of apoptosis; IKZF1, zinc finger protein Ikaros; IKZF3, zinc finger protein Aiolos; LC-MS, liquid chromatography–mass spectrometry; MDM2, murine double minute 2; MM, multiple myeloma; NMR, nuclear magnetic resonance; PROTAC, proteolysis targeting chimera; PS-TPP, polymer-bound triphenylphosphine; RING, really interesting new gene; SMAC, second mitochondria-derived activator of caspases; TBAHS, tetrabutylammonium hydrogen sulfate; TEMPO, (2,2,6,6-tetramethylpiperidin-1-yl)oxyl; TFA, trifluoroacetic acid; THP, tetrahydropyran; TLC, thin-layer chromatography; TNF- $\alpha$ , tumor necrosis factor alpha; VHL, von Hippel-Lindau; XIAP, X-chromosome-linked IAP

## REFERENCES

- (1) Luh, L. M.; Scheib, U.; Juenemann, K.; Wortmann, L.; Brands, M.; Cromm, P. M. Prey for the Proteasome: Targeted Protein Degradation—A Medicinal Chemist's Perspective. *Angew. Chem., Int. Ed.* **2020**, *59*, 15448–15466.
- (2) Nalawansa, D. A.; Crews, C. M. PROTACs: An Emerging Therapeutic Modality in Precision Medicine. *Cell Chem. Biol.* **2020**, *27*, 998–1014.
- (3) Naito, M. Targeted Protein Degradation and Drug Discovery. *J. Biochem.* **2022**, *172*, 61–69.
- (4) Mullard, A. Targeted Protein Degradation Crowds into the Clinic. *Nat. Rev. Drug Discovery* **2021**, *20*, 247–250.
- (5) Li, K.; Crews, C. M. PROTACs: Past, Present and Future. *Chem. Soc. Rev.* **2022**, *51*, 5214–5236.
- (6) Békés, M.; Langley, D. R.; Crews, C. M. PROTAC Targeted Protein Degradation: The Past Is Prologue. *Nat. Rev. Drug Discovery* **2022**, *21*, 181–200.
- (7) Chamberlain, P. P.; Hamann, L. G. Development of Targeted Protein Degradation Therapeutics. *Nat. Chem. Biol.* **2019**, *15*, 937–944.
- (8) Burslem, G. M.; Crews, C. M. Proteolysis-Targeting Chimeras as Therapeutics and Tools for Biological Discovery. *Cell* **2020**, *181*, 102–114.
- (9) Maneiro, M.; De Vita, E.; Conole, D.; Kounde, C. S.; Zhang, Q.; Tate, E. W. PROTACs, Molecular Glues and Bifunctionals from



- Bench to Bedside: Unlocking the Clinical Potential of Catalytic Drugs. *Prog. Med. Chem.* **2021**, *60*, 67–190.
- (10) Zheng, N.; Shabek, N. Ubiquitin Ligases: Structure, Function, and Regulation. *Annu. Rev. Biochem.* **2017**, *86*, 129–157.
- (11) Bulatov, E.; Ciulli, A. Targeting Cullin–RING E3 Ubiquitin Ligases for Drug Discovery: Structure, Assembly and Small-Molecule Modulation. *Biochem. J.* **2015**, *467*, 365–386.
- (12) Burslem, G. M.; Crews, C. M. Small-Molecule Modulation of Protein Homeostasis. *Chem. Rev.* **2017**, *117*, 11269–11301.
- (13) Galdeano, C. Drugging the Undruggable: Targeting Challenging E3 Ligases for Personalized Medicine. *Future Med. Chem.* **2017**, *9*, 347–350.
- (14) Bulatov, E.; Zagidullin, A.; Valiullina, A.; Sayarova, R.; Rizvanov, A. Small Molecule Modulators of RING-Type E3 Ligases: MDM and Cullin Families as Targets. *Front. Pharmacol.* **2018**, *9*, 450.
- (15) Blaquiére, N.; Villemure, E.; Staben, S. T. Medicinal Chemistry of Inhibiting RING-Type E3 Ubiquitin Ligases. *J. Med. Chem.* **2020**, *63*, 7957–7985.
- (16) Steinebach, C.; Lindner, S.; Udeshi, N. D.; Mani, D. C.; Kehm, H.; Köpf, S.; Carr, S. A.; Gütschow, M.; Krönke, J. Homo-PROTACs for the Chemical Knockdown of Cereblon. *ACS Chem. Biol.* **2018**, *13*, 2771–2782.
- (17) Maniaci, C.; Hughes, S. J.; Testa, A.; Chen, W.; Lamont, D. J.; Rocha, S.; Alessi, D. R.; Romeo, R.; Ciulli, A. Homo-PROTACs: Bivalent Small-Molecule Dimerizers of the VHL E3 Ubiquitin Ligase to Induce Self-Degradation. *Nat. Commun.* **2017**, *8*, 830.
- (18) He, S.; Ma, J.; Fang, Y.; Liu, Y.; Wu, S.; Dong, G.; Wang, W.; Sheng, C. Homo-PROTAC Mediated Suicide of MDM2 to Treat Non-Small Cell Lung Cancer. *Acta Pharm. Sin. B* **2021**, *11*, 1617–1628.
- (19) Yan, J.; Li, T.; Miao, Z.; Wang, P.; Sheng, C.; Zhuang, C. Homobivalent, Trivalent, and Covalent PROTACs: Emerging Strategies for Protein Degradation. *J. Med. Chem.* **2022**, *65*, 8798–8827.
- (20) Steinebach, C.; Kehm, H.; Lindner, S.; Vu, L. P.; Köpf, S.; López Marmol, A.; Weiler, C.; Wagner, K. G.; Reichenzeller, M.; Krönke, J.; Gütschow, M. PROTAC-Mediated Crosstalk between E3 Ligases. *Chem. Commun.* **2019**, *55*, 1821–1824.
- (21) Girardini, M.; Maniaci, C.; Hughes, S. J.; Testa, A.; Ciulli, A. Cereblon versus VHL: Hijacking E3 Ligases against Each Other Using PROTACs. *Bioorg. Med. Chem.* **2019**, *27*, 2466–2479.
- (22) Li, Y.; Yang, J.; Aguilar, A.; McEachern, D.; Przybranowski, S.; Liu, L.; Yang, C.-Y.; Wang, M.; Han, X.; Wang, S. Discovery of MD-224 as a First-in-Class, Highly Potent, and Efficacious Proteolysis Targeting Chimera Murine Double Minute 2 Degradable Capable of Achieving Complete and Durable Tumor Regression. *J. Med. Chem.* **2019**, *62*, 448–466.
- (23) Wang, B.; Wu, S.; Liu, J.; Yang, K.; Xie, H.; Tang, W. Development of Selective Small Molecule MDM2 Degraders Based on Nutlin. *Eur. J. Med. Chem.* **2019**, *176*, 476–491.
- (24) Chen, H.; Nguyen, N. H.; Magtoto, C. M.; Cobbold, S. A.; Bidgood, G. M.; Meza Guzman, L. G.; Richardson, L. W.; Corbin, J.; Au, A. E.; Lechtenberg, B. C.; Feltham, R.; Sutherland, K. D.; Grohmann, C.; Nicholson, S. E.; Sleebs, B. E. Design and Characterization of a Heterobifunctional Degradable of KEAP1. *Redox Biol.* **2023**, *59*, 102552.
- (25) Du, G.; Jiang, J.; Henning, N. J.; Safaei, N.; Koide, E.; Nowak, R. P.; Donovan, K. A.; Yoon, H.; You, L.; Yue, H.; Eleuteri, N. A.; He, Z.; Li, Z.; Huang, H. T.; Che, J.; Nabet, B.; Zhang, T.; Fischer, E. S.; Gray, N. S. Exploring the Target Scope of KEAP1 E3 Ligase-Based PROTACs. *Cell Chem. Biol.* **2022**, *29*, 1470–1481.e31.
- (26) Salvesen, G. S.; Duckett, C. S. IAP Proteins: Blocking the Road to Death's Door. *Nat. Rev. Mol. Cell Biol.* **2002**, *3*, 401–410.
- (27) Deveraux, Q. L.; Reed, J. C. IAP Family Proteins—Suppressors of Apoptosis. *Genes Dev.* **1999**, *13*, 239–252.
- (28) Dubrez, L.; Berthelet, J.; Glorian, V. IAP Proteins as Targets for Drug Development in Oncology. *Oncotargets Ther.* **2013**, *6*, 1285–1304.
- (29) Fulda, S.; Vucic, D. Targeting IAP Proteins for Therapeutic Intervention in Cancer. *Nat. Rev. Drug Discovery* **2012**, *11*, 109–124.
- (30) Wu, G.; Chai, J.; Suber, T. L.; Wu, J.-W.; Du, C.; Wang, X.; Shi, Y. Structural Basis of IAP Recognition by Smac/DIABLO. *Nature* **2000**, *408*, 1008–1012.
- (31) Liu, Z.; Sun, C.; Olejniczak, E. T.; Meadows, R. P.; Betz, S. F.; Oost, T.; Herrmann, J.; Wu, J. C.; Fesik, S. W. Structural Basis for Binding of Smac/DIABLO to the XIAP BIR3 Domain. *Nature* **2000**, *408*, 1004–1008.
- (32) Chai, J.; Du, C.; Wu, J.-W.; Kyin, S.; Wang, X.; Shi, Y. Structural and Biochemical Basis of Apoptotic Activation by Smac/DIABLO. *Nature* **2000**, *406*, 855–862.
- (33) Du, C.; Fang, M.; Li, Y.; Li, L.; Wang, X. Smac, a Mitochondrial Protein That Promotes Cytochrome c-Dependent Caspase Activation by Eliminating IAP Inhibition. *Cell* **2000**, *102*, 33–42.
- (34) Verhagen, A. M.; Erkert, P. G.; Pakusch, M.; Silke, J.; Connolly, L. M.; Reid, G. E.; Moritz, R. L.; Simpson, R. J.; Vaux, D. L. Identification of DIABLO, a Mammalian Protein That Promotes Apoptosis by Binding to and Antagonizing IAP Proteins. *Cell* **2000**, *102*, 43–53.
- (35) Fulda, S. Promises and Challenges of Smac Mimetics as Cancer Therapeutics. *Clin. Cancer Res.* **2015**, *21*, 5030–5036.
- (36) Cong, H.; Xu, L.; Wu, Y.; Qu, Z.; Bian, T.; Zhang, W.; Xing, C.; Zhuang, C. Inhibitor of Apoptosis Protein (IAP) Antagonists in Anticancer Agent Discovery: Current Status and Perspectives. *J. Med. Chem.* **2019**, *62*, 5750–5772.
- (37) Morrish, E.; Brumatti, G.; Silke, J. Future Therapeutic Directions for Smac-Mimetics. *Cells* **2020**, *9*, 406.
- (38) Varfolomeev, E.; Blankenship, J. W.; Wayson, S. M.; Fedorova, A. V.; Kayagaki, N.; Garg, P.; Zobel, K.; Dynek, J. N.; Elliott, L. O.; Wallweber, H. J. A.; Flygare, J. A.; Fairbrother, W. J.; Deshayes, K.; Dixit, V. M.; Vucic, D. IAP Antagonists Induce Autoubiquitination of C-IAPs, NF- $\kappa$ B Activation, and TNF $\alpha$ -Dependent Apoptosis. *Cell* **2007**, *131*, 669–681.
- (39) Vince, J. E.; Wong, W. W.-L.; Khan, N.; Feltham, R.; Chau, D.; Ahmed, A. U.; Benetatos, C. A.; Chunduru, S. K.; Condon, S. M.; McKinlay, M.; Brink, R.; Leverkus, M.; Tergaonkar, V.; Schneider, P.; Callus, B. A.; Koentgen, F.; Vaux, D. L.; Silke, J. IAP Antagonists Target CIAP1 to Induce TNF $\alpha$ -Dependent Apoptosis. *Cell* **2007**, *131*, 682–693.
- (40) Dueber, E. C.; Schoeffler, A. J.; Lingel, A.; Elliott, J. M.; Fedorova, A. V.; Giannetti, A. M.; Zobel, K.; Maurer, B.; Varfolomeev, E.; Wu, P.; Wallweber, H. J. A.; Hymowitz, S. G.; Deshayes, K.; Vucic, D.; Fairbrother, W. J. Antagonists Induce a Conformational Change in CIAP1 That Promotes Autoubiquitination. *Science* **2011**, *334*, 376–380.
- (41) Feltham, R.; Bettjeman, B.; Budhidarmo, R.; Mace, P. D.; Shirley, S.; Condon, S. M.; Chunduru, S. K.; McKinlay, M. A.; Vaux, D. L.; Silke, J.; Day, C. L. Smac Mimetics Activate the E3 Ligase Activity of CIAP1 Protein by Promoting RING Domain Dimerization. *J. Biol. Chem.* **2011**, *286*, 17015–17028.
- (42) Naito, M.; Ohoka, N.; Shibata, N. SNIPERs—Hijacking IAP Activity to Induce Protein Degradation. *Drug Discovery Today: Technol.* **2019**, *31*, 35–42.
- (43) Ohoka, N.; Morita, Y.; Nagai, K.; Shimokawa, K.; Ujikawa, O.; Fujimori, I.; Ito, M.; Hayase, Y.; Okuhira, K.; Shibata, N.; Hattori, T.; Sameshima, T.; Sano, O.; Koyama, R.; Imaeda, Y.; Nara, H.; Cho, N.; Naito, M. Derivatization of Inhibitor of Apoptosis Protein (IAP) Ligands Yields Improved Inducers of Estrogen Receptor  $\alpha$  Degradation. *J. Biol. Chem.* **2018**, *293*, 6776–6790.
- (44) Troup, R. I.; Fallan, C.; Baud, M. G. J. Current Strategies for the Design of PROTAC Linkers: A Critical Review. *Explor Target Antitumor Ther.* **2020**, *1*, 273–312.
- (45) Bemis, T. A.; La Clair, J. J.; Burkart, M. D. Unraveling the Role of Linker Design in Proteolysis Targeting Chimeras: Miniperspective. *J. Med. Chem.* **2021**, *64*, 8042–8052.
- (46) Galdeano, C.; Gadd, M. S.; Soares, P.; Scalfidi, S.; Van Molle, I.; Birced, I.; Hewitt, S.; Dias, D. M.; Ciulli, A. Structure-Guided Design and Optimization of Small Molecules Targeting the Protein—

- Protein Interaction between the von Hippel–Lindau (VHL) E3 Ubiquitin Ligase and the Hypoxia Inducible Factor (HIF) Alpha Subunit with in Vitro Nanomolar Affinities. *J. Med. Chem.* **2014**, *57*, 8657–8663.
- (47) Han, X.; Wang, C.; Qin, C.; Xiang, W.; Fernandez-Salas, E.; Yang, C.-Y.; Wang, M.; Zhao, L.; Xu, T.; Chinnaswamy, K.; Delproposto, J.; Stuckey, J.; Wang, S. Discovery of ARD-69 as a Highly Potent Proteolysis Targeting Chimera (PROTAC) Degrader of Androgen Receptor (AR) for the Treatment of Prostate Cancer. *J. Med. Chem.* **2019**, *62*, 941–964.
- (48) Smith, B. E.; Wang, S. L.; Jaime-Figueroa, S.; Harbin, A.; Wang, J.; Hamman, B. D.; Crews, C. M. Differential PROTAC Substrate Specificity Dictated by Orientation of Recruited E3 Ligase. *Nat. Commun.* **2019**, *10*, 131.
- (49) Tovell, H.; Testa, A.; Maniaci, C.; Zhou, H.; Prescott, A. R.; Macartney, T.; Ciulli, A.; Alessi, D. R. Rapid and Reversible Knockdown of Endogenously Tagged Endosomal Proteins via an Optimized HaloPROTAC Degrader. *ACS Chem. Biol.* **2019**, *14*, 882–892.
- (50) Powell, C. E.; Du, G.; Bushman, J. W.; He, Z.; Zhang, T.; Fischer, E. S.; Gray, N. S. Selective Degradation-Inducing Probes for Studying Cereblon (CRBN) Biology. *RSC Med. Chem.* **2021**, *12*, 1381–1390.
- (51) Frost, J.; Rocha, S.; Ciulli, A. Von Hippel–Lindau (VHL) Small-Molecule Inhibitor Binding Increases Stability and Intracellular Levels of VHL Protein. *J. Biol. Chem.* **2021**, *297*, 100910.
- (52) Cecchini, C.; Pannilunghi, S.; Tardy, S.; Scapozza, L. From Conception to Development: Investigating PROTACs Features for Improved Cell Permeability and Successful Protein Degradation. *Front. Chem.* **2021**, *9*, 672267.
- (53) Oost, T. K.; Sun, C.; Armstrong, R. C.; Al-Assaad, A.-S.; Betz, S. F.; Deckwerth, T. L.; Ding, H.; Elmore, S. W.; Meadows, R. P.; Olejniczak, E. T.; Oleksijew, A.; Oltersdorf, T.; Rosenberg, S. H.; Shoemaker, A. R.; Tomaselli, K. J.; Zou, H.; Fesik, S. W. Discovery of Potent Antagonists of the Antiapoptotic Protein XIAP for the Treatment of Cancer. *J. Med. Chem.* **2004**, *47*, 4417–4426.
- (54) Meier, F.; Brunner, A.-D.; Frank, M.; Ha, A.; Bludau, I.; Voytik, E.; Kaspar-Schoenefeld, S.; Lubeck, M.; Raether, O.; Bache, N.; Aebersold, R.; Collins, B. C.; Röst, H. L.; Mann, M. DiaPASEF: Parallel Accumulation–Serial Fragmentation Combined with Data-Independent Acquisition. *Nat. Methods* **2020**, *17*, 1229–1236.
- (55) Petersen, S. L.; Wang, L.; Yalcin-Chin, A.; Li, L.; Peyton, M.; Minna, J.; Harran, P.; Wang, X. Autocrine TNF $\alpha$  Signaling Renders Human Cancer Cells Susceptible to Smac-Mimetic-Induced Apoptosis. *Cancer Cell* **2007**, *12*, 445–456.
- (56) Li, B.-X.; Wang, H.-B.; Qiu, M.-Z.; Luo, Q.-Y.; Yi, H.-J.; Yan, X.-L.; Pan, W.-T.; Yuan, L.-P.; Zhang, Y.-X.; Xu, J.-H.; Zhang, L.; Yang, D.-J. Novel Smac Mimetic APG-1387 Elicits Ovarian Cancer Cell Killing through TNF-Alpha, Ripoptosome and Autophagy Mediated Cell Death Pathway. *J. Exp. Clin. Cancer Res.* **2018**, *37*, 53.
- (57) Li, N.; Feng, L.; Han, H.-Q.; Yuan, J.; Qi, X.-K.; Lian, Y.-F.; Kuang, B.-H.; Zhang, Y.-C.; Deng, C.-C.; Zhang, H.-J.; Yao, Y.-Y.; Xu, M.; He, G.-P.; Zhao, B.-C.; Gao, L.; Feng, Q.-S.; Chen, L.-Z.; Yang, L.; Yang, D.; Zeng, Y.-X. A Novel Smac Mimetic APG-1387 Demonstrates Potent Antitumor Activity in Nasopharyngeal Carcinoma Cells by Inducing Apoptosis. *Cancer Lett.* **2016**, *381*, 14–22.
- (58) McComb, S.; Aguadé-Gorgorió, J.; Harder, L.; Marovca, B.; Cario, G.; Eckert, C.; Schrappe, M.; Stanulla, M.; von Stackelberg, A.; Bourquin, J.-P.; Bornhauser, B. C. Activation of Concurrent Apoptosis and Necroptosis by SMAC Mimetics for the Treatment of Refractory and Relapsed ALL. *Sci. Transl. Med.* **2016**, *8*, 339ra70.
- (59) Ward, G. A.; Lewis, E. J.; Ahn, J. S.; Johnson, C. N.; Lyons, J. F.; Martins, V.; Munck, J. M.; Rich, S. J.; Smyth, T.; Thompson, N. T.; Williams, P. A.; Wilsher, N. E.; Wallis, N. G.; Chessari, G. ASTX660, a Novel Non-Peptidomimetic Antagonist of CIAP1/2 and XIAP, Potently Induces TNF $\alpha$ -Dependent Apoptosis in Cancer Cell Lines and Inhibits Tumor Growth. *Mol. Cancer Ther.* **2018**, *17*, 1381–1391.
- (60) Steinebach, C.; Ng, Y. L. D.; Sosić, I.; Lee, C.-S.; Chen, S.; Lindner, S.; Vu, L. P.; Bricelj, A.; Haschemi, R.; Monschke, M.; Steinwarz, E.; Wagner, K. G.; Bendas, G.; Luo, J.; Gütschow, M.; Krönke, J. Systematic Exploration of Different E3 Ubiquitin Ligases: An Approach towards Potent and Selective CDK6 Degraders. *Chem. Sci.* **2020**, *11*, 3474–3486.
- (61) Raina, K.; Lu, J.; Qian, Y.; Altieri, M.; Gordon, D.; Rossi, A. M. K.; Wang, J.; Chen, X.; Dong, H.; Siu, K.; Winkler, J. D.; Crew, A. P.; Crews, C. M.; Coleman, K. G. PROTAC-Induced BET Protein Degradation as a Therapy for Castration-Resistant Prostate Cancer. *Proc. Natl. Acad. Sci. U.S.A.* **2016**, *113*, 7124–7129.
- (62) Hu, J.; Hu, B.; Wang, M.; Xu, F.; Miao, B.; Yang, C.-Y.; Wang, M.; Liu, Z.; Hayes, D. F.; Chinnaswamy, K.; Delproposto, J.; Stuckey, J.; Wang, S. Discovery of ERD-308 as a Highly Potent Proteolysis Targeting Chimera (PROTAC) Degrader of Estrogen Receptor (ER). *J. Med. Chem.* **2019**, *62*, 1420–1442.
- (63) Zengerle, M.; Chan, K.-H.; Ciulli, A. Selective Small Molecule Induced Degradation of the BET Bromodomain Protein BRD4. *ACS Chem. Biol.* **2015**, *10*, 1770–1777.
- (64) Donovan, K. A.; An, J.; Nowak, R. P.; Yuan, J. C.; Fink, E. C.; Berry, B. C.; Ebert, B. L.; Fischer, E. S. Thalidomide Promotes Degradation of SALL4, a Transcription Factor Implicated in Duane Radial Ray Syndrome. *Elife* **2018**, *7*, No. e38430.
- (65) Demichev, V.; Messner, C. B.; Vernardis, S. I.; Lilley, K. S.; Ralser, M. DIA-NN: neural networks and interference correction enable deep proteome coverage in high throughput. *Nat. Methods* **2020**, *17*, 41–44.
- (66) Kerns, E. H.; Di, L.; Petusky, S.; Kleintop, T.; Huryn, D.; McConnell, O.; Carter, G. Pharmaceutical Profiling Method for Lipophilicity and Integrity Using Liquid Chromatography–Mass Spectrometry. *J. Chromatogr. B* **2003**, *791*, 381–388.
- (67) Valko, K.; Nunhuck, S.; Bevan, C.; Abraham, M. H.; Reynolds, D. P. Fast Gradient HPLC Method to Determine Compounds Binding to Human Serum Albumin. Relationships with Octanol/Water and Immobilized Artificial Membrane Lipophilicity. *J. Pharm. Sci.* **2003**, *92*, 2236–2248.
- (68) Ng, Y. L. D.; Bricelj, A.; Jansen, J. A.; Murgai, A.; Gütschow, M.; Krönke, J.; Steinebach, C.; Sosić, I. Heterobifunctional Ligase Recruiters Enable Pan-Degradation of Inhibitor of Apoptosis Proteins. *Chemistry* **2022**, DOI: 10.26434/chemrxiv-2022-pt7gi.
- (69) Park, S.; Kim, D.; Lee, W.; Cho, J. H.; Kim, S.; Lee, G. S.; Moon, J. H.; Kim, J.-A.; Ha, J. D.; Kim, J.-H.; Kim, H. J. Discovery of Pan-IAP Degraders via a CRBN Recruiting Mechanism. *Eur. J. Med. Chem.* **2023**, *245*, 114910.

---

## Supplementary Information

### **Heterobifunctional Ligase Recruiters Enable Pan-Degradation of Inhibitor of Apoptosis Proteins**

Yuen Lam Dora Ng,<sup>+[a]</sup> Aleša Bricelj,<sup>+[b]</sup> Jacqueline A. Jansen,<sup>[a]</sup>  
Arunima Murgai,<sup>[a,c]</sup> Kirsten Peter,<sup>[a]</sup> Katherine A. Donovan,<sup>[d,e]</sup>  
Michael Gütschow,<sup>[f]</sup> Jan Krönke,<sup>[a,c]</sup> Christian Steinebach,<sup>\*[f]</sup> Izidor Sosič<sup>\*[b]</sup>

<sup>[a]</sup> Department of Hematology, Oncology and Cancer Immunology, Charité - Universitätsmedizin  
Berlin, corporate member of Freie Universität Berlin and Humboldt-Universität zu Berlin,  
D-12203 Berlin, Germany.

<sup>[b]</sup> Faculty of Pharmacy, University of Ljubljana,  
Aškerčeva cesta 7, SI-1000 Ljubljana, Slovenia.

<sup>[c]</sup> German Cancer Consortium (DKTK) partner site Berlin and German Cancer Research Center (DKFZ),  
D- 69120 Heidelberg, Germany

<sup>[d]</sup> Department of Cancer Biology, Dana-Farber Cancer Institute, Boston, MA 02215, USA

<sup>[e]</sup> Biological Chemistry and Molecular Pharmacology, Harvard Medical School, Boston, MA 02215,  
USA

<sup>[f]</sup> Pharmaceutical Institute, Department of Pharmaceutical & Medicinal Chemistry,  
University of Bonn, An der Immenburg 4, D-53121 Bonn, Germany.



## Table of Contents

<b>Supplementary Tables, Schemes, and Figures .....</b>	<b>3</b>
<b>Selected NMR and MS spectra .....</b>	<b>34</b>
<b>References.....</b>	<b>78</b>
<b>Table of Intermediates.....</b>	<b>79</b>

## Supplementary Tables, Schemes, and Figures

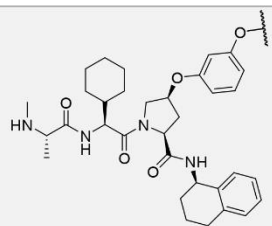
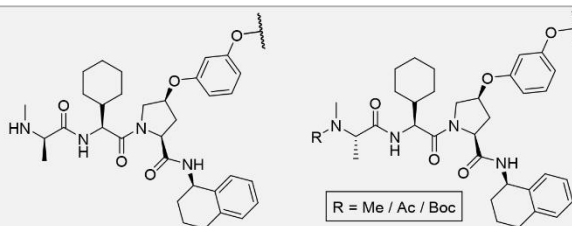
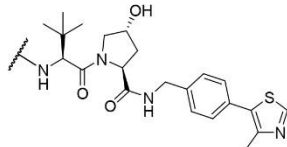
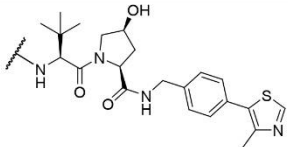
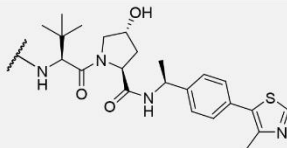
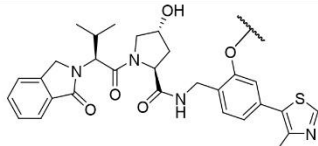
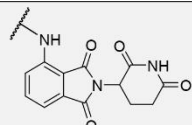
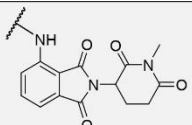
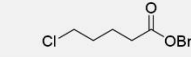
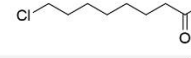
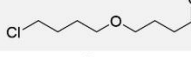

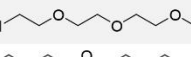



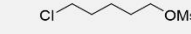
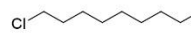
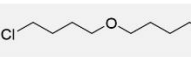
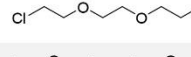
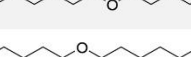
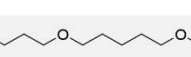
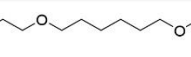

	E3 ligase ligands	Negative control ligands
IAP	 <p>IAP ligand</p>	 <p>(-) IAP ligands R = Me / Ac / Boc</p>
VHL1 Series	 <p>VHL1 ligand</p>	 <p>(-) VHL1 ligand</p>
	 <p>Me-VHL1 ligand</p>	--
VHL2 Series	 <p>VHL2 ligand</p>	--
CRBN Series	 <p>CRBN ligand</p>	 <p>(-) CRBN ligand</p>

Table S1. Overview of different E3 ligase ligands incorporated into final hetero-PROTACs.

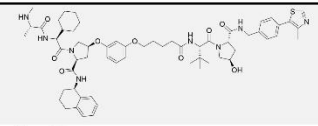
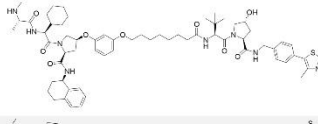
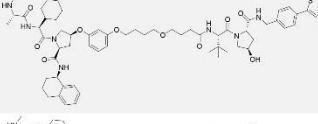
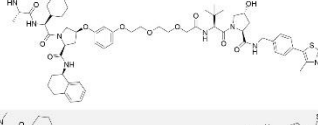
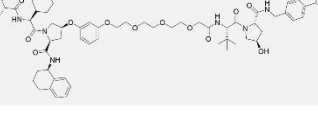
Linker	Pattern	Structure
L1a	5	
L2a	8	
L3a	4-4	
L4a	2-2-2	
L5a	2-2-2-2	
L6a	6-6-2	
L7a	6-5-5	
L8a	6-6-6	

**Table S2.** Structures of linkers used in the IAP-VHL Series 1 PROTACs.

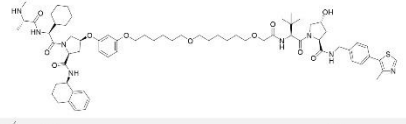
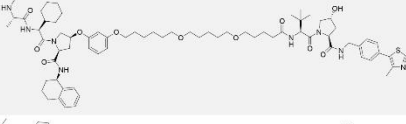
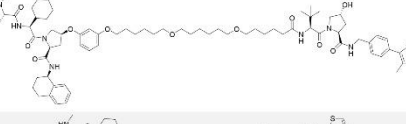
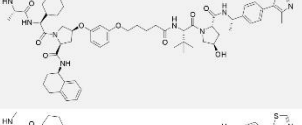
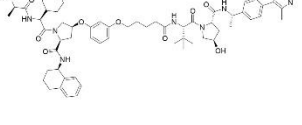
Linker	Pattern	Structure
L1b	5	
L2b	8	
L3b	4-4	
L4b	2-2-2	
L5b	2-2-2-2	
L6b	6-6-2	
L7b	6-5-5	
L8b	6-6-6	

**Table S3.** Structures of linkers used in the IAP-VHL Series 2 and IAP-CRBN Series PROTACs.

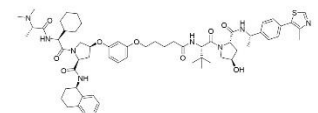
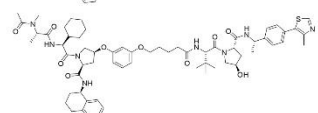
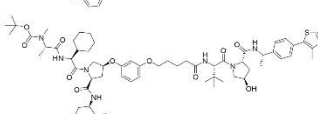
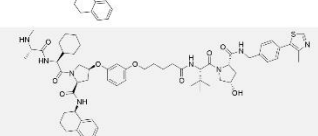


Cmpd	MW (g/mol)	logD <sup>a</sup>	PPB <sup>b</sup> (%)	TPSA <sup>c</sup> (Å <sup>2</sup> )	NRotB <sup>d</sup>	HBD <sup>e</sup>	HBA <sup>f</sup>	Structure
1	1089	3.8	96	249	29	6	11	
2	1131	4.4	96	249	32	6	11	
3	1147	4.0	95	258	33	6	12	
4	1135	3.7	95	267	32	6	13	
5	1179	3.7	94	277	35	6	14	

S5

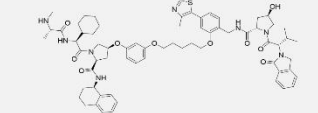
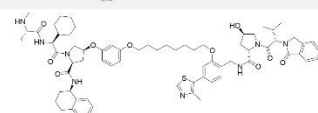
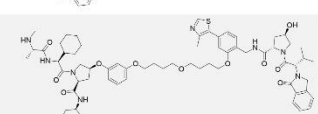
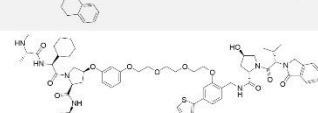
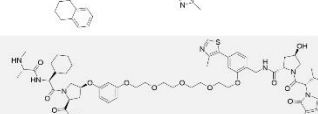
6	1247	5.5	n.d.	267	40	6	13	
7	1276	5.3	96	267	42	6	13	
8	1304	5.8	n.d. <sup>g</sup>	267	44	6	13	
9 (CST626)	1103	3.4	95	249	30	6	11	
10a	1103	3.2	n.d.	249	30	6	11	

S6

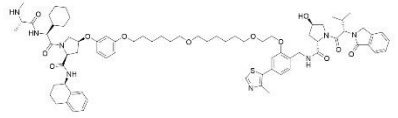
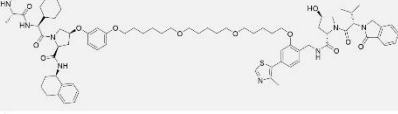
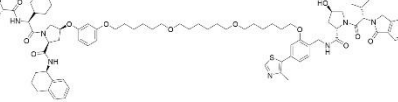
<b>10b</b>	1117	n.d.	n.d.	212	31	5	10	
<b>10c</b>	1145	n.d.	n.d.	229	31	5	11	
<b>10d (115)</b>	1204	n.d.	n.d.	238	31	5	11	
<b>11</b>	1089	3.3	n.d.	249	29	6	11	

**Table S4.** Overview on synthesized hetero-PROTACs: IAP-VHL series 1. <sup>a</sup> Experimental partition coefficient at pH 7.4 determined by a fast-gradient HPLC method. <sup>b</sup> Plasma protein binding (PPB) values were estimated by an HPLC-based method. <sup>c</sup> Topological polar surface area is given in Å<sup>2</sup>. <sup>d</sup> Number of rotatable bonds. Values were obtained using LigandScout 4.4.3. <sup>e</sup> Number of hydrogen bond donors. <sup>f</sup> Number of hydrogen bond acceptors. <sup>g</sup> Not determined. Very lipophilic compounds (logD > 5.5) may cause damage to the HSA column.

S7

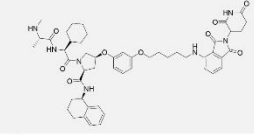
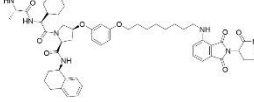
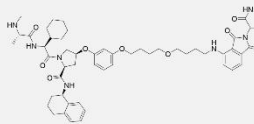
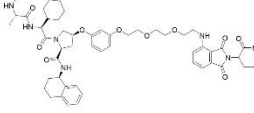
Cmpd	MW (g/mol)	logD <sup>g</sup>	PPB <sup>b</sup> (%)	TPSA <sup>c</sup> (Å <sup>2</sup> )	NRotB <sup>d</sup>	HBD <sup>e</sup>	HBA <sup>f</sup>	Structure
<b>12</b>	1193	4.0	96	249	30	5	12	
<b>13</b>	1235	4.8	97	249	33	8	12	
<b>14</b>	1252	4.2	96	259	34	5	13	
<b>15</b>	1240	3.4	95	268	33	5	14	
<b>16</b>	1284	3.3	95	277	36	5	15	

S8

17	1352	5.2	97	268	41	5	14	
18	1380	5.6	n.d.	268	43	5	14	
19	1408	6.3	n.d.	268	45	5	14	

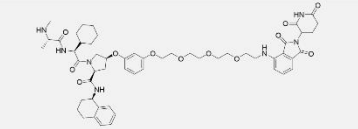
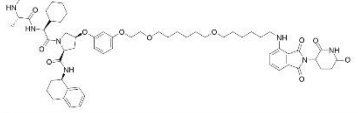

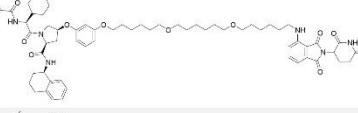
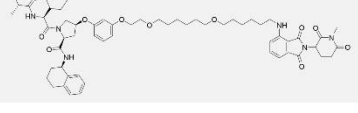
**Table S5.** Overview on synthesized hetero-PROTACs: IAP-VHL series 2. <sup>a</sup> Experimental partition coefficient at pH 7.4 determined by a fast-gradient HPLC method. <sup>b</sup> Plasma protein binding (PPB) values were estimated by an HPLC-based method. <sup>c</sup> Topological polar surface area is given in Å<sup>2</sup>. <sup>d</sup> Number of rotatable bonds. Values were obtained using LigandScout 4.4.3. <sup>e</sup> Number of hydrogen bond donors. <sup>f</sup> Number of hydrogen bond acceptors. <sup>g</sup> Not determined. Very lipophilic compounds (logD > 5.5) may cause damage to the HSA column.

S9

Cmpd	MW (g/mol)	logD <sup>a</sup>	PPB <sup>b</sup> (%)	TPSA <sup>c</sup> (Å <sup>2</sup> )	NRotB <sup>d</sup>	HBD <sup>e</sup>	HBA <sup>f</sup>	Structure
20	918	4.6	96	204	20	5	10	
21	960	5.7	n.d.	204	23	5	10	
22	976	4.9	96	213	24	5	11	
23	964	3.9	95	223	23	5	12	

S10



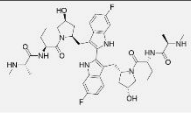
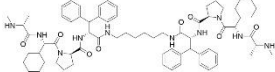
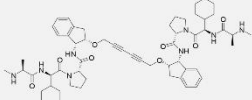
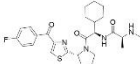
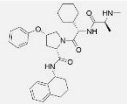
24	1008	3.9	94	232	26	5	13	
25 (SAB141)	1076	6.0	n.d.	223	31	5	12	
26	1104	6.5	n.d.	223	33	5	12	
27 (SAB142)	1132	7.2	n.d.	223	35	5	12	
28	1090	6.0	n.d.	214	32	4	12	

S11

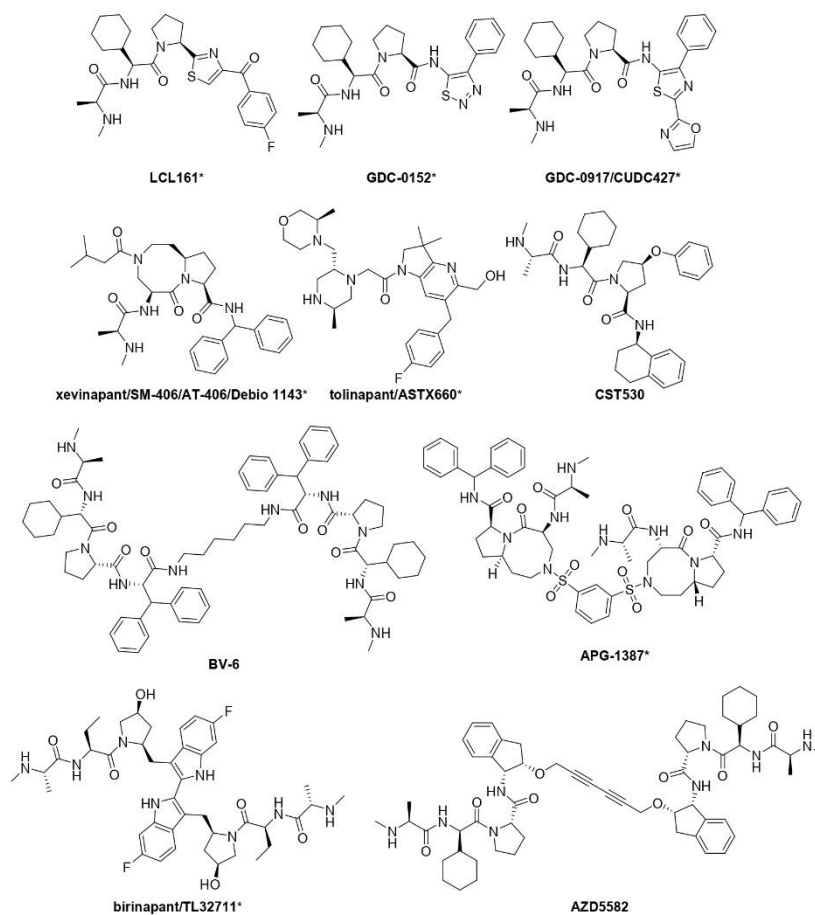
29	1146	7.4	n.d.	214	36	4	12	
----	------	-----	------	-----	----	---	----	--

**Table S6.** Overview on synthesized hetero-PROTACs: IAP-CRBN series. <sup>a</sup> Experimental partition coefficient at pH 7.4 determined by a fast-gradient HPLC method. <sup>b</sup> Plasma protein binding (PPB) values were estimated by an HPLC-based method. <sup>c</sup> Topological polar surface area is given in Å<sup>2</sup>. <sup>d</sup> Number of rotatable bonds. Values were obtained using LigandScout 4.4.3. <sup>e</sup> Number of hydrogen bond donors. <sup>f</sup> Number of hydrogen bond acceptors. <sup>g</sup> Not determined. Very lipophilic compounds (logD > 5.5) may cause damage to the HSA column.

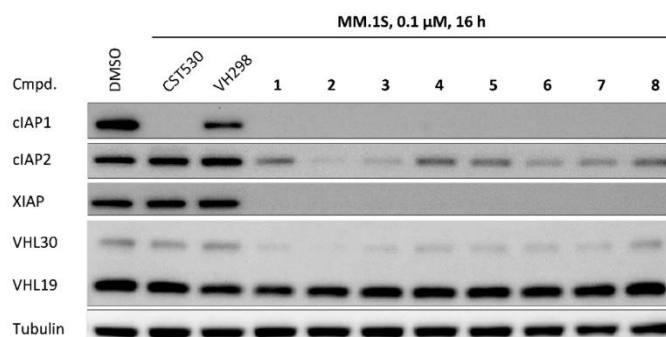
S12

Cmpd	MW (g/mol)	logD <sup>a</sup>	PPB <sup>b</sup> (%)	TPSA <sup>c</sup> (Å <sup>2</sup> )	NRotB <sup>d</sup>	HBD <sup>e</sup>	HBA <sup>f</sup>	Structure
Birinapant	807	3.4	95	195	23	8	10	
BV6	1206	3.4	n.d. <sup>g</sup>	239	33	8	10	
AZD5582	1015	4.1	94	200	22	6	10	
LCL161	501	3.3	88	138	10	2	6	
CST530	561	3.1	94	163	11	3	5	

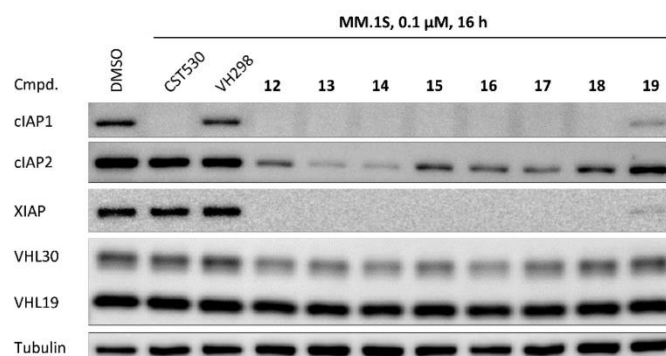
**Table S7.** Overview on mono- and bivalent SMAC mimetics. <sup>a</sup> Experimental partition coefficient at pH 7.4 determined by a fast-gradient HPLC method. <sup>b</sup> Plasma protein binding (PPB) values were estimated by an HPLC-based method. <sup>c</sup> Topological polar surface area is given in Å<sup>2</sup>. <sup>d</sup> Number of rotatable bonds. Values were obtained using LigandScout 4.4.3. <sup>e</sup> Number of hydrogen bond donors. <sup>f</sup> Number of hydrogen bond acceptors. <sup>g</sup> Not determined.



**Figure S1.** The most promising small molecules targeting IAPs are mimicking the IAP-binding motif of SMAC. Compounds that entered clinical trials are marked with an asterisk (please note that AEG40826 and BI 891065 are two additional clinically evaluated SMAC mimetics, but their structures are undisclosed). SMAC mimetics bind to XIAP, cIAP1, and cIAP2 and antagonize their functions, *e.g.* association with caspases and with regulators of the nuclear factor- $\kappa$ B signaling pathways.<sup>1-3</sup> They also prevent XIAP-mediated inhibition of caspases-3/7/9.<sup>4</sup> Bivalent IAP antagonists are composed of two monovalent units that are connected through a linker. Since these can bind to two IAP proteins they are better at triggering dimerization and autodegradation of cIAPs.<sup>5-7</sup> Moreover, they generally display higher binding affinities than monovalent compounds for IAPs.<sup>4,8,9</sup>

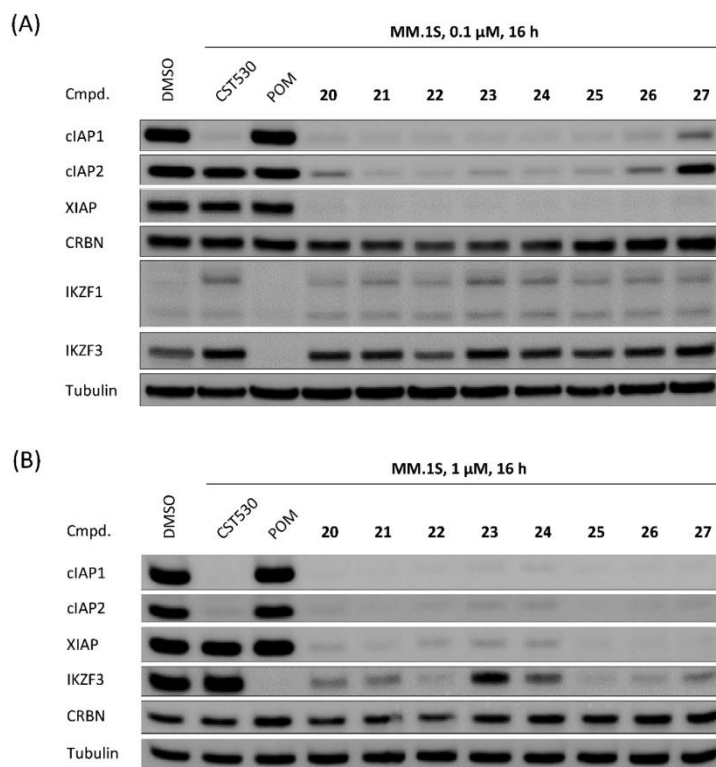


**Figure S2.** IAP-VHL Series 1 hetero-PROTACs induce strong cIAP1, cIAP2 (in certain cases), XIAP, as well as VHL30 degradation. MM.1S cells were treated for 16 h with 0.1  $\mu$ M IAP ligand CST530, VHL ligand VH298, and hetero-PROTACs **1-8**.

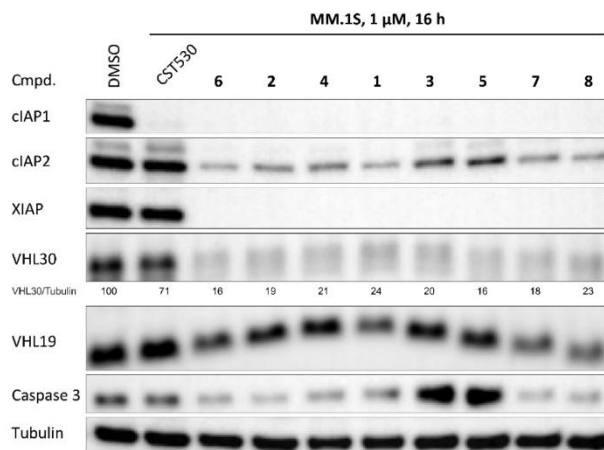


**Figure S3.** IAP-VHL Series 2 hetero-PROTACs induce strong cIAP1, cIAP2 (in certain cases), and XIAP degradation. MM.1S cells were treated for 16 h with 0.1  $\mu$ M IAP ligand CST530, VHL ligand VH298, and hetero-PROTACs **12-19**.

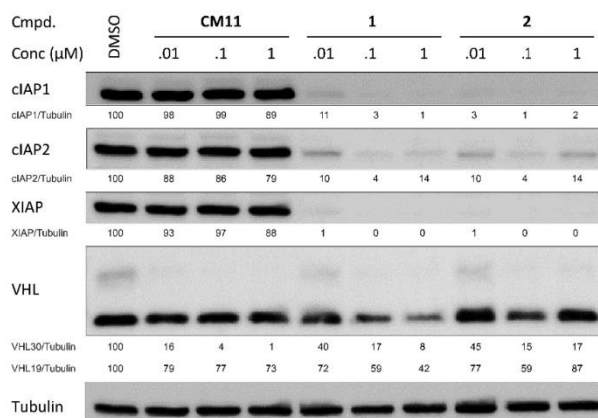




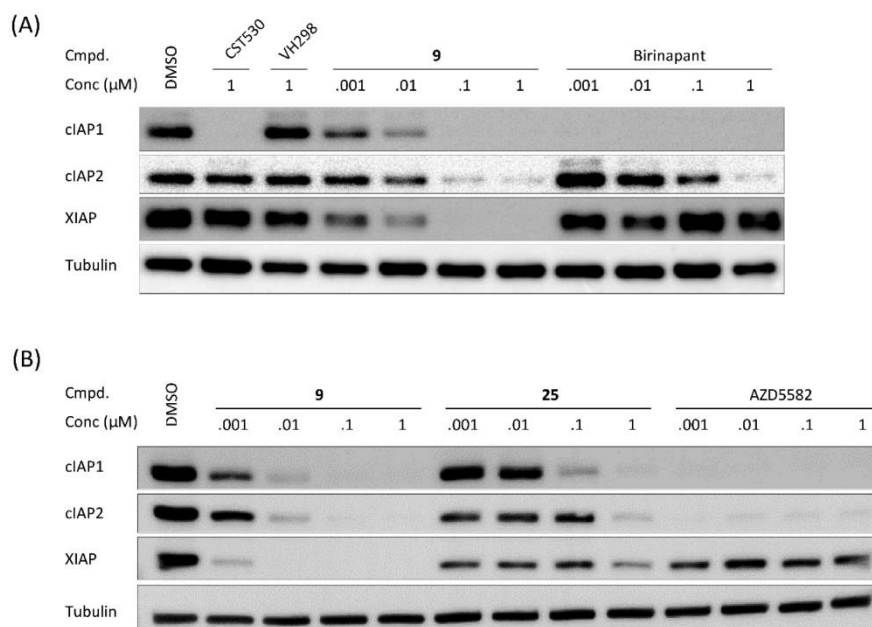
**Figure S4.** IAP-CRBN hetero-PROTACs induce strong degradation of IAPs. MM.1S cells were treated for 16 h with 0.1  $\mu$ M (A) or 1  $\mu$ M (B) IAP ligand CST530, VHL ligand VH298, and hetero-PROTACs **20-27**.



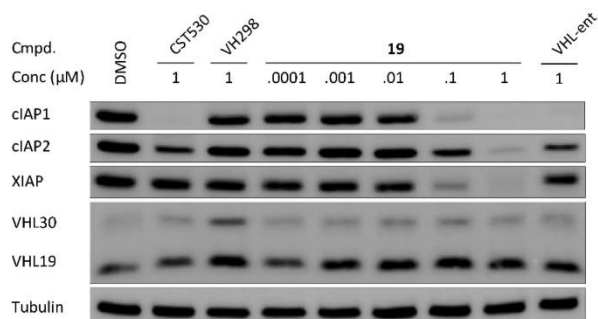
**Figure S5.** IAP-VHL Series 1 hetero-PROTACs **1-8** strongly degrade cIAP1 and XIAP, as well as VHL30 at 1  $\mu$ M. MM.1S cells were treated with compounds for 16 h.



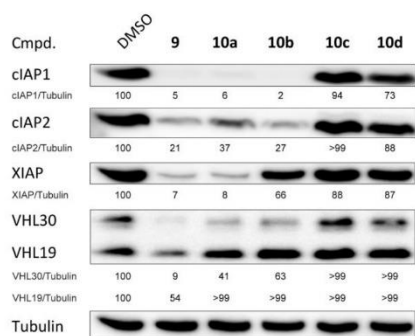
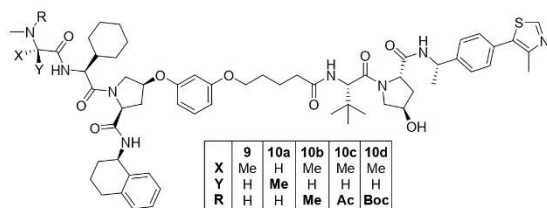
**Figure S6.** CM11 and hetero-PROTACs **1** and **2** induce strong and dose-dependent VHL30 degradation. A slight hook effect for VHL19 degradation is seen for hetero-PROTAC **2**. MM.1S cells were treated with PROTACs at indicated concentrations for 16 h.



**Figure S7.** (A) Hetero-PROTAC **9** depletes clAP2 more potently than birinapant, and induces XIAP degradation. MM.1S cells were treated with **9** and birinapant at indicated concentrations for 16 h. (B) AZD5582 potently degrades both clAPs, but does not have an influence on XIAP levels. MM.1S cells were treated with hetero-PROTACs and AZD5582 at indicated concentrations for 16 h.

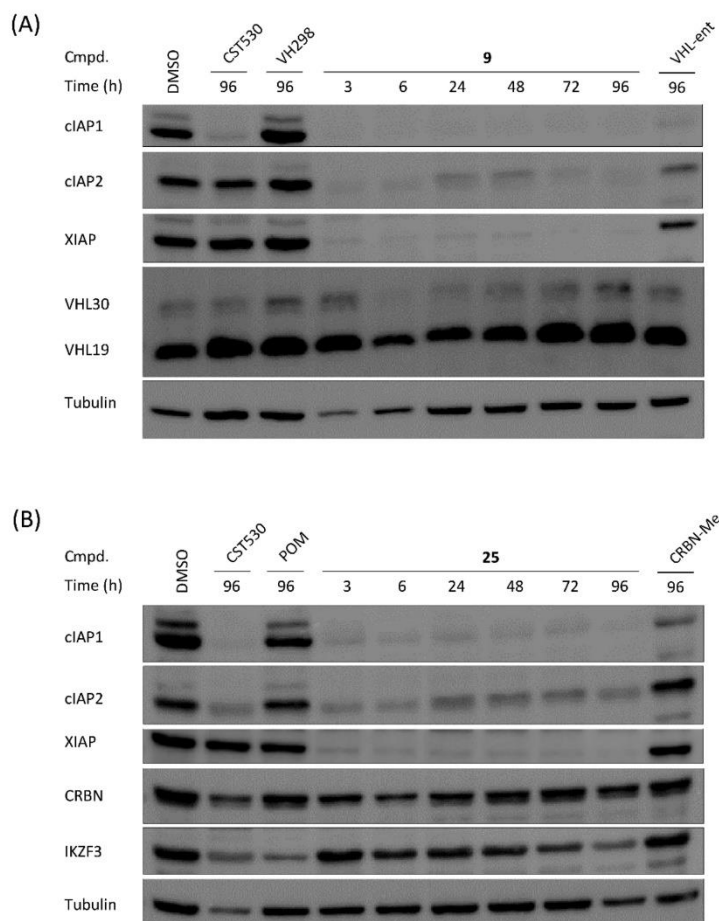


**Figure S8.** IAP-VHL hetero-PROTAC **19** induces IAPs degradation in a dose-dependent manner. MM.1S cells were treated with **19** at indicated concentrations for 16 h.

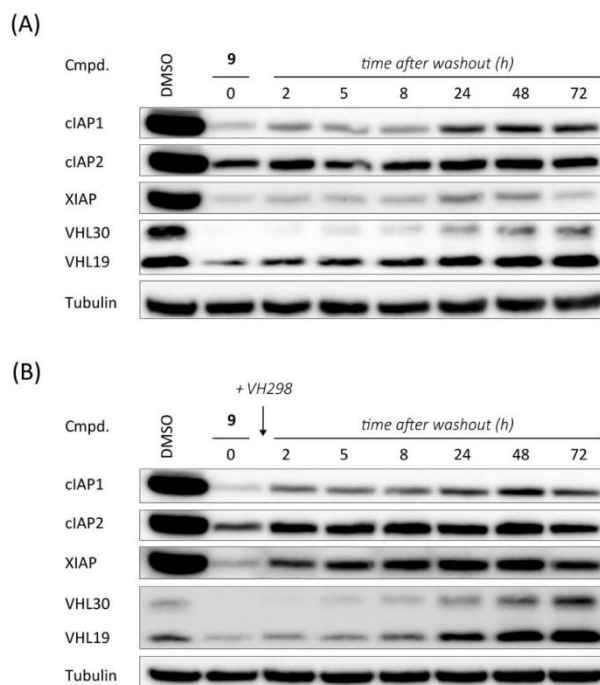


**Figure S9.** Testing of the IAP-VHL hetero-PROTAC **9** (CST626) and a series of putative IAP non-binding control compounds (**10a–10d**). MM.1S cells were treated with compounds at 1 μM for 16 h. Quantification in this representative blot refers to mean of replicates (n=3).

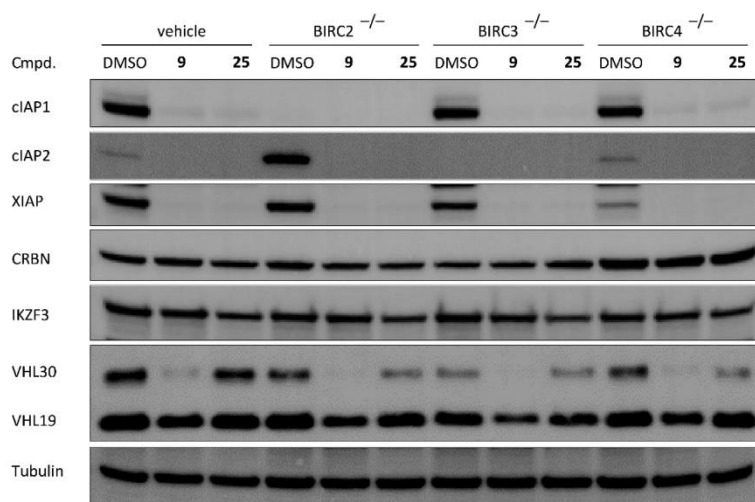




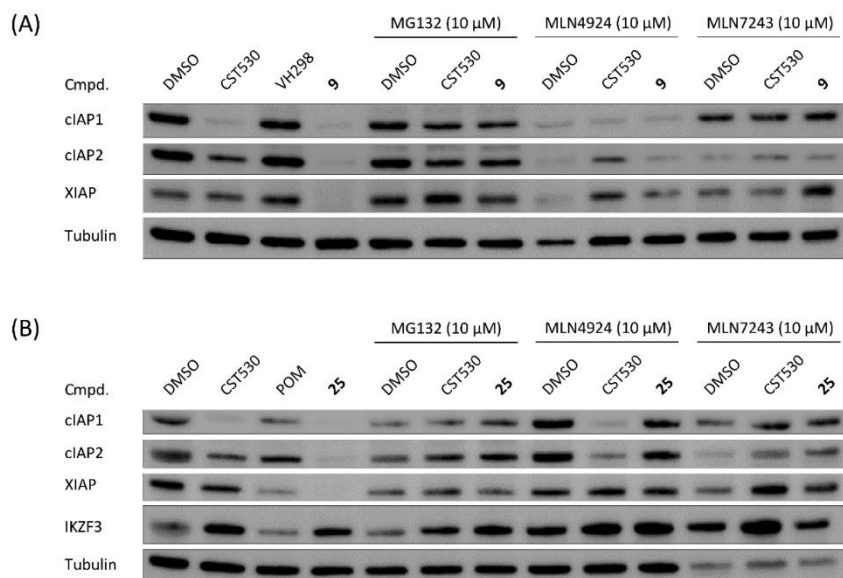
**Figure S10.** (A) Time course experiment with hetero-PROTAC **9**. MM.1S cells were treated with compounds at 0.1  $\mu$ M for the indicated time. (B) Time course experiment with hetero-PROTAC **25**. MM.1S cells were treated with compounds at 0.1  $\mu$ M for the indicated time.



**Figure S11.** Persisting effects of hetero-PROTAC **9** on IAPs degradation after compound washout from the cell medium. MM.1S cells were treated with **9** at 1  $\mu$ M for 16 h before washout (= 0 h), and then kept in plain media (A) in the absence or (B) in the presence of 1  $\mu$ M VH298 until indicated time points.

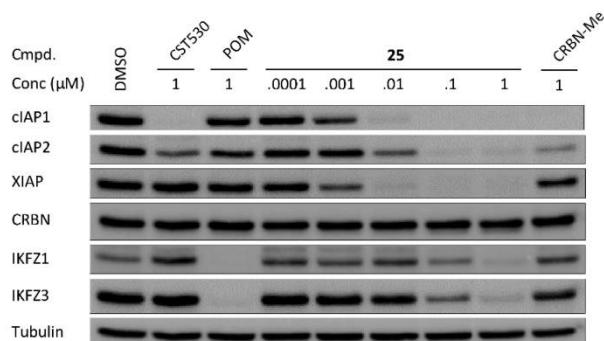


**Figure S12.** Knockout of individual IAPs in MM.1S cells do not influence VHL30 degradation by hetero-PROTAC 9. Individual IAP knock-out cells were treated with hetero-PROTACs at 0.1 μM for 16 h.

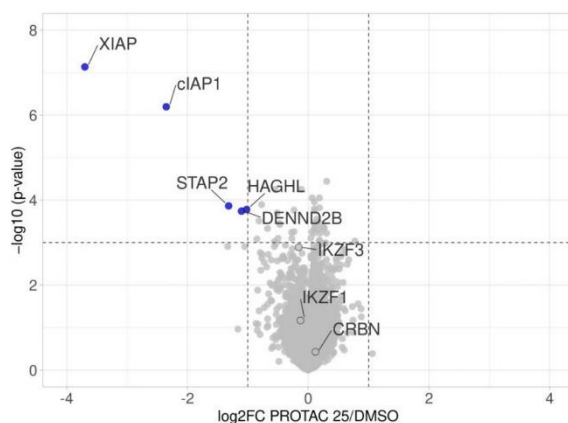


**Figure S13.** (A) Degradation of IAPs induced by hetero-PROTAC **9** is mediated *via* the ubiquitin-proteasome system. MG132, MLN4924, and MLN7243 prevent proteasomal degradation of IAPs. MM.1S cells were treated with 10  $\mu$ M MG132, MLN4924, or MLN7243 for 1 h before the addition of **9** for additional 3 h. (B) Degradation of IAPs induced by hetero-PROTAC **25** is mediated *via* the ubiquitin-proteasome system. MG132, MLN4924, and MLN7243 prevent proteasomal degradation of IAPs. MM.1S cells were treated with 10  $\mu$ M MG132, MLN4924, or MLN7243 for 1 h before the addition of **25** for further 3 h.

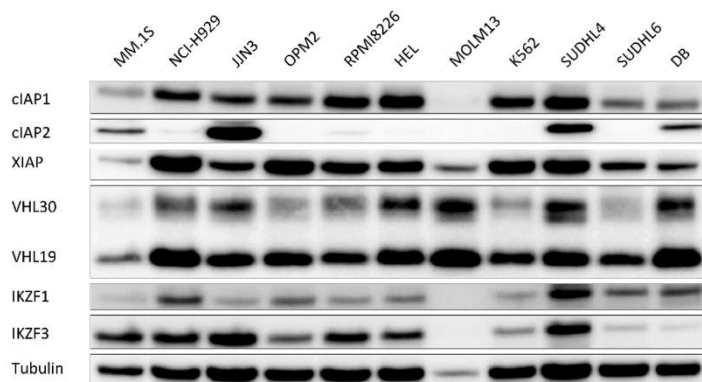




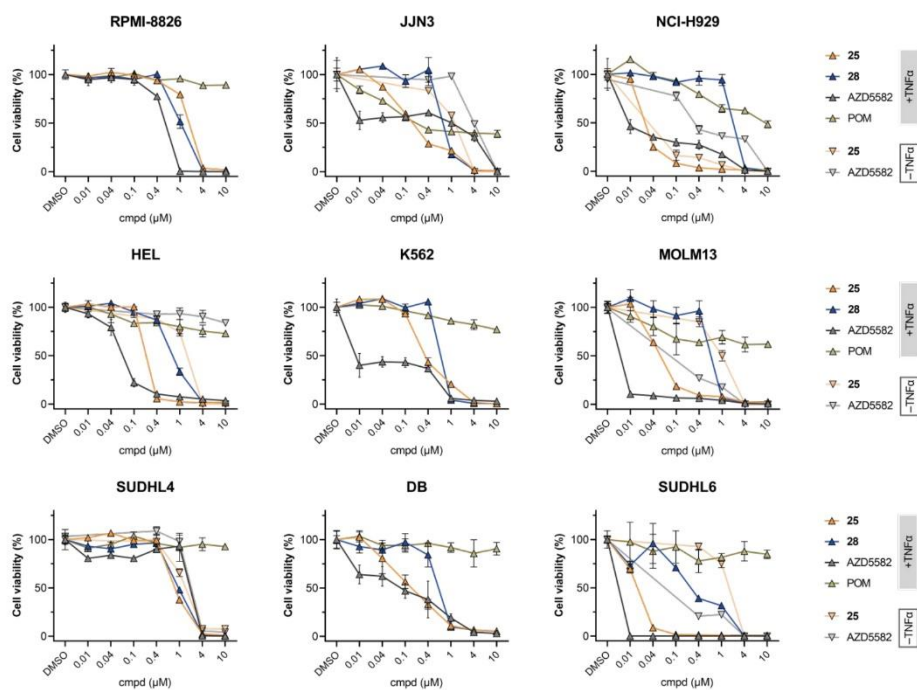
**Figure S14.** IAP-CRBN hetero-PROTAC **25** (SAB141) induces cIAP1, cIAP2, XIAP, IKZF1, and IKZF3 in a dose-dependent manner. CRBN-non-binding control **28** (CRBN-Me) only marginally degrades XIAP, IKZF1, and IKZF3. MM.1S cells were treated with compounds at indicated concentrations for 16 h.



**Figure S15.** diaPASEF quantitative proteomics for PROTAC **25**. MM.1S cells were treated with compound **25** at 0.1 μM for 3 h. The identified proteins were plotted as log<sub>2</sub> fold change (PROTAC/DMSO) versus -log<sub>10</sub> of p-value. Proteins with -log<sub>10</sub> (p-value) >3 (p-value <0.001) and log<sub>2</sub> fold change >1 or <-1 (translating to 2-fold up- or down-regulation) were considered to have significantly changed in abundance. Data are mean of biological duplicates.



**Figure S16.** Baseline expression of IAPs in a panel of hematological cell lines.



**Figure S17.** Cell viability screenings in 9 different hematological cancer cell lines with pan-IAP degrader **25**, its CRBN non-binding control **28**, as well as the advanced bivalent IAP antagonist AZD5582 and the CRBN binder pomalidomide (POM) as respective controls. In certain cases, viability inhibition was assessed in the presence and absence of TNF- $\alpha$ . Multiple myeloma, acute myeloid leukemia, and lymphoma cell lines were treated with the respective compounds at indicated concentrations for 96 h. Viability is normalized to their respective DMSO controls. Data represent means  $\pm$  s.d. of at least three independent biological replicates.

cell line	disease <sup>[a]</sup>	IC <sub>50</sub> (μM)			
		<b>25</b>	<b>28</b>	<b>AZD5582</b>	<b>POM</b>
<b>RPMI-8826</b>	MM	1.52	1.01	0.47	>10
<b>JJN3</b>	MM	0.18	0.90	0.20	0.042
<b>NCI-H929</b>	MM	0.027	1.99	0.014	>10
<b>HEL</b>	AML	0.30	0.77	0.064	>10
<b>K562</b>	AML	0.38	0.84	0.019	>10
<b>MOLM13</b>	AML	0.052	0.63	0.0020	>10
<b>SUDHL4</b>	DLBCL	0.92	1.00	1.64	>10
<b>DB</b>	DLBCL	0.16	0.57	0.073	>10
<b>SUDHL6</b>	DLBCL	0.014	0.44	0.0015	>10

[a] MM, multiple myeloma; AML, acute myeloid leukemia; DLBCL, diffuse large B-cell lymphoma.

**Table S8.** Cell viability profiles (IC<sub>50</sub> values) of the CRBN-recruiting PROTAC **25**, the CRBN non-binding control **28**, as well as the bivalent IAP antagonist AZD5582 and the CRBN ligand pomalidomide (POM) for comparison. Values correspond to TNF $\alpha$ -challenged conditions.



## **Curriculum Vitae**

My curriculum vitae does not appear in the electronic version of my paper for reasons of data protection.

## Publication list

Johannes Sievers, Rabea Voget, Feiteng Lu, Cindy H. Chau, **Yuen Lam Dora Ng**, Kathleen M. Garchitoren, Christian Steinebach, William D. Figg, Jan Krönke, and Michael Gütschow. “Revisiting the antiangiogenic mechanism of fluorinated thalidomide derivatives” *Bioorganic & Medicinal Chemistry Letters* 110, 129858 (2024)

Evelyn Ramberger, Valeriia Sapozhnikova, **Yuen Lam Dora Ng**, Anna Dolnik, Matthias Ziehm, Oliver Popp, Eric Sträng, Miriam Kull, Florian Grünschläger, Josefine Krüger, Manuela Benary, Sina Müller, Xiang Gao, Arunima Murgai, Mohamed Haji, Annika Schmidt, Raphael Lutz, Axel Nogai, Jan Braune, Dominik Laue, Christian Langer, Cyrus Kandhanpour, Florian Bassermann, Hartmut Döhner, Monika Engelhardt, Christian Straka, Michael Hundemer, Dieter Beule, Simon Haas, Ulrich Keller, Hermann Einsele, Lars Bullinger, Stefan Knop, Philipp Mertins, Jan Krönke. “Proteogenomic landscape of multiple myeloma.” *Nature Cancer* (2024)

Aleša Bricelj, **Yuen Lam Dora Ng**, Martina Gobec, Robert Kuchta, Wanyi Hu, Špela Javornik, Miha Rožič, Michael Gütschow, Guangrong Zheng, Jan Krönke, Christian Steinebach, and Izidor Sosič. “Design, Synthesis, and Evaluation of BCL-2 Targeting PROTACs.” *Chemistry—A European Journal* (2024)

Zefeng Wang\*, Shabnam Shaabani\*, Xiang Gao\*, **Yuen Lam Dora Ng**, Valeriia Sapozhnikova, Philipp Mertins, Jan Krönke, Alexander Dömling. “Direct-to-biology, automated, nano-scale synthesis, and phenotypic screening-enabled E3 ligase modulator discovery.” *Nat Commun* 14, 8437 (2023)

Christian Steinebach\*, Aleša Bricelj\*, Arunima Murgai\*, Izidor Sosič, Luca Bischof, **Yuen Lam Dora Ng**, Christopher Heim, Samuel Maiwald, Matic Proj, Rabea Voget, Felix Feller, Janez Košmrlj, Valeriia Sapozhnikova, Annika Schmidt, Maximilian Rudolf Zuleeg, Patricia Lemnitzer, Philipp Mertins, Finn K. Hansen, Michael Gütschow, Jan Krönke, and Marcus D. Hartmann. “Leveraging Ligand Affinity and Properties: Discovery of Novel Benzamide-Type Cereblon Binders for the Design of PROTACs.” *J Med Chem* 66, 21, 14513–14543 (2023)

**Yuen Lam Dora Ng\***, Aleša Bricelj\*, Jacqueline A. Jansen, Arunima Murgai, Kirsten Peter, Katherine A. Donovan, Michael Gütschow, Jan Krönke, Christian Steinebach, Izidor Sosič. “Heterobifunctional Ligase Recruiters Enable Pan-Degradation of Inhibitor of Apoptosis Proteins.” *J Med Chem* 66, 7, 4703–4733 (2023) (\*equal contribution)

Robert Kuchta, Christopher Heim, Alexander Herrmann, Samuel Maiwald, **Yuen Lam Dora Ng**, Izidor Sosič, Tim Keuler, Jan Krönke, Michael Gütschow, Marcus D. Hartmann, Christian Steinebach. “Accessing three-branched high-affinity cereblon ligands for molecular glue and protein degrader design.” *RSC Chemical Biology* 4, 229-234 (2023)

Guus J J E Heynen, Francis Baumgartner, Michael Heider, Upayan Patra, Maximilian Holz, Jan Braune, Melanie Kaiser, Isabell Schäffer, Stefanos A Bamopoulos, Evelyn Ramberger, Arunima Murgai, **Yuen Lam Dora Ng**, Uta Margareta Demel, Dominik Laue, Sven Liebig, Josefine Krüger, Martin Janz, Axel Nogai, Markus Schick, Philipp Mertins, Stefan Müller, Florian Bassermann, Jan Krönke, Ulrich Keller, Matthias Wirth. “SUMOylation inhibition overcomes proteasome inhibitor resistance in multiple myeloma.” *Blood Adv.* 7(4): 469–481 (2022)

**Yuen Lam Dora Ng\***, Evelyn Ramberger\*, Stephan Bohl, Anna Dolnik, Oliver Popp, Christian Steinebach, Miriam Kull, Mohamad Haji, Michael Gütschow, Hartmut Döhner, Lars Bullinger, Philipp Mertins, Jan Krönke. “Proteomic profiling reveals CDK6 upregulation as a targetable resistance mechanism for lenalidomide in multiple myeloma.” *Nat Commun* 13, 1009 (2022) (\*equal contribution)

Aleša Bricelj\*, **Yuen Lam Dora Ng\***, Dominic Ferber, Robert Kuchta, Sina Müller, Marius Monschke, Karl G. Wagner, Jan Krönke, Izidor Sosič, Michael Gütschow and Christian Steinebach. “Influence of Linker Attachment Points on Stability and Neosubstrate Degradation of Cereblon Ligands.” *ACS Med. Chem. Lett.* 12, 11, 1733–1738 (2021) (\*equal contribution)

Linda Röhner\*, **Yuen Lam Dora Ng\***, Annika Scheffold, Stefanie Lindner, Simon Köpff, Andreas Brandl, Andreas Beilhack, Jan Krönke. “Generation of a lenalidomide-sensitive syngeneic murine in vivo multiple myeloma model by expression of Crbn I391V.” *Exp Hematol.* 93, 61-69 (2021) (\*equal contribution)

Christian Steinebach\*, **Yuen Lam Dora Ng\***, Izidor Sosič, Chih-Shia Lee, Sirui Chen, Stefanie Lindner, Lan Phuong Vu, Aleša Bricelj, Reza Haschemi, Marius Monschke, Elisabeth Steinwarz, Karl G. Wagner, Gerd Bendas, Ji Luo, Michael Gütschow, Jan Krönke. “Systematic exploration of different E3 ubiquitin ligases: an approach towards potent and selective CDK6 degraders.” *Chemical Science* 11, 3474-3486 (2020) (\*equal contribution)

Christian Steinebach, Izidor Sosič, Stefanie Lindner, Aleša Bricelj, Franziska Kohl, **Yuen Lam Dora Ng**, Marius Monschke, Karl G. Wagner, Jan Krönke and Michael Gütschow. “A MedChem Toolbox for Cereblon-directed PROTACs.” *Med. Chem. Comm.* 10, 1037-1041 (2019)

Hansen, Carsten G, **Yuen Lam Dora Ng**, Wai-Ling Macrina Lam, Steven W. Plouffe, and Kun-Liang Guan. “The Hippo Pathway Effectors YAP and TAZ Promote Cell Growth by Modulating Amino Acid Signaling to mTORC1.” *Cell Research* 25, 1299–1313 (2015)

## Acknowledgments

I would like to express my heartfelt gratitude to Jan Krönke for our several years of endeavors spanning from Ulm to Berlin. From setting up the laboratory to embracing senior responsibilities, every step has been enriched with invaluable lessons and opportunities, and Jan has challenged me to learn continuously while providing immense support and encouragement. The culture of openness and respect under his mentorship has cultivated an environment where ideas are not only heard but valued, transforming discussions into avenues of ingenious insight. For this profound influence, I extend my sincere appreciation to Jan, whose mentorship has not only played a pivotal role in shaping my career trajectory but has consistently challenged me to strive for excellence throughout my doctoral studies. This experience would not only shape me both professionally and personally, but the inspiration and passion will prevail in my future scientific ventures.

My sincere gratitude extends to esteemed members of my doctoral committee Lars Bullinger and Philipp Mertins, for their generous investment of time and insightful discussions pertaining to my research endeavors. I am deeply grateful for their unwavering support throughout my academic pursuits and their approachability and collegiality, making professional interactions both productive and enjoyable.

To exceptionally brilliant and driven principal investigators Christian Steinebach, Izidor Sosič, Michael Gütschow, Alexander Dömling; and accomplished scientists Evelyn Ramberger, Valeria Sapozhnikova, Aleša Bricelj, and Anna Dolnik, all of whom I have had the privilege to collaborate closely with: you inspire me. I am grateful for everyone's patience throughout my learning process and willingness to share their expertise. Their drive and vision for the projects have undoubtedly enriched my understanding of the various research topics and have served as a great source of inspiration.

I would like to extend my gratitude to all members of the Krönke lab who have made it an exceptional workplace. I am particularly proud of the students I have had the pleasure to mentor: their scientific accomplishments, exceptional theses, and commitment to advancing their academic research and education are commendable. These meaningful experiences and personal growth as a scientist have been immensely fulfilling and gratifying for me. I would also like to acknowledge all colleagues from the neighboring labs. While there are too many to mention individually, their kind assistance and friendliness have been greatly appreciated.

My acknowledgment would not be complete without mentioning my greatest pillar of support during my doctoral studies, Nikita Singh. My best friend and my partner in crime who has been standing by me unconditionally through my highs and lows, I have learned much from you in and out of the lab, and my appreciation for your unchanging support is ineffable. My dear friends Yuexin Chen, Tarada



Tripetchr, Alexandra Niedermayer, Hannah Strobel, Sabrina Skambraks, Tatjana Meyer, Hazal Köse, and Sara Uhan, I cannot imagine how different my journey would have been without your tremendous support.

Lastly, I wish to convey my deepest and sincere gratitude to my parents and siblings for their unwavering support. I've dedicated nearly half of my life far away from home in pursuit of my aspirations and your unconditional sacrifice, unhesitating faith, and steadfast trust in my decisions have meant the world to me and have kept me going. I am eternally grateful and could not have asked for more. As I embark on the next phases of my career, no matter where in the world I may find myself, I strive to make you proud.